A Very Positive Image of Boron: Triarylborane Chromophores for Live Cell Imaging

Dissertation zur Erlangung des naturwissenschaftlichen Doktorgrades

der Julius-Maximilians-Universität Würzburg

Stefanie Ingrid Griesbeck

aus Eschenbach i. d. Opf.

Würzburg, 2019

Eingereicht bei der Fakultät für Chemie und Pharmazie am

_____

Gutachter der schriftlichen Arbeit

1. Gutachter: Prof. Dr. Dr. h. c. Todd B. Marder

2. Gutachter: Prof. Dr. Christoph Lambert

Prüfer des öffentlichen Promotionskolloquiums

1. Prüfer: Prof. Dr. Dr. h. c. Todd B. Marder

2. Prüfer: Prof. Dr. Christoph Lambert

3. Prüfer:

Datum des öffentlichen Promotionskolloquiums

_____

Doktorurkunde ausgehändigt am

_____

Für meine Familie

"I am among those who think that science has great beauty.
A scientist in his laboratory is not only a technician: he is also a child placed
before natural phenomena which impress him like a fairy tale."

Marie Curie, 1933

Die Experimente zur vorliegenden Arbeit wurden in der Zeit von Januar 2015 bis Februar 2019 am Institut für Anorganische Chemie der Julius-Maximilians-Universität Würzburg unter der Aufsicht von Prof. Dr. Dr. h. c. Todd B. Marder durchgeführt.

ACKNOWLEDGEMENT

First of all, I would like to thank **Prof. Dr. Dr. h. c. Todd B. Marder** for the infinite support during the last four years. I really appreciate the huge scientific freedom I had, the trust you always had in my work and myself, and the many advisory conversations about science and life. I will never forget your teasing regarding an academic career. Furthermore, I want to thank you for the great opportunities provided for me to be able to spend several months abroad. I had a fantastic time in Croatia and Japan and learned, in addition to the huge amount of chemistry, a lot about cultural diversity. I also enjoyed my time at several conferences (BORAM, IC3EM and the various Borchemikertreffen) and would like to thank you for these opportunites. It is an honor and pleasure to be part of the "Marder" family, and therefore, I would also like to thank Anne and Ian for the great time I had with you in Lisbon, Leeds or Würzburg.

I would like to thank **Prof. Dr. Shigehiro Yamaguchi** for the great opportunity to stay twice for several months in Nagoya. I will never forget when we met at the GRK conference in Würzburg and you invited me at the dinner to work with you. I had an amazing time and it was a pleasure to come back one year later. I learned so much during these two stays, and I am very thankful for all the help, explanations and discussions. Therefore, I also would like to thank your Associate Professors **Dr. Masayasu Taki**, **Dr. Yoshikatsu Sato**, **Dr. Aiko Fukazawa** and **Dr. Ogi Soichiro** for proofreading of manuscripts, discussions and translations from Japanese to English. Of course, I want to thank **Wang-san** and **Ogasawara-san**, for all their help regarding cell work, explanations thereof, proofreading and for the great time we had. Furthermore, I would like to thank **Marek**, **Paresh**, **Raul**, **Asraah**, **Cem**, **Philippa**, **Magnus**, **Johannes**, and **Ethan** for the international coffee breaks, lunches, ramen Tuesdays and the amazing weekend trips. I thank, the Japan Society for the Promotion of Science (JSPS) and the DAAD for providing the funding for my first trip to Japan. Concerning the JSPS I would also like to thank **Kathi**, **Niklas**, **Björn**, **Karina**, **Anna** and especially **Dianne** for the awesome time I had with you in Japan.

I would also like to thank my cooperation partners in Croatia **Dr. Ivo Piantanida**, **Dr. Željka Ban** and **Dr. Ivo Crnolatac**. Thank you very much for training me regarding DNA titrations, CD spectra, *etc*. and providing a better understanding of the behavior of my compounds. I am also very thankful for the time you invested to show me Zagreb and surroundings as well as the traditional Croatian food. I thank the DAAD and the Ministry of Science, Education and Sport of the Republic of Croatia for funding this travel.

I want to thank **Dr. Mireille Blanchard-Desce** and her co-workers **Adina Lazar** and **Guillaume Clermont** for the two-photon measurements and the two-photon imaging in Chapter 2.

Furthermore, I would like to thank my “in-house” collaboration partners. **Prof. Dr. Christoph Lambert** and his working group for thorough proofreading of the manuscripts, the opportunity to use their fluorescence spectrometer when my lifetimes were too short for our machine, and sharing of equipment, *e.g*. laser diodes. Especially, I would like to thank **Michail Evripidis** for all the TPA measurements. I want to thank **Prof. Dr. Lorenz Meinel** and his working group for the nice cooperation regarding my first paper and the DFG grant. Special thanks go to **Dr. Tessa Lühmann**, **Dr. Marcus Gutmann**, **Dr. Jennifer Ritzer** and **Martina Raschig** for their support regarding imaging, toxicology, as well as introductions to your equipment and other help.

Most important is, of course, the Marder group, without whom I would never have accomplished the research resulting in this thesis. Therefore, I would like to thank the permanent senior researchers **Prof. Dr. Andreas Steffen** (thank you for teaching me the secrets of spectroscopy), **Dr. Stephan Wagner** (thank you for the discussions on mass spectra and the massive number of GC-MS repair services), **Dr. Alexandra Friedrich** (thank you for solving plenty of crystal structures and proofreading) and **Dr. Rüdiger Bertermann** (thank you for conducting all my special NMR experiments, especially the solid-state ones and the help with the VT-NMRs). Of course I want to thank the boron materials team: **Dr. Zuolun Zhang** (thank you for introducing me to the wonderful world of boron and the start of my PhD topic), **Dr. Lei Ji** (thank you for the many discussions and the productive work on our review), **Julia Merz** (thank you for listening to all my problems while we were running, eating cheese cake or sushi or in any other situation. Thank you for being a great friend), **Florian Rauch** (thank you for the numerous discussions, synthetic advices, and calculations and for joining the back workout at the gym – I am not resentful of any “postponed” appointment – Hereby, I transfer to you the rule of the boron kingdom), **Matthias Ferger** and **Sarina Berger** (thank you both for the great time in lab 120, enduring my “Pur”, 90s and what so ever days, and the many, many, many discussions, help and support. I am very happy that you two take over my thesis topic, and I would also like to thank you for your hard work as my masters interns), and **Jiang He**, **Johannes Krebs**, **Dr. Jian Zhao**, **Dr. Xiangqing Jia** and **Zhu Whu**. Furthermore, I would like to thank the rest of the group, especially **Dr. Robert M. Edkins** (thank you for introducing me to the fluorescence spectrometer, you did an incredible job, and I still draw on many of your explanations. I also want to thank you for the help with the calculations, explanations and proofreading of the manuscripts), **Dr. Martin Eck** (it was a pleasure to share the lab with you and I am very thankful for everything – and I know it was a lot – you did for this group), **Dr. Lujia Mao**, **Dr. Emily Neeve** and **Dr. Goutam Kumar Kole** (thank you for being part of lab 120, and a lot of help and discussions), **Dr. Jörn Nitsch** (thank you for many calculations, discussions and proofreading of manuscripts), **Dr. Martin Haehnel**, **Dr. Antonius Eichhorn** and **Dr. Daniel Sieh** (thank you for solving my crystal structures – I know

it was not always an easy job with my thin needles), and **Jan Maier**, **Dr. Hashem Amini**, **Florian Kerner**, **Laura Kuehn**, and **Robert Ricker**.

Special thank goes to the AK Steffen. Especially, **Benjamin Hupp** (thank you for the incredible amount of organization, work and dealing with problems of our group – a Benni is irreplacable), **Markus Gernert** (thank you for many discussions and cheering me up with your moaning).

I would also like to thank all my interns: My bachelor students **Marvin Schock**, **Lukas Gerstner** (I am still impressed with how many coffees one can drink) and especially **Corinna Czernetzki** (thank you for your enthusiastic and optimistic manner - you always made me smile in the lab – and the enormous amount of work you did) and my masters students **Matthias Ferger**, **Sarina Berger** and **Theresa Zhang** (thank you for the large amount of reactions you did for me).

Of course, I also want to thank the technical staff of the Institute. **Sabine Lorenzen** (thank you so much for all the synthetic work you did for me, especially in the last few months. Assisting me with the re-synthesis of the diketopyrrolopyrrole dye was an enormous help. Furthermore, I would like to thank you for every task you did or problem you solved for the group: waste disposal, filling the SPS system, training of new students, … the list is endless), **Yannik Reuß** and **Tamara Stawski** (thank you for providing me with starting materials), **Helga Dietrich** and **Hildegard Holzinger** (thank you for ordering chemicals and plenty of consumables), **Christoph Mahler** (thank you for the measurements of uncountable mass spectra, the help for every jammed canula or flask and every “funny” email), **Marie-Luise Schäfer** (thank you for running my NMR spectra and for help with the VT-NMRs), **Sabine Timmroth** and **Liselotte Michels** (thank you for the elemental analysis measurements), **Gertrud Wunderling** (thank you for being the soul of this Institute – without you it would be a huge mess here), **Alfred Schertzer** (thank you for the argon and dry ice supply), the glass blower **Berthold Fertig** and the workshop team **Alois Ruf**, **Wolfgang Obert**, **Frank Förtsch**, **Michael Ramold**, **Manfred Reinhart** (thank you for the maintenance and repair of my equipment, a special thanks goes to Manny for solving every rotary evaporator problem immediately and spending many hours in our “organic” lab)

Furthermore, I would like to thank all the secretaries **Eleonore Klaus** (thank you for welcoming me so nicely in this group and your effort even after you left our Institute), **Bianca Putz**, **Stefanie Ziegler**, **Birgit Zepke** and especially **Maria Eckhardt** and **Cornelia Walter** (thank you for your enormous help in so many ways, last minute contracts, accounting of all my foreign travels,…)

Last but not least, I want to thank my friends and family. My mensa-connection and friends from university studies **Chrissi** and **Andrea** (thank you for your support and discussions, when the chemistry went wrong, but also for all the great days and evenings at wine festivals, Christmas

markets, the Escalera, …) and **Tina** (thank you for always having an open ear and the awesome travel time in Japan). I also want to thank my Würzburg girls **Nico** and **Juli** (thank you for all the cake/ice cream/sushi/wine we had together, and for always being there when I needed you) and **Caro** (thank you for listening when I came home dejected from work, and our time together in the shared flat or our "Wohnzimmer"). My friends from home, **Franzi**, **Steffi** and **Resi** thank you for the great coffee hangouts and relaxing days at the spa. My brother **Michi** (thank you for being you – I will always feel like I have to take care of you, no matter what you do), my sister **Sabrina** (thank you for being the best sister in the world and always being there for me). I want to thank especially **Julian** (thank you for going through the hard writing time with me – I know I was not easy to handle in the last months – I love you) and my **parents** (thank you for always standing by me, no matter what I do, for your infinite support especially during the last years, listening and giving advice, whenever I got stuck).

Thank You

LIST OF PUBLICATIONS

The publications listed below are partly reproduced in this dissertation with permission from the Royal Society of Chemistry and Wiley-VCH. The table itemizes at which position in this work the paper have been reproduced.

Publication	Position
J. Lei, S. Griesbeck, T. B. Marder, *Chem. Sci.* **2017**, *8*, 846-863.	Chapter 1
S. Griesbeck, Z. Zhang, M. Gutmann, T. Lühmann, R. M. Edkins, G. Clermont, A. N. Lazar, M. Haehnel, K. Edkins, A. Eichhorn, M. Blanchard-Desce, L. Meinel, T. B. Marder, *Chem. Eur. J.* **2016**, *22*, 14701-14706.	Chapter 2
S. Griesbeck, M. Evripidis, C. Wang, H. Ogasawara, S. Lorenzen, L. Gerstner, T. Zang, J. Nitsch, Y. Sato, R. Bertermann, M. Taki, C. Lambert, S. Yamaguchi, T. B. Marder, *submitted*.	Chapter 3
S. Griesbeck, M. Ferger, C. Czernetzki, C. Wang, R. Bertermann, A. Friedrich, M. Haehnel, D. Sieh, M. Taki, S. Yamaguchi, T. B. Marder, *submitted.*	Chapter 5

Further publications:

- M. Steeger, S. Griesbeck, A. Schmiedel, M. Holzapfel, I. Krummenacher, H. Braunschweig, C. Lambert, *Phys. Chem. Chem. Phys.* **2015**, *17*, 11848-11867.

- T. E. Stennett, P. Bissinger, S. Griesbeck, S. Ullrich, I. Krummenacher, M. Auth, A. Sperlich, M. Stolte, K. Radacki, C.-J. Yao, F. Würthner, A. Steffen, T. B. Marder, H. Braunschweig, *Angew. Chem. Int. Ed.* **2019**, 10.1002/anie.201900889, *Angew. Chem.* **2019**, 10.1002/ange.201900889

LIST OF ABBREVIATIONS

A	acceptor
Å	Ångström (1 Å = 10^{-10} m)
abs	absorption
AOTF	acousto-optic tunable filter
APCI	atmospheric-pressure chemical ionization
ATP	adenosine triphosphate
bipy	2,2'-bipyridine
Boc	*tert*-butyloxycarbonyl
br	broad
C_Q	quadrupole coupling constant
COD	1,5-cyclooctadiene
CT	charge transfer
D	donor
d	doublet
dba	dibenzylideneacetone
DFT	density functional theory
DLS	dynamic light scattering
DMEM	Dulbecco's Modified Eagle's Medium
DMSO	dimethyl sulfoxide
dtbpy	di-*tert*-butyl-2,2'-dipyridine
EPR	electron paramagnetic resonance
em	emission
FBS	fetal bovine serum
FLP	frustrated Lewis pair

FWHM	full-width-at-half-maximum
g	gerade
GM	Göppert-Mayer (1 GM = 10^{-50} cm^4 s $photon^{-1}$)
GSD	ground state depletion
HESI	heated-electrospray ionization
HOMO	highest occupied molecular orbital
i	*iso*
ICT	intramolecular charge transfer
IRF	instrument response function
k_r	radiative decay rate
k_{nr}	non-radiative decay rate
LD	laser diode
LE	locally excited
LIFDI	liquid injection field description ionization
LUMO	lowest unoccupied molecular orbital
m	multiplet
m	*meta*
MAS	magic-angle spinning
Mes	mesityl, 2,4,6-methylbenzene
Mes*	2,4,6-tri-*tert*-butylphenyl
MS	mass spectrometry
MTT	3-(4,5-dimethylthazol-2-yl)-2,5-diphenyltetrazolium bromide
m.w.	molecular weight
NHC	*N*-heterocyclic carbene
NIR	near-infrared

NLO	non-linear optics
NMR	nuclear magnetic resonance
NTO	natural transition orbital
o	*ortho*
OD	optical density
OFET	organic field-effect transistor
OLED	organic light emitting diode
OPA	one-photon absorption
OTf^-	triflate
PAH	polycyclic aromatic hydrocarbons
PALM	photoactivated localization microscopy
PBS	phosphate buffered saline
PCM	polarizable continuum model
PFA	*para*-formaldehyde
PHOLED	phosphorescent organic light-emitting diode
pin	pinacolato
Pfp	4-(pentafluorophenyl)-2,5-dimethylphenyl
q	quartet
RISC	reverse intersystem crossing
RNA	ribonucleic acid
RNS	reactive nitrogen species
ROS	reactive oxgen species
R_r	Pearson value, Pearson correlation coefficient
RSS	reactive sulfur species
r.t.	room temperature

S	singlet
s	singlet
SPhos	2-dicyclohexylphosphino-2',6'-dimethoxybiphenyl
SSIM	saturated structured illumination microscopy
STED	stimulated emission depletion
STORM	stochastic optical reconstruction microscopy
SOFI	super-resolution optical fluctuation imaging
T	triplet
t	triplet
t	*tert*
$t_{1/2}$	half-life
TADF	thermally activated delayed fluorescence
TCSPC	time-correlated single-photon counting
TD-DFT	time-dependent density functional theory
Tfp	4-(3,5-di(trifluoromethyl)-phenyl)-2,5-dimethylphenyl
THF	tetrahydrofuran
TICT	twisted intramolecular charge transfer
Tip	2,4,6-tri-*iso*-propylphenyl
TLC	thin-layer chromatography
TPA	two-photon absorption
TPEF	two-photon excited fluorescence
u	ungerade
UV	ultraviolet
V	coupling constant
Vis	visible

VT	variable temperature
WLL	white light laser
WST-1	4-[3-(4-iodophenyl)-2-(4-nitrophenyl)-2*H*-5-tetrazolio]-1,3-benzene disulfonate
β	first-order molecular hyper-polarizability
γ	second-order molecular hyper-polarizability
δ	chemical shift
ΔG^{00}	rotation barrier
ε	extinction coefficient
Φ_f	fluorescence quantum yield
λ	wavelength
ΔM_{01}	transition dipole moment difference between ground and excited state
$\Delta\mu_{01}$	dipole moment difference between ground and excited state
η_{EQE}	external quantum efficiencies
η_Q	quadrupolar asymmetry parameter
σ_2	two-photon cross-section
τ	fluorescence lifetime
τ_0	natural lifetime
$\tilde{\upsilon}$	wavenumber

ANNOTATION

I am aware that the dipole moment μ in charged compounds is origin dependent and not an observable quantity.[1] For simplification, I use the term dipole moment to describe the electron density distribution in the charged compounds. Thus, the terms dipole, quadrupole and octupole are used accordingly.

TABLE OF CONTENTS

CHAPTER ONE

-

INTRODUCTION

1 Introduction

The discovery of cells, cellular organelles and their processes relate to the development of microscopes, since Hooke coined the term “cell”, after observation of a piece of cork with his simple light microscope in 1665.[2] Two different kinds of microscopes are distinguished, namely electron and light microscopy and, depending on the scientific question, one or the other is more applicable. Although electron microscopes have much higher resolution (0.2 nm) than light microscopes, they are more expensive and technically more difficult to operate.[2a] Dynamic processes of live cells cannot be observed, as the cells need to be fixed and stained, which can introduce artefacts.[2a] With light microscopes, live cells can be studied, which provide information about cell structures and processes in real time.[3] Observations of dynamic changes provide more insight into the operations of a cell than a snapshot of the fixed cells can tell.[3] Although the diffraction of light limits the spatial resolution to 0.22 μm, with a light microscope subcellular structures can be observed using fluorescent probes.[2a] Recently, the development of super-resolution light microscopy techniques broke the diffraction barrier and increased the resolution of fluorescence microscopy to the range of 10-100 nm.[2a] Live-cell imaging has applications in examining structural components of a cell, studying dynamic cell processes and localization of molecules.[3] Furthermore, cell integrity, endocytosis, exocytosis, protein trafficking, signal transduction and enzyme activity can be observed.[3] How molecules translocate, interact or respond to environmental cues or other molecules can be monitored within live animals.[3] For each of these applications, different light microscopes may be applicable. The use of the different transmission light microscopy techniques, bright-field, phase-contrast or differential interference-contrast microscopy, is the easiest approach.[2] However, fluorescence microscopy, which uses reflected rather than transmitted light, has the advantage that the molecule, protein or organelle of interest is labeled with a fluorescent dye and that different fluorescent dyes can be applied simultaneously to stain different or the same components of the cell and can be detected simultaneously.[2a, 3] The images obtained by conventional wide-field fluorescence microscopy are blurred as a result of out-of-focus fluorescence, leading to reduction of contrast and resolution.[2a, 3] This can be improved by image deconvolution, a computational approach, or the use of a confocal microscope.[2a] This suppresses this problem, as the sample is excited by a focused laser beam only at a single point at a particular depth (in the focus plane).[2a, 3] A precisely placed pinhole aperture at the point where light emitted from the chosen plane comes to a focus, selects the emitted light, whereby only light emitted from the focus plane is able to reach the detector after passing through the pinhole.[2a, 3] More advanced fluorescence microscopy techniques include two-photon excited fluorescence (TPEF) microscopy and the super-resolution techniques.

With the super-resolution techniques, Abbe's diffraction barrier was broken (*vide infra*) and highly resolved images could be obtained.[4] The key to overcome the diffraction limit is spatial and/or temporal modulation of the transition between two molecular states of a fluorophore.[4] Super-resolution can be achieved by three different techniques. Narrowing the point spread function, the apparent shape of a point target as it appears in the output image, with stimulated emission depletion (STED), ground-state depletion (GSD) and saturated structured illumination microscopy (SSIM) is one method.[4] Another is the detection of a single molecule, which includes photoactivated localization microscopy (PALM), stochastic optical reconstruction microscopy (STORM) and more specific techniques.[4] The newest one is super-resolution optical fluctuation imaging (SOFI), which uses the fact that the emission of each single fluorescent emitter fluctuates independently.[5] The recent development of super-resolution imaging techniques has enabled the visualization of cellular features with previously unimagined detail.[4] Nevertheless, super-resolution microscopes are still very expensive, the required instrumentation complicated and fluorescent probes limit the performance of super-resolution imaging.[4] For STED microscopy, fluorophores need to be highly fluorescent and photostable, due to the powerful STED laser beam, while chromophores used for PALM or STORM techniques require reversible or irreversible photoactivatable or photoshiftable behavior. Dyes for SOFI imaging need fluctuating fluorescence intensities under the illumination of the laser beam.[5]

Two-photon microscopy is the healthy choice for live-cell imaging, as the excitation only occurs within a very limited region and with longer wavelengths.[6] Two-photon excitation is based on the simultaneous absorption of two photons by a single fluorophore molecule. Therefore, TPEF microscopy is inherently confocal as the simultaneous absorption only occurs in the highly photon-dense laser focal volume (~ 1 femto liter).[7] As two photons are used for excitation, less energetic light can be used to reach the excited state. The longer wavelength light combined with fluorescence only at the focus of the laser beam leads to less phototoxicity and allows much deeper penetration (~ 1 mm), as it scatters less within the tissue.[6-7] For thick specimens, live animals or in tissue-slice cultures, such as *in vivo* imaging, or where the dye would normally require UV excitation, TPEF microscopy is an excellent and often the only choice.[6-7] Although existing one-photon probes can be used, high laser power is often required to obtain clear images owing to the small two-photon absorption cross-section.[8]

As the development of new microscopy techniques is rapidly advancing, the need of new bright fluorescent material is necessary. Fluorescent probes should be smaller, exceptionally photostable, biocompatible and bearing large extinction coefficients and high fluorescence quantum yields to allow video-rate imaging with molecular resolution in the future.[4-5]

Within this work, a new class of dyes, triarylboranes, will be applied for fluorescence microscopy, especially two-photon excited fluorescence live-cell imaging, as this sort of compounds is known for its efficient use in non-linear optics (Chapter 1.7). At the start of this thesis, no triarylborane chromophore was applied in live-cell imaging. Many different aspects need to be investigated in this completely new field. Water-solubility and stability (Chapter 2) must be achieved, the two-photon properties optimized in aqueous conditions (Chapter 3 and 4) and the fluorescence quantum yield enhanced, while maintaining stability (Chapter 5). In the following introduction, a general overview of the applications of this class of dyes is given.

The following section is slightly modified and reproduced from ref. [9] with permission from the Royal Society of Chemistry.

1.1 General Introduction to Triarylboranes

Three-coordinate boron has a trigonal-planar geometry with an empty p_z-orbital and is isoelectronic with a carbonium ion. While such compounds are well-known as Lewis acids, binding Lewis bases *via* the empty orbital, suitable steric hindrance can inhibit such interactions leading to what are now termed "Frustrated Lewis Pairs" or FLPs.[10] Interest in FLPs has grown rapidly with their demonstrated ability to activate small molecules such as H_2. However, what is often overlooked is the fact that steric hindrance around the boron center was recognized several decades ago as providing a useful way to prepare air-stable triarylboranes in which the protected empty p_z-orbital on boron can act as a strong π-acceptor (A) in conjugated organic π-systems.[11] Thus, in the 1970's, a group at Kodak first examined the solvatochromic emission properties of compounds of the form 4-D–C_6H_4–$BMes_2$ where D is a π-donor, such as Me_2N, and Mes is the bulky mesityl group, 2,4,6-$Me_3C_6H_2$.[12] In fact, these were indeed FLPs insofar as the Lewis basic Me_2N-group was inhibited by the bulk of the $BMes_2$ moiety from forming N–B dative bonds. Thus, the propeller arrangements of the *ortho*-methyl substituted benzenes generally shields the boron p_z-orbital from attack by Lewis bases or nucleophiles with the exception of very small anions such as F^- and CN^-. As such, compounds of this type have been developed recently as selective anion sensors.[13] In fact, 4-D–C_6H_4–$BMes_2$ represents an excellent and simple example of a compound exhibiting intramolecular charge transfer (ICT) behavior upon photoexcitation, as illustrated by its strongly solvatochromic fluorescence emission. Historically, Marder's and Lequan's group recognized the ability of (aryl)–$BMes_2$ systems to exhibit interesting second order non-linear optical (NLO) properties as early as 1990,[14] and Marder and co-workers reported on the 2nd order NLO behavior of a series of D–π–A (A = $BMes_2$ acceptor) compounds then, with more detailed experimental and theoretical studies following sometime later.[15] They also prepared a series of compounds incorporating diarylphosphino π-donor

groups, namely *trans*-Ph_2P–CH=CH–$BMes_2$, Ph_2P–C≡C–$BMes_2$ and 1,4-Ph_2P–C_6H_4–$BMes_2$ in the early 1990's,[14a, 14f] setting the stage for the fascinating 1,4-Ar_2P–C_6F_4–$B(C_6F_5)_2$ FLPs developed by Welch and Stephan *et al.* in 2006.[10a] Early on, Marder and co-workers also recognized the potential of centrosymmetric compounds containing two terminal $BMes_2$ moieties linked by an extended organic π-system to function as third order NLO materials.[16] Subsequently, they and many research groups have reported a wide range of interesting electronic and optical properties of three-coordinate boron and related compounds and polymers, and Marder's group reviewed the early work in this field in 2002 and 2004.[17] The applications of three-coordinate boron compounds in electronic and optical materials have expanded very rapidly over the past two decades.[13b, 18] In this chapter, a few recent contributions using $BMes_2$ moieties along with the development of alternative strong B-based π-acceptors by the Marder group and others are highlighted, focusing on systems which retain or enhance the air-stability of such species, a property which is most desirable for ease of preparation and handling, and thus for use in electronic or optical devices and other applications.

1.2 Modifying the Electronic Properties of Three-Coordinate Boron

The solvatochromic behavior of many D–π–A compounds using dimesitylboryl or related three-coordinate boron moieties as the electron accepting group has been widely explored. Below, the most important recent examples are highlighted. Lambert reported a very interesting octupolar trigonal compound **1-1** with *tris*(2,6-xylyl)boron as the core, attached to three carbazole donors at the 4-positions (Scheme 1-1).[19] They showed in solution, using polarized steady-state fluorescence spectroscopy, a symmetry-broken ground state. Upon photoexcitation, an inversion of the dipole moment takes place, leading to a negative solvatochromism for the charge transfer absorption band, while the emission spectrum is positively affected. Furthermore, they proposed a dynamic dipole moment in the excited state, which can hop between the branches of the otherwise symmetric molecule.[20] Thereby, the dipole moment can respond to the solvent relaxation and change its direction according to the local field of the solvation shell, thus leading to a faster energy relaxation compared to a model compound with just one donor moiety.

By employing $BMes_2$ as the acceptor, Wang and co-workers have reported the first few examples of through-space ICT in such compounds, which included the U-shaped 1,8-naphthylenediyl and V-shaped silylene-spaced donor acceptor compounds **1-2** and **1-3**.[21] These compounds are strongly emissive and can be used as F^- sensors. More recently, Zhao and co-workers reported a simpler compound exhibiting through-space ICT, with a dimesitylborane and a dimethylamine incorporated at the *o*, *o*'-positions of a biphenyl framework **1-4**.[22] The Lambert group reported

a hexaarylbenzene with three triarylamine donors and three triarylborane acceptors with weak donor-acceptor interactions due to through-space charge transfer.[23] Additionally, the excitation energy can be redistributed between the aryl substituents within the fluorescence lifetime. Highly fluorescent *N*-borylated 2,5-diarylpyrroles with dimesitylborane as the acceptor moiety were reported by Yamaguchi in 2013.[24] These molecules show a twisted conformation in the ground state, which is planarized in the excited state, leading to an increased electron-donating ability of the nitrogen by enhanced π-delocalization. Therefore, the ICT character is increased by stronger donors, resulting in a more red-shifted emission. Müllen reported boron-nitrogen containing 'dendrimers', the optical properties of which can be controlled by the donor/acceptor ratio. A ratio of 1:1 exhibits a more efficient charge transfer than the 1:2 analogue, and therefore a stronger solvent dependence.[25]

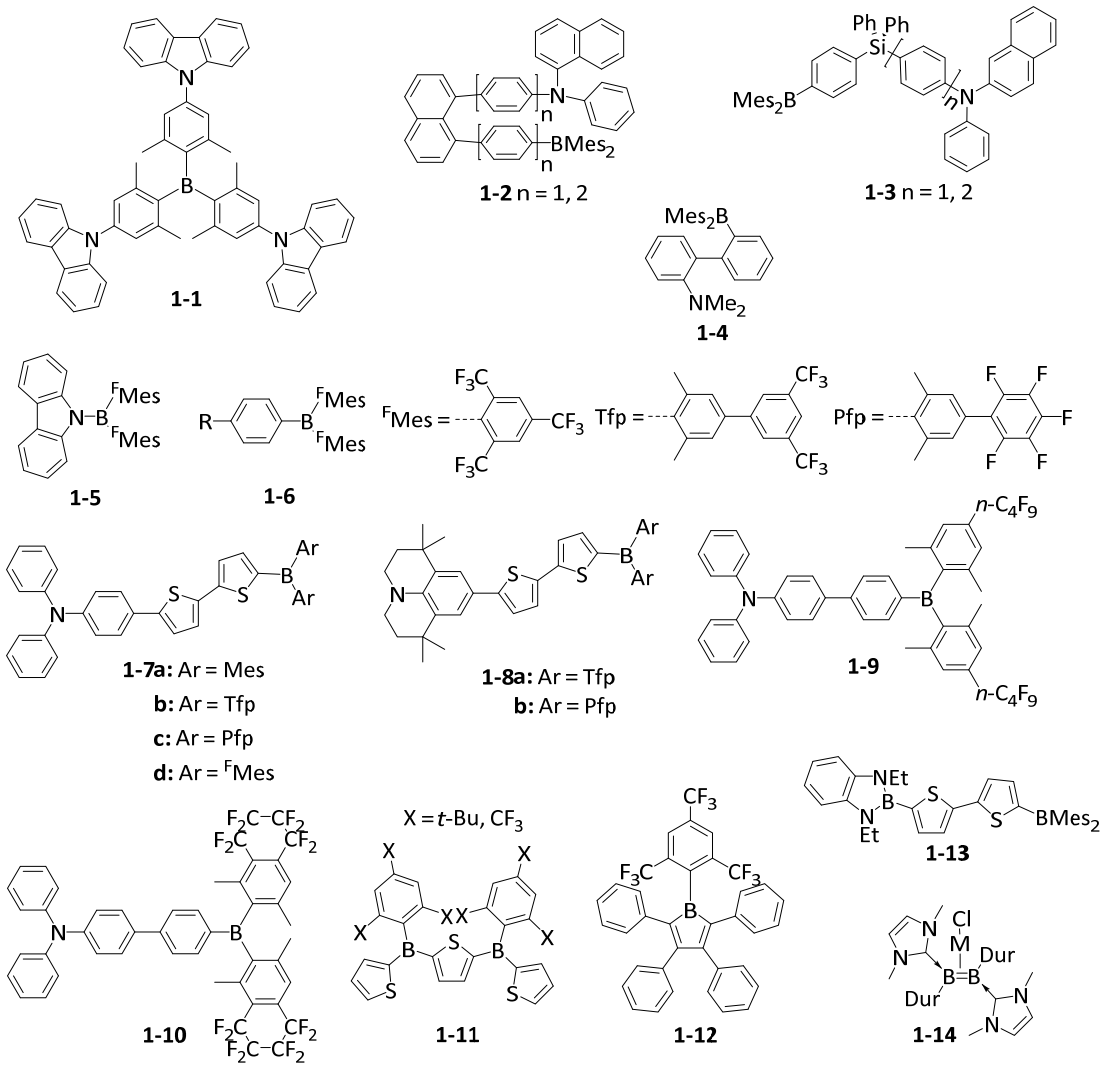

Scheme 1-1. Three-coordinate boron compounds with different electronic properties.

In 2003, working with K. Dillon, Marder's group reported the synthesis of $FB(^FMes)_2$ (^FMes = 2,4,6-$(CF_3)_3C_6H_2$), the trifluoromethyl analogue of $FBMes_2$, and this is a useful precursor to a series of compounds containing the $B(^FMes)_2$ group.[26] In addition, they decided to explore,

theoretically, the electronic effect of substituents, X, on boron on the HOMO and LUMO in a consistent series of compounds of the form 2,5′-$(BX_2)_2$–$(C_4H_2S)_2$, *i.e.*, related to and including 2,5′-$(BMes_2)_2$–dithiophene previously employed by Shirota as an electron transporter in OLEDs (*vide infra*).[27] Examination of X = C_6F_5 and 2,4,6-$(CF_3)_3C_6H_2$, i.e., ^{F}Mes, showed that these two fluorinated arenes had fairly similar electronic effects, dropping the LUMO by *ca*. 1 eV with respect to X = Mes. While Jäkle had used $B(C_6F_5)_2$ moieties successfully to provide strong Lewis acidity, these systems are not stable to water.[28] In contrast, Marder and co-workers found that electronically similar but sterically very demanding ^{F}Mes provides new air-stable, readily reducible boron compounds with strongly enhanced π-acceptor character.

With this in mind, Marder and Yamaguchi began to explore the optical properties of donor-substituted $B(^FMes)_2$ compounds. While Marder's work was in progress, Yamaguchi thus reported the synthesis of carbazole directly bonded to a $B(^FMes)_2$ group *via* its N-atom **1-5**.[29] They observed a strong red shift in emission compared with the $BMes_2$ analogue, and also noted evidence for a twisted intramolecular charge transfer (TICT) excited state, with their calculations suggesting that this state maintained 2-fold rotational symmetry. Recently, Thilagar and co-workers have reported the TICT behavior of 4-$BMes_2$aniline.[30] Marder's group prepared two compounds of the form 4-R–C_6H_4–$B(^FMes)_2$ **1-6**, wherein R = *t*-Bu or the strong π-donor Ph_2N.[31] For comparison, they also prepared the known 4-Ph_2N–C_6H_4–$BMes_2$ analogue. In addition, Stephan's group had simultaneously prepared $PhB(^FMes)_2$ and had shown that it was so sterically hindered at the boron center that it did not form FLPs with phosphines that were capable of activating even the smallest molecule, H_2. In contrast, the less hindered compound $HB(^FMes)_2$ was shown to exhibit interesting chemical reactivity.[32]

Marder and co-workers first measured the redox properties of their aryl-$B(^FMes)_2$ compounds and, as expected, these showed reduction potentials which were *ca*. 1 V lower than that of 1,4-Ph_2N–C_6H_4–$BMes_2$, consistent with their previous calculations on the thienyl-bridged three-coordinate boron compounds, *vide supra*. They then explored the photophysical behavior of the new $ArB(^FMes)_2$ compounds. Having shown that $B(^FMes)_2$ is an exceptional π-acceptor, they also noted that this led to quenching of emission in more polar solvents due to TICT behavior, in which, in contrast to the study by Yamaguchi,[29] it appears that one ^{F}Mes group rotates into the BC_3 plane in the excited state.[31]

Marder and co-workers thus decided to prepare analogues with acceptor strengths lying between those of $BMes_2$ and $B(^FMes)_2$ in order to tune the properties of their systems, as the $BMes_2$ compounds they had examined thus far did not show signs of TICT behavior.[33] A straightforward approach was to make use of the steric selectivety of the Ir-catalyzed C–H

borylation methodology.[34] Thus, direct borylation of 1-Br-2,6-Me_2-C_6H_3 gave 1-Br-2,6-Me_2-4-Bpin-C_6H_2 which was then coupled with either 1-Br-3,5-$(CF_3)_2C_6H_3$ or BrC_6F_5 yielding the two respective 1-Br-2,6-Me_2-4-Ar^F-C_6H_2 derivatives Tfp–Br and Pfp–Br (for the structures of Tfp and Pfp see Scheme 1-1) *via* Pd-catalyzed Suzuki-Miyaura reactions. Thus, they synthesized two series of D–π–A compounds, each with triphenylamine (**1-7**) or julolidine (**1-8**) as the donor, where A is BAr_2 (Ar = Mes, Tfp, Pfp, ^{F}Mes). These compounds show high quantum yields up to unity. By comparing their photophysical properties and cyclic voltammetry, they established the order of acceptor strength as $BMes_2 < B(Pfp)_2 \approx B(Tfp)_2 << B(^FMes)_2$.[33] In contrast to the $B(^FMes)_2$ compounds, these systems showed strong emission in the red-NIR region in polar solvents. Wakamiya and Yamaguchi recently reported compounds **1-9** and **1-10**, which bear *n*-C_4F_9 at the 4-position or a $–CF_2CF_2CF_2CF_2–$ loop at the 3,4-positions of 2,6-xylyl group.[35] Both systems show enhanced strong acceptor properties, while maintaining high fluorescence quantum yields in polar solvents.

A single ^{F}Mes on boron is sufficient to provide a dramatic enhancement of stability and greatly improved acceptor ability with respect to Mes. Thus, Jäkle and Marder reported a series of air- and moisture-stable conjugated thienylboranes **1-11**, which are inert even to acids and strong bases, due to their bulky ^{F}Mes or 2,4,6-tri-*tert*-butylphenyl (Mes*) groups.[36] In contrast to the Mes* groups, the ^{F}Mes compounds also exhibit a high Lewis acidity towards very small anions, because of their highly electron-withdrawing character.

Boroles ($RBC_4R'_4$) represent another interesting class of electron-deficient three-coordinate boron compounds, being 4π-antiaromatic analogues of $[C_5H_5]^+$.[37] They are, however, notoriously sensitive to air, water and various dimerization processes.[38] Marder and co-workers recently demonstrated a *ca*. 600-fold improvement in stability towards water for pentaarylborole **1-12**, with a bulky ^{F}Mes group on the boron, compared to its mesityl analogue, whilst at the same time enhancing the electron-deficient character of the borole.[39] This borole was prepared through a new and general method for borole synthesis, by reaction of $Li[(^FMes)BF_3]$ with 1,4-dilithio-1,3-butadiene reagents,[40] and it shows good thermal stability without dimerizing or isomerizing as reported for some other boroles. Thus, an air-stable $ArBF_3$ salt can serve as the electrophile in place of more sensitive $ArBX_2$ compounds.[41] Meanwhile, Wagner and co-workers reported the preparation of triarylboranes by nucleophilic reaction of aryllithium reagents with an $ArBF_3K$ salt.[42] Dixon, Rupar and co-workers reported the stability of dibenzoborole (borafluorenes) with various substituents on the boron atom. They disclosed that ^{F}Mes is an outstanding protecting group comparable with the Tip group (Tip = 2,4,6-

*i*Pr$_3$C$_6$H$_2$). The ^{F}Mes protected dibenzoborole could be isolated by silica column chromatography in air and only 5% decomposition after 24 hours in solution under air occurred.

In 2009, as part of an experimental and theoretical study of the optical properties of another type of three-coordinate boron center, namely the benzodiazaboroles of L. Weber *et al*., Marder's group noted that these species could unexpectedly serve as a π-donor, a novel observation for a three-coordinate boron moiety.[27, 43] This allowed the development of a series, *e.g*. **1-13**, of π-linked dipolar compounds featuring three-coordinate boron centers in the role of both π-donor and π-acceptor.[43b-d] A new group of three-coordinate boron compounds in which the very electron-rich B=B double bond can serve as a strong π-donor **1-14** has been reported by the Braunschweig group. Neutral NHC-stabilized diborenes coordinate to Ag^I and Cu^I in an olefin-like η^2 mode, which is mostly of electrostatic nature due to the high electron density on the B=B double bond.[44] These metal complexes are highly luminescent compared to their olefin analogues.

1.3 Three-Coordinate Boron-Based Radicals

As a consequence of the strong π-acceptor properties of the three-coordinate boron unit, triarylboranes have been demonstrated to be good negative-charge and spin carriers.[45] Most of the boron-containing radical anions can be prepared by reduction with alkali metals or other strong reducing agents. Bulky groups are needed to protect the boron radical center from the formation of diamagnetic clusters. The $BMes_3$ radical anion has been studied in detail since the 1950s, demonstrating that the negative charge resides mostly on the boron center, but is also delocalized into the mesityl groups to some extent.[46] Its lithium salt was isolated and characterized by single crystal X-ray diffraction in 1986 by Power and co-workers.[47] They reported that the geometry of the radical anion of $BMes_3$ is very similar to that of the neutral $BMes_3$, with a slight elongation of the B–C bonds. Subsequently, the study of boron-based radicals, the formation of boron-boron one-electron bonds, and arene-bridged mixed valent diboranes has attracted much attention.[48]

Early on, Kaim also recognized the π-acceptor ability of the $BMes_2$ group, examining the electrochemical reduction of, for example, 1,4-Mes_2B–C_6H_4–$BMes_2$ (**1-15**) and 4,4'-Mes_2B–$(C_6H_4)_2$–$BMes_2$ (**1-16**), showing that the extra electron in the radical anion was completely delocalized over the two boron centers as well as the bridging phenylene or biphenylene group, resulting in what has been referred to as a boron mixed-valence compound, analogous to widely studied transition metal mixed-valence-species (Scheme 1-2).[49] Indeed, compounds such as **1-16** are the inverse of the 4,4'-Ar_2N–$(C_6H_4)_2$–NAr_2 systems, which are widely used as hole transport materials in OLEDs due to their ease of oxidation to their respective radical cations.[50]

Shirota has employed thienyl-bridged $Mes_2B–(C_4H_2S)_n–BMes_2$ compounds (n = 2,3) as electron transporters in OLEDs.[51] Marder and co-workers have recently confirmed, by isolation of its anion salt and determination of its molecular structure by single-crystal X-ray diffraction, that in the radical anion of **1-15** the unpaired electron is fully delocalized between the two $BMes_2$ group and the phenylene bridge.[52]

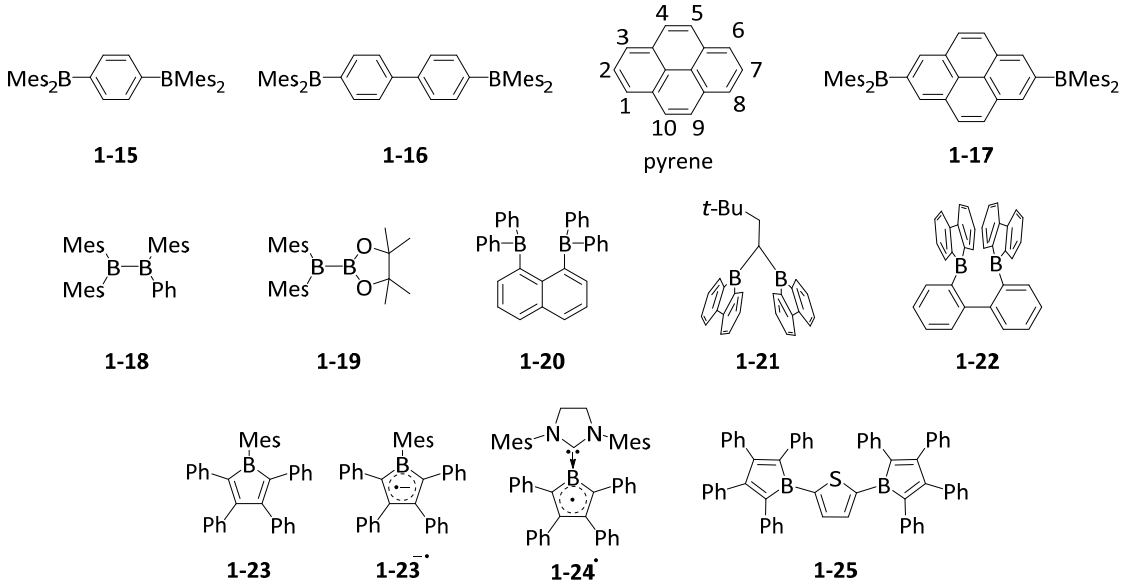

Scheme 1-2. Three-coordinate boron radicals and their precursors.

Pyrene is a prototypical luminescent polycyclic aromatic compound which exhibits highly efficient fluorescence and an unusual long singlet lifetime.[53] Thus, pyrene and its derivatives have been widely employed in numerous applications. Interestingly, however, both the HOMO and the LUMO of pyrene possess a nodal plane perpendicular to the molecular plane and passing through carbon atoms 2 and 7 (Scheme 1-2) lying along the long molecular 2-fold axis. As such, neither electrophilic nor nucleophilic aromatic substitutions typically take place at C_2 or C_7. However, as these are the least sterically demanding sites, iridium-catalyzed direct C–H borylation of pyrene with B_2pin_2 (pin = $OCMe_2CMe_2O$) takes place exactly at these positions, as steric effects dominate over electronic ones.[34, 54] This has allowed Marder's group to prepare 2,7-*bis*(Bpin)pyrene in excellent yield and on a large scale directly from pyrene, and the product can also be readily converted to 2,7-dibromopyrene in the same pot.[55] This has opened up a new avenue in pyrene chemistry by providing an efficient, rapid route to a wide variety of desirable 2,7-pyrene derivatives *via* simple pyrene reagents which can act as formal nucleophilic or electrophilic partners, respectively, in cross-coupling reactions as well as being useful precursors for classical organic reactions.

Normally, substituting the 2- or 2,7-positions with odd-electron substituents does not cause strong communication between the substituents and pyrene, which would generate high spin

radicals at room temperature.[56] This is due to the lack of mixing between the HOMO and LUMO of pyrene and those of the substituents. In fact, Marder and co-workers have reported the electronic structure and photophysical properties of 2-($BMes_2$)pyrene in 2011.[57] In that paper, they noted that the introduction of the strong π-acceptor $BMes_2$ groups allows mixing of the empty p_z-orbital of the boron with the LUMO+1 orbital of pyrene (it cannot mix with the LUMO due to its nodal properties, *vide supra*).[57] This stabilizes what was the pyrene LUMO+1 sufficiently to drop it below the "pyrene-LUMO" in energy, reversing the order of these two virtual frontier orbitals. This is a particularly nice illustration of the excellent π-acceptor properties of $BMes_2$ and its ability to conjugate with organic π-systems. As a result, reduction of 2- and 2,7-$BMes_2$-substituted pyrenes would be expected to show electron delocalization between the boron and pyrene. Thus, they prepared **1-17**, which can be readily reduced to its radical monoanion and its diamagnetic dianion, all of which have been characterized by single-crystal X-ray diffraction.[52] All three compounds are crystallographically centrosymmetric, and experimental and theoretical studies confirm the full delocalization of the "extra" 1 and 2 electrons in the radical anion and the dianion over the pyrenylene bridge as well as the two boron centers. As an aside, they note that the introduction of strong π-donors (*e.g.*, R_2N) at the 2- or 2,7-positions allows mixing with the HOMO-1 of pyrene (recall that mixing with the pyrene HOMO is also excluded due to its nodal properties) raising it in energy above what was the pyrene HOMO.[58] Thus, not only the order of LUMO and LUMO+1 can be reversed, but also that of HOMO and HOMO-1 by judicious choice of substituents.[59]

Beyond the arene bridged diboranes, the formation of B–B bonds during reduction is very important for the development of bonding theory. In organic diboron compounds such as **1-18** and **1-19**,[60] one- and two-electron reductions lead to the formation of one-electron B–B π-bonds and B=B double bonds, respectively.[61] Recently, the formation of a one-electron σ-bond by reduction of *bis*(organoboron) compounds, when appropriately spatially separated, has been disclosed. In 2000, Gabbaï and co-workers reported the one-electron reduction of 1,8-*bis*(diphenylboryl)naphthalene (**1-20**), in which the two boron centers are spatially close to one another.[62] The EPR spectrum of the radical anion of **1-20** reveals the delocalization of the unpaired electron between the two boron centers. DFT calculations show that there is a strong one-electron σ-bond between the two boron centers, with a slight decrease of the B–B distance and pyramidalization of the BC_3 moieties. The formation of another B–B one-electron σ-bond was recently reported by Wagner *et al*.[63] The X-ray crystal structures of the radical anions of **1-21** and **1-22** reveal a decrease of the B–B distance compared to the neutral compounds. EPR spectroscopy and DFT calculations further confirmed the formation of a B–B one-electron σ-bond.

Another interesting boron radical system is the one-electron reduced anti-aromatic free borole **1-23**. The hyperfine coupling constant of its boron (3.44 G) is much smaller than that of triarylborane radical anions, indicating a much stronger delocalization of the unpaired electron into the borole ring.[41] The change in bond length alternation confirms the delocalization of the unpaired electron. However, trapping of the radical anion with dibenzoyl peroxide reveals that the spin is still largely populated on the boron atom. Recently, Braunschweig and co-workers reported a neutral borole radical **1-24•**, in which the boron was stabilized by an NHC.[64] The EPR spectrum of this borole radical ($A(^{11}B)$ = 3.02 G) shows more delocalization of the unpaired electron within the five-membered ring compared to the afore-mentioned pentaaryl borole radical anion.[64-65]

Interestingly, the dianion of 2,5-diborolylthiophene **1-25** also shows complete delocalization of the unpaired electron. The single-crystal X-ray structure and theoretical studies of the dianion of the diborolylthiophene reveal its quinoidal structure with singlet biradical character.[66]

1.4 Boron-Containing Polycyclic π-Systems

Polycyclic aromatic hydrocarbons (PAHs) are very important in organic electronics, for example, as hole/charge transporters in organic field-effect transistors (OFETs). Depending on the demands of the device, different heteroatoms are introduced into the π-systems, to adjust the HOMO and LUMO levels of PAHs and thus their photophysical and electrochemical properties. Although many hetero PAHs with electron-rich sulfur and nitrogen have been reported, compounds with electron-deficient boron atoms, which have empty p_z-orbitals,[67] have rarely been studied, although BN-containing systems have received considerable attention.[68] Fundamental studies of the aromatic/anti-aromatic, chemical, and photophysical properties of the fused 5-membered boroles[69] and the 7-membered borepin[70] have been discussed in the last decade, and they have been reviewed in detail recently.[18a, 35, 67, 71]

In 2012, Yamaguchi and co-workers found that planarized triarylboranes can be stabilized by structural constraints.[72] They found that planar triarylboron compounds **1-26** and **1-27** are stable to water and air without the steric protection usually required in the vertical direction (Scheme 1-3). The B–C bonds in **1-27** are much shorter than those in BPh_3, as a result of structural constraints. Compound **1-27** can, however, bind fluoride with a similar binding affinity as $BMes_3$, and thus is still a good Lewis acid. Interestingly, the reduction potential of **1-27** does not differ from that of $BMes_3$, and reduction is still reversible, indicating no dimer formation, in contrast to the unprotected BPh_3.[46c] This demonstrates that these compounds are especially useful as potential electron-transporting materials. Indeed, the radical anion of **1-27** has been isolated and the EPR spectrum, X-ray structure, and DFT calculations reveal a stronger

delocalization of the spin compared to the BPh_3 radical anion.[73] This demonstrates more mixing of the boron p_z-orbital with the π^*-orbitals of the aromatic system in **1-27**. The hyperfine coupling constants for the protons in the EPR spectrum of the radical anion of **1-27** are similar to those of its neutral, isoelectronic carbon radical species, demonstrating an effective delocalization of the unpaired electron over the whole planar molecule.

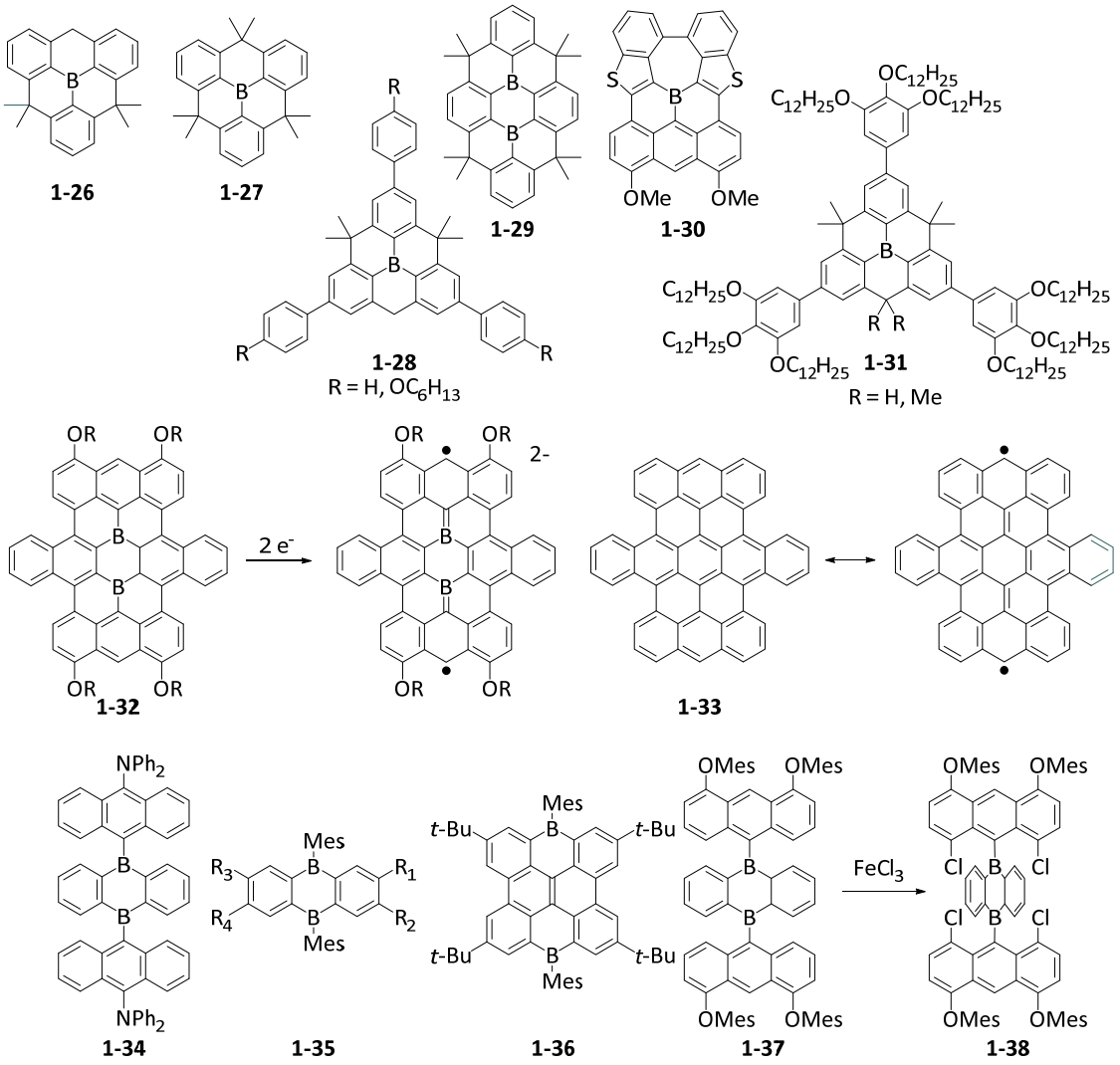

Scheme 1-3. Boron-containing polycyclic π-systems.

Interestingly, the radical anion of **1-27** can change between bowl-shaped and co-planar conformations at room temperature. This suggested that there could be two conformations in the excited state of the constrained triarylborane. Recent studies reveal that photoexcited **1-26** and **1-27** both show dual emission at room temperature, with different ratios in THF and 3-methylpentane.[74] Transient absorption, fluorescence lifetime measurements, and DFT calculations reveal a higher energy planar and a lower energy bowl-shaped excited state. At room temperature, the lower energy emission dominates the fluorescence spectra. However, because the lowest energy ground state structure is planar, the planar excited state is more

easily formed. The ratio of the two emission bands from the planar and the bowl-shaped excited states are thus dependent on temperature in 3-methylpentane. With decreasing temperature (in most cases, below 100 K), fluorescence is observed only from the higher energy planarized excited state. This is possibly the consequence of the fact that the activation energy for the transformation from the planarized to the bowl-shaped excited state cannot be overcome at very low temperatures. This is the case for the π-extended compound **1-28**.[74]

Since 2012, a considerable number of large boron-doped PAHs, such as **1-29** – **1-32**, have been synthesized,[29, 72-75] many of which have been examined for use as electron-transporting materials,[75e] liquid crystals,[75f] battery electrodes,[75g] *etc*. The planarization of the triarylborane makes π-π stacking easier, thus, *e.g*. **1-31** (R = H) forms discotic liquid crystals at room temperature, with an electron mobility value of *ca*. 10^{-3} cm^2 $V^{-1}s^{-1}$.[75f]

An enlarged, boron-doped graphene **1-32**, containing two boron centers, has also been reported.[75b, 75g] The X-ray crystal structure shows the molecule to be planar, except for the two side phenyl rings in the middle row, which twist out of the plane due to H–H repulsions. These compounds are very Lewis acidic and can be used as amine sensors, as binding of an amine causes fluorescence "turn-on". These compounds show two reversible reduction waves by cyclic voltammetry. While their full hydrocarbon analogue **1-33** has open-shell singlet character in its ground state, due to Clar's sextets rule, **1-32** has a closed-shell ground state. The two-electron reduced [**1-32**]$^{2-}$, species isoelectronic with **1-33**, has a triplet ground state with a triplet-singlet energy gap of 0.45 kJ mol^{-1} (estimated by temperature-dependent EPR spectroscopy). Compound **1-32** (R = *n*-butyl) has also been used as a battery electrode material, instead of graphene, and it shows excellent performance.[75g]

One of the most important series of PAHs, the acenes (anthracene, tetracene, pentacene, *etc*.), are not stable when there are more than six rings in a row, because the molecules tend to split into Clar's sextets, thus generating biradical character. Introducing heteroatoms could enhance the stability of large acenes.[76] Recently, a stable *N*-heteroacene with 13 rings in a row has been synthesized and its structure has been confirmed by single crystal X-ray diffraction.[77] However, insertion of two sp^2 boron atoms in place of the two *para* carbon atoms of a benzene ring has not been well studied. Wagner and co-workers have recently reported many compounds based on 9,10-diboraanthracene.[78] The 9,10-diboraanthracenes have been successfully applied as catalysts for dihydrogen activation[79] and the inverse-electron-demand Diels-Alder reaction.[80] When the boron atoms are protected by bulky substituents, such as 9-anthrancenyl or 2-mesityl, the diboraanthracenes **1-34** – **1-36** are stable in air for several hours or days, and could be isolated following chromatography on a silica column. However, degradation was observed in

dilute solutions (10^{-5} M) of **1-37** during photophysical measurements.[81] Yamaguchi and co-workers found that the introduction of two chloro atoms at the 1,8-positions of the 9-naphthalenyl substituent could stabilize the boron *via* Cl–B interactions. This results in a weak Cl–B–Cl three-center, four-electron bond and a nominally five-coordinate boron center. This compound could be worked up with water and isolated following chromatography on silica without any precautions. Interestingly, the $S_1 \leftarrow S_0$ transition in **1-38** is simply a π-π^* transition, while **1-37** shows an ICT transition. Indeed, the LUMOs of most of the diboraanthracene-containing compounds are located on the diboraanthracene core, while the HOMOs are located on the bulky boron substituents. The $S_1 \leftarrow S_0$ transition (absorption/emission) thus involves charge transfer from the boron substituents to the diboraanthracene core.

1.5 Anion Sensors

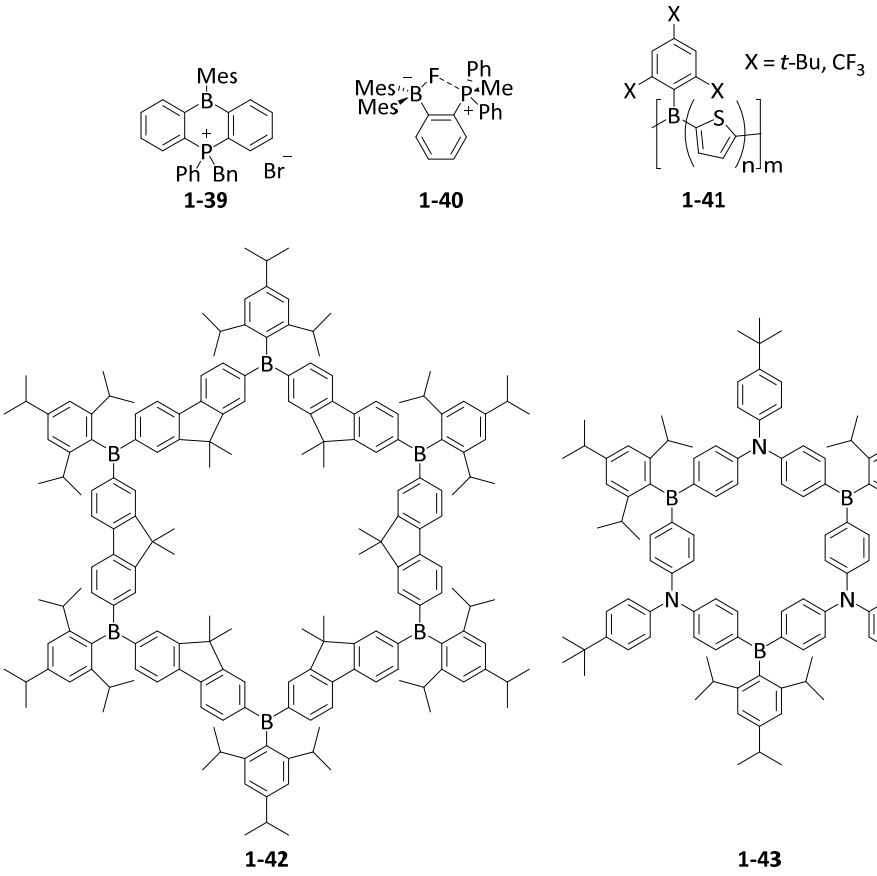

Scheme 1-4. Triarylboranes as anion sensors.

As mentioned above, typically only small anions such as F^- and CN^- can overcome the steric bulk of $BMes_2$ and attack the free p_z-orbital at the boron.[13] Thus, (aryl)–$BMes_2$ compounds can act as selective sensors for these specific anions. The absorption and emission spectra change upon the addition of F^- and CN^- due to interruption of the π-conjugation. Interestingly, at temperatures below 253 K, coordination of bromide ion to dibenzopnictogenborin **1-39** (Scheme 1-4) was observed by Kawashima.[82] The complexation of anions can be followed stepwise by

incorporating more than one trigonal boron moiety into a compound.[83] Furthermore, ratiometric sensing is observed for compounds where the binding of an anion inhibits an energy transfer resulting in a new emission band.[84] The Wang group developed "turn-off" (emission is completely quenched after the addition of F^-) and "turn-on" (emission color changes with complexation of F^-) sensors by investigating the afore-mentioned U- and V-shaped bridges between triarylborane acceptors and triarylamine donors.[21] Furthermore, they reported metal complexes as "turn-on" sensors, especially Pt^{II} complexes with bipy ligands with triarylborane and triarylamine substituents,[85] as well as some lanthanide complexes.[86] Recently, compounds with a triarylborane as well as a dicyanovinyl acceptor were reported for colorimetric discrimination, by the naked eye, between the two interfering anions, F^- and CN^-.[87]

Gabbaï and co-workers enhanced the fluoride binding affinity by incorporation of a hydrogen-bond donor near to the triarylborane,[88] as well as by using bidentate Lewis acids. For other studies of bidentate boron Lewis acids and their role in olefin polymerization catalysis, see: reference [89]. The proximity of two neutral Lewis acidic centers, one or two of them being triarylboranes, enforced by the 1,8-naphthalenediyl backbone, promotes F^- binding by chelation and leads to very high binding constants.[90] Incorporation of one cationic binding site, *e.g.* **1-40**, at the bidentate ligand results in cooperative, favorable Coulombic effects which enhance the binding affinity.[91] They also reported linear cationic compounds for fluoride sensing in water, in which the Lewis acidity at the boron is enhanced sufficiently to overcome the large hydration enthalpy of fluoride.[92]

Jäkle and co-workers synthesized oligomers and polymers with $BMes_2$ groups in the side-chain, and observed remarkable "turn-on" fluorescence by anion complexation, in contrast to polymers with boron in the main-chain.[93] Yamaguchi previously reported side-chain $BMes_2$-containing systems to be very efficient solid-state fluorescent materials.[94] Enhanced anion binding strength by introduction of cationic groups was also reported for the side-chain polymers.[95] Interestingly, Jäkle and co-workers also reported a polymer with BTip(OH) in the side-chain with tunable properties stimulated by F^- and temperature.[96] A new approach for air- and moisture-stable polythiophenes with boron in the main chain was reported 2016.[97] The Jäkle group used Mes* or ^{F}Mes for steric protection of the boron atom against hydrolysis. Polymers of the type **1-41** showed unusually intense luminescence in the solid state favored by the rigid, planar structure enforced by the bulky pendent groups.

A highly luminescent conjugated organoboron macrocycle with six Lewis acidic boron centers **1-42** was also used as "turn-off" sensor for F^- and CN^-. Interestingly, reversible reductions occur at more negative potentials than those for the linear oligomeric analogue due to larger

Coulombic repulsion within the cyclic framework.[98] Comparison with the first ambipolar π-conjugated B–N macrocycle **1-43** shows a smaller HOMO-LUMO gap for the latter one.[99] The CN^- sensing by this "π-expanded borazine" is very different from that of the respective boracyclophane **1-42**. Whereas the emission from CT states of the partially complexed species [**1-43**(CN)]$^-$ and [**1-43**$(CN)_2]_2^-$ remains strong, [**1-42**(CN)]$^-$ shows a very weakly emissive low-energy CT state. New design strategies utilizing carbazoles as donors gave access to unstrained ambipolar macrocycles. Electronic communication between the boron centers is influenced by the π-bridge in the cycle. Complexation of CN^- changes the geometry of the macrocycle and leads to the appearance of strong CT emission bands for the *bis*(cyanide) complex.[100]

A completely different building block is a diboraanthracene **1-35** (R_1, R_4 = Br and R_2, R_3 = H or R_1, R_3 = Br and R_2, R_4 = H) (Scheme 1-3), which was used to prepare air- and water-stable oligomers,[78h] after earlier polymers formed by hydroboration polymerization of 9,10-dihydro-9,10-diboraanthracene were found to be sensitive towards air and moisture.[78a] The new oligomers were prepared by Stille-type C–C coupling reactions with thiophenes. Polymers are not necessary, because the oligomers have already reached the limit of conjugation length and form free-standing thin films.

1.6 OLEDs

Organic light-emitting diodes (OLEDs) are very important in lighting applications and in flat panel display screens with high energy efficiency and resolution. In the organic emitting layer of OLEDs, the recombination of holes and electrons populates the excited states of the molecules. These excited molecules then emit photons and generate light. During the formation of excitons, the singlet:triplet ratio is expected to be 1:3. Thus, there should be two ways of emitting: fluorescence and phosphorescence to the singlet ground state. In an organic molecule without any heavy atom, fluorescence is usually very fast and the lack of spin-orbit coupling leads to slower, inefficient intersystem crossing between singlet and triplet manifolds. Thus, phosphorescence, which would arise from the $S_0 \leftarrow T_1$ transition, is forbidden because of the spin-selection rule. Traditional OLEDs using pure organic boron-containing materials as the emitting layer present very low external quantum efficiencies (η_{EQE}) because only a quarter at most of the electrochemically generated excitons can be converted to light. After introducing three-coordinate boranes into OLEDs as very efficient electron transporters,[51] Shirota and co-workers examined several pure organic boranes for use as the electroluminescent layer.[101] Many pure organic boranes have been reported by Wang and others for use in electroluminescent layers, mostly based on fluorescence.[102] However, their η_{EQE} are limited to a few percent.

One way of utilizing the triplet excitons is to introduce heavy atoms into the system to relax the spin selection rule and facilitate the $S_0 \leftarrow T_1$ transition because of their strong spin-orbit coupling. Due to the fact that the energy of the S_1 state is higher than that of the T_1 state in most cases, the S_1 state can relax to the T_1 state *via* intersystem crossing, often within femtoseconds. Thus, in theory, the excited state could be populated to give 100% triplets, and the external quantum efficiency of phosphorescent OLEDs (PHOLEDs) could be much higher than that of fluorescent OLEDs. Several boron-containing transition metal complexes have been designed as PHOLED emitters with high η_{EQE}. In collaboration with Wong and co-workers, Marder's group has reported a red-emitting $BMes_2$-substituted Ir-2-phenylpyridinecomplex (**1-44**) with a high η_{EQE} of 9.4%.[103] The external quantum efficiency of a Pt^{II} complex (**1-45**) reported by Wang and co-workers reached 21%.[104] However, most of the organometallic PHOLEDs emit at lower energy in the color range from yellow to red.[13b] The design of PHOLEDs with a larger band-gap is challenging. By employing $BMes_2$ as a substituent to decrease the energy of the HOMO of phenylimidazole as the ligand (compound **1-46**), Wang and co-workers reported high energy blue emitting OLEDs with high η_{EQE}.[105]

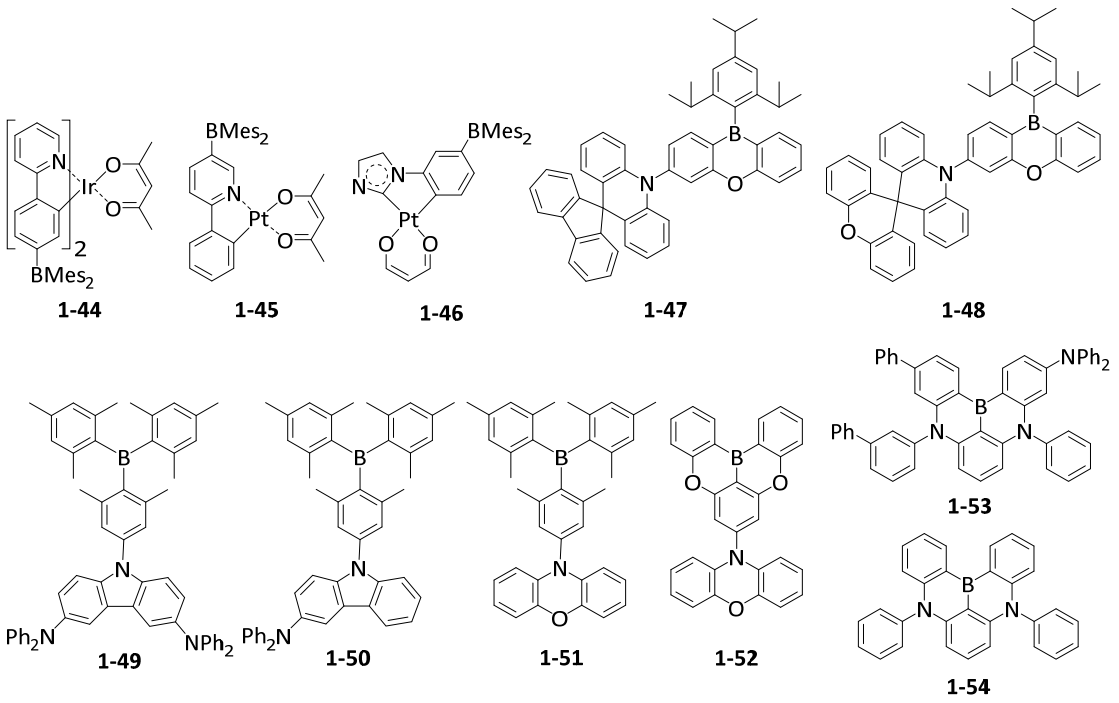

Scheme 1-5. Triarylboranes used in OLEDs.

Most PHOLEDs utilize expensive third-row transition metals to achieve efficient phosphorescence. However, another way of making use of the triplet state was recently reported by Adachi and co-workers.[106] In some highly twisted compounds, the triplet state energy is not much lower than that of the singlet excited state. This is due to the lack of efficient spatial overlap of the HOMO and LUMO as a result of the large dihedral angle between the donor

and acceptor moieties. Thus, it appears possible for the singlet excited state to be repopulated from the triplet state at room temperature by thermally activated reverse intersystem-crossing (RISC) and then it can relax to the ground state by fluorescence. This process is termed thermally-activated delayed fluorescence (TADF). The speed and efficiency of TADF are affected by the temperature and the S_1-T_1 gap. Indeed, Marder and Wang have both reported long-lived emissions, presumably from the triplet excited states of triarylboranes, including **1-6** (R = *tert*-butyl).[31, 107] The energy difference between the singlet and triplet excited state (as indicated by the emission spectra measured at 77 K) of **1-6** (R = *tert*-butyl) is very small.

Hatakeyama, Adachi, and Kaji reported TADF-based OLEDs which use twisted three-coordinate organoboranes (**1-47** – **1-54**) as emitters.[108] The highest η_{EQE} of the first TADF-based OLED device using triarylborane **1-48** as the luminescence layer was *ca.* 20%, which is comparable to the most efficient PHOLEDs (Scheme 1-5).[108b] The blue emitters **1-49** and **1-51** show the highest η_{EQE} (21.6% and 22.8%) among the TADF-based OLEDs. The recent interest in three-coordinate organoboranes as the emitting layer of OLEDs again demonstrates the wide array of applications of triarylboranes in material science.

1.7 Three-Coordinate Boron in Chromophores Exhibiting Strong TPA

Two-photon absorption (TPA) is a phenomenon in which a molecule absorbs two photons, to reach the S_n excited state.[109] In particular, in this chapter the focus is on those cases in which the absorption of two photons occurs essentially simultaneously, *via* a virtual state, with each photon having less energy than the S_0-S_1 gap (S_0-S_2 gap for centrosymmetric molecules). An indication of TPA is emission at higher energy than that of either of the two absorbed photons, a phenomenon known as two-photon excited fluorescence (TPEF). TPA is proportional to the square of the light intensity and the intrinsic TPA coefficient of the organic dye, the latter being known as its two-photon cross-section (σ_2). The units of σ_2 are $cm^4 \cdot s \cdot photon^{-1}$, which is too large for most TPA dyes. Thus, units of Göppert-Mayer (GM), named for the person who first predicted TPA theoretically, are used, where 1 GM is $10^{-50}\,cm^4 \cdot s \cdot photon^{-1}$. Compounds with $\sigma_{2,max} > 50$ GM are considered to be excellent TPA dyes. Compared to one-photon absorption, TPA has the advantages of long-wavelength absorption and squared light intensity dependence leading to excellent 3D resolution (*i.e.*, especially depth resolution at the focus of a laser beam). Thus, it can be used effectively in bioimaging (which will be discussed in Chapter 1.8), 3D optical data storage, microfabrication, optical power-limiting, photodynamic therapy, *etc*. Thus, designing organic molecules with large σ_2 values is highly desirable. Due to the fact that the two-photon cross-section is proportional to the square of the transition dipole moment (ΔM_{01}) and the square of the dipole moment change between S_0 and S_1 ($\Delta\mu_{01}$) for dipolar molecules, for

example, compounds bearing strong donors and acceptors with strong ICT transitions normally have large σ_2 values. Also important is the structural design of the chromophore. Quadrupolar and octupolar compounds have also been studied in detail and show very strong TPA, both theoretically and experimentally.[110] Within the context of the afore-mentioned electron-deficient and excitation-induced charge transfer properties of the three-coordinate boron compounds, Fang, Liu and coworkers as well as Marder's group have developed various dipolar, quadrupolar and octupolar compounds featuring $BMes_2$ -acceptor moieties, which show strong TPA and TPEF behaviour.[111] Scheme 1-6 shows several typical three-coordinate boron compounds which have large σ_2 values.[111-112]

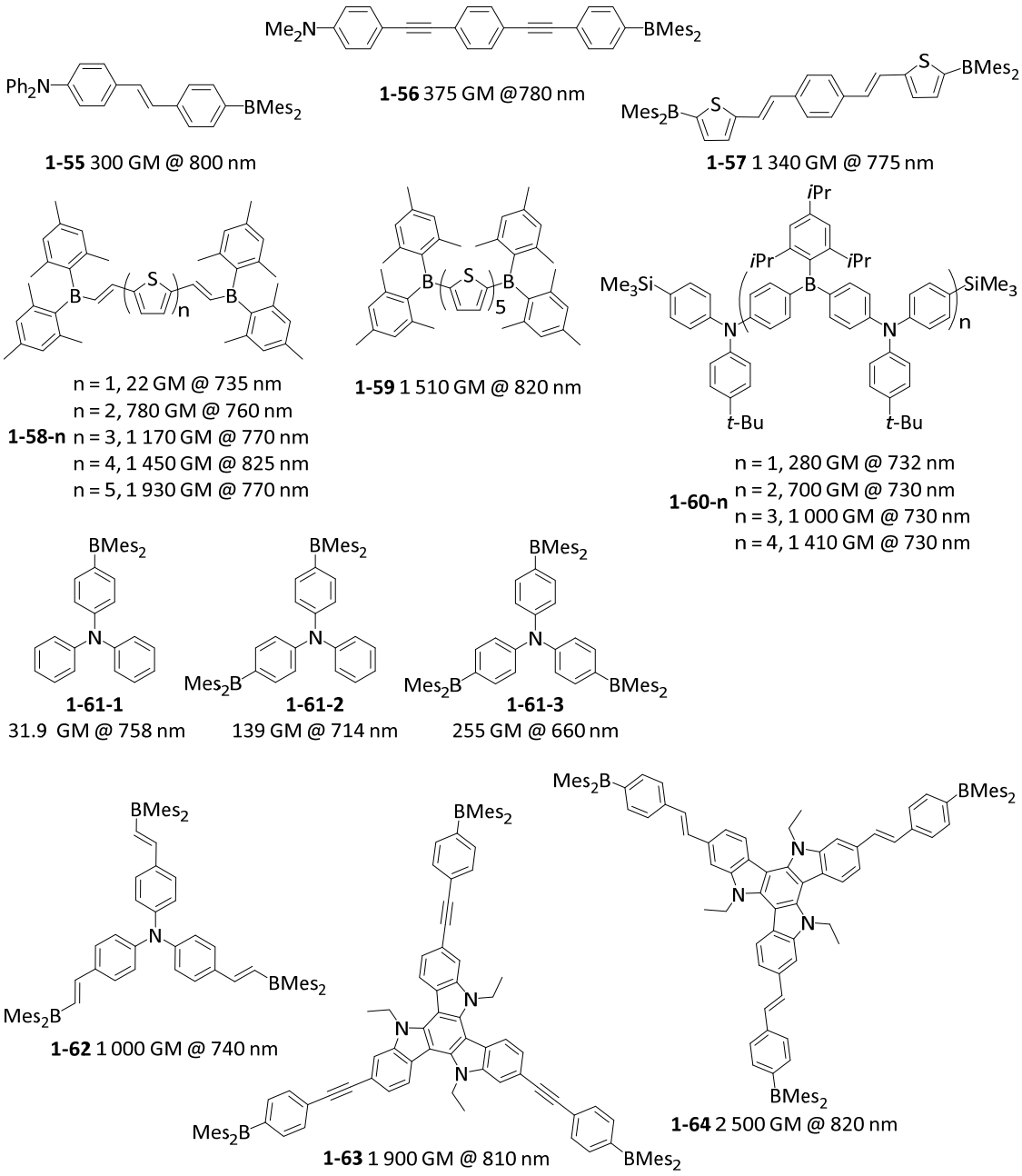

Scheme 1-6. Three-coordinate boron compounds with large TPA cross-sections.

Compound **1-55** is a very typical dipolar compound, which has a very strong electron acceptor ($BMes_2$) and donor (NPh_2). The emission is strongly solvent-dependent, indicating a large dipole moment in the excited states, and thus a large $\Delta\mu_{01}$. This compound has $\sigma_{2,max}$ of 300 GM at 800 nm, which is much larger than most dipolar dyes of similar size.[111b] The energy of the lowest TPA-allowed transition of this compound is the same as its $S_1 \leftarrow S_0$ transition in the one-photon absorption spectrum. Thus, λ_{max} for TPA = $2\lambda_{max}$ for one-photon absorption. By using longer bridges between the donor and the acceptor, compound **1-56** shows a larger $\sigma_{2,max}$ of 375 GM, despite the fact that alkynyl moieties are typically not as good as alkenyl ones in the π-bridge for TPA dyes.[111g]

Quadrupolar molecules have been reported to have considerably enhanced TPA compared to their dipolar counterparts.[110a] Due to the fact that the parity selection rule is different for one- *vs*. two-photon absorption in quadrupoles, the $S_1 \leftarrow S_0$ transition is allowed for one-photon absorption but forbidden for TPA, while the $S_2 \leftarrow S_0$ transition is allowed for TPA but forbidden for one-photon absorption.[110a] Thus, the energy of the TPA maximum is higher than half of the energy of the one-photon absorption. Compound **1-57** is a representative quadrupolar molecule.[111c] The $\sigma_{2,max}$ of **1-57** is 1 340 GM (at 775 nm), which is about four times that of the similar size dipolar compound **1-56**. Recently, Marder and co-workers have reported a series of thiophene- and thiophene-vinyl-bridged dyes **1-58-n** and **1-59**. In the case of **1-58-n**, as the number of thiophenes increases from one to four, the $\sigma_{2,max}$ of the $S_2 \leftarrow S_0$ TPA increases from 22 to 1 450 GM with a concomitant red shifting of the TPA band. However, the increase in TPA plateaus around four thienyl units. Although **1-58-5** displays a $\sigma_{2,max}$ of 1 930 GM at 770 nm, it seems likely that this is due to a higher energy transition than the $S_2 \leftarrow S_0$ one. Thus, the $S_2 \leftarrow S_0$ TPA band of **1-58-5** only red-shifts from **1-58-4** without obvious enhancement. With the same conjugated bridge length, **1-59** shows a similar two-photon absorption band and intensity as **1-58-4**. More recently, Jäkle and co-workers have reported a series of quadrupolar molecules **60-n**. The σ_2 values increase linearly with increasing number n of the D–A subunits, but σ_2/n is not enhanced in these compounds with rising n.[112b]

Another important series of TPA dyes are octupolar compounds. Their lowest one-photon allowed transition, $S_1 \leftarrow S_0$, is also two-photon allowed. In addition, octupolar compounds can have a much stronger, higher energy two-photon allowed band which is forbidden for one-photon transitions.[110b] The *mono*-, *bis*- and *tris*-$BMes_2$ substituted triphenylamines have been compared recently.[112a] Compound **1-61-1** has a two-photon excited $S_1 \leftarrow S_0$ transition band with $\sigma_{2,max}$ = 32 GM (at 758 nm). However, the two-photon absorption of this transition ($S_1 \leftarrow S_0$) in the *bis*-substituted compound (quasi-quadrupolar) **1-61-2** is very weak (σ_2 = 2.9 GM, at 808 nm),

but it has a very strong TPA band at 714 nm ($\sigma_{2,max}$ = 139 GM), for the $S_2 \leftarrow S_0$ transition. In comparison, the $S_2 \leftarrow S_0$ two-photon absorption band of the three-branched octupolar compound **1-61-3** has a large $\sigma_{2,max}$ of 255 GM at 660 nm. These strongly suggest that the octupolar compounds have much larger TPA cross-sections. Another factor that affects the TPA cross-section is the size of the molecule. By introduction of one more ethylene bridge, the $\sigma_{2,max}$ of **1-62** increases to 200 GM (at 880 nm) for the $S_1 \leftarrow S_0$ transition and 1 000 GM (at 740 nm) for the $S_2 \leftarrow S_0$ transition.[111g] With three nitrogen π-donors and larger π-systems, **1-63** (1 900 GM at 810 nm) and **1-64** (2 500 GM at 820 nm) bear the largest two-photon cross-sections among the octupolar triarylboranes reported to date.[111h] Due to the fact that the wavelength window of the measurement was very narrow and the TPA maximum is very close to the one-photon absorption maximum, another much stronger higher energy TPA absorption band is also possible in the shorter wavelength region.

1.8 Bioimaging

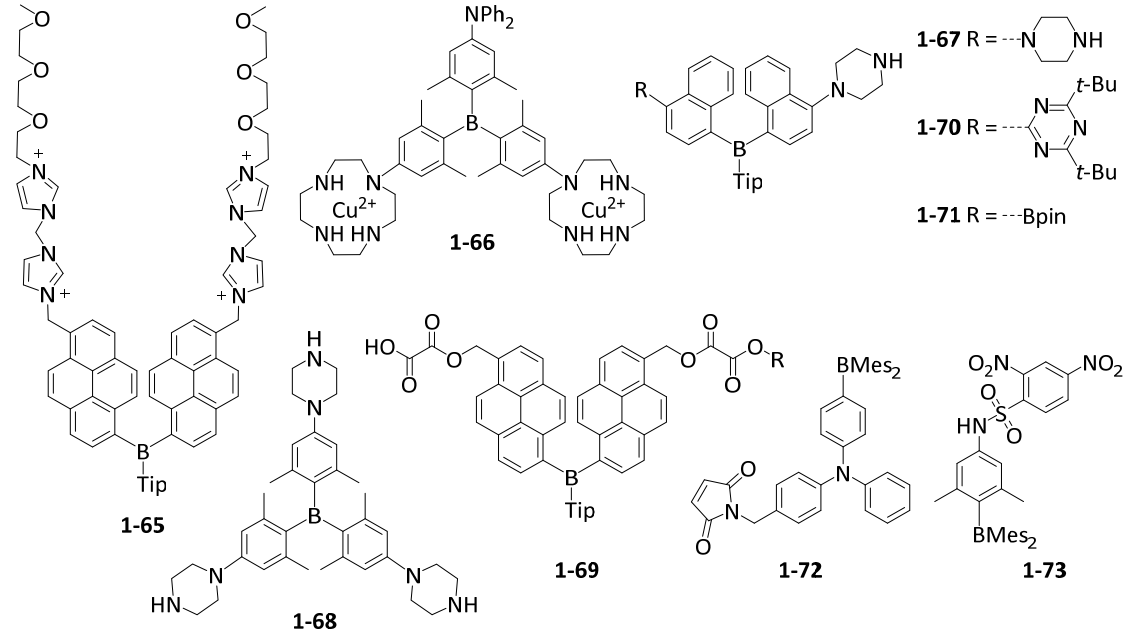

Scheme 1-7. Triarylboranes used as biological imaging agents.

Very recently, a new application of triarylboranes in cell imaging has emerged. Yang and co-workers reported the water-soluble, non-ionic triarylborane **1-65**, incorporating polyethylene glycol chains as the hydrophilic groups, as an efficient fluorescence indicator for ATP in the cytoplasm and cell membrane (Scheme 1-7).[113] Furthermore, they could sense hydrogen sulfide release with another water-soluble triarylborane **1-66**.[114] By addition of hydrogen sulfide, **1-66** acts as a two-photon excited "turn-on" fluorescence sensor as the emission is quenched in the absence of H_2S. They utilized their chromophore for fluorescence lifetime imaging and TPEF imaging of live cells and found moderate TPA cross-sections with a maximum of 60 GM in DMSO

They demonstrate cell-membrane permeability and a preferential distribution in mitochondria, while the same compound, without Cu^{II}, was reported one year later to stain nucleoli and cytoplasm.[115] Two other triarylboranes **1-67** and **1-68** with piperazine in *para* position were reported, recently.[116] They are, to some degree, water-soluble and found to stain nucleoli, as well as the nuclear membrane, nuclear matrix, nuclear pore and the cytoplasm, while binding to RNA. Further three-coordinate boron containing dyes were used for imaging (**1-69** – **1-72**), although they were not water-soluble. By loading them into nanogels, these were cell membrane permeable, stained the cytoplasm and could be applied as temperature, viscosity, pH, H_2O_2, and biothiol sensors.[117] Another intracellular "turn-on"-sensor **1-73** for thiophenol was published by Thilagar and co-workers very recently.[118]

1.9 Conclusions and Perspectives

Studies of the synthesis and applications of three-coordinate boron compounds in material science have increased dramatically in the last few decades. Due to the empty p_z-orbital, the three-coordinate boron compounds are efficient electron and spin carriers. Thus, such compounds can be used as electron-transporting materials both in devices and liquid crystals. For this aspect, planarized, constrained triarylboranes are highly promising as the intermolecular stacking is easier than for the sterically-protected triarylboranes. Although acenes and azaacenes have been studied as semiconductors for many years, the study of boraacences has just begun. Exchanging some of the sp^2 carbons by boron atoms could stabilize the LUMO of acenes and strongly enhance their electron-transporting properties. The spin-carrier character of the three-coordinate boron also makes boron radicals intrinsic magnetic materials.

Although the application of triarylboranes as TADF emitters is a very new field, the external quantum efficiencies reported for several devices using new triarylboranes are the highest among the TADF-based OLEDs. One can anticipate that this area will attract much attention as TADF emitters based on triarylboranes could be employed in the next generation of OLEDs.

Triarylboranes are also efficient π-acceptors in chromophores with strong absorptivities and high fluorescence quantum yields. The process of exciting a D–π–boron chromophore results in a charge transfer from the donor to the electron-deficient three-coordinate boron group. The three-coordinate boron atom can also lower the energy of an unoccupied orbital of a molecule by mixing the empty boron p_z-orbital with the unoccupied molecular orbital, thus generating a lower-lying excited state and a red-shifted emission. When the empty p_z-orbital mixes with a higher unoccupied molecular orbital efficiently, such as in the case of pyrene derivative **1-17**, a switching of the energy ordering of the unoccupied molecular orbitals can occur. By introducing stronger electron-withdrawing substituents in $B(aryl)_2$ groups, such as changing Mes to ^{F}Mes or

other electron-acceptors, the LUMO of the molecule is further lowered, the ICT is enhanced, and the fluorescence is further red-shifted. It should be noted that the strong ICT of these D–π–A triarylboranes makes them efficient TPA materials. Bearing in mind the red-shifted emissions and high fluorescence quantum yields of triarylboranes, these compounds can be applied as two-photon excited fluorescence sensors in bioimaging as long as they are water-soluble and water-stable. Triarylboranes modified to be water-soluble and water-stable, red-emissive and strongly two-photon absorbing could be very interesting for bioimaging. Clearly, three-coordinate boron chemistry has a bright future!

Chapter Two

-

Water-Soluble and Water-Stable Triarylborane Chromophores

2 WATER-SOLUBLE AND WATER-STABLE TRIARYLBORANE CHROMOPHORES

This section is slightly modified and reproduced from ref. [119] with permission from Wiley-VCH. Furthermore, preliminary aspects of some of these results were included in my Master's Thesis entitled "Synthesis of potential water-soluble triarylboranes and studies of their optical properties", prepared at the Institute of Inorganic Chemistry, Julius-Maximilians-Universität Würzburg in 2014. The preliminary synthetic procedures reported in the above-mentioned thesis, were significantly improved and mentioned here for the sake of completeness. New analytical data and more detailed photophysical studies are reported in the current work.

2.1 Introduction

Three-coordinate organoboron compounds have aroused much interest for various optical and electronic applications.[13d, 17, 18b, 120] Due to its vacant p_z-orbital, three-coordinate boron is a strong π-electron acceptor when connected to a conjugated π-system. The trigonal planar geometry and Lewis acidity of the boron atom facilitate attack by nucleophiles, resulting in bond cleavage or the formation of a four-coordinate boron species, which inhibits the boron atom from being part of the delocalized π-system. To prevent the attack of nucleophiles such as water, kinetic stabilization can be achieved by introducing sterically demanding substituents, such as mesityl (Mes) or 2,4,6-$(CF_3)_3C_6H_2$ (^{F}Mes),[31] to the boron atom, or by incorporation of the boron atom in a rigid, planar structure.[121] Only small anions, such as fluoride or cyanide, are able to overcome the steric bulk and attack the boron center, which is exploited for anion-selective sensing.[13a-c, 122] Triarylboranes are also used in organic light-emitting diodes (OLEDs) as electron-transporting, emitting and hole-blocking materials.[75e, 102d, 123]

The large change in dipole moment upon excitation of compounds including a triarylborane moiety as an electron acceptor results in large first and second-order molecular hyperpolarizabilities β and γ.[14a, 14e, 15-16] These interesting 2nd and 3rd order non-linear optical properties indicate that triarylboranes should be excellent components of chromophores that undergo two-photon absorption (TPA). Several octupolar and quadrupolar compounds using this boron acceptor were reported and their TPA cross-sections (σ_2) and fluorescence quantum yields (Φ_f) were measured to develop structure-TPA relationships.[111a-h, 112a, 124] In previous work, Marder's group reported that the insertion of thiophene rings into the π-bridge of A–π–A chromophores (A = boryl acceptor; here, $B(Mes)_2$) results in a remarkable increase of the TPA cross-section, and synthesized a quadrupolar compound with a TPA cross-section of 1 930 GM at 770 nm that is, as far as known, the highest σ_2/m.w. of all compounds containing $B(Mes)_2$ and thiophene groups reported to date.[111i] Because the TPA maximum of each of these

chromophores is located in the near-infrared (NIR) biological transparent window, the reported chromophores are potentially good candidates for two-photon excited fluorescence (TPEF) microscopy of living cells and tissues. However, these prototype compounds were not designed to be water-soluble, posing formidable challenges for *in vitro* or *in vivo* application, and it is this important aspect is addressed in this chapter, *i.e.*, water-soluble chromophores were developed while maintaining their aqueous stability and favorable optical properties.

Only a few examples of water-soluble triarylboranes have been reported to date.[125] Gabbaï and co-workers achieved water-solubility by successively replacing the *para*-methyl groups of trimesitylborane with cationic ammonio substituents, and used two such compounds as efficient cyanide sensors in water.[126] They and two other groups made use of a similar method for the preparation of water-soluble triarylboranes with phosphonio substituents for anion sensing.[127] Recently, a water-soluble, non-ionic triarylborane, containing polyethylene glycol chains as the hydrophilic groups, was reported by Yang and co-workers as an efficient fluorescence indicator for ATP in the cytoplasm and cell membrane.[128] Furthermore, while this work was in progress, the same authors reported a water-soluble triarylborane containing Cu^{II}-cyclen. While non-fluorescent itself, it can serve as a one- and two-photon excited fluorescence turn-on probe for H_2S at mitochondria.[129]

For TPEF imaging in biological systems, analogues of the previous quadrupolar compounds were prepared with trimethylammonio substituents for enhanced water-solubility. These substituents are not just promising due to their hydrophilic character, but are also expected to enhance the accumulation in the mitochondria.[130] These features profile the molecules as potential sensors for the mitochondrial membrane potential, providing direct information about the status of a cell's power plants.[131] Importantly, the use of such dyes, if amenable for TPA, is potentially beyond *in vitro* use on single cells, populations of cells, or united cell structures, but may very well expand into *in vivo* applications by virtue of the afore-mentioned accessibility of deeper cell layers and tissues for NIR light. Measurements of time-lapse acute mitochondrial responses to, *e.g.*, drug exposure, inducible gene knock-in/-out or exposure to other challenges could provide immediate information on secondary respiratory challenges to mitochondria, thereby providing on-the-fly read-out of cell damage. Other potential applications include live-cell imaging of diseased *vs*. healthy tissue, *e.g.*, to understand the underlying mechanisms of dynamic transport in neurodegenerative diseases such as glaucoma[132] or Alzheimer's disease.[133]

In this chapter, three quadrupolar chromophores, **2-1M** – **2-3M**, containing cationic triarylborane acceptors (Scheme 2-1) are investigated. The π-bridge has been modified by the

number of thiophene spacers and the nature of the aryl substituent adjacent to the boron atom. Their linear photophysical properties were examined experimentally and theoretically. With the water-stable derivative **2-3M** one- and two-photon excited fluorescence imaging of the mitochondria in cells will be demonstrated, due to its remarkable fluorescence quantum yield and high two-photon cross-section in water. Co-localization and cytotoxicity studies show that dye **2-3M** is an excellent candidate for the use as a new mitochondrial imaging agent.

2.2 Results and Discussion

2.2.1 Directly Connected Thiophene-Boron Chromophores 2-1M and 2-2M

2.2.1.1 Synthesis

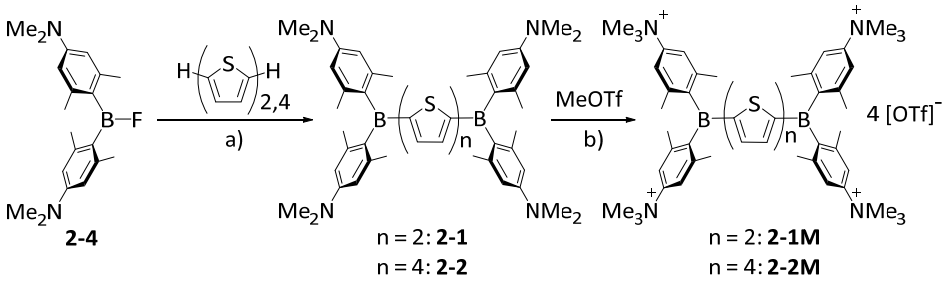

Scheme 2-1. Synthesis of the compounds **2-1M** – **2-2M**. a) *n*-BuLi, THF, -78 °C to r.t.; b) CH_2Cl_2, r.t.

The synthesis of the compounds **2-1M** and **2-2M** is summarized in Scheme 2-1. Compounds **2-1** and **2-2** were prepared *via* reaction of *bis*[4-(*N*,*N*-dimethylamino)-2,6-xylyl]fluoroborane **2-4**[134] with dilithiated bithiophene or quaterthiophene. Neutral compounds **2-1** and **2-2** were methylated with methyl triflate in CH_2Cl_2, and the products **2-1M** and **2-2M** precipitated in quantitative yield. Both compounds **2-1M** and **2-2M** were found to be water-soluble at concentrations suitable for fluorescence microscopy, especially noting that commercially available chromophores for mitochondrial imaging are generally dissolved in dimethyl sulfoxide (DMSO).

2.2.1.2 Linear Optical Properties

The absorption and emission spectra of the methylated dyes **2-1M** and **2-2M** were measured in water and MeCN (Figure 2-1). The absorption spectra recorded in water exhibit a broad band at 426 nm for compound **2-1M**, whereas an elongated quaterthiophene π-system shifts the absorption by *ca*. 1640 cm^{-1} to the red for chromophore **2-2M**. The extinction coefficients, measured in MeCN, due to enhanced stability (*vide infra*) and solubility, range from 28 000 to 48 000 $M^{-1}\,cm^{-1}$ (Table 2-1). The emission spectra are broad, with maxima spread over a *ca.* 5020 cm^{-1} range for the different compounds. The smaller quadrupolar compound, **2-1M**, has an emission maximum in water at 451 nm, with a small Stokes shift of 1 300 cm^{-1}. By insertion of two more thiophene rings into the bridging unit, the emission of **2-2M** is bathochromically

shifted by more than 5020 cm^{-1}, resulting in a much larger Stokes shift. The fluorescence quantum yields of **2-1M** and **2-2M** in water are remarkably large at 0.19 and 0.20, respectively, whereas they are even larger in MeCN, both being 0.41. The fluorescence lifetimes are relatively short being 1.2 and 0.7 ns in water, respectively, and are similar in MeCN.

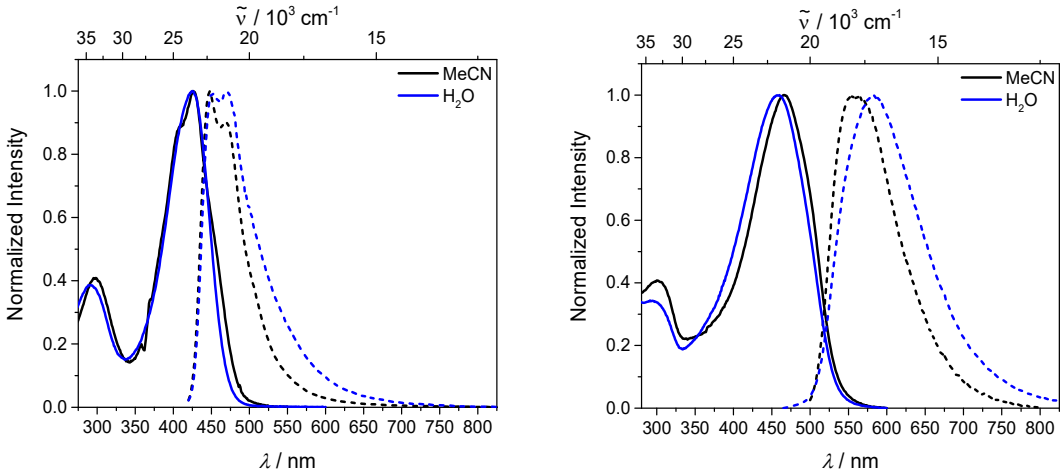

Figure 2-1. Absorption (solid) and emission (dashed) spectra of **2-1M** (left) and **2-2M** (right) in MeCN (black) and water (blue).

Table 2-1. Photophysical data for the chromophores **2-1M** and **2-2M**.

	solvent	λ_{abs} / nm	ε / M^{-1} cm^{-1}	λ_{em} / nm	Stokes shift / cm^{-1}	Φ_f	τ / ns	k_r / 10^8 s	k_{nr} / 10^8 s	τ_0 / ns
2-1M	H_2O	426	-	451	1 300	0.19	1.2	1.6	6.8	6.3
	MeCN	426	28 000	448	1 200	0.41	1.7	2.3	3.4	4.2
2-2M	H_2O	458	-	583	4 700	0.20	0.7	2.8	11.4	3.5
	MeCN	467	48 000	555	3 400	0.41	0.7	5.9	8.5	1.7

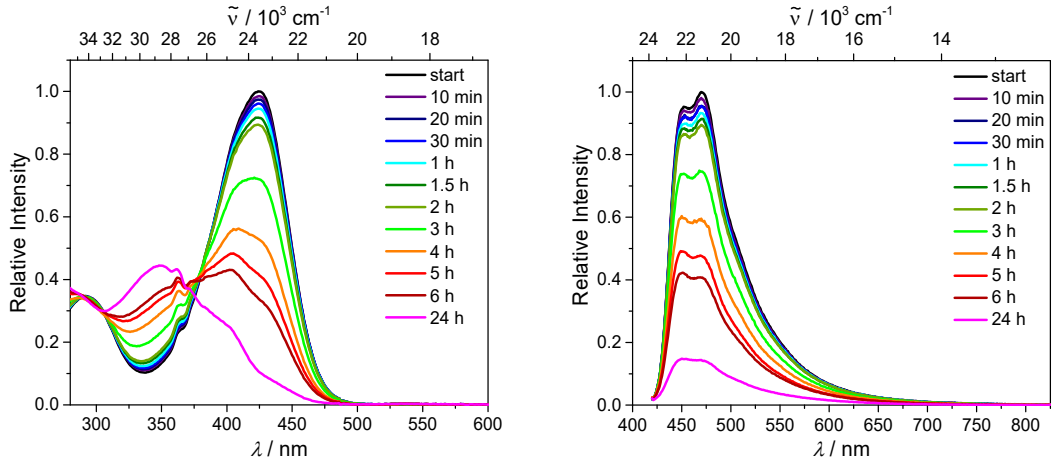

Figure 2-2. Absorption (left) and emission (right) spectra of **2-1M** in H_2O as a function of time. Sample kept in the dark between measurements.

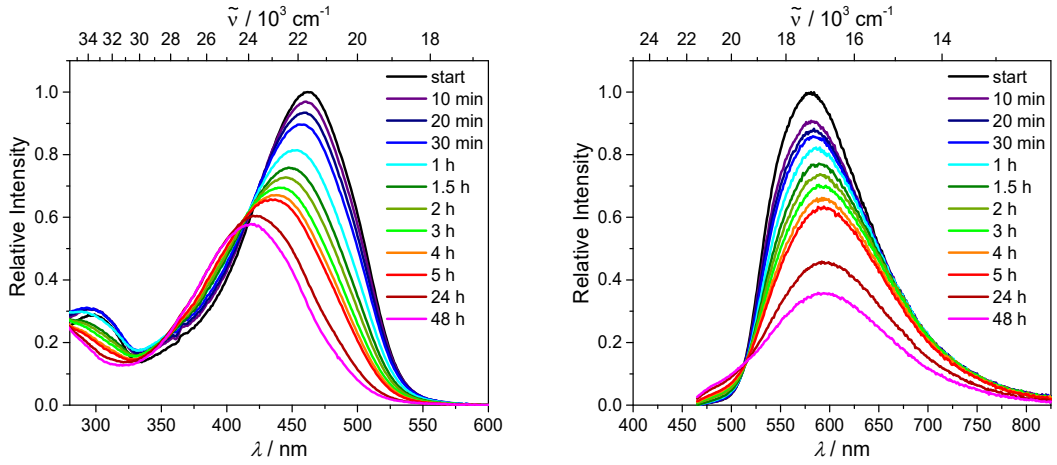

Figure 2-3. Absorption (left) and emission (right) spectra of **2-2M** in H_2O as a function of time. Sample kept in the dark between measurements.

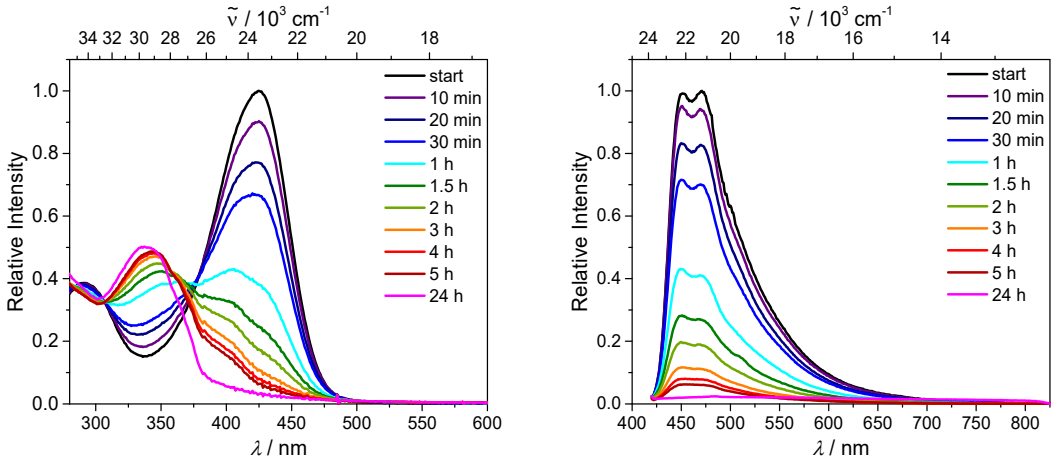

Figure 2-4. Absorption (left) and emission (right) spectra of **2-1M** in H_2O as a function of time. Sample exposed to room light between the measurements.

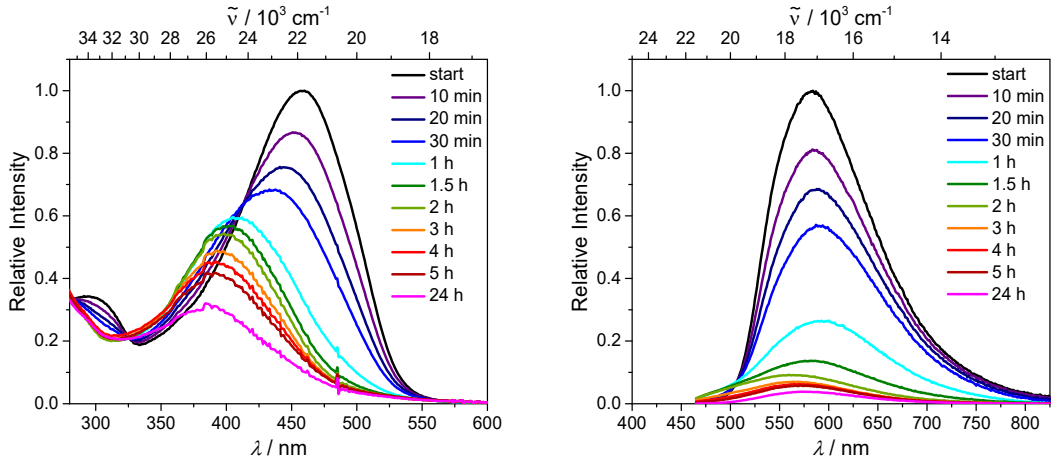

Figure 2-5. Absorption (left) and emission (right) spectra of **2-2M** in H_2O as a function of time. Sample exposed to room light between the measurements.

UV/Vis absorption and emission spectra monitored over extended time periods demonstrate slow degradation of **2-1M** and **2-2M** in water as shown in Figures 2-2 and 2-3. Mass spectrometry

of the degradation product confirmed hydrolysis at the boron center. The intensities of the absorption maxima were plotted *versus* time and the decays were fitted with an exponential function $y = y_0 + A \times e^{(-k \times t)}$, whereby half times could be calculated (Table 2-2 and Figure 2-7). Thus, **2-2M** decomposes in about half of the time of **2-1M**. Light and oxygen enhance the rate of decomposition of **2-1M** and **2-2M** (Figures 2-4, 2-5 and 2-6). When exposed to light, **2-1M** and **2-2M** have the same decomposition rates ($t_{1/2} \approx 40$ min), which can be slowed in a degassed solution in water ($t_{1/2} \approx 100$ min).

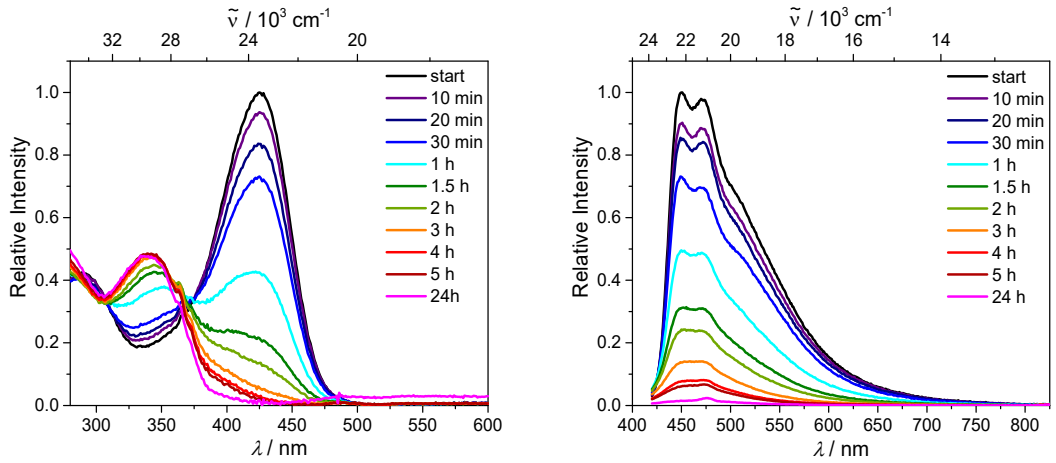

Figure 2-6. Absorption (left) and emission (right) spectra of **2-1M** in degassed H_2O as a function of time. Sample exposed to room light between the measurements.

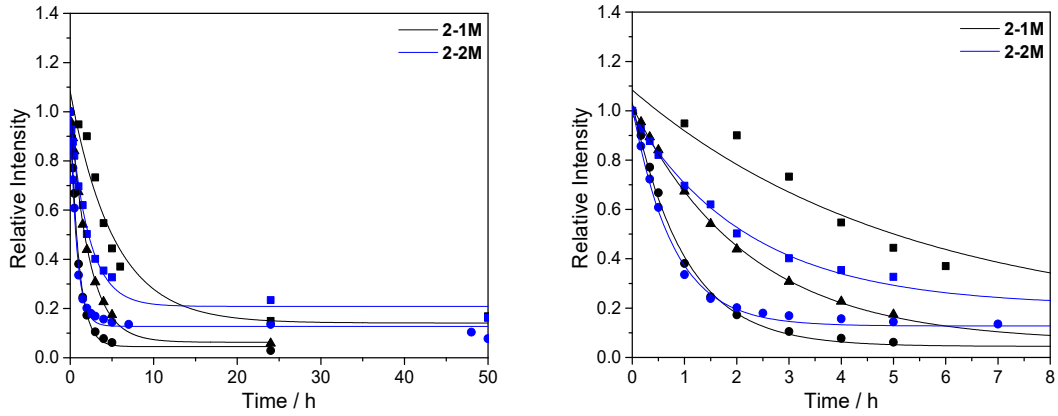

Figure 2-7. Intensity of the absorption maximum *vs*. time for compounds **2-1M** (black) and **2-2M** (blue). Decays for measurements with the sample in the light (●), in the dark (■) and in the light without oxygen (▲) between the measurements. The data for **2-1M** and **2-2M** are fit with an exponential function: $y = y_0 + A \times e^{(-k \times t)}$. The values for the parameters of the function are given in Table 2-2.

Table 2-2. Parameters for the functions depicted in Figure 2-7, and the resulting half-lives $t_{1/2}$.

	-k	y_0	$t_{1/2}$
2-1M without light	0.00321	0.14101	4.4 h
2-1M with light	0.01667	0.04511	0.7 h
2-1M with light without oxygen	0.00748	0.06295	1.7 h
2-2M without light	0.00742	0.20879	2.1 h
2-2M with light	0.02151	0.12762	0.6 h

2.2.2 Water-Stable Chromophore 2-3M

2.2.2.1 Synthesis

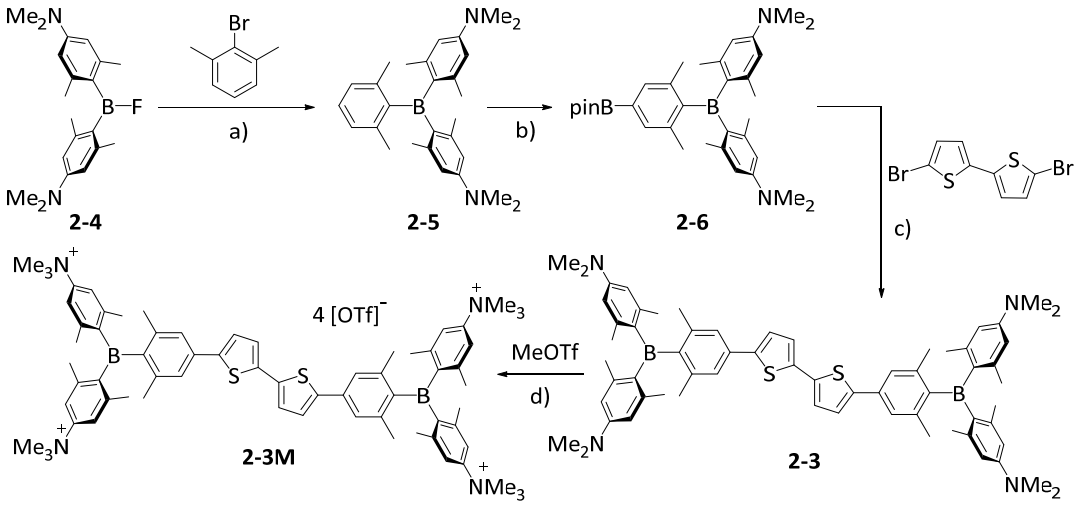

Scheme 2-2. Synthesis of the compound **2-3M**. a) *t*-BuLi, THF, -78 °C to r.t.; b) B_2pin_2, [Ir(μ-OMe)(COD)]$_2$, dtbpy, THF, 80 °C; c) $Pd_2(dba)_3{\cdot}CHCl_3$, SPhos, KOH, toluene, H_2O, 85 °C; d) MeOTf, CH_2Cl_2/Et_2O 1:3, r.t.

To improve the water-stability of the chromophore for bioimaging applications, compound **2-3M**, in which the additional two *ortho*-methyl groups provide significantly enhanced steric protection at the boron center, was synthesized. Therefore, **2-4** was reacted with 2-lithio-*m*-xylene giving *bis*[4-(*N*,*N*-dimethylamino)-2,6-xylyl]-2,6-xylylborane, **2-5**, in 63% isolated yield (Scheme 2-2). For use in Suzuki-Miyaura reactions, the *para*-position of this borane was borylated in an iridium-catalyzed C–H-activation reaction in 91% isolated yield.[34] Borylated species **2-6** was coupled with 5,5′-dibromo-2,2′-bithiophene to prepare the neutral precursor **2-3** in 82% isolated yield, using $Pd_2(dba)_3{\cdot}CHCl_3$ as the catalyst precursor, SPhos as the ligand and potassium hydroxide as the base. Methylation of **2-3** was achieved with methyl triflate in a CH_2Cl_2/Et_2O mixture giving a 76% isolated yield of **2-3M**. Compound **2-3M** is air- and moisture-stable and can be stored on the bench as a solid at room temperature, in contrast to the commercially available MitoTrackers™, for which storage at less than -20 °C and exclusion of light are recommended in their instructions.[135] Chromophore **2-3M** was also found to be water-soluble in the required concentration range.

2.2.2.2 *Linear Optical Properties*

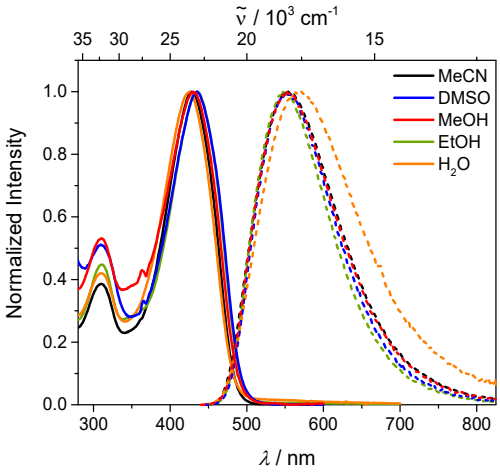

Figure 2-8. Absorption (solid) and emission (dashed) spectra of **2-3M** MeCN (black), DMSO (blue), MeOH (red), EtOH (green) and water (orange).

The absorption maximum of **2-3M** (Figure 2-8) shifts hypsochromically to 425 nm in water, compared to **2-2M**. This blue shift can be explained by somewhat diminished electron delocalization between the planar π-system and the boron p_z-orbital, as shown in TD-DFT calculations (Figures 2-13 – 2-15), as a result of increased twisting in the ground state due to the increased steric hindrance at the boron center. The emission maximum is not affected as much as the absorption maximum; hence, the Stokes shift is further increased to 6 000 cm^{-1}. The fluorescence quantum yield of **2-3M** in MeCN of 0.41 is the same as those of **2-1M** and **2-2M**, whereas in water it is 0.10 which, while lower than the other two chromophores, is still remarkable (Table 2-1 and 2-3). This decrease is a result of the *ca*. ten-times higher non-radiative decay rate in H_2O compared to MeCN. While there is almost no difference between these two solvents for compounds **2-1M** and **2-2M**, the lifetime is shortened drastically from 1.9 ns to 300 ps for **2-3M** with increasing solvent polarity. Chromophore **2-3M** shows almost no solvatochromism in its absorption spectra. A small progressive blue-shift of the emission is observed on going from water to (polar aprotic or protic) organic solvents of decreasing polarity.

Table 2-3. Photophysical data for chromophore **2-3M**.

	solvent	λ_{abs} / nm	ε / M^{-1} cm^{-1}	λ_{em} / nm	Stokes shift / cm^{-1}	Φ_f	τ / ns	k_r / 10^8 s	k_{nr} / 10^8 s	τ_0 / ns
2-3M	MeCN	428	51 000	554	5 300	0.41	1.9	2.2	3.1	4.6
	DMSO	435		551	4 800	0.45				
	MeOH	430		552	5 100	0.45				
	EtOH	435		545	4 600	0.41				
	H_2O	425	-	570	6 000	0.10	0.3	3.3	30	3.0

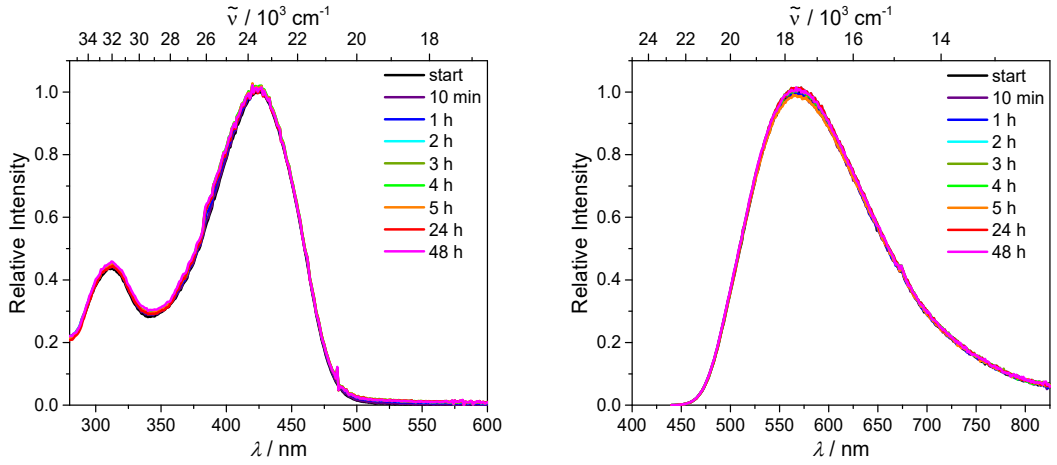

Figure 2-9. Absorption (left) and emission (right) spectra of **2-3M** in H_2O as a function of time. Sample kept in the dark between measurements.

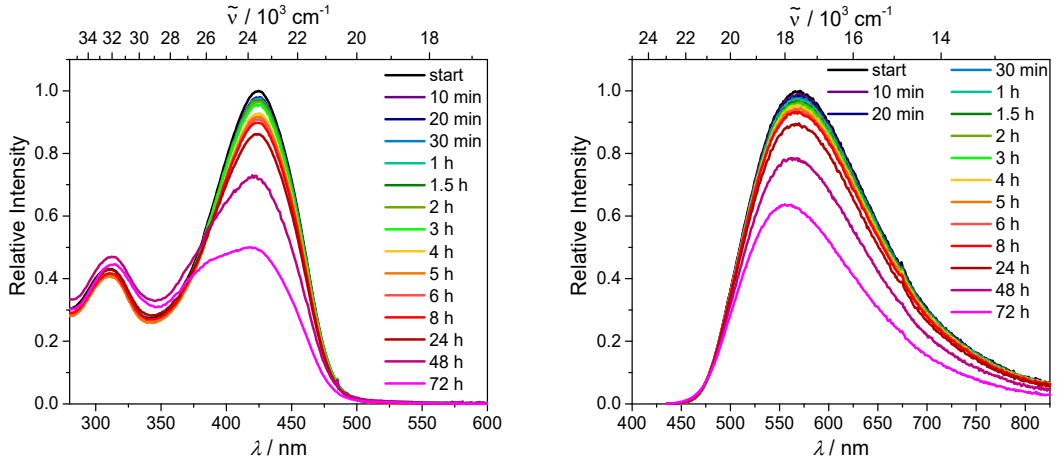

Figure 2-10. Absorption (left) and emission (right) spectra of **2-3M** in H_2O as a function of time. Sample exposed to room light between the measurements.

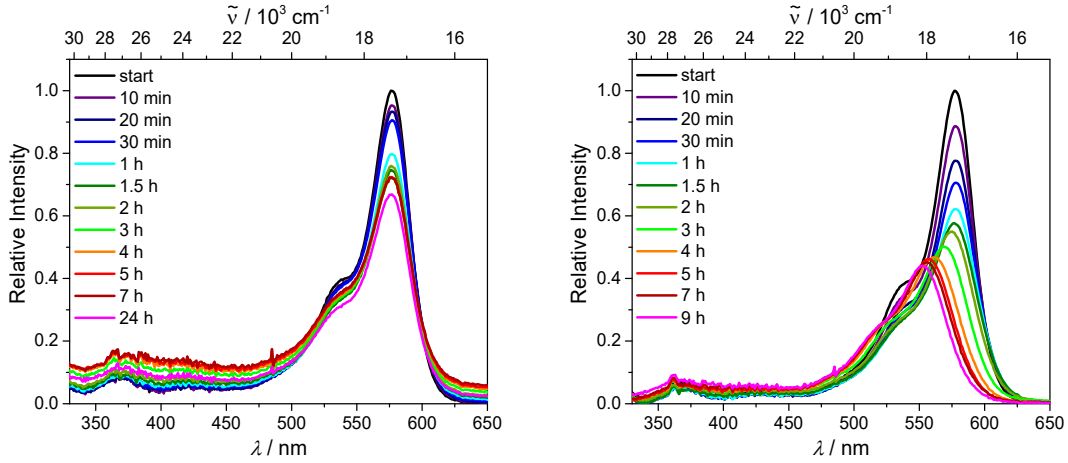

Figure 2-11. Absorption spectra of MitoTracker™ Red CMXRos in H_2O as a function of time. Sample kept in the dark (left) and exposed to room light (right) between the measurements.

UV/Vis measurements over 48 h clearly demonstrate that the increased steric protection provided by the additional methyl groups in **2-3M** dramatically enhances stability in water

(Figure 2-9). As for the dyes **2-1M** and **2-2M**, light enhances their decomposition rate (Figure 2-10). The intensities of the absorption spectra were plotted *versus* time and fit with a linear function. The half-lives of compound **2-3M** were calculated to be 698 h and 79 h, respectively (Figure 2-12 and Table 2-4). Therefore, light decreases the stability by a factor of 9. Furthermore, **2-3M** is more stable in water than the commercially available imaging chromophore MitoTracker™ Red CMXRos (Figure 2-11); the latter data could be fit with an exponential function. This dye has a half-life of only *ca*. 2 h.

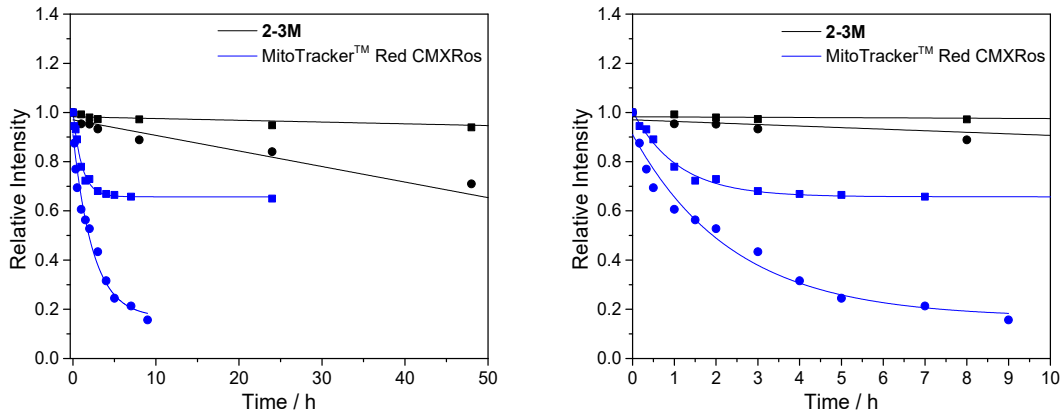

Figure 2-12. Intensity of the absorption maximum *vs*. time for compounds **2-3M** (black) and MitoTracker™ Red CMXRos (blue). Decays for measurements with the sample in the light (●), in the dark (■) between the measurements. The data for MitoTracker™ Red CMXRos are fit with an exponential function: $y = y_0 + A \times e^{(-k \times t)}$ and for **2-3M** with a linear function: $y = m \times t + y_0$. The values for the parameters of the functions are given in Table 2-4.

Table 2-4. Parameter for the functions depicted in Figure 2-12, and the resulting half-lives $t_{1/2}$.

	-k or m	y_0	$t_{1/2}$
2-3M without light	1.19324×10^{-5}	0.98263	698 h
2-3M with light	1.05449×10^{-4}	0.97019	79 h
MitoTracker™ Red CMXRos without light	0.0155	0.65737	1.9 h
MitoTracker™ Red CMXRos with light	0.00695	0.16583	2.1 h

2.2.3 DFT-Calculations

Density functional theory (DFT) calculations were carried out in order to examine the effects of the linker groups on the dihedral angles around the boron center and its influence on conjugation. The geometry of each of the compounds **2-1M** – **2-3M** was optimized using DFT (B3LYP/6-31G(d), gas phase). The structures all show the expected propeller arrangement of the aryl groups about the rigorously trigonal planar boron center. The exchange of the thiendiyl linkers at the boron atom in **2-1M** and **2-2M** for xylylene groups in **2-3M**, leads to an increased twist of the aryl group with respect to the BC_3 plane (**2-1M**: 16.2°; **2-2M**: 13.7°; and **2-3M**: 43.2°). This reduced conjugation with the boron atom leads to the LUMO of **2-3M** being 0.37 eV higher in energy than that of **2-2M**. The π-bridge backbone remains relatively planar in all cases (inter-ring dihedral angles **2-1M**: 14.3°; **2-2M**: 1.5 and 10.3°; and **2-3M**: 18.9 and 12.4°).

Time-dependent-DFT (TD-DFT) calculations (CAM-B3LYP/6-31G(d)) were carried out in order to obtain information on the nature of the optical transitions, and to compute the expected UV/Vis absorption spectra of the compounds and compare this with the experimental spectra. TD-DFT calculations excellently reproduced the experimental absorption maxima of the lowest energy bands, the deviation in energy being within 0.02 – 0.15 eV in simulated MeCN solution. Full details of these results and those in the gas phase are presented in the Figures 2-13 – 2-15. Introduction of the xylylene groups in **2-3M** leads to a hypsochromically shifted absorption spectrum relative to **2-2M**, in line with the experimental spectra. As seen in the natural transition orbitals (NTOs) (Figures 2-13 – 2-15) the $S_1 \leftarrow S_0$ transitions of all three compounds contain a significant contribution from population of the empty boron p_z-orbital, albeit that the transitions are predominantly π-π^*. The boron acceptor thus increases the conjugation length of the π-system. For TPA and TPEF applications, the $S_2 \leftarrow S_0$ transitions were also considered, as this is the lowest energy allowed TPA transition in a quadrupolar chromophore; thus, the NTOs for these transitions are plotted in Figures 2-13 – 2-15.

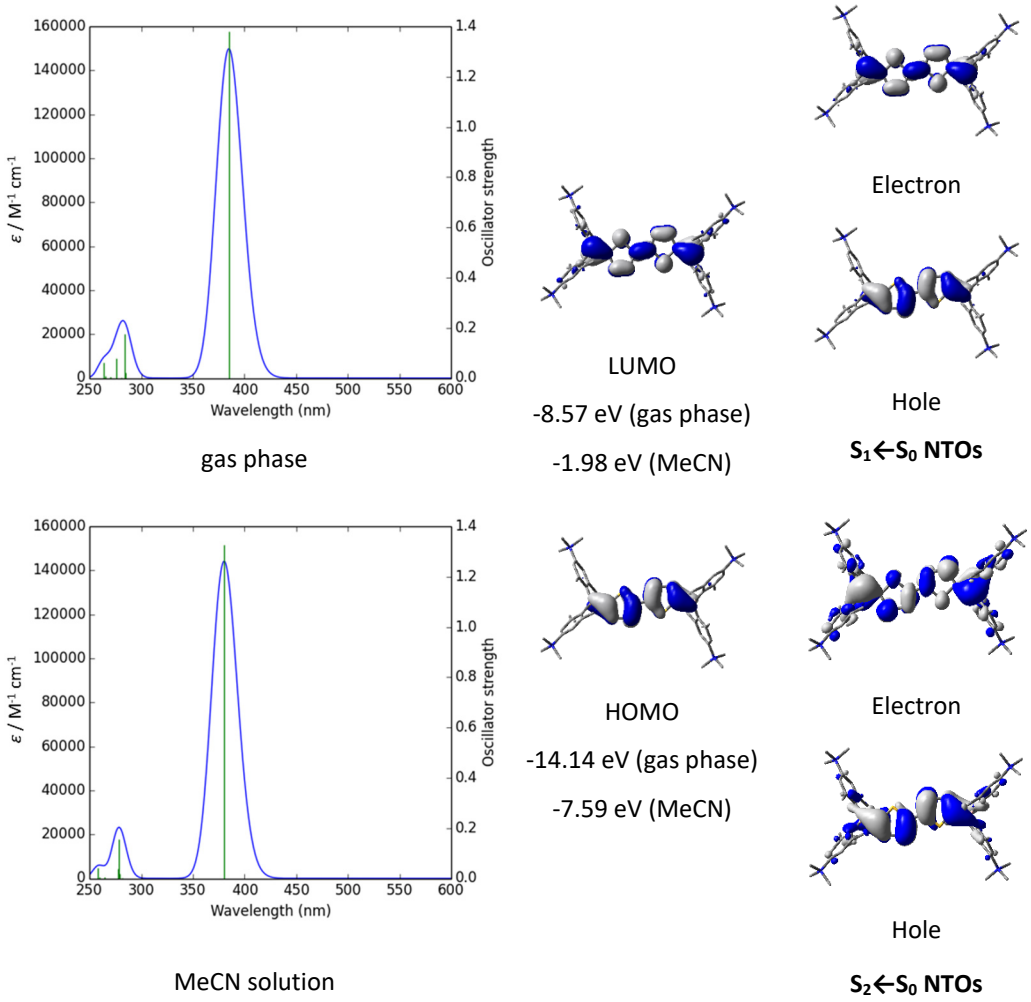

Figure 2-13. TD-DFT calculations for compound **2-1M**. Simulated absorption spectrum (left). FWHM = 2000 cm^{-1}. Orbitals relevant to the $S_1 \leftarrow S_0$ transition (center). H atoms omitted for clarity. Note orbital energies are for the naked tetracation, *i.e.* triflate counterions have not been considered. $S_1 \leftarrow S_0$ and $S_2 \leftarrow S_0$ natural transition orbitals (NTOs) (right).

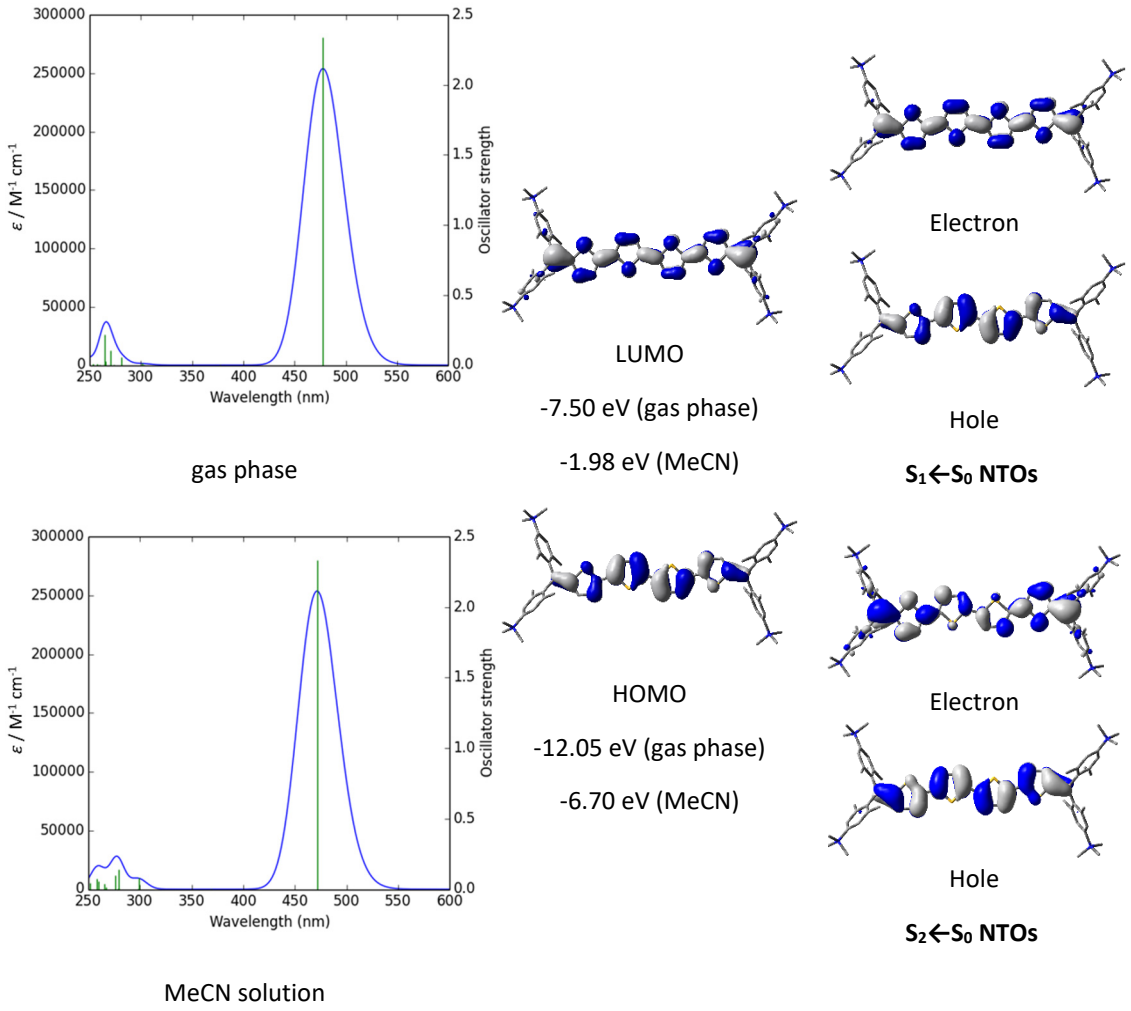

Figure 2-14. TD-DFT calculations for compound **2-2M**. Simulated absorption spectrum (left). FWHM = 2000 cm^{-1}. Orbitals relevant to the $S_1 \leftarrow S_0$ transition (center). H atoms omitted for clarity. Note orbital energies are for the naked tetracation, *i.e*. triflate counterions have not been considered. $S_1 \leftarrow S_0$ and $S_2 \leftarrow S_0$ natural transition orbitals (NTOs) (right).

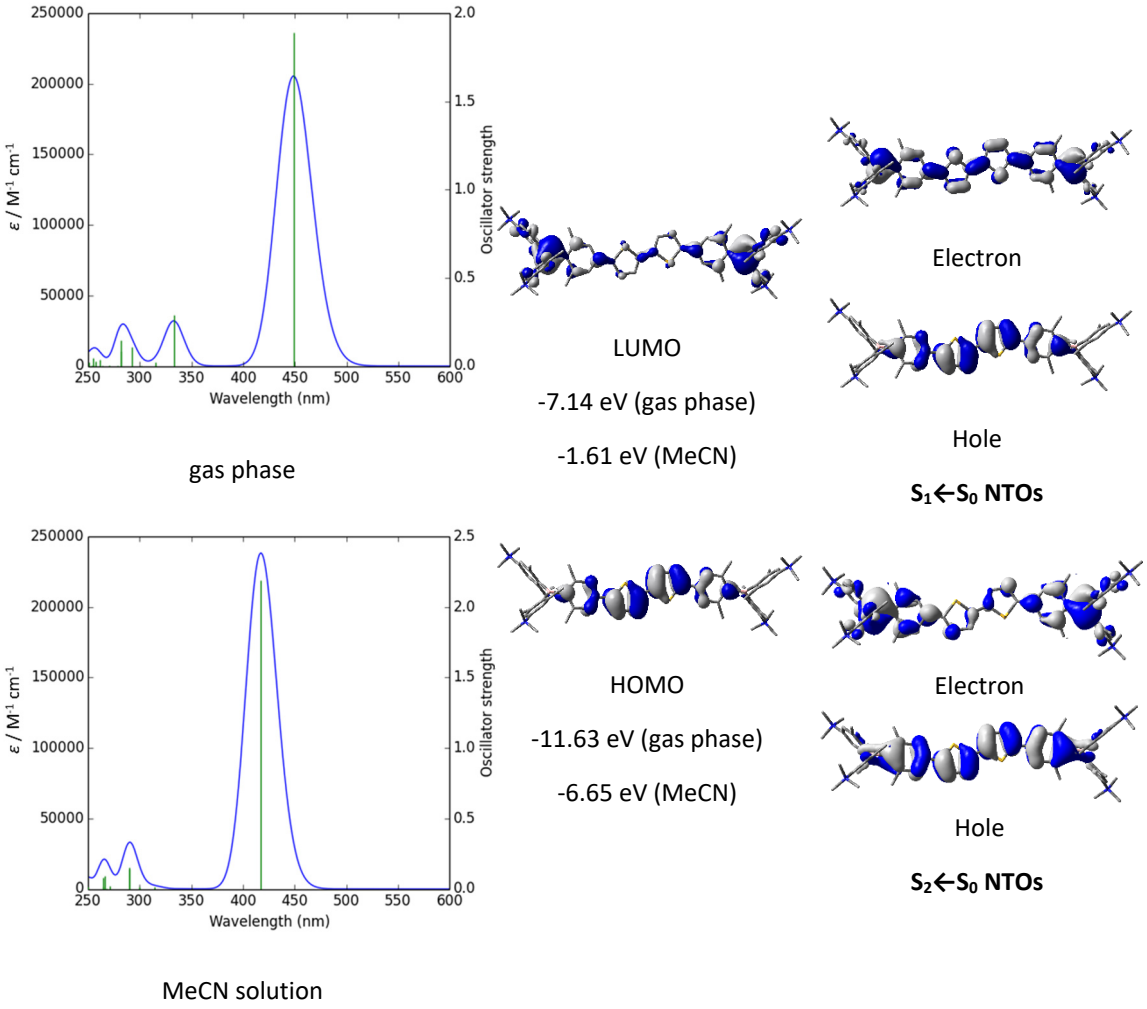

Figure 2-15. TD-DFT calculations for compound **2-3M**. Simulated absorption spectrum (left). FWHM = 2000 cm^{-1}. Orbitals relevant to the $S_1 \leftarrow S_0$ transition (center). H atoms omitted for clarity. Note orbital energies are for the naked tetracation, *i.e.* triflate counterions have not been considered. $S_1 \leftarrow S_0$ and $S_2 \leftarrow S_0$ natural transition orbitals (NTOs) (right).

2.2.4 Two-Photon Absorption

Table 2-5 summarizes the results of TPA measurements of chromophore **2-3M** by using a two-photon excited fluorescence method.[136] Due to the quantum selection rules for centrosymmetric molecules, the TPA maximum does not occur at the doubled wavelength of the one-photon absorption (OPA) maximum, but is located at a shorter wavelength. Indeed, as observed in Figure 2-16, in which the TPA and rescaled OPA are compared, the TPA maximum is observed at higher energy, corresponding to an excited state which is not one-photon allowed. This is in agreement with the typical behavior of quadrupolar molecules.[137] The lowest-excited state is, however, slightly TPA allowed (as indicated by the shoulder between 850 and 900 nm), most probably due to vibrational coupling of an A_u state with an a_u vibrational mode, which makes the overall wavefunction gerade, and therefore TPA allowed.

Table 2-5. Two-photon absorption data for chromophore **2-3M**.

	solvent	λ_{abs} / nm	Φ_f	$2\lambda_{OPA}$ / nm	λ_{TPA}^{max} / nm	$\sigma_2^{max}\Phi_f$ / GM	σ_2^{max} / GM
2-3M	MeCN	428	0.41	856	800	285	693
					870	58	140
	H_2O	425	0.10	850	800	27	268
					870	6	58

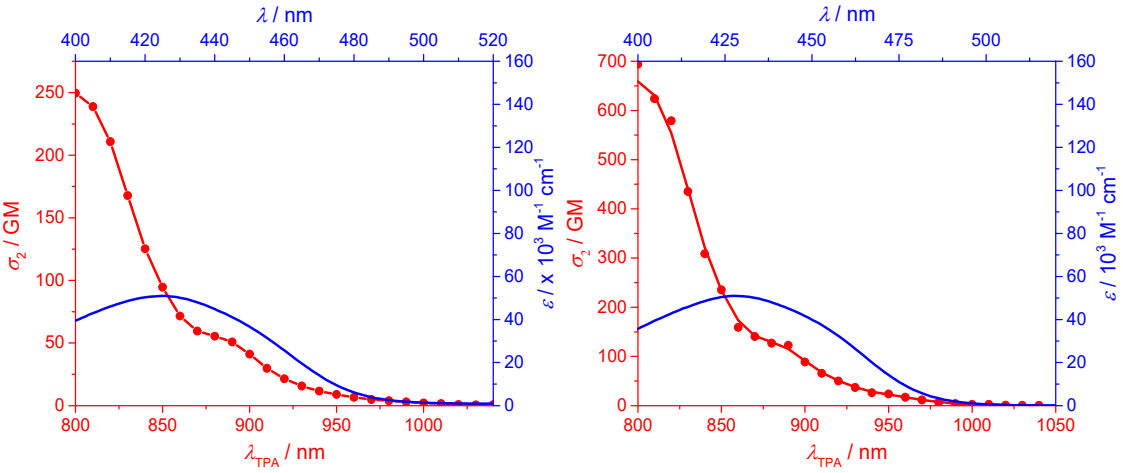

Figure 2-16. One-photon absorption (OPA) (blue) and two-photon absorption (TPA) spectra (red) of **2-3M** in water (left) and MeCN (right).

It was not possible to determine the actual maximum of the TPA (Figure 2-16), which is calculated to be at 792 nm (Table 7-8), as no measurement beyond 800 nm was done, but at 800 nm, a very large TPA cross-section of 268 GM in H_2O was observed, which is increased to 693 GM in MeCN (Figure 2-16). Due to the sizeable fluorescence quantum yields, relatively large values of the two-photon brightness (27 and 285 GM in water and MeCN, respectively) were measured, making dye **2-3M** promising for two-photon imaging in tissues.

2.2.5 Cell Cytotoxicity and Cell Imaging

In light of the above photophysical properties and water-stability of **2-3M**, and thus its potential as a chromophore for live-cell imaging, its possible cytotoxicity in cells was examined. Therefore, three different cell lines - murine-fibroblasts (NIH 3T3), human embryonal kidney (HEK 293T), and human-hepatic origin (HepG2-16) - were exposed to serial dilutions of **2-3M** and also LiOTf and studied the cell metabolic activity with a colorimetric (WST-1) assay (Figures 2-17 and 2-18). These experiments confirmed that compound **2-3M** did not influence the cell viability at concentrations as high as 10 μM. The triflate counterion, as its lithium salt, was also examined for cytotoxicity and showed no toxicity up to 100 μM. Therefore, compound **2-3M** can be safely used in live-cell imaging applications, and this class of compounds shows great potential for the development of *in vivo* diagnostics to probe mitochondrial function and for other live-cell imaging applications.

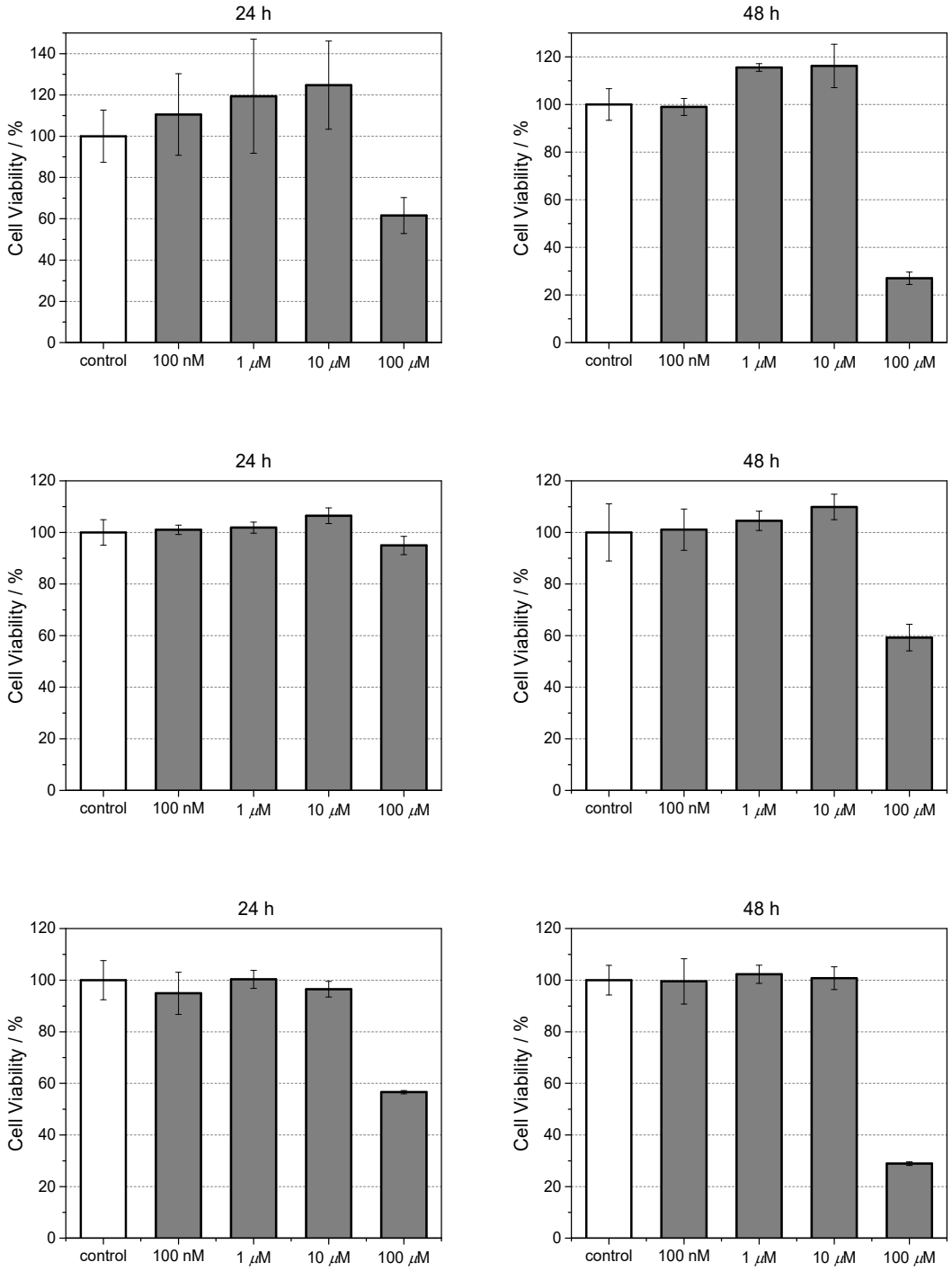

Figure 2-17. The cell viability of NIH 3T3 (first row), HEK 293T (second row) and HEPG2-16 cells was measured after 24 h (left panels) or 48 h incubation (right panels) with serial dilution of compound **2-3M** by using a colorimetric WST-1 assay. The results are presented as the relative viability shown as a percent of the DMSO-treated control (white bars) + the standard deviation.

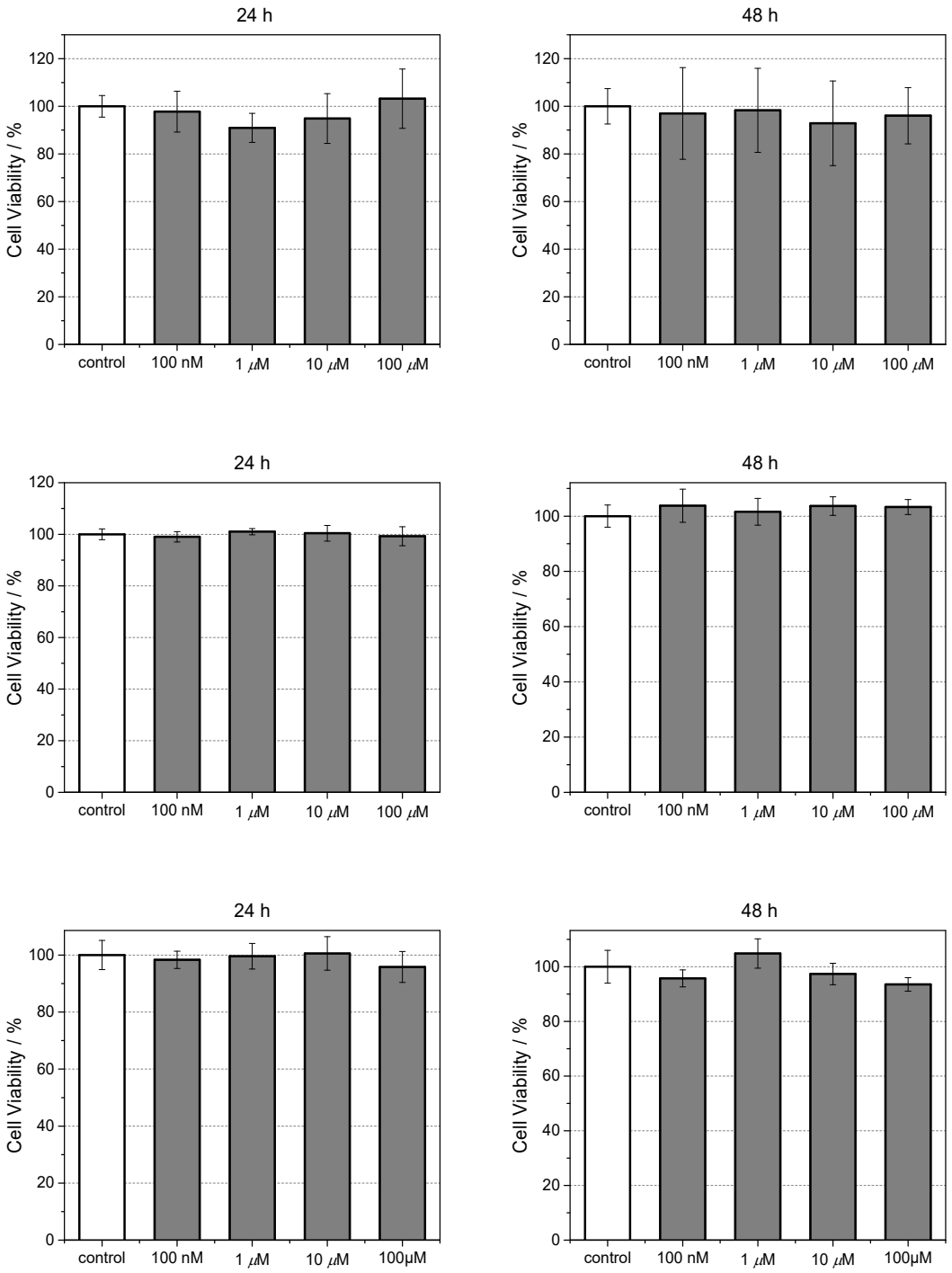

Figure 2-18. The cell viability of NIH 3T3 (first row), HEK 293T (second row) and HEPG2-16 cells was measured after 24 h (left panels) or 48 h incubation (right panels) with serial dilution of LiOTf by using a colorimetric WST-1 assay. The results are presented as the relative viability shown as a percent of the DMSO-treated control (white bars) + the standard deviation.

Thus, living mouse embryo fibroblast cells (NIH 3T3) were treated with a 10 μM concentration of chromophore **2-3M**. Visualization by confocal laser scanning fluorescence microscopy showed that **2-3M** penetrated the cell membrane of living cells and localized at the mitochondria as confirmed by co-localization experiments with the commercial mitochondrial imaging agent MitoTracker™ Red CMXRos (Figure 2-19).

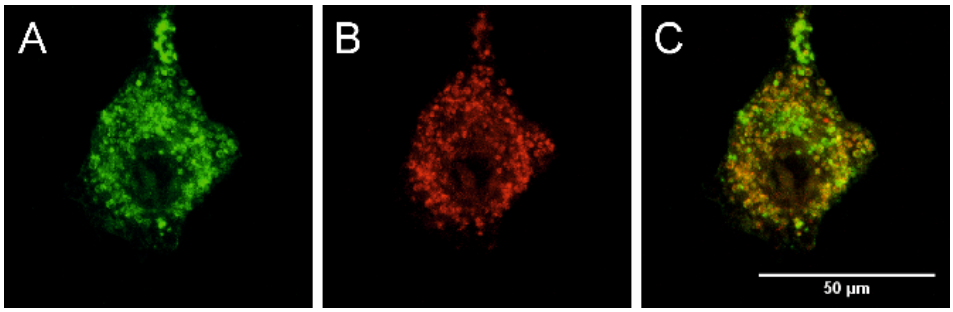

Figure 2-19. Confocal microscope live-cell image of murine NIH 3T3 fibroblast cells with (A) 10 μM of dye **2-3M** and (B) 125 nM of MitoTracker™ Red CMXRos. (C) Merged image indicating the co-localization of compound **2-3M** with MitoTracker™ Red CMXRos.

Based on the sizeable two-photon brightness of dye **2-3M** in water, it was tested as a two-photon dye to stain POS 1 cells - a cell line derived from an osteosarcoma tumor. The two-photon imaging experiments (and parallel confocal imaging under one-photon excitation) were performed using a 300 nM concentration.

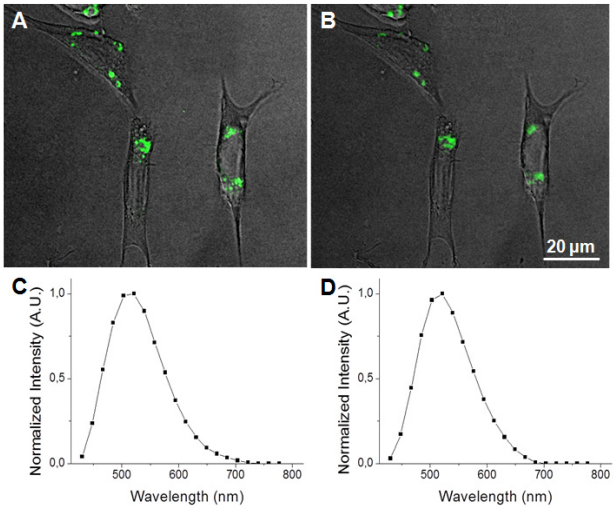

Figure 2-20. Confocal microscope image of POS 1 cells after 8 h of incubation with dye **2-3M** (300 nM in the media): merge of transmission image (grey) and fluorescence image (green) showing the internalization of the dye within the cells: (A) one-photon excitation (λ_{ex} = 405 nm; λ_{em} = 500 – 600 nm) and (B) two-photon excitation (λ_{ex} = 800 nm; λ_{em} = 500 – 600 nm); (C) emission spectrum upon one-photon excitation (λ_{ex} = 405 nm; 20 nm step) of the dye within the cell; (D) emission spectrum upon two-photon excitation (λ_{ex} = 800 nm; 20 nm step) of the dye within the cell.

As clearly shown in Figure 2-20, fluorescence images under standard one-photon and two-photon excitation show the same localization of the dye. Furthermore, emission spectra of the uptaken dyes were acquired demonstrating that the dye structure is retained upon internalization in the cells. Hence, the steric protection around the empty p_z-orbital at the boron atom not only confers stability of dye **2-3M** in pure water, but is also sufficient to make it stable in a cellular environment. The blue-shifted emission compared to that observed in pure water can be related to environmental effects, suggesting that the dye is located in a less polar environment.

2.3 Conclusions

In conclusion, three water-soluble quadrupolar chromophores with triarylborane acceptors were synthesized. The two compounds **2-1M** and **2-2M** are bright emitters in water, but were shown to decompose, due to hydrolysis at the boron center. In contrast, **2-3M** has enough steric protection around the empty p_z-orbital at the boron atom that it is sufficiently stable in water. Furthermore, **2-3M** localizes at mitochondria, which was confirmed by co-localization experiments, and is not toxic at concentrations suitable for imaging purposes. It was demonstrated that **2-3M** is more stable than the commercial available MitoTracker™ Red CMXRos. In this chapter, the first TPA cross-section measurement of a triarylborane in water was reported, being 268 GM at 800 nm, which is very large; hence, **2-3M** is suitable for two-photon live-cell microscopy. Herein, a three-coordinate boron-containing chromophore for mitochondrial TPEF imaging was reported, profiling this compound as a water-soluble, biocompatible mitochondrial tracker for *in vitro* live-cell imaging applications. Future application as a diagnostic tool for clinical use should, in spite of the promising data set obtained with respect to (cellular) biocompatibility, be re-assessed in light of the outcome from robust (pre-)clinical safety studies. Optimization of such chromophores to enhance quantum yields and TPA cross-sections and to tune emission wavelengths is described in Chapters 3, 4 and 5.

Chapter Three

-

Tuning the π-Bridge of Quadrupolar Triarylborane Chromophores

3 TUNING THE π-BRIDGE OF QUADRUPOLAR TRIARYLBORANE CHROMOPHORES

3.1 Introduction

The synthesis and applications of triarylboranes have increased tremendously in the last few decades.[9, 13b, 17, 18b, 18e, 120a, 138] The three-coordinate boron moiety is a strong π-electron acceptor (A) due to its vacant p_z-orbital. The trigonal-planar geometry of the boron atom must be maintained, due to its strong Lewis acidity which can otherwise lead to binding of Lewis bases and/or hydrolytic decomposition. This can be accomplished by the use of sterically demanding substituents, such as mesityl (Mes) or 2,4,6-$(CF_3)_3C_6H_2$ (^{F}Mes),[139] or by physical constraint, *via* incorporation in a rigid, planar structure.[121] While the latter strategy prevents the formation of a four-coordinate boron species by inhibiting structural deformation, the former builds a propeller-like structure around the empty p_z-orbital and obstructs the attack of nucleophiles, such as water, *via* the formation of a protective cage. Only small anions, such as fluoride and cyanide, can overcome the steric bulk and bind to the free p_z-orbital at the boron.[13a, 13c, 13d] For this reason, triarylborane acceptors are often used as selective F^- and CN^- sensors, as the emission spectra change quite significantly upon anion binding.[140] Three-coordinate boron species are also applied as emitting/electron transporting materials in organic light emitting diodes.[101c, 103, 105] As they are known to be excellent acceptors for thermally activated delayed fluorescence (TADF) emitters, a new generation of OLEDs has been established.[108c, 108d, 141] They can be used as electron-transporting materials, as they are efficient electron and spin carriers.[45, 75e, 101c, 105, 123a, 142] This allows chemical and electrochemical reduction of the triarylborane unit and makes boron radicals intrinsic magnetic materials.[49f, 52, 59, 143] Furthermore, the electron deficiency of BAr_3 acceptor units, make them especially useful in intramolecular charge transfer compounds, when conjugated to a π-donor (D) moiety.[12, 15, 31, 33, 43d, 111g, 144] As excitation induced charge transfer properties increase the two-photon absorption (TPA) probability, triarylborane acceptors have great potential for use in TPA and for two-photon excited fluorescence (TPEF).[145]

TPA is the simultaneous absorption of two photons *via* a virtual state, which is proportional to the square of the light intensity, whereas one-photon absorption is a linear process obeying Beer's Law.[109b, 109d, 146] For this reason, two-photon optics enables excitation of molecules within a very small volume (~ femto liter) at the focus of a laser beam, which is useful for many applications. There is thus a strong demand for efficient two-photon absorption dyes for microfabrication,[147] three-dimensional data-storage,[148] optical power limiting,[149] laser up-conversion,[150] photodynamic therapy[151] and biological imaging.[145, 152] Especially for the latter application, relatively few small organic molecules have been studied, as they need to be highly

specific for their biological target, highly photostable, water-stable and at least somewhat water-soluble to stain cells and tissues. In addition, the two-photon brightness ($\sigma_2\Phi_f$), where σ_2 is the two-photon absorption cross-section (comparable to an extinction coefficient) in GM and Φ_f is the fluorescence quantum yield, should be at least 50 GM to observe bright two-photon microscope images.[145] Such probes have been applied as sensors of biomolecules (*e.g*. ions, reactive oxygen species (ROS), reactive sulfur species (RSS) and reactive nitrogen species (RNS)) and changes inside cells (pH, viscosity and polarity).[153] However, two-photon dyes for monitoring and visualizing mitochondria and lysosomes are still limited.

Lysosomes are acidic (pH 4.5-5.0) organelles in eukaryotic cells and are responsible for intracellular digestion degradation, secretion, plasma membrane repair, cell signaling, energy metabolism and endocrine regulation.[154] Lysosomes are filled with more than 60 enzymes, the synthesis of which is controlled by nuclear genes. Mutations of these genes lead to lysosomal storage diseases, such as neurodegenerative disorders, *e.g*. Parkinson's disease and Alzheimer's disease, cardiovascular diseases and cancer.[155] As they are acidic organelles, usually organic bases, such as morpholine, pyridine and dimethylamino groups, lead to accumulation in lysosomes. These terminal groups are typically attached to common dyes, such as naphthalene,[156] 1,8-naphthalimide,[157] indole,[48c] coumarin,[158] chromene[159] and fluorenone.[160] Most of them are lysosome trackers,[156a, 156b, 157f, 159-160] while others can sense Zn^{2+},[157b] HClO,[156d, 157c] H_2S,[48c, 157g] thiols,[157d] NO,[157a] β-galactosidase,[157i] pH[156c, 157e, 157h] or polarity[158] within the lysosome. While all of the above-mentioned dyes are dipolar, quadrupolar chromophores for two-photon imaging of lysosomes are rare. It should be noted that efficient two-photon absorbing dyes bear the common structural motifs of dipolar, push-pull systems (D–A), quadrupolar (D–π–D, A–π–A) or octupolar systems (D–A_3, A–D_3), with the latter two being often more efficient than dipoles.[109d, 146c] While the TPA properties of many quadrupoles have been studied, only a handful of those are used for imaging, especially of the lysosome. All eight such compounds which are, to our knowledge, the only ones, are depicted in Scheme 3-1.

In 2010, Belfield and co-workers reported[161] the first quadrupolar TPEF imaging agent for lysosomes (**3-A**) which exhibited a very high two-photon brightness of 431 GM in toluene. The dye localized in the lysosome, was found to be not toxic and photostable. One year later, the same group reported three other compounds, **3-B1**, **3-B2** and **3-C**, with $\sigma_2\Phi_f$ of 1 444, 1 887 and 788 GM, respectively, in cyclohexane.[162] In the more polar solvent THF, the two-photon brightness of **3-B1** decreased to 1/3 and for compound **3-C**, $\sigma_2\Phi_f$ decreased to 1/9 of its original value in a "5 wt% aqueous DMSO" solution. The brightness is usually much smaller in aqueous solution, due to the reduced quantum yield. Nevertheless, the three compounds show

remarkably large values, due to their large conjugation lengths, but have relatively high molecular weights. Furthermore, these compounds are not water-soluble and must be premixed with Pluronic F-127, which is a block copolymer based on ethylene oxide and propylene oxide that is used for drug delivery. It encapsulates the chromophores upon formation of micelles facilitating dye uptake by the cells. In 2015, Cho's group reported the water-soluble dye **3-D**.[163] Due to its negligible fluorescence in water, they measured its TPEF properties in a dioxane-water mixture and reported a brightness of 116 GM. The fluorenone dye **3-E** does not show bright fluorescence in water (Φ_f = 0.07); thus, its TPEF properties were measured in toluene ($\sigma_2\Phi_f$ = 150 GM).[164] The small size of the molecule might be the reason for its more modest two-photon brightness. Compounds **3-F** and **3-G** are two pH-sensitive dyes for lysosome imaging.[165] The pyridine moiety acts as a ratiometric sensor for pH changes, as the protonation of the pyridine enhances intramolecular charge transfer. The two-photon cross-section increases, while the quantum yield drops at lower pH values. Therefore, the two-photon brightness maxima occur at pH 7 for **3-F** (130 GM) and at pH 3 for **3-G** (99 GM). Unfortunately, the selectivity of the dyes in the lysosome is less than excellent, as co-localization experiments showed an overlap with LysoTracker™ at lower pH, but also distribution in the cytosol at neutral pH.

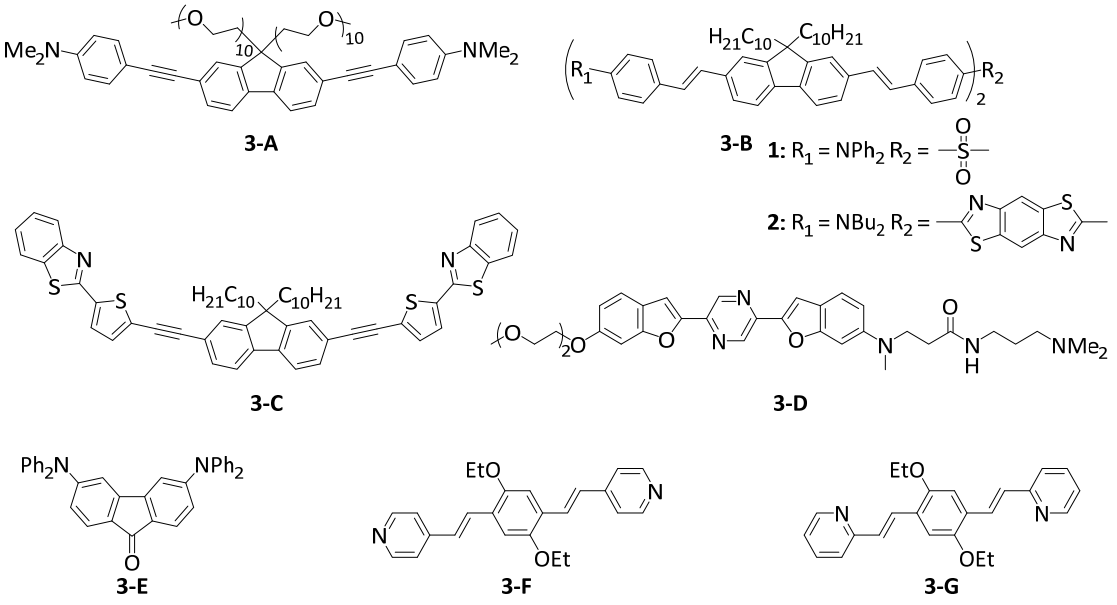

Scheme 3-1. Previously reported quadrupolar chromophores for two-photon excited fluorescence (TPEF) imaging of lysosomes.[161-165]

As the Marder group has shown[16, 111e-g, 111i] that quadrupolar compounds (A–π–A), with three-coordinate boron moieties as acceptors, exhibit large TPA cross-sections, they wanted to apply them for imaging, but only a few water-soluble triarylboranes were known. Gabbaï and co-workers used trimethylammonio groups at the *para*-positions of triarylboranes to achieve water-solubility for sensing of cyanide in aqueous solution.[166] They and other groups also introduced cationic phosphonio substituents onto triarylboranes for further anion sensing

studies.[127] Yang and co-workers were the first to report water-soluble three-coordinate boron compounds for imaging purposes. They substituted a triarylborane with polyethylene glycol chains for ATP sensing in the cytoplasm and cell membrane.[128] Furthermore, they could sense H_2S with a Cu^{II}-cyclen-substituted triarylborane.[129] They reported cell-membrane permeability and a preferential distribution at mitochondria,[129] while the same compound, without Cu^{II} binding, was used one year later to stain nucleoli and cytoplasm.[115] However, a two-photon brightness of only 30 GM in DMSO was measured for this compound. Two other triarylboranes with piperazine in the *para*-position were recently reported. They are water-soluble to some degree and were found to stain nucleoli as well as the nuclear membrane, nuclear matrix, nuclear pore and the cytoplasm, while binding to RNA.[116] Further three-coordinate boron containing dyes were used for imaging, although they were not water-soluble.[117, 167] By loading them into nanogels, they became cell membrane permeable, stained the cytoplasm and could be applied as temperature, viscosity, pH, H_2O_2 and biothiol sensors.[117, 167] Another intracellular "turn-on"-sensor for thiophenol, based on a triarylborane moiety, was very recently published by Thilagar and co-workers.[118] In chapter 2 the only water-soluble quadrupolar three-coordinate boron compound for imaging (**2-3M**) is reported, which exhibits a very reasonable two-photon brightness of 285 GM in MeCN (Scheme 3-2).[119]

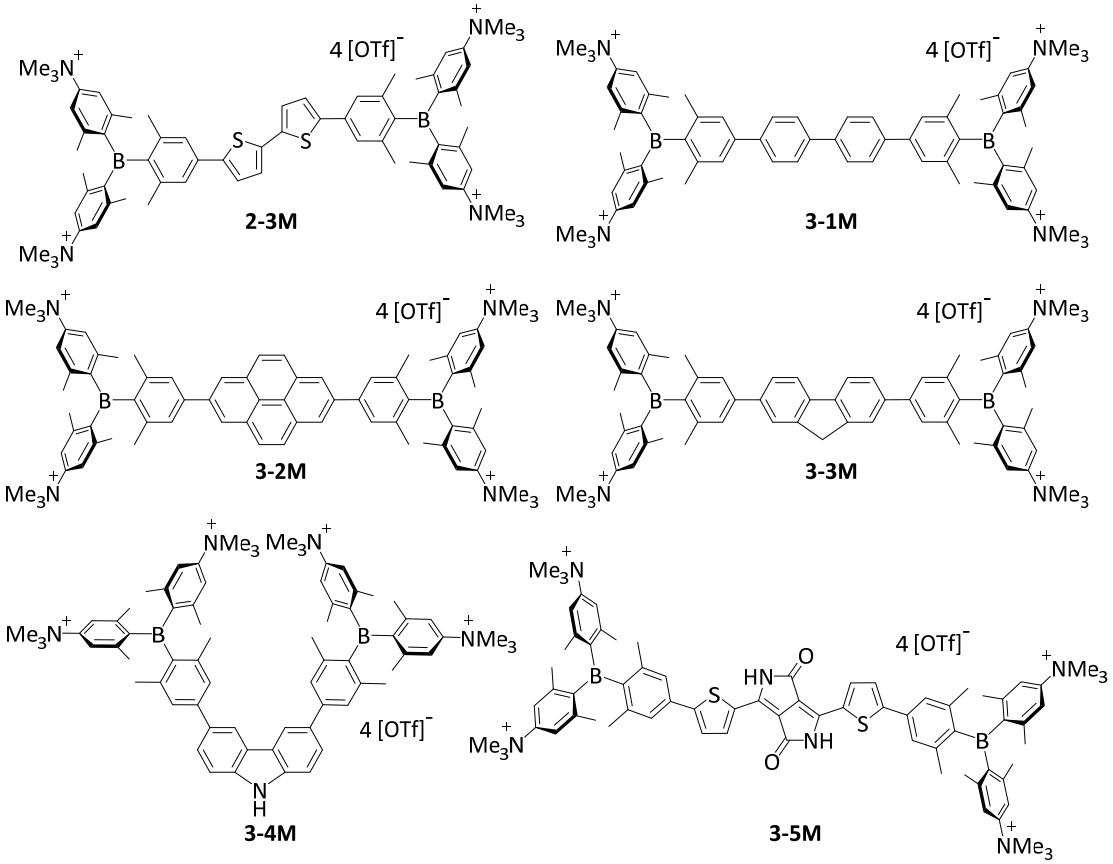

Scheme 3-2. Quadrupolar chromophores for TPEF imaging **2-3M**, **3-1M** – **3-5M**.

With the very promising initial results of **2-3M**, the optimization of the imaging dye is the next step. Tuning the emission color, enhancing the quantum yield, TPA cross-section and photostability, maintaining low cytotoxicity, determining co-localization as well as examining the cellular uptake pathway are the main goals. For this purpose, the new dyes **3-1M** – **3-5M** shown in Scheme 3-2 were designed, all of which contain trimethylammonio groups for water-solubility.[166] Due to the inductive withdrawing character of the ammonium cations, these triarylborane moieties are much stronger acceptors than the normally used aryldimesitylborane. In the present chapter, the role of the π-bridge in the A–π–A system, employing 4,4'-biphenyl, 2,7-pyrenyl, 2,7-fluorenyl, 3,6-carbazolyl and 5,5'-di(thien-2-yl)-3,6-diketopyrrolopyrrolyl bridges, will be investigated. Thus, more rigid π-bridges are introduced, to compare with the biphenyl compound **3-1M**, to achieve more planar ground state structures, resulting in a better delocalized π-system and therefore enhanced TPA/TPEF properties. Furthermore, enhanced donor character was introduced into the π-bridge *via* the carbazole, while incorporation of the dithienyl-diketopyrrolopyrrole moiety leads to an A–D–A–D–A-type chromophore, allowing enhanced intramolecular charge transfers. The diketopyrrolopyrrole moiety is known for its high photostability and TPA cross-section,[168] *e.g*. when connected to two porphyrin groups (up to 4 000 GM at 910 nm in CH_2Cl_2).[169]

3.2 Results and Discussion

3.2.1 Synthesis

The synthesis of the neutral compounds **3-1** – **3-5** was achieved *via* Suzuki-Miyaura coupling of the different dibrominated π-bridges with the borylated triarylborane **2-6**[119] using $Pd_2(dba)_3{\cdot}CHCl_3$ as the catalyst, SPhos as the ligand and KOH as the base (Scheme 3-3). The neutral compounds were methylated with methyl triflate in dichloromethane and the products **3-1M** – **3-3M** precipitated in almost quantitative yields. The methylation needs to be carried out in basic glassware, such as soda-lime glass, as otherwise the reaction does not go to completion, and the product is contaminated with the three-times methylated species. When using the two *Boc*-protected bridges, carbazole **3-4** and dithienyl-diketopyrrolopyrrole **3-5**, the reaction time needs to be carefully controlled, as too short a reaction time leads to incomplete methylation, whereas too long a reaction time results in deprotection and subsequent methylation of the amine in the bridge. The latter two *Boc*-protected tetracationic compounds were subsequently deprotected with triflic acid to yield the final compounds **3-4M** and **3-5M**.

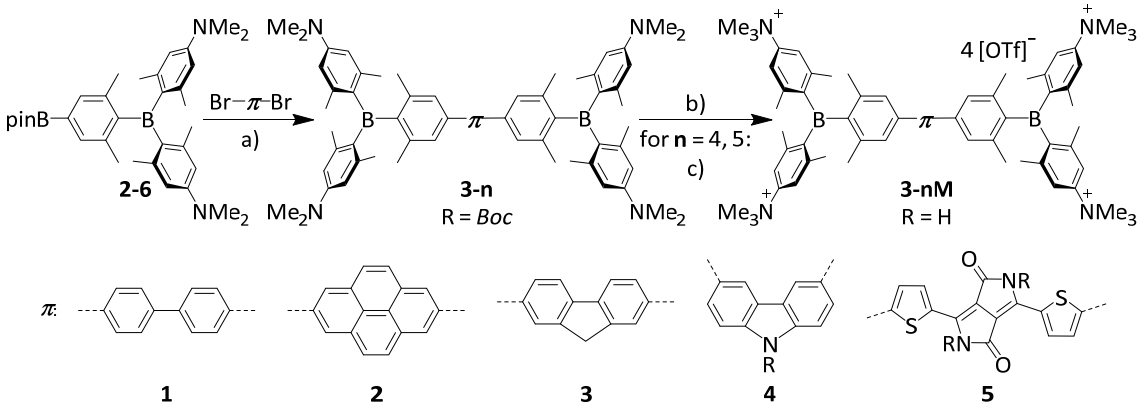

Scheme 3-3. Synthesis of compounds **3-1M** – **3-5M**. a) $Pd_2(dba)_3{\cdot}CHCl_3$, SPhos, KOH, toluene, H_2O, 85 °C; b) MeOTf, CH_2Cl_2; c) TfOH, MeOH.

3.2.2 Linear Optical Properties and TD-DFT Calculations

The neutral chromophores behave in a very similar manner, with the exception of compound **3-5**. The absorption spectra of **3-1** – **3-4** (Figure 3-1 and 3-2, Table 3-1) show a low energy band corresponding charge transfer from the *para*-(*N*,*N*-dimethylamino)xylyl donor to the π-bridge and boron acceptor, as confirmed by TD-DFT calculations, *vide infra*. As compounds **3-1** – **3-4** are so similar, in the following compound **3-1** will be discussed in detail as an example. Thus, for the biphenyl compound **3-1**, the above described absorption band occurs at 392 nm (calculated at 354 nm) resulting from the coincidental overlap of the weak $S_1 \leftarrow S_0$ and stronger $S_2 \leftarrow S_0$ transitions (Table 3-2). The HOMO-1 and HOMO are nearly degenerate, and both orbitals are localized at the *para*-(*N*,*N*-dimethylamino)xylyl groups, while the LUMO and LUMO+1 are located at the π-bridge and the boron atoms (Figure 3-3). The higher energy absorption bands have charge-transfer character, but with increasing energy the π-π^* character at the π-bridge becomes increasingly dominant. The $S_3 \leftarrow S_0$ and $S_5 \leftarrow S_0$ transitions at 372 and 328 nm, respectively, were calculated to be at 335 and 296 nm, with contributions of HOMO-4 of 11 and 55%, respectively (Table 3-2). HOMO-4 is delocalized over the whole π-bridge (Figure 3-3). Very similar results were calculated for compounds **3-2** – **3-4**. All compounds show different high energy absorption bands, as the π-π^* contributions of the π-bridges become more and more important. For example, compound **3-2** shows one additional absorption band at 342 nm, which is calculated to arise from the $S_6 \leftarrow S_0$ transition from HOMO-6 to LUMO, and is a classic pyrene π-π^* transition, with the typical nodal plane through the 2,7-positions (Figure 3-3).[52, 57-58, 59] The dithienyl-diketopyrrolopyrrole dye **3-5** is an exception, as the HOMO is located at the π-bridge (Figure 3-4). Therefore, the $S_1 \leftarrow S_0$ transition is a locally excited (LE) HOMO to LUMO transition at the π-bridge, while higher energy transitions show the same charge transfer character as noted above for **3-1** – **3-4** (Table 3-2). For **3-5**, the HOMO-1 and HOMO-2 are nearly degenerate and are each localized at two *para*-(*N*,*N*-dimethylamino)xylyl groups. Note that the TD-DFT

calculations were carried out for the geometry optimized (lowest energy) structure and not for the highest possible symmetry (C_i) of these molecules. Therefore, the corresponding $S_2 \leftarrow S_0$ and $S_4 \leftarrow S_0$ transitions are isoenergetic and exhibit charge transfer character from the nitrogens to the boron atom.

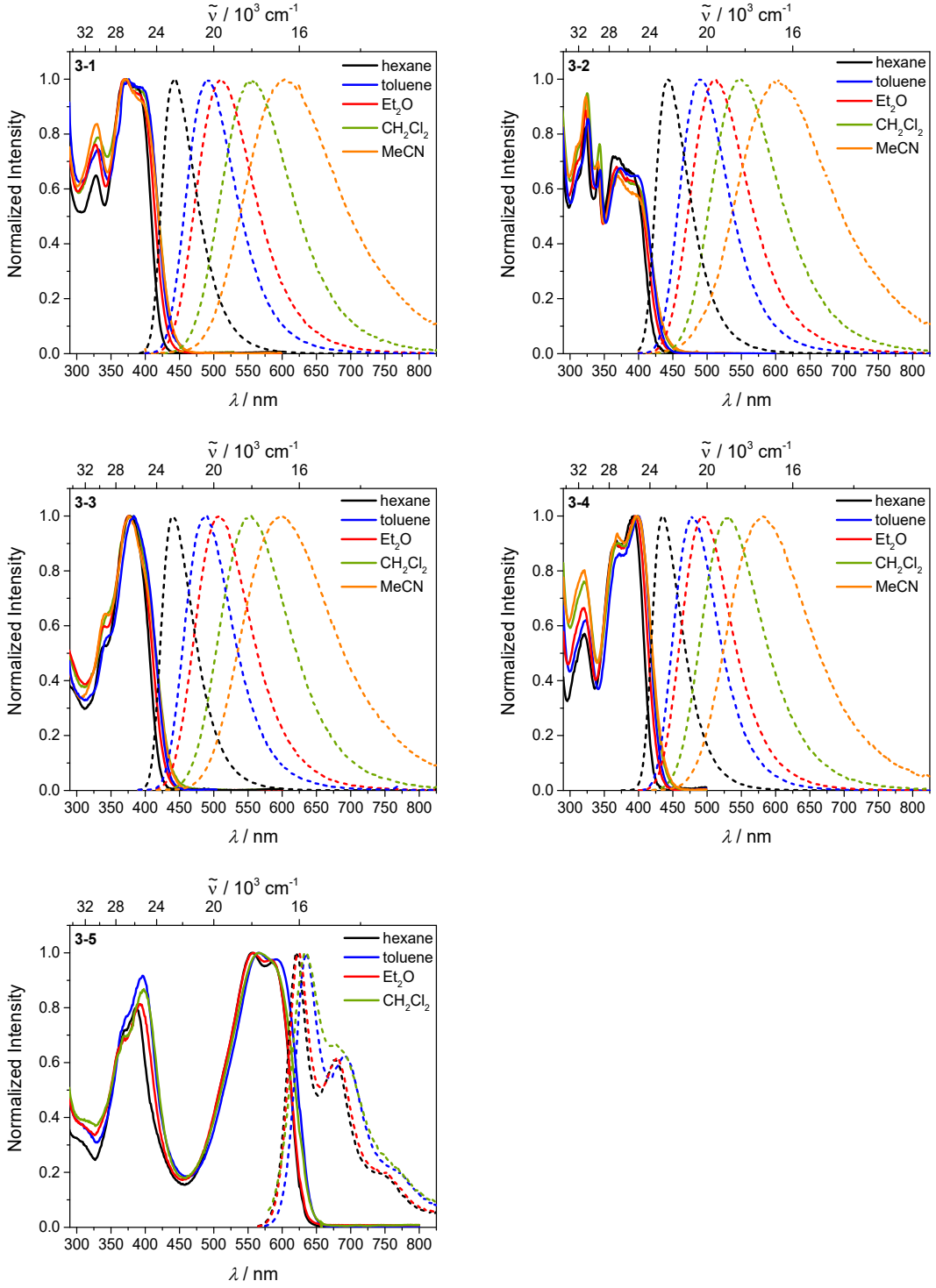

Figure 3-1. Absorption and emission spectra of **3-1** (first row, left), **3-2** (first row, right), **3-3** (second row, left), **3-4** (second row, right) and **3-5** (third row, left) in various solvents (hexane: black, toluene: blue, diethylether: red, dichloromethane: green, MeCN: orange).

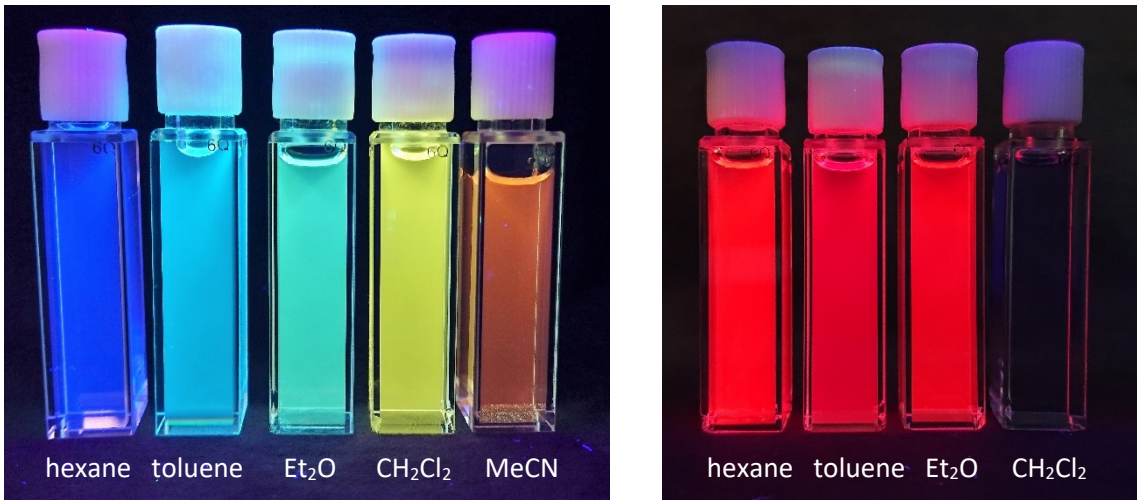

Figure 3-2. Pictures of the solutions under UV irradiation (bottom) of **3-1** (left) and **3-5** (right) in various solvents.

Table 3-1. Photophysical data of compounds **3-1** – **3-5** in various solvents.

	solvent	λ_{abs} / nm	ε / M^{-1} cm^{-1}	λ_{em} / nm	Stokes shift / cm^{-1}	Φ_f	τ / ns	k_r / 10^8 s	k_{nr} / 10^8 s
3-1	Hexane	372	69 000	442	4 300	0.14	1.5	0.9	5.8
	toluene	376		493	6 300	0.20	3.4	0.6	2.3
	Et_2O	369		511	7 500	0.24	5.9	0.4	1.3
	CH_2Cl_2	373		556	8 800	0.30	8.8	0.3	0.8
	MeCN	371		603	10 400	0.08	2.5	0.3	3.7
3-2	Hexane	366	70 000	445	4 900	0.14	1.5	0.9	5.8
	toluene	372		490	6 500	0.23	3.6	0.6	2.2
	Et_2O	368		511	7 600	0.27	6.4	0.4	1.2
	CH_2Cl_2	371		545	8 600	0.34	9.6	0.4	0.6
	MeCN	370		603	10 400	0.08	2.9	0.3	3.1
3-3	Hexane	378	82 000	441	3 800	0.16	1.5	1.1	5.6
	toluene	383		491	5 700	0.21	3.3	0.6	2.4
	Et_2O	375		509	7 000	0.23	6.5	0.4	1.1
	CH_2Cl_2	383		555	8 100	0.29	8.1	0.4	0.8
	MeCN	377		596	9 700	0.09	3.3	0.3	2.7
3-4	Hexane	393	56 000	436	2 500	0.12	1.4	0.9	6.2
	toluene	399		479	4 200	0.23	3.3	0.7	2.3
	Et_2O	395		495	5 100	0.25	5.0	0.5	2.0
	CH_2Cl_2	399		530	6 200	0.41	10.3	0.4	0.6
	MeCN	398		581	7 900	0.15	6.3	0.2	1.4
3-5	Hexane	557	59 000	622	1 900	0.57	2.4	2.4	1.8
	toluene	566		635	1 900	0.55	2.3	2.4	1.9
	Et_2O	558		624	1 900	0.40	2.0	2.0	3.0
	CH_2Cl_2	568		635	1 900	0.004	2.3	0.02	4.3

Table 3-2. TD-DFT-calculated photophysical data for **3-1** and **3-5** at the CAM-B3LYP/6-31G(d) level in hexane:[a]

	transition (f)	E / eV[b]	λ / nm[b]	dominant components[c]
3-1	$S_1 \leftarrow S_0$ (0.054)	3.50 (3.16)	354 (392)	LUMO+1←HOMO-1 (44%), LUMO←HOMO (38%)
	$S_2 \leftarrow S_0$ (0.736)	3.50 (3.16)	354 (392)	LUMO←HOMO-1 (38%), LUMO+1←HOMO (44%)
	$S_3 \leftarrow S_0$ (1.496)	3.70 (3.33)	335 (372)	LUMO←HOMO-4 (11%), LUMO+1←HOMO-3 (29%), LUMO←HOMO-2 (37%)
	$S_5 \leftarrow S_0$ (0.778)	4.19 (3.78)	296 (328)	LUMO←HOMO-4 (55%), LUMO+1←HOMO-3 (15%)
3-5	$S_1 \leftarrow S_0$ (1.739)	2.31 (2.23)	537 (554)	LUMO←HOMO (94%)
	$S_2 \leftarrow S_0$ (0.294)	3.35 (3.20)	370 (388)	LUMO←HOMO-2 (33%), LUMO+1←HOMO-2 (20%), LUMO+2←HOMO-2 (27%), LUMO+3←HOMO-2 (10%)
	$S_4 \leftarrow S_0$ (0.260)	3.38 (3.20)	367 (388)	LUMO←HOMO-1 (28%), LUMO+1←HOMO-1 (24%), LUMO+2←HOMO-1 (26%), LUMO+3←HOMO-1 (13%)

[a] Transitions with modest to high oscillator strength f are displayed in this table. Others are shown in the Tables 7-11 – 7-15; [b] Values in parentheses are experimental absorption maxima in hexane; [c] components with greater than 10% contribution shown. Percentage contribution approximated by $2 \times (c_i)^2 \times 100\%$, where c_i is the coefficient for the particular 'orbital rotation'.

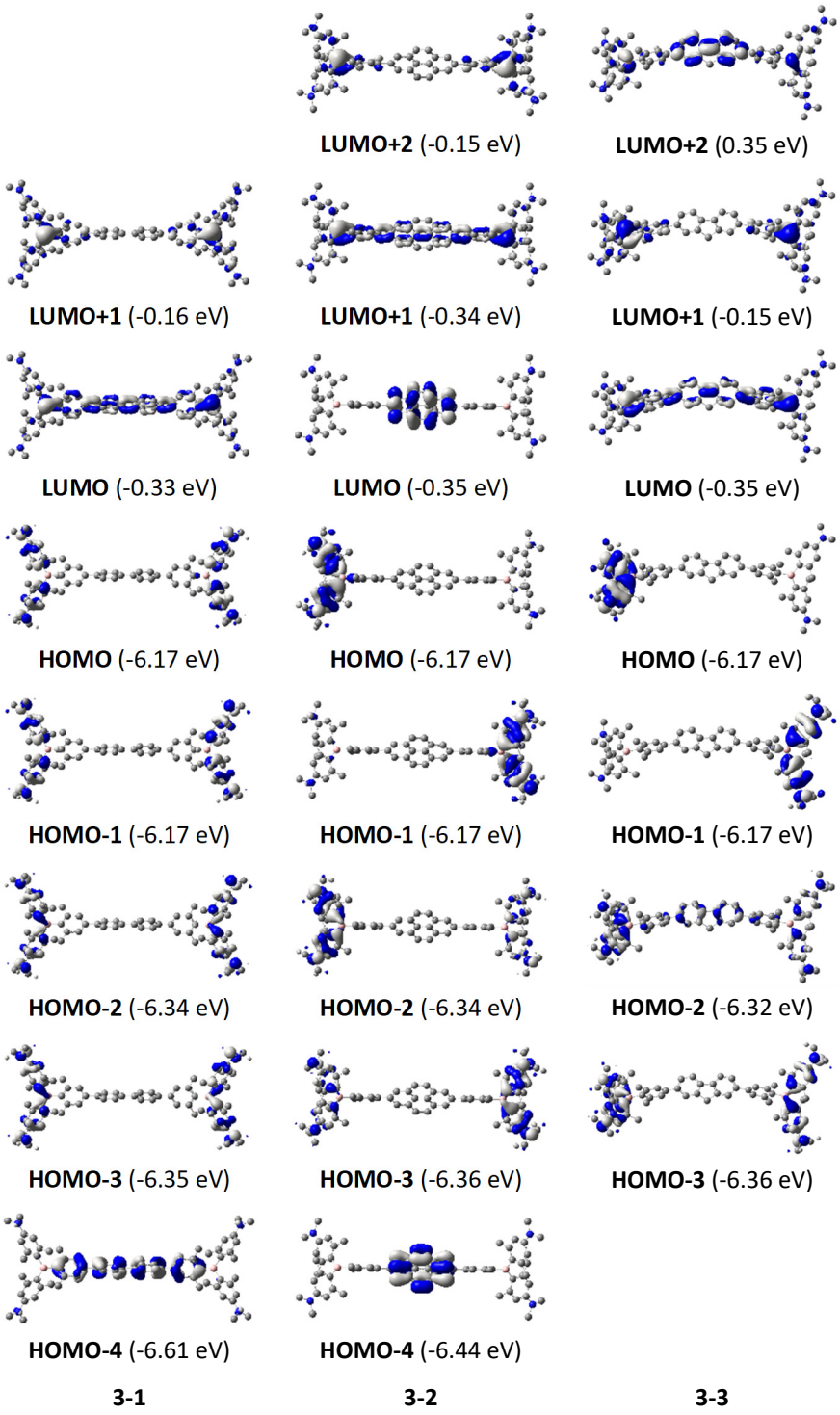

Figure 3-3. DFT (CAM-B3LYP/6-31 G(d))-calculated relevant orbitals for **3-1** – **3-3**. Hydrogen atoms are omitted for clarity. Surface isovalue: ± 0.03 $[e\ a_0^{-3}]^{1/2}$.

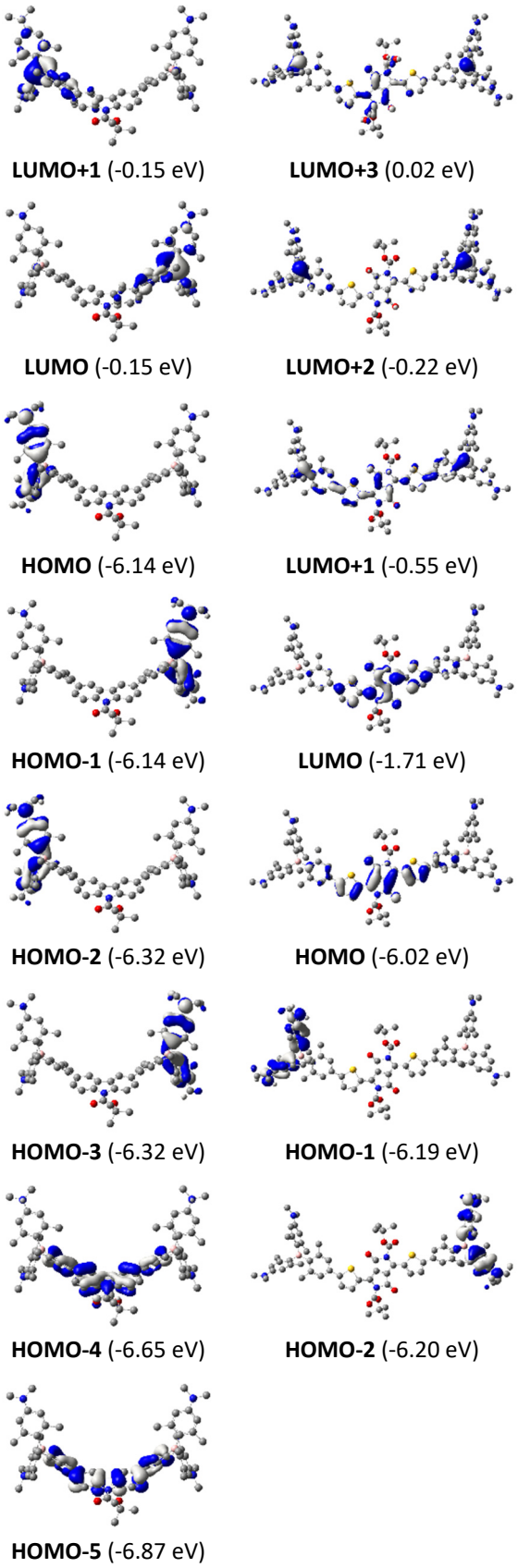

Figure 3-4. DFT (B3LYP/6-31 G(d))-calculated frontier orbitals for **2**-**4**. Hydrogen atoms are omitted for clarity. Surface isovalue: ± 0.03 $[e\ a_0^{-3}]^{1/2}$.

As the lowest energy absorption bands of **3-1** – **3-4** have charge-transfer character, their emission spectra display strong solvatochromism. Upon going from nonpolar hexane ($\lambda_{em,max}$ = 442 nm) to polar MeCN ($\lambda_{em,max}$ = 603 nm), the emission maximum of **3-1** is bathochromically shifted by 6 040 cm^{-1}, which results in an increase of the Stokes shift by 6 100 cm^{-1}, *i.e.*, from 4 300 to 10 400 cm^{-1} (Figure 1 and Table 1). This positive solvatochromism with increasing solvent polarity results from a large dipole moment in the excited-state. As the lowest absorption band results from *para*-(*N*,*N*-dimethylamino)xylyl-to-boron charge transfer for **3-1** – **3-4**, which all of those compounds have in common, the emission spectra are identical regardless of the nature of the π-bridge. The emission band of **3-4** is slightly blue-shifted, as the LUMO is a little higher in energy (~0.15 eV) than for **3-1** – **3-3**. The LUMO of compound **3-4** is more localized at the boron than the bridge, because the carbazole bridge also acts as a donor. The fluorescence quantum yields and lifetimes are essentially the same for **3-1** – **3-4** (Table 3-1). Interestingly, they do not follow the expected dependence on solvent polarity. Thus, with increasing solvent polarity, the excited state is more stabilized as shown by the bathochromic shift of the emission maximum. As ΔG^{00} decreases, following the energy gap law,[170] it is expected that the non-radiative decay rate k_{nr} should increase and therefore the quantum yield should decrease. Our compounds **3-1** – **3-4** show the opposite behavior. With increasing solvent polarity, the non-radiative decay rate decreases and the quantum yield is enhanced. Also, the experimentally determined fluorescence lifetimes increase with increasing solvent polarity, while the radiative decay rates k_r decrease with decreasing emission energy in qualitative accordance with the Strickler-Berg equation.[171] This formula predicts a proportionality of the radiative decay rate k_r with the cube of the fluorescence wavenumber $\tilde{\nu}_f^3$. Furthermore, in MeCN, compounds **3-1** – **3-4** do not follow the afore-mentioned trend. In this solvent, the quantum yields are smaller, and the fluorescence lifetimes shorter compared with CH_2Cl_2 solutions. This behavior was observed previously for nitrogen donor - boron acceptor compounds[19, 31, 172] and has its origin in symmetry breaking in the excited state. The symmetry breaking is more enhanced in polar solvents than nonpolar solvents, leading to the unusual solvent behavior seen above.[173] The dithienyl-diketopyrrolopyrrole dye **3-5** is again an exception. As the low-energy absorption is an LE transition, this compound shows no solvatochromism on the solvents examined. In all solvents it emits pink light (~630 nm), and the quantum yield is *ca*. 0.55, but drops significantly in CH_2Cl_2, as the non-radiative decay rate rises.

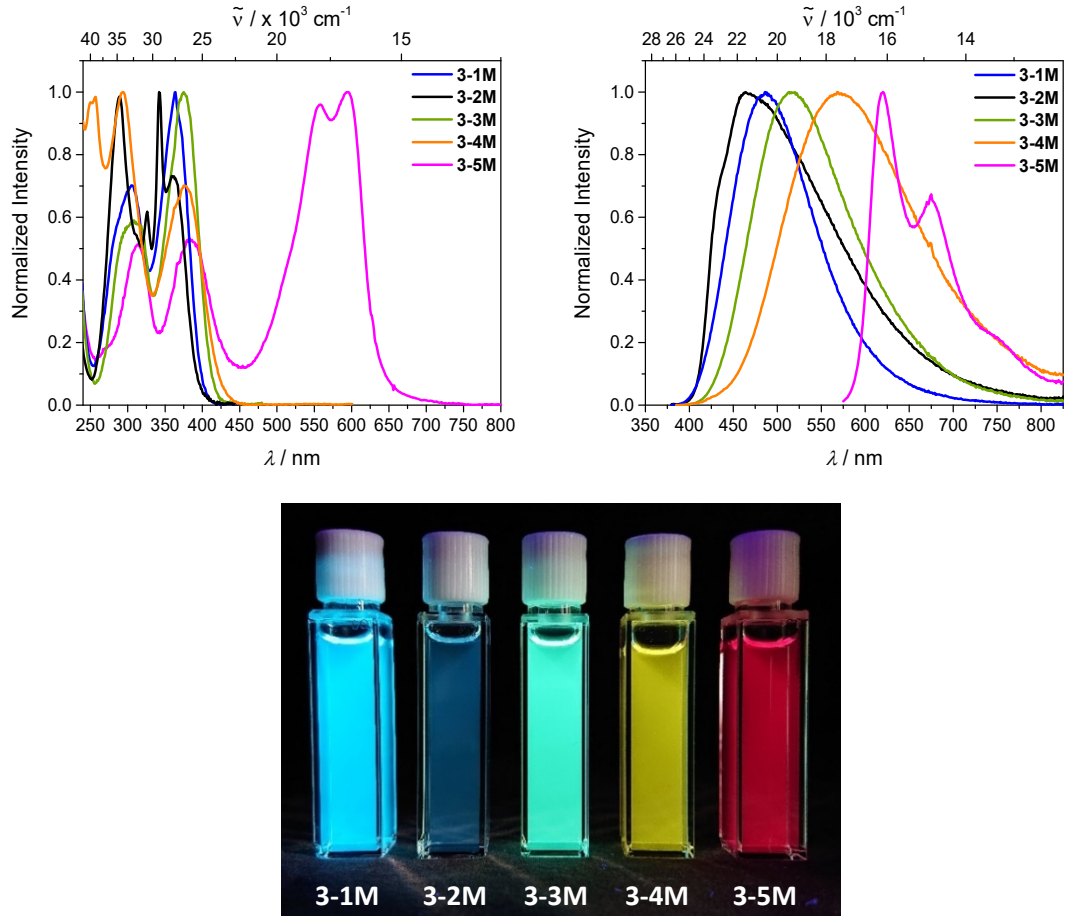

Figure 3-3. Absorption (top, left) and emission spectra (top, right) of **3-1M** – **3-5M** in water. Compound **3-2M** was dissolved in 10% MeCN in water. Picture of the solutions (bottom) of **3-1M** – **3-5M** in MeCN under UV irradiation.

Table 3-3. One- and two-photon photophysical data of compounds **3-1M** – **3-5M** in various solvents.

	solvent	λ_{abs} / nm	ε / M^{-1} cm^{-1}	λ_{em} / nm	Stokes shift / cm^{-1}	Φ_f	τ / ns	k_r / 10^8 s^{-1}	k_{nr} / 10^8 s^{-1}	$\lambda_{TPA,max}$ / nm	σ_2 / GM
	EtOH	373		470	5 500	0.71	4.9	1.4	0.6		
3-1M	MeCN	368	57 000	478	6 300	0.73	5.2	1.4	0.5	720	72
	H_2O	364		486	6 900	0.58	6.6	0.9	0.6		
	EtOH	371		465	5 400	0.20	14.3	0.1	0.6		
3-2M	MeCN	368	61 000	462	5 500	0.12	12.6	0.1	0.7	750	79
	H_2O[a]	365		467	6 000	0.12	19.5	0.1	0.4		
	EtOH	389		492	5 400	0.71	5.0	1.4	0.6		
3-3M	MeCN	383	62 000	501	6 100	0.61	5.3	1.2	0.7	730	162
	H_2O	375		513	7 200	0.33	3.7	0.9	1.8		
	EtOH	397		565	7 500	0.45	7.4	0.6	0.7		
3-4M	MeCN	385	33 000	568	8 400	0.38	7.9	0.5	0.8	760	134
	H_2O	376		568	9 000	0.03	-[b]	-	-		
	EtOH	599		624	6 700	0.40	2.2	1.8	2.7		
3-5M	MeCN	593	50 000	617	6 600	0.56	2.9	1.9	1.5	740	4 560
	H_2O	594		620	7 100	0.13	1.1	1.2	7.9		

[a] measured in 10% MeCN in water; [b] not measurable.

Upon methylation of the neutral precursors **3-1** – **3-5**, and subsequent deprotection of **3-4** and **3-5**, the charge transfer from the amine to the boron moiety is no longer present, so the linear optical properties of the chromophores **3-1M** – **3-5M** are completely different from those of **3-1** – **3-5**. Figure 3-3 shows the absorption spectra of **3-1M** – **3-5M** in water. Due to solubility issues, compound **3-2M** was dissolved in 10% MeCN in water. The various absorption bands are

attributed to the π-π* transitions of the individual π-bridges. TD-DFT calculations show that the computed low-energy absorption bands at 338, 351, 335, 346 and 544 nm, respectively, for **3-1M** – **3-5M** (experimentally: 363, 375, 361, 376 and 594 nm, respectively) are located on the π-bridge (Table 3-4 and Figures 3-4 and 3-5).

Table 3-4. TD-DFT-calculated photophysical data for **3-1M** – **3-5M** at the CAM-B3LYP/6-31G(d) level in water.

	state	symmetry	f	E / eV	λ / nm	dominant components[b]
3-1M	S_1	A	1.709	3.66	338	H-1 → L+1 (28%), H → L (53%)
	S_1	A_u	1.857	3.63	341	H-1 → L+1 (26%), H → L (56%)
	S_2	A	0.000	3.80	326	H-1 → L (38%), H → L+1 (40%)
	S_2	A_g	0.000	3.80	326	H-1 → L (37%), H → L+1 (40%)
	S_3	A	0.013	4.18	296	H-3 → L+1 (31%), H-2 → L (36%)
	S_3	A_g	0.000	4.18	297	H-3 → L (36%), H-2 → L+1 (31%)
3-2M	S_1	A	0.004	3.65	339	H-1 → L+2 (29%), H → L (33%), H → L+3 (28%)
	S_1	A_u	0.005	3.51	354	H-1 → L+2 (27%), H → L (39%), H → L+3 (25%)
	S_2	A	1.733	3.69	335	H-2 → L+1 (30%), H-1 → L (52%)
	S_2	A_u	1.801	3.58	347	H-2 → L+1 (24%), H-1 → L (61%)
	S_3	A	0.012	3.81	325	H-2 → L (38%), H-1 → L+1 (39%)
	S_3	A_g	0.000	3.75	330	H-2 → L (37%), H-1 → L+1 (43%)
3-3M	S_1	A	1.905	3.53	351	H-1 → L+1 (21%), H → L (60%)
	S_2	A	0.023	3.74	332	H-5 → L+1 (11%), H-1 → L (34%), H-1 → L+1 (44%)
	S_3	A	0.018	4.16	298	H-2 → L (32%), H-2 → L+1 (24%)
3-4M	S_1	A	1.113	3.58	346	H-5 → L (11%), H-2 → L+1 (12%), H-1 → L+1 (16%), H → L (48%)
	S_2	A	0.298	3.70	335	H-5 → L+1 (15%), H-2 → L (14%), H-1 → L (20%), H → L+1 (40%)
	S_3	A	0.013	4.19	296	H-3 → L (41%), H-3 → L+1 (23%)
3-5M	S_1	A	1.802	2.28	544	H → L (93%)
	S_1	A_u	1.596	2.33	532	H → L (94%)
	S_2	A	0.138	3.29	376	H-1 → L (22%), H → L+1 (53%), H → L+3 (10%)
	S_2	A_g	0.000	3.36	369	H-1 → L (25%), H → L+1 (45%), H → L+3 (11%)
	S_3	A	0.777	3.57	347	H-2 → L (28%), H-1 → L+1 (23%), H → L+2 (34%)
	S_3	A_u	0.917	3.59	345	H-2 → L (26%), H-1 → L+1 (24%), H → L+2 (32%)

[a] black: without symmetry constraints, red: in C_i symmetry; [b] components with greater than 10% contribution shown. Percentage contribution approximated by $2 \times (c_i)^2 \times 100\%$, where c_i is the coefficient for the particular 'orbital rotation'.

For the biphenyl (**3-1M**) and fluorene (**3-3M**) compounds, this is an $S_1 \leftarrow S_0$ transition, with LUMO+1←HOMO-1 and LUMO←HOMO contributions, where the HOMO and HOMO-1 are located at the π-bridge and the LUMO and LUMO+1 are mostly localized at the boron atoms (Table 3-4 and Figure 3-4). Pyrene derivative **3-2M** has the same behavior, but the transition is $S_2 \leftarrow S_0$ with the main contributions being LUMO+1←HOMO-2 and LUMO←HOMO-1. As the HOMO is located only at the pyrene, and has a nodal plane through the substituted 2,7-positions, it does not take part in the first allowed, low energy, transition. The LUMO+2←HOMO transition is the $S_4 \leftarrow S_0$ absorption, which is a higher energy absorption band of **3-2M** at 316 nm (experimentally: 342 nm) (Table 7-17 and Figure 3-4). In the case of the carbazole bridged derivative **3-4M**, the calculations indicate that the $S_1 \leftarrow S_0$ absorption has LUMO←HOMO-5 (11%), LUMO+1←HOMO-2 (12%), LUMO+1←HOMO-1 (16%) and LUMO←HOMO (48%) contributions. For **3-1M** – **3-4M**, the HOMOs which contribute are located at the π-bridges and LUMO and LUMO+1 are mainly localized at the boron atom. The $S_1 \leftarrow S_0$ transition of the dithienyl-diketopyrrolopyrrole dye **3-5M** is a simple LUMO←HOMO LE transition localized at the π-bridge, with a small contribution from the borons.

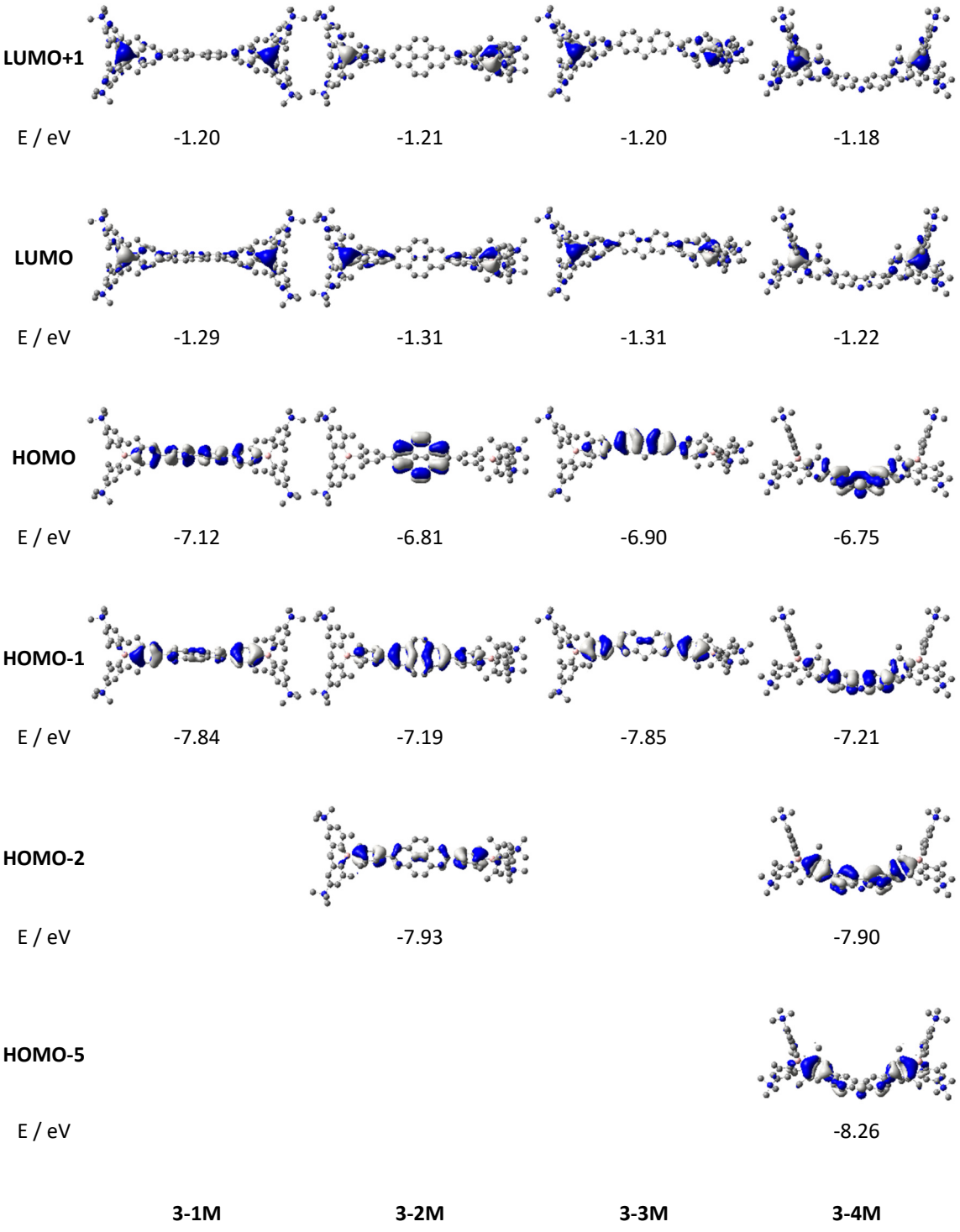

Figure 3-4. DFT (CAM-B3LYP/6-31 G(d))-calculated relevant orbitals for **3-1M** – **3-4M**. Hydrogen atoms are omitted for clarity. Surface isovalue: ± 0.03 $[e\ a_0^{-3}]^{1/2}$.

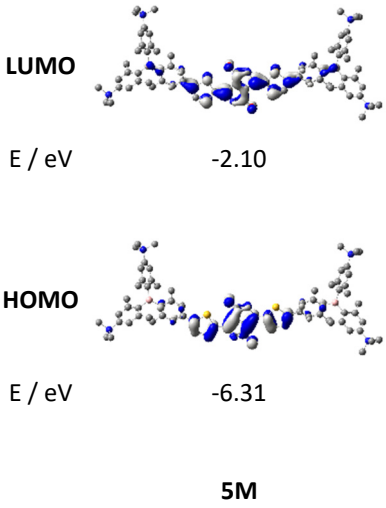

Figure 3-5. DFT (CAM-B3LYP/6-31 G(d))-calculated frontier orbitals for **3-5M**. Hydrogen atoms are omitted for clarity. Surface isovalue: ± 0.03 [e a_0^{-3}]$^{1/2}$.

Due to the strong acceptor strength of the boron moiety, which lowers the energies of the virtual orbitals, the low-energy absorption maxima are red-shifted by up to 4 334 cm^{-1} compared with those of the analogous compounds **3-1A** – **3-5A** (Scheme 3-4). Compounds **3-1A** – **3-4A** were previously reported,[57, 174] whereas compound **3-5A** was synthesized as part of the present study.

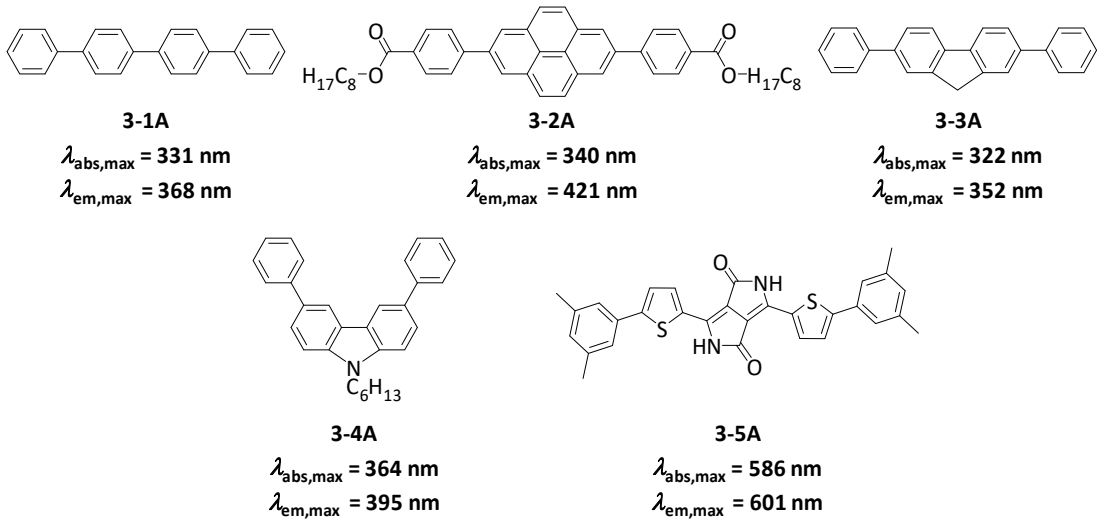

Scheme 3-4. Non-boron containing analogues; **3-1A** was measured in acetone,[174a] **3-2A** in toluene,[57] **3-3A** in ethyl acetate,[174c] **3-4A** in MeCN[174b] and **3-5A** in DMSO.

As the nature of the transitions vary somewhat for the various π-bridges, the emission color can be tuned from blue to pink (Figure 3-3). The emission maxima shift from 467 nm (**3-2M**) to 620 nm (**3-5M**) and follow the trend of the HOMO energy, as the LUMO energy stays nearly constant and is mainly boron centered (except for **3-5M**). Furthermore, for compound **3-2M** the HOMO-1 needs to be considered, as the HOMO is only localized on the pyrene and is not involved in the strongest low-energy $S_2 \leftarrow S_0$ excitation ($S_1 \leftarrow S_0$ has an oscillator strength near zero). The higher the HOMO energy, the more bathochromically shifted the emission band. Our

variety of π-bridged water-soluble, quadrupolar three-coordinate boron chromophores thus provides a wide color range spanning most of the visible spectrum. Furthermore, the compounds are not solvatochromic, as shown in Figure 3-6. This proves that the transitions do not involve significant change in dipole moment. The only observed effect is a broadening of the emission spectra in more polar solvents. Using Jortner's theory,[175] the full width at half maximum of the bell-shaped curve of a transition depends on the reciprocal value of the reorganization energy of the solvent, so the broadening of the emission bands in more polar solvents is expected. The strong π-acceptor boron moieties also shift the emission maxima compared to those of the non-boron analogues **3-1A** – **3-5A** (Scheme 3-4) between 509 and 8 916 cm^{-1} to the red, depending on the contribution of the boron atoms.

The fluorescence quantum yields and lifetimes were measured in aqueous solution (Table 3-3). As the fluorescence of the carbazole compound **3-4M** is very weak in aqueous solution, the lifetime could not be determined. For all other compounds **3-1M** – **3-3M** and **3-5M** the radiative and non-radiative decay rates were calculated and the radiative decay rates are very similar for all compounds, except for **3-2M**. This may be due to the use of 10% MeCN to improve solubility. The variation in the quantum yields is thus due to differences in the non-radiative decay rates. Apart from **3-4M**, all compounds show remarkably high fluorescence quantum yields in aqueous solution, especially compound **3-1M**. In other solvents as EtOH or MeCN, the fluorescence quantum yields increase, as the non-radiative decay rates decrease or the radiative decay rates increase for all compounds.

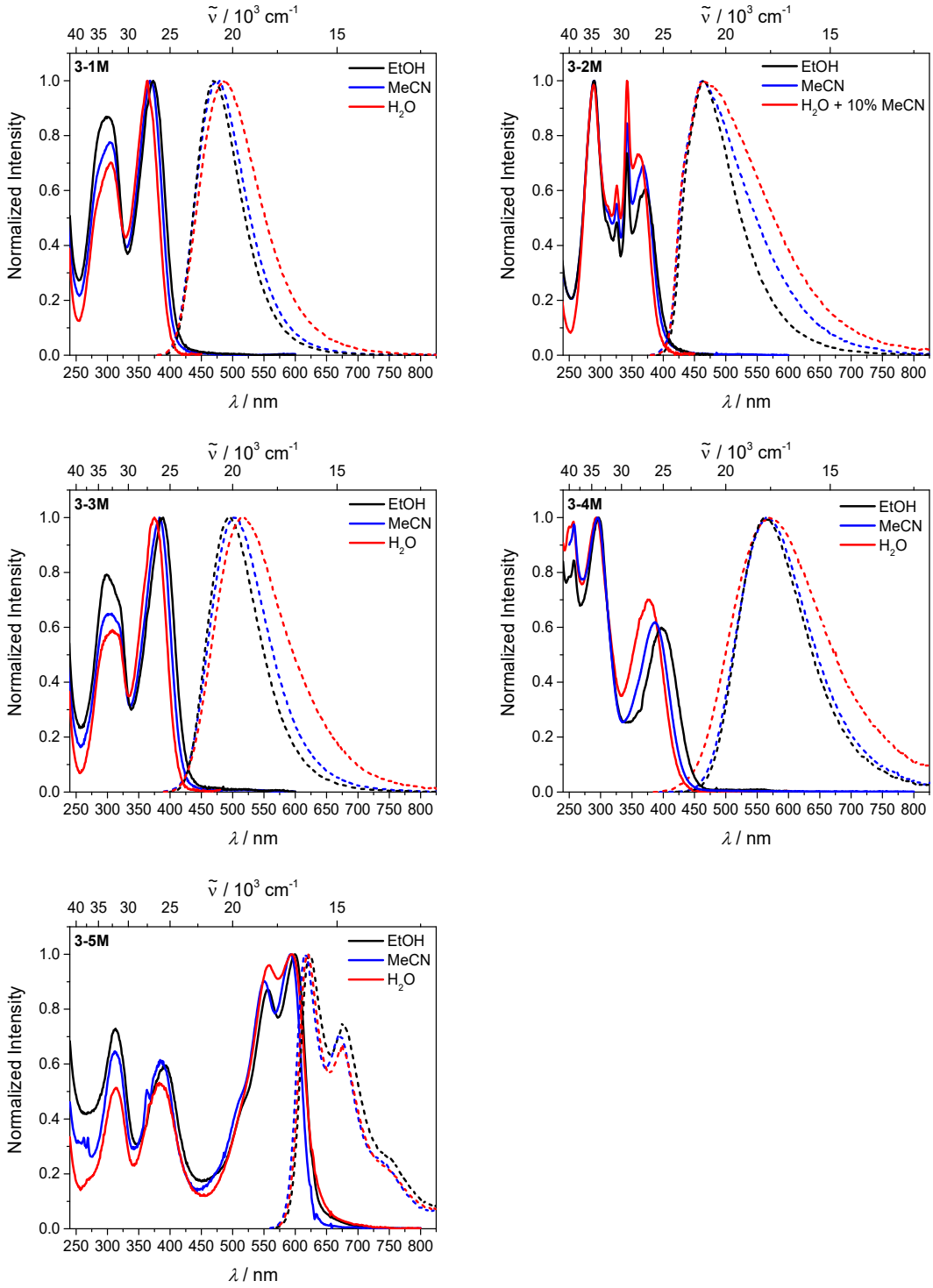

Figure 3-6. Absorption and emission spectra of **3-1M** (first row, left), **3-2M** (first row, right), **3-3M** (second row, left), **3-4M** (second row, right) and **3-5M** (third row, left) in various solvents (ethanol: black, MeCN: blue, H_2O: red).

3.2.3 Two-Photon Absorption

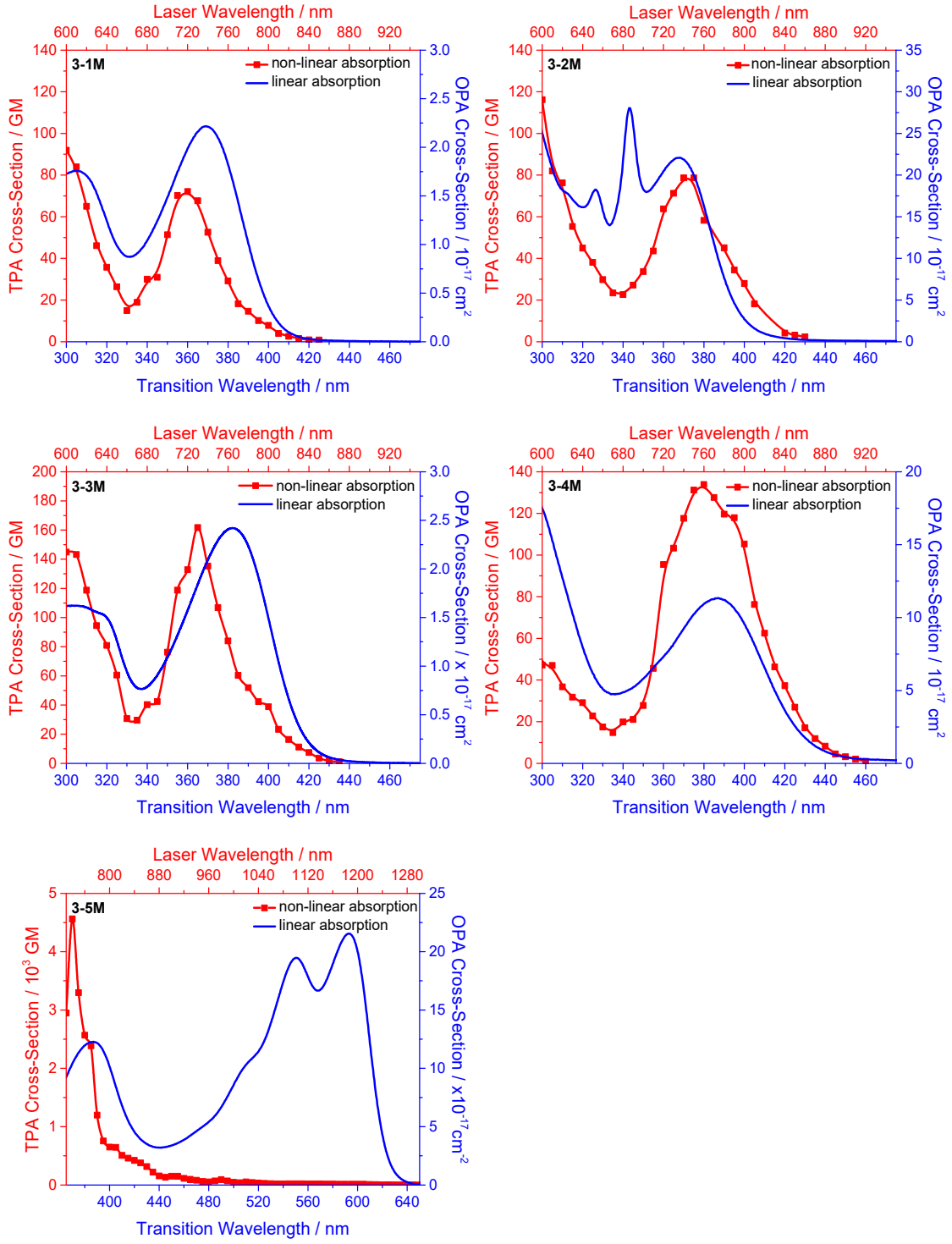

Figure 3-7. One-photon absorption (blue) and two-photon absorption spectra (red) of **3-1M** (first row, left), **3-2M** (first row, right), **3-3M** (second row, left), **3-4M** (second row, right) and **3-5M** (third row, left) in MeCN.

The two-photon absorption spectra of **3-1M** – **3-5M** were measured in MeCN, as the polarity within cells is rather like MeCN than water,[130c, 176] using the two-photon excited fluorescence technique. Following the electronic selection rules for centrosymmetric molecules (C_i symmetry), **3-1M**, **3-2M** and **3-5M**, the TPA maximum does not occur at the one-photon absorption maximum, as the $S_1 \leftarrow S_0$ transition ($A_u \leftarrow A_g$ symmetry) is symmetry forbidden for two-

photon absorption, but is located at higher energy where TPA allowed transitions of $A_g \leftarrow A_g$ symmetry occur ($S_2 \leftarrow S_0$ transition for **3-1M** and **3-5M** and $S_3 \leftarrow S_0$ transition for **3-2M**). The other two molecules **3-3M** and **3-4M** have C_{2v} as their highest possible symmetry, thus lacking an inversion center, which is why all transitions are one- and two-photon allowed. Therefore, we applied C_i symmetry for **3-1M**, **3-2M** and **3-5M** and performed TD-DFT calculations (Table 3-4, red), to obtain more insight into which transitions are one- and/or two-photon allowed. In Figure 3-7, in which the TPA and rescaled one-photon absorption (OPA) are compared, for **3-1M** we observed a TPA maximum at 720 nm, corresponding to $S_2 \leftarrow S_0$ which has A_g symmetry, and therefore is two-photon allowed but one-photon forbidden. The first excited state is, however, slightly TPA allowed as indicated by the shoulder, because of vibrational coupling of the A_u state with an a_u vibrational mode, which makes the overall wavefunction gerade.[177] From calculations on **3-2M** in C_i symmetry, we can assign the two-photon allowed transition to the $S_3 \leftarrow S_0$ transition ($A_g \leftarrow A_g$ symmetry). However, the experimental spectrum shows a TPA maximum at 750 nm, which is at the energy of the $S_1 \leftarrow S_0$ transition. This transition has a very small oscillator strength (f = 0.005) and is therefore not observable in the OPA spectrum, although the first excited state is ungerade. It might be TPA allowed because of vibrational coupling of the $1A_u$ and/or $2A_u$ state with an a_u vibrational mode, as the energy difference between S_1 and S_3 is only 1 936 cm^{-1}.[177] Compound **3-5M** shows a TPA maximum at 740 nm, which correlates with the second excited state. This state is gerade and therefore the transition should be only TPA allowed. Excitation to the ungerade first excited state is forbidden for the two photon process, and is therefore only observed in the OPA spectrum at 600 nm. Vibrational coupling in this molecule is very unlikely as the first and second excited states are 8 308 cm^{-1} apart from each other.[177] The two other molecules **3-3M** and **3-4M** have no inversion centers; therefore, all transitions are both OPA and TPA allowed. However, the transitions have different oscillator strength. For compound **3-3M** the TPA maximum at 730 nm corresponds to the S_2 state, which has a higher oscillator strength for TPA than OPA. The S_1 state has a lower oscillator strength for TPA and is indicated by the shoulder. For compound **3-4M** the TPA maximum at 760 nm corresponds to the S_2 state, but the transition to the first excited state is also highly allowed. Therefore, the two-photon cross-sections for both transitions are not very different, while the one-photon cross-sections are.

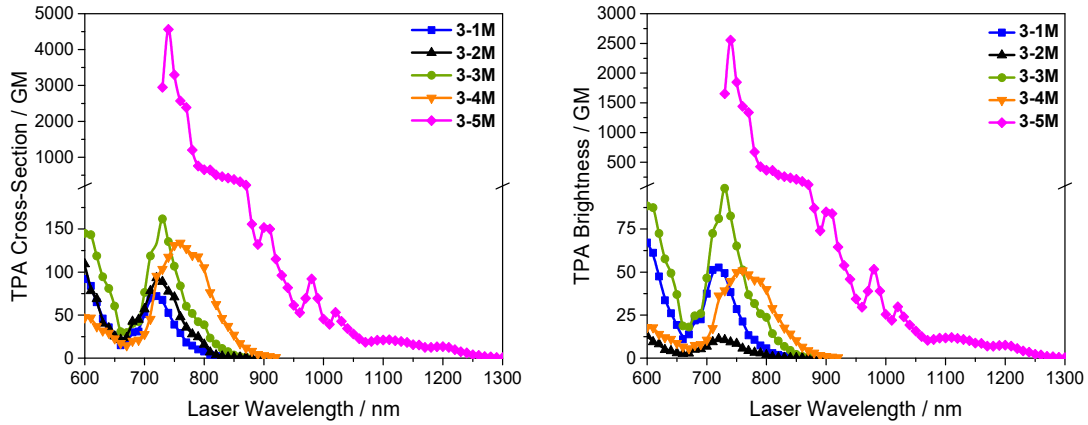

Figure 3-8. Two-photon absorption spectra (left) and two-photon brightness ($\sigma_2\Phi_f$) (right) of **3-1M** – **3-5M** in MeCN.

In the following discussion, the geometry optimized structures were used to explain the magnitudes of the TPA cross-sections. As expected, the biphenyl compound **3-1M** has the smallest TPA cross-section, being 72 GM, as this compound is the most twisted in its ground state structure (Figures 3-8 and 3-9). The twist angles between the xylylene and phenylene rings are *ca*. 37° and the angle between the two phenyl rings of the flexible biphenyl bridge is also 37° (Table 3-5). Conjugation within the π-system in **3-1M** is less efficient due to the rotational degree of freedom around the central C–C bond and, therefore, the TPA cross-section is reduced. With increasing planarity in **3-2M** – **3-4M**, in which two phenyl rings are rigidified by incorporation into the pyrene, fluorene or carbazole moieties, the two-photon cross-sections are increased to 79, 162, and 134 GM, respectively. The ground state structures show that the angles between the xylylene group and the π-bridge are again *ca*. 37° for the three compounds, while the two "phenylene" rings have no twist at all, as they are constrained. To explain the rather different results for the three compounds, the different ways, beside co-planarity, to improve the two-photon absorption cross-section must be discussed. It was shown that increasing the length or efficiency of a conjugated system leads to an enhanced two-photon absorption cross-section.[109b, 109d, 146] Therefore, compound **3-4M** should have the smallest value, as the xylylene groups are linked *via* the 3,6-positions rather than the 2,7-positions of the π-bridge, which leads to a less efficient conjugation. Furthermore, increasing intramolecular charge transfer enhances the two-photon absorption cross-section.[109b, 109d, 146] It is known that A–π–D–π–A systems are more efficient than A–π–A systems.[109b, 109d, 146] The donor-strength of the π-bridge can be correlated with the HOMO energy, which rises from pyrene (-8.47 eV (HOMO-1)) to fluorene (-7.84 eV) to carbazole (-7.21 eV). In the case of pyrene, the HOMO-1 must be considered as the HOMO has a nodal plane at the 2,7-positions. Therefore, the two-photon cross-section should be enhanced from pyrene **3-2M**, to fluorene **3-3M** to carbazole **3-4M**. The latter one **3-4M**, has, however, a shorter conjugation length than **3-3M**, and the effect of the reduced conjugation

(*vide supra*) lowers the TPA cross-section. The dithienyl-diketopyrrolopyrrole compound **3-5M** has by far the highest two-photon absorption value, being 4 560 GM. Its conjugated π-system is elongated, and the calculated ground state structure is almost planar. The angles between the xylylene and the thiophene groups are 15°, and thus much smaller than in the other compounds and the twist between the thiophenes and the diketopyrrolopyrrole is only 2 - 4°. Furthermore, the two-photon brightness shows the same trend, with the exception that compound **3-1M** has a higher value than **3-2M** and **3-4M**, due to its much higher fluorescence quantum yield (Figure 3-8). Overall, the two-photon brightness of **3-5M** is exceptionally high, being 2 545 GM in MeCN.

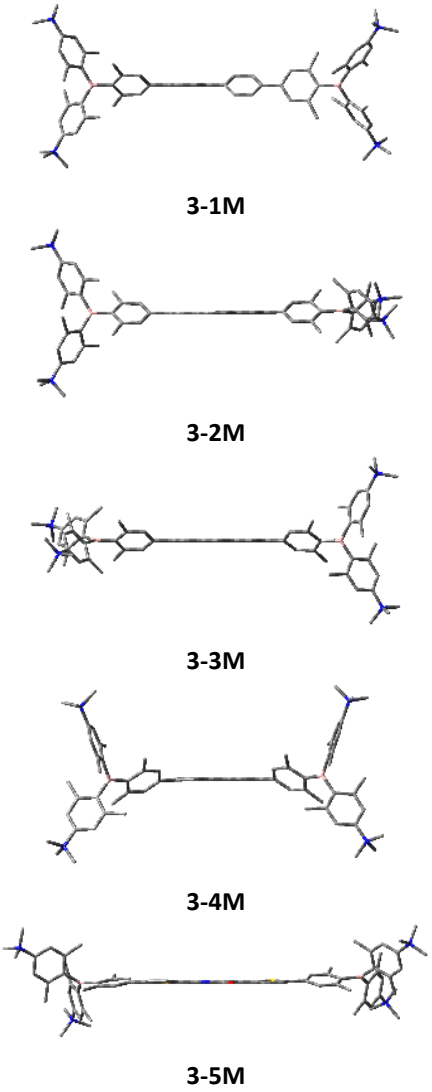

Figure 3-9. Side view of the geometries of the DFT-optimized S_0 states of **3-1M** – **3-5M** at the B3LYP/6-31G(d) level of theory. Atom color code: carbon (grey), boron (pink), sulfur (yellow), nitrogen (blue), oxygen (red). Hydrogen atoms are omitted for clarity.

Table 3-5. Selected angles (°) for **3-1M** - **3-5M** in the S_0 states. Calculations were performed by using the B3LYP density functional and the 6-31G(d) basis set.

angles	3-1M	3-2M	3-3M	3-4M	3-5M
∠ B1C$_3$-xylyl (terminal)	54.005	53.653	53.693	54.050	53.626
	54.358	53.264	53.700	54.602	53.754
∠ B1C$_3$-xylyl (central)	44.328	44.441	44.399	43.330	44.023
∠ xylyl (central)-aryl1	36.558	36.084	35.580	38.267	14.634
∠ aryl1-aryl2	37.464	0.286	0.863	2.240	3.545
∠ aryl2-aryl3					1.993
∠ aryl2/3-xylyl (central)	36.557	37.100	33.891	40.320	16.020
∠ xylyl (central)-B2C$_3$	44.338	43.858	44.598	44.783	44.020
∠ xylyl (terminal)- B2C$_3$-	54.357	54.053	53.347	54.203	54.191
	53.993	54.054	53.822	54.159	53.139

Furthermore, the two-photon absorption of **3-5M** was compared with its non-boron analogue **3-5A**. While the linear optical properties (absorption and emission) of **3-5M** were only slightly red-shifted compared to those of **3-5A**, the TPA data are quite different. The two-photon absorption cross-section of **3-5M** is *ca*. 8.7 times higher than that of its analogue **3-5A** in DMSO solution (Figure 3-10). These data show that our boron-based acceptor moiety strongly enhances the TPA properties.

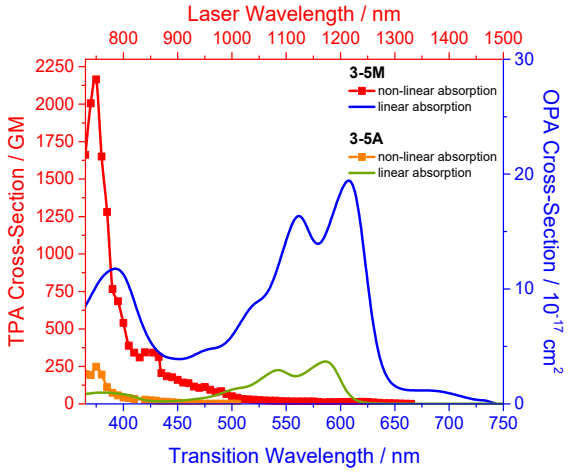

Figure 3-10. Two-photon absorption spectra of **3-5M** (red) and **3-5A** (orange) and one-photon absorption spectra of **3-5M** (blue) and **3-5A** (green) in DMSO.

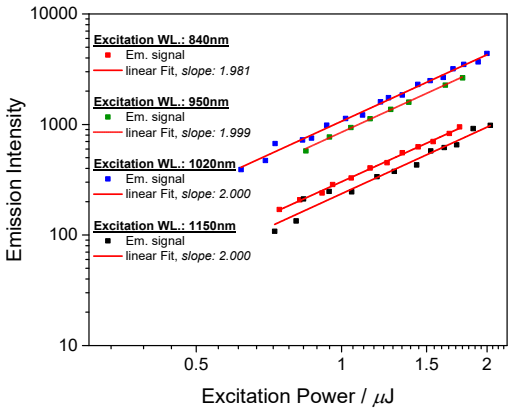

Figure 3-11. Power dependence of the emission intensity of **3-5M** in MeCN at selected excitation wavelengths.

3.2.4 Imaging

As none of the neutral compounds **3-1** – **3-5** are soluble in Dulbecco's Modified Eagle Medium (DMEM), they formed nanoparticles (Table 3-6) in that medium and were not taken up by HeLa or HepG2 cells (Figure 3-12). In addition, pre-mixing of chromophores **3-1** – **3-5** with Pluronic F-127 was not successful. The compounds did dissolve in that medium, yet no cellular uptake was observable (Figure 3-13).

Table 3-6. Measured particle sizes of the neutral compounds in PBS containing 0.5% DMSO with DLS.

compound	particle size [nm]	error [± nm]
3-1	413.6	50.79
3-2	441.0	54.45
3-3	425.1	54.09

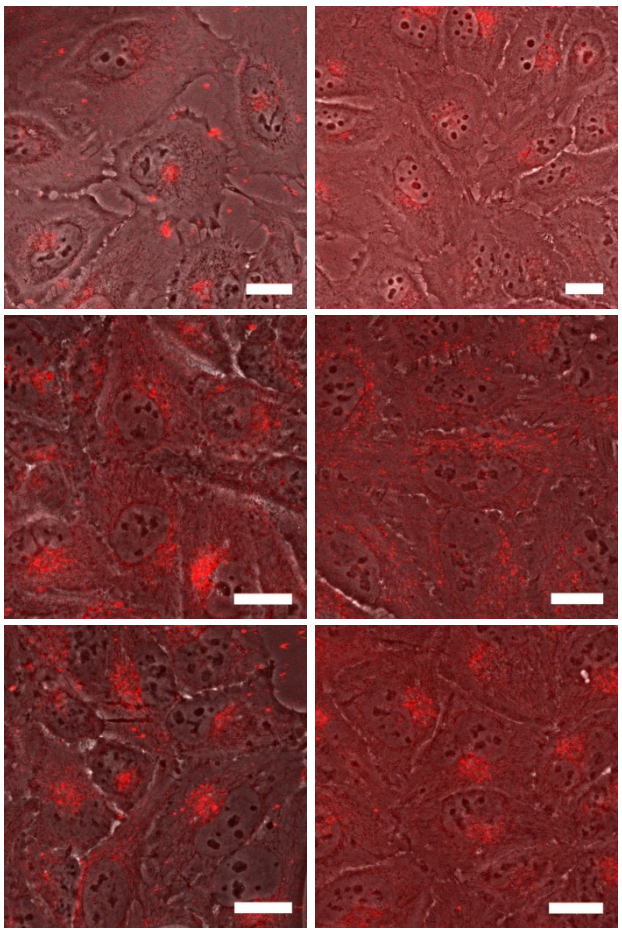

Figure 3-12. Confocal microscope image of HeLa cells after 1 h of incubation at 37 °C with **3-1** (5 μM) (first row), **3-2** (5 μM) (second row) and **3-3** (5 μM) (third row). Merged bright field image with fluorescence image (λ_{ex} = 405 nm; λ_{em} = 570 – 670 nm) before washing (left) shows the formation of nanoparticles, while after washing (right) a nominal uptake of the dye by the cell can be observed. Scale bars: 20 μm.

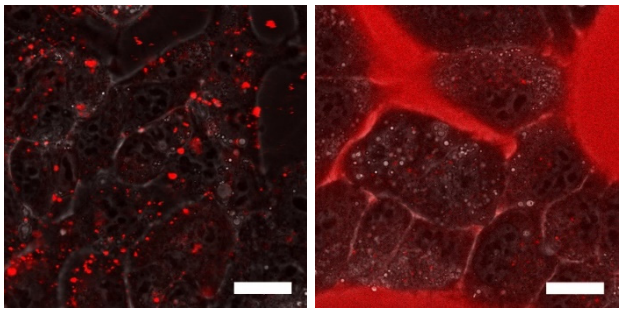

Figure 3-13. HepG2 cells challenged with fatty acids for 24 h and stained with **3-1** (5 μM) 24 h at 37 °C. Merged bright field image with fluorescence image (λ_{ex} = 405 nm; λ_{em} = 570 – 670 nm) without Pluronic F-127 (left) shows the formation of nanoparticles, while with the addition of 0.04% Pluronic F-127 (right) it shows the solution of the dye, but also no cellular uptake. Scale bars: 20 μm.

Thus, the methylated species **3-1M** – **3-5M**, designed to be water-soluble, were used for cell imaging. HeLa cells were treated with 500 nM concentrations of all five compounds. Visualization with a confocal laser scanning fluorescence microscope showed cellular uptake for **3-1M** – **3-5M** (Figure 3-14 – 3-18). Co-staining experiments with commercially available LysoTrackers™ confirmed their localization in acidic intracellular compartments such as endosomes and lysosomes. The Pearson values (R_r), indicative of the degree of co-localization, were all higher than 0.73, while for **3-4M** and **3-5M** values of 0.83 and 0.81, respectively, were reached.

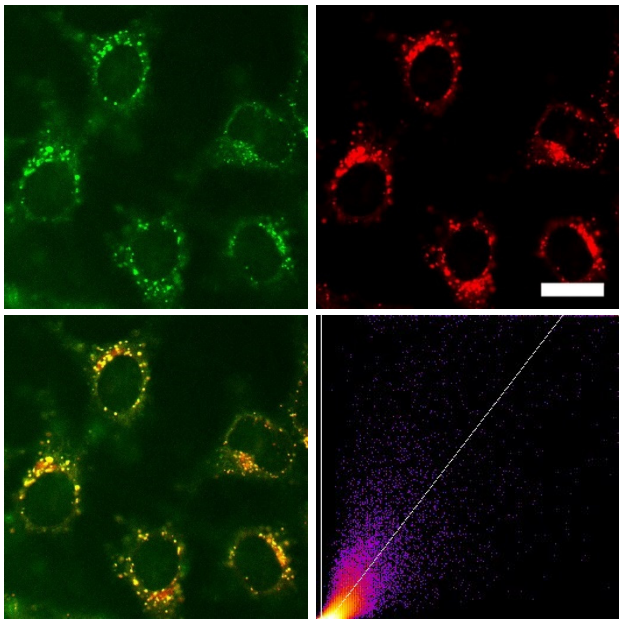

Figure 3-14. Co-staining experiment of HeLa cells with **3-1M** and LysoTracker™ Red. The cells were loaded with **3-1M** (0.5 μM, 2 h) and LysoTracker™ Red (0.1 μM, 20 min) under 5% CO_2 at 37 °C. Fluorescence images of **3-1M** (top, left: λ_{ex} = 405 nm; λ_{em} = 450 – 550 nm) and LysoTracker™ Red (top, right: λ_{ex} = 561 nm; λ_{em} = 600 – 750 nm). The merged fluorescence images (bottom, left) and the correlation plot of the intensities (bottom, right: R_r = 0.80), show co-localization of the dye **3-1M** in the lysosomes. Scale bar: 20 μm.

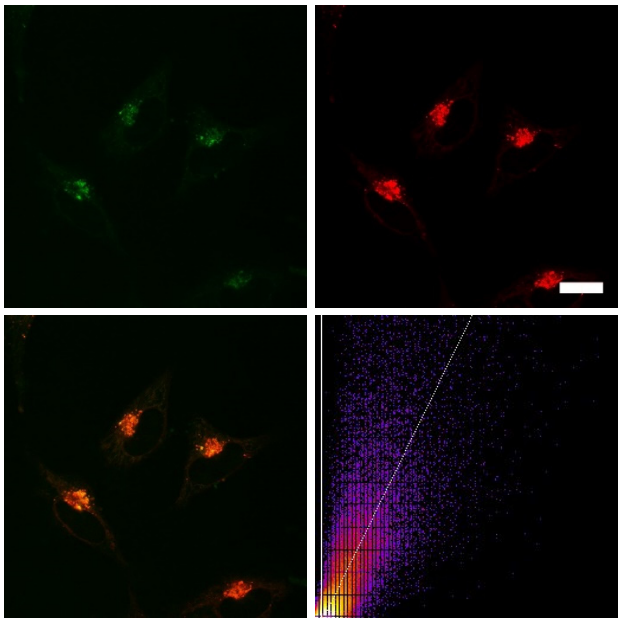

Figure 3-15. Co-staining experiment of HeLa cells with **3-2M** and LysoTracker™ Red. The cells were loaded with **3-2M** (0.5 μM, 2 h) and LysoTracker™ Red (0.1 μM, 20 min) under 5% CO_2 at 37 °C. Fluorescence images of **3-2M** (top, left: λ_{ex} = 405 nm; λ_{em} = 450 – 550 nm) and LysoTracker™ Red (top, right: λ_{ex} = 561 nm; λ_{em} = 600 – 750 nm). The merged fluorescence images (bottom, left) and the correlation plot of the intensities (bottom, right: R_r = 0.73), show co-localization of the dye **3-2M** in the lysosomes. Scale bar: 20 μm.

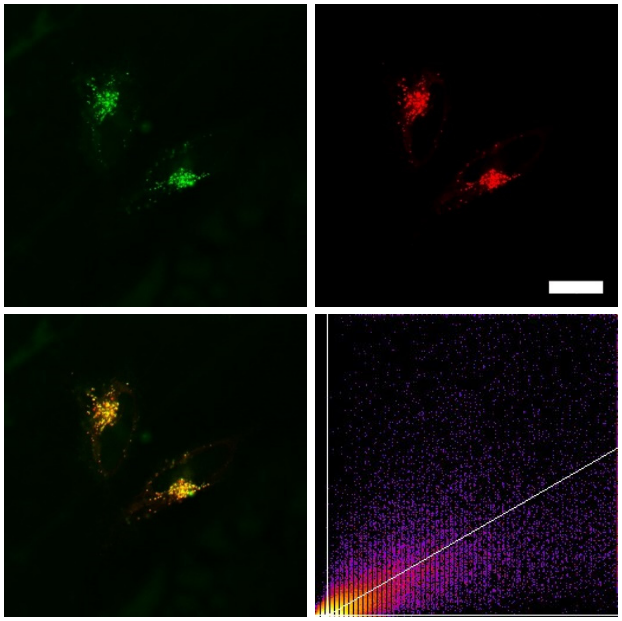

Figure 3-16. Co-staining experiment of HeLa cells with **3-3M** and LysoTracker™ Red. The cells were loaded with **3-3M** (0.5 μM, 2 h) and LysoTracker™ Red (0.1 μM, 20 min) under 5% CO_2 at 37 °C. Fluorescence images of **3-3M** (top, left: λ_{ex} = 405 nm; λ_{em} = 450 – 550 nm) and LysoTracker™ Red (top, right: λ_{ex} = 561 nm; λ_{em} = 600 – 750 nm). The merged fluorescence images (bottom, left) and the correlation plot of the intensities (bottom, right: R_r = 0.75), show co-localization of the dye **3-3M** in the lysosomes. Scale bar: 20 μm.

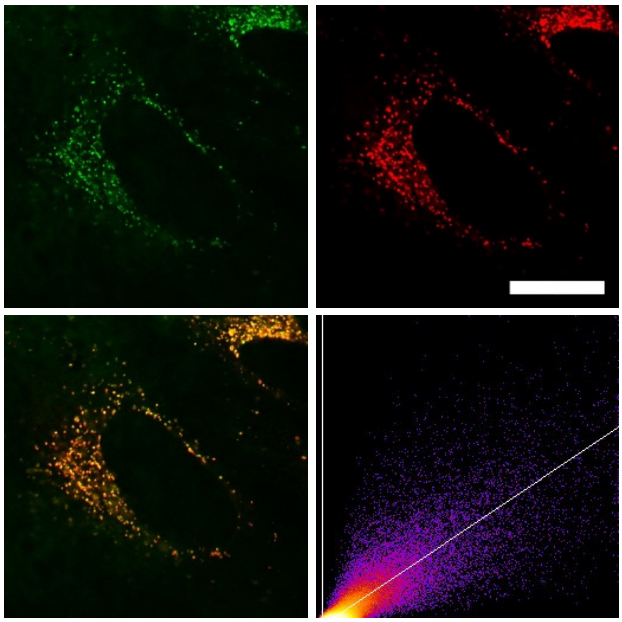

Figure 3-17. Co-staining experiment of HeLa cells with **3-4M** and LysoTracker™ Red. The cells were loaded with **3-4M** (0.5 μM, 2 h) and LysoTracker™ Red (0.1 μM, 20 min) under 5% CO_2 at 37 °C. Fluorescence images of **3-4M** (top, left: λ_{ex} = 405 nm; λ_{em} = 500 – 605 nm) and LysoTracker™ Red (top, right: λ_{ex} = 561 nm; λ_{em} = 607 – 786 nm). The merged fluorescence images (bottom, left) and the correlation plot of the intensities (bottom, right: R_r = 0.83), show co-localization of the dye **3-4M** in the lysosomes. Scale bar: 20 μm.

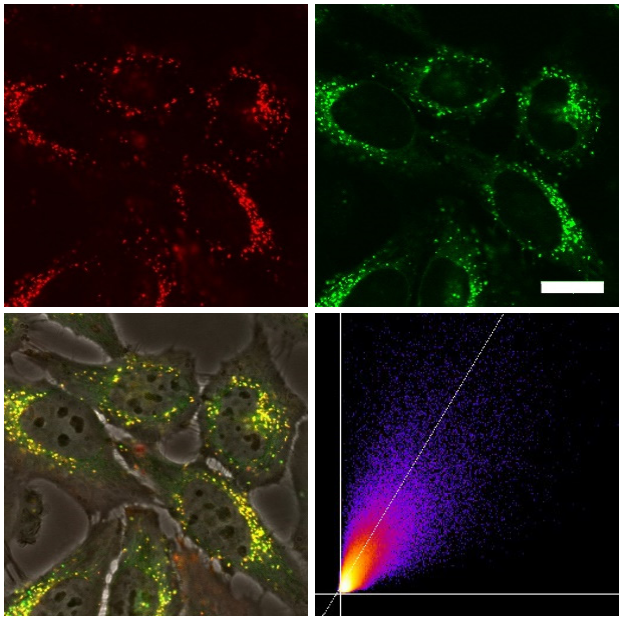

Figure 3-18. Co-staining experiment of HeLa cells with **3-5M** and LysoTracker™ Green. The cells were loaded with **3-5M** (500 nM, 2 h) and LysoTracker™ Green (100 nM, 20 min) under 5% CO_2 at 37 °C. Fluorescence images of **3-5M** (top, left: λ_{ex} = 559 nm; λ_{em} = 570 – 670 nm) and LysoTracker™ Green (top, right: λ_{ex} = 473 nm; λ_{em} = 490 – 540 nm). The merged image of the bright field image and both fluorescence images (bottom, left), and the correlation plot of the intensities (bottom, right: R_r = 0.81), show co-localization of the dye **3-5M** in the lysosomes. Scale bar: 20 μm.

Furthermore, cell viability experiments were performed to investigate the potential of chromophores **3-1M** – **3-5M** for live-cell imaging. HeLa cells were treated with serial dilutions of **3-1M** – **3-5M** and the cell metabolic activity was studied using a colorimetric (MTT) assay (Figure 3-19). These confirmed that compounds **3-1M** – **3-5M** did not influence the cell viability at concentrations as high as 5 μM after 24 h incubation time, and some of them were non-toxic to

cells even at higher concentrations (10 μM). As the dithienyl-diketopyrrolopyrrole dye **3-5M** has the most red-shifted absorption and emission bands and, by far, the highest TPA cross-section and brightness, further imaging experiments were done for this one.

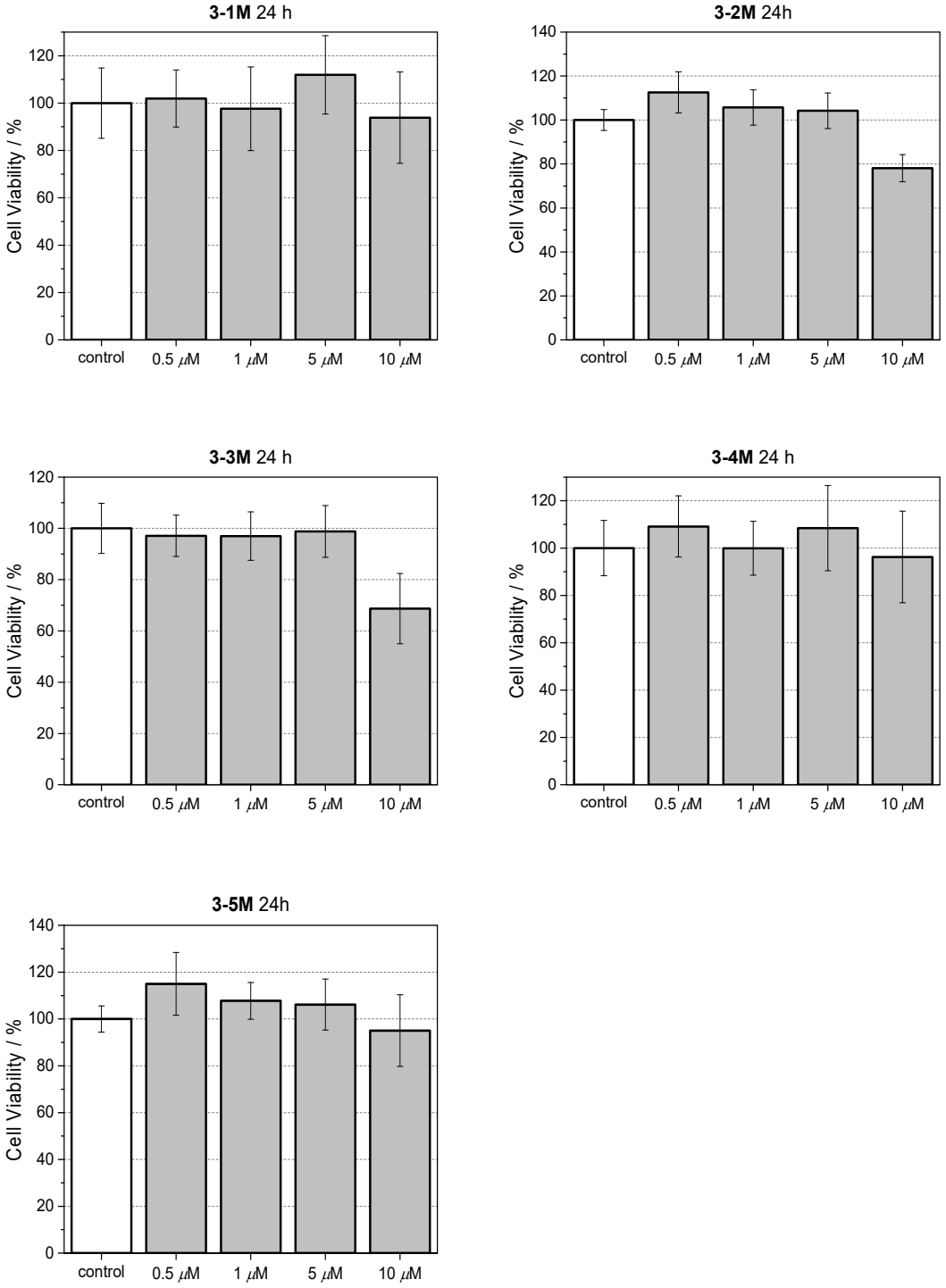

Figure 3-19. Cell viability of **3-1M** – **3-5M** loaded HeLa cells determined by MTT assay. The cells were incubated with **3-1M** – **3-5M** (0, 0.5, 1, 5, 10 μM) in DMEM containing 0.5% DMSO in a CO_2 incubator for 24 h. The results are expressed as percentages of the dye-free controls. All data are presented as mean standard deviation (*n* = 10).

The process by which cell internalization of our dye **3-5M** takes place was observed *via* time-lapse confocal microscopy for 2 h (Figure 3-20). The cultured medium of HeLa cells was replaced

with the dye-containing DMEM and images were recorded every 10 min without any washing process. The dye first attaches to the cell membrane and, after 50 min, small bright spots in the intracellular region are observed. With further incubation time, additional chromophore enters the cell and the signal-to-noise ratio improves as the residual dye in the medium is consumed. Furthermore, HeLa cells were stained at 4 °C or at 37 °C with the presence of 0.1% NaN_3 (Figure 3-21); both sets of conditions inhibit endocytosis. Both experiments showed much lower fluorescence intensity in comparison with the control experiment, therefore, suggesting endocytosis as the mechanism by which **3-5M** enters cells.

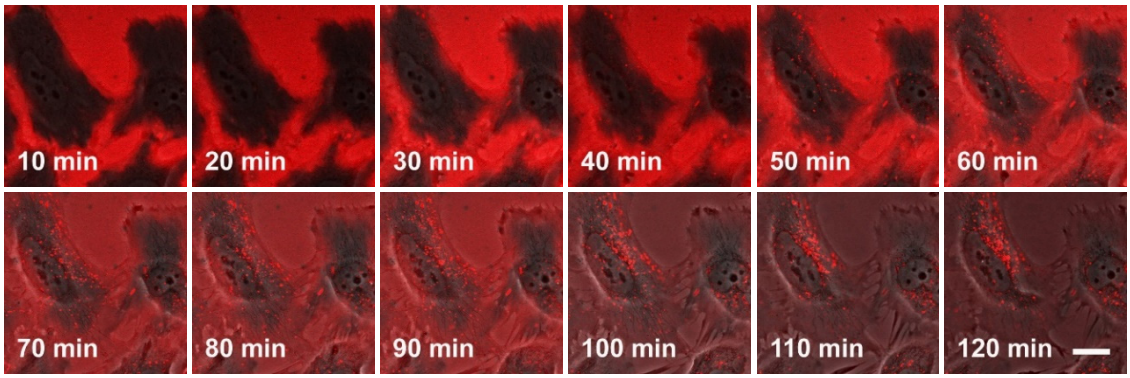

Figure 3-20. Confocal microscope images of HeLa cells at 37 °C with **3-5M** (500 nM). Merged bright field image with fluorescence image (λ_{ex} = 559 nm; λ_{em} = 570 – 670 nm) between 10 min and 120 min after staining. Scale bar: 20 μm.

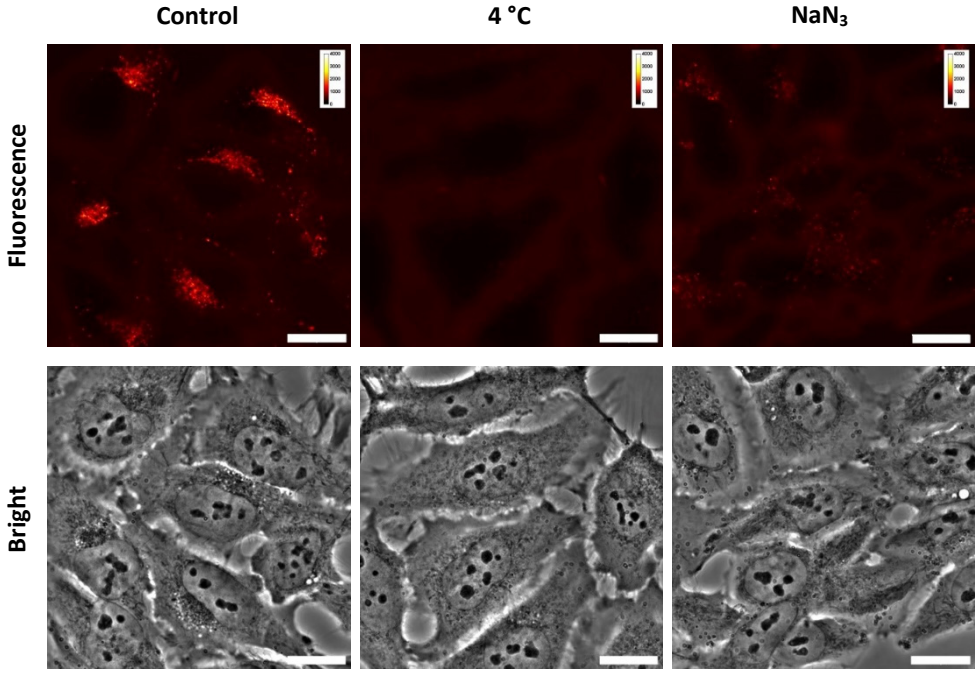

Figure 3-21. Cell staining with 500 nM of **3-5M** in DMEM for 2 h at 37 °C (left), for 2 h at 4°C (middle) and for 2 h at 37 °C with 0.1% NaN_3 (right). Fluorescence images of **3-5M** (top, λ_{ex} = 559 nm; λ_{em} = 570 – 670 nm) and bright field images (bottom) suggest an endocytosis pathway. Scale bars: 20 μm.

The photostability of our dye **3-5M** was tested by repetitive imaging of HeLa cells after staining. Over 95% of the initial fluorescence intensity of **3-5M** was retained after irradiation with an excitation laser at 561 nm for 50 images. When using the commercially available LysoTracker™

Red under the same imaging conditions, the emission intensity decreased by 45% (Figure 3-22). This result revealed the outstanding photostability of **3-5M**, which is highly desired for time-lapse imaging of live cells.

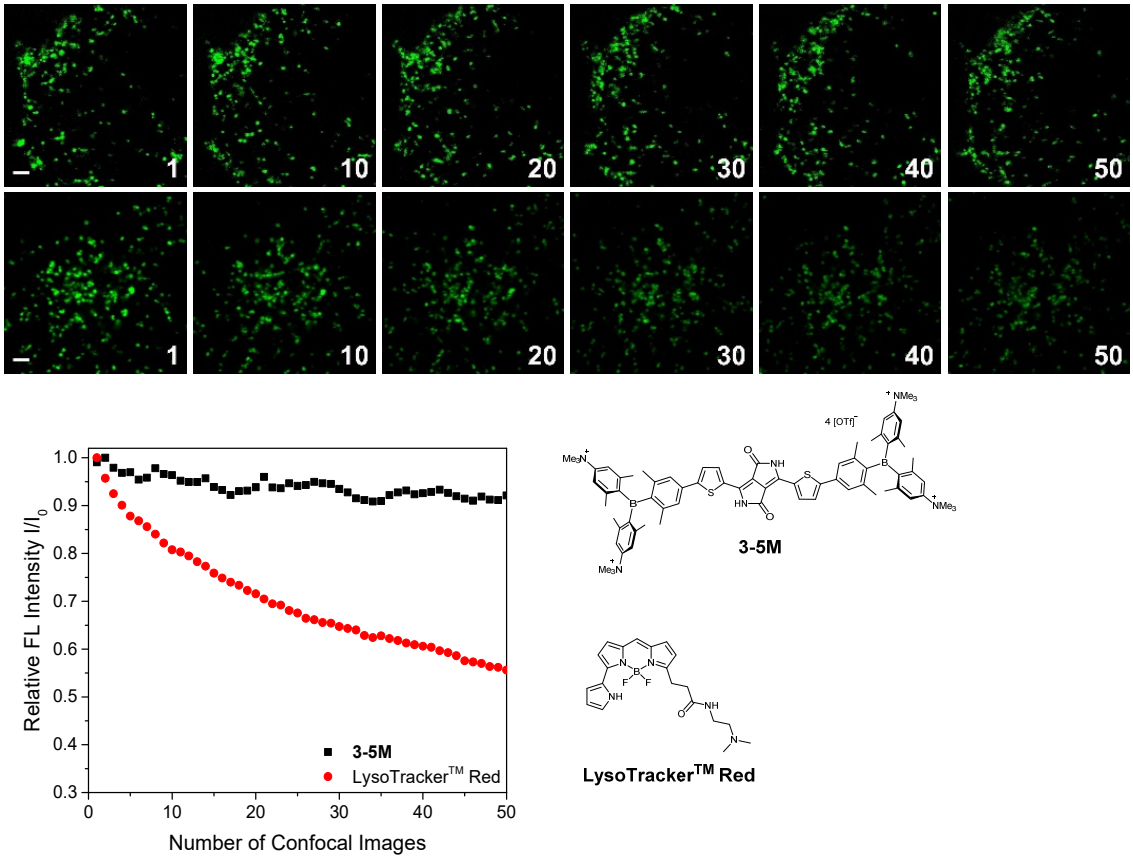

Figure 3-22. Comparison of the repeated fluorescence images of HeLa cells stained with **3-5M** (first row) and LysoTracker™ Red (second row) under irradiation with a confocal laser at 561 nm (WLL, output power 70%, AOTF 2%). Each number indicates the number of recorded confocal images. Scale bar: 2 μm. Plots of integrated fluorescence intensities (I) relative to the initial value (I_0) as a function of the number of recorded images (third row).

As chromophore **3-5M** has an outstanding two-photon brightness of 2 545 GM (at 740 nm) and showed good imaging and cell viability properties, **3-5M** was also tested as a two-photon excited fluorescence dye to stain HeLa cells. The two-photon imaging experiments were performed at 500 nM concentration. As clearly shown in Figure 3-23, dye **3-5M** again stained the cell also at the lysosomes and is a very effective two-photon imaging agent.

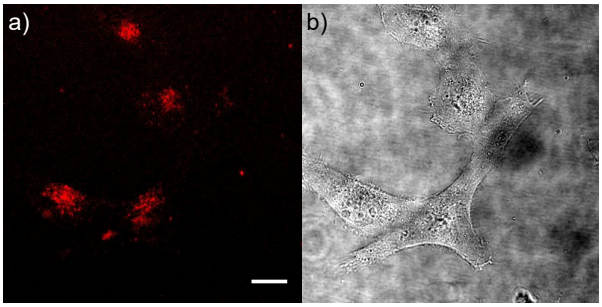

Figure 3-23. (a) Two-photon excited fluorescence and (b) bright-field images of HeLa cells stained with **3-5M** (500 nM). The TPEF image was recorded under excitation at 720 nm (AOTF 38%) using an HyD detector with a bandpass filter 650/50 and an HC Fluotar L 25 × 0.95 W VISIR objective. Scale bar: 20 μm.

3.3 Conclusions

We have synthesized a series of quadrupolar A–π–A chromophores with five different π-bridges, namely biphenyl, pyrene, fluorene, carbazole and dithienyl-diketopyrrolopyrrole all containing triarylborane π-acceptor groups functionalized to enhance water solubility. While the neutral precursor molecules **3-1** – **3-5** are not water-soluble and are not taken up by the cells, they show interesting photophysical properties. Except for compound **3-5**, the neutral dyes are highly solvatochromic as the excited state results from charge transfer from the nitrogens to the boron atoms. As the *para*-(*N*,*N*-dimethylamino)xylyl group is present in all of the neutral chromophores, the photophysical properties of those compounds are very similar. After methylation of the four nitrogen atoms, this charge transfer is no longer possible and, therefore, the tetracationic compounds **3-1M** – **3-5M** display completely different optical properties. The emission of the different cationic compounds covers nearly the entire visible spectrum depending on the selected π-bridge. The color can be tuned from blue to pink over a range of 5 300 cm^{-1}, while the emission spectra of the compounds themselves are not solvatochromic. The TPA cross-sections correlate with the planarity of the π-bridge, thus, the more planar the π-bridge, the higher the two-photon absorption cross-section. The two-photon absorption cross-section also correlates well with the donor ability of the π-bridge and the length of the conjugated π-system. The dithienyl-diketopyrrolopyrrole dye **3-5M** has the highest two-photon cross-section of 4 560 GM in MeCN and due to its high fluorescence quantum yield, also exhibits a remarkable two-photon brightness of 2 545 GM.

We carried out live-cell imaging with all five cationic compounds **3-1M** – **3-5M**. All of our cationic dyes were taken up by the HeLa cells and localize at the lysosomes. Furthermore, they do not show any effect on cell viability up to concentrations of 5 μM, which is much higher than the concentration needed for imaging purposes (500 nM). Further experiments were performed with compound **3-5M**, which shows the most red-shifted absorption and emission, the highest TPA cross-section, no cell toxicity up to 20 times the staining concentration, and a very good co-

localization pattern (R_r = 0.83) with the lysosomes. We showed that this dye is taken up by the endocytosis pathway of the HeLa cells, that compound **3-5M** is far more photostable than the commercially available LysoTracker™ Red, and that it is an excellent dye for TPEF imaging. In summary, we have designed and synthesized a series of fluorescent three-coordinate boron-containing quadrupolar dyes for one- and two-photon excited fluorescence imaging of lysosomes. Incorporation of our boron acceptor groups greatly enhances the TPA cross-sections and, *via* tuning of the π-bridge, we obtained two-photon absorption cross-sections up to 4 560 GM and a two-photon brightness up to 2 545 GM in MeCN, which are by far the highest values reported for a lysosomal imaging dye.

Chapter Four

-

Dipole *vs*. Octupole

4 DIPOLE *VS*. OCTUPOLE

Preliminary aspects of some of these results were included in my Master's Thesis entitled "Synthesis of potential water-soluble triarylboranes and studies of their optical properties", prepared at the Institute of Inorganic Chemistry, Julius-Maximilians-Universität Würzburg in 2014. The synthetic procedures reported in the above-mentioned thesis, were mentioned here for the sake of completeness. Additional analytical data and more detailed photophysical studies are reported in the current work.

4.1 Introduction

Triarylboranes have aroused much interest in materials applications in the last few decades.[9, 13b, 17, 18b, 18e, 120a, 138] Due to the empty p_z-orbital of the three-coordinate boron atom, they are used as strong π-acceptors (A), when conjugated to a π-donor (D). In 1971, Williams and co-workers at Kodak explored the photophysical properties of several *para*-substituted aryldimesitylboranes.[12] While the absorption maxima were only slightly affected by solvent polarity, the fluorescence maxima showed a large bathochromic shift with increasing solvent polarity. This suggests a small dipole moment in the ground state and a large increase in the dipole moment in the first excited singlet state, which can be better stabilized in polar solvents. Thus, triarylboranes are excellent π-acceptors in intramolecular charge transfer compounds, *e.g.* in dipolar chromophores, as they show highly solvatochromic emission.[31, 33, 144a, 144b] Furthermore, excitation-induced charge transfer properties increase the two-photon absorption (TPA) probability.[145] Therefore, three-coordinate boron compounds have great potential for TPA[111a-d, 111f, 111h, 124, 178] and other non-linear optical (NLO) applications.[14a-c, 14e, 15-16, 179]

Degenerate two-photon absorption is a third-order non-linear optical process, which involves the simultaneous absorption of two photons.[109b, 109d, 146b, 146c] As the final state is reached by two photon absorption *via* a virtual state, the energy of the photons is half of the actual energy gap between the ground and excited states. This is highly desirable for fluorescence microscopy of live cells and tissues, because of the deeper tissue penetration of these longer wavelength photons. There are three characteristic structural motifs known for efficient organic TPA dyes, namely dipole (D–A), quadrupole (D–π–D, A–π–A) or octupole (D–A_3, A–D_3). Attention has progressively moved from well-known push-pull systems to quadrupoles and octupoles, as they exhibit larger TPA cross-sections (σ_2). Quadrupolar dyes are the most studied for two-photon excited fluorescence, and we have also studied them for live-cell imaging.[119] In this chapter, the differences between dipolar and octupolar borane dyes are investigated.[111f] Properly speaking, the latter are three dipoles connected by a trigonal core which can display cooperative

(> 3 × σ_2(dipole)), additive (3 × σ_2(dipole)) or suppressive (< 3 × σ_2(dipole)) effects of the branching.[109d] Prasad first demonstrated the cooperative effect with a triphenylamine donor core, branched with three 2-phenyl-5-(4-*tert*-butylphenyl)-1,3,4-oxadiazole acceptors.[180] Further studies of octupolar systems showed that the effect of branching depends on the nature and strength of the coupling between the three arms and also the nature of the core.[181] While triphenylbenzene **4-A**,[182] triphenylphosphine oxide **4-B** and triphenylphosphine sulfide **4-C**[183] as a core exhibit only an additive effect, tricyanobenzene **4-D**,[184] pyridinium **4-E**,[185] *s*-triazine **4-F**,[186] truxene **4-G**[110c] and triphenylamine **4-H**[111g, 180, 187] showed highly cooperative behavior (Scheme 4-1). To understand the influence of the coupling, several models were investigated.[187e, 188] The Frenkel exciton model, in which only electrostatic interactions of the dipole units are considered, led to qualitatively good results and a correct order of the excited states for octupolar compounds but, as the donor or acceptor in the core is shared by the three arms, this model does not provide quantitative estimations of non-linear properties. As soon as the coupling becomes stronger and the charge more delocalized over the three branches, electron-vibration interactions and/or solvent effects must be taken into account. Therefore, essential-state models or correlated quantum chemical approaches are more accurate. Fang and co-workers compared octupolar dyes with a triphenylamine core, a conjugated central moiety, and a triethanolamine core, which is non-conjugated.[189] As the non-conjugated moiety is not able to couple electronically, and no cooperative enhancement was observed, it was demonstrated that electronic coupling still plays the major role, while the vibronic coupling is often overrated. Therefore, the Frenkel exciton model gives a qualitatively good approximation of the two-photon absorption enhancement. Müllen classified the electronic coupling constant *V* as being 'small' (≤ 0.05 eV), 'increased' (0.05 eV ≤ *V* ≤ 0.15 eV) or 'strong' (0.15 eV ≤ *V* ≤ 0.25 eV).[188b] While the weak coupling only leads to additive enhancement and no interaction in the excited states, increased coupling yields cooperative enhancement. However, the interaction between the branches in the excited state is not dominant, as the excitation localizes on a dipolar chromophore branch prior to emission.[190] The strong coupling case is more complex, and leads to strong enhancement, as the exciton is completely delocalized and emission occurs from the entire system.

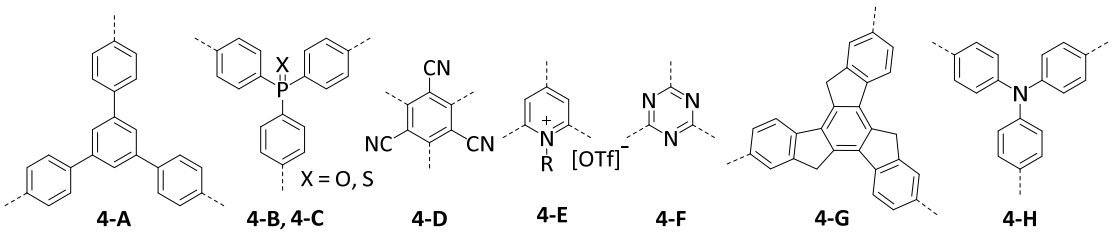

Scheme 4-1. Schematic drawing of the different cores **4-A** – **4-H**.

Only a few octupolar dyes have been explored for two-photon excited fluorescence imaging (TPEF) thus far. In 2007, the first octupolar dye, with a triphenylamine core branched to three pyridinium acceptor moieties for solubility and electron-withdrawing strength, was reported to have a two-photon absorption cross-section of 700 GM in glycerol.[191] Unfortunately, the two-photon absorption cross-section was not measured in buffer as the dye is almost non-emissive (0.02), but it acts as a turn-on sensor when binding to DNA occurs. In fixed CHO-K1 cells, the dye was found to localize in the nucleus and bind selectively to DNA. This dye was further improved by the same group by using *N*-methyl benzimidazolium moieties as the acceptor units, leading to a higher fluorescence quantum yield and DNA affinity.[192] Blanchard-Desce and co-workers also examined octupolar systems for TPEF. In 2011, their first report involved the preparation of nanoparticles with molecules containing a triphenylamine core and 2-formylthiophene as the acceptor unit, but these were found to aggregate very rapidly and deposit in small blood vessels,[193] thereby hindering blood flow, leading to the death of the tadpole they were studying. Two years later, they reported two symmetric octupolar dyes for cell imaging,[181] both of which have a triphenylamine core and $SO_2CH_2CH_2OH$ as the peripheral acceptor for improved solubility. The donor and acceptor groups were connected by phenyl-ethynyl and phenyl-vinyl bridges. The TPA brightness ($\sigma_2\Phi_f$, where Φ_f is the fluorescence quantum yield) of the two compounds in ethanol solution were found to be 250 and 268 GM, respectively, and TPEF images showed the localization of the dyes in the cytoplasm of HEK 293 cells. Another octupolar dye that selectively stains the cytoplasm was reported by Tian and co-workers.[194] This dye bears a triphenylamine core and *bis*-cyano-substituted isophorones as acceptors. Very recently, an octupolar dye was reported, which stains nucleoli as well as nuclear membrane, nuclear matrix, nuclear pore and the cytoplasm, while binding to RNA.[116] This dye comprises a triarylborane acceptor core branched by three piperazine donors, and has a two-photon brightness of 90 GM.

Thus far, there have been no studies on the difference between dipolar and octupolar systems in cell imaging, comparing their selectivity and toxicity. Therefore, a dipolar dye with a triphenylamine donor and a triarylborane acceptor was synthesized. As triphenylamine is an efficient core for cooperative TPA enhancement (*vide supra*), this core was used for an octupolar system and connected to three triarylborane acceptors. The triarylborane acceptors are substituted with trimethylammonio groups to achieve good water solubility.[166] In this chapter, a comparison of the linear and non-linear optical properties is reported as well as the differences between the two dyes when used for live-cell fluorescence imaging.

4.2 Results and Discussion

4.2.1 Synthesis

The neutral dyes **4-1** and **4-2** were prepared *via* Suzuki-Miyaura cross-coupling reactions. Thus, the borylated triarylborane **2-6**, which was already synthesized in Chapter 2,[119] and 4-bromo-*N*,*N*-diphenylaniline or *tris*(4-bromophenyl)amine were coupled using $Pd_2(dba)_3 \cdot CHCl_3$ as the catalyst, SPhos as the ligand and potassium hydroxide as the base. To strengthen the acceptor ability of the boron center, and to enhance water solubility, the neutral dyes were methylated with methyl triflate to yield the cationic dyes **4-1M** and **4-2M** in almost quantitative yields. Unfortunately, neither dye was soluble in water, but they could be dissolved upon addition of 0.5% DMSO, with no nanoparticles observable *via* dynamic light scattering (DLS) measurements.

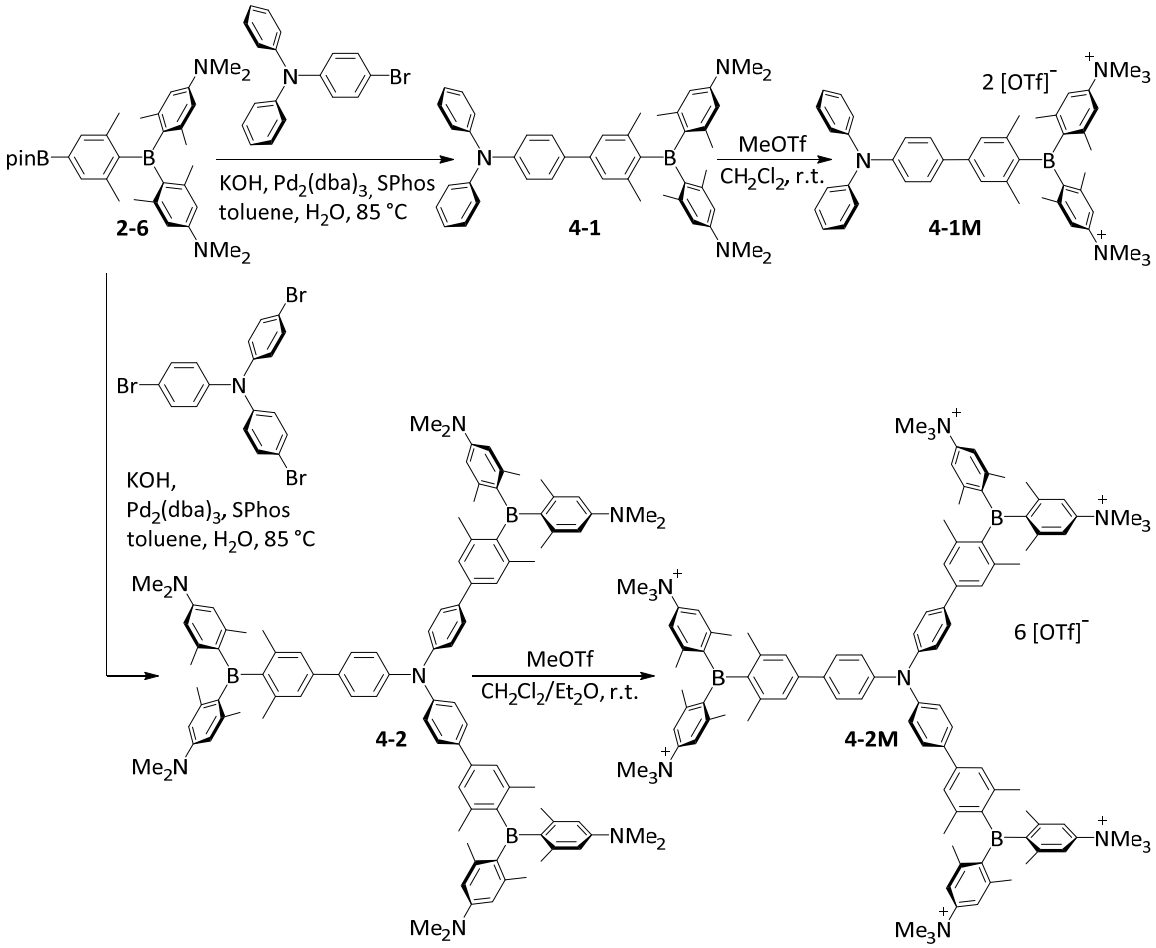

Scheme 4-2. Synthesis of the target molecules **4-1M** and **4-2M**.

4.2.2 Linear Optical Properties and TD-DFT Calculations of **4-1** and **4-2**

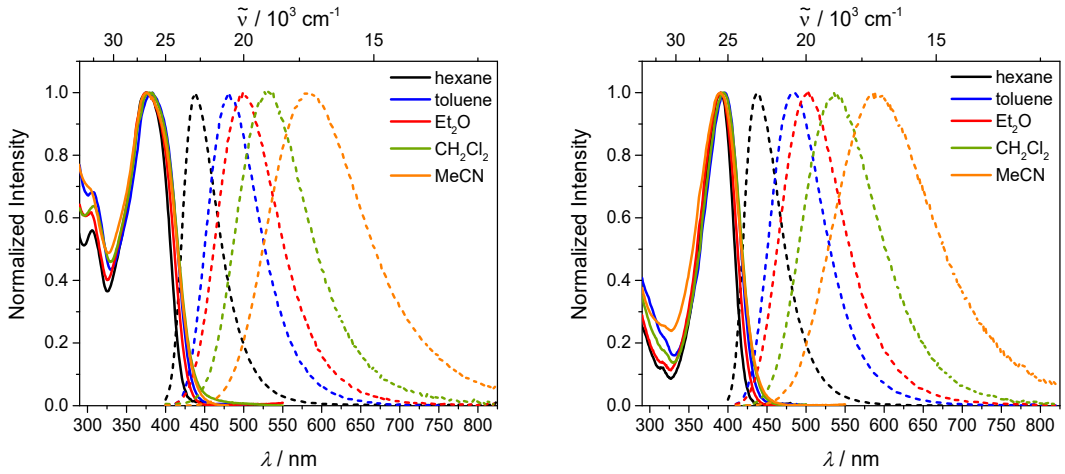

Figure 4-1. Absorption and emission spectra of **4-1** (left) and **4-2** (right) in various solvents (hexane: black, toluene: blue, diethylether: red, dichloromethane: green, MeCN: orange).

Table 4-1. Photophysical data for the compounds **4-1** and **4-2** in various solvents.

	solvent	λ_{abs} / nm	ε / M^{-1} cm^{-1}	λ_{em} / nm	Stokes shift / cm^{-1}	Φ_f	τ / ns	k_r / 10^8 s^{-1}	k_{nr} / 10^8 s^{-1}	τ_0 / ns
4-1	hexane	375	58 000	438	3 800	0.13	1.6	0.8	5.5	12.3
	toluene	383		481	5 300	0.21	3.1	0.7	2.5	14.8
	Et_2O	375		499	6 600	0.22	4.7	0.5	1.6	21.4
	CH_2Cl_2	383		527	7 100	0.31	8.5	0.4	0.8	27.4
	MeCN	376		583	9 400	0.12	5.0	0.2	1.8	41.7
4-2	hexane	391	186 000	439	2 800	0.17	1.4	1.2	5.9	8.2
	toluene	396		481	4 700	0.23	3.2	0.7	2.4	13.9
	Et_2O	390		503	5 800	0.23	4.9	0.5	1.5	21.3
	CH_2Cl_2	394		536	6 700	0.33	8.5	0.4	0.8	25.8
	MeCN	391		588	8 600	0.13	4.8	0.3	1.8	36.9

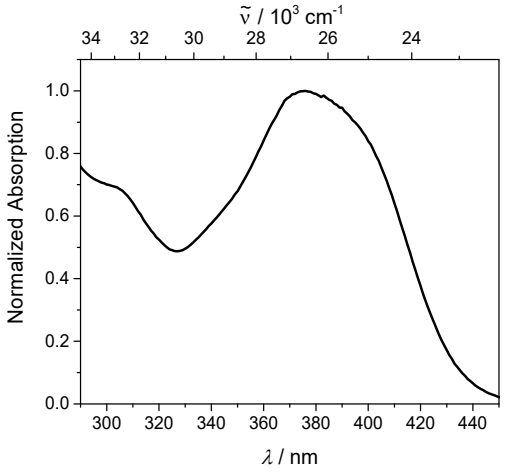

Figure 4-2. Absorption spectrum of **4-1** in MeCN.

The absorption spectra of **4-1** and **4-2** display one broad absorption band at wavelengths greater then 300 nm, which shows almost no solvatochromism (Figure 4-1 and Table 4-1). In compound **4-1** the absorption maximum is at *ca*. 380 nm ($S_2 \leftarrow S_0$ transition) with a shoulder around 392 nm

($S_1 \leftarrow S_0$ transition), which is exactly the absorption maximum of **4-2** (see Figure 4-2 for an enlarged display of the absorption band).

DFT (B3LYP/6-31G(d)) and TD-DFT (31G(d)) calculations were performed in the gas phase for both compounds **4-1** and **4-2** to obtain a better understanding of the absorption spectra. The HOMO is localized on the triphenylamine, and HOMO-1 (and HOMO-2, HOMO-3 for **4-2**) are localized on the dimethylamine (Figure 4-3). The HOMO and HOMO-1 are isoenergetic for compound **4-1**, while in compound **4-2** the HOMO is slightly higher in energy than the isoenergetic HOMO-1, HOMO-2 and HOMO-3. The TD-DFT calculations of the $S_1 \leftarrow S_0$ transition in the neutral compounds **4-1** and **4-2** show that the short-range CT from the dimethylamino groups to the boron atom predominates over the long-range CT from the triphenylamine to the boron center, even though the HOMO is localized on the triphenylamine. In the geometry optimized structures, the phenyl group(s) of the triphenylamine involved in the link(s) between N and B and the xylyl group(s) of the boron moiety have a torsion angle of 35° in both molecules (**4-1** and **4-2**), which hinders efficient long-range charge transfer. However, the higher energy transitions, $S_2 \leftarrow S_0$ and $S_3 \leftarrow S_0$, of **4-1** have increasing contributions from the long-range CT as they have greater HOMO contributions (Table 4-2).

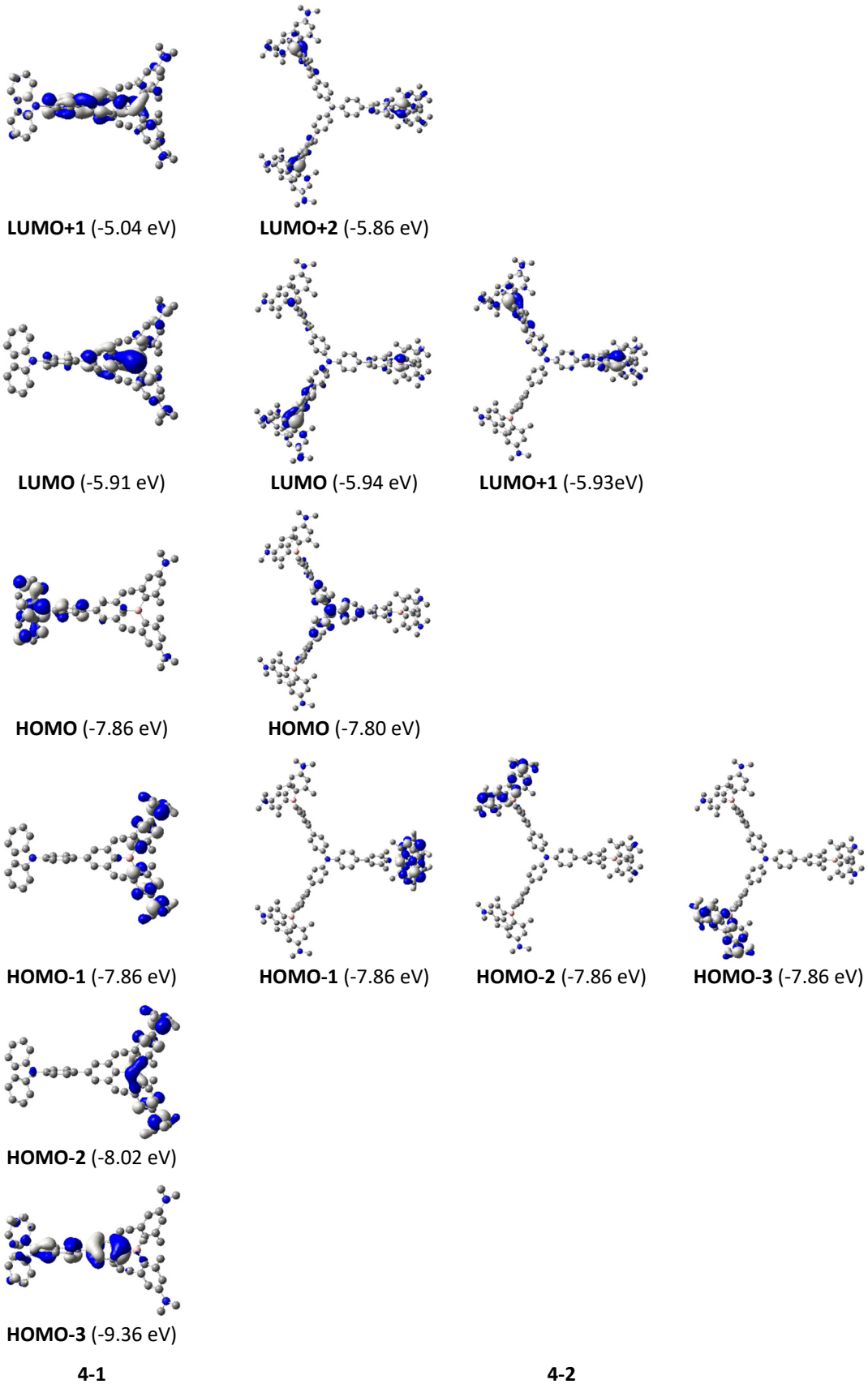

Figure 4-3. DFT (CAM-B3LYP/6-31 G(d))-calculated frontier orbitals for **4-1** and **4-2**. Hydrogen atoms are omitted for clarity. Surface isovalue: ± 0.03 $[e\ a_0^{-3}]^{1/2}$. LUMO and LUMO+1, as well as HOMO-1, HOMO-2 and HOMO-3 of **4-2** are isoenergetic.

Table 4-2. TD-DFT calculations on **4-1** and **4-2** in the gas phase.

	state	symmetry	E / eV	λ / nm	f	major (> 10%) contributions
	S_1	A	3.56	349	0.327	H-1 → L (86%)
4-1	S_2	A	3.75	331	0.708	H-3 → L (13%), H-2 → L (41%), H → L (32%)
	S_3	A	4.15	299	0.320	H-2 → L (42%), H → L (23%), H → L+1 (24%)
	S_1	E	3.56	348	0.161	H-3 → L (27%), H-2 → L+1 (13%), H-2 → L+2 (25%), H-1 → L (13%)
4-2 C_3	S_2	E	3.56	348	0.161	H-3 → L+1 (27%), H-2 → L (13%), H-1 → L+1 (13%), H-1 → L+2 (25%)
	S_3	A	3.56	348	0.611	H-3 → L+2 (29%), H-2 → L (28%), H-1 → L+1 (28%)
	S_1	A	3.56	348	0.161	H-3 → L (12%), H-2 → L (11%), H-1 → L+1 (19%), H-1 → L+2 (26%)
4-2 C_1	S_2	A	3.56	348	0.161	H-3 → L (21%), H-3 → L+1 (15%), H-2 → L+1 (14%), H-2 → L+2 (28%)
	S_3	A	3.56	348	0.611	H-3 → L+2 (27%), H-2 → L (20%), H-1 → L+1 (19%)

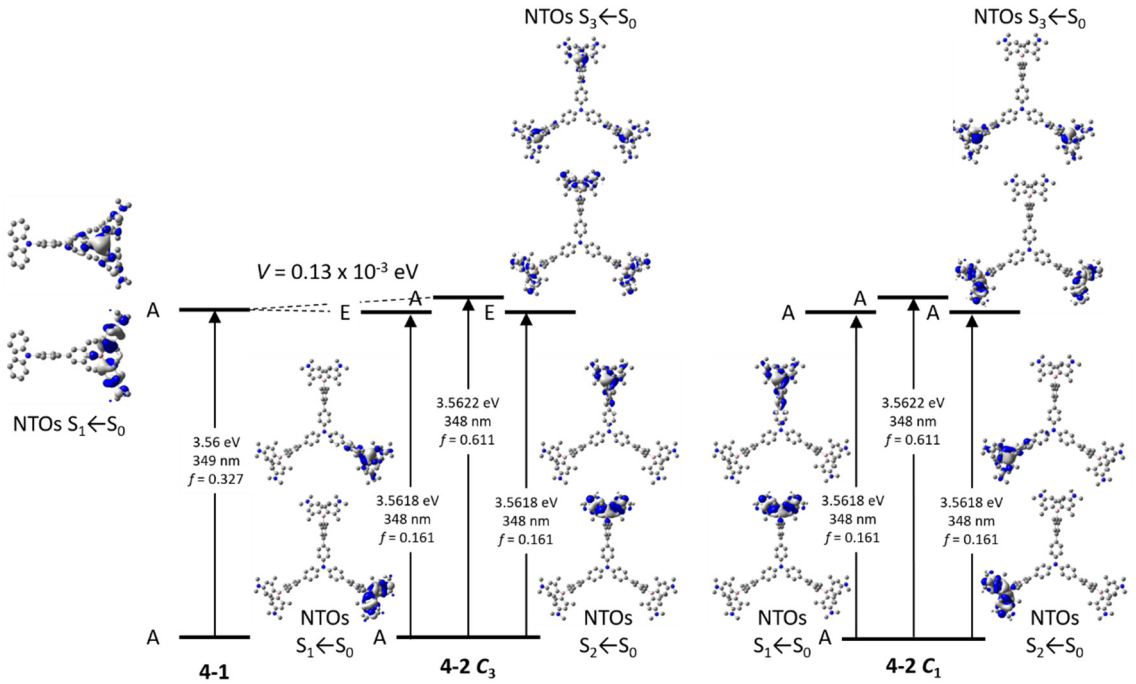

Figure 4-4. Excited state splitting of **4-2** with respect to **4-1**. The natural transition orbitals (NTOs) of S_1←S_0, S_2←S_0 and S_3←S_0 are depicted from TD-DFT calculations in the gas phase.

To investigate the coupling between the three branches of **4-2**, we use the exciton coupling model. Coupling of the three excited states in C_3 symmetry leads to two degenerate excited states (S_1 and S_2), which are stabilized by the coupling constant V and have E symmetry, and one excited state (S_3), which is destabilized by $2V$ and has A symmetry (Figure 4-4). As excitation from S_0 (A symmetry) is only allowed to S_1 and S_2 (E symmetry), one might observe the coupling constant V from the shift of the S_1←S_0 absorption bands. Comparing the calculated S_1←S_0 absorption band of **4-1** with that of **4-2** (optimized gas phase geometry for **4-1** and **4-2** and also C_3 symmetrized geometry for **4-2**) gives a negligible difference; therefore, coupling between the three arms is very small or non-existent and the coupling constant V is ~0.00 eV.[188b] The experimentally determined absorption bands at 392 nm (the shoulder in the absorption spectrum of **4-1**) and 391 nm (the absorption maximum of **4-2**) confirm this. Furthermore, the extinction coefficient ε = 186 000 measured for **4-2** being *ca*. 3 × that of **4-1** (ε = 58 000) shows

additive behavior as the three individual branches in **4-2** can be excited, but the emission occurs from a localized single branch. That is why the emission spectra as well as the fluorescence quantum yields and lifetimes of **4-1** and **4-2** are similar (Table 4-1). The emission maximum red-shifts with increasing solvent polarity, as the CT excited state becomes more stabilized, which is well known for D–A compounds. However, fluorescence quantum yields and lifetimes do not follow the expected dependence on solvent polarity. The quantum yields increase from nonpolar to polar solvents, while the non-radiative decay rates k_{nr} decrease. This is exactly the opposite of what would be expected from the energy gap law.[170] Usually, the non-radiative decay rate k_{nr} increases and, therefore, the quantum yield decreases. The fluorescence lifetimes become longer with increasing solvent polarity, while the radiative decay rates k_r are in qualitative accordance with the Strickler-Berg equation,[171] decreasing with decreasing emission energy. Furthermore, in MeCN, both compounds do not follow the afore-mentioned trend, as the quantum yields are decreased and fluorescence lifetimes are shorter compared with dichloromethane solutions. This behavior was observed previously for nitrogen donor – boron acceptor compounds[19, 31, 172b, 195] and has its origin in symmetry breaking in the excited state. The symmetry breaking is more enhanced in polar solvents than in nonpolar solvents, leading to the unusual solvent behavior seen above.[173] As the two short-range CTs in compound **4-1** are arranged in C_2 symmetry, the symmetry can break in the excited state, resulting in the observed unusual behavior of the fluorescence quantum yields and lifetimes in polar solvents. The long-range CT is parallel to the C_2 axis and, therefore, would not show symmetry breaking, and hence, no solvatochromism. In the branched compound **4-2**, the short-range CT is the most dominant. In C_3 symmetry, as well as in C_1 symmetry, coupling between the three subchromophore branches was not observed as the exciton coupling constant V between the three arms is negligibly small, being 0.13×10^{-3} eV (Figure 4-4). This is not astonishing as the triphenylamine core does not take part in the transitions. Therefore, chromophore **4-2** can be considered to be comprised of three independent subchromophors, each directly analogous to **4-1**. Thus, **4-2** exhibits the same photophysical properties as **4-1**.

4.2.3 Linear Optical Properties and TD-DFT Calculations of **4-1M** and **4-2M**

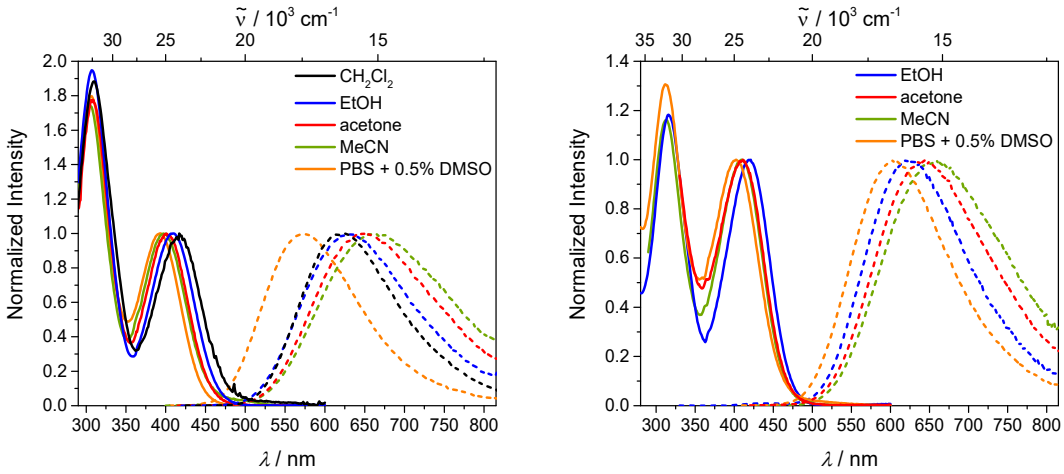

Figure 4-5. Absorption and emission spectra of **4-1M** (left) and **4-2M** (right) in various solvents (dichloromethane: black, ethanol: blue, acetone: red, MeCN: green, PBS + 0.5% DMSO: orange).

Table 4-3. Photophysical data of the cationic compounds **4-1M** and **4-2M** in various solvents.

	solvent	λ_{abs} / nm	ε / M^{-1} cm^{-1}	λ_{em} / nm	Stokes shift / cm^{-1}	Φ_f	τ / ns	τ_0 / ns	k_r / 10^8 s^{-1}	k_{nr} / 10^8 s^{-1}
4-1M	CH_2Cl_2	417		622	7 900	0.61	9.0	14.8	0.7	0.4
	EtOH	407		633	8 800	0.31	4.9	15.8	0.6	1.4
	acetone	401		649	9 500	0.23	4.7	20.4	0.5	1.6
	MeCN	397	19 000	659	10 000	0.19	3.4	17.9	0.6	2.3
	PBS + 0.5% DMSO	393		573	8 000	0.09	10.6	117.8	0.08	0.9
4-2M	EtOH	419		624	7 800	0.44	6.4	14.5	0.7	0.9
	acetone	411		643	8 800	0.29	5.9	20.3	0.5	1.2
	MeCN	410	55 000	660	9 200	0.26	5.0	19.2	0.5	1.5
	PBS + 0.5% DMSO	402		604	8 300	0.15	7.4	49.3	0.2	1.1

Upon methylation of all dimethylamino groups in the neutral dyes **4-1** and **4-2**, the photophysical properties of the chromophores change completely. The absorption spectra of **4-1M** and **4-2M** exhibit two absorption bands (Figure 4-5). While the higher energy absorption bands at *ca*. 305 and 314 nm, respectively, are almost solvent independent, the low-energy absorption band is significantly hypsochromically shifted with increasing solvent polarity. Within the limited range of solvents in which the compounds are readily soluble, the observed trend in the absorption maxima tracks with the dipole moment of the solvent rather than (ε–1/2ε+1)-(n^2-1/2n^2+1) as used for Lippert-Mataga plots. Strong deviations in the solvatochromic behavior might occur, as the compounds are di-cations/hexa-cations and their counterions and, therefore, differences in the separation of the ion pairs are possible in the various solvents. As compound **4-2M** shows solvatochromism, it must have a symmetry lower than C_3 to possess a dipole moment. Therefore, symmetry breaking occurs in the ground state. Comparing the absorption spectra of **4-1M** and **4-2M** in EtOH shows a bathochromic shift of 704 cm^{-1}. Using the exciton coupling model (*vide supra*) a coupling constant of 0.09 eV was calculated. The branching leads to a delocalization and therefore a red-shifted absorption.[111g, 187c] As this is 'increased' but not

'strong' coupling, as classified by Müllen (*vide supra*), the extinction coefficient shows approximately additive behavior (Table 4-3). Furthermore, the excitation localizes on a dipolar chromophore branch prior to emission. Therefore, the compound also has an excited state dipole moment. Thus, the emission maxima are bathochromically shifted, except for the PBS (phosphate buffered saline) + 0.5% DMSO solution in which special ion-ion interactions might occur. As the absorption is hypsochromically shifted, and the emission is bathochromically shifted in more polar solvents, an inversion of the dipole moment upon excitation occurs. This contrasts with the short-range CT transition of compounds **4-1** and **4-2**, in which the absorption is not solvatochromic and the emission shows positive solvatochromism, which implies that the dipole moment retains its original direction. The charge transfer behavior of dipolar and trigonal boron chromophores in the ground and excited state as it occurs in the neutral dyes **4-1** and **4-2** and the cationic dyes **4-1M** and **4-2M** was already explained by Lambert and co-workers in 2006.[19] In the less-hindered chromophores **4-1** and **4-2** (one xylyl between the nitrogen and the boron) the ground state polarization is dominated by mesomeric effects, leading to a charge-separated quinoidal contribution with a partially negative boron and a positive nitrogen, as is the case to a greater extent after the charge transfer upon excitation. In contrast, the chromophores **4-1M** and **4-2M** have less effective π-conjugation as the xylyl and the phenyl group are twisted. Therefore, the ground-state polarization is mainly influenced by inductive effects, *i.e*. boron as a σ-donor and nitrogen as a σ-acceptor. This leads to an inversion of the direction of the ground *vs*. excited state dipole moments. As the solvatochromism is more pronounced in the emission than the excitation, $\vec{\mu}_e$ must be larger than $\vec{\mu}_g$ for both cationic compounds **4-1M** and **4-2M**. The value of $\vec{\mu}_g$ of **4-2M** must be smaller than $\vec{\mu}_g$ of **4-1M**, as the two other branches also have a small contribution to the dipole moment, as illustrated in Figure 4-6. That this is the case is demonstrated by the smaller negative solvatochromism observed for **4-2M** (shift of 524 cm^{-1} from EtOH to MeCN) than for the **4-1M** analogue (shift of 618 cm^{-1} from EtOH to MeCN). In comparison, the positive solvatochromism is more enhanced for **4-2M** than **4-1M**, resulting in a larger $\vec{\mu}_e$ (-624 cm^{-1} and -874 cm^{-1} from EtOH to MeCN, respectively).

However, the quantum yields are consistent with normal CT behavior for both compounds, following the energy gap law.[170] They decrease for each compound with increasing solvent polarity, as the non-radiative decay rate k_{nr} increases, while the radiative decay rate k_r remains constant. In the PBS solution, the chromophores again behave differently; the fluorescence lifetimes increase, as the radiative decay rates k_r decrease dramatically, while the non-radiative decay rate k_{nr} is not as strongly affected. Branching leads to a slightly enhanced quantum yield as observed previously, due to the smaller non-radiative decay rates k_{nr}.[111g, 187c]

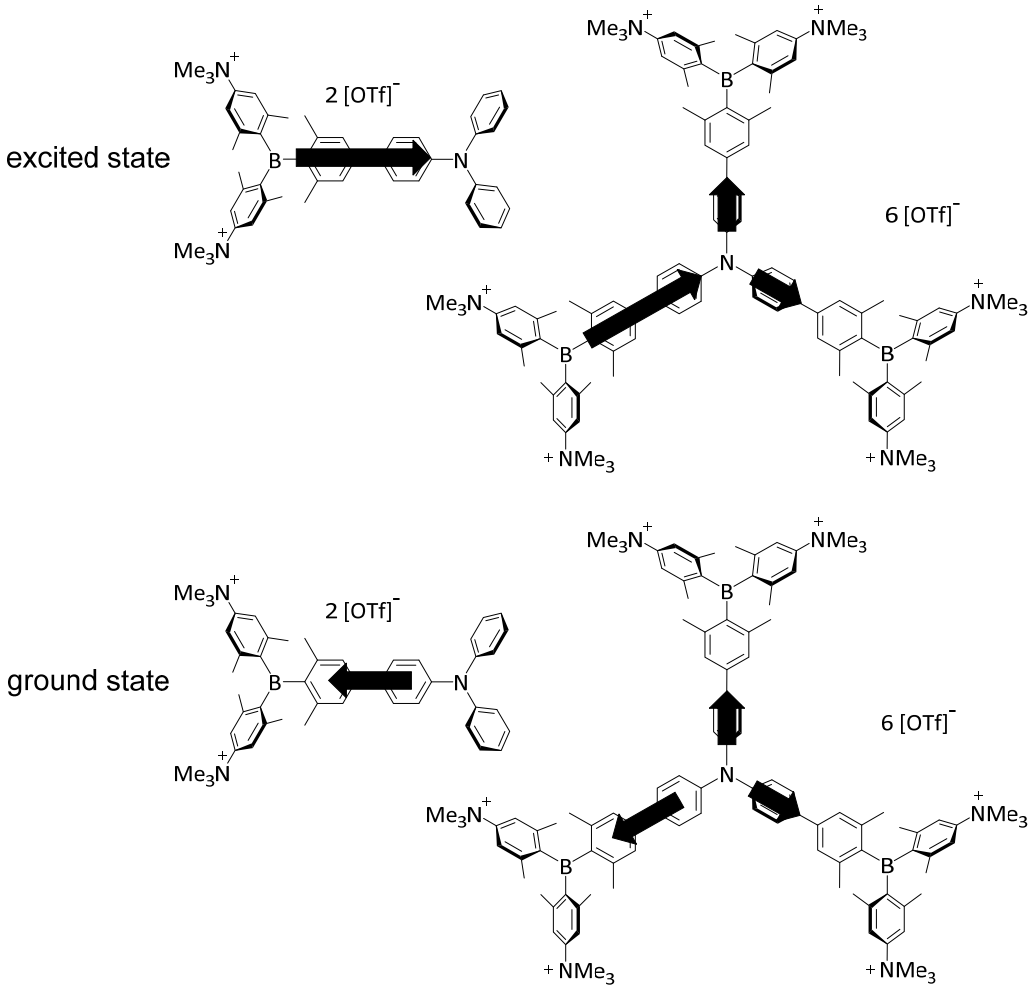

Figure 4-6. Schematic representation of the ground- and excited state dipole moments of **4-1M** and **4-2M**. The length of the arrows is not to scale with the absolute values of the dipole moments.

Methylation of compounds **4-1** and **4-2** destroys the short-range CT between the lone pairs on the dimethylamino groups and the boron center and, concomitantly, the acceptor strength of the triarylborane units is enhanced by the inductive effect of the cationic trimethylammonio substituents. Therefore, in **4-1M** and **4-2M**, the transitions all involve CT from the triphenylamine to the borons. DFT calculations on compounds **4-1M** and **4-2M** were carried out in the gas phase using the B3LYP functional in combination with the 6-31G(d) basis set. The torsion angles between the phenyl groups of the triphenylamine and the xylyl groups of the boron moiety are reduced to 25° and 31° in **4-1M** and **4-2M**, respectively, compared to the neutral dyes **4-1** and **4-2**. Comparing the results from the TD-DFT calculations (CAM-B3LYP/6-31G(d)) in the gas phase and EtOH show, especially for **4-1M**, a strong hypsochromic shift as the CT is weaker in the polar solvents (Figure 4-7) as both of the natural transition orbitals (NTOs) are more delocalized over the π-system in EtOH than the gas phase.

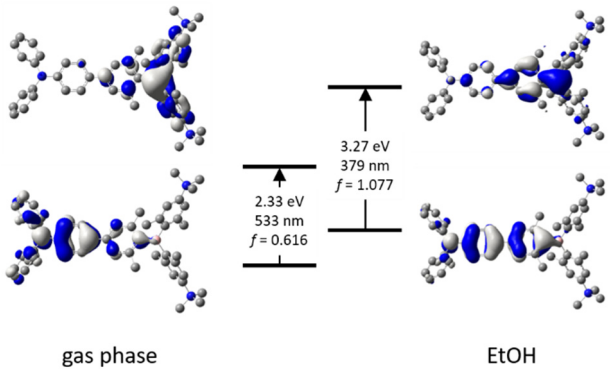

Figure 4-7. The natural transition orbitals (NTOs) of $S_1 \leftarrow S_0$ transition of compound **4-1M** are depicted based on TD-DFT calculations in the gas phase and in EtOH.

In the octupole **4-2M**, charge transfers from the central triphenylamine to one of the boron atoms of the three branches. As the central triphenylamine contributes, the branches couple with each other. Because of the C_3 symmetry, the S_1 and S_2 excited states are degenerate, stabilized by the coupling constant V, and excitation from S_0 is allowed (E symmetry, f = 1.407), while S_3 is destabilized by $2V$ and $S_3 \leftarrow S_0$ is forbidden (A symmetry, f = 0.000) (Table 4-4). From the exciton coupling model, the coupling constant V was calculated to be 0.09 eV, *i.e*. one third of the energy difference between the TD-DFT-computed excited E and A symmetry states. This is exactly the same as the value obtained from the experimental shift between **4-1M** and **4-2M** in the UV/Vis spectra. Both molecules show weak solvatochromism in their absorption spectra which indicates a small dipole moment in the ground state. However, as the solvatochromism is quite pronounced in the fluorescence spectra, a moderate to large excited state dipole moment can be anticipated, caused by symmetry breaking in the excited state. Therefore, **4-2M** does not have ideal C_3 symmetry in both the ground and excited states, but only C_1 symmetry (Figure 4-8), resulting in a non-zero dipole moment.

Table 4-4. TD-DFT calculations on **4-1M** and **4-2M** in ethanol solution.

	state	symmetry	E / eV	λ / nm	f	major (> 10%) contributions
	S_1	A	3.27	379	1.077	H-1 → L (16%), H → L (72%)
4-1M	S_2	B	4.12	301	0.011	H-2 → L (82%)
	S_3	A	4.20	295	0.167	H-9 → L (12%), H-1 → L (31%), H → L+1 (30%)
	S_1	E	3.40	365	1.407	H → L (54%), H → L+3 (11%)
4-2M C_3	S_2	E	3.40	365	1.408	H → L+1 (54%), H → L+4 (11%)
	S_3	A	3.66	339	0.000	H-2 → L (13%), H-1 → L+1 (13%), H → L+2 (48%),
	S_1	A	3.40	365	1.407	H → L (56%), H → L+3 (11%)
4-2M C_1	S_2	A	3.40	365	1.408	H → L+1 (56%), H → L+4 (11%)
	S_3	A	3.66	339	0.000	H-2 → L (16%), H-1 → L+1 (16%), H → L+2 (48%),

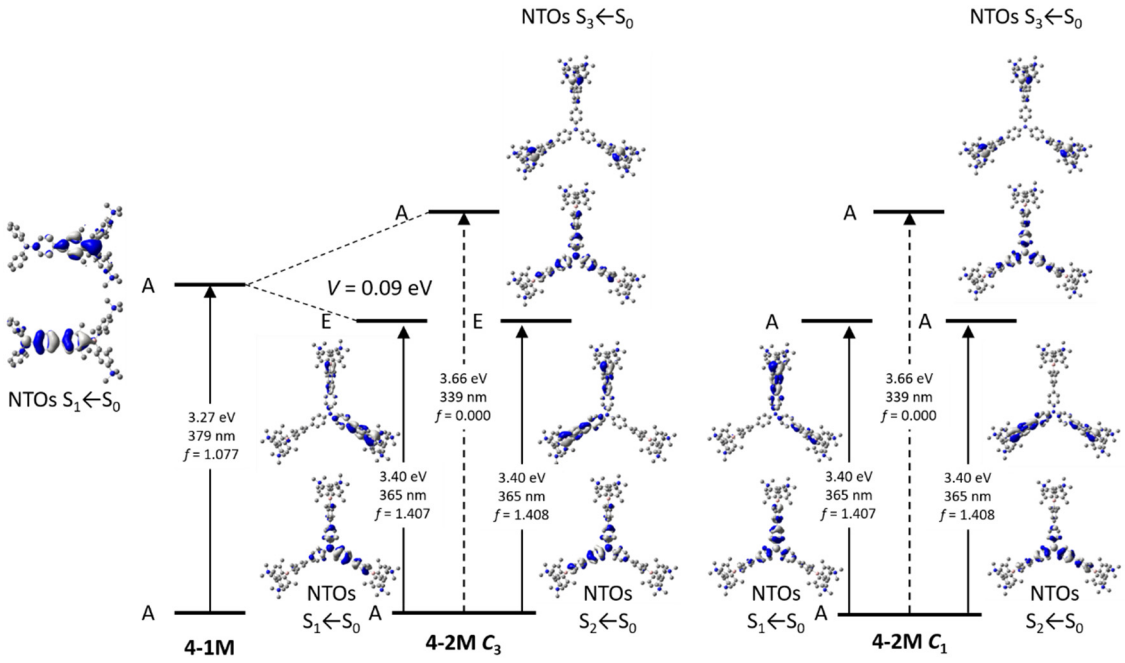

Figure 4-8. Excited state splitting of **4-2M** with respect to **4-1M**. The natural transition orbitals (NTOs) of $S_1 \leftarrow S_0$, $S_2 \leftarrow S_0$ and $S_3 \leftarrow S_0$ are depicted from TD-DFT calculations in ethanol.

4.2.4 Two-Photon Absorption

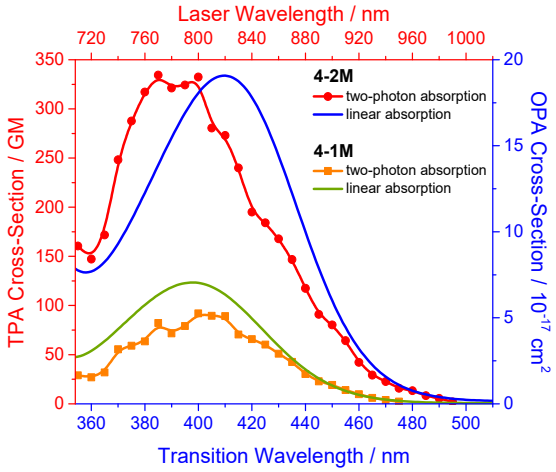

Figure 4-9. One-photon absorption spectra of **4-1M** (green) and **4-2M** (blue) and two-photon absorption spectra of **4-1M** (orange) and **4-2M** (red) in MeCN.

We measured the two-photon absorption spectra of both cationic dyes **4-1M** and **4-2M** in MeCN *via* two-photon excited fluorescence (Figure 4-9). While for **4-1M** the two-photon absorption (TPA) coincides with twice the wavelength of the one-photon absorption (OPA), the maximum of the TPA spectrum for **2M** is clearly shifted to shorter wavelength (higher energy). This is because two-photon absorption from the A symmetry ground state is allowed into the A symmetry excited state. The energy difference between the TPA energy and the OPA allowed E symmetry states thus gives a direct estimate for 3*V* which is 0.16 eV in reasonable agreement with the DFT computations (3*V* = 0.26 eV, see Table 4-4). The TPA cross-section of the dipolar chromophore **4-1M** is 91 GM in MeCN, which is increased upon branching to 335 GM for **4-2M**.

For comparison, normalizing the TPA cross-section by the number of branches leads to a value of 112 GM for **4-2M** in MeCN, and thus there is a small cooperative branching effect for **4-2M**. However, given the general error of the TPA measurement (ca. 10%) and the expected cooperative behavior (some 10% at best) we are reluctant to overstress this observation. Despite this conservative assessment, the two-photon brightness is greatly enhanced by branching as the fluorescence quantum yield also increases with the number of branches. While dipolar **4-1M** shows a TPA brightness of 17 GM, the value for octupolar **4-2M** is enhanced by a factor of *ca*. 5 to 87 GM.

4.2.5 Imaging

Before applying the two cationic dyes **4-1M** and **4-2M** for live-cell imaging, their influence on the cell viability of HeLa cells was tested. Thus, HeLa cells were treated with serial dilutions of the two compounds, and the cell metabolic activity was studied with a colorimetric (MTT) assay after 24 h (Figure 4-10). Up to a concentration of 1 μM, cell viability is unaffected by either dye, but higher concentrations led to reduced viability. The octupolar chromophore **4-2M** is less toxic than its dipolar analogue **4-1M**, for which the cell viability is reduced to 40% with a staining concentration of 10 μM.

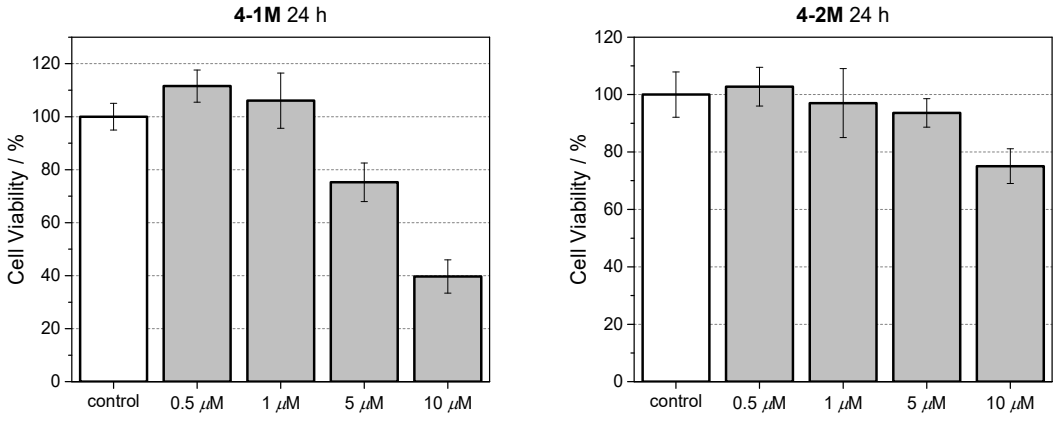

Figure 4-10. Cell viability of **4-1M**-loaded (left) and **4-2M**-loaded (right) HeLa cells determined by MTT assay. The cells were incubated with **4-1M** or **4-2M** (0, 0.5, 1, 5, 10 μM) in DMEM containing 0.5% DMSO in a CO_2 incubator for 24 h. The results are expressed as percentages of the dye-free controls. All data are presented as a mean with standard deviation (n = 10).

Having demonstrated that the dyes do not affect the cell viability up to 1 μM after 24 h, we stained HeLa cells with the two dyes **4-1M** and **4-2M** (0.5 μM). Using a confocal laser scanning fluorescence microscope, we observed cellular uptake of both dyes (Figures 4-11 and 4-12). Furthermore, *via* co-localization studies with commercially available LysoTracker™ Red, we demonstrate that the octupolar compound **4-2M** has a very good selectivity for lysosomes (R_r = 0.81), whereas the dipolar compound **4-1M** localizes to a lesser extent in lysosomes (R_r = 0.48),

and is clearly observed elsewhere in the cells. The fiber-like structures observed in the microscope images may be indicative of some degree of localization in mitochondria. Therefore, the octupolar compound **4-2M** is more selective than the dipolar compound **4-1M**, which may be ascribed to three factors, namely the increased number of cationic groups, the more hydrophilic character, and the larger size of compound **4-2M**. Furthermore, we applied both dyes for TPEF imaging, as shown in Figure 4-13, and the same staining pattern was observed as in the confocal microscopic imaging using one-photon excited fluorescence.

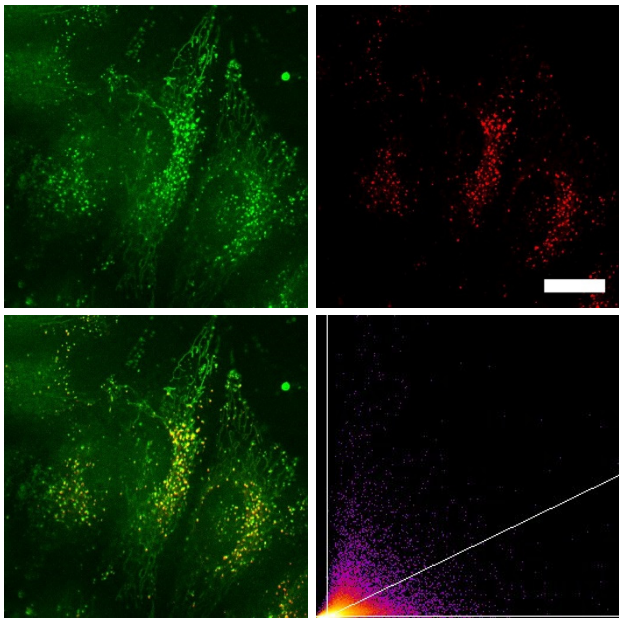

Figure 4-11. Co-staining experiment of HeLa cells with **4-1M** and LysoTracker™ Red. The cells were loaded with **4-1M** (0.5 μM, 2 h) and LysoTracker™ Red (0.1 μM, 20 min) at 37 °C. Fluorescence images of **4-1M** (top, left: λ_{ex} = 405 nm; λ_{em} = 500 – 605 nm) and LysoTracker™ Red (top, right: λ_{ex} = 561 nm; λ_{em} = 607 – 786 nm). The merged fluorescence images (bottom, left) and the correlation plot of the intensities (bottom, right: R_r = 0.48) show a modest degree of co-localization of the dye **4-1M** in lysosomes. Scale bar: 20 μm.

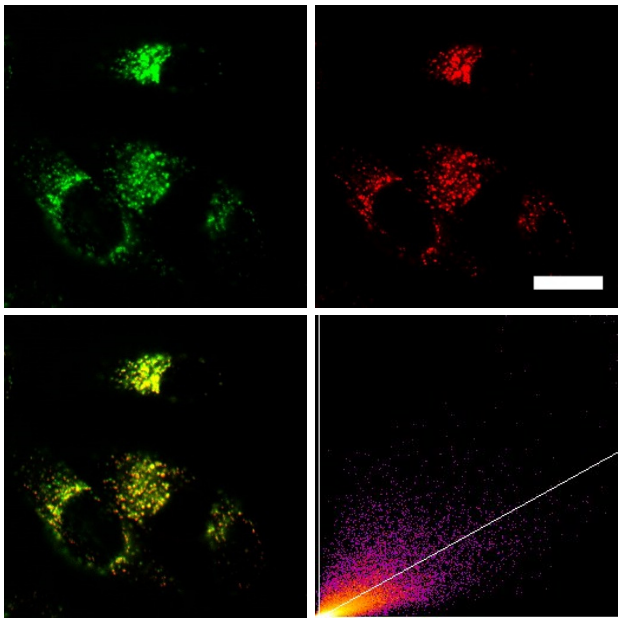

Figure 4-12. Co-staining experiment of HeLa cells with **4-2M** and LysoTracker™ Red. The cells were loaded with **4-2M** (0.5 μM, 2 h) and LysoTracker™ Red (0.1 μM, 20 min) at 37 °C. Fluorescence images of **4-2M** (top, left: λ_{ex} = 405 nm; λ_{em} = 500 – 605 nm) and LysoTracker™ Red (top, right: λ_{ex} = 561 nm; λ_{em} = 607 – 786 nm). The merged fluorescence images (bottom, left) and the correlation plot of the intensities (bottom, right: R_r = 0.81) show good co-localization of the dye **4-2M** in lysosomes. Scale bar: 20 μm.

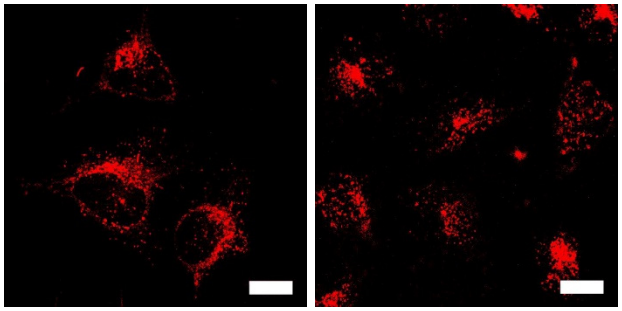

Figure 4-13. Two-photon excited fluorescence image of HeLa cells stained with 0.5 μM **4-1M** (left) or **4-2M** (right). The TPEF images were recorded with excitation at 800 nm (AOTF 10%) using an HyD1 detector through a 585/40 bandpass filter and an HCX APO L 40 × 0.80 W UVI objective. Scale bars: 20 μm.

4.3 Conclusions

In this chapter, two different chromophores, namely dipolar dicationic **4-1M** with a triphenylamine donor and a dicationic triarylborane acceptor and octupolar hexacationic **4-2M**, with a triphenylamine core branched by three dicationic triarylborane acceptors, were synthesized. The neutral precursors **4-1** and **4-2** show short-range charge transfer from the dimethylamine donor to the boron acceptor. Therefore, the three subchromophores do not couple with each other as the triphenylamine core is not involved. After methylation, the cationic dyes **4-1M** and **4-2M**, behave completely differently. There is a coupling (V = 0.09 eV) of the three branches observable in the UV/Vis absorption spectrum, as the absorption maxima redshift upon branching. Both systems show a hypsochromic shift with increasing solvent polarity in the absorption spectra, while the emission maxima are bathochromically shifted. The cationic dyes **4-1M** and **4-2M** show modest cooperative enhancement (factor of 3.7) of the TPA

cross-section, and an even larger increase (factor of 5.1) in the two-photon brightness ($\sigma_2\Phi_f$ = 87 GM) for octupole **4-2M**. The dyes were applied in TPEF imaging of live cells, and different behaviors of the two systems observed. The octupolar system **4-2M** is more biocompatible than the dipolar one **4-1M**, as the former shows lower cytotoxicity at higher concentrations. Furthermore, the selectivity of the dye **4-2M** for lysosomes is much better due to the increased number of cationic groups and therefore, more hydrophilic character, and the larger size of the molecule. In summary, the octupolar system **4-2M** is more suitable for TPEF imaging than the dipolar system **4-1M**, as the former has a much higher TPA brightness, is less toxic and is more selective for lysosomes.

Chapter Five

-

Optimization of

Aqueous Stability *vs.* π-Conjugation

5 OPTIMIZATION OF AQUEOUS STABILITY *VS.* π-CONJUGATION

5.1 Introduction

Over the last few decades, three-coordinate boranes with three aryl substituents have become increasingly important in materials research.[9, 13b, 17, 18b, 18e, 120a, 138, 144a] The empty p_z-orbital which is perpendicular to the BC_3 plane, makes these molecules strong π-acceptors and readily reducable units, but can be easily attacked by nucleophiles, such as water. To obtain easy to handle and durable materials, especially for applications such as live-cell imaging, this orbital needs to be protected. One way is to incorporate the triarylborane into a rigid, planar structure, thus inhibiting the formation of a tetrahedral geometry *via* structural constraints.[121] More common is the kinetic stabilization of the p_z-orbital by use of sterically demanding substituents. The first studies in this field were done by Krause and co-workers in 1924.[196] They found that BPh_3 was unstable in air, while tri-α-naphthylborane was almost air-stable.[197] Wittig and co-workers synthesized tri-(*o*-diphenyl)borane and tri-4-(*N*,*N*-dimethylamino)phenylborane, which were both found to be air-stable for *ca*. one week.[198] They explained the stability of the former compound by steric protection and of the latter by the electronic +M effect of the amine substituents. In 1957, Brown and Dodson reported the synthesis of the first completely air-stable triarylborane, namely trimesitylborane (2,4,6-trimethylphenyl = mesityl = Mes), and concluded, after oxygen reactivity tests, that the stability increases with the "shielding of the boron atom by the surrounding aryl groups".[46a] Later, it was found that two mesityl groups can provide enough protection for stability towards air and moisture in the solid state and in typical organic solvents.[12, 14a, 14b, 16, 111g, 123a, 199] In all cases, the aryl-rings form a more or less pronounced propeller-like structure around the boron atom leading to complete steric protection of the empty p_z-orbital. Due to their C_3 (D_3) symmetry, the molecules are necessarily chiral and crystallize as different rotational isomers. This phenomenon was first observed by Brown in 1948, while studying tri-α-naphthylborane as a reference Lewis acid.[200] He observed two polymorphic forms due to restricted rotation, which interconverted at elevated temperature. The dynamics of the conformational interconversion were studied by Gust and Mislow, as well as Weismann and Schug, by temperature dependent NMR measurements.[201] They observed mixtures of stereoisomers at low temperature, which interconverted at elevated temperature by a two-ring flip, which is the lowest-energy mechanism. Thus, two rings rotate about their respective B–C bonds through planes perpendicular to the BC_3 plane, while the remaining ring rotates in the opposite direction through the BC_3 plane. The activation energy of the stereoisomerization was estimated by the coalescence temperatures observed in the VT-NMR spectra. Comparison of Mes_2B–(aryl) compounds indicates that the activation energy decreases

with less steric demand of the aryl substituent, *e.g*. Mes_2B–(2-methylnaphthyl) (15.4 kcal/mol), Mes_2B–(9-anthryl) (13.8 kcal/mol), Mes_2B–(*o*-tolyl) (11 kcal/mol).[201c] Unfortunately, for $BMes_3$ no coalescence temperature is observable, as the two isomers are enantiomers. However, Wang and co-workers reported[102c] activation energies of Mes_2B–(duryl) and Mes_2B–(phenyl) compounds of 16.6 and 10.3 kcal/mol, respectively, which are consistent with the previous reported studies.[201c]

In addition to sterics, electronic effects are the most important tool to tune the properties of functional materials. Thus, it is worth noting that as soon as the Lewis acidity and electron affinity of the three-coordinate borane is enhanced compared to Mes_2B–(aryl), many of them tend to decompose upon exposure to air and moisture.[85a, 202] Only a few air-stable examples have been reported to date. Many of them used the 2,4,6-*tris*(trifluoromethyl)phenyl (^{F}Mes) substituent to enhance the electron deficiency while simultaneously stabilizing the triarylborane, due to its highly electron-withdrawing nature and increased steric bulk.[31, 39, 69h, 139, 194, 203] Without the sterically demanding ^{F}Mes group, it is very difficult to achieve higher stability and enhanced electron deficiency of the borane. The more the reduction potential of the boron moiety is increased, the more protection around the boron atom is required to maintain stability to air and moisture. Song and co-workers prepared triarylboranes with *para*-cyano substituents with reduction potentials of *ca*. -1.83 V, bearing six *ortho*-methyl groups for steric protection.[204] Marder and co-workers fine tuned the electron-accepting ability of donor-acceptor thienyl $BMes_2$ compounds by substitution of the *para*-methyl group of the mesityl moieties by C_6F_5 (Pfp) or 3,5-$(CF_3)_2$-C_6H_3 (Tfp).[33] The reduction potential is increased to -2.04 V for both compounds compared to Mes_2B–(thiophene) ($E^{1/2}_{red}$ = -2.23 V) but the four *ortho*-methyl groups are still sufficient to provide adequate steric protection. Gabbaï and co-workers introduced trimethylammonio cations at the *para*-positions of $BMes_3$.[166] Each substitution increases the reduction potential by 0.24 V. Two substitutions lead to a water-soluble triarylborane with $E^{1/2}_{red}$ = -2.09 V. This compound was stable even at low concentrations in aqueous solution, as it bears six *ortho*-methyl groups around the boron. This was recently used to synthesize water-soluble and stable quadrupolar dyes for live-cell imaging (see Chapter 2).[119] Changing the third unsubstituted mesityl group to a thienyl group led to a relatively air- and moisture-stable compound; however, at the very low concentrations in aqueous solution required for luminescence or imaging studies ($10^{-5} – 10^{-6}$ M) the compound decomposed significantly over a period of 24 hours. Therefore, the steric protection provided by four *ortho*-methyl groups in that system is not enough for aqueous applications. However, six *ortho*-methyl groups are sufficient for stabilization, as compound **2-3M** was stable in highly diluted aqueous solutions for more than three days.[119]

In this chapter, the stability of various triarylboranes in dilute aqueous solution will be investigated to asses the design features required for the synthesis of useful live-cell imaging agents. The design of these dyes is based on a quadrupolar structure (A–π–A), which was shown by Marder and co-workers to possess excellent two-photon absorption (TPA) properties.[111e, 111f, 111i] Therefore, the (*para*-(*N*,*N*,*N*-trimethylammonio)xylyl)$_2$B–(linker)–B(*para*-(*N*,*N*,*N*-trimethylammonio)xylyl)$_2$ motif developed in the previous chapters was employed.[119] As linkers, 1,4-phenylene (**5-1M**), 2,2‴-(3,3‴-dimethyl)-5,2′:5′,2″:5″,5‴-quaterthiophene (**5-2M**), 9,10-anthracenylene (**5-3M**) and 4,4‴-(5′-(3,5-dimethylphenyl))(5″-(3‴,5‴-dimethylphenyl))-2′,2″-bithiophene (**2-3M**) were explored to provide a gradual increase in steric demand and, therefore, protection around the boron atoms (Scheme 5-1). As increasing steric protection also reduces π-conjugation between the borons and the π-linker of the molecules, the aim of our study was to find the limit of stability of triarylboranes in dilute aqueous solution, *i.e*. to optimize the stability *vs*. π-conjugation trade-off.

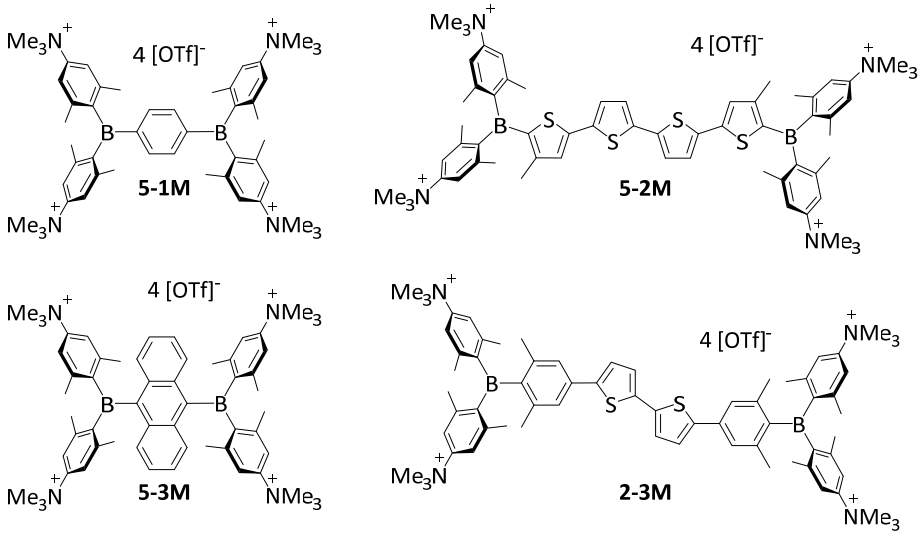

Scheme 5-1. Target molecules **5-1M** – **5-3M** and **2-3M**.

5.2 Results and Discussion

5.2.1 Synthesis

New compounds **5-1M** – **5-3M** were synthesized in this study, while compound **2-3M** was synthesized already in Chapter 2.[119] The neutral phenylene and anthracenylene compounds **5-1** and **5-3** were synthesized by lithiation of 1,4-dibromobenzene and 9,10-dibromoanthracene, respectively, and subsequent addition of fluoroborane **2-4** (Scheme 5-2). This strategy was unsuccessful for the tetrathiophene compound **5-1**, as the dibrominated thiophene bridge was insoluble in all suitable solvents. Therefore, 2-bromo-3-methylthiophene was lithiated and the fluoroborane **2-4** was added. The resulting triarylborane **5-4** was borylated *via* iridium-catalyzed C–H borylation[34] at the 5-position of the thiophene and then coupled to 5,5′-dibromo-2,2′-

bithiophene in a Suzuki-Miyaura cross-coupling reaction, giving the neutral tetrathiophene compound **5-2**. All three neutral compounds **5-1** – **5-3** were methylated with methyl triflate in CH_2Cl_2. The target molecules **5-1M** – **5-3M** precipitated directly from the reaction mixtures. The methylation needs to be done in basic glassware, such as soda-lime glass, as otherwise the reaction does not go to completion, and the product is contaminated with the three-times methylated species.

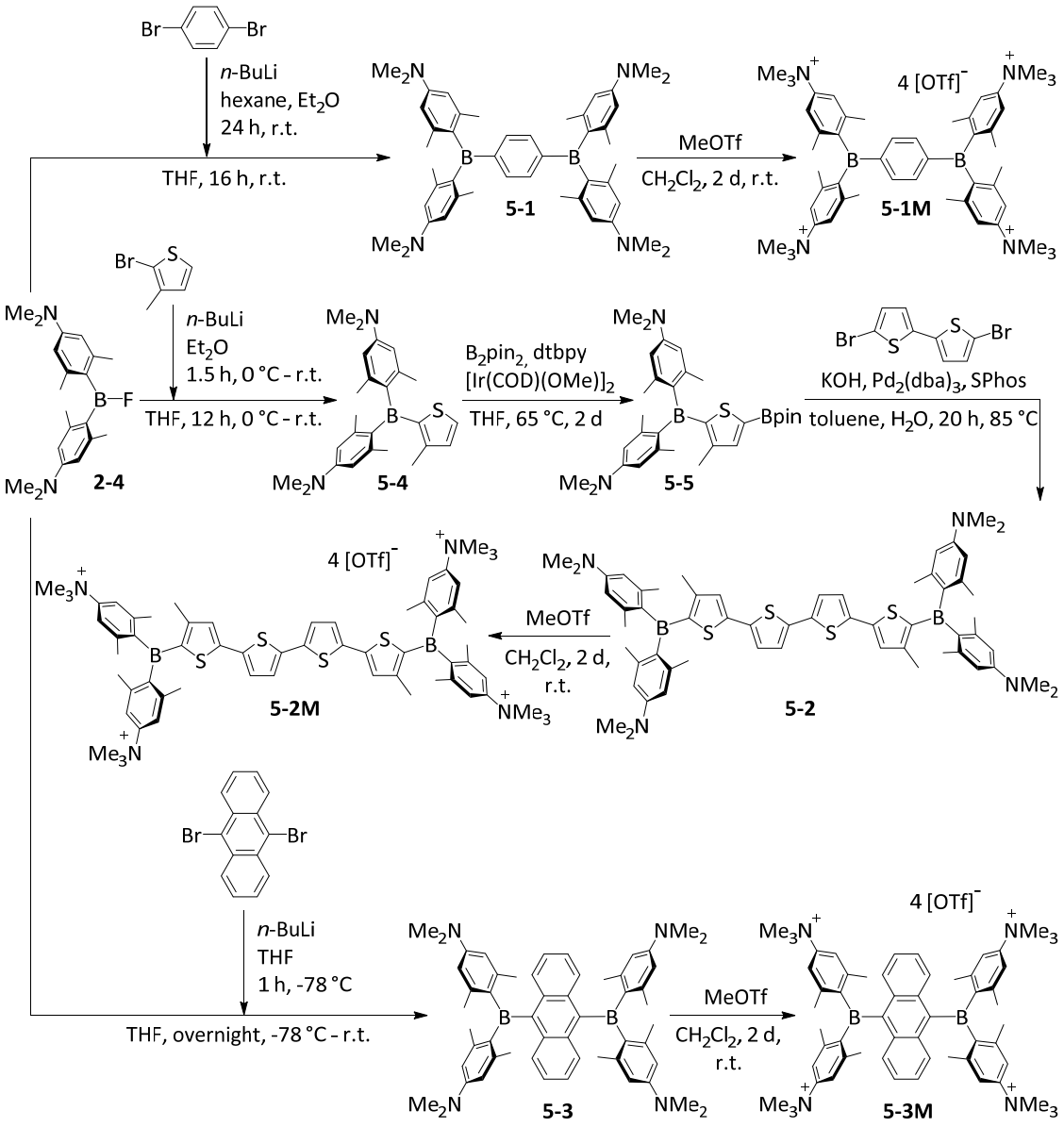

Scheme 5-2. Synthesis of compounds **5-1M** – **5-3M**.

5.2.2 Crystal Structure Analysis

Single crystals of neutral precursors **5-1** and **5-3** were obtained by slow evaporation of hexane/EtOAc or MeCN solutions, respectively, while methylated compounds **5-1M** and **5-3M** were both crystallized by slow diffusion of Et_2O into saturated MeCN/THF solutions. Unfortunately, single crystals suitable for X-ray diffraction of the larger thiophene compounds

5-2, **5-2M**, **2-3** and **2-3M** could not be obtained. However, their borylated triarylborane precursors, **5-5** and **2-6**[119] were crystallized by cooling saturated MeCN solutions. The molecular structures obtained are shown in Figure 5-1. Selected bond lengths and dihedral angles are listed in Table 5-1. The boron-centered BC_3 moieties are planar with the sum of the C–B–C bond angles equal to 360°. In **5-1**, **5-5**, **5-3** and **2-6**, the BC_3 planes and the *para*-(*N*,*N*-dimethylamino)xylyl rings form interplanar angles ranging from 41-58°. These values are similar to those in previously reported triarylborane compounds.[15-16, 33, 179b, 194] The angles between the third boron-bonded aryl ring and the BC_3 plane correlate with the steric demand of the aryl ring. The compounds with the smaller phenyl and methylthienyl rings exhibit twists of 27° and 39° for **5-1** and 35° for **5-5** with respect to the BC_3 plane. For the sterically more demanding anthracenyl and xylyl moieties, the twist angle with respect to the BC_3 plane nearly doubles to 64° (**5-3**) and 59° (**2-6**). A similar behavior was also observed for the $BMes_2$ analogues **5-6** (twist of 24° between the BC_3 plane and the central phenyl ring) and **5-7** (twists of 53° and 56° between the BC_3 plane and the central anthracenyl moieties) (Table 5-1).[16] While the interplanar angles of the four compounds show dramatic differences, the B–C bond lengths of **5-1**, **5-5**, **5-3** and **2-6** (1.560(2)-1.592(2)) are very similar and lie in the expected region. In methylated compounds **5-1M** and **5-3M**, the interplanar angles of the terminal *para*-(*N*,*N*,*N*-trimethylammonio)xylyl rings are also in the expected range of 46°-56° with respect to the BC_3 plane.[15, 33, 179b, 194] The central phenyl ring of compound **5-1M** is twisted by 27° and 25° out of the two BC_3 planes, while the twist angle of the anthracenyl moiety of compound **5-3M**, again, roughly doubles to 59° and 58°. Compared to neutral analogues **5-1** and **5-3**, the interplanar angles are slightly smaller with respect to the central ring, but still correlate well with the steric demand of the aryl substituent. Furthermore, the B–C bond lengths are not significantly affected by the methylation, and thus lie in the expected range (1.563(7)-1.597(9)).

Table 5-1: Selected bond lengths (Å) and angles (°) of **5-1**, **5-5**, **5-3**, **2-6**, **5-1M**, **5-3M**, **5-6** and **5-7**.

	5-1	5-5	5-3	2-6[119]	5-1M	5-3M	5-6[16]	5-7[16]
B1–C	1.567(3)	1.568(2)	1.585(3)	1.592(2)	1.563(7)	1.587(6)	1.571(3)	1.589(3)
	1.568(3)	1.563(2)	1.568(3)	1.571(2)	1.573(8)	1.585(5)	1.572(3)	1.589(3)
	1.574(2)	1.560(2)	1.569(3)	1.567(2)	1.570(9)	1.575(6)	1.582(3)	1.577(3)
B2–C	1.563(3)		= B1–C		1.564(7)	1.581(6)	= B1–C	1.593(2)
	1.567(3)				1.597(9)	1.585(6)		1.571(3)
	1.577(2)				1.567(9)	1.580(6)		1.582(3)
∠B1C3-R1 (central)	27.01(8)	35.10(6)	63.50(10)	58.94(6)	27.4(2)	58.7(1)	23.8(1)	52.8(1)
∠B1C3-R2 (terminal)	41.32(7)	54.55(6)	46.94(8)	42.39(6)	53.0(2)	51.7(2)	54.2(1)	50.8(1)
∠B1C3-R3 (terminal)	57.98(7)	46.04(6)	49.70(7)	45.80(4)	52.1(2)	46.2(2)	60.1(1)	53.0(1)
∠B2C3-R1 (central)	38.97(7)				24.8(1)	58.3(1)		56.1(1)
∠B2C3-R4 (terminal)	48.27(6)				52.3(2)	47.6(1)		44.0(1)
∠B2C3-R5 (terminal)	55.37(8)				55.8(2)	49.1(2)		50.4(1)
Sum ∠ CB1C	360.0(1)	360.0(1)	360.0(2)	360.0(1)	360.0(5)	360.0(4)	360.0(2)	360.0(1)
Sum ∠ CB2C	360.0(1)				360.0(5)	360.0(3)		360.0(1)

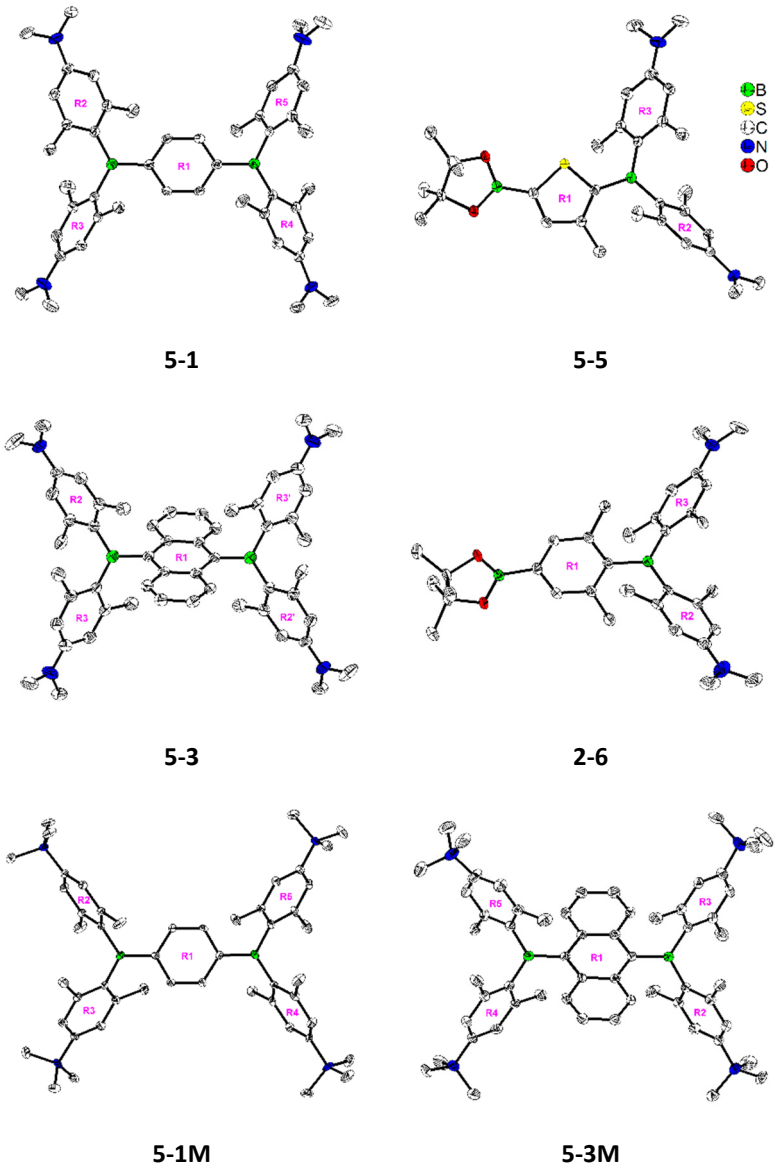

Figure 5-1. Solid state molecular structures of **5-1**, **5-3**, **5-5**, **2-6**,[119] **5-1M** and **5-3M** from single-crystal X-ray diffraction at 100 K. Atomic displacement ellipsoids are drawn at the 50% probability level, and H atoms and counter anions are omitted for clarity. With regard to the aryl rings bonded to boron atoms, the central ring is labelled R1 and the terminal rings are labelled R2 and R3 if bonded to B1, and R4 and R5 if bonded to B2, respectively.

5.2.3 NMR Spectroscopy

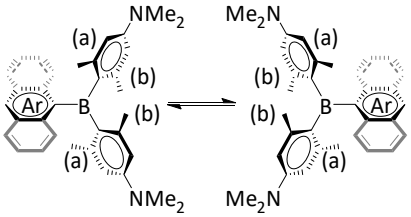

Figure 5-2. Interconversion between the two enantiomers on the NMR time scale due to restricted rotation of the *para*-(*N*,*N*-dimethylamino)xylyl rings around the boron center. Methyl groups closer to and farther from the aryl linker moiety are labelled (a) and (b), respectively.

At room temperature, the *ortho*-methyl groups of the *para*-(*N*,*N*-dimethylamino)xylyl rings of **5-1** and **5-2** exhibit one sharp singlet at 1.95 and 2.09 ppm, respectively, while the analogous methyl groups of **5-3** show one broad singlet at 1.94 ppm. For compound **2-3**, two sharp singlets

at 2.37 and 2.29 ppm with a 1:1 ratio are observed. According to previous studies[201] on the stereoisomerization of triarylboranes (*vide supra*), slow exchange between the two enantiomers of the racemic mixture is possible *via* rotations of the aryl rings around the B–C bonds (Figure 5-2). The broadening and decoalescence of the NMR signals with decreasing temperature is ascribed to this dynamic interconversion. As compounds **5-1** and **5-2** exhibit one sharp singlet at room temperature, the exchange is very fast and the rotation barrier very small. Thus, the stereoisomerization of **5-3** and **2-3** is slower, as a broad signal and two sharp signals, respectively, are observed at room temperature. Variable temperature (VT) ^{1}H NMR experiments on the neutral and methylated compounds at 300 MHz were conducted, which are displayed in Figures 5-3 and 5-4. When the temperature is decreased from 298 K to 183 K, the sharp signal of compound **5-1** becomes slightly broader, but no coalescence point was observed. Due to the melting point of CD_2Cl_2, NMR spectra could not be recorded at lower temperatures. Repeating the VT-NMR measurements with compound **5-2** shows a broadening of the singlet upon cooling to 223 K (the coalescence temperature), below which it splits into two singlets. Decreasing the temperature further to 213 K and 183 K leads to an additional splitting of both singlets, as the methylthiophene ring has no C_2 axis. The rotational barrier was calculated to be 11.0 kcal/mol. The broad signal of compound **5-3** at room temperature shows that 298 K is the coalescence temperature. The signal splits upon decreasing the temperature, resulting in two signals which are very sharp at 233 K. These suggest a very slow exchange, which makes the two methyl groups positioned closer to the anthracene linker (labelled (a) in Figure 5-2) inequivalent to the remaining two methyl groups (labelled (b) in Figure 5-2), which are located further away. A similar dynamic process due to restricted rotation was observed previously.[201c] From the difference in their resonance frequencies in Hz and the coalescence temperature, the energy barrier of the stereoisomerization was calculated to be higher (13.9 kcal/mol) than for compound **5-2**. To study the rotational barrier of compound **2-3**, the NMR sample must be heated as, at room temperature, the spectrum displays two sharp singlets, suggesting slow exchange. The coalescence temperature was found to be 348 K, which gives the highest rotational barrier of 17.7 kcal/mol. There is a clear trend for the rotational barriers of the *para*-(*N*,*N*-dimethylamino)xylyl rings, based on the observed broadening and decoalescence of the NMR signals. The rotational barriers increase with increasing steric demand of the linker in the order 1,4-phenylene **5-1** < 2,2‴-(3,3‴-dimethyl)-5,2′:5′,2″:5″,5‴-quaterthiophene **5-2** < 9,10-anthracenylene **5-3** < 4,4‴-(5′-(3,5-dimethyl-phenyl))(5″-(3‴,5‴-dimethylphenyl))-2′,2″-bithiophene **2-3**. Therefore, the rotational barrier of **5-1** must be smaller than 11.0 kcal/mol.

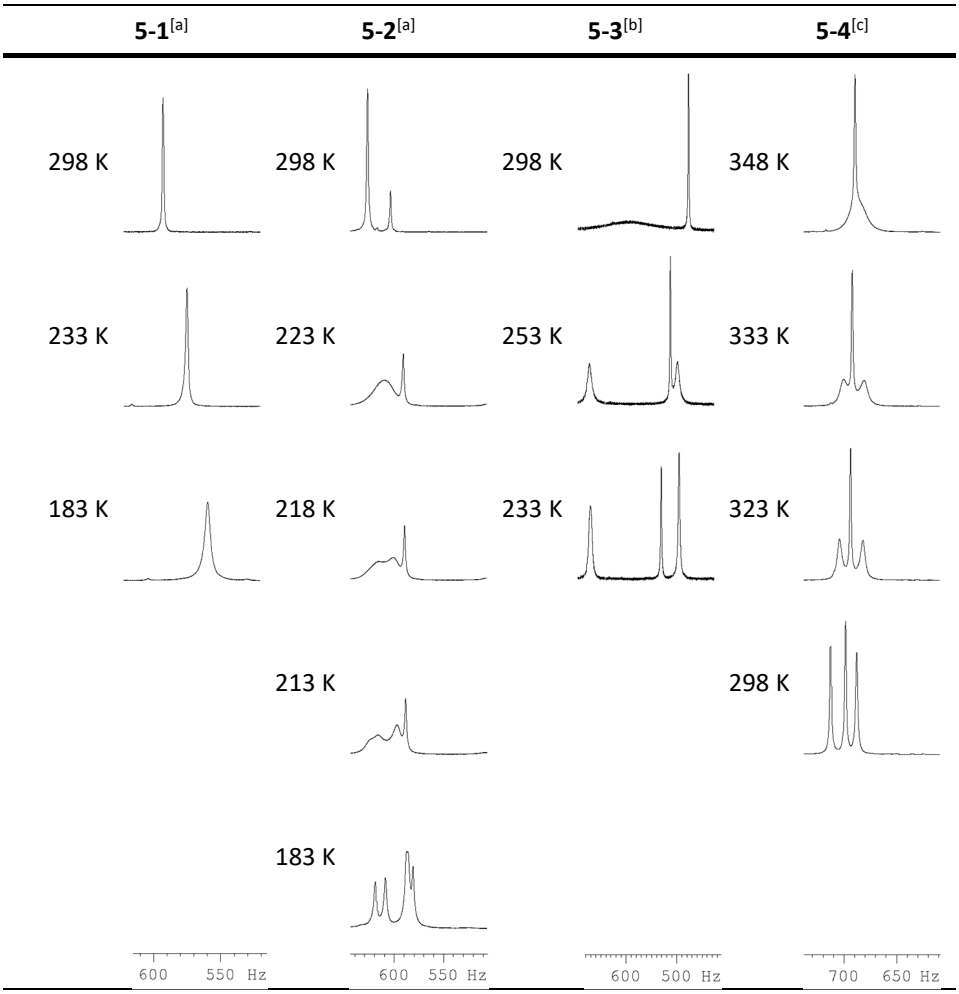

[a] measured in CD_2Cl_2; [b] measured in $CDCl_3$; [c] measured in C_6D_6.

Figure 5-3. ^{1}H NMR spectra (300 MHz) of the methyl resonance of compounds **5-1** – **5-3** and **2-3** at various temperatures.

Methylated compounds **5-1M** – **5-3M** and **2-3M** show the same trend as their respective neutral species **5-1** – **5-3** and **2-3**, and the coalescence temperatures are higher (Figure 5-4). Again, no rotational barrier could be calculated for compound **5-1M**. The low temperature limiting spectrum, at which no exchange occurs on the NMR time scale, could not be reached due to the melting point of CD_3OD, but the coalescence temperature was found to be 203 K. Calculations using the difference of the resonance frequencies 10 K below the coalescence temperature indicate a rotational barrier lower than 9.7 kcal/mol. The rotational barrier for compound **5-2M** was calculated to be 15.5 kcal/mol. The coalescence temperature was found to be 298 K. Decreasing the temperature leads to a splitting of the signal into two singlets, which sharpen until 253 K, where there is still more than 20% overlap between the two signals. Interestingly, further cooling leads to a broadening of the two signals and increasing overlap, presumably due to specific solvation effects. For compound **5-3M**, two broad singlets are observed at room temperature, which sharpen with decreasing temperature. The calculated rotational barrier (15.3 kcal/mol) at the coalescence temperature of 323 K is higher than that of the neutral

analogue **5-3** (13.9 kcal/mol). However, compound **2-3M** shows a coalescence temperature of 338 K, which is almost the same as that of the neutral analogue **2-3**, yielding a similar rotational barrier of 17.0 kcal/mol. Thus, as for the neutral compounds, the rotational barriers correlate with steric demand, following a similar trend (**5-1M** < **5-2M** ~ **5-3M** < **2-3M**).

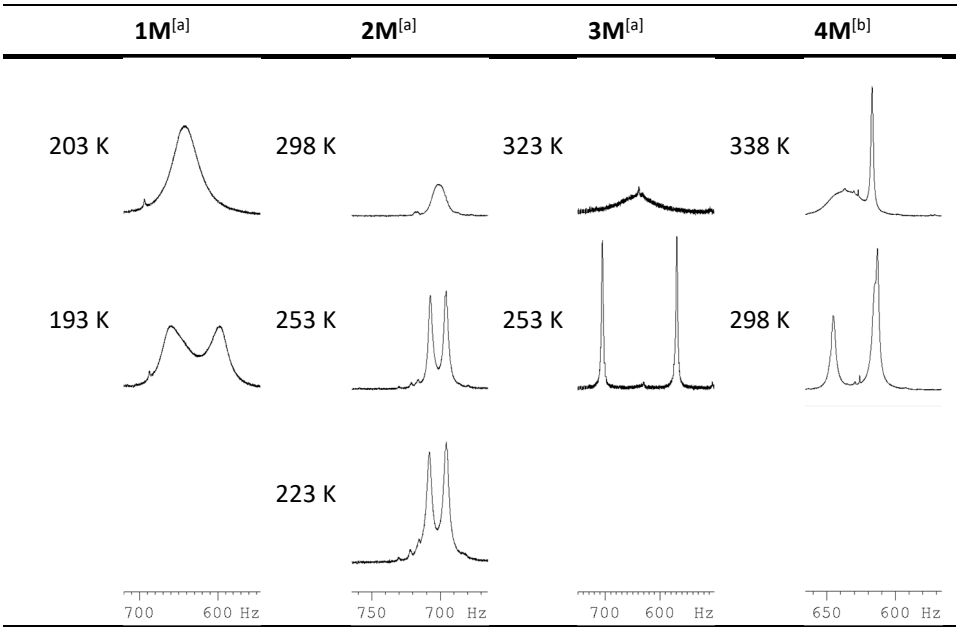

[a] measured in d_4-MeOH; [b] measured in d_6-DMSO.

Figure 5-4. ^{1}H NMR spectra (300 MHz) of the methyl resonance of compounds **5-1M** – **5-3M** and **2-3M** at various temperatures.

5.2.4 Stability

While all neutral compounds **5-1** – **5-3** and **2-3** are air- and moisture-stable in the solid-state and organic solvents, they are not soluble in water. The methylated derivatives **5-1M** – **5-3M** and **2-3M** exhibit different stabilities in aqueous solution, depending on the steric hindrance of the aryl linker substituent. Aqueous solutions of **5-2M**, **5-3M** and **2-3M** are stable over a period of days, while **5-1M**, with the smallest aryl substituent, namely phenylene, shows evidence of decomposition as determined by NMR spectroscopy. The NMR spectrum of **5-1M** was measured in CD_3OD, containing traces of water, and the aromatic region was plotted at different times (Figure 5-5). Direct NMR measurement after dilution of the sample confirmed its purity and displayed two distinct signals with an integrated ratio of 2:1. With time, the two signals decrease in intensity, while many other signals appear, due to decomposition of the compound. After three weeks, crystals precipitated in this NMR tube. Washing and dissolving the crystals in CD_3OD showed there to be only one species in the NMR spectrum. The isolated crystals were also examined by X-ray diffraction (Figure 5-6a). A B–C bond cleavage was observed, due to the attack of water as a nucleophile, leading to the unexpected product $[4\text{-}Me_3N\text{–}C_6H_4\text{–}OH]^+$ $[OTf]^-$. Oxygen was expected to attack the Lewis acidic boron atom rather than carbon, given the higher

electron-deficiency of boron due to its empty p_z-orbital. Mulliken charges obtained from DFT calculations, *vide infra*, are also consistent with such a picture (Figure 5-6c). However, a space filling model of the structure obtained from X-ray crystallographic data shows that the boron atom is not easy to access due to the steric protection provided by the *ortho*-methyl groups (Figure 5-6d). A water molecule does not fit easily into the pocket, but the *ipso*-carbon atom of the B–aryl linker group can be attacked, as it is more accessible. The other hydrolysis products were not identified.

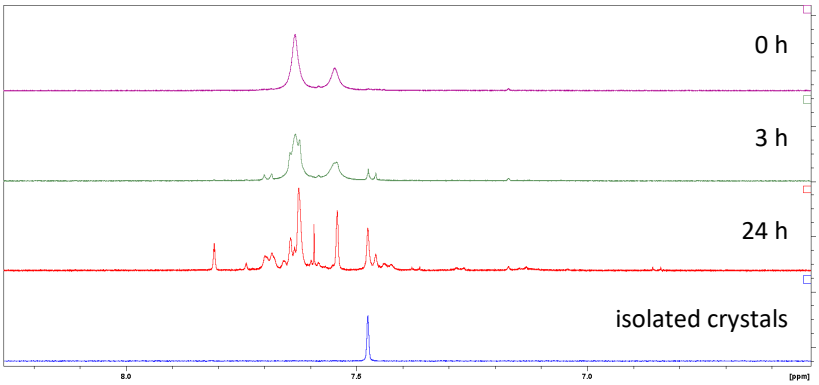

Figure 5-5. Aromatic region of ^{1}H NMR of **5-1M** in CD_3OD at different times (purple: t = 0 h, green: 3 h, red: 24 h, blue: isolated species after 3 weeks by crystallization).

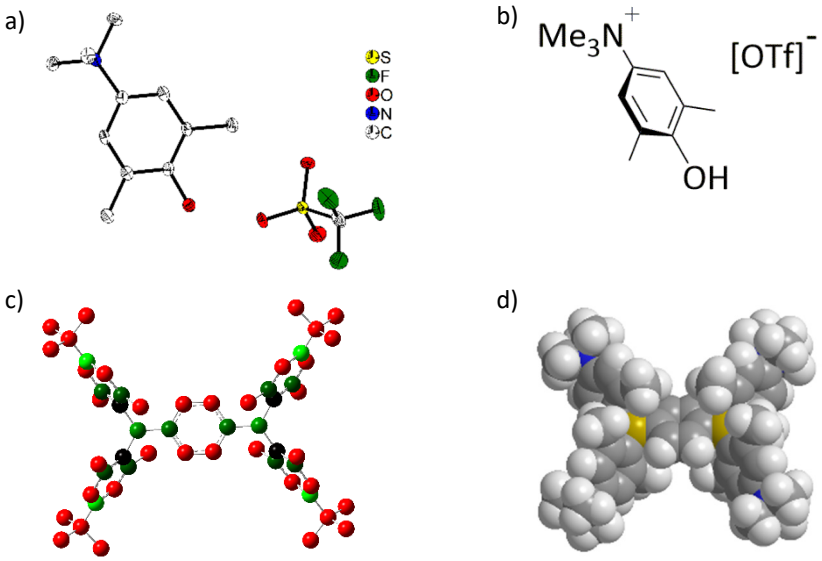

Figure 5-6. a) Molecular structure of the decomposition (hydrolysis) product of **5-1M** found in the crystals formed after 3 weeks in CD_3OD/H_2O (hydrogens are omitted for clarity and thermal ellipsoids are shown at 50% probability); b) Schematic drawing of the isolated decomposition product; c) Mulliken charges of the calculated structure of **5-1M** (CAM-B3LYP/6-31G(d)) in water (red: negative, black: 0, green: positive); d) Space filling model of the crystal structure of **5-1M** with Chem3D.

The stabilities of **5-1M** – **5-3M** and **2-3M** were examined *via* UV/Vis spectroscopy at lower concentrations (10^{-5} M) in water (Figure 5-7) than possible by NMR spectroscopy. It can be seen that compound **5-1M** started to decompose immediately, even before the compound was completely dissolved. This can be concluded from the raised baseline between 350 and 500 nm, due to scattered light from undissolved solid. The methylthiophene containing compound **5-2M**

is more stable, due to the additional methyl group at the 3-position of the thiophene ring and the electron-donating ability of methylthienyl moiety. It starts to decompose only after 4 h, but it is still not stable enough for cellular imaging. In contrast, compounds **5-3M** and **2-3M** showed no evidence of decomposition over 48 h. In aqueous solution, a xylene group or a substituent of similar steric demand, *e.g*. anthracene, is thus necessary to protect the boron atom from nucleophilic attack by water.

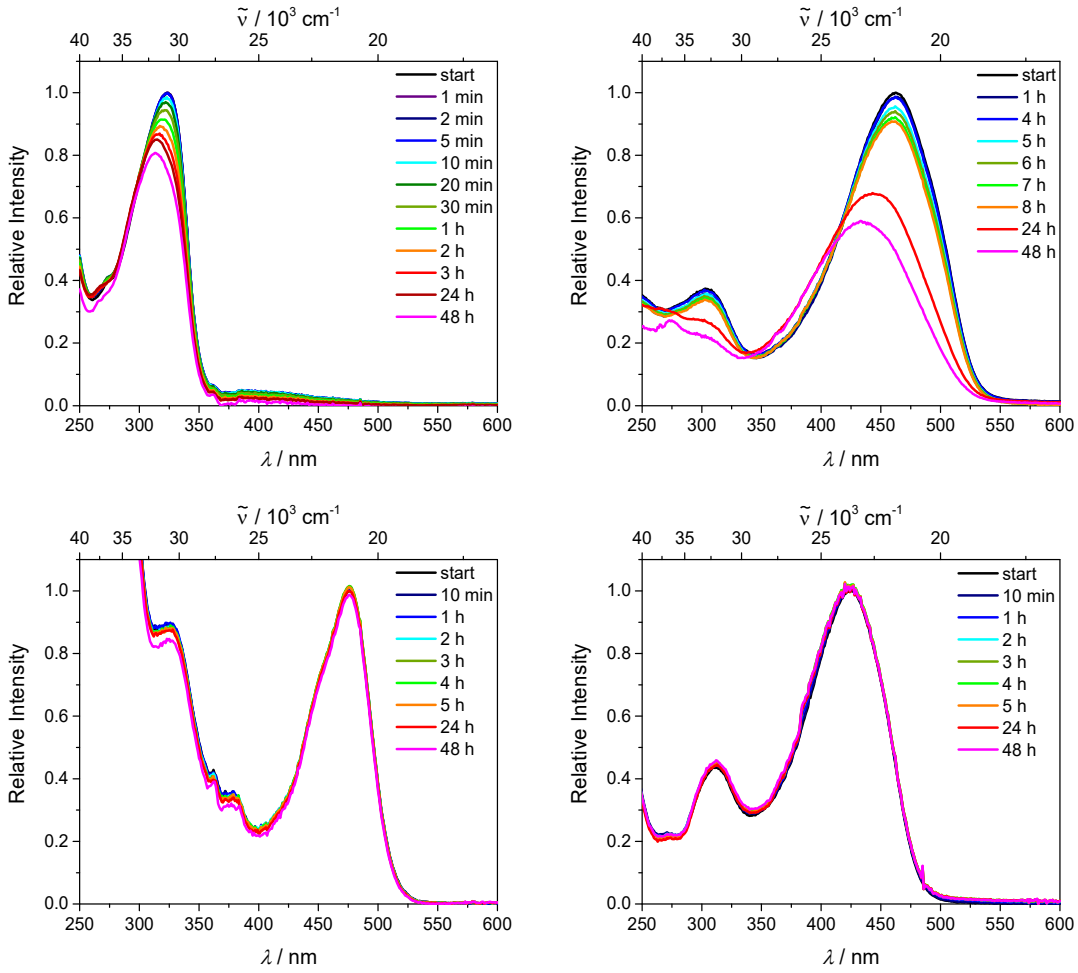

Figure 5-7. UV/Vis spectra of the relative intensities of compounds **5-1M** (top, left: OD at t = 0 min: 0.16), **5-2M** (top, right: OD at t = 0 min: 0.14), **5-3M** (bottom, left: OD at t = 0 min: 0.07) and **2-3M** (bottom, right: OD at t = 0 min: 0.10) over a 48 h time interval in water. Stock solutions with the same concentrations of **5-1M** – **5-3M** and **2-3M** could not be prepared, as the dilution takes time and an absorption spectrum at t = 0 min would not be possible.

5.2.5 Linear Optical Properties and TD-DFT Calculations

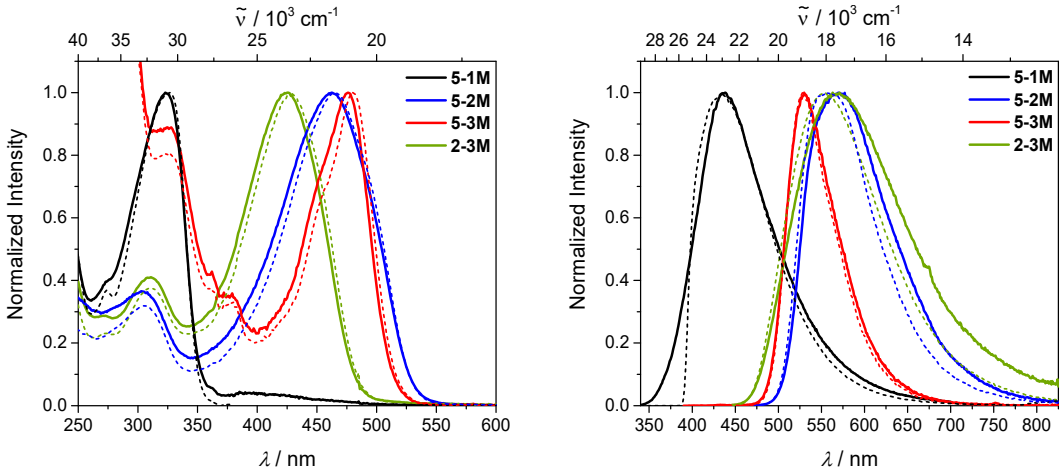

Figure 5-8. Absorption (left) and emission (right) spectra of compounds **5-1M** – **5-3M** and **2-3M** in water (solid) and MeCN (dashed).

Table 5-2. Photophysical data for compounds **5-1M** – **5-3M** and **2-3M** in water and MeCN.

	solvent	λ_{abs} / nm	ε / M^{-1} cm^{-1}	λ_{em} / nm	Stokes shift / cm^{-1}	Φ_f	τ / ns	k_r / 10^8 s	k_{nr} / 10^8 s
5-1M	MeCN	326	-[a]	434	7 600	-[a]	-[a]		
	H_2O	324		438	8 000	-[a]	-[a]		
5-2M	MeCN	464	47 000	558	3 600	0.27	0.44	6.1	16.6
	H_2O	463		570	4 100	0.21	0.64	3.3	13.4
5-3M	MeCN	481	14 000	528	1 900	0.82[b]	14.0	0.6	0.1
	H_2O	476		530	2 100	0.86[b]	14.9	0.6	0.1
2-3M	MeCN	428	51 000	554	5 300	0.41	1.9	2.2	3.1
	H_2O	425		563	5 800	0.10	0.3	3.3	30.0

[a] not measurable due to rapid decomposition; [b] excitation at 445 nm.

The absorption spectra of compounds **5-1M** – **5-3M** and **2-3M** were measured in water and MeCN (Figure 5-8). The absorption maximum of the phenyl compound **5-1M** occurs at 324 nm, while the other compounds **5-2M** – **5-4M** are much more red shifted, with λ_{max} occurring at 463, 476 and 425 nm, respectively (Table 5-2). The red shift in compounds **5-2M** and **5-4M**, results from the enhanced conjugation length between the two boron centers, and **5-3M**, due to its increased conjugation length in the direction perpendicular to the bridge. TD-DFT calculations (Table 5-3 and Figure 5-9) show that the $S_1 \leftarrow S_0$ transitions are allowed, and for **5-2M**, **5-3M** and **2-3M**, result from HOMO to LUMO excitation. The phenylene compound **5-1M** is an exception, as the $S_1 \leftarrow S_0$ transition involves mainly excitation from HOMO-2 to LUMO. The HOMO and HOMO-1 are located at the *para*-(*N*,*N*,*N*-trimethylammonio)xylyl groups and, therefore, the overlap with the LUMO is very small. In fact, the $S_6 \leftarrow S_0$ transition is mainly HOMO to LUMO and HOMO-1 to LUMO+1. The HOMO (HOMO-2 for **5-1M**) and LUMO are located at the π-bridge between the two boron atoms and the transitions are of π-π^* nature with a significant contribution from boron to the LUMO. The emission spectra of the four chromophores in water are depicted in Figure 5-8. Again, the phenylene compound **5-1M** has the most blue shifted

maximum at 438 nm, but the apparent Stokes shift of 8 000 cm^{-1} is the largest of all compounds. The methylthiophene and xylene derivatives **5-2M** and **2-3M** are similar to one another with emission maxima at 570 and 563 nm, respectively. The apparent Stokes shifts are smaller, being 4 100 and 5 800 cm^{-1}, respectively, compared to **5-1M**. The anthracene derivative **5-3M** has the smallest apparent Stokes shift of 2 100 cm^{-1} and an emission maximum at 530 nm. The mainly π-π* character of the transitions does not significantly alter the dipole moment and thus none of the compounds showed significant solvatochromism (Figure 5-8). As compound **5-1M** is not stable in water, fluorescence quantum yields and lifetimes were measured only for compounds **5-2M**, **5-3M** and **2-3M** (Table 5-2). The quantum yield of **2-3M** is a third of the one of **5-2M**, because the non-radiative decay rate is enhanced by a factor of more than two and the radiative decay rate is decreased by a third. The anthracene compound **5-3M** is outstanding compared to the other three dyes. The fluorescence quantum yield of 86% is extremely high in aqueous solution, and the fluorescence lifetime is very long (14.9 ns). These interesting properties result from the fact that the radiative decay rate is six times faster than the non-radiative one.

Table 5-3. TD-DFT-calculated photophysical data for the lowest energy transitions for **5-1M** – **5-4M** at the CAM-B3LYP/6-31G(d) level in water.

	transition (*f*)	*E* / eV[a]	λ / nm[a]	dominant components[b]
5-1M	$S_1 \leftarrow S_0$ (0.716)	4.15 (3.83)	299 (324)	LUMO←HOMO-2 (84%)
5-2M	$S_1 \leftarrow S_0$ (2.212)	2.68 (2.68)	463 (463)	LUMO←HOMO (88%)
5-3M	$S_1 \leftarrow S_0$ (0.333)	2.72 (2.60)	455 (476)	LUMO←HOMO (97%)
2-3M	$S_1 \leftarrow S_0$ (2.182)	2.97 (2.92)	417 (425)	LUMO←HOMO (78%)

[a] Values in parentheses are experimental absorption maxima in water; [b] Components with greater than 10% contribution shown. Percentage contribution approximated by $2 \times (c_i)^2 \times 100\%$, where c_i is the coefficient for the particular orbital rotation. Further details are provided in Tables 7-10, 7-29 – 7-31.

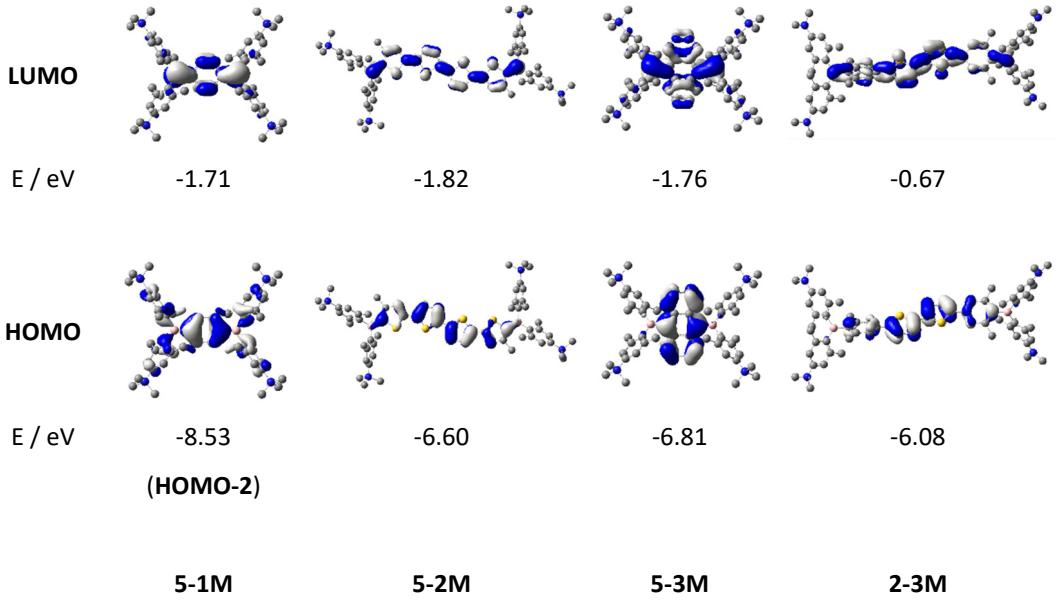

Figure 5-9. TD-DFT (CAM-B3LYP/6-31 G(d))-calculated frontier orbitals for **5-1M** – **5-3M** and **2-3M**. Hydrogen atoms were omitted for clarity. Surface isovalue: ± 0.03 [e a_0^{-3}]$^{1/2}$.

5.2.6 Cell Viability and Imaging

As the anthracene compound **5-3M** is stable in water and has excellent photophysical properties, *i.e.*, the most red shifted absorption band and an extremely high quantum yield, it was focused on this derivative for cell imaging experiments. First, cell viability was tested to investigate the potential of **5-3M** as a live-cell imaging chromophore. HeLa cells were treated with serial dilutions (0, 0.5, 1, 5, 10 μM) of **5-3M** and the cell metabolic activity was analyzed using a colorimetric (MTT) assay (Figure 5-10). This experiment confirmed that compound **5-3M** does not influence the cell viability at concentrations up to at least 5 μM after 24 h incubation time.

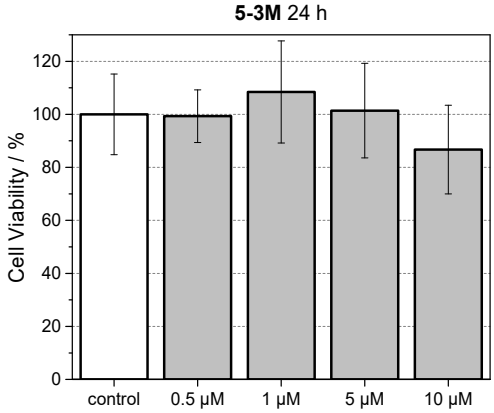

Figure 5-10. Cell viability of **5-3M** loaded HeLa cells determined by MTT assay. The cells were incubated with **5-3M** (0, 0.5, 1, 5, 10 μM) in DMEM containing 0.5% DMSO in a CO_2 incubator for 24 h. The results are expressed as percentages of the dye-free controls. All data are presented as mean standard deviation (n = 10).

Therefore, the tetracationic compound **5-3M** was used for live-cell imaging. HeLa cells were treated with a 5 μM solution of **5-3M** in culture medium DMEM and its cellular uptake was observed by visualization with a confocal laser scanning fluorescence microscope (Figure 5-11). Co-localization studies with the commercially available LysoTracker™ Red gave a very high Pearson value (R_r) of 0.86 indicative of the high degree of co-localization in the lysosomes.

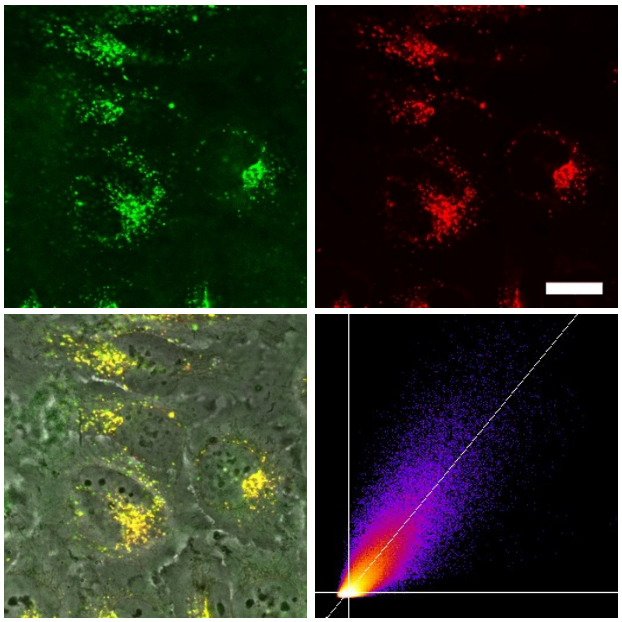

Figure 5-11. Co-staining experiment of HeLa cells with **5-3M** and LysoTracker™ Red. The cells were loaded with **5-3M** (5 μM, 1 h) and LysoTracker™ Red (0.1 μM, 20 min) at 37 °C. Fluorescence images of **5-3M** (top, left: λ_{ex} = 473 nm; λ_{em} = 490 – 540 nm) and LysoTracker™ Red (top, right: λ_{ex} = 559 nm; λ_{em} = 570 – 670 nm). The merged image of the bright field image and both fluorescence images (bottom, left) and the correlation plot of the intensities (bottom, right: R_r = 0.86) show excellent co-localization of the dye **5-3M** with LysoTracker™ Red in the lysosomes. Scale bar: 20 μm.

5.3 Conclusions

Four tetracationic quadrupolar compounds **5-1M** – **5-3M** and **2-3M**, with different conjugated linkers between the two boron moieties, were synthesized. These linkers, namely 1,4-phenylene, 2,2‴-(3,3‴-dimethyl)-5,2′:5′,2″:5″,5‴-quaterthiophene, 9,10-anthracenylene and 4,4‴-(5′-(3,5-dimethylphenyl))(5″-(3‴,5‴-dimethyl-phenyl))-2′,2″-bithiophene, have different steric demands, observable *via* increasing dihedral angles from crystal structure analyses, which are obviously correlated with the size of the linker. Furthermore, the steric demand of the linker was also observed by NMR spectroscopy, as the rotational barrier for the exchange of the enantiomers increases with the size of the arene. The smallest phenylene linker **5-1M** was unstable in CD_3OD containing traces of water at NMR concentrations. Compound **5-2M**, containing the slightly larger methylthiophene moiety, was found to be stable in the NMR study as well as being air- and moisture-stable on the bench for several months, while at the low concentrations employed for UV/Vis measurements (10^{-5} M), some decomposition after 4 h was observed in water. The other two compounds **5-3M** and **2-3M** are stable even at very low concentrations for at least two days. Therefore, the very strongly accepting, and thus Lewis acidic, dicationic boron moiety requires the substitution of both *ortho*-positions of the aryl linker, *e.g*. xylene and anthracene, to protect the boron-carbon bond from cleavage by water when the compounds are employed at micromolar concentrations. The stable anthracene compound **5-3M** exhibits impressive photophysical properties in water. A very red shifted

absorption band for its small size (476 nm) and a fluorescence quantum yield of 86% indicate that this dye is a very good candidate for live-cell imaging. Its low cytotoxicity and high selectivity for lysosomes proved this to be the case.

Chapter Six

-

Summary / Zusammenfassung

6 SUMMARY / ZUSAMMENFASSUNG

6.1 Summary

Efficient quadrupolar chromophores (A–π–A) with triarylborane moieties as acceptors have been studied by the Marder group regarding their non-linear optical properties and two-photon absorption ability for many years. Within the present work, this class of dyes found applications in live-cell imaging. Therefore, the dyes need to be water-soluble and water-stable in diluted aqueous solutions, which was examined in Chapter 2. Furthermore, the influence of the π-bridge on absorption and emission maxima, fluorescence quantum yields and especially the two-photon absorption properties of the chromophores was investigated in Chapter 3. In Chapter 4, a different strategy for the design of efficient two-photon excited fluorescence imaging dyes was explored using dipoles (D–A) and octupoles (DA_3). Finding the optimum balance between water-stability and π-conjugation and, therefore, red-shifted absorption and emission and high fluorescence quantum yields, was investigated in Chapter 5.

6.1.1 Chapter Two

Using the concept of Gabbaï and co-workers, the introduction of ammonio groups at the *para*-postion of a dixylylborane moiety, three quadrupolar compounds were synthesized, namely **2-1M** – **2-3M** (Scheme 6-1).

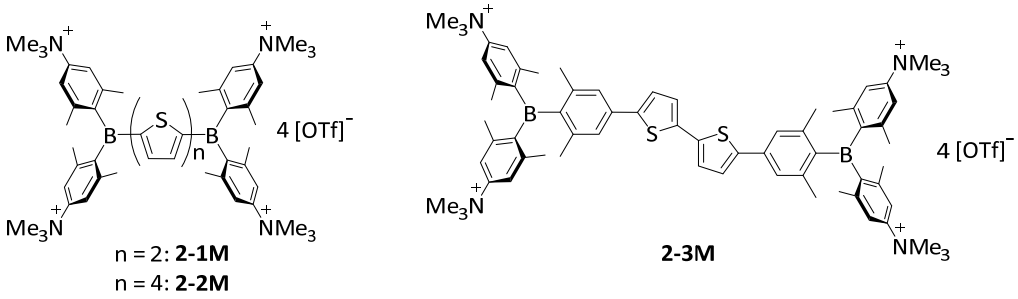

Scheme 6-1. Target Molecules **2-1M** – **2-3M**.

The three compounds bear four ammonio groups, each at the *para*-positions of the xylyl groups attached to the boron atoms. While in **2-1M** and **2-2M** the boron acceptor moiety is directly attached to the thiophene, in **2-3M** additional xylyl rings are incorporated for increased steric protection of the boron atom. All compounds are water-soluble, but the two compounds **2-1M** and **2-2M** without the additional protection are not stable in dilute aqueous solution. They decompose in water with half-lives of 4.4 and 2.1 h, respectively (Figure 6-1). Light and oxygen enhance the rate of hydrolysis of **2-1M** and **2-2M**.

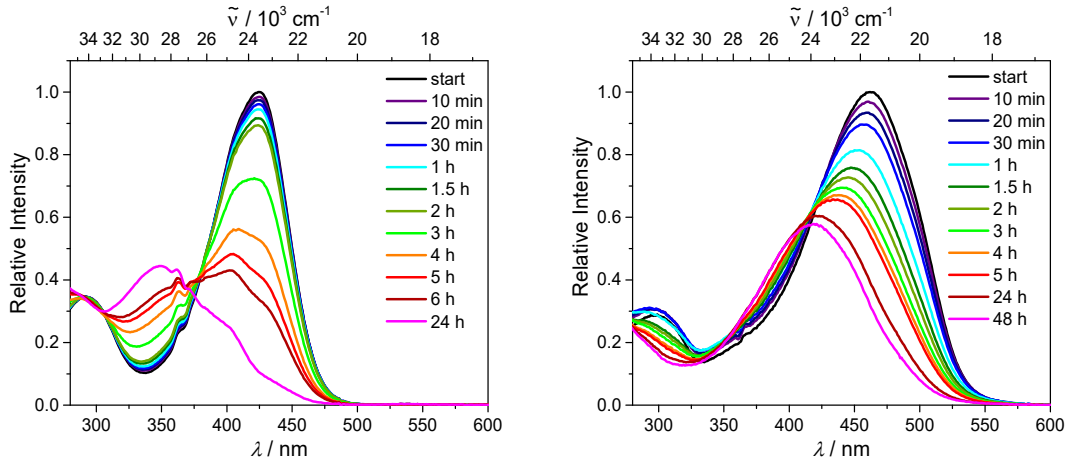

Figure 6-1. Absorption spectra of **2-1M** (left) and **2-2M** (right) in H_2O as a function of time. Sample kept in the dark between measurements.

The additional xylyl group at the boron atom leads to adequate steric protection resulting in a stable compound in aqueous solution (Figure 6-2).

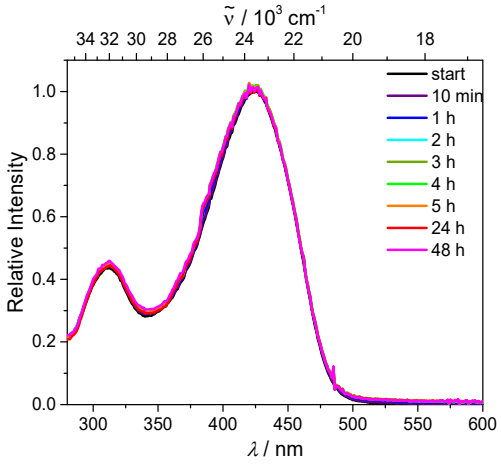

Figure 6-2. Absorption spectra of **2-3M** in H_2O as a function of time. Sample kept in the dark between measurements.

While the elongation of the π-bridge by two thiophenes (**2-1M** to **2-2M**) leads to a red-shifted absorption and emission, the quantum yield is constant at 0.20 in water. The incorporation of the xylyl groups into **2-1M** does not shift the absorption maxima at all, and shifts the emission maxima only slightly to the red. The fluorescence quantum yield is also decreased to 10%. This may be due to less π-conjugation between the two boron acceptors, as the xylyl groups twist out of the BC_3 plane. This was confirmed by TD-DFT calculations and optimization of the B-attached linker moiety is described in Chapter 5.

However, the first water-soluble and water-stable quadrupolar triarylborane dye was synthesized and its TPEF imaging applicability was investigated. Due to its centrosymmetric geometry, the dye **2-3M** exhibits strong two-photon absorption at 800 nm for the $S_2 \leftarrow S_0$ transition, but only weakly at 870 nm for the $S_1 \leftarrow S_0$ transition. The compound exhibits a TPA

cross-section of 693 GM in MeCN, which is very high. Furthermore, the cytotoxicity of the dye was tested. Three different cell lines, were exposed to serial dilutions of **2-3M** which confirmed that **2-3M** does not influence the cell viability at concentrations as high as 10 μM. Therefore, NIH 3T3 cells were treated with the dye, and confocal laser scanning fluorescence microscopy showed a localization of the dye within the cells. The dye co-localized with the commercially available mitochondrial imaging agent MitoTracker™ Red CMXRos. Given the above-mentioned successful tests, the dye was used for two-photon excited fluorescence imaging in POS 1 cells (Figure 6-3).

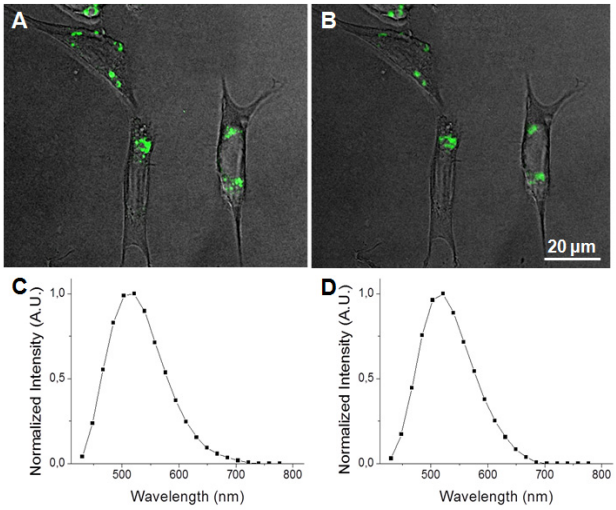

Figure 6-3. Confocal microscope image of POS 1 cells after 8 h of incubation with dye **2-3M** (300 nM in the media): merge of transmission image (grey) and fluorescence image (green) showing the internalization of the dye within the cells: (A) one-photon excitation (λ_{ex} = 405 nm; λ_{em} = 500-600 nm) and (B) two-photon excitation (λ_{ex} = 800 nm; λ_{em} = 500-600 nm); (C) emission spectrum upon one-photon excitation (λ_{ex} = 405 nm; 20 nm step) of the dye within the cell; (D) emission spectrum upon two-photon excitation (λ_{ex} = 800 nm; 20 nm step) of the dye within the cell.

6.1.2 Chapter Three

In this chapter of the thesis, the very encouraging previous results obtained for compound **2-3M** were further improved upon investigation of the nature of the π-bridge. The bithiophene unit was exchanged for 4,4'-biphenylene, 2,7-pyrene, 2,7-fluorene, 3,6-carbazole and 5,5'-di(thien-2-yl)-3,6-diketopyrrolo-pyrrole (Scheme 6-2) moieties. The new tetracationic compounds are water-soluble (**3-2M** only with the addition of 10% MeCN) and, due to the additional xylyl group, they are stable even in dilute aqueous solution.

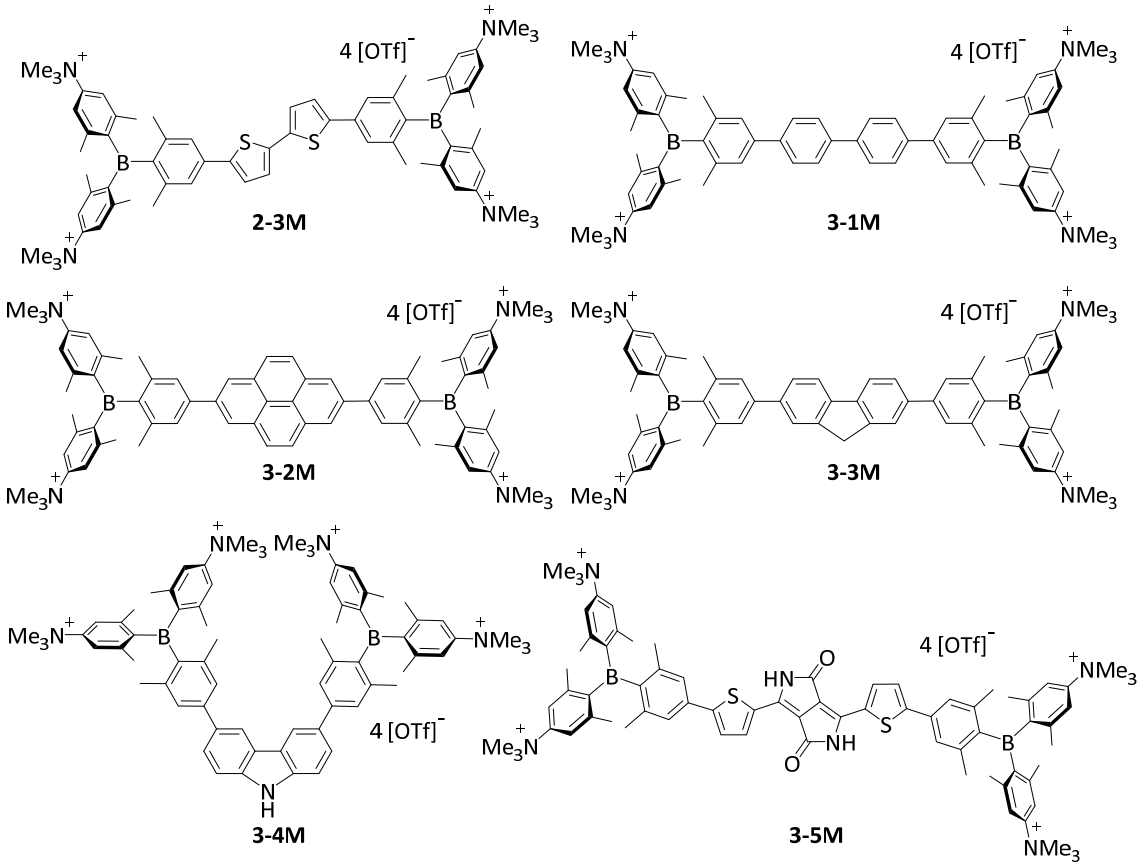

Scheme 6-2. Quadrupolar chromophores for TPEF imaging **2-3M**, **3-1M** – **3-5M**.

Changing the π-bridge influences the absorption and emission spectra enormously, as the lowest energy transitions are mainly of π-π* nature and located on the π-bridge. Therefore, depending on the π-bridge, the emission color can be tuned from blue to pink, and follows the trend of the HOMO energy, as the LUMO energy stays nearly constant (except for **3-5M**). The compounds are not solvatochromic, which further proves the π-π* nature of the transitions. Apart from **3-4M**, all compounds show remarkably high fluorescence quantum yields in aqueous solutions.

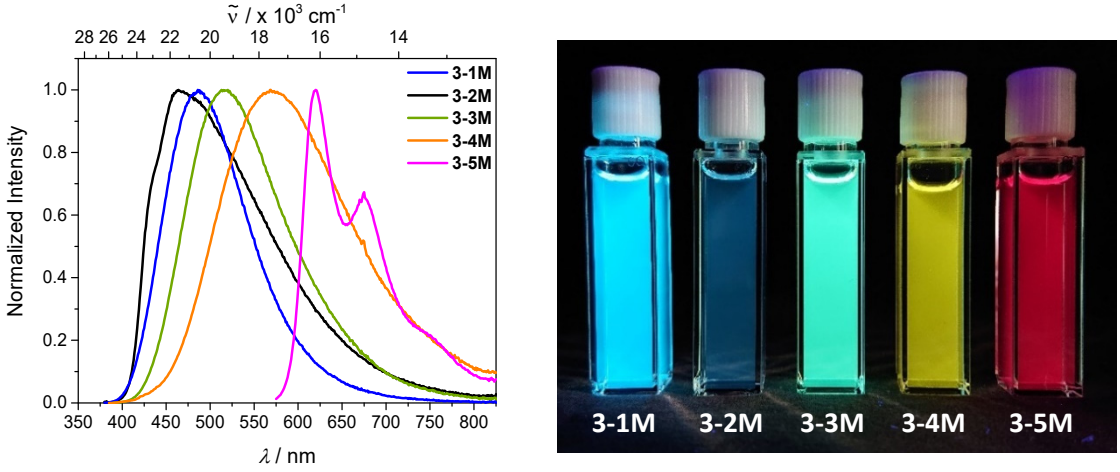

Figure 6-4. Emission spectra (left) of **3-1M** – **3-5M** in water. Compound **3-2M** was dissolved in 10% MeCN in water. Picture of the solutions (right) of **3-1M** – **3-5M** in MeCN under UV irradiation.

As known for quadrupolar (A–π–A) compounds, the π-bridge has an enormous effect on the two-photon absorption cross-section. Following the electronic selection rules for centrosymmetric molecules, **3-1M**, **3-2M** and **3-5M**, the TPA maximum does not occur at the one-photon absorption maximum, as the $S_1 \leftarrow S_0$ transition ($A_u \leftarrow A_g$ symmetry) is symmetry forbidden for two-photon absorption, but is located at higher energy where TPA allowed transitions of $A_g \leftarrow A_g$ symmetry occur ($S_2 \leftarrow S_0$ transition for **3-1M** and **3-5M** and $S_3 \leftarrow S_0$ transition for **3-2M**). The other two molecules, **3-3M** and **3-4M**, have C_{2v} as their highest possible symmetry, and thus do not have an inversion center, which is why all transitions are one- and two-photon allowed. As expected, the biphenyl compound **3-1M** has the smallest TPA cross-section of 72 GM, as this compound is the most twisted in its ground state structure (Figure 6-5). With increasing planarity, **3-2M** – **3-4M**, in which the two phenyl rings are linked by incorporation into the pyrene, fluorene or carbazole moieties, the two-photon cross-section is increased to 79, 162, and 134 GM, respectively. Furthermore, increasing intramolecular charge transfer enhances the two-photon absorption cross-section. [109b, 109d, 146] It is known that A–π–D–π–A systems are more efficient than A–π–A systems. [109b, 109d, 146] The donor-strength of the π-bridge can be correlated with the HOMO energy, therefore, the two-photon cross-section should be enhanced from pyrene **3-2M**, to fluorene **3-3M** to carbazole **3-4M**. The latter compound **3-4M**, however, has a shorter conjugation length than **3-3M**, and the effect of the reduced conjugation lowers the TPA cross-section. The dithienyl-diketopyrrolopyrrole compound **3-5M** has by far the highest two-photon absorption value, being 4 560 GM. Its conjugated π-system is elongated, and the calculated ground state structure is almost planar.

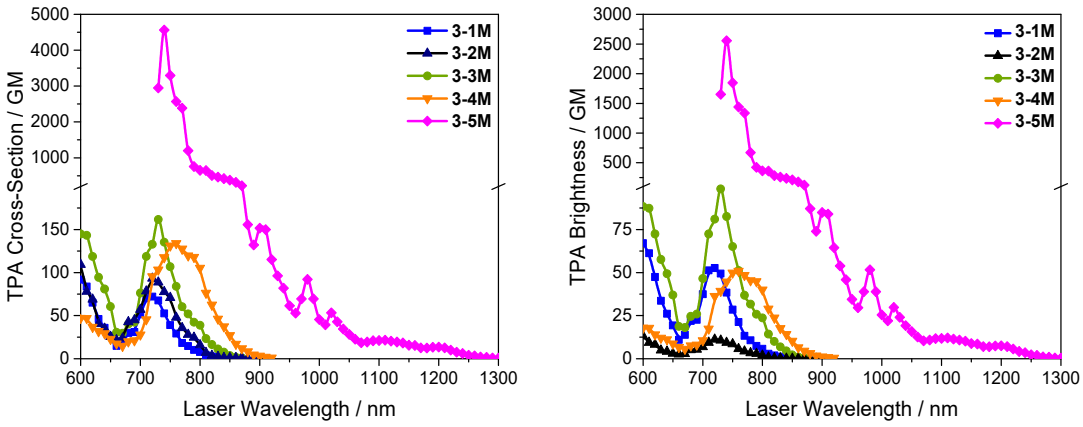

Figure 6-5. Two-photon absorption spectra (left) and two-photon brightness (right) of **3-1M** – **3-5M** in MeCN.

The cytotoxicity of the methylated compounds **3-1M** – **3-5M** were investigated by cell viability studies which confirmed that the compounds are non-toxic to the cells at concentrations as high as 5 μM after a 24 h incubation time. Therefore, the dyes were used for confocal laser scanning

fluorescence microscopy, which demonstrated the cellular uptake for all of them. Co-staining experiments confirmed their localization in acidic intracellular compartments, such as lysosomes (Figure 6-6). As the dithienyl-diketopyrrolopyrrole dye **3-5M** has the most red-shifted absorption and emission bands and, by far, the highest TPA cross-section and brightness, further imaging experiments were done using this compound.

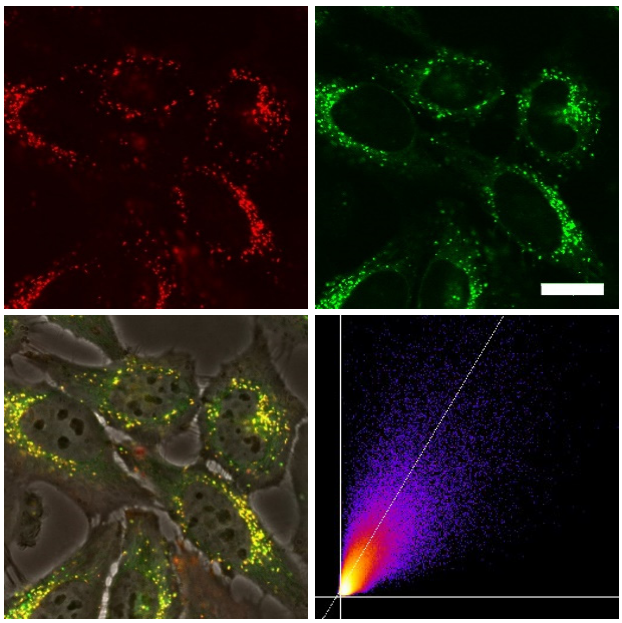

Figure 6-6. Co-staining experiment of HeLa cells with **3-5M** and LysoTracker™ Green. The cells were loaded with **3-5M** (500 nM, 2 h) and LysoTracker™ Green (100 nM, 20 min) under 5% CO_2 at 37 °C. Fluorescence images of **3-5M** (top, left: λ_{ex} = 559 nm; λ_{em} = 570 – 670 nm) and LysoTracker™ Green (top, right: λ_{ex} = 473 nm; λ_{em} = 490 – 540 nm). The merged image of the bright field image and both fluorescence images (bottom, left), and the correlation plot of the intensities (bottom, right: R_r = 0.81), show co-localization of the dye **3-5M** in the lysosomes. Scale bar: 20 μm.

The process for cell internalization of the dye **3-5M** was observed *via* time-lapse imaging over 2 h, indicating the endocytosis mechanism. The proof of this mechanism was achieved by staining the cells at 4 °C, or at 37 °C in the presence of 0.1% NaN_3, as both conditions inhibit endocytosis. Indeed, both experiments showed much lower fluorescence intensity in comparison to the control experiment. Furthermore, the photostability of the dye **3-5M** was tested by repetitive imaging of HeLa cells after staining. Over 95% of the initial fluorescence intensity was retained after irradiation with an excitation laser at 561 nm for 50 images, while the commercially available LysoTracker™ Red showed 45% decrease in emission intensity under the same conditions. Furthermore, due to the outstanding two-photon brightness of **3-5M**, the chromophore was applied for two-photon excited fluorescence imaging.

6.1.3 Chapter Four

As dipoles and octupoles are also known to be efficient design motifs for TPA chromophores, both were studied in this chapter. As triphenylamine is an efficient core for cooperative TPA enhancement, this moiety was used as the donor. The dicationic triarylborane discussed in the

previous chapters was used as the acceptor moiety, resulting in a dipole (**4-1M**) and an octupole (**4-2M**). Furthermore, the neutral precursors **4-1** and **4-2** were studied.

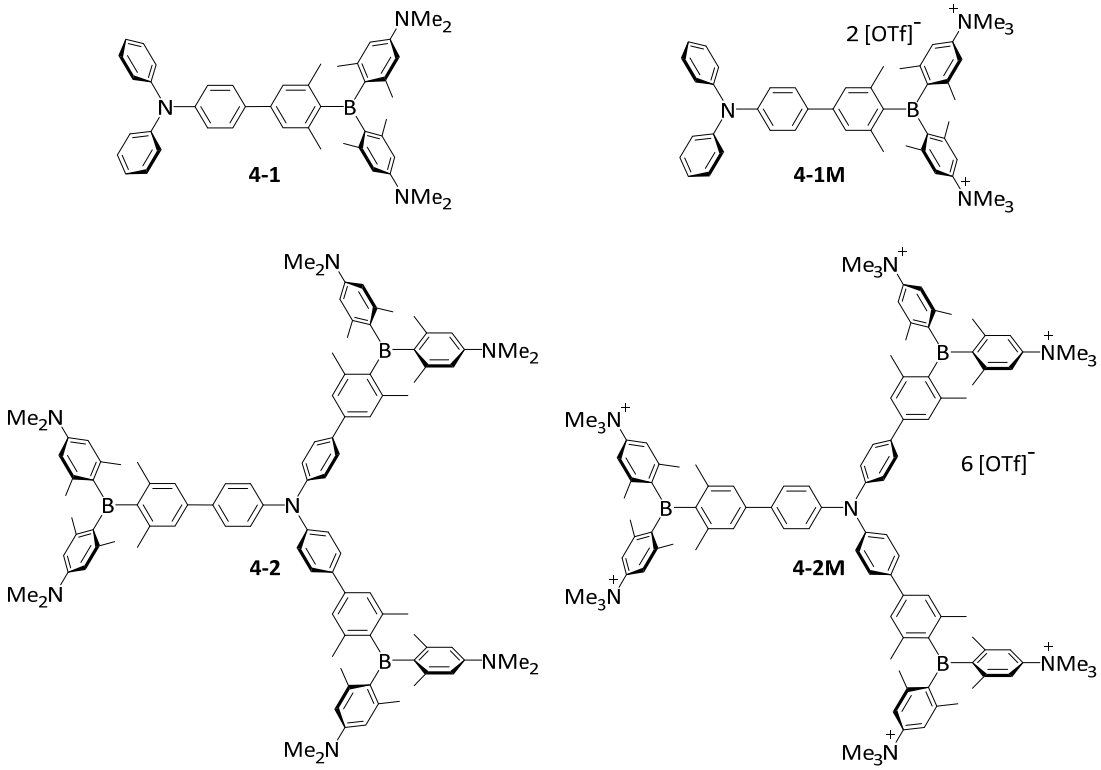

Scheme 6-3. Target molecules **4-1**, **4-2**, **4-1M** and **4-2M**.

In those neutral precursors, the triphenylamine does not play a role in the low energy optical transitions. The dominant charge transfer is always from the dimethylamine group to the boron moiety at the periphery of the molecules. Therefore, the photophysical properties of **4-1** and **4-2** are similar and the branching has no effect on the absorption and emission maximum, and an additive effect on the extinction coefficient.

Upon methylation, charge transfer between the dimethylamine and the boron center is no longer possible and, furthermore, the acceptor strength of the boron moiety is increased due to the inductive effect of the cationic trimethylammonio group. Therefore, the long-range charge transfer from the triphenylamine to the cationic boron moiety becomes the dominant transition. While the lowest energy absorption band is hypsochromically shifted with increasing solvent polarity, the emission maximum is bathochromically shifted (Figure 6-7). The reversed solvatochromism for absorption and emission was previously observed by Lambert and co-workers and results from an inversion of the dipole moment upon excitation.[19] Furthermore, the absorption band of **4-2M** is shifted by 704 cm^{-1} compared to that of **4-1M**, as a result of the coupling of the three branches in **4-2M**. From the exciton coupling model (Figure 6-8), a coupling constant *V* of 0.09 eV was calculated from the experimental absorption spectra.

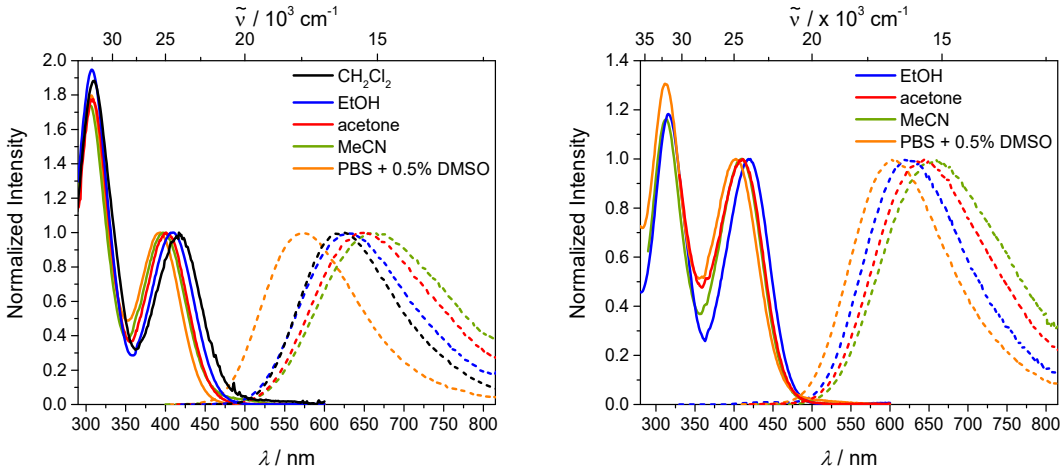

Figure 6-7. Absorption and emission spectra of **4-1M** (left) and **4-2M** (right) in various solvents (dichloromethane: black, ethanol: blue, acetone: red, MeCN: green, PBS + 0.5% DMSO: orange).

TD-DFT calculations also showed the contribution of the triphenylamine and, therefore, coupling of the three branches. Because of the C_3 symmetry, the excited states S_1 and S_2 are degenerate, stabilized by the coupling constant V and the excitation from the S_0 is allowed (E symmetry, f = 1.407), while the S_3 is destabilized by $2V$ and is forbidden (A symmetry, f = 0.000). From the exciton coupling model, a coupling constant V of 0.09 eV was calculated, being one third of the energy difference between the TD-DFT computed E and A symmetry excited states. This is exactly the same value as obtained from the experimental shift in the UV/Vis spectra. As the molecule is solvatochromic, it must possess a dipole moment. This is caused by symmetry breaking, as **4-2M** does not have ideal C_3 symmetry, but only C_1 symmetry.

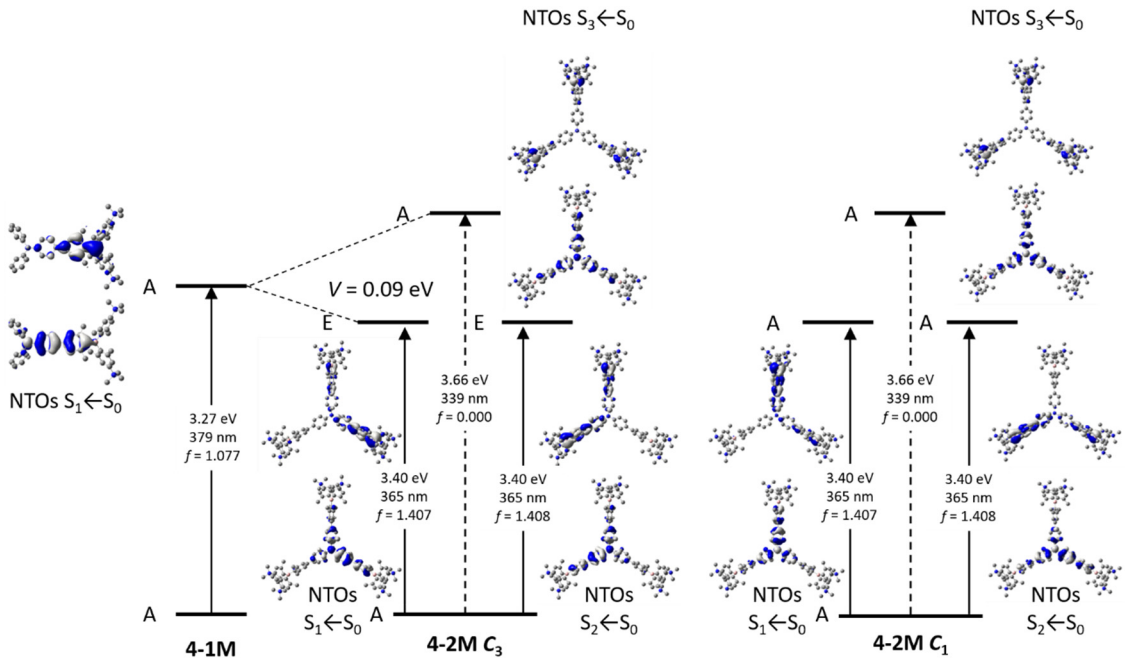

Figure 6-8. Excited state splitting of **4-1M** with respect to **4-2M**. The natural transition orbitals (NTOs) of S_1←S_0, S_2←S_0 and S_3←S_0 are depicted from TD-DFT calculations in the gas phase.

The two-photon absorption spectra of both cationic dyes **4-1M** and **4-2M** were measured in MeCN. While for **4-1M** the TPA maximum occurs at double the wavelength of the OPA maximum, the maximum of the TPA spectrum of **4-2M** is clearly blue shifted. This is because the two-photon absorption results from the $S_3 \leftarrow S_0$ transition (A←A symmetry), as excitations to S_1 and S_2 are symmetry forbidden (E symmetry). The TPA cross-section of the dipolar chromophore **4-1M** is 91 GM in MeCN, which increases upon branching to 335 GM (**4-2M**).

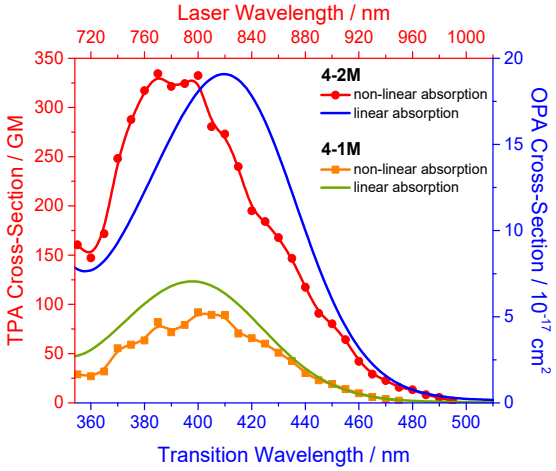

Figure 6-9. One-photon absorption spectra of **4-1M** (green) and **4-2M** (blue) and two-photon absorption spectra of **4-1M** (orange) and **4-2M** (red) in MeCN.

Staining HeLa cells with both dyes **4-1M** and **4-2M** gave quite different responses. The octupolar chromophore is less toxic after 24 h incubation time and is much more selective for lysosomal staining. The dipolar chromophore also localizes in the mitochondria as indicated by the fiber-like structures observed in the microscope image. This may be ascribed to three factors, the increasing number of cationic groups, the more hydrophilic character, and the larger size of compound **4-2M**.

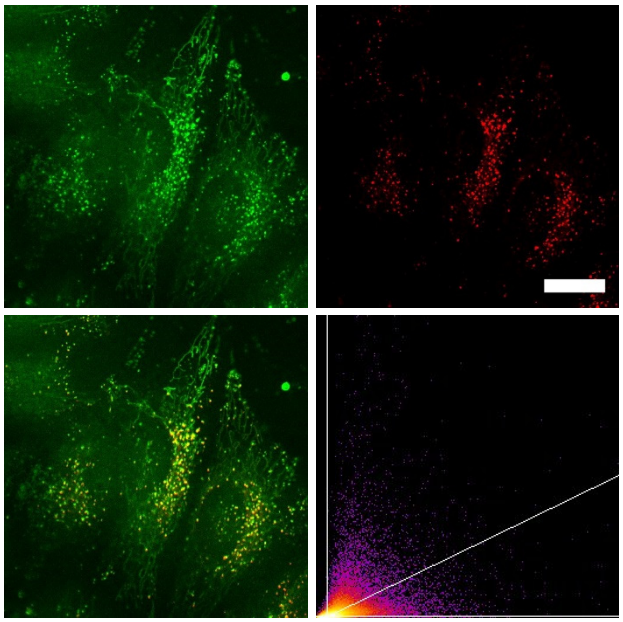

Figure 6-10. Co-staining experiment of HeLa cells with **4-1M** and LysoTracker™ Red. The cells were loaded with **4-1M** (0.5 μM, 2 h) and LysoTracker™ Red (0.1 μM, 20 min) at 37 °C. Fluorescence images of **4-1M** (top, left: λ_{ex} = 405 nm; λ_{em} = 500 – 605 nm) and LysoTracker™ Red (top, right: λ_{ex} = 561 nm; λ_{em} = 607 – 786 nm). The merged fluorescence images (bottom, left) and the correlation plot of the intensities (bottom, right: R_r = 0.48), show a modest degree of co-localization of the dye **4-1M** in lysosomes. Scale bar: 20 μm.

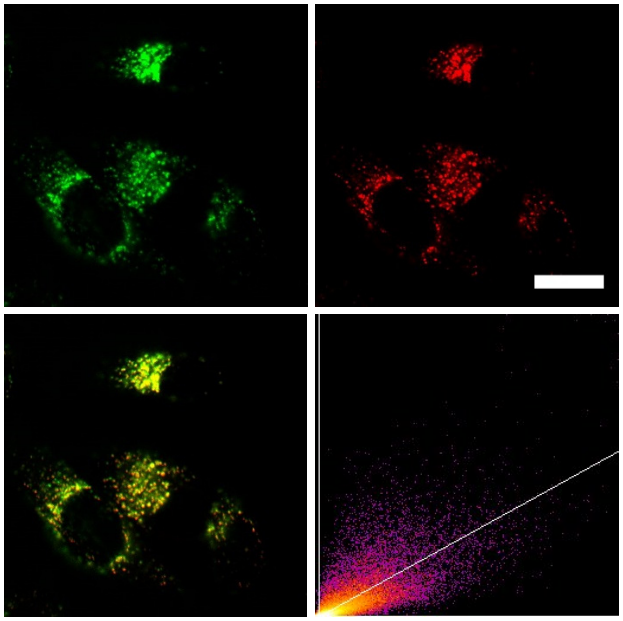

Figure 6-11. Co-staining experiment of HeLa cells with **4-2M** and LysoTracker™ Red. The cells were loaded with **4-2M** (0.5 μM, 2 h) and LysoTracker™ Red (0.1 μM, 20 min) at 37 °C. Fluorescence images of **4-2M** (top, left: λ_{ex} = 405 nm; λ_{em} = 500 – 605 nm) and LysoTracker™ Red (top, right: λ_{ex} = 561 nm; λ_{em} = 607 – 786 nm). The merged fluorescence images (bottom, left) and the correlation plot of the intensities (bottom, right: R_r = 0.81), show good co-localization of the dye **4-2M** in lysosomes. Scale bar: 20 μm.

6.1.4 Chapter Five

The last part of this thesis contains the investigation of the stability of various triarylboranes in dilute aqueous solution. The design of these dyes is based on a quadrupolar structure (A–π–A), which was already discussed in Chapters 2 and 3. Therefore, 1,4-phenylene (**5-1M**), 2,2‴-(3,3‴-dimethyl)-5,2′:5′,2″:5″,5‴-quaterthiophene (**5-2M**), 9,10-anthracenylene (**5-3M**) and 4,4‴-(5′-

(3,5-dimethylphenyl))(5''-(3''',5'''-dimethylphenyl))-2',2''-bithiophene (**2-3M**) were explored as linkers of the (*para*-(*N*,*N*,*N*-trimethylammonio)xylyl)$_2$B–(linker)–B(*para*-(*N*,*N*,*N*-trimethyl-ammonio)xylyl)$_2$ motif.

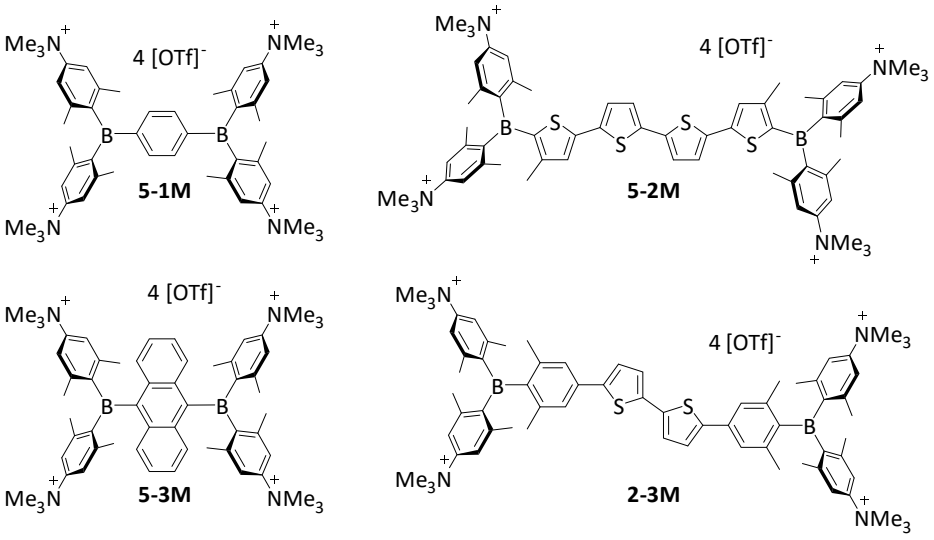

Scheme 6-4. Target molecules **5-1M** – **5-3M** and **2-3M**.

The different steric demands of the four aryl linkers are evident from the corresponding crystal structures of the neutral analogues **5-1**, **5-5**, **5-3** and **2-6** (Figure 6-12). The compounds with the smaller phenyl and methylthienyl rings exhibit twists of the aryl ring of 27° and 39° for **5-1** and 35° for **5-5** with respect to the BC_3 plane. For the sterically more demanding anthracenyl and xylyl moieties, the twist angle of the aryl linker with respect to the BC_3 plane nearly doubles to 64° (**5-3**) and 59° (**2-6**).

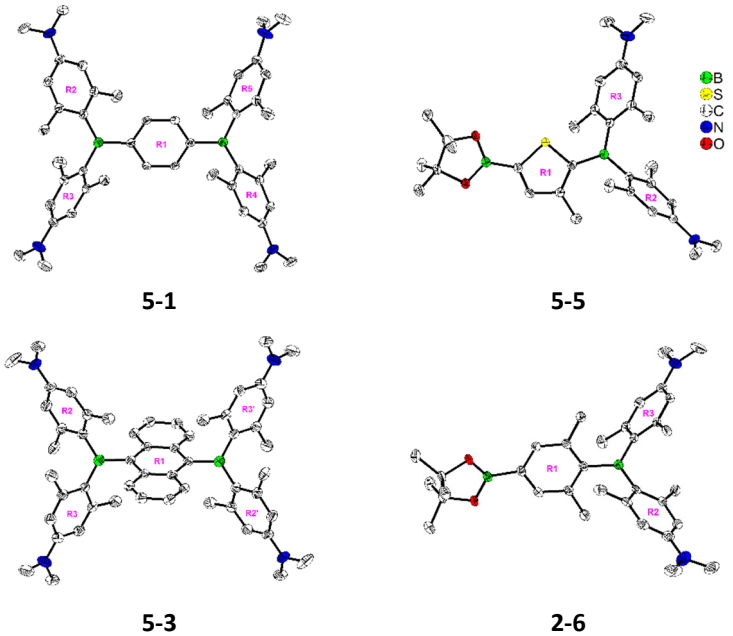

Figure 6-12. Solid state molecular structures of **5-1**, **5-5**, **5-3** and **2-6**[119] from single-crystal X-ray diffraction at 100 K. Atomic displacement ellipsoids are drawn at the 50% probability level, and H atoms are omitted for clarity. With regards to the aryl rings bonded to boron atoms, the central ring is labelled R1 and the terminal rings are labelled R2 and R3 if bonded to B1 and R4 and R5 if bonded to B2, respectively.

This trend was confirmed to be the case in solution by measuring the magnitude of the rotational barriers by NMR spectroscopy. The NMR signals of the *ortho*-methyl groups of the *para*-(*N*,*N*-dimethylamino)xylyl rings broaden and decoalescence with decreasing temperature, due to the slower stereoisomerization of the triarylboranes. The rotational barriers (Figure 6-13) increase with increasing steric demand of the linker in the order 1,4-phenylene **5-1** < 2,2‴-(3,3‴-dimethyl)-5,2′:5′,2″:5″,5‴-quaterthiophene **5-2** < 9,10-anthracenylene **5-3** < 4,4‴-(5′-(3,5-dimethylphenyl))(5″-(3‴,5‴-dimethylphenyl))-2′,2″-bithiophene **2-3**. The lack of decoalescence of the signals for **5-1** even at 183 K suggest strongly that the rotational barrier of **5-1** must be smaller than 11.0 kcal/mol.

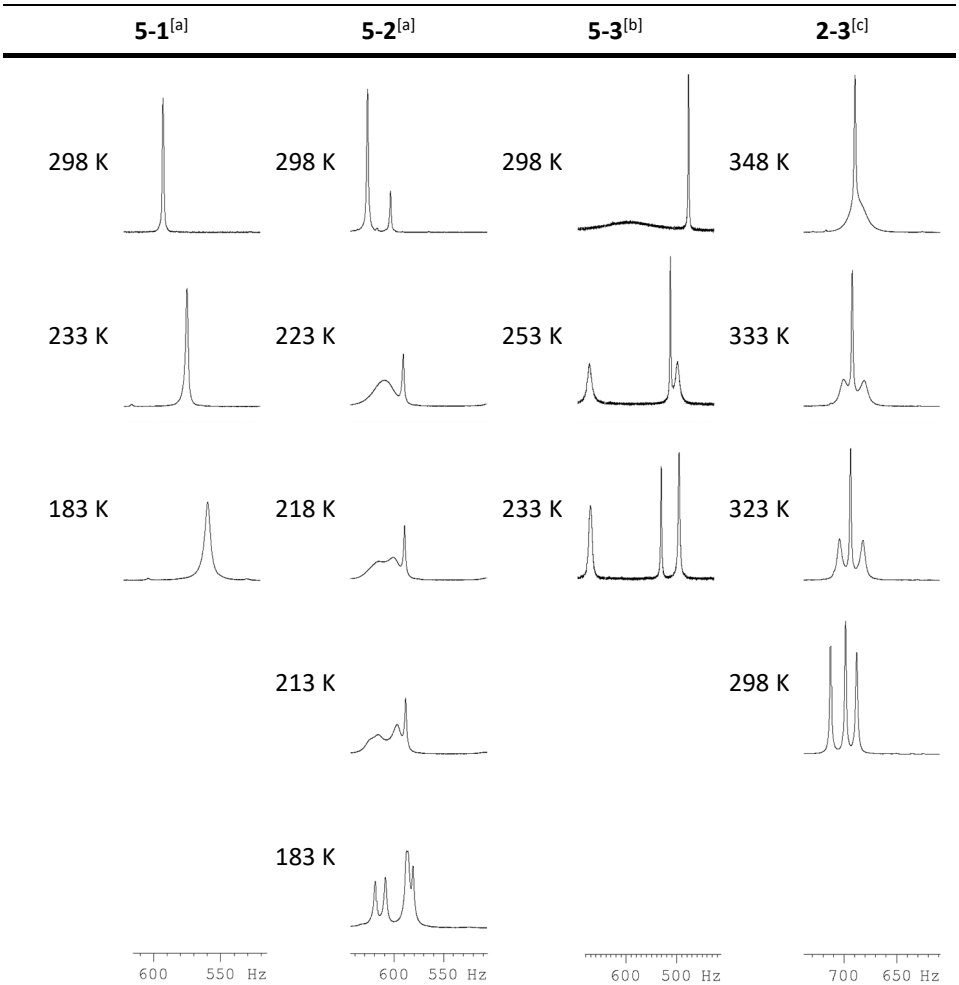

[a] measured in CD_2Cl_2; [b] measured in $CDCl_3$; [c] measured in C_6D_6.

Figure 6-13. ^{1}H NMR spectra of the methyl resonance of the compounds **5-1** – **5-3** and **2-3** at various temperatures at 300 MHz.

While all neutral compounds **5-1** – **5-3** and **2-3** are air- and moisture-stable in the solid-state and in solution, they are not soluble in water. The methylated derivatives **5-1M** – **5-3M** and **2-3M** exhibit different stabilities in aqueous solution, depending on the steric hindrance of the aryl linker substituent. At NMR concentrations, aqueous solutions of **5-2M**, **5-3M** and **2-3M** appear

to be stable over a period of days, while **5-1M**, with the smallest aryl substituent, namely phenylene, shows evidence of decomposition as determined by NMR spectroscopy. *Via* UV/Vis spectroscopy, the stabilities of **5-1M** – **5-3M** and **2-3M** were examined at lower concentrations (10^{-5} M) in water (Figure 6-14) than is possible by NMR spectroscopy.

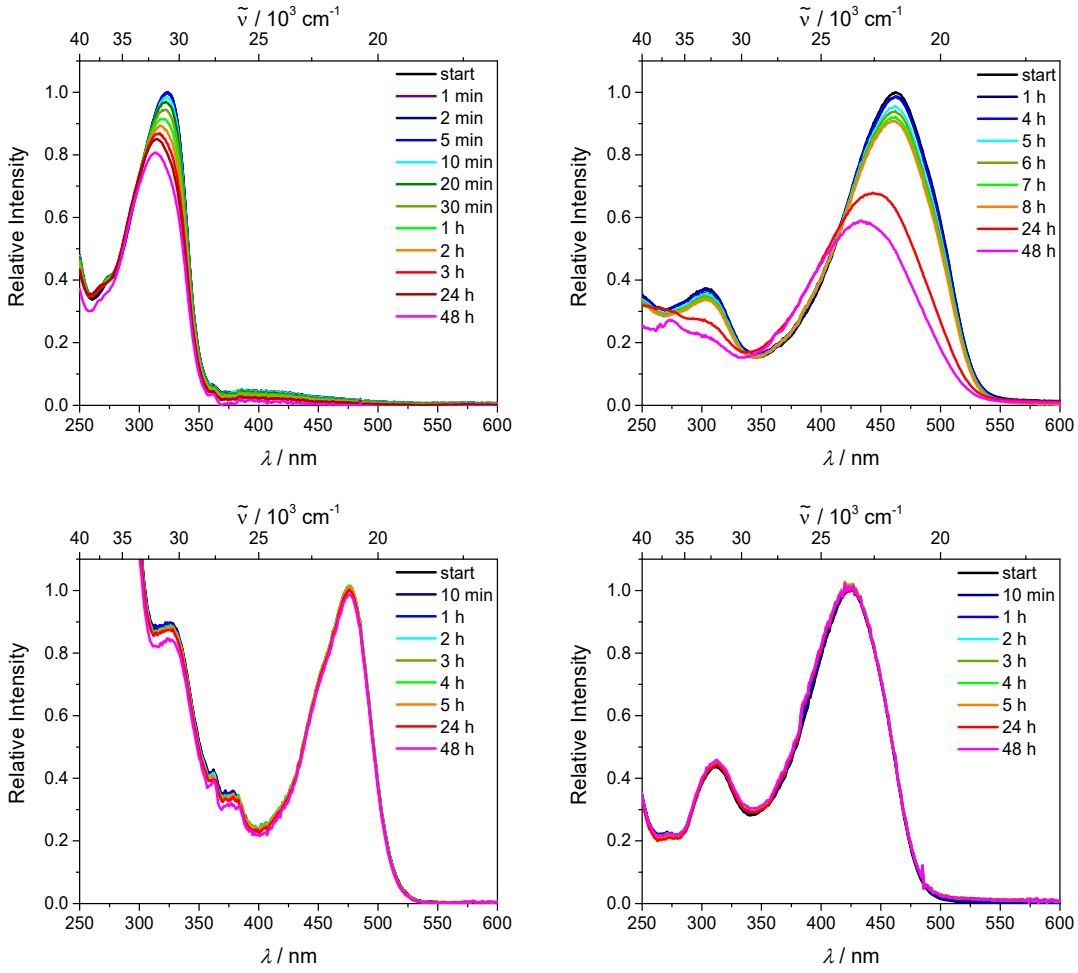

Figure 6-14. UV/Vis spectra of the relative intensities of compounds **5-1M** (top, left: OD at t = 0 min: 0.16), **5-2M** (top, right: OD at t = 0 min: 0.14), **5-3M** (bottom, left: OD at t = 0 min: 0.07) and **2-3M** (bottom, right: OD at t = 0 min: 0.10) over a 48 h time interval in water. Stock solutions with the same concentration of **5-1M** – **5-3M** and **2-3M** could not be prepared, as the dilution costs time and an absorption spectrum at t = 0 min would not be possible.

Compound **5-1M** started to decompose immediately, while the methylthiophene-containing compound **5-2M** is more stable, due to the additional methyl group at the 3-position of the thiophene ring and the electron-donating ability of methylthienyl-moiety. It starts to decompose only after 4 h, but it is still not stable enough for cellular imaging. In contrast, compounds **5-3M** and **2-3M** showed no evidence of decomposition over 48 h. In aqueous solution, a xylene group or a substituent of similar steric demand, *e.g*. anthracene, is thus necessary to protect the boron atom from nucleophilic attack by water.

Regarding their photophysical properties, the absorption maximum of **5-3M** is red-shifted compared to the other dyes, due to its increased conjugation length in the direction

perpendicular to the bridge (Figure 6-15). Due to the small reorganization energy in the exited state, the Stokes shift (2 100 cm^{-1}) of **5-3M** is very small and, therefore, the emission maximum is slightly hypsochromic shifted compared to **5-2M** and **2-3M**. However, the non-radiative decay rate is negligibly small in water, which is why the anthracene dye **5-3M** gives an exceptional high fluorescence quantum yield of 0.86 in water.

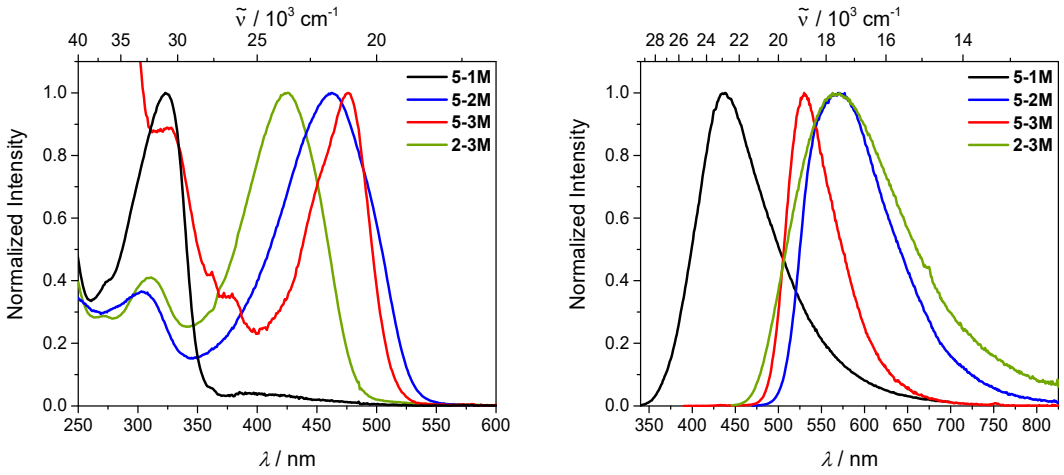

Figure 6-15. Absorption (left) and emission (right) spectra of compounds **5-1M** – **5-3M** and **2-3M** in water.

As the anthracene compound **5-3M** is stable in water and has excellent photophysical properties, *i.e.*, the most red shifted absorption band and an extremely high quantum yield, cell imaging experiments were conducted with this dye. Compound **5-3M** shows no cytotoxicity in HeLa cells at a concentration of 5 μM after 24 h. Furthermore, cellular uptake of **5-3M** was observed by confocal laser scanning fluorescence microscopy and localization in the lysosomes was confirmed by its co-localization with the commercially available LysoTracker™ Red.

6.2 Zusammenfassung

Effiziente quadrupole Farbstoffe (A–π–A) mit Triarylboraneinheiten als Akzeptoren wurden innerhalb der letzten Jahre von der Arbeitsgruppe Marder bezüglich ihrer nicht-linearen optischen Eigenschaften und Zweiphotonenabsorptionsfähigkeiten untersucht. In der vorliegenden Arbeit wurde diese Farbstoffklasse zur Untersuchung lebender Zellen mittels Fluoreszenzmikroskopie angewendet. Hierzu müssen die Farbstoffe wasserlöslich und in verdünnten wässrigen Lösungen stabil sein. Dies wurde in Kapitel 2 untersucht. Außerdem wurde der Einfluss der π-Brücke auf das Absorptions- und Emissionsmaximum, die Fluoreszenzquantenausbeute und vor allem die Zweiphotonenabsorptionsfähigkeit untersucht (Kapitel 3). In Kapitel 4 wurden andere molekulare Designstrategien verfolgt um effiziente Zweiphotonenangeregtenfluoreszenzfarbstoffe zu erhalten. Dazu zählen die Strukturmotive des Dipols (D–A) und des Oktupols (DA_3). Bestandteil des Kapitels 5 war die Optimierung zwischen Wasserstabilität und π-Konjugation und eine damit verbundene rotverschobene Absorption und Emission, sowie eine hohe Fluoreszenzquantenausbeute.

6.2.1 Kapitel Zwei

Durch die Nutzung des Konzepts von Gabbaï und Mitarbeitern - der Einführung von Ammoniogruppen in der *para*-Position von $BMes_3$ - wurden die drei quadrupolen Verbindungen **2-1M** – **2-3M** synthetisiert (Schema 6-1).

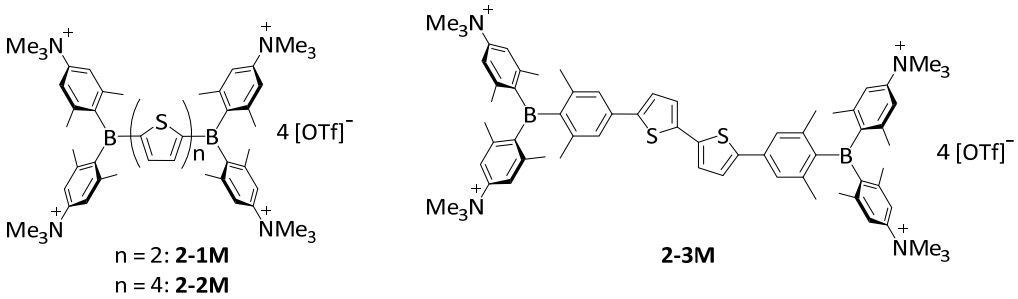

Schema 6-1. Zielmoleküle **2-1M** – **2-3M**.

Diese drei Verbindungen beinhalten je vier Ammoniogruppen, welche sich jeweils in der *para*-Position der Xylylsubstituenten am Boratom befinden. Während in **2-1M** und **2-2M** die Borakzeptoreinheit direkt mit einem Thiophen verbunden ist, wurden in **2-3M** zusätzliche Xylylgruppen eingefügt, um eine erhöhte sterische Abschirmung des Boratoms zu erhalten. Alle Verbindungen sind wasserlöslich, allerdings zeigen die zwei Verbindungen **2-1M** und **2-2M** ohne den zusätzlichen Schutz Zersetzung in verdünnter wässriger Lösung. Sie zersetzen sich in Wasser mit Halbwertszeiten von 4.4 bzw 2.1 h (Abbildung 6-1). Licht und Sauerstoff beschleunigen die Hydrolyse von **2-1M** und **2-2M**.

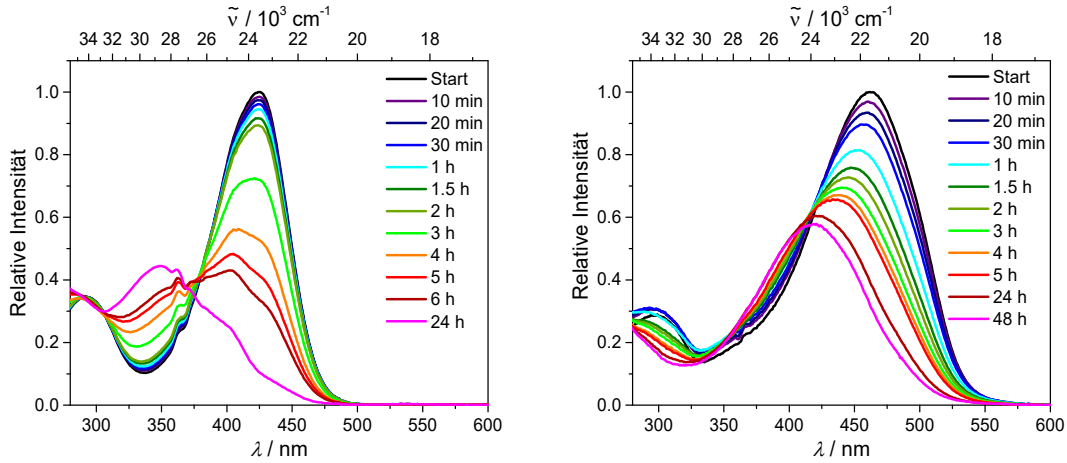

Abbildung 6-1. Absorptionspektren von **2-1M** (links) and **2-2M** (rechts) in H_2O als Funktion der Zeit. Die Probe wurde zwischen den Messungen im Dunkeln aufbewahrt.

Die zusätzliche Xylylgruppe am Boratom gibt der Verbindung den nötigen sterischen Schutz und resultiert in der Stabilität der Verbindung in wässriger Lösung (Abbildung 6-2).

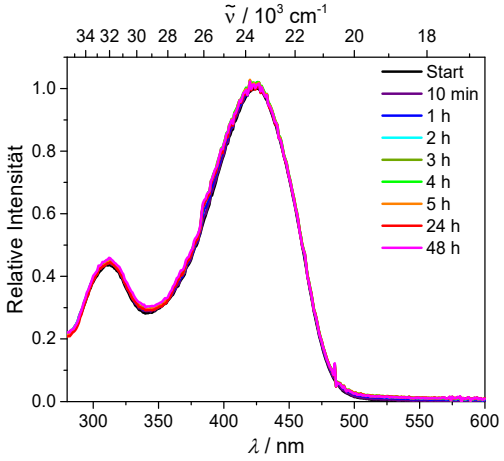

Abbildung 6-2. Absorptionsspektrum von **2-3M** in H_2O als Funktion der Zeit. Die Probe wurde zwischen den Messungen im Dunkeln aufbewahrt.

Während die Verlängerung der π-Brücke um zwei Thiophene (**2-1M** zu **2-2M**) zu einer rotverschobenen Absorption und Emission führt, bleibt die Fluoreszenzquantenausbeute in Wasser konstant bei 0.20. Das Einfügen der Xylylgruppen in **2-1M** verschiebt das Absorptionsmaximum hingegen nicht, das Emissionsmaximum dagegen nur leicht ins Rote. Außerdem sinkt die Fluoreszenzquantenausbeute auf 10%. Dies geht wahrscheinlich mit der verringerten π-Konjugation einher, da die Xylylgruppen aus der Ebene herausgedreht sind. Dies wurde durch TD-DFT Rechnungen bestätigt und eine dahingehende Optimierung wurde in Kapitel 5 durchgeführt.

Jedoch konnte der erste wasserlösliche und wasserstabile quadrupolare Triarylboranfarbstoff synthetisiert werden und hinsichtlich seiner Zweiphotonangeregtenfluoreszenzfähigkeit untersucht werden. Aufgrund der zentralsymmetrischen Symmetrie ist das Molekül **2-3M** bei

800 nm, dem $S_2 \leftarrow S_0$ Übergang, und nur minimal bei 870 nm, dem $S_1 \leftarrow S_0$ Übergang, anregbar. Die Verbindung besitzt einen sehr hohen Zweiphotonenabsorptionsquerschnitt von 693 GM in MeCN. Des Weiteren wurde der Farbstoff bezüglich seiner Toxizität getestet. Drei verschiedene Zelllinien wurden mit Lösungen konsekutiver Verdünnung von **2-3M** versetzt und damit gezeigt, dass **2-3M** in Konzentrationen bis zu 10 μM keine Auswirkungen auf die Zellviabilität hat. Zusätzlich wurden NIH 3T3 Zellen mit dem Farbstoff behandelt, wobei durch konfokale Fluoreszenzmikroskopie eine Lokalisation des Farbstoffes innerhalb der Zelle beobachtet werden konnte. Die Verbindung kolokalisiert mit dem kommerziell erhältlichen Mitochondrienanfärbereagenz MitoTracker™ Red CMXRos. Aufgrund aller oben aufgeführten erfolgreich bestandenen Kriterien wurde der Farbstoff in der Zweiphotonenangeregten-fluoreszenzmikroskopie in POS 1 Zellen eingesetzt (Abbildung 6-3).

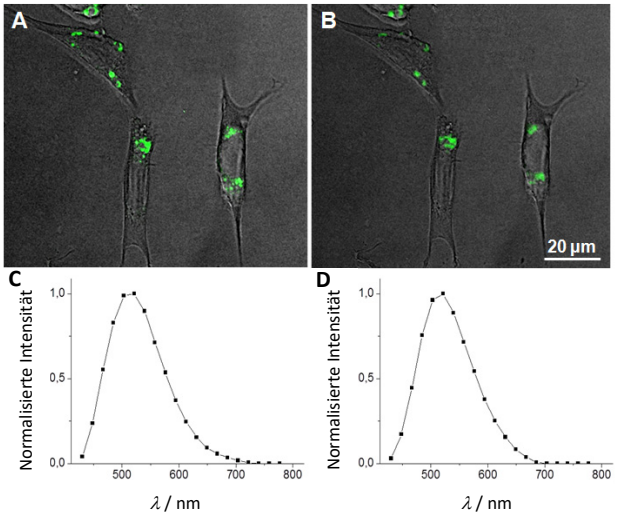

Abbildung 6-3. Konfokale Mikroskopabbildung von POS 1 Zellen nach 8 h Inkubation mit dem Farbstoff **2-3M** (300 nM im Medium): Übereinanderlegen des Transmissionsabbilds (grau) und des Fluoreszenzabbilds (grün) zeigt den Einschluss des Farbstoffes innerhalb der Zellen: (A) Einphotonenanregung (λ_{ex} = 405 nm; λ_{em} = 500 – 600 nm) und (B) Zweiphotonenanregung (λ_{ex} = 800 nm; λ_{em} = 500 – 600 nm); (C) Emissionsspektrum nach Einphotonenanregung (λ_{ex} = 405 nm; 20 nm Schritt) des Farbstoffes in der Zelle; (D) Emissionsspektrum nach Zweiphotonenanregung (λ_{ex} = 800 nm; 20 nm Schritt) des Farbstoffes in der Zelle.

6.2.2 Kapitel Drei

In diesem Kapitel der Doktorarbeit wurden die vielversprechenden, bereits erhaltenen Ergebnisse der Verbindung **2-3M** weiter verbessert und der Einfluss der π-Brücke untersucht. Die Bithiophenbrücke wurde durch 4,4'-Biphenylen, 2,7-Pyren, 2,7-Fluoren, 3,6-Carbazol und 5,5'-Di(thien-2-yl)-3,6-diketopyrrolopyrrol ersetzt (Schema 6-2). Die neuen vierfachkationischen Verbindungen sind wasserlöslich (**3-2M** nur nach Zugabe von 10% MeCN) und aufgrund der zusätzlichen Xylylgruppe wasserstabil.

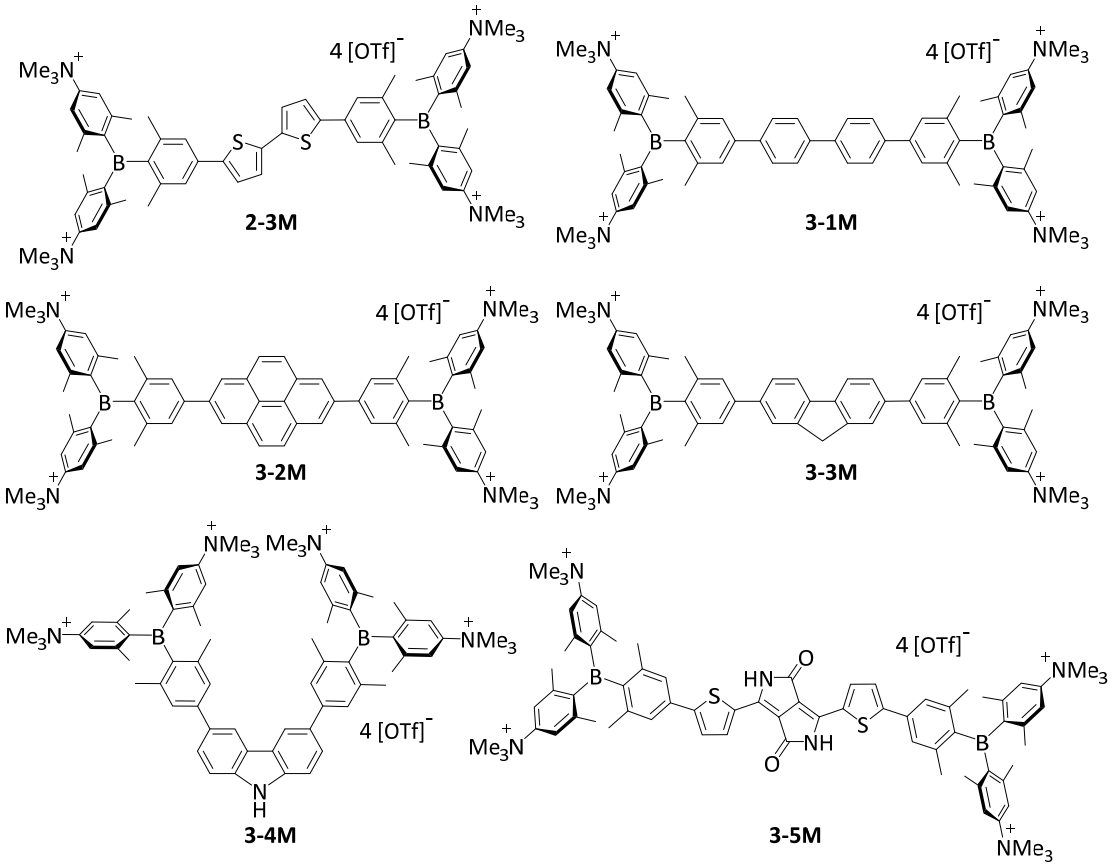

Schema 6-2. Quadrupole Farbstoffe für Zweiphotonenangeregtefluoreszenzmikroskopie **2-3M**, **3-1M** – **3-5M**.

Das Austauschen der π-Brücke beeinflusst die Absorptions- und Emissionsspektren extrem, da die Anregung hauptsächlich auf der π-Brücke lokalisiert ist und einen π-π* Übergang darstellt. Demnach kann je nach Wahl der π-Brücke die Emissionsfarbe von blau nach pink verändert werden. Diese folgt der Energie des HOMOs, da die LUMO Energie nahezu konstant bleibt (mit Ausnahme von **3-5M**). Die Verbindungen sind nicht solvatochrom was die Art des Übergangs (π-π*) weiter bestätigt. Alle Moleküle, ausgenommen **3-4M**, zeigen hohe Fluoreszenzquantenausbeuten in wässriger Lösung.

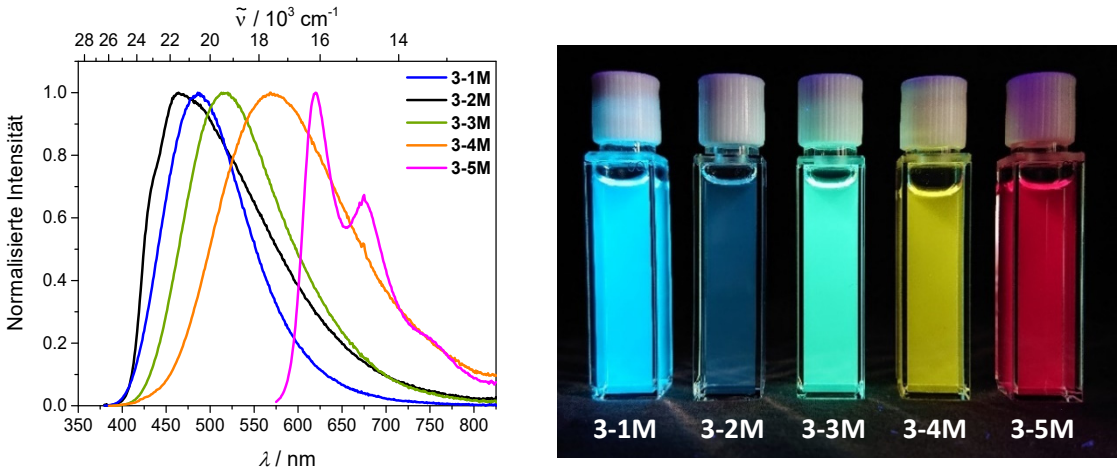

Abbildung 6-4. Emissionsspektrum (links) von **3-1M** – **3-5M** in Wasser. Verbindung **3-2M** wurde in 10% MeCN in Wasser gelöst. Bild der Lösungen (rechts) von **3-1M** – **3-5M** in MeCN unter UV-Bestrahlung.

Wie bekannt für quadrupole Verbindungen (A–π–A) hat die π-Brücke einen entscheidenden Einfluss auf den Zweiphotonenabsorptionsquerschnitt. Aufgrund der elektronischen Auswahlregeln für zentrosymmetrische Moleküle, **3-1M**, **3-2M** und **3-5M**, befindet sich das Zweiphotonenabsorptionsmaximum nicht bei dem Einphotonenabsorptionsmaximum, da der $S_1 \leftarrow S_0$ Übergang ($A_u \leftarrow A_g$ Symmetrie) für die Zweiphotonenabsorption symmetrieverboten ist. Das Zweiphotonenabsorptionsmaximum liegt bei höherer Energie bei der der zweiphotonabsorptionerlaubte Übergang mit $A_g \leftarrow A_g$ Symmetrie stattfindet ($S_2 \leftarrow S_0$ Übergang für **3-1M** und **3-5M** und $S_3 \leftarrow S_0$ Übergang für **3-2M**). Die anderen beiden Moleküle **3-3M** und **3-4M** weisen C_{2v} als höchstmöglichste Symmetrie auf und besitzen daher kein Inversionszentrum, weswegen alle Übergänge sowohl für die Ein- als auch die Zweiphotonenabsorption erlaubt sind. Wie erwartet zeigt die Biphenylenverbindung **3-1M** den kleinsten Zweiphotonenabsorptions-querschnitt (72 GM), da diese im Grundzustand am meisten verdreht ist (Abbildung 6-5). Durch Planarisierung der beiden Phenylringe, wie im Pyren, Fluoren und Carbazol, **3-2M** – **3-4M**, wird der Zweiphotonenabsorptionsquerschnitt erhöht (79, 162 bzw. 134 GM). Des Weiteren wird der Zweiphotonabsorptionsquerschnitt durch verbesserten intramolekularen Ladungstransfer gesteigert.[109b, 109d, 146] Es ist bekannt, dass A–π–D–π–A Systeme effizienter sind als A–π–A Systeme. [109b, 109d, 146] Die Donorstärke der π-Brücke korreliert dabei mit der HOMO Energie, weswegen der Zweiphotonabsorptionsquerschnitt vom Pyren **3-2M** zum Fluoren **3-3M** zum Carbazol **3-4M** ansteigen sollte. Letztere Verbindung zeigt jedoch einen kleineren Zweiphotonenabsorptionsquerschnitt, was auf die kürzere Konjugationslänge zurückzuführen ist. Die Dithienyldiketopyrrolopyrrolverbindung **3-5M** zeigt den mit Abstand höchsten Zweiphotonenabsorptionsquerschnitt (4 560 GM), da das konjugierte π-System verlängert und die Struktur im berechneten Grundzustand nahezu planar ist.

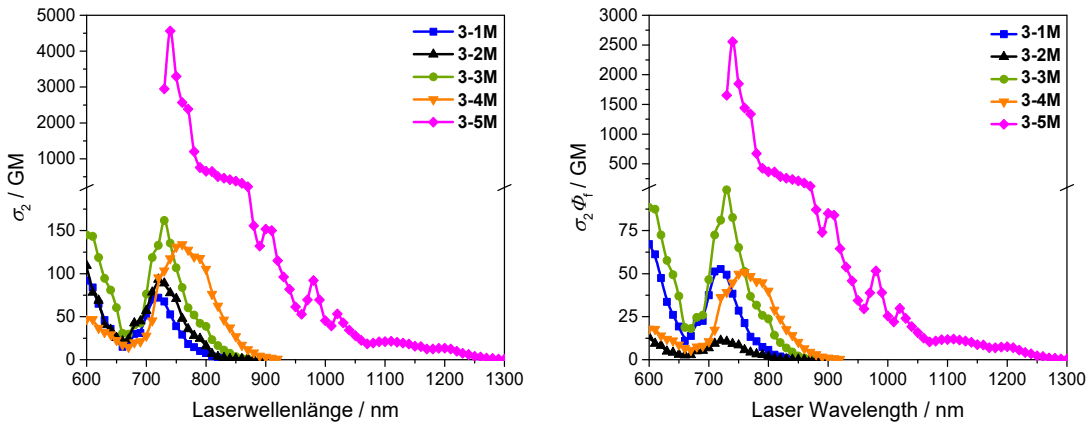

Abbildung 6-5. Zweiphotonabsorptionsspektren (links) und Zweiphotonenabsorptionsspektren multipliziert mit der Fluoreszenzquantenausbeute (rechts) von **3-1M** – **3-5M** in MeCN.

Die methylierten Verbindungen **3-1M** – **3-5M** wurden bezüglich Zytotoxizität getestet und zeigen keine Beeinträchtigung der Zellviabilität bis zu 5 μM nach 24 h Inkubationszeit. Deswegen wurden die Farbstoffe in der konfokalen Fluoreszenzmikroskopie eingesetzt und eine zelluläre Aufnahme beobachtet. Kolokalisierungsexperimente bestätigen die Lokalisation in sauren intrazellulären Kompartimenten, z. B. Lysosomen (Abbildung 6-6). Da der Dithienyldiketo-pyrrolopyrrolfarbstoff **3-5M** das am meisten rotverschobene Absorptions- und Emissionsmaximum, sowie den mit Abstand höchsten Zweiphotonenabsorptionsquerschnitt aufweist, wurden weitere Zellexperimente mit diesem durchgeführt.

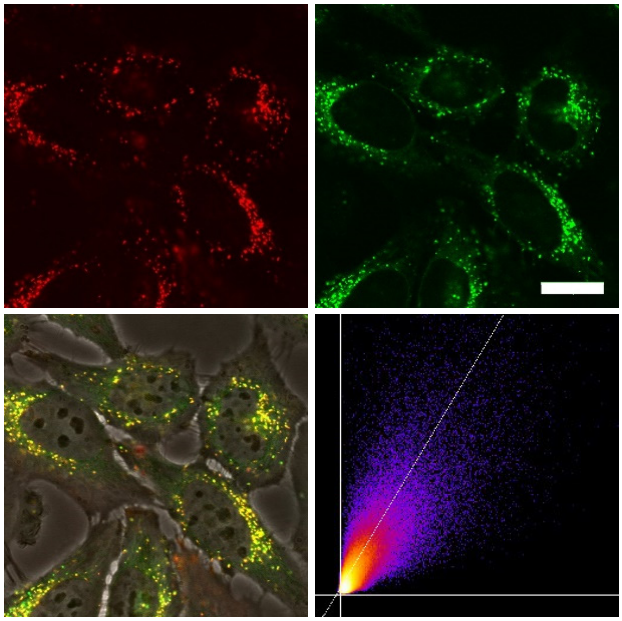

Abbildung 6-6. Kolokalisierungsexperiment mit HeLa Zellen mit **3-5M** und LysoTracker™ Green. Die Zellen wurden mit **3-5M** (500 nM, 2 h) und LysoTracker™ Green (100 nM, 20 min) unter 5% CO_2 bei 37 °C versetzt. Fluoreszenzabbildungen von **3-5M** (oben, links: λ_{ex} = 559 nm; λ_{em} = 570 – 670 nm) und LysoTracker™ Green (oben, rechts: λ_{ex} = 473 nm; λ_{em} = 490 – 590 nm). Das Übereinanderlegen des Hellfeldabbilds und der beiden Fluoreszenzabbildungen (unten, links), und das Korrelationsdiagramm der Intensitäten (unten, rechts: R_r = 0.81) zeigen die Lokalisierung des Farbstoffes **3-5M** in den Lysosomen. Maßstabsleiste: 20 μm.

Der Mechanismus der Zellinternalisierung des Farbstoffes **3-5M** wurde durch Zeitraffermikroskopie über 2 h als Endozytose bestimmt. Dies konnte durch weitere Experimente bestätigt werden. Dazu wurden die Zellen bei 4 °C bzw. bei 37 °C mit dem Zusatz von 0.1% NaN_3 angefärbt, da beide Bedingungen die Endozytose verhindern. Beide Experimente zeigten eine viel geringere Fluoreszenz innerhalb der Zelle als das Kontrollexperiment. Des Weiteren konnte die Photostabilität des Farbstoffes **3-5M** durch wiederholte Bildgebung der angefärbten HeLa Zellen bestätigt werden. Mehr als 95% der Anfangsfluoreszenzintensität waren nach der Aufnahme von 50 Bildern durch Bestrahlung mit einem 561 nm Anregungslaser erhalten, während unter denselben Bedingungen die Fluoreszenzintensität des kommerziell erhältlichen LysoTracker™ Red um 45% sank. Außerdem konnte der Farbstoff **3-5M** aufgrund

des hervorragenden Zweiphotonenabsorptionsquerschnittes in der Zweiphotonen-mikroskopie an lebenden Zellen angewendet werden.

6.2.3 Kapitel Vier

Da Dipole und Oktupole ebenfalls ein Designmotiv effizienter Zweiphotonenabsorptions-farbstoffe sind, wurden beide Strukturmotive in diesem Kapitel untersucht. Triphenylamin ist ein effizientes Zentrum für die Zweiphotonenabsorptionsverstärkung in Oktupolen und wurde deswegen als Donor benutzt. Als Akzeptor wurde das dikationische Triarylboran der vorherigen Kapitel benutzt. Der erhaltene Dipol (**4-1M**) und Oktupol (**4-2M**) sowie die neutralen Vorstufen **4-1** und **4-2** wurden untersucht.

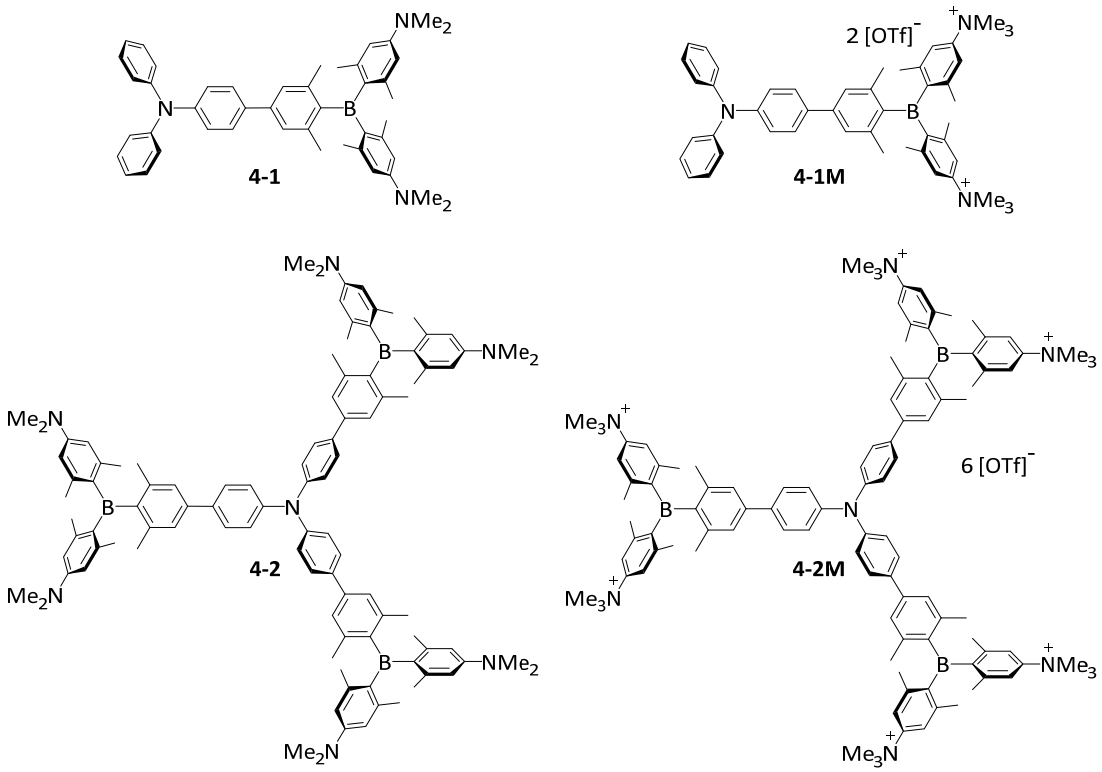

Schema 6-3. Zielmoleküle **4-1**, **4-2**, **4-1M** und **4-2M**.

In diesen neutralen Vorstufen spielt das Triphenylamin bezüglich der photophysikalischen Eigenschaften keine Rolle. Der Ladungstransfer findet immer vom Dimethylamin zur Boreinheit in der äußeren Peripherie der Moleküle statt. Deswegen sind die photophysikalischen Eigenschaften von **4-1** und **4-2** sehr ähnlich und die Verzweigung hat keinen Effekt.

Durch die Methylierung wird der Ladungstransfer vom Dimethylamin zum Borzentrum verhindert und gleichzeitig die Akzeptorstärke der Boreinheit erhöht. Deswegen ist der Ladungstransfer vom Triphenylamin zur kationischen Boreinheit der dominante Übergang. Obwohl die höher energetische Absorptionsbande mit steigender Lösungsmittelpolarität hypsochrom verschoben wird, wird das Emissionsmaximum bathochrom verschoben (Abbildung

6-7). Der entgegengesetzte Solvatochromismus für Absorption und Emission wurde bereits von Lambert und Mitarbeitern beobachtet und resultiert aus einer Inversion des Dipolmoments durch Anregung.[19] Desweiteren ist die Absorptionsbande von **4-2M** um 704 cm^{-1} von **4-1M** verschoben. Dieser Effekt basiert auf der Kopplung der drei Arme in **4-2M**. Durch das Exciton Kopplungsmodell (Abbildung 6-8) wurde eine Kopplungskonstante von 0.09 eV bestimmt.

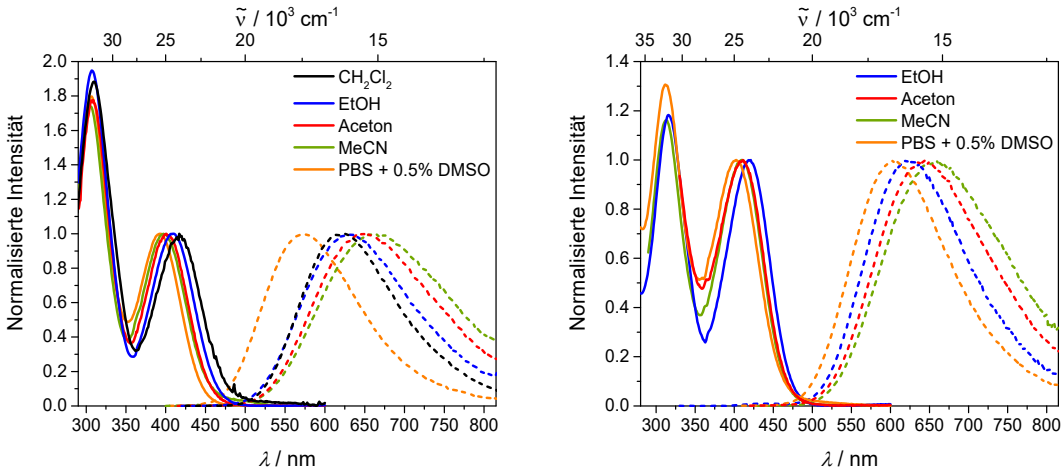

Abbildung 6-7. Absorptions- und Emissionsspektren von **4-1M** (links) und **4-2M** (rechts) in verschiedenen Lösungsmitteln (Dichlormethan: schwarz, Ethanol: blau, Aceton: rot, MeCN: grün, PBS + 0.5% DMSO: orange).

Auch TD-DFT Rechnungen zeigen die Beteiligung des Triphenylamines und dadurch die Kupplung der drei Arme. Aufgrund der C_3 Symmetrie des Moleküls sind die angeregten Zustände S_1 und S_2 entartet, um die Kopplungskonstante *V* stabilisiert und die Anregung vom S_0 Grundzustand ist erlaubt (E Symmetrie, $f = 1.407$). Zudem ist der S_3 Zustand um $2V$ destabilisiert und die Anregung verboten (A Symmetrie, $f = 0.000$). Durch das Exciton Kopplungsmodell konnte eine Kopplungskonstante *V* von 0.09 eV als ein Drittel der Energiedifferenz zwischen den durch DFT berechneten angeregten Zuständen (E und A Symmetrie) bestimmt werden. Dies ist exakt der selbe Wert wie experimentell im UV/Vis durch die Verschiebung der Absorptionsbande bestimmt. Da das Molekül **4-2M** Solvatochromie zeigt muss ein Dipolmoment vorhanden sein. Dies ergibt sich durch die Aufbrechung der Symmetrie, da **4-2M** nicht ideal C_3 symmetrisch ist.

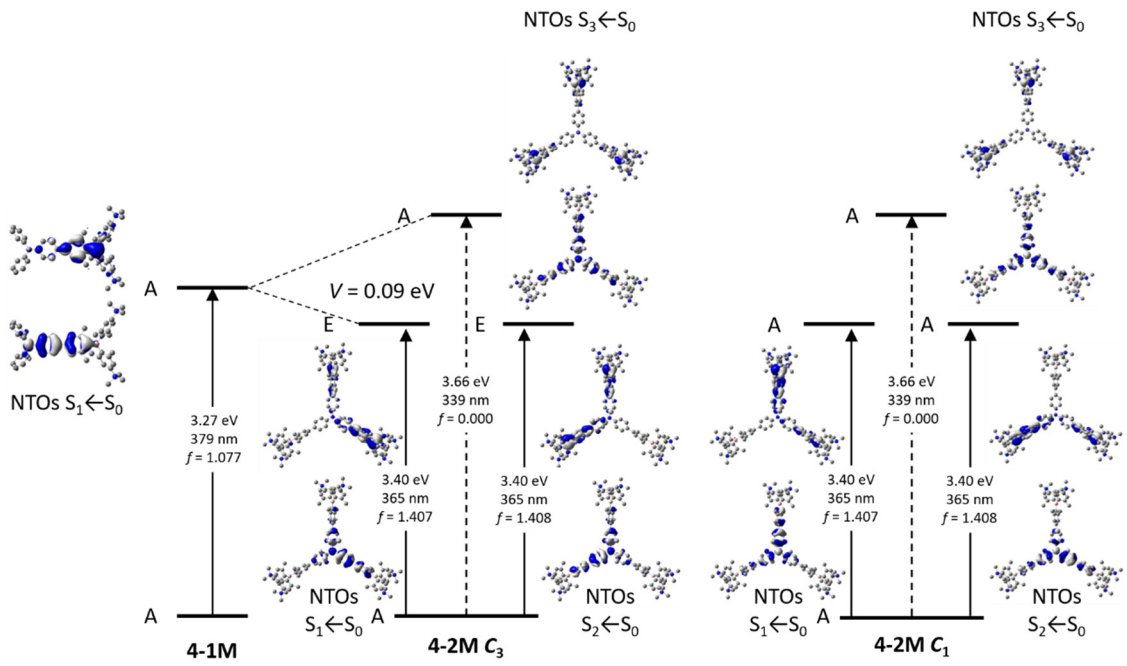

Abbildung 6-8. Aufspalten des angeregten Zustandes von **4-1M** bezüglich **4-2M**. Die natürlichen Übergangsorbitale (NTOs) von $S_1 \leftarrow S_0$, $S_2 \leftarrow S_0$ und $S_3 \leftarrow S_0$ sind durch TD-DFT Rechnungen in der Gasphase dargestellt.

Die Zweiphotonenabsorptionsspektren der beiden kationischen Farbstoffe **4-1M** und **4-2M** wurden in MeCN gemessen. Während für **4-1M** das Zweiphotonenabsorptionsspektrum der doppelten Wellenlänge des Einphotonenabsorptionsspektrum folgt, ist das Maximum der Zweiphotonenspektroskopie für **4-2M** blau verschoben, da in **4-2M** mittels Zweiphotonenabsorption der $S_3 \leftarrow S_0$ Übergang (A←A Symmetrie) angeregt wird. Der Zweiphotonenabsorptionsquerschnitt des Dipoles **4-1M** ist 91 GM in MeCN, welcher durch die Verzweigung in **4-2M** auf 335 GM gesteigert werden kann.

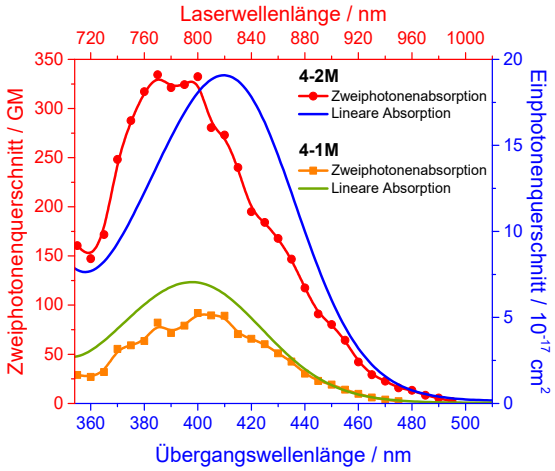

Abbildung 6-9. Einphotonenabsorptionsspektrum von **4-1M** (grün) und **4-2M** (blau) und Zweiphotonenabsorptionsspektrum von **4-1M** (orange) und **4-2M** (rot) in MeCN.

Das Anfärben von HeLa Zellen mit den Farbstoffen **4-1M** und **4-2M** ergibt sehr unterschiedliche Ergebnisse. Der oktupole Farbstoff ist nach 24 h Inkubationszeit weniger toxisch und deutlich

selektiver für das Anfärben der Lysosomen. Der Dipol lokalisiert neben den Lysosomen ebenso in den Mitochondrien, was an der faserartigen Struktur im Mikroskopiebild erkannt werden kann. Dies kann auf drei Faktoren zurückzuführen sein: Die erhöhte Anzahl der kationischen Gruppen, der hydrophilere Charakter oder die Größe von **4-2M**.

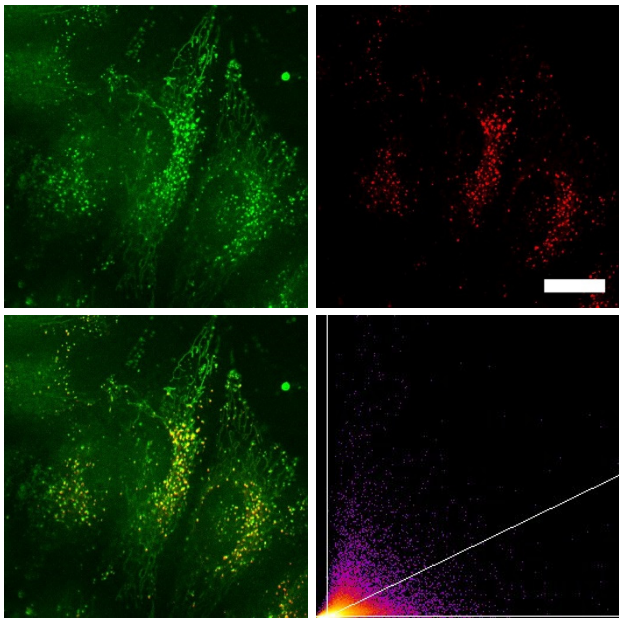

Abbildung 6-10. Kolokalisierungsexperiment mit HeLa Zellen mit **4-1M** und LysoTracker™ Red. Die Zellen wurden mit **4-1M** (500 nM, 2 h) und LysoTracker™ Red (100 nM, 20 min) unter 5% CO_2 bei 37 °C versetzt. Fluoreszenzabbildungen von **4-1M** (oben, links: λ_{ex} = 405 nm; λ_{em} = 500 – 605 nm) und LysoTracker™ Red (oben, rechts: λ_{ex} = 561 nm; λ_{em} = 607 – 786 nm). Das Übereinanderlegen der beiden Fluoreszenzabbildungen (unten, links), und das Korrelationsdiagramm der Intensitäten (unten, rechts: R_r = 0.48) zeigen eine geringe Lokalisierung des Farbstoffes **4-1M** in den Lysosomen. Maßstabsleiste: 20 μm.

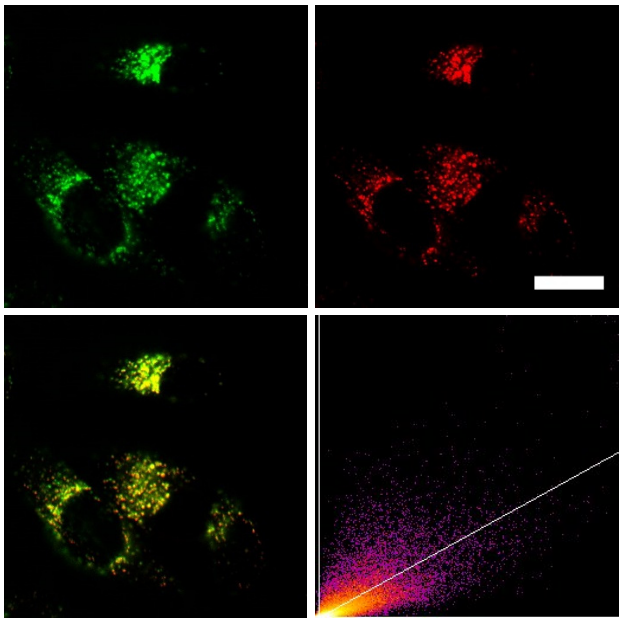

Abbildung 6-11. Kolokalisierungsexperiment mit HeLa Zellen mit **4-2M** und LysoTracker™ Red. Die Zellen wurden mit **4-2M** (500 nM, 2 h) und LysoTracker™ Red (100 nM, 20 min) unter 5% CO_2 bei 37 °C versetzt. Fluoreszenzabbildungen von **4-2M** (oben, links: λ_{ex} = 405 nm; λ_{em} = 500 – 605 nm) und LysoTracker™ Red (oben, rechts: λ_{ex} = 561 nm; λ_{em} = 607 – 786 nm). Das Übereinanderlegen der beiden Fluoreszenzabbildungen (unten, links), und das Korrelationsdiagramm der Intensitäten (unten, rechts: R_r = 0.81) zeigen eine gute Lokalisierung des Farbstoffes **4-2M** in den Lysosomen. Maßstabsleiste: 20 μm.

6.2.4 Kapitel Fünf

Der letzte Teil dieser Doktorarbeit befasst sich mit der Untersuchung der Stabilität verschiedener Triarylborane in verdünnter, wässriger Lösung. Das Design der Farbstoffe basiert auf der quadrupolen Struktur (A–π–A), welche bereits in Kapitel 2 und 3 verwendet wurde. Dazu wurden 1,4-Phenylen (**5-1M**), 2,2‴-(3,3‴-Dimethyl)-5,2′:5′,2″:5″,5‴-quaterthiophen (**5-2M**), 9,10-Anthracenylen (**5-3M**) und 4,4‴-(5′-(3,5-Dimethylphenyl))(5″-(3‴,5‴-dimethylphenyl))-2′,2″-bithiophen (**2-3M**) als Brücke im (*para*-(*N*,*N*,*N*-trimethylammonio)xylyl)$_2$B–(Brücke)–B(*para*-(*N*,*N*,*N*-trimethyl-ammonio)xylyl)$_2$-Motiv verwendet.

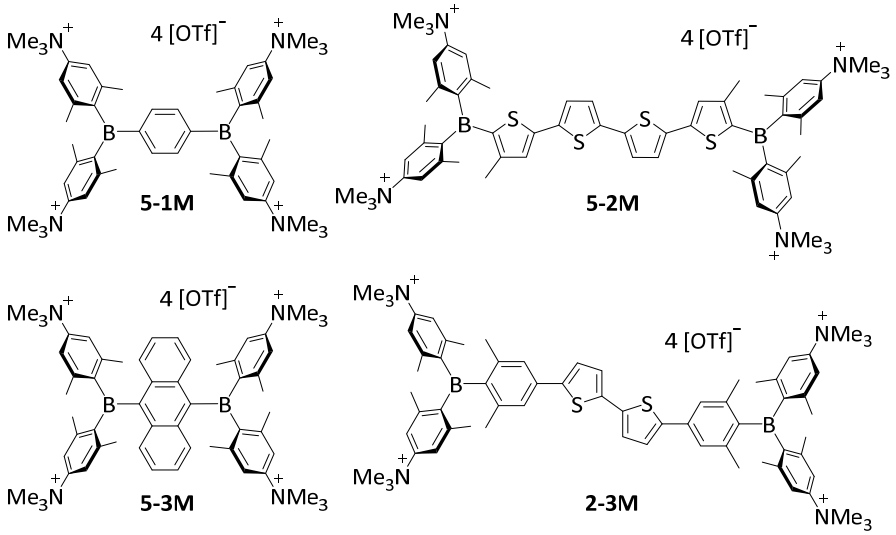

Schema 6-4. Zielmoleküle **5-1M** – **5-3M** und **2-3M**.

Der unterschiedliche sterische Anspruch der vier Aromaten zeigt sich bereits in den entsprechenden Kristallstrukturen der neutralen Analoga **5-1**, **5-5**, **5-3** und **2-6** (Abbildung 6-12). Die Verbindungen mit dem kleineren Phenyl- und Methylthiophenaromaten zeigen Verdrehungen um 27° und 39° bei **5-1** und 35° bei **5-5** gegenüber der BC_3 Ebene. Bei den sterisch anspruchsvolleren Anthracenyl- und Xylylgruppen beträgt der Drehwinkel gegenüber der BC_3 Ebene mit 64° (**5-3**) und 59° (**2-6**) fast doppelt so viel.

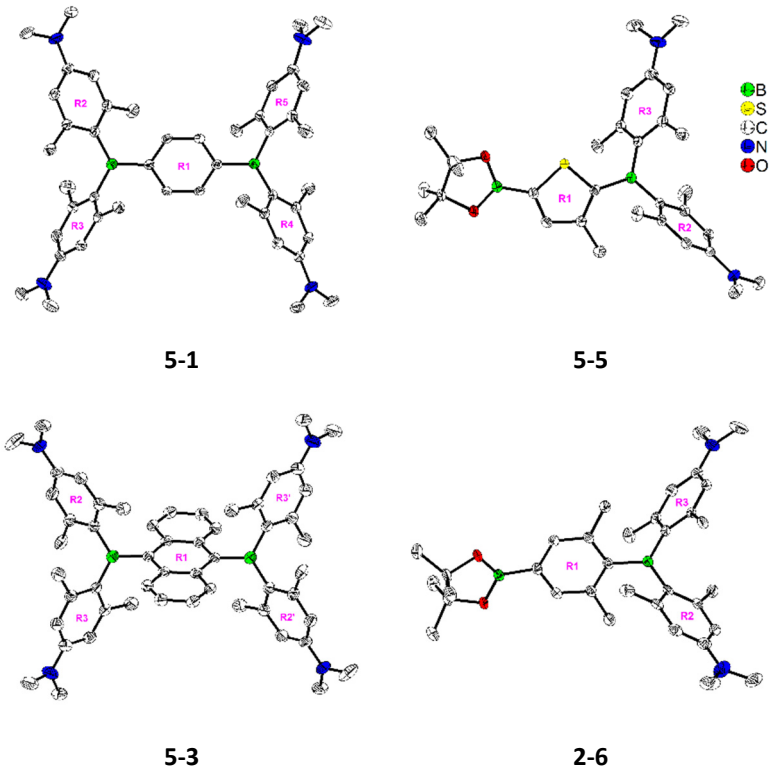

Abbildung 6-12. Festkörpermolekülstrukturen von **5-1**, **5-5**, **5-3** und **2-6**[119] durch Einkristallröntgendiffraktometrie bei 100 K. Die thermischen Ellipsoide sind auf dem 50%-Wahrscheinlichkeitsniveau abgebildet und H Atome aus Gründen der Übersichtlichkeit nicht dargestellt. Die zentralen Arylgruppen, die an das Boratom gebunden sind, wurden mit R1 beschriftet, wohingegen die terminalen Arylgruppen mit R2 und R3 beschriftet wurden, sofern sie mit B1 verbunden sind, bzw. mit R4 und R5 beschriftet, sofern sie mit B2 verbunden sind.

Dieser Trend konnte durch die Ordnung der Rotationsbarrieren, die mittels NMR Spektroskopie bestimmt wurden, genauer spezifiziert werden. Die NMR Signale der *ortho*-Methylgruppen des *para*-(*N*,*N*-Dimethylamino)xylylaromatens werden mit sinkender Temperatur breiter und spalten auf, da die Stereoisomerisierung der Triarylborane abnimmt. Die Rotationsbarrieren (Abbildung 6-13) nehmen mit zunehmendem sterischem Anspruch der Brücke zu: 1,4-Phenylen **5-1** < 2,2‘‘‘-(3,3‘‘‘-Dimethyl)-5,2‘:5‘,2‘‘:5‘‘,5‘‘‘-quaterthiophen **5-2** < 9,10-Anthracenylen **5-3** < 4,4‘‘‘-(5‘-(3,5-Dimethylphenyl))(5‘‘-(3‘‘‘,5‘‘‘-dimethylphenyl))-2‘,2‘‘-bithiophen **2-3**. Deswegen muss die Rotationsbarriere von **5-1** kleiner als 11.0 kcal/mol sein.

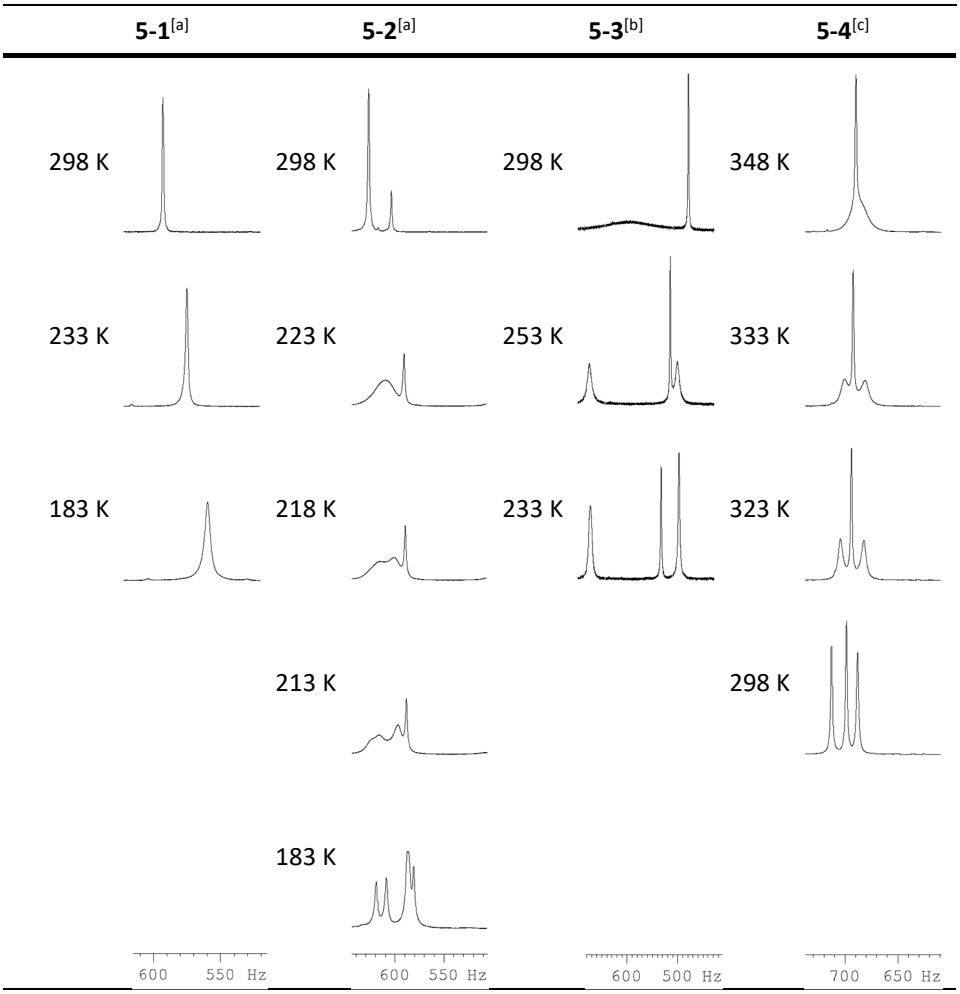

[a] wurden in CD_2Cl_2 gemessen; [b] wurde in $CDCl_3$ gemessen; [c] wurde in C_6D_6 gemessen.

Abbildung 6-13. ^{1}H NMR Spektren der Methylresonanz der Verbindungen **5-1** – **5-3** und **2-3** bei verschiedenen Temperaturen bei 300 MHz.

Alle Neutralverbindungen **5-1** – **5-3** und **2-3** sind im Festkörper und in Lösung stabil gegenüber Luft und Feuchtigkeit, aber nicht wasserlöslich. Die methylierten Derivate **5-1M** – **5-3M** und **2-3M** zeigen unterschiedliche Stabilitäten in wässriger Lösung abhängig vom sterischen Anspruch der Arylbrücke. Wässrige Lösungen von **5-2M**, **5-3M** und **2-3M** sind über mehrere Tage stabil, während **5-1M**, die Verbindung mit dem kleinsten Arylsubstituenten, dem Phenyl, Zersetzung im NMR Spektrum zeigt. Mittels UV/Vis Spektroskopie wurde die Stabilität von **5-1M** – **5-3M** und **2-3M** bei niedrigeren Konzentrationen (10^{-5} M) in Wasser untersucht (Abbildung 6-14).

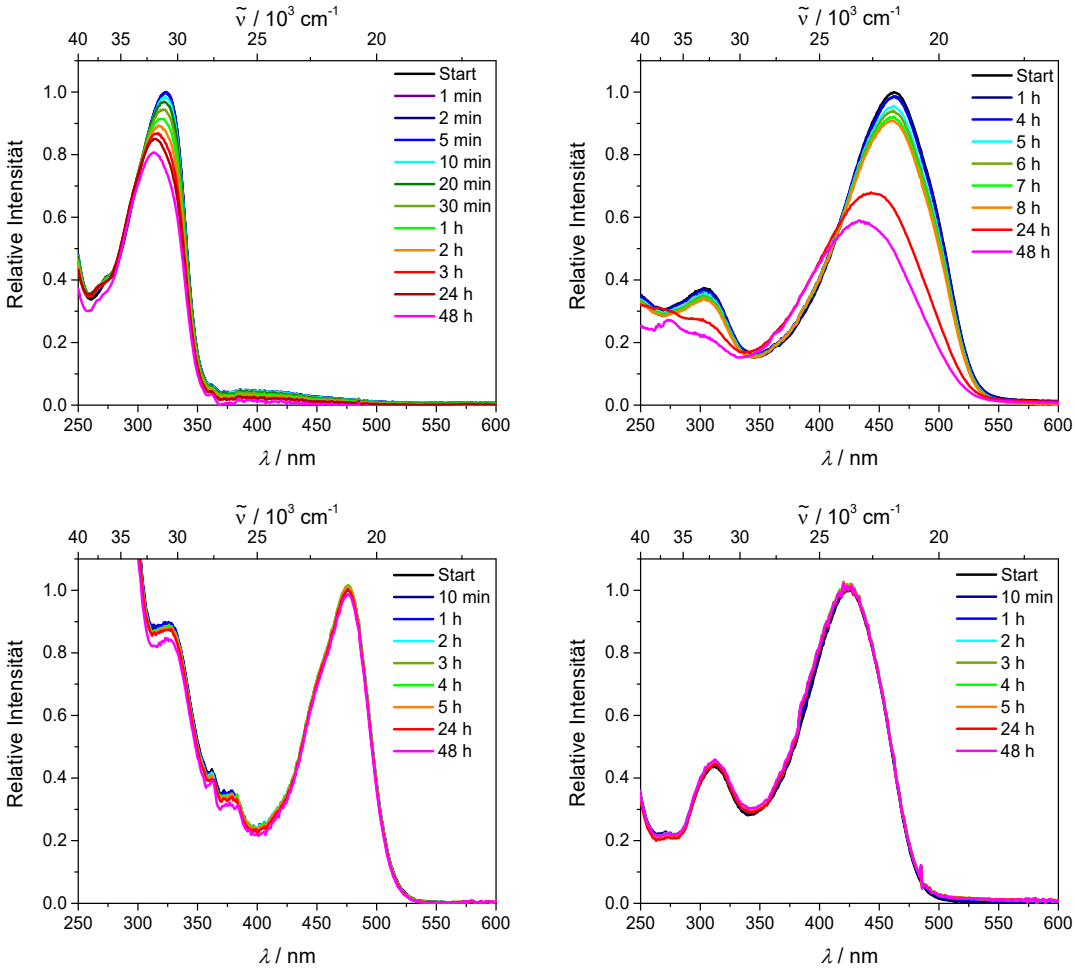

Abbildung 6-14. UV/Vis Spektren mit den relativen Intensitäten der Verbindungen **5-1M** (oben, links: OD bei t = 0 min: 0.16), **5-2M** (oben, rechts: OD bei t = 0 min: 0.14), **5-3M** (unten, links: OD bei t = 0 min: 0.07) und **2-3M** (unten, rechts: OD bei t = 0 min: 0.10) über 48 h in Wasser. Lösungen derselben Konzentration von **5-1M** – **5-3M** und **2-3M** konnten nicht hergestellt werden, da die Verdünnung Zeit kostet und ein Absorptionsspektrum bei t = 0 min nicht realisierbar ist.

Verbindung **5-1M** zersetzt sich sofort, während die Methylthiophenverbindung **5-2M** stabiler ist, aufgrund der zusätzlichen Methylgruppe an der 3-Position des Thiophens und der elektronenschiebenden Eigenschaften der Methylthiophenegruppe. Dadurch zersetzt sich die Verbindung erst nach 4 h was allerdings für die Zellmikroskopie nicht ausreichend ist. Im Gegensatz dazu zeigen die Verbindungen **5-3M** und **2-3M** für mindestens 48 h keine Zersetzung. In wässriger Lösung ist ein Xylylsubstituent oder ein Substituent mit ähnlichem sterischem Anspruch, z. B. Anthracen, notwendig um das Boratom von einem nucleophilen Angriff durch Wasser zu schützen.

Bei der Untersuchung der photophysikalischen Eigenschaften wurde festgestellt, dass sich das Absorptionsmaximum von **5-3M** verglichen mit den anderen Verbindungen bathochrom verschiebt. Dies liegt an der Verlängerung der Konjugationslänge senkrecht zur Brücke (Abbildung 6-15). Aufgrund der kleinen Reorganisationsenergie im angeregten Zustand ist der Stokes Shift (2 100 cm^{-1}) von Verbindung **5-3M** sehr klein, weswegen das Emissionsmaximum

verglichen zu **5-2M** and **2-3M** hypsochrom verschoben ist. Der nicht-radiative Zerfall ist in Wasser vernachlässigbar klein, weshalb die Anthracenverbindung **5-3M** in Wasser eine außerordentlich hohe Fluoreszenzquantenausbeute von 0.86 zeigt.

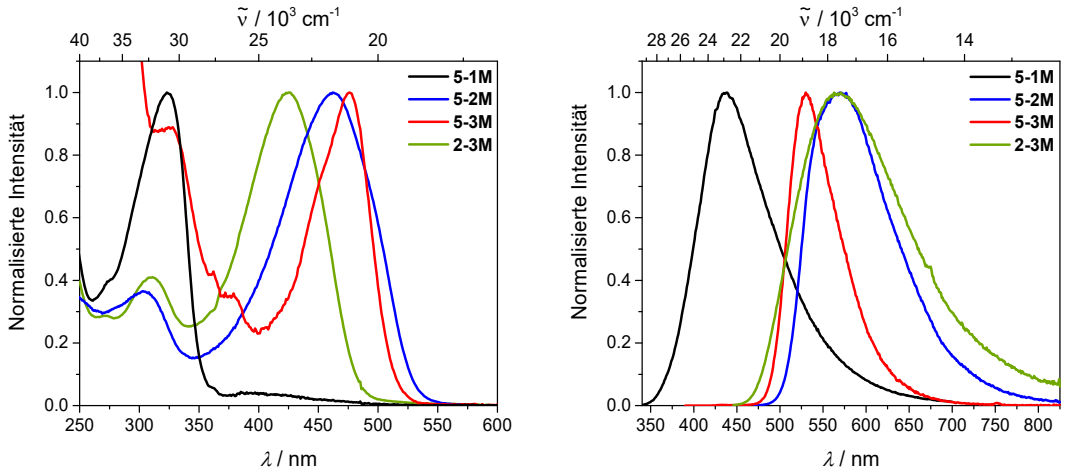

Abbildung 6-15. Absorptions- (links) und Emissionsspektren (rechts) von **5-1M** – **5-3M** und **2-3M** in Wasser.

Da die Anthracenverbindung **5-3M** wasserstabil ist und exzellente photopysikalische Eigenschaften zeigt, z. B. die am meisten rotverschobene Absorptionsbande und eine außerordentlich hohe Fluoreszenzquantenausbeute, wurde diese für ihren Einsatz in Experimenten an lebenden Zellen getestet. Verbindung **5-3M** zeigt keine Toxizität gegenüber HeLa Zellen bis zu einer Konzentration von 5 μM über 24 h. Außerdem wurde eine zelluläre Aufnahme durch konfokale Fluoreszenzmikroskopie beobachtet und Kolokalisierung mit den Lysosomen durch Kolokalisierungsexperimente mit dem kommerziell erhältlichen LysoTracker™ Red bestätigt.

Chapter Seven

-

Experimental

7 EXPERIMENTAL

7.1 Gerneral Information

Unless otherwise noted, the following conditions apply. Reactions were performed using standard Schlenk or glovebox (Innovative Technology Inc.) techniques under an atmosphere of argon. Only oven-dried glassware was used. Solvents used for reactions were HPLC grade, dried using an Innovative Technology Inc. Pure Solvent Purification System, and further deoxygenated. *Bis*[4-(*N*,*N*-dimethylamino)-2,6-xylyl]fluoroborane[134] **2-4**, 2,2′:5′,2′′:5′′,2′′′-quaterthiophene,[205] [Ir(COD)(μ-OMe)]$_2$ (COD = 1,5-cyclooctadiene),[206] 2,7-dibromopyrene,[55] *tris*(dibenzylideneacetone)-dipalladium(0),[207] *N*-*tert*-butoxycarbonyl-3,6-dibromo-9*H*-carbazole,[208] di-*tert*-butyl-3,6-*bis*(5-bromothiophen-2-yl)-1,4-dioxopyrrolo[3,4-c]pyrrole-2,5-(1*H*,4*H*)-dicarboxylate,[209] 2-(3,5-dimethylphenyl)-4,4,5,5-tetramethyl-1,3,2-dioxaborolane,[210] and 2-bromo-3-methylthiophene[211] were synthesized according to literature procedures. All other starting materials were purchased from commercial sources and were used without further purification.

Reaction progress was monitored using thin layer chromatography (TLC) plates pre-coated with a layer of silica (Polygram® Sil G/UV254) with fluorescent indicator UV254 from Marcherey-Nagel. Column chromatography was performed using either Silica Gel 60 (40-63 microns) or Al_2O_3 as the stationary phase and the solvent system indicated. Automated flash column chromatography was performed using a Biotage® Isolera Four system with silica gel (Biotage SNAP cartridge KP-Sil 50 g or KP-Sil 100 g obtained from Biotage) as the stationary phase and the solvent system indicated. Solvents were generally removed *in vacuo* using a rotary evaporator at a maximum temperature of 50 °C.

^{1}H, ^{13}C{^{1}H}, and ^{11}B{^{1}H} solution NMR spectroscopic data were obtained at ambient temperature using a Bruker Avance 500 NMR spectrometer (operating at 500 MHz for ^{1}H and 125 MHz for ^{13}C{^{1}H} and 160 MHz for ^{11}B{^{1}H}). Chemical shifts (δ) were referenced to solvent peaks as follows: ^{1}H NMR spectra were referenced to residual protiated solvent in CD_2Cl_2 (5.32 ppm), CD_3OD (3.31 ppm) or d_6-DMSO (2.50 ppm); and ^{13}C{^{1}H} spectra were referenced to CD_2Cl_2 (53.84 ppm), CD_3OD (49.00 ppm) or d_6-DMSO (39.52 ppm); and ^{11}B{^{1}H} NMR signals were referenced to external $BF_3{\cdot}Et_2O$. VT-NMR spectroscopic data were obtained at various temperatures using a Bruker Avance III HD 300 NMR spectrometer (operating at 300 MHz for ^{1}H). Temperature was calibrated using a sample of 4% MeOH in CD_3OD for temperatures below 298 K or a sample of 80% 1,2-ethanediol in d_6-DMSO for temperatures above 298 K according to Ref. [212]. The solid-state magic-angle spinning (MAS) NMR spectra were recorded using a Bruker DSX-400 or a Bruker Avance Neo 400 WB spectrometer operating at 128.38 MHz for ^{11}B and a 4 mm rotor (o.

d.). Spectra are referenced to external $BF_3{\cdot}Et_2O$. Isotropic chemical shifts were estimated by simulating the observed spectrum using the Solid Line Shape Analysis 2.2.4 (SOLA) in Bruker TopSpin. Due to the very small amount of sample of **3-4M**, **3-5M**, **4-2M** and **5-1M** – **5-3M**, a residual boron signal of the boron nitride stator is observable at -30 to 20 ppm.

Elemental analyses were performed on an Elementar vario MICRO cube elemental analyzer. As is common for related organo-$BMes_2$ compounds, carbon analysis of **2-1M**, **2-2M**, **3-2**, **3-1M**, **3-2M**, **3-4M**, **3-5M**, **4-2M**, **5-1**, **5-2**, **5-4**, **5-1M**, **5-2M** and **5-3M** were up to 3.6% below the calculated value, while hydrogen, nitrogen and sulfur analyses were satisfactory. This has been ascribed previously to the formation of boron carbide.[213] High resolution mass spectrometry (MS) was performed with a Thermo Fisher Scientific Exactive Plus Orbitrap MS System with either an atmospheric-pressure chemical ionization (APCI), liquid injection field desorption ionization (LIFDI) or a heated-electrospray ionization (HESI) probe.

7.2 Single-Crystal X-Ray Diffraction

Crystals suitable for single-crystal X-ray diffraction were selected, coated in perfluoropolyether oil, and mounted on MiTeGen sample holders. Diffraction data were collected on Bruker Apex II 4-circle diffractometers with CCD area detectors, using Mo-K_α radiation monochromated by graphite (**2-4**, **2-5**, **2-6**, **2-2M**, **5-4**, **5-5**) or multi-layer focussing mirrors (**2-1**, **5-1**, **5-3**, **5-6**, **5-1M**, **5-3M**). Oxford Cryostreams or Bruker Kryoflex II low-temperature devices. Data were collected at 100 K. The images were processed and corrected for Lorentz-polarization effects and absorption as implemented in the Bruker software packages. The structures were solved using the intrinsic phasing method (SHELXT)[214] and Fourier expansion technique. All non-hydrogen atoms were refined in anisotropic approximation, with hydrogen atoms 'riding' in idealized positions, by full-matrix least squares against F^2 of all data, using SHELXL[215] software and the SHELXLE graphical user interface.[216] The crystal structure of **5-1M** and **5-3M** were refined as racemic twins. Crystals of **5-1M** and **5-3M** desolvate very quickly forming cracks resulting in a decrease of the crystal quality. Furthermore, several acetonitrile solvent molecules and triflate anions are strongly disordered in these compounds and, hence, were modelled using restraints. Diamond[217] software was used for graphical representation. Crystal data and experimental details are listed in Table 7-1 – 7-3; full structural information has been deposited with Cambridge Crystallographic Data Centre. CCDC-1476258 to 1476262 and CCDC-1892920 to 1892926.

7.3 General Photophysical Measurements

All measurements were performed in standard quartz cuvettes (1 cm × 1 cm cross-section), except for **3-5M** in DMSO (plastic of silylated cuvettes were used), in air unless otherwise stated. UV-visible absorption spectra were recorded using an Agilent 8453 diode array UV-visible spectrophotometer. The molar extinction coefficients were calculated from three independently prepared samples in MeCN (**2-1M** – **2-3M**, **3-1M** – **3-5M**, **4-1M** – **4-2M**, **5-1M** – **5-3M**) and hexane (**3-1** – **3-5**, **4-1** – **4-2**) solution. The emission spectra were recorded using an Edinburgh Instruments FLSP920 spectrometer equipped with a double monochromator for both excitation and emission, operating in right-angle geometry mode, and all spectra were fully corrected for the spectral response of the instrument. All solutions used in photophysical measurements had a concentration lower than 5×10^{-6} M to minimize inner filter effects during fluorescence measurements.

7.4 Fluorescence Quantum Yield Measurements

The fluorescence quantum yields were measured using a calibrated integrating sphere (inner diameter: 150 mm) from Edinburgh Instruments combined with the FLSP920 spectrometer described above. For solution-state measurements, the longest-wavelength absorption maximum of the compound in the respective solvent was chosen as the excitation wavelength, unless stated otherwise.

7.5 Lifetime Measurements

Fluorescence lifetimes were recorded using the time-correlated single-photon counting (TCSPC) method using an Edinburgh Instruments FLS980 spectrometer equipped with a high speed photomultiplier tube positioned after a single emission monochromator. Measurements were made in right-angle geometry mode, and the emission was collected through a polarizer set to the magic angle. Solutions were excited with a pulsed diode laser at a wavelength of 376 nm (**3-1** – **3-4**, **3-1M** – **3-4M**, **4-1** – **4-2**), 419 nm (**2-1M** – **2-3M**, **4-1M** – **4-2M**, **5-2M**), 470 nm (**5-3M**) and 509 nm (**3-5**, and **3-5M**) at repetition rates of 10 or 20 MHz, as appropriate. The full-width-at-half-maximum (FWHM) of the pulse from the diode laser was *ca.* 80 ps with an instrument response function (IRF) of *ca.* 230 ps FWHM, *ca.* 90 ps with an instrument response function (IRF) of *ca.* 260 ps FWHM, *ca.* 90 ps with an instrument response function (IRF) of *ca.* 900 ps FWHM, and *ca.* 200 ps with an instrument response function (IRF) of *ca.* 1 120 ps FWHM, respectively. The IRFs were measured from the scatter of an aqueous suspension of Ludox at the excitation wavelength. Decays were recorded to 10 000 counts in the peak channel with a record length of 8 192 channels. The band pass of the emission monochromator and a variable neutral density filter on the excitation side were adjusted to give a signal count rate of <60 kHz.

Iterative reconvolution of the IRF with one decay function and non-linear least-squares analysis were used to analyse the data. The quality of all decay fits was judged to be satisfactory, based on the calculated values of the reduced χ^2 and Durbin-Watson parameters and visual inspection of the weighted residuals.

7.6 Two-Photon Induced Fluorescence Spectroscopy

In Chapter 2: TPA cross-sections (σ_2) were derived from the two-photon excited fluorescence (TPEF) cross-sections ($\sigma_2\Phi_f$) and the fluorescence emission quantum yield (Φ_f). TPEF cross-sections were measured relative to fluorescein in 0.01 M aqueous NaOH,[136b] using the well-established method described by Xu and Webb[136a, 218] and the appropriate solvent-related refractive index corrections.[219] The quadratic dependence of the fluorescence intensity on the excitation power was checked for each sample and all wavelengths. Measurements were conducted using an excitation source delivering fs pulses. A Chameleon Ultra II (COHERENT) was used generating 140 fs pulses at 80 MHz repetition rate. The excitation was focused into the cuvette through a microscope objective (10x, NA 0.25). The fluorescence was detected in epifluorescence mode *via* a dichroic mirror (Chroma 675dcxru) and a barrier filter (Chroma e650sp-2p) by a compact CCD spectrometer module BWTek BTC112E. Total fluorescence intensities were obtained by integrating the corrected emission spectrum.

In Chapter 3 and 4: The two-photon absorption cross-section of the compounds was determined by the relative two-photon induced fluorescence technique. In detail, the fundamental laser source used is an amplified Ti:sapphire laser (Solstice, Spectra Physics) operating at 1 KHz repetition rate with 100 fs pulses at 800 nm. 70% of the available energy seeds a computer-controlled optical parametric amplifier (TOPAS-C, Light Conversion), which produces pulses in the range of 290 – 2 600 nm. Excitation of the samples was achieved using a protected silver parabolic mirror, and vertically polarized light with the excitation energy varying in the 0.2 – 3 μJ range. The latter conditions established by using a series of three thin broadband polarizers and a mechanical rotational mount. Maintenance of identical excitation conditions for both reference and samples was achieved using a high precision motorized rotational stage to ensure that the unknown compounds and the secondary reference standard are subjected to the same excitation conditions. Perylene in CH_2Cl_2, Coumarin 540A in CCl_4, Rhodamine 6G in CH_3OH and Styryl 9M in $CHCl_3$ were used as reference compounds.[218, 220] The emitted fluorescence signal was detected at 90° with respect to the excitation beam, and recorded using a compact CCD spectrometer. Two-photon excitation was verified by log-log plots of fluorescence intensities *vs*. excitation power at various wavelengths, all giving slopes of 2.

7.7 Theoretical Studies

All calculations (DFT and TD-DFT) were carried out with the Gaussian 09 (Rev. D/E.01) program package [221] and were performed on a parallel cluster system. GaussView 5.0.9 was used to visualize the results, to measure calculated structural parameters, and to plot orbital surfaces (isovalue: ±0.03 [e a_0^{-3}]$^{1/2}$). The ground-state geometries were optimized using the B3LYP functional[222] in combination with the 6-31G(d) basis set.[223] The optimized geometries were confirmed to be local minima by performing frequency calculations and obtaining only positive (real) frequencies. Where optimized structures of a higher symmetry (>C_1) were determined as local minima by frequency calculation, the symmetry was included in the subsequent calculations as well. Stability analysis showed the wavefunction to be stable in each case. Based on these optimized structures, the lowest-energy gas-phase vertical transitions were calculated (singlets, 10 states) by TD-DFT, using the Coulomb-attenuated functional CAM-B3LYP[224] in combination with the 6-31G(d) basis set.[222a, 222b] The CAM-B3LYP functional has been shown to be effective for the ICT systems, hence its selection here.[225] Natural transition orbitals were calculated for the lowest energy transition in each case using Multiwfn[226] and simulated absorption spectra were created using GaussSum 3.0.[227] The optimizations were conducted with inclusion of hexane (**3-1** – **3-5**), MeCN (**2-1M** – **2-3M**), EtOH (**4-1M**, **4-2M**) or water (**3-1M** – **3-5M**, **5-1M** – **5-3M**) solvation through the polarizable continuum model (PCM).[228] The ultrafine integration grid was used throughout.

7.8 Cell Culture

In Chapter 2: HepG2-16 cells (ATCC-Number 59159, ATCC Manassas, VA) were maintained in 100 mm culture dishes in growth medium (DMEM containing 10% heat inactivated FBS, 0.1 mM nonessential amino acids, 100 U/mL penicillin G and 100 μg/mL streptomycin) at 37 °C and 5% CO_2. For the cytotoxic experiments, the cells were seeded at a density of 4×10^4 cells/mL (using 125 μL per well) in 96-well plates in growth medium and were grown for 24 h at 37 °C and 5% CO_2. NIH 3T3 cells (ATCC-Number CRL-1658, ATCC, Manassas, VA) and HEK 293T cells (ATCC-Number CRL-1573, ATCC, Manassas, VA) were cultured in 100 mm culture dishes in growth medium (DMEM containing 10% heat inactivated FBS, 100 U/mL penicillin G and 100 μg/mL streptomycin) at 37 °C and 5% CO_2. For the cytotoxic experiments, the cells were seeded at a density of 1.6×10^4 cells/mL (using 125 μL per well) in 96-well plates in growth medium and were grown for 24 h at 37 °C and 5% CO_2. For mitochondrial staining, NIH 3T3 cells were cultured at a density of 2.0×10^4 cells/mL (using 500 μL per well) in Nunc™ Lab-Tek™ II Chamber Slide™ 8-well system in growth medium for 24 h at 37 °C and 5% CO_2. POS-1 cells were cultivated on glass coverslips up to 30% confluence. The cells were further incubated for 8 h with compound

2-3M at a final concentration in the culture media of 300 nM. Cells were then rinsed with PBS, fixed with 4% PFA and mounted using a Fluoromoun aqueous mounting medium.

In Chapter 3: HeLa and HepG2 cells (RIKEN Cell Bank, Japan) were cultured in Dulbecco's modified Eagle's medium (DMEM, Wako) containing 10% fetal bovine serum (FBS, Biosera) and 1% Antibiotic-Antimycotic (AA, Wako) at 37 °C in a 5% CO_2/95% air incubator. Cells (5×10^4) were seeded in poly-lysine coated glass-bottom dishes three days before imaging. In order to facilitate the generation of lipid droplets, the HepG2 cells were treated with fatty acids (oleic acid:palmitic acid = 2:1, 1 mM) in DMEM for 24 h before staining with dyes.

In Chapter 4 and 5: HeLa cells (RIKEN Cell Bank, Japan) were cultured in Dulbecco's modified Eagle's medium (DMEM, Wako) containing 10% fetal bovine serum (FBS, Biosera) and 1% Antibiotic-Antimycotic (AA, Wako) at 37 °C in a 5% CO_2/95% air incubator. Cells (5×10^4) were seeded in poly-lysine coated glass-bottom dishes three days before imaging.

7.9 Staining Experiments

In Chapter 3: The incubation medium was removed from the HeLa cells, and the cells were further incubated with 5 μM **3-1** – **3-3** in DMEM containing 0.5% DMSO for 1 h in a 5% CO_2 incubator. Afterwards, the cells were rinsed with DMEM three times and the dish was filled with 1.5 mL of DMEM. Fluorescence images before and after washing were obtained with a FV10i-DOC confocal laser-scanning microscope (OLYMPUS), with a 405 nm LD laser for excitation. The fluorescence signals were collected between 570 – 670 nm.

The incubation medium was removed from the HepG2 cells and the cells were further incubated with 5 μM of **3-1** or 5 μM of **3-1** premixed with 0.04% Pluronic F-127 in DMEM containing 0.5% DMSO for 24 h in a 5% CO_2 incubator. Fluorescence images before and after washing were obtained with a FV10i-DOC confocal laser-scanning microscope (OLYMPUS), with a 405 nm LD laser for excitation. The fluorescence signals were collected between 570 – 670 nm.

7.10 Co-Staining Experiments

In Chapter 2: NIH 3T3 cells were seeded in Lab-Tek II Chamber Slide 8-well system and were grown for 24 h before mitochondrial staining. After 24 h, the medium was gently aspirated and the cells were washed twice with phosphate buffered saline (PBS). The cells were stained for 45 min at 37 °C and 5% CO_2 using a mixture of 125 nM MitoTracker™ Red CMXRos and 10 μM **2-3M** dissolved in DMEM without any supplements. After washing with PBS five times, the cells were subsequently analysed with a high resolution Leica AOBS SP2 confocal laser scanning microscope (Leica Microsystem, Wetzlar, Germany) using a 63 x oil objective. To avoid cross-talk among the channels, the emission signals were collected independently. Image processing was

performed using ImageJ. Two-photon imaging was performed with a Leica DM 6000TCS SP5 MP FLIM confocal microscope.

In Chapter 3 and 4: The incubation medium was removed from the cells, and the cells were further incubated with 0.5 μM dye (**3-1M** – **3-5M**, **4-1M** – **4-2M**) in DMEM containing 0.5% DMSO for 2 h in a 5% CO_2 incubator. Then the cells were rinsed with DMEM three times and the dish was filled with 2.0 mL of DMEM containing 0.1 μM LysoTracker™ Green or LysoTracker™ Red (Invitrogen) and further incubated for 20 min in a CO_2 incubator. Fluorescence images were obtained with a confocal microscope (TCS SP8 STED 3X; Leica), including an inverted DMI6000 CS microscope equipped with a laser diode (405 nm), a tunable (470 – 670 nm) pulsed white light laser (WLL; repetition rate of 78 MHz) for excitation. For confocal imaging, a HyD detector and 100 × oil-immersion objective (NA 1.4) were used. The dyes were excited with the 405 nm diode laser (**3-1M** – **3-4M**, **4-1M** – **4-2M**), and the 561 nm wavelength of the WLL (LysoTracker™ Red). The fluorescence signals were collected between 450 and 550 nm (**3-1M** – **3-3M**), 500 and 605 nm (**3-4M**, **4-1M** – **4-2M**), 600 and 750 nm (LysoTracker™ Red in the co-staining experiment with **3-1M** – **3-3M**) and 607 and 786 nm (LysoTracker™ Red in the co-staining experiment with **3-4M**) with a time gating interval of 0.1 − 12 ns. Each image was recorded with a line average of 4. To avoid crosstalk among the channels, the emission signals were collected independently in the sequential scanning mode. Fluorescence images (**3-5M**) were obtained with an FV10i-DOC confocal laser-scanning microscope (OLYMPUS), using LD lasers of 473 nm and 559 nm were used for the excitation of LysoTracker™ Green and **3-5M**, respectively. The fluorescence signals were collected between 490 and 540 nm (LysoTracker™ Green) and 570 and 670 nm (**3-5M**). Images were processed with Fiji software.

In Chapter 5: The incubation medium was removed from the cells, and the cells were further incubated with 5 μM **5-3M** in DMEM containing 0.5% DMSO for 1 h in a CO_2 incubator. Then the cells were rinsed with DMEM three times and the dish was filled with 1.5 mL of DMEM containing 0.1 μM LysoTracker™ Red (Invitrogen) and further incubated for 20 min in a 5% CO_2 incubator. Fluorescence images were obtained with an FV10i-DOC confocal laser-scanning microscope (OLYMPUS), where LD lasers of 473 nm and 559 nm were used for the excitation of **5-3M** and LysoTracker™ Red, respectively. Images were processed with Fiji software.

7.11 Cytotoxicity Evaluation.

In Chapter 2: NIH 3T3, HEK 293T and HepG2-16 were seeded in quadruplets using 96-well plates and were grown for 24 h. After incubation of 24 h, the cells were treated with increasing concentrations of the compounds **2-1M**, **2-2M** and **2-3M** dissolved in growth medium ranging from 0.1 μM to 100 μM for 24 and 48 h. Untreated cells were used as control. Cell viability was

assessed using the WST-1 colorimetric assay following the manufacturer's instructions. The medium was gently aspirated and replaced while adding 10 μL WST-1 after 24 and 48 h. After 4 h of incubation at 37 °C and 5% CO_2, the absorbance of the formed soluble formazan was measured at 450 and 630 nm using a SPECTRAmax 250 automated microtiter plate reader (Molecular Devices, Sunnyvale, USA).

In Chapter 3, 4 and 5: HeLa cells were seeded into a flat-bottomed 96-well plate (1 $\times 10^4$ cells/well) and incubated in DMEM at 37 °C in a 5% CO_2/95% air incubator for 24 h. The medium was then replaced with culture medium (100 μL/well) containing various concentrations of **3-1M** – **3-5M**, **4-1M** – **4-2M**, **5-3M** (0, 0.5, 1, 5, and 10 μM) in DMEM (0.5% DMSO). Then the cells were incubated for 24 h at 37 °C, MTT reagent (10 μL/well, 0.5 mg/mL) in PBS was added to each well, and the plates were incubated for another 4 h in a 5% CO_2 incubator. The medium was then removed, the formazan crystals were solubilized in DMSO (100 μL/well) for 10 min at room temperature, and the absorbance of each well was measured at 535 nm using a SpectraMax i3 (Molecular Devices).

7.12 Uptake Pathway

In Chapter 3: The incubation medium was removed from the cells, and the cells were incubated with 0.5 μM **3-5M** in 1.5 mL DMEM. Fluorescence images (**3-5M**) were obtained with a FV10i-DOC confocal laser-scanning microscope (OLYMPUS), and a 559 nm LD laser was used for the excitation of **3-5M**. The fluorescence signals were collected between 570 and 670 nm every 10 min over a period of 2 hours. Images were processed with Fiji software. In the cellular uptake control experiment, cells were stained at 37 °C with 500 nM of **3-5M** in DMEM, washed with fresh DMEM and subsequent imaging. In the cellular uptake experiment at 4 °C experiment, cells were incubated at 4 °C for 30 min, then grown in DMEM containing **3-5M** (500 nM) for 2 h at 4 °C, washed with fresh DMEM and subsequent imaging. In the cellular uptake experiment in the presence of NaN_3 cells were first pretreated at 37 °C for 30 min with DMEM containing 0.1% NaN_3 and then incubated with DMEM containing **3-5M** (500 nM) and 0.1% NaN_3 for 2 h at 37 °C. Afterwards, the cells were washed with fresh DMEM followed by imaging. Fluorescence images were obtained with a FV10i-DOC confocal laser-scanning microscope (OLYMPUS), and a 559 nm LD laser was used for the excitation of **3-5M**. The fluorescence signals were collected between 570 and 670 nm.

7.13 Photostability

In Chapter 3: The incubation medium was removed from the cells, and the cells were further incubated with 0.5 μM **3-5M** or 0.1 μM LysoTracker™ Red (Invitrogen) in DMEM in a 5% CO_2 incubator for 2 h or 20 min, respectively. Then cells stained with **3-5M** were rinsed with DMEM

three times and the dish was filled with 1.5 mL of DMEM. Imaging experiments were conducted using a Leica TCS SP8 STED 3X system (Leica Microsystems), including an inverted DMI6000 CS microscope equipped with a tunable (470 – 670 nm) pulsed white light laser (WLL; repetition rate of 78 MHz) for excitation. For confocal imaging, a HyD detector and 100 × oil-immersion objective (NA 1.4) were used. For the evaluation of photostability under confocal conditions, dye-stained cells prepared above were irradiated with a WLL at 561 nm, the fluorescence signals were collected between 570 and 770 nm and images were acquired at the following setting: 1 024 × 1 024 pixels; scan speed of 100 Hz; bidirectional model; zoom factor of 5; line average of 4; frame average of 1. The total signal intensity of each image was normalized to the value of the first image and plotted as a function of the number of recorded confocal images.

7.14 TPA Imaging

In Chapter 3: The incubation medium was removed from the cells, and the cells were further incubated with 0.5 μM **3-5M** in DMEM in a CO_2 incubator for 2 h. Then the cells were rinsed with DMEM three times and the dish was filled with 15 mL of DMEM containing 20 mM HEPES (pH = 7.4). Imaging experiments were conducted using a Leica SP8-MP system (Leica Microsystems), equipped with a tunable (680 – 1 300 nm) for laser two-photon excitation. For TPA imaging, a HyD detector with a 650/50 bandpass filter and Lens HC Fluotar L 25 × 0.95 W VisIR objective were used. The dye was excited with the 720 nm wavelength of the laser and fluorescence signals were collected between 600 and 700 nm.

In Chapter 5: The incubation medium was removed from the cells, and the cells were further incubated with 0.5 μM **4-1M** or **4-2M** in DMEM in a CO_2 incubator for 2 h. Then the cells were rinsed with DMEM three times and the dish was filled with 15 mL of DMEM containing 20 mM HEPES (pH = 7.4). Imaging experiments were conducted using a Leica SP8-MP system (Leica Microsystems), equipped with a tunable (680 – 1 300 nm) laser for two-photon excitation. For TPA imaging, a HyD detector with a 585/40 bandpass filter and a Lens HCX APO L 40 × 0.80 W UVI objective were used. The dyes were excited with the 800 nm wavelength of the laser and fluorescence signals were collected through a 585/40 band pass filter.

7.15 Synthesis

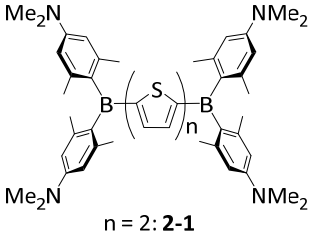

n = 2: **2-1**

5,5'-*Bis*[*bis*[4-(*N,N*-dimethylamino)-2,6-xylyl]boryl]-2,2'-bithiophene (2-1). *n*-BuLi (1.6 M in hexane, 1.18 mL, 1.90 mmol, 2.2 eq.) was added to a solution of 2,2'-bithiophene (143 mg, 0.86 mmol, 1.0 eq.) in THF (2.6 mL) at -78 °C. After addition, the mixture was stirred at -78 °C for 15 min and then warmed to r.t. After cooling to -78 °C again, a solution of *bis*[4-(*N*,*N*-dimethylamino)-2,6-xylyl]fluoroborane **2-4** (700 mg, 2.14 mmol, 2.5 eq.) in THF (3 mL) was added. The mixture was warmed to r.t., stirred for 1 h, and then heated at 40 °C for 15 min. The solvent was removed under vacuum, and the residue was purified by column chromatography on Al_2O_3 with hexane:CH_2Cl_2 1:1 as the eluent to remove forerunning impurities and then with the addition of 10% Et_2O to elute the product. The solvent of the product fraction was removed under reduced pressure and the solid residue was dissolved in a CH_2Cl_2/MeOH mixture. Partial evaporation led to the precipitation of the product **2-1**, which was then collected by filtration and dried (305 mg, 46%). Single crystals were obtained by slow evaporation of a CH_2Cl_2/MeOH solution.

^{1}H NMR (500 MHz, CD_2Cl_2): δ = 7.37 (d, *J* = 4 Hz, 2H), 7.24 (d, *J* = 4 Hz, 2H), 6.38 (s, 8H), 2.96 (s, 24H), 2.09 (s, 24H) ppm.

^{13}C{^{1}H} NMR (125 MHz, CD_2Cl_2): δ = 152.6, 151.5, 148.3, 143.0, 140.2, 133.5, 126.8, 111.7, 40.3, 24.3 ppm.

^{11}B{^{1}H} NMR (160 MHz, CD_2Cl_2): δ = 65 ppm.

HRMS (ESI$^+$): *m/z* found: $[M+H]^+$ 779.4493 [M+H]; calc. for $[C_{48}H_{61}B_2N_4S_2]^+$ 779.4518 (|Δ| = 3.21 ppm).

Elem. Anal. Calc. (%) for $C_{48}H_{60}B_2N_4S_2$: C 74.03, H 7.77, N 7.19, S 8.23; found: C 74.31, H 7.86, N 7.39, S 8.01.

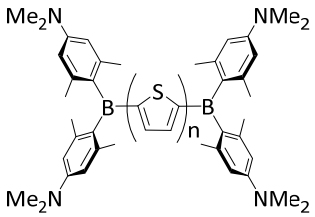

n = 4: **2-2**

5,5‴-*Bis*[*bis*[4-(*N*,*N*-dimethylamino)-2,6-xylyl]boryl]-2,2′:5′,2″:5″,2‴-quaterthiophene (2-2). *n*-BuLi (1.6 M in hexane, 1.01 mL, 1.60 mmol, 2.2 eq.) was added to a solution of 2,2′:5′,2″:5″,2‴-quaterthiophene (243 mg, 0.74 mmol, 1.0 eq.) in THF (15 mL) at -78 °C. After addition, the mixture was warmed to r.t. and stirred for 2 h. The solution was cooled again to -78 °C, and then a solution of *bis*[4-(*N*,*N*-dimethylamino)-2,6-xylyl]fluoroborane **2-4** (600 mg, 1.83 mmol, 2.5 eq.) in THF (4 mL) was added. The mixture was warmed to r.t. and stirred overnight. The solvent was removed under vacuum, and the residue was dissolved in CH_2Cl_2 and eluted through a silica gel pad, firstly using CH_2Cl_2 as the eluent to remove forerunning impurities and then with the addition of 10% Et_2O to elute the product. The product fraction was reduced to dryness and the solid residue was dissolved in a mixture of Et_2O and MeOH. Partial evaporation led to the precipitation of the product **2-2**, which was then collected by filtration and dried (362 mg, 51%).

^{1}H NMR (500 MHz, CD_2Cl_2): δ = 7.32 (d, *J* = 4 Hz, 2H), 7.28 (d, *J* = 4 Hz, 2H), 7.20 (d, *J* = 4 Hz, 2H), 7.11 (d, *J* = 4 Hz, 2H), 6.41 (s, 8H), 2.98 (s, 24H), 2.13 (s, 24H) ppm.

^{13}C{^{1}H} NMR (125 MHz, CD_2Cl_2): δ = 152.0, 151.4, 147.7, 143.0, 140.2, 137.1, 137.0, 133.4, 126.1, 125.7, 125.1, 111.7, 40.3, 24.3 ppm.

^{11}B{^{1}H} NMR (160 MHz, CD_2Cl_2): δ = 66 ppm.

HRMS (ESI$^+$): *m*/*z* found: 943.4263 $[M+H]^+$; calc. for $[C_{56}H_{65}B_2N_4S_4]^+$ 943.4273 (|Δ| = 1.06 ppm).

Elem. Anal. Calc. (%) for $C_{56}H_{64}B_2N_4S_4$: C 71.32, H 6.84, N 5.94, S 13.06; found: C 71.63, H 6.96, N 6.09, S 13.45.

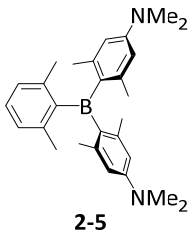

2-5

***Bis*[4-(*N*,*N*-dimethylamino)-2,6-dimethylphenyl]-2,6-dimethylphenylborane 2-5.** A degassed solution of 2-bromo-*m*-xylene (3.90 g, 21.1 mmol, 1.0 eq.) in THF (20 mL) was cooled to -78 °C and *t*-BuLi (1.7 M in pentane, 25.0 mL, 42.2 mmol, 2.0 eq.) was added dropwise over 45 min. After addition of *t*-BuLi, the reaction was allowed to warm to r.t. A solution of *bis*[4-(*N*,*N*-dimethylamino)-2,6-xylyl]fluoroborane **2-4** (5.00 g, 15.3 mmol, 1.0 eq.) in THF (5 mL) was added, and the reaction mixture was stirred overnight at r.t. The reaction was quenched with H_2O (20 mL), and the aqueous layer was extracted with hexane (3 × 50 mL). The combined organic phases were dried over $MgSO_4$, filtered and concentrated under reduced pressure. Recrystallization from Et_2O afforded the title compound as a pale-yellow solid (4.85 g, 77%).

^{1}H NMR (500 MHz, CD_2Cl_2): δ = 7.09 (t, *J* = 7.5 Hz, 1H) 6.90 (d, *J* = 7.5 Hz, 2H), 6.33 (br s, 2H), 6.32 (br s, 2H), 2.96 (s, 12H), 2.04 (s, 6H), 2.03 (s, 6H), 1.94 (s, 6H) ppm.

^{13}C{^{1}H} NMR (125 MHz, CD_2Cl_2): δ = 151.6, 149.7, 143.2, 142.8, 140.3, 136.2, 128.6, 127.6, 111.9, 111.8, 40.2, 24.1, 23.7, 23.0 ppm.

^{11}B{^{1}H} NMR (160 MHz, CD_2Cl_2): δ = 73 ppm.

HRMS (ESI^+): *m*/*z* found: 413.3117 $[M+H]^+$; calc. for $[C_{28}H_{38}BN_2]^+$ 413.3123 (|Δ| = 1.45 ppm).

Elem. Anal. Calc. (%) for $C_{28}H_{37}BN_2$: C 81.54, H 9.04, N 6.79; found: C 81.93, H 9.19, N 7.07.

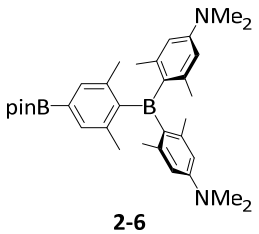

2-6

***Bis*[4-(*N*,*N*-dimethylamino)-2,6-xylyl]-2,6-dimethyl-4-(4,4,5,5-tetramethyl-1,3,2-dioxaborlan-2-yl)phenylborane 2-6.** Compound **2-5** (2.60 g, 6.31 mmol, 1.0 eq.), B_2pin_2 (pin = pinacolato) (1.92 g, 7.57 mmol, 1.2 eq.), 4,4′-di-*tert*-butyl-2,2′-bipyridine (dtbpy) (33.9 mg, 0.13 mmol, 2 mol%) and $[Ir(COD)(\mu\text{-OMe})]_2$ (COD = 1,5-cyclooctadiene) (41.8 mg, 0.06 mmol, 1 mol%) were dissolved in THF (10 mL) and heated at 70 °C for 3 d. After the solvent was removed, the resulting solid was purified by filtration through a silica pad with CH_2Cl_2 and recrystallized in MeCN to afford the title compound as a yellow solid (3.25 g, 96%).

^{1}H NMR (500 MHz, CD_2Cl_2): δ = 7.27 (s, 2H), 6.31 (br s, 2H), 6.30 (br s, 2H), 2.95 (s, 12H), 2.04 (s, 6H), 2.01 (s, 6H), 1.90 (s, 6H), 1.33 (s, 12H) ppm.

^{13}C{^{1}H} NMR (125 MHz, CD_2Cl_2): δ = 153.3, 151.7, 143.3, 142.9, 139.4, 135.9, 133.7, 128.9, 111.9, 111.8, 83.9, 40.1, 25.1, 24.0, 23.7, 22.8 ppm.

^{11}B{^{1}H} NMR (160 MHz, CD_2Cl_2): δ = 74, 30 ppm.

HRMS (ESI^+): *m*/*z* found: 538.3901 $[M]^+$; calc. for $[C_{34}H_{48}B_2N_2O_2]^+$ 538.3896 ($|\Delta|$ = 0.93 ppm).

Elem. Anal. Calc. (%) for $C_{34}H_{48}B_2N_2O_2$: C 75.85, H 8.99, N 5.20; found: C 75.65, H 8.94, N 5.18.

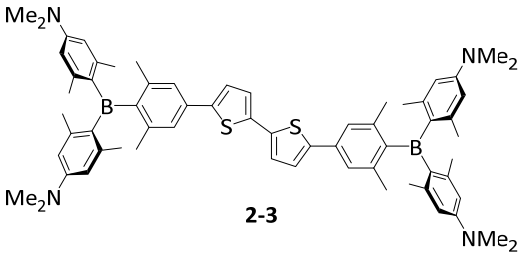

2-3

5,5'-*Bis*[4-[*bis*[4-(*N*,*N*-dimethylamino)-2,6-xylyl]boryl]-3,5-xylyl]-2,2'-bithiophene (2-3).

Compound **2-6** (1.00 g, 1.86 mmol, 2.2 eq.), 5,5'-dibromo-2,2'-bithiophene (274 mg, 0.85 mmol, 1.0 eq.), KOH (285 mg, 5.07 mmol, 6.0 eq.) and SPhos (2-dicyclohexylphosphino-2',6'-dimethoxybiphenyl) (52.5 mg, 0.05 mmol, 20 mol%) were dissolved in a degassed mixture of toluene (10 mL) and H_2O (5 mL). The reaction mixture was degassed and $Pd_2(dba)_3 \cdot CHCl_3$ (dba = dibenzylideneacetone) (24.0 mg, 0.02 mmol, 5 mol%) was added. The reaction was heated to 85 °C and stirred for 20 h. Reaction monitoring by TLC (hexane:EtOAc 5:1) indicated that the starting material was consumed. Therefore, the phases were separated, and the aqueous solution was extracted with hexane (3 × 10 mL). The combined organic layers were concentrated under reduced pressure and the residue was purified by column chromatography (silica gel, hexane:EtOAc 5:1). The obtained yellow solid was dissolved in Et_2O and crystallized by adding MeOH to afford **2-3** as a yellow solid (360 mg, 82%).

^{1}H NMR (500 MHz, CD_2Cl_2): δ = 7.29 (d, *J* = 3.8 Hz, 2H), 7.19 (s, 4H), 7.18 (d, *J* = 3.8 Hz, 2H), 6.32 (br s, 4H), 6.32 (br s, 4H), 2.95 (s, 24H), 2.07 (s, 12H), 2.02 (s, 12H), 1.97 (s, 12H) ppm.

^{13}C{^{1}H} NMR (125 MHz, CD_2Cl_2): δ = 151.7, 149.8, 143.9, 143.2, 142.9, 141.3, 136.6, 136.0, 133.7, 124.7, 124.5, 123.7, 111.9, 111.8, 40.1, 24.0, 23.8, 23.0 ppm.

^{11}B{^{1}H} NMR (160 MHz, CD_2Cl_2): δ = 74 ppm.

HRMS (ESI^+): *m*/*z* found: 987.5751 $[M+H]^+$; calc. for $[C_{64}H_{77}B_2N_4S_2]^+$ 987.5770 (|Δ| = 1.92 ppm).

Elem. Anal. Calc. (%) for $C_{64}H_{76}B_2N_4S_2$: C 77.88, H 7.76, N 5.68, S 6.50; found: C 77.92, H 7.74, N 5.76, S 6.22.

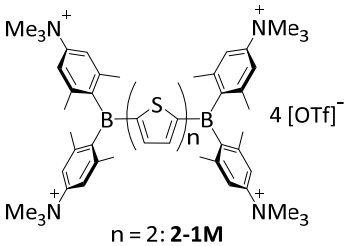

n = 2: **2-1M**

5,5′-*Bis*[*bis*[4-(*N*,*N*,*N*-trimethylammonio)-2,6-xylyl]boryl]-2,2′-bithiophene tetratriflate (2-1M). Methyl triflate (220 μL, 2.00 mmol, 10.0 eq.) was added to a solution of **2-1** (150 mg, 0.19 mmol, 1.0 eq.) in CH_2Cl_2 (6 mL) at r.t. The mixture was stirred overnight at r.t. and then filtered. The solid was washed with CH_2Cl_2 and dried to obtain the product **2-1M** (280 mg, 100%).

^{1}H NMR (500 MHz, CD_3OD): δ = 7.69 (d, *J* = 4 Hz, 2H), 7.62 (s, 8H), 7.50 (d, *J* = 4 Hz, 2H), 3.68 (s, 36H), 2.32 (s, 24H) ppm.

^{13}C{^{1}H} NMR (125 MHz, CD_3OD): δ = 152.2, 149.8, 149.3, 146.3, 145.1, 145.1, 129.9, 121.8 (q, *J* = 319 Hz), 119.7, 57.5, 24.2 ppm.

Solid-State ^{11}B{^{1}H} NMR (128 MHz): Isotropic chemical shift δ_{iso} = 64.2 ppm, quadrupole coupling constant C_Q = 4.39 MHz, quadrupolar asymmetry parameter η_{Quad} = 0.0.

HRMS (ESI$^+$) *m*/*z* found: $[M\text{-}2OTf]^{2+}$ 568.22049; calc. for $[C_{54}H_{72}B_2N_4S_4O_6F_6]^{2+}$ 568.22070 (|Δ| = 0.37 ppm).

Elem. Anal. Calc. (%) for $C_{56}H_{72}B_2F_{12}N_4O_{12}S_6$: C 46.87, H 5.06, N 3.90, S 13.41; found: C 46.08, H 5.31, N 3.94, S 13.42.

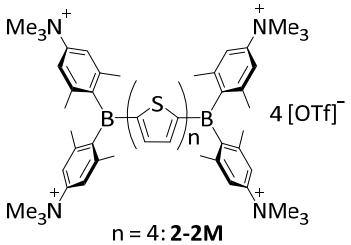

n = 4: **2-2M**

5,5‴-*Bis*[*bis*[4-(*N*,*N*,*N*-trimethylammonio)-2,6-xylyl]boryl]-2,2′:5′,2″:5″,2‴-quarterthiophene tetratriflate (2-1M). Methyl triflate (180 μL, 1.64 mmol, 10.0 eq.) was added to a solution of **2-1** (150 mg, 0.16 mmol, 1.0 eq.) in CH_2Cl_2 (15 mL) at r.t., and then the mixture was stirred for 48 h and filtered. The solid was washed with CH_2Cl_2 and dried to obtain **2-1M** (259 mg, 100%).

^{1}H NMR (500 MHz, CD_3OD): δ = 7.63 (s, 8H), 7.56 (d, *J* = 3.5 Hz, 2H), 7.48 (d, *J* = 3.5 Hz, 2H), 7.41 (d, *J* = 4 Hz, 2H), 7.31 (d, *J* = 4 Hz, 2H), 3.69 (s, 36H), 2.34 (s, 24H) ppm.

^{13}C{^{1}H} NMR (125 MHz, CD_3OD): δ = 153.5, 149.2, 147.8, 146.5, 145.4, 145.1, 139.2, 137.0, 128.5, 128.1, 127.0, 121.8 (q, *J* = 319 Hz), 119.6, 57.5, 24.2 ppm.

Solid-State ^{11}B{^{1}H} NMR (128 MHz): Isotropic chemical shift δ_{iso} = 62.6 ppm, quadrupole coupling constant C_Q = 4.31 MHz, quadrupolar asymmetry parameter η_{Quad} = 0.0.

HRMS (ESI) *m*/*z* found: $[M\text{-}2OTf]^{2+}$ 650.2082; calc. for $[C_{62}H_{76}B_2F_6N_4O_6S_6]^{2+}$ 650.2084 (|Δ| = 0.31 ppm).

Elem. Anal. Calc. (%) for $C_{64}H_{76}B_2F_{12}N_4O_{12}S_8$: C 48.06, H 4.79, N 3.50, S 16.04; found: C 46.52, H 5.10, N 3.67, S 15.89.

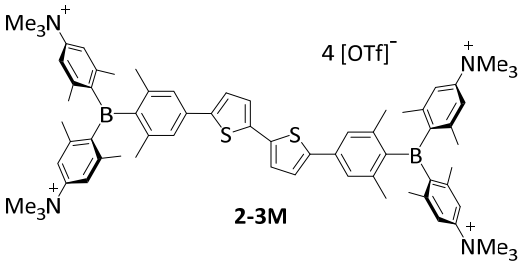

2-3M

5,5′-*Bis*[4-[*bis*[4-(*N*,*N*,*N*-trimethylammonio)-2,6-xylyl]boryl]-3,5-xylyl]-2,2′-bithiophene tetratriflate (2-3M). The neutral compound **2-3** (100 mg, 0.10 mmol, 1.0 eq.) was dissolved in dry CH_2Cl_2 (10 mL) and Et_2O (3.5 mL) and treated with methyl triflate (115 μL, 1.0 mmol, 10.0 eq.). The reaction mixture was stirred for 20 h at r.t. A yellow solid was precipitated by adding Et_2O (20 mL), which was collected by filtration and washed with Et_2O to afford **2-3M** as a yellow solid (126 mg, 76%).

^{1}H NMR (500 MHz, CD_3OD): δ = 7.58 (br s, 4H), 7.57 (br s, 4H), 7.47 (d, *J* = 3.9 Hz, 2H), 7.35 (s, 4H), 7.29 (d, *J* = 3.9 Hz, 2H), 3.66 (s, 36H), 2.25 (s, 12H), 2.16 (s, 12H), 2.08 (s, 12H) ppm.

^{13}C{^{1}H} NMR (125 MHz, CD_3OD): δ = 149.7, 149.4, 144.9, 144.5, 143.7, 143.2, 138.4, 137.8, 126.2, 126.2, 126.1, 121.8 (q, *J* = 318 Hz), 120.1, 57.5, 23.6, 23.4 ppm.

Solid-State ^{11}B{^{1}H} NMR (128 MHz): Isotropic chemical shift δ_{iso} = 77.0 ppm, quadrupole coupling constant C_Q = 4.77 MHz, quadrupolar asymmetry parameter η_{Quad} = 0.0.

HRMS (ESI^+): *m/z* found: 672.28265 $[M\text{-}2OTf]^{2+}$; calc. for $[C_{70}H_{88}B_2F_6N_4O_6S_4]^{2+}$ 672.28330 (|Δ| = 0.97 ppm).

Elem. Anal. Calc. (%) for $C_{72}H_{88}B_2N_4F_{12}O_{12}S_6$: C 52.62, H 5.40, N 3.41, S 11.71; found: C 52.20, H 5.57, N 3.45, S 11.57.

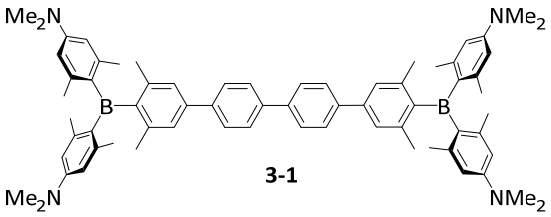

3-1

4,4'-*Bis*[4-[*bis*[4-(*N*,*N*-dimethylamino)-2,6-xylyl]boryl]-3,5-xylyl]-1,1'-biphenyl (3-1).

Compound **2-6** (500 mg, 0.93 mmol, 2.1 eq.), 4,4'-dibromobiphenyl (138 mg, 0.44 mmol, 1.0 eq.) and KOH (149 mg, 2.66 mmol, 6.0 eq.) were dissolved in a degassed mixture of H_2O (5 mL) and toluene (10 mL). The reaction mixture was degassed for 15 min and SPhos (36.4 mg, 88.7 μmol, 20 mol%) and $Pd_2(dba)_3{\cdot}CHCl_3$ (24.3 mg, 23.5 μmol, 5 mol%) were added. After heating to 85 °C for 3 d, the aqueous layer was extracted with hexane (3 × 30 mL). The solvent was evaporated and the crude product was purified by automated flash column chromatography (KP-Sil 50 g, hexane:ethylacetate 5:1) to obtain compound **3-1** as a yellow solid (310 mg, 72%).

^{1}H NMR (500 MHz, CD_2Cl_2): δ = 7.77 – 7.73 (m, 8H), 7.25 (s, 4H), 6.33 (s, 4H), 6.33 (s, 4H), 2.96 (s, 24H), 2.12 (s, 12H), 2.03 (s, 12H), 1.99 (s, 12H) ppm.

^{13}C{^{1}H} NMR (125 MHz, CD_2Cl_2): δ = 151.7, 149.0, 143.2, 142.9, 141.1, 140.4, 140.2, 139.6, 136.2, 127.5, 127.4, 126.0, 111.9, 111.8, 40.2, 24.0, 23.8, 23.1 ppm.

Solid-State ^{11}B{^{1}H} NMR (128 MHz): Isotropic chemical shift δ_{iso} = 72.8 ppm, quadrupole coupling constant C_Q = 4.49 MHz, quadrupolar asymmetry parameter η_{Quad} = 0.0.

HRMS (ESI$^+$): *m/z* found: $[M]^+$ 975.6637; calc. for $[C_{68}H_{80}B_2N_4]^+$ 975.6642 ($|\Delta|$ = 0.51 ppm).

Elem. Anal. Calc. (%) for $C_{68}H_{80}B_2N_4$: C 83.77, H 8.27, N 5.75; found: C 83.83, H 8.28, N 5.49.

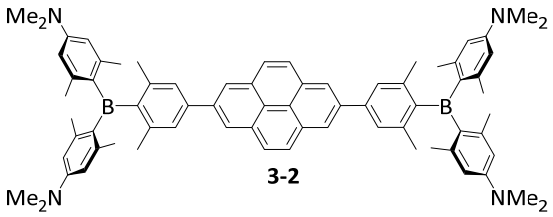

3-2

2,7-*Bis*[4-[*bis*[4-(*N*,*N*-dimethylamino)-2,6-xylyl]boryl]-3,5-xylyl]-pyrene (3-2). Compound **2-6** (1.00 g, 1.86 mmol, 2.2 eq.), 2,7-dibromopyrene (304 mg, 0.85 mmol, 1.0 eq.) and KOH (285 mg, 5.07 mmol, 6.0 eq.) were dissolved in a degassed mixture of H_2O (5 mL) and toluene (10 mL). The reaction mixture was degassed for 15 min and SPhos (104 mg, 254 μmol, 30 mol%) and $Pd_2(dba)_3{\cdot}CHCl_3$ (52.5 mg, 50.7 μmol, 6 mol%) were added. After heating to 85 °C for 16 h, the aqueous layer was extracted with hexane (3 × 30 mL). The solvent was evaporated and the crude product was purified by automated flash column chromatography (KP-Sil 100 g, hexane:ethylacetate 9:1). The yellow solid obtained was dissolved in CH_2Cl_2 and crystallized by adding MeOH to afford **3-2** as a yellow solid (399 mg, 46%).

^{1}H NMR (500 MHz, CD_2Cl_2): δ = 8.49 (s, 4H), 8.15 (s, 4H), 7.51 (s, 4H), 6.36 (s, 8H), 2.97 (s, 24H), 2.21 (s, 12H), 2.07 (s, 12H), 2.05 (s, 12H) ppm.

^{13}C{^{1}H} NMR (125 MHz, CD_2Cl_2): δ = 151.7, 149.1, 143.3, 143.0, 141.4, 141.0, 139.3, 136.2, 131.9, 128.2, 127.0, 124.1, 123.9, 111.9, 111.9, 40.2, 24.1, 23.9, 23.2 ppm.

Solid-State ^{11}B{^{1}H} NMR (128 MHz): Isotropic chemical shift δ_{iso} = 71.9 ppm, quadrupole coupling constant C_Q = 4.51 MHz, quadrupolar asymmetry parameter η_{Quad} = 0.0.

HRMS (ESI$^+$): *m/z* found: $[M]^+$ 987.6623; calc. for $[C_{69}H_{80}B_2N_4]^+$ 987.6642 ($|\Delta|$ = 1.92 ppm).

Elem. Anal. Calc. (%) for $C_{72}H_{82}B_2N_4$: C 84.36, H 8.06, N 5.47; found: C 82.87, H 8.05, N 5.33.

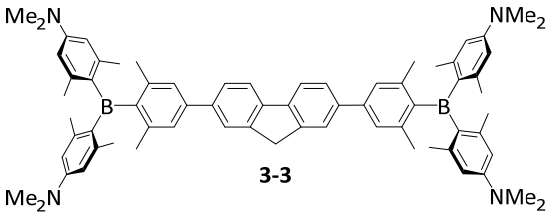

3-3

2,7-*Bis*[4-[*bis*[4-(*N*,*N*-dimethylamino)-2,6-xylyl]-boryl]-3,5-xylyl]-fluorene (3-3). Compound **2-6** (1.00 g, 1.86 mmol, 2.2 eq.), 2,7-dibromofluorene (274 mg, 0.85 mmol, 1.0 eq.) and KOH (285 mg, 5.08 mmol, 6.0 eq.) were dissolved in a degassed mixture of H_2O (5 mL) and toluene (10 mL). The reaction mixture was degassed for 15 min and SPhos (104 mg, 253 μmol, 30 mol%) and $Pd_2(dba)_3{\cdot}CHCl_3$ (52.5 mg, 50.7 μmol, 6 mol%) were added. After heating to 85 °C for 16 h, the aqueous layer was extracted with hexane (3 × 30 mL). The solvent was evaporated and the crude product was purified by automated flash column chromatography (KP-Sil 100 g, hexane:ethylacetate 98:2). The yellow solid obtained was dissolved in Et_2O and crystallized by adding MeOH to afford **3-3** as a yellow solid (511 mg, 61%).

^{1}H NMR (500 MHz, CD_2Cl_2): δ = 7.88 – 7.85 (m, 4H), 7.72 – 7.70 (m, 2H), 7.28 (s, 4H), 6.35 (s, 4H), 6.35 (s, 4H), 4.03 (s, 2H), 2.97 (s, 24H), 2.14 (s, 12H), 2.06 (s, 12H), 2.02 (s, 12H) ppm.

^{13}C{^{1}H} NMR (125 MHz, CD_2Cl_2): δ = 151.7, 148.8, 144.7, 143.2, 142.9, 141.1, 141.1, 140.9, 140.1, 136.3, 126.2, 126.0, 123.8, 120.4, 111.9, 111.9, 40.2, 37.4, 24.0, 23.8, 23.2 ppm.

Solid-State ^{11}B{^{1}H} NMR (128 MHz): Isotropic chemical shift δ_{iso} = 73.0 ppm, quadrupole coupling constant C_Q = 4.53 MHz, quadrupolar asymmetry parameter η_{Quad} = 0.0.

HRMS (ESI$^+$): *m/z* found: $[M]^+$ 987.6623; calc. for $[C_{69}H_{80}B_2N_4]^+$ 987.6642 ($|\Delta|$ = 1.92 ppm).

Elem. Anal. Calc. (%) for $C_{69}H_{80}B_2N_4$: C 83.96, H 8.17, N 5.68; found: C 83.94, H 8.38, N 5.71.

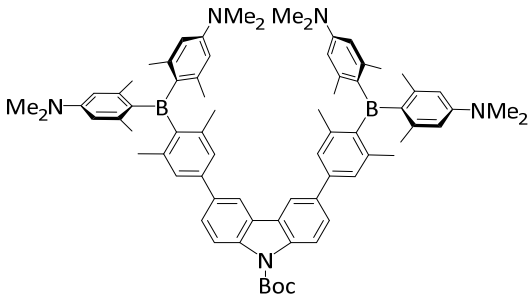

3-4

3,6-*Bis*[4-[*bis*[4-(*N*,*N*-dimethylamino)-2,6-xylyl]boryl]-3,5-xylyl]-*N*-*Boc*-carbazole (3-4).

Compound **2-6** (1.00 g, 1.86 mmol, 2.2 eq.), 3,6-dibromo-*N*-*Boc*-carbazole (359 mg, 0.84 mol, 1.0 eq.) and KOH (283 mg, 5.04 mmol, 6.0 eq.) were dissolved in a degassed mixture of H_2O (10 mL) and toluene (20 mL). The reaction mixture was degassed for 15 min and SPhos (103 mg, 252 μmol, 30 mol%) and $Pd_2(dba)_3{\cdot}CHCl_3$ (52.2 mg, 50.4 μmol, 6 mol%) were added. After heating to 85 °C for 3 d, the aqueous layer was extracted with hexane (3 × 30 mL). The solvent was evaporated and the crude product was purified by automated flash column chromatography (KP-Sil 100 g, hexane:ethylacetate 97:3 → 95:5 → 90:10) to obtain compound **3-4** as a yellow solid (757 mg, 83%).

^{1}H NMR (500 MHz, CD_2Cl_2): δ = 8.42 - 8.41 (m, 2H), 8.40 - 8.39 (m, 2H), 7.87 - 7.85 (m, 2H), 7.40 (s, 4H), 6.39 - 6.38 (m, 8H), 3.00 (s, 24H), 2.21 (s, 12H), 2.10 (s, 12H), 2.08 (s, 12H), 1.84 (s, 9H) ppm.

^{13}C{^{1}H} NMR (125 MHz, CD_2Cl_2): δ = 151.7, 151.4, 148.7, 143.2, 142.9, 141.2, 140.8, 138.7, 136.6, 136.3, 126.7, 126.4, 126.3, 118.0, 116.9, 112.0, 111.9, 84.4, 40.2, 28.6, 24.1, 23.9, 23.3 ppm.

^{11}B{^{1}H} NMR (160 MHz, CD_2Cl_2): δ = 73 ppm.

HRMS (ESI$^+$): *m/z* found: $[M+H]^+$ 1088.7112; calc. for $[C_{73}H_{88}B_2N_5O_2]^+$ 1088.7119 ($|\Delta|$ = 0.64 ppm).

Elem. Anal. Calc. (%) for $C_{73}H_{87}B_2N_5O_2$: C 80.58, H 8.06, N 6.44; found: C 80.65, H 8.24, N 6.53.

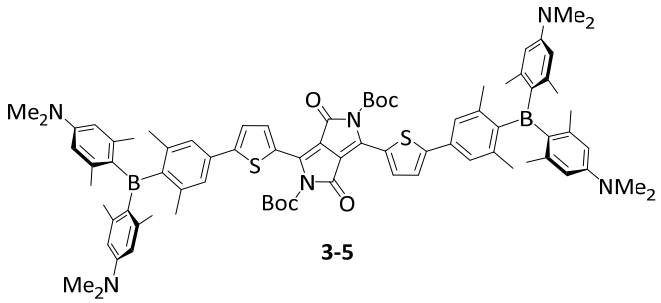

3-5

2,5-Di-*N*-*Boc*-3,6-*bis*[5-[4-[*bis*[4-(*N*,*N*-dimethylamino)-2,6-xylyl]boryl]-3,5-xylyl]-2-thienyl]-1,4-diketopyrrolo[3,4-c]pyrrole (3-5). Compound **2-6** (4.59 g, 8.83 mmol, 2.2 eq.), 2,5-di-*N*-*Boc*-3,6-di(5-bromo-thien-2-yl)-1,4-diketopyrrolo[3,4-c]pyrrole (2.55 g, 3.87 mol, 1.0 eq.) and KOH (1.30 g, 23.2 mmol, 6.0 eq.) were dissolved in a degassed mixture of H_2O (46 mL) and toluene (93 mL). The reaction mixture was degassed for 15 min and SPhos (479 mg, 1.17 mmol, 30 mol%) and $Pd_2(dba)_3{\cdot}CHCl_3$ (277.0 mg, 0.27 mmol, 7 mol%) were added. After heating to 85 °C for 3 d, the aqueous layer was extracted with CH_2Cl_2 (7 × 100 mL) and dried over Na_2SO_4. The solvent was evaporated and the crude product was purified by automated flash column chromatography (KP-Sil 100 g, hexane:ethylacetate 9:1 → 5:1) to obtain compound **3-5** as a violet solid (1.48 g, 29%).

^{1}H NMR (500 MHz, CD_2Cl_2): δ = 8.23 (d, *J* = 4.2 Hz, 2H), 7.47 (d, *J* = 4.2 Hz, 2H), 7.26 (s, 4H), 6.33 (s, 4H), 6.32 (s, 4H), 2.96 (s, 24H), 2.09 (s, 12H), 2.03 (s, 12H), 1.97 (s, 12H), 1.63 (s, 18H) ppm.

^{13}C{^{1}H} NMR (125 MHz, CD_2Cl_2): δ = 159.4, 152.2, 151.8, 151.6, 149.4, 143.4, 142.9, 141.5, 137.2, 135.8, 135.4, 132.8, 128.6, 125.2, 124.1, 111.9, 110.5, 86.1, 40.2, 27.9, 24.1, 23.9, 23.0 ppm.

Solid-State ^{11}B{^{1}H} NMR (128 MHz): Isotropic chemical shift δ_{iso} = 72.5 ppm, quadrupole coupling constant C_Q = 4.49 MHz, quadrupolar asymmetry parameter η_{Quad} = 0.1.

HRMS (LIFDI): *m/z* found: $[M]^+$ 1320.6856; calc. for $[C_{80}H_{94}B_2N_6O_6S_2]^+$ 1320.6857 ($|\Delta|$ = 0.08 ppm).

Elem. Anal. Calc. (%) for $C_{80}H_{94}B_2N_6O_6S_2$: C 72.72, H 7.17, N 6.36, S 4.85; found: C 72.97, H 7.40, N 6.49, S 4.52.

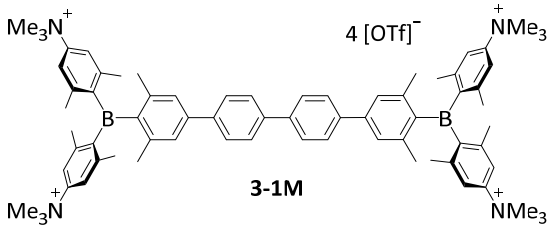

4,4'-*Bis*[4-[*bis*[4-(*N*,*N*,*N*-trimethylammonio)-2,6-xylyl]-boryl]-3,5-xylyl]-1,1'-biphenyl tetra-triflate (3-1M). In a soda-lime glass vial, compound **3-1** (15.0 mg, 15.4 μmol, 1.0 eq.) was dissolved in degassed CH_2Cl_2 (2.0 mL). After the addition of methyl triflate (7.74 μL, 69.2 μmol, 4.5 eq.), the reaction mixture was stirred at r.t. for 2 d. The white precipitate was collected by filtration and washed with Et_2O (6.0 mL) to obtain compound **3-1M** as a pale-yellow solid (19.6 mg, 78%).

^{1}H NMR (500 MHz, CD_3OD): δ = 7.80 (s, 8H), 7.58 (s, 4H), 7.58 (s, 4H), 7.40 (s, 4H), 3.67 (s, 36H), 2.26 (s, 12H), 2.18 (s, 12H), 2.13 (s, 12H) ppm.

^{13}C{^{1}H} NMR (125 MHz, CD_3OD): δ = 149.7, 149.5, 145.2, 145.0, 144.5, 144.4, 142.9, 141.2, 140.5, 128.4, 128.3, 127.8, 121.8 (q, *J* = 319 Hz), 120.1, 57.5, 23.6, 23.6, 23.4 ppm.

Solid-State ^{11}B{^{1}H} NMR (128 MHz): Isotropic chemical shift δ_{iso} = 79.2 ppm, quadrupole coupling constant C_Q = 4.86 MHz, quadrupolar asymmetry parameter η_{Quad} = 0.0.

HRMS (ESI$^+$): *m/z* found: $[M\text{-}2OTf]^{2+}$ 666.3266; calc. for $[C_{74}H_{92}B_2F_6N_4O_6S_2]^{2+}$ 666.3269 ($|\Delta|$ = 0.45 ppm).

Elem. Anal. Calc. (%) for $C_{76}H_{92}B_2F_{12}N_4O_{12}S_4$: C 55.95, H 5.68, N 3.43, S 7.86; found: C 54.76, H 5.88, N 3.53, S 7.62.

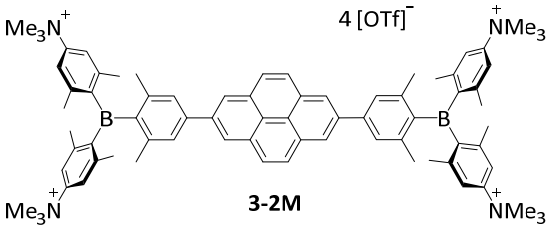

3-2M

2,7-*Bis*[4-[*bis*[4-(*N*,*N*,*N*-trimethylammonio)-2,6-xylyl]-boryl]-3,5-xylyl]-pyrene tetratriflate (3-2M). In a soda-lime glass vial, compound **3-2** (15.0 mg, 14.6 μmol, 1.0 eq.) was dissolved in degassed CH_2Cl_2 (3.0 mL). After the addition of methyl triflate (7.47 μL, 65.7 μmol, 4.5 eq.), the reaction mixture was stirred at r.t. for 2 d. The precipitate was collected by filtration and washed with Et_2O (6.0 mL) to obtain compound **3-2M** as a brown solid (21.4 mg, 91%).

^{1}H NMR (500 MHz, CD_3OD): δ = 8.55 (s, 4H), 8.23 (s, 4H), 7.69 (s, 4H), 7.62 (br s, 4H), 7.62 (br s, 4H), 3.67 (s, 36H), 2.33 (s, 12H), 2.23 (s, 12H), 2.22 (s, 12H) ppm.

^{13}C{^{1}H} NMR (125 MHz, CD_3OD): δ = 149.7, 149.5, 145.3, 145.2, 145.0, 144.5, 143.0, 139.4, 133.1, 129.1, 128.8, 125.1, 124.7, 121.8 (q, *J* = 319 Hz), 120.1, 57.5, 23.6, 23.5 ppm.

Solid-State ^{11}B{^{1}H} NMR (128 MHz): Isotropic chemical shift δ_{iso} = 77.2 ppm, quadrupole coupling constant C_Q = 4.78 MHz, quadrupolar asymmetry parameter η_{Quad} = 0.0.

HRMS (ESI$^+$): *m/z* found: $[M\text{-}4OTf]^{4+}$ 270.6869; calc. for $[C_{76}H_{92}B_2N_4]^{4+}$ 270.6872 ($|\Delta|$ = 1.11 ppm).

Elem. Anal. Calc. (%) for $C_{80}H_{92}B_2F_{12}N_4O_{12}S_4$: C 57.21, H 5.52, N 3.34 S 7.64; found: C 56.17, H 5.75, N 3.39, S 7.37.

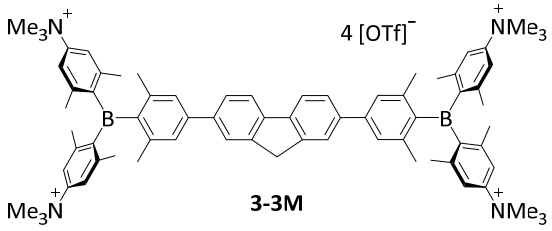

3-3M

2,7-*Bis*[4-[*bis*[4-(*N*,*N*,*N*-trimethylammonio)-2,6-xylyl]-boryl]-3,5-xylyl]-fluorene tetratriflate (3-3M). In a soda-lime glass vial, compound **3-3** (15.0 mg, 15.2 μmol, 1.0 eq.) was dissolved in degassed CH_2Cl_2 (2.0 mL). After the addition of methyl triflate (7.74 μL, 68.4 μmol, 4.5 eq.), the reaction mixture was stirred at r.t. for 2 d. The yellow precipitate was collected by filtration and washed with Et_2O (6.0 mL) to obtain compound **3-3M** as a yellow solid (22.8 mg, 91%).

^{1}H NMR (500 MHz, CD_3OD): δ = 7.93 – 7.92 (m, 2H), 7.91 - 7.90 (m, 2H), 7.73 - 7.72 (m, 2H), 7.58 (s, 8H), 7.41 (s, 4H), 4.06 (s, 2H), 3.67 (s, 36H), 2.27 (s, 12H), 2.18 (s, 12H), 2.13 (s, 12H) ppm.

^{13}C{^{1}H} NMR (125 MHz, CD_3OD): δ = 149.6, 149.5, 145.8, 145.3, 144.9, 144.5, 142.9, 142.4, 140.3, 127.9, 127.0, 124.6, 121.8 (q, *J* = 319 Hz), 121.4, 120.1, 57.5, 37.8, 23.6, 23.4 ppm.

Solid-State ^{11}B{^{1}H} NMR (128 MHz): Isotropic chemical shift δ_{iso} = 77.1 ppm, quadrupole coupling constant C_Q = 4.76 MHz, quadrupolar asymmetry parameter η_{Quad} = 0.0.

HRMS (ESI$^+$): *m/z* found: $[M\text{-}4OTf]^{4+}$ 261.6870; calc. for $[C_{73}H_{92}B_2N_4]^{4+}$ 261.6872 ($|\Delta|$ = 0.76 ppm).

Elem. Anal. Calc. (%) for $C_{77}H_{92}B_2F_{12}N_4O_{12}S_4$: C 56.28, H 5.64, N 3.41 S 7.80; found: C 56.38, H 5.94, N 3.56 S 7.63.

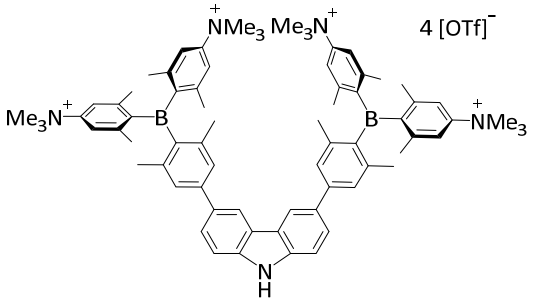

3-4M

3,6-*Bis*[4-[*bis*[4-(*N*,*N*,*N*-trimethylammonio)-2,6-xylyl]-boryl]-3,5-xylyl]-9*H*-carbazole tetratriflate (3-4M). In a soda-lime glass vial, compound **3-4** (44.0 mg, 40.1 μmol, 1.0 eq.) was dissolved in degassed CH_2Cl_2 (6.0 mL). After the addition of methyl triflate (20.6 μL, 183 μmol, 4.5 eq.), the reaction mixture was stirred at r.t. for 18 h. The pale-yellow precipitate was collected by filtration and washed with Et_2O (18 mL) to obtain the methylated compound as a pale-yellow solid (50.0 mg, 71%). The crude product (50.0 mg, 28.7 μmol, 1.0 eq.) was directly deprotected and therefore dissolved in MeOH (1.0 mL) in a soda-lime glass vial. After the addition of a solution of TfOH (3.0 mL) in MeOH (5.0 mL), the reaction mixture was stirred at r.t. for 1 h. The reaction mixture was quenched with water (8.0 mL) and the precipitate was collected by centrifugation and washed with water until the washing solution was pH neutral. The compound **3-4M** was isolated as a yellow solid (32.0 mg, 68%).

^{1}H NMR (500 MHz, CD_3OD): δ = 8.49 (d, *J* = 1.3 Hz, 2H), 7.77 – 7.75 (m, 2H), 7.56 (s, 8H), 7.56 – 7.54 (m, 2H), 7.47 (s, 4H), 3.65 (s, 36H), 2.27 (s, 12H), 2.16 (s, 12H), 2.13 (s, 12H) ppm.

^{13}C{^{1}H} NMR (125 MHz, CD_3OD): δ= 149.7, 149.5, 146.2, 144.9, 144.4, 144.1, 142.9, 141.9, 132.5, 127.9, 126.1, 125.1, 121.8 (q, *J* = 319 Hz), 120.0, 120.0, 119.6, 112.3, 57.5, 23.7, 23.6, 23.4 ppm.

Solid-State ^{11}B{^{1}H} NMR (128 MHz): Isotropic chemical shift δ_{iso} = 77.0 ppm, quadrupole coupling constant C_Q = 4.77 MHz, quadrupolar asymmetry parameter η_{Quad} = 0.1.

HRMS (ESI$^+$): *m/z* found: $[M\text{-}2OTf]^{2+}$ 672.8241; calc. for $[C_{74}H_{91}B_2F_6N_5O_6S_2]^{2+}$ 672.8245 ($|\Delta|$ = 0.59 ppm).

Elem. Anal. Calc. (%) for $C_{76}H_{91}B_2F_{12}N_5O_{12}S_4$: C 55.51, H 5.58, N 4.26, S 7.80; found: C 53.52, H 5.71, N 4.30, S 7.51.

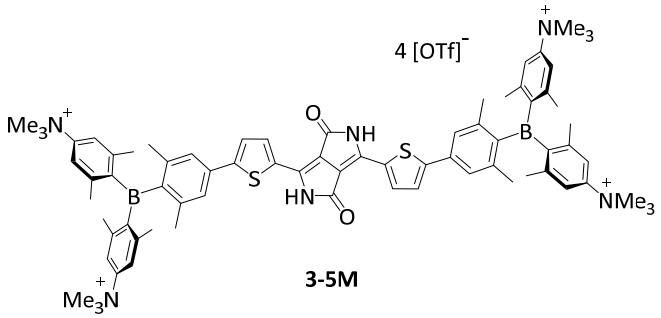

3-5M

3,6-*Bis*[5-[4-[*bis*[4-(*N*,*N*,*N*-trimethylammonio)-2,6-xylyl]boryl]-3,5-xylyl]-2-thienyl]-1,4-diketopyrrolo[3,4-c]pyrrole tetratriflate (3-5M). In a soda-lime glass vial, compound **3-5** (15.0 mg, 11.4 μmol, 1.0 eq.) was dissolved in degassed CH_2Cl_2 (2.0 mL). After the addition of methyl triflate (5.78 μL, 51.1 μmol, 4.5 eq.), the reaction mixture was stirred at r.t. for 7 h. The violet precipitate was collected by filtration and washed with Et_2O (6 mL) to obtain the methylated compound as a violet solid (22.0 mg, 97%). The crude product (22.0 mg, 11.1 μmol, 1.0 eq.) was directly deprotected and therefore dissolved in MeOH (0.2 mL) in a borosilicate glass vial. After the addition of a solution of TfOH (0.8 mL) in MeOH (2.0 mL), the reaction mixture was stirred at r.t. for 1.5 h. The reaction mixture was quenched with water (9.0 mL) and the precipitate was collected by centrifugation and washed with water until the washing solution was pH neutral. The compound **3-5M** was isolated as a violet solid (17.0 mg, 86%).

^{1}H NMR (500 MHz, CD_3OD): δ = 8.23 (d, *J* = 4.1 Hz, 2H), 7.69 (d, *J* = 4.1 Hz, 2H), 7.59 (s, 4H), 7.58 (s, 4H), 7.48 (s, 4H), 3.67 (s, 36H), 2.25 (s, 12H), 2.17 (s, 12H), 2.11 (s, 12H) ppm.

^{13}C{^{1}H} NMR (125 MHz, CD_3OD): δ = 163.7, 150.8, 149.8, 149.2, 147.0, 144.9, 144.6, 143.3, 137.9, 137.0, 134.2, 131.7, 126.8, 126.7, 112.8 (q, *J* = 319 Hz), 120.2, 120.2, 111.0, 57.5, 23.6, 23.5, 23.4 ppm.

Solid-State ^{11}B{^{1}H} NMR (128 MHz): Isotropic chemical shift δ_{iso} = 77.1 ppm, quadrupole coupling constant C_Q = 4.79 MHz, quadrupolar asymmetry parameter η_{Quad} = 0.0.

HRMS (ESI$^+$): *m/z* found: $[M\text{-}4OTf]^{4+}$ 295.1685; calc. for $[C_{74}H_{90}B_2N_6O_2S_2]^{4+}$ 295.1683 ($|\Delta|$ = 0.68 ppm).

Elem. Anal. Calc. (%) for $C_{78}H_{90}B_2F_{12}N_6O_{14}S_6$: C 52.70, H 5.10, N 4.73, S 10.82; found: C 51.49, H 5.40, N 4.48, S 10.14.

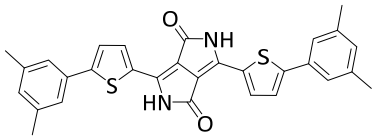

3-5A

3,6-*Bis*[5-[4-[*bis*[3,5-xylyl]-2-thienyl]-1,4-diketopyrrolo[3,4-c]pyrrole (3-5A). 2-(3,5-dimethyl-phenyl)-4,4,5,5-tetramethyl-1,3,2-dioxaborolane (140 mg, 0.60 mmol, 2.2 eq.), 2,5-di-*N*-*Boc*-3,6-di(5-bromo-thien-2-yl)-1,4-diketopyrrolo[3,4-c]pyrrole (180 mg, 0.27 mol, 1.0 eq.) and KOH (92.0 mg, 1.64 mmol, 6.0 eq.) were dissolved in a degassed mixture of H_2O (1.5 mL) and toluene (3 mL). The reaction mixture was degassed for 5 min and SPhos (33 mg, 82.0 μmol, 30 mol%) and $Pd_2(dba)_3{\cdot}CHCl_3$ (16.6 mg, 16.4 μmol, 6 mol%) were added. After heating to 85 °C for 3 d, the aqueous layer was extracted with CH_2Cl_2 (3 × 30 mL). The solvent was evaporated and the crude product was purified by automated flash column chromatography (KP-Sil 100 g, hexane:ethylacetate 99:1 → 97:3 → 95:5 → 90:10) to obtain the coupled compound as a violet solid (100 mg, 52%). The crude product (50.0 mg, 70.4 μmol, 1.0 eq.) was directly deprotected and therefore dissolved in CH_2Cl_2 (1.0 mL) in a borosilicate glass vial. After the addition of a solution of TfOH (0.2 mL) in CH_2Cl_2 (1.0 mL), the reaction mixture was stirred at r.t. for 1 h. The precipitate was collected by centrifugation and washed with water until the washing solution was pH neutral. The compound **3-5A** was isolated as a violet solid (30.0 mg, 84%).

^{1}H NMR (500 MHz, d_6-DMSO): δ = 11.23 (s, 2H), 8.17 (d, *J* = 4.0 Hz, 2H), 7.68 (d, *J* = 4.0 Hz, 2H), 7.36 (s, 4H), 7.05 (s, 2H), 2.34 (s, 12H) ppm.

^{13}C{^{1}H} NMR (125 MHz, d_6-DMSO): δ = 161.6, 149.4, 138.6, 135.5, 132.7, 132.5, 130.5, 129.5, 125.2, 123.6, 109.1, 20.9 ppm.

HRMS (ASAP$^-$): *m/z* found: $[M]^-$ 508.1281; calc. for $[C_{30}H_{24}N_2O_2S_2]^-$ 508.1285 ($|\Delta|$ = 0.79 ppm).

Elem. Anal. Calc. (%) for $C_{30}H_{24}N_2O_2S_2$: C 70.84, H 4.76, N 5.51, S 12.61; found: C 66.23, H 4.95, N 5.37, S 11.73.

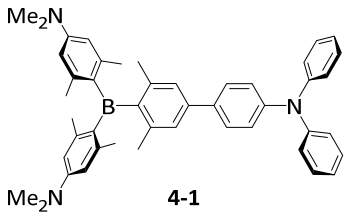

4-1

4-[4-[*Bis*[4-(dimethylamino)-2,6-xylyl]boryl]-3,5-xylyl]-phenyl-*N*,*N*-diphenylamine (4-1). Compound **2-6** (537 mg, 0.93 mmol, 1.1 eq.), 4-bromo-*N*,*N*-diphenylaniline (273 mg, 0.85 mmol, 1.0 eq.), KOH (157 mg, 2.79 mmol, 3.0 eq.) and SPhos (38 mg, 0.09 mmol, 10 mol%) were dissolved in a degassed mixture of toluene (10 mL) and H_2O (5 mL). The reaction mixture was degassed and $Pd_2(dba)_3{\cdot}CHCl_3$ (26 mg, 0.03 mmol, 3 mol%) was added. The reaction was heated to 85 °C and stirred for 20 h. Reaction monitoring by TLC (hexane:EtOAc 8:1) indicated that the starting material was fully consumed. Therefore, the phases were separated, and the aqueous solution was extracted with hexane (3 × 10 mL). The combined organic layers were concentrated under reduced pressure and purified by column chromatography (silica gel, hexane:EtOAc 12:1). The yellow solid was dissolved in Et_2O and crystallized by adding MeOH to afford **4-1** as a yellow solid (441 mg, 79%).

^{1}H NMR (500 MHz, CD_2Cl_2): δ = 7.56 – 7.54 (m, 2H), 7.28 – 7.25 (m, 4H), 7.15 (s, 2H), 7.12 – 7.09 (m, 6H), 7.05 – 7.01 (m, 2H), 6.32 (br s, 2H), 6.31 (br s, 2H), 2.95 (s, 12H), 2.08 (s, 6H), 2.02 (s, 6H), 1.97 (s, 6H) ppm.

^{13}C{^{1}H} NMR (125 MHz, CD_2Cl_2): δ = 151.7, 148.4, 148.2, 147.4, 143.2, 142.9, 141.1, 140.2, 136.2, 135.6, 129.6, 127.7, 125.6, 124.7, 124.4, 123.2, 111.9, 111.8, 40.2, 24.0, 23.8, 23.1 ppm.

^{11}B{^{1}H} NMR (160 MHz, CD_2Cl_2): δ = 74 ppm.

HRMS ($APCI^+$): *m/z* found: $[M+H]^+$ 656.4160; calc. for $[C_{46}H_{51}BN_3]^+$ 656.4171 ($|\Delta|$ = 1.68 ppm).

Elem. Anal. Calc. (%) for $C_{46}H_{50}BN_3$: C 84.26, H 7.69, N 6.41; found: C 84.39, H 7.67, N 6.35.

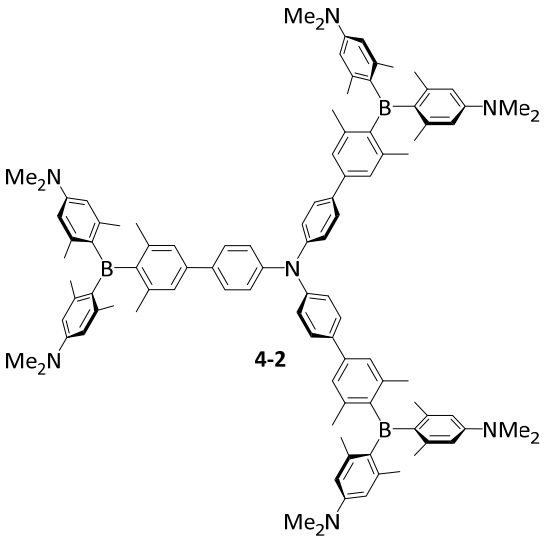

***Tris*[4-[4-[*bis*[4-(dimethylamino)-2,6-xylyl]boryl]-3,5-xylyl]-phenyl]amine (4-2).** Compound **2-6** (500 mg, 0.93 mmol, 3.1 eq.), 4,4',4''-tribromotriphenylamine (144 mg, 0.30 mmol, 1.0 eq.), KOH (152 mg, 2.70 mmol, 9.0 eq.) and SPhos (37 mg, 0.09 mmol, 30 mol%) were dissolved in a degassed mixture of toluene (10 mL) and H_2O (5 mL). The reaction mixture was degassed and $Pd_2(dba)_3{\cdot}CHCl_3$ (25 mg, 0.02 mmol, 8 mol%) was added. The reaction was heated to 85 °C and stirred for 20 h. Reaction monitoring by TLC (hexane:EtOAc 3:1) indicated that the starting material was consumed. Therefore, the phases were separated, and the aqueous solution was extracted with hexane (3 × 10 mL). The combined organic layers were concentrated under reduced pressure, and the residue was purified by column chromatography (silica gel, hexane:EtOAc 3:1). The yellow solid was dissolved in Et_2O and crystallized by adding MeOH to afford **4-2** as a yellow solid (389 mg, 88%).

^{1}H NMR (500 MHz, CD_2Cl_2): δ = 7.60 – 7.58 (m, 6H), 7.21 – 7.19 (m, 6H), 7.18 (s, 6H), 6.33 (br s, 6H), 6.32 (br s, 6H), 2.95 (s, 36H), 2.09 (s, 18H), 2.02 (s, 18H), 1.98 (s, 18H) ppm.

^{13}C{^{1}H} NMR (125 MHz, CD_2Cl_2): δ = 151.6, 148.5, 147.1, 143.2, 142.9, 141.1, 140.2, 136.2, 135.8, 127.8, 125.6, 124.7, 111.9, 111.8, 40.2, 24.0, 23.8, 23.1 ppm.

Solid-State ^{11}B{^{1}H} NMR (128 MHz): Isotropic chemical shift δ_{iso} = 73.2 ppm, quadrupole coupling constant C_Q = 4.53 MHz, quadrupolar asymmetry parameter η_{Quad} = 0.0.

HRMS (APCI$^+$): *m/z* found: $[M+H]^+$ 1476.9989; calc. for $[C_{102}H_{121}B_3N_7]^+$ 1476.9969 ($|\Delta|$ = 0.40 ppm).

Elem. Anal. Calc. (%) for $C_{102}H_{120}B_3N_7$: C 82.97, H 8.19, N 6.64; found: C 82.70, H 8.25, N 6.47.

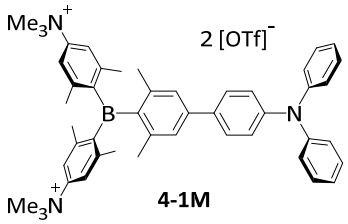

4-1M

4-[4-[*Bis*[4-(trimethylammonio)-2,6-xylyl]boryl]-3,5-xylyl]-phenyl-*N*,*N*-diphenylamine ditriflate (4-1M). The neutral donor-acceptor compound **4-1** (100 mg, 0.15 mmol, 1.0 eq.) was dissolved in dry CH_2Cl_2 (15 mL) and then methyl triflate (86 μL, 0.76 mmol, 5.0 eq.) was added. The reaction mixture was stirred for 20 h at r.t. The yellow solid which precipitated upon addition of Et_2O (20 mL) was collected by filtration and washed with Et_2O to afford **4-1M** (152 mg, 97%).

^{1}H NMR (500 MHz, CD_3OD): δ = 7.57 – 7.56 (m, 6H), 7.30 – 7.27 (m, 6H), 7.09 – 7.04 (m, 8H), 3.66 (s, 18H), 2.24 (s, 6H), 2.16 (s, 6H), 2.08 (s, 6H) ppm.

^{13}C{^{1}H} NMR (125 MHz, CD_3OD): δ = 149.6, 149.2, 149.0, 144.9, 144.5, 144.4, 142.8, 135.0, 130.5, 128.7, 127.3, 125.8, 124.4, 124.4 121.8 (q, *J* = 318 Hz), 120.1, 120.0, 57.5, 23.6, 23.4 ppm.

Solid-State ^{11}B{^{1}H} NMR (128 MHz): Isotropic chemical shift δ_{iso} = 76.0 and 77.6 ppm, quadrupole coupling constant C_Q = 4.76 and 4.78 MHz, quadrupolar asymmetry parameter η_{Quad} = 0.0 and 0.0. Since no further side products are observable *via* NMR spectroscopy in solution, it can be assumed that the two signals correspond to two isomers, which exist in the solid state. An integration of the signals gives a ratio of 1:1.

HRMS (ESI^+): *m/z* found: $[M\text{-}OTf]^+$ 834.4074; calc. for $[C_{49}H_{56}BN_3SO_3F_3]^+$ 834.4082 ($|\Delta|$ = 0.96 ppm).

Elem. Anal. Calc. (%) for $C_{50}H_{56}BN_3F_6O_6S_2$: C 61.03, H 5.74, N 4.27, S 6.52; found: C 60.74, H 5.74, N 4.50, S 6.36.

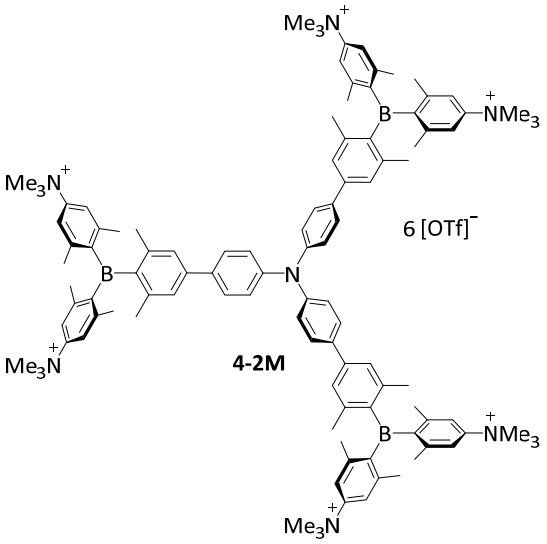

***Tris*[4-[4-[*bis*[4-(trimethylammonio)-2,6-xylyl]boryl]-3,5-xylyl]-phenyl]amine hexatriflate (4-2M).** The neutral trigonal donor-acceptor compound **4-2** (70 mg, 0.05 mmol, 1.0 eq.) was dissolved in dry CH_2Cl_2 (4.7 mL) and Et_2O (1.6 mL) and then methyl triflate (80 μL, 0.71 mmol, 15.0 eq.) was added. The reaction mixture was stirred for 20 h at r.t. The yellow solid which precipitated upon addition of Et_2O (20 mL) was collected by filtration and washed with Et_2O to afford **4-2M** as a yellow solid (107 mg, 92%).

^{1}H NMR (500 MHz, CD_3OD): δ = 7.67 – 7.65 (m, 6H), 7.57 (br s, 6H), 7.57 (br s, 6H), 7.34 (s, 6H), 7.23 – 7.21 (m, 6H), 3.66 (s, 54H), 2.25 (s, 18H), 2.16 (s, 18H), 2.10 (s, 18H) ppm.

^{13}C{^{1}H} NMR (125 MHz, CD_3OD): δ = 149.6, 149.5, 148.6, 144.9, 144.8, 144.5, 144.4, 142.9, 136.1, 128.9, 127.4, 125.6, 121.8 (q, J = 316 Hz), 120.1, 120.1, 57.5, 23.6, 23.6, 23.4 ppm.

Solid-State ^{11}B{^{1}H} NMR (128 MHz): Isotropic chemical shift δ_{iso} = 77.6 ppm, quadrupole coupling constant C_Q = 4.79 MHz, quadrupolar asymmetry parameter η_{Quad} = 0.1.

HRMS (ESI$^+$): *m/z* found: $[M\text{-}6OTf]^{6+}$ 261.0216; calc. for $[C_{108}H_{138}B_3N_7]^+$ 261.0210 ($|\Delta|$ = 2.30 ppm).

Elem. Anal. Calc. (%) for $C_{114}H_{138}B_3N_7F_{18}O_{18}S_6$: C 55.63, H 5.65, N 3.98, S 7.82; found: C 54.45, H 5.89, N 3.99, S 7.53.

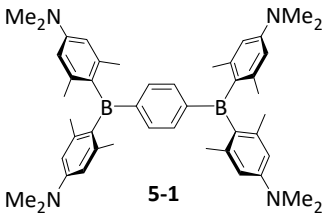

5-1

1,4-*Bis*[*bis*[4-(*N*,*N*-dimethylamino)-2,6-xylyl]boryl]-benzene (5-1). To a solution of 1,4-dibromobenzene (2.00 g, 8.48 mmol, 1.0 eq.) in hexane (60 mL) and Et_2O (60 mL), *n*-BuLi (6.80 mL, 2.5 M in hexane, 17.0 mmol, 2.0 eq.) was added slowly. The solution was stirred for 24 h at r.t. Fluoroborane **2-4** (5.53 g, 17.0 mmol, 2.0 eq.) was dissolved in THF (17 mL) and added to the reaction mixture. The reaction was stirred for a further 16 h at r.t. and quenched with H_2O (100 mL). The phases were separated, and the aqueous phase was extracted with CH_2Cl_2 (4 × 70 mL). The combined organic phases were dried over $MgSO_4$ and the solvent was removed *in vacuo*. The residue was dissolved in MeCN (30 mL) and crystallized in a freezer. The resulting yellow crystals were collected by filtration (458 mg, 8%). Single crystals suitable for X-ray diffraction were grown from hexane/EtOAc (1:1).

^{1}H NMR (500 MHz, CD_2Cl_2): δ = 7.38 (s, 4H), 6.36 (s, 8H), 2.95 (s, 24H), 1.96 (s, 24H) ppm.

^{13}C{^{1}H} NMR (125 MHz, CD_2Cl_2): δ = 151.5, 151.5, 143.1, 134.8, 134.5, 111.7, 40.3, 24.3 ppm.

Solid-State ^{11}B{^{1}H} NMR (128 MHz): Isotrope chemical shift δ_{iso} = 71.2 ppm, quadrupole coupling constant C_Q = 4.54 MHz, quadrupolar asymmetry parameter η_{Quad} = 0.0.

HRMS ($APCI^+$): *m/z* found: $[M+H]^+$ 691.5071; calc. for $[C_{46}H_{61}B_2N_4]^+$ 691.5077 ($|\Delta|$ = 0.87 ppm).

Elem. Anal. Calc. (%) for $C_{46}H_{60}B_2N_4$: C 80.00, H 8.76, N 8.11; found: C 79.36, H 8.75, N 8.23.

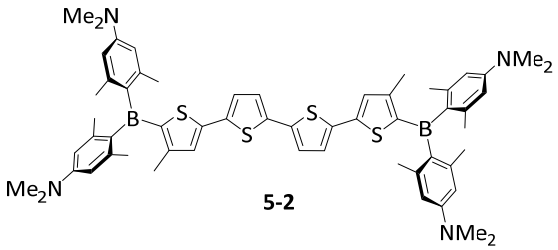

5-2

5,5‴-*Bis*[*bis*[4-(*N*,*N*-dimethylamino)-2,6-xylyl]boryl]-4,4‴-dimethyl-2,2′:5′,2″:5″,2‴-quarterthiophene (5-2). Compound **5-5** (1.10 g, 2.07 mmol, 2.2 eq.), 5,5′-dibromo-2,2′-bithiophene (305 mg, 0.94 mmol, 1.0 eq.) and KOH (316 mg, 5.63 mmol, 6.0 eq.) were dissolved in a degassed mixture of toluene (14 mL) and H_2O (7 mL). The reaction mixture was degassed and $Pd_2(dba)_3{\cdot}CHCl_3$ (57.3 mg, 0.06 mmol, 6 mol%) and SPhos (116 mg, 0.28 mmol, 30 mol%) were added. The reaction was heated to 85 °C and stirred for 20 h. Reaction monitoring by TLC (hexane:EtOAc 9:1) indicated that the starting material was consumed. The phases were separated, and the aqueous phase was extracted with hexane (3 × 70 mL). The combined organic layers were concentrated under reduced pressure. After column chromatography (silica gel, hexane:EtOAc 97:3), the orange solid was dissolved in Et_2O and crystallized by adding MeOH to afford the neutral compound **5-2** (406 mg, 44%).

^{1}H NMR (500 MHz, CD_2Cl_2): δ = 7.15 (s, 2H), 7.14 (d, *J* = 3.8 Hz, 2H), 7.08 (d, *J* = 3.8 Hz, 2H), 6.39 (s, 8H), 2.97 (s, 24H), 2.11 (s, 24H), 2.02 (s, 6H) ppm.

^{13}C{^{1}H} NMR (125 MHz, CD_2Cl_2): δ = 151.4, 148.6, 147.1, 145.2, 142.7, 137.1, 136.7, 134.2, 129.5, 125.4, 125.0, 111.7, 40.3, 23.8, 16.2 ppm.

^{11}B NMR (160 MHz, CD_2Cl_2): δ = 66 ppm.

HRMS ($APCI^+$): m/z found: $[M+H]^+$ 971.4564; calc. for $[C_{58}H_{69}B_2N_4S_4]^+$ 971.4586 ($|\Delta|$ = 2.26 ppm).

Elem. Anal. Calc. (%) for $C_{58}H_{68}B_2N_4S_4$: C 71.74 H 7.06 N 5.77 S 13.21; found: C 71.19, H 7.18, N 5.81, S 13.15.

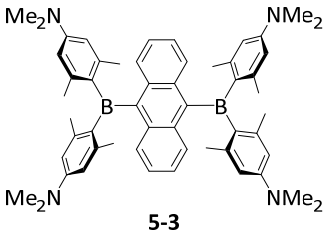

5-3

1,4-*Bis*[*bis*[4-(*N*,*N*-dimethylamino)-2,6-xylyl]boryl]-anthracene (5-3). To a suspension of 9,10-dibromoanthracene (1.00 g, 3.00 mmol, 1.0 eq.) in THF (30 mL) at -78 °C, *n*-BuLi (3.00 mL, 2.5 M in pentane, 7.50 mmol, 2.5 eq.) was added. After 1 h, a solution of compound **2-4** (1.96 g, 6.00 mmol, 2.0 eq.) in THF (20 mL) was added dropwise. The temperature was allowed to rise slowly to r.t. and the reaction mixture was stirred overnight. The solution turned from dark brown to yellow with the formation of a yellow precipitate. The THF solvent was removed *in vacuo* and the residue was washed with Et_2O (300 mL) to obtain compound **5-3** (142 mg, 6%) as a yellow powder. Single crystals suitable for X-ray diffraction were grown from MeCN.

^{1}H NMR (500 MHz, CD_2Cl_2, 298 K): δ = 8.10 – 8.08 (m, 4H), 7.10 - 7.08 (m, 4H), 6.32 (br s, 8H), 2.95 (s, 24H), 2.17 (br s, 12H), 1.66 (br s, 12H) ppm.

^{13}C{^{1}H} NMR (125 MHz, CD_2Cl_2, 298 K): δ= 151.8, 150.7, 143.3, 138.0, 133.9, 130.2, 124.0, 112.0, 40.1, 24.6 ppm.

^{1}H NMR (500 MHz, CD_2Cl_2, 235 K): δ = 8.03 – 8.00 (m, 4H), 7.10 - 7.06 (m, 4H), 6.41 (br s, 2H), 6.40 (br s, 2H),6.14 - 6.12 (m, 4H), 2.92 (s, 24H), 2.16 (br s, 6H), 2.15 (br s, 6H) 1.55 (s, 12H) ppm.

^{13}C{^{1}H} NMR (125 MHz, CD_2Cl_2, 235 K): δ= 151.0, 150.9, 150.1, 149.9, 142.8, 142.6, 142.5, 136.8, 133.0, 129.7, 123.6, 111.2, 111.0, 111.0, 39.8, 24.6, 24.4, 24.4 ppm.

Solid-State ^{11}B{^{1}H} NMR (128 MHz, 298 K): Isotrope chemical shift δ_{iso} = 73.6 ppm, quadrupole coupling constant C_Q = 4.47 MHz, quadrupolar asymmetry parameter η_{Quad} = 0.1.

HRMS (APCI$^+$): *m/z* found: $[M+H]^+$ 791.5375; calc. for $[C_{54}H_{65}B_2N_4]^+$ 791.5390 ($|\Delta|$ = 1.90 ppm).

Elem. Anal. Calc. (%) for $C_{54}H_{64}B_2N_4$: C 82.02, H 8.16, N 7.09; found: C 82.10, H 8.30, N 7.13.

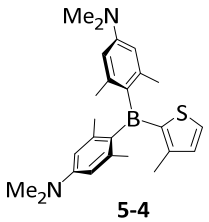

5-4

***Bis*[4-(*N*,*N*-dimethylamino)-2,6-xylyl]-2-(3-methylthiophene)-borane (5-4).** 2-Bromo-3-methylthiophene (4.50 g, 25.4 mmol, 1.1 eq.) was dissolved in dry Et_2O (20 mL). The reaction mixture was cooled to 0 °C and treated with *n*-BuLi (11.1 mL, 2.5 M in pentane, 28.0 mmol, 1.2 eq.). After addition, the cooling bath was removed and the reaction mixture was stirred for 1.5 h at r.t. A solution of compound **2-4** (7.54 g, 23.1 mmol, 1.0 eq.) in THF (90 mL) was added at 0 °C, and the reaction mixture was stirred overnight at r.t. The reaction was quenched with H_2O (120 mL), and the aqueous layer was extracted with CH_2Cl_2 (5 × 150 mL). The combined organic phases were dried over $MgSO_4$, filtered and concentrated under reduced pressure. The resulting solid was purified by crystallization from acetone, which afforded **5-4** (2.99 g, 32%) as a yellow solid. Single crystals suitable for X-ray diffraction were grown from MeCN.

^{1}H NMR (500 MHz, CD_2Cl_2): δ = 7.67 (m, 1H), 7.01 (m, 1H), 6.36 (s, 4H), 2.96 (s, 12H), 2.04 (m, 12H), 2.04 (m, 3H) ppm.

^{13}C{^{1}H} NMR (125 MHz, CD_2Cl_2): δ = 151.4, 147.4, 147.1, 142.6, 134.6, 134.3, 132.7, 111.6, 40.3, 23.7, 16.0 ppm.

^{11}B NMR (160 MHz, CD_2Cl_2): δ = 66 ppm.

HRMS (APCI$^+$): m/z found: $[M+H]^+$ 405.2524; calc. for $[C_{25}H_{34}BN_2S]^+$ 405.2530 ($|\Delta|$ = 1.48 ppm).

Elem. Anal. Calc. (%) for $C_{25}H_{33}BN_2S$: C 74.25 H 8.23 N 6.93 S 7.93; found: C 71.94, H 8.04, N 6.74, S 7.38.

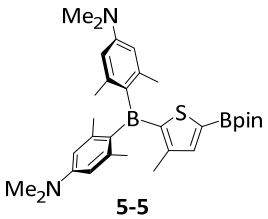

5-5

***Bis*[4-(*N*,*N*-dimethylamino)-2,6-xylyl]-2-[3-methyl-5-(4,4,5,5-tetramethyl-1,3,2 dioxaborlan-2-yl)thiophene]-borane (5-5).** Compound **5-4** (1.50 g, 3.71 mmol, 1.0 eq.), B_2pin_2 (1.13 g, 4.45 mmol, 1.2 eq.), dtbpy (40.2 mg, 0.16 mmol, 4 mol%) and $[Ir(COD)(\mu\text{-OMe})]_2$ (50.0 mg, 0.08 mmol, 2 mol%) were dissolved in THF (40 mL) and heated at 65 °C for 2 d. After the solvent was removed, the resulting solid was purified by column chromatography (silica gel, hexane:EtOAc 9:1) and crystallized from MeCN to afford the title compound **5-5** as a yellow solid (1.65 g, 84%). Single crystals suitable for X-ray diffraction were grown from MeCN.

^{1}H NMR (500 MHz, CD_2Cl_2): δ = 7.42 (m, 1H), 6.36 (s, 4H), 2.96 (s, 12H), 2.04 (m, 3H), 2.03 (s, 12H), 1.31 (s, 12H) ppm.

^{13}C{^{1}H} NMR (125 MHz, CD_2Cl_2): δ = 154.6, 151.5, 147.4, 142.7, 141.6, 137.7, 134.4, 111.6, 84.4, 40.3, 25.0, 23.7, 15.7 ppm.

^{11}B NMR (160 MHz, CD_2Cl_2): δ = 66, 29 ppm.

HRMS (APCI$^+$): m/z found: $[M+H]^+$ 531.3381; calc. for $[C_{31}H_{45}B_2N_2O_2S]^+$ 531.3382 (|Δ| = 0.19 ppm)

Elem. Anal. Calc. (%) for $C_{31}H_{44}B_2N_2O_2S$: C 70.20 H 8.36 N 5.28 S 6.04; found: C 69.98, H 8.68, N 5.28, S 5.69.

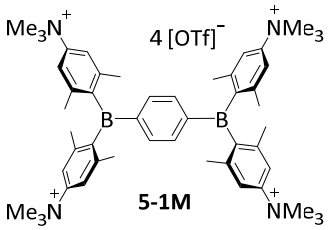

5-1M

1,4-*Bis*[*bis*[4-(*N*,*N*,*N*-trimethylammonio)-2,6-xylyl]-boryl]-benzene tetratriflate (5-1M). In a soda-lime glass vial, compound **5-1** (15.0 mg, 21.7 μmol, 1.0 eq.) was dissolved in degassed CH_2Cl_2 (3.0 mL). After the addition of methyl triflate (11.2 μL, 97.7 μmol, 4.5 eq.), the reaction mixture was stirred at r.t. for 2 d. The white precipitate was collected by filtration and washed with Et_2O (6.0 mL) to obtain compound **5-1M** as a white solid (29.0 mg, 99%). Single crystals suitable for X-ray diffraction were grown from slow diffusion of Et_2O into a saturated MeCN/THF solution.

^{1}H NMR (500 MHz, CD_3OD): δ = 7.62 (s, 8H), 7.53 (s, 4H), 3.67 (s, 36H), 2.18 (s, 24H) ppm.

^{13}C{^{1}H} NMR (125 MHz, CD_3OD): δ = 150.1, 149.5, 146.8, 145.0, 136.9, 121.8 (q, *J* = 319 Hz), 119.8, 57.5, 24.1 ppm.

Solid-State ^{11}B{^{1}H} NMR (128 MHz): Isotrope chemical shift δ_{iso} = 74.6 ppm, quadrupole coupling constant C_Q = 4.73 MHz, quadrupolar asymmetry parameter η_{Quad} = 0.0.

HRMS (ESI$^+$): *m/z* found: $[M\text{-}3OTf]^{3+}$ 299.8482; calc. for $[C_{51}H_{72}B_2N_4S_1O_3F_3]^{3+}$ 299.8482 ($|\Delta|$ = 0.00 ppm).

Elem. Anal. Calc. (%) for $C_{54}H_{72}B_2F_{12}N_4O_{12}S_4$: C 48.15, H 5.39, N 4.16, S 9.52; found: C 46.65, H 5.50, N 4.29, S 9.10.

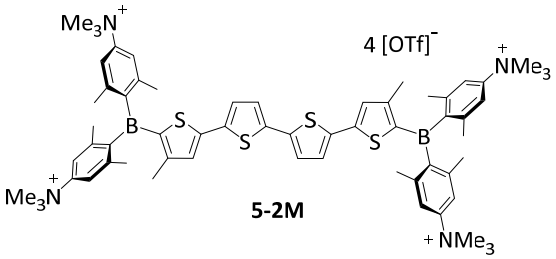

5-2M

5,5‴-*Bis*[*bis*[4-(trimethylammonio)-2,6-xylyl]boryl]-4,4‴-dimethyl-2,2′:5′,2″:5″,2‴-quaterthiophene tetratriflate (5-2M). In a soda-lime glass vial, compound **5-2** (15.0 mg, 15.4 μmol, 1.0 eq.) was dissolved in degassed CH_2Cl_2 (2.0 mL). After the addition of methyl triflate (7.87 μL, 69.5 μmol, 4.5 eq.), the reaction mixture was stirred at r.t. for 2 d. The red precipitate was collected by filtration and washed with Et_2O (6.0 mL) to obtain compound **5-2M** as a red solid (19.7 mg, 81%).

^{1}H NMR (500 MHz, CH_3OD): δ = 7.61 (s, 4H), 7.60 (s, 4H), 7.40 (s, 2H), 7.33 - 7.32 (m, 2H), 7.26 - 7.25 (m, 2H), 3.68 (s, 36H), 2.35 (s, 12H), 2.32 (s, 12H), 2.05 (s, 6H) ppm.

^{13}C{^{1}H} NMR (125 MHz, CH_3OD): δ = 155.0, 150.9, 149.3, 149.2, 147.7, 146.8, 145.2, 144.5, 143.4, 138.9, 136.9, 131.4, 128.1, 126.7, 121.8 (q, *J* = 319 Hz), 119.8, 119.5, 57.5, 23.9, 23.5, 16.8 ppm.

Solid-State ^{11}B{^{1}H} NMR (128 MHz): Isotrope chemical shift δ_{iso} = 64.0 ppm, quadrupole coupling constant C_Q = 4.31 MHz, quadrupolar asymmetry parameter η_{Quad} = 0.0.

HRMS (ESI^+): m/z found: $[M\text{-}2OTf]^{2+}$ 664.2235; calc. for $[C_{64}H_{80}B_2F_6N_4O_6S_6]^{2+}$ 664.2241 (|Δ| = 0.90 ppm).

Elem. Anal. Calc. (%) for $C_{66}H_{80}B_2F_{12}N_4O_{12}S_8$: C 48.71 H 4.95 N 3.44 S 15.76; found: C 47.13, H 5.22, N 3.65, S 15.33.

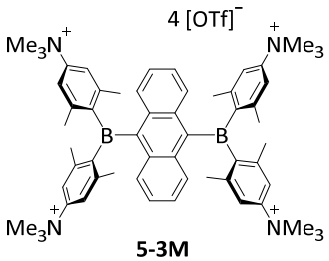

5-3M

1,4-*Bis*[*bis*[4-(*N*,*N*,*N*-trimethylammonio)-2,6-xylyl]-boryl]-anthracene tetratriflate (5-3M). In a soda-lime glass vial, compound **5-3** (15.0 mg, 19.0 μmol, 1.0 eq.) was dissolved in degassed CH_2Cl_2 (3.0 mL). After the addition of methyl triflate (9.67 μL, 85.5 μmol, 4.5 eq.), the reaction mixture was stirred at r.t. for 2 d. The precipitate was collected by filtration and washed with Et_2O (6.0 mL) to obtain compound **5-3M** as a yellow solid (26.0 mg, 95%). Single crystals suitable for X-ray diffraction were grown by slow diffusion of Et_2O into a saturated MeCN/THF solution.

^{1}H NMR (500 MHz, CD_3OD): δ = 7.98 - 7.96 (m, 4H), 7.72 (br s, 4H), 7.49 (br s, 4H), 7.25 - 7.23 (m, 4H), 3.66 (s, 36H), 2.34 (br s, 12H), 1.91 (br s, 12H) ppm.

^{13}C{^{1}H} NMR (125 MHz, CD_3OD): δ = 150.3, 150.0, 148.6, 145.3, 144.7, 134.5, 130.0, 127.1, 121.8 (q, *J* = 319 Hz), 120.7, 57.5, 24.0 ppm.

Solid-State ^{11}B{^{1}H} NMR (128 MHz): Isotrope chemical shift δ_{iso} = 79.0 ppm, quadrupole coupling constant C_Q = 4.78 MHz, quadrupolar asymmetry parameter η_{Quad} = 0.0.

HRMS (ESI^+): *m/z* found: $[M\text{-}4OTf]^{4+}$ 212.6560; calc. for $[C_{58}H_{76}B_2N_4]^{4+}$ 212.6559 ($|\Delta|$ = 0.47 ppm).

Elem. Anal. Calc. (%) for $C_{62}H_{76}B_2F_{12}N_4O_{12}S_4 \cdot (C_4H_8O)$: C 52.32, H 5.32, N 3.70, S 8.46; found: C 48.68, H 5.43, N 4.02, S 8.31.

7.16 X-Ray

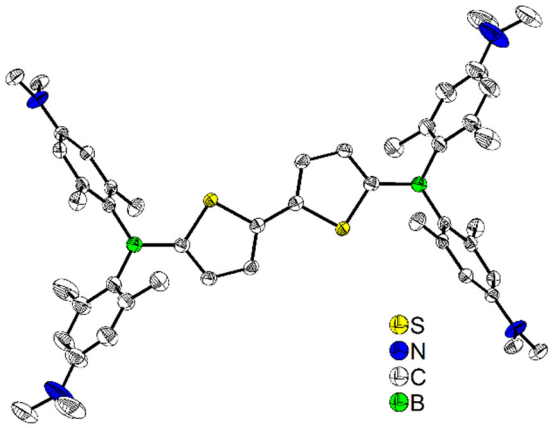

Figure 7-1. Molecular structure of **2-1** in the solid state at 100 K. Hydrogen atoms are omitted for clarity. Atomic displacement ellipsoids are drawn at 50% probability level. Angles between the plane of the BC_3-core (defined by B1, C1, C11 and C21) and the planes of the adjacent aryl rings: 55.7(2)° for C1; 56.6(2)° for C11; 21.0(2)° for C21.

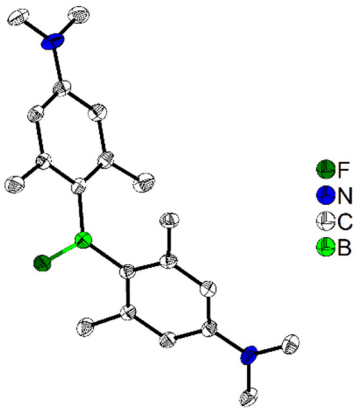

Figure 7-2. Molecular structure of **2-4** in the solid state at 100 K. Hydrogen atoms are omitted for clarity. Atomic displacement ellipsoids are drawn at 50% probability level.

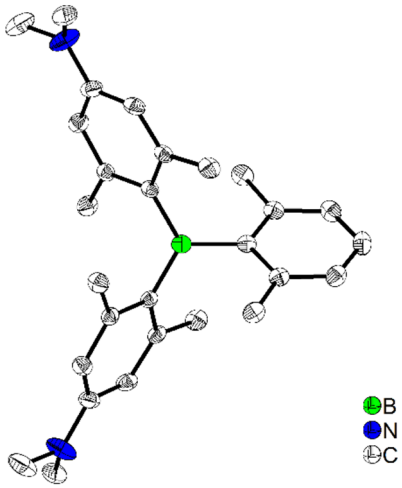

Figure 7-3. Molecular structure of **2-5** in the solid state at 100 K. Hydrogen atoms are omitted for clarity. Atomic displacement ellipsoids are drawn at 50% probability level. Angles between the plane of the BC_3-core (defined by B1, C1, C1A and C11) and the planes of the adjacent aryl rings: 53.0(1)° for C1 and C1A; 56.7(1)° for C11.

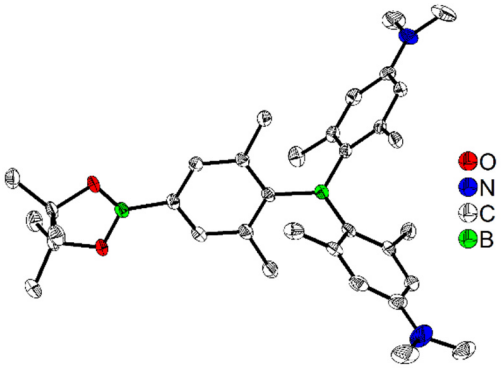

Figure 7-4. Molecular structure of **2-6** in the solid state at 100 K. Hydrogen atoms are omitted for clarity. Atomic displacement ellipsoids are drawn at 50% probability level. Angles between the plane of the BC_3-core (defined by B1, C5, C9 and C19) and the planes of the adjacent aryl rings: 58.9(1)° for C5; 42.4(1)° for C9; 45.8(1)° for C19.

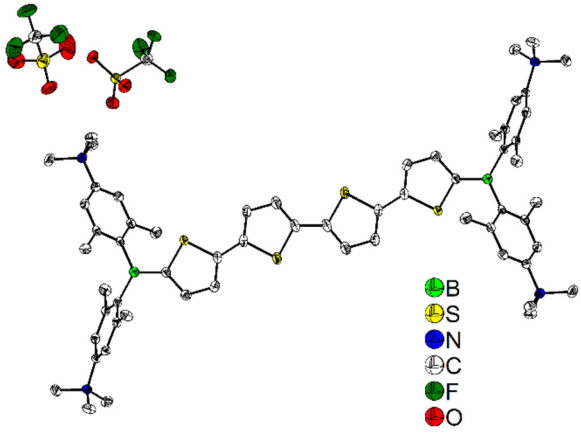

Figure 7-5. Molecular structure of **2-2M** in the solid state at 100 K. The triflate anions, co-crystallized solvent (acetonitrile) and hydrogen atoms are omitted for clarity. Atomic displacement ellipsoids are drawn at 50% probability level. Angles between the plane of the BC_3-core (defined by B1, C1, C12 and C23) and the planes of the adjacent aryl rings: 64.1(1)° for C1; 56.4(1)° for C12; 17.6(2)° for C23. Angle between the thienyl planes: 6.9(2)°.

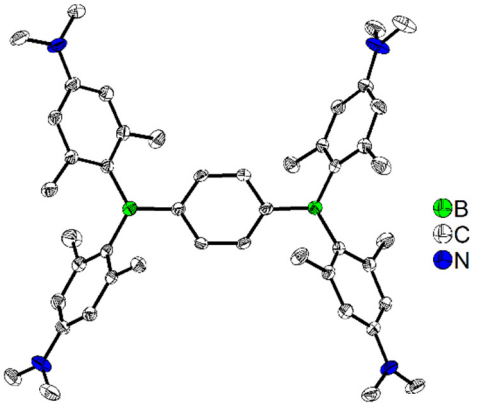

Figure 7-6. Molecular structure of **5-1** in the solid state at 100 K. Atomic displacement ellipsoids are drawn at the 50% probability level, and H atoms are omitted for clarity.

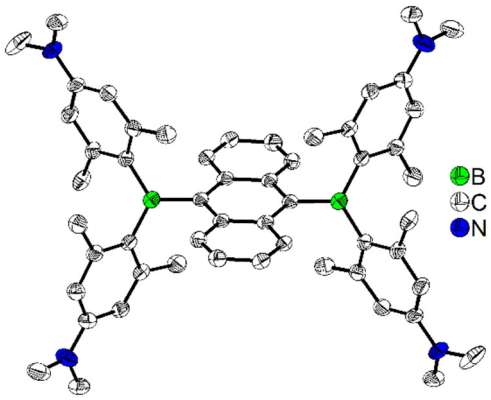

Figure 7-7. Molecular structure of **5-3** in the solid state at 100 K. Atomic displacement ellipsoids are drawn at the 50% probability level, and H atoms are omitted for clarity.

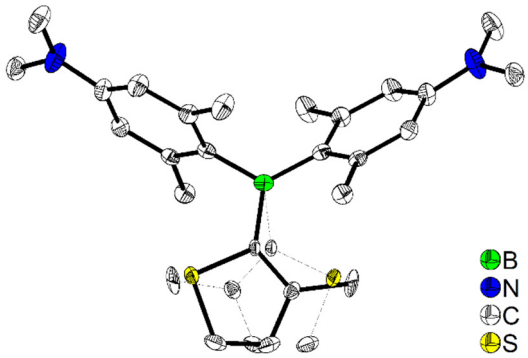

Figure 7-8. Molecular structure of **5-4** in the solid state at 100 K. Atomic displacement ellipsoids are drawn at the 50% probability level, and H atoms are omitted for clarity. The methylthiophene moiety is disordered by 50% *via* symmetry. The symmetry-related part is shown with thin, dashed bonds.

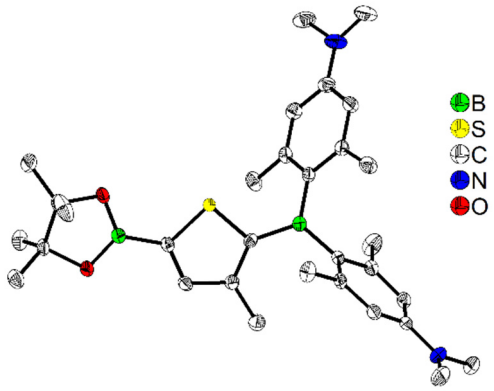

Figure 7-9. Molecular structure of **5-5** in the solid state at 100 K. Atomic displacement ellipsoids are drawn at the 50% probability level, and H atoms are omitted for clarity. The BPin moiety is disordered and only the part with 89% occupancy is shown.

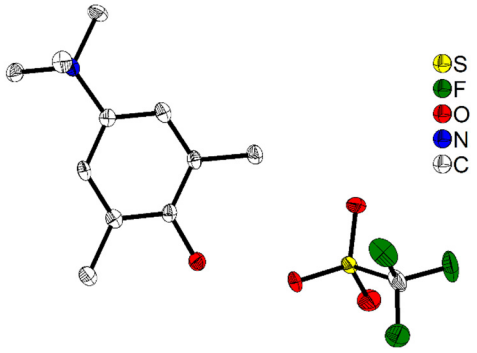

Figure 7-10. Molecular structure of **5-6** in the solid state at 100 K. Atomic displacement ellipsoids are drawn at the 50% probability level, and H atoms are omitted for clarity.

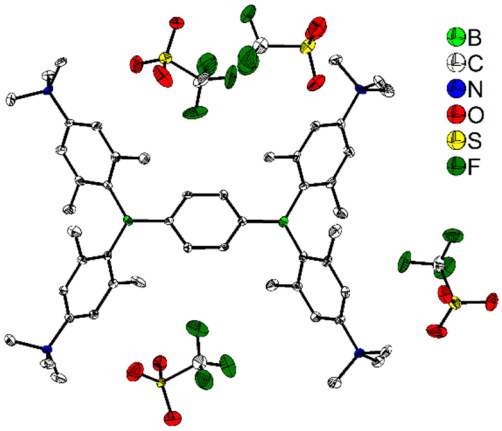

Figure 7-11. Molecular structure of **5-1M** in the solid state at 100 K. Atomic displacement ellipsoids are drawn at the 50% probability level, and H atoms are omitted for clarity. One of the anions is disordered and the part with 62% occupancy is shown.

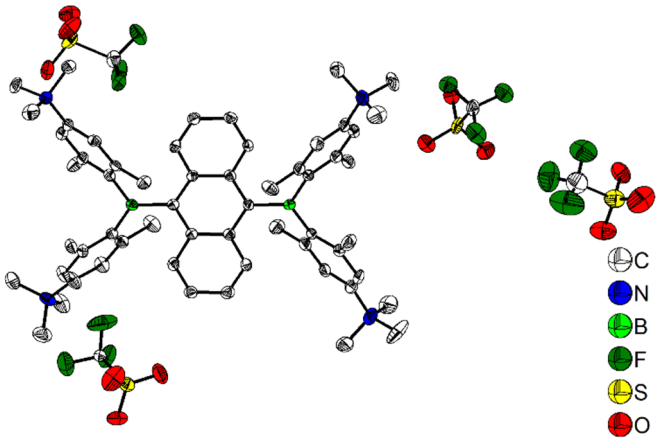

Figure 7-12. Molecular structure of **5-3M** in the solid state at 100 K. Atomic displacement ellipsoids are drawn at the 50% probability level, and H atoms are omitted for clarity. One of the (*N*,*N*,*N*-trimethylammonio)xylyl moieties is disordered and only the part with 63% occupancy is shown. Of the disordered anions, only the part with the highest occupancy is shown.

Table 7-1. Single-crystal X-ray diffraction data and structure refinements of **2-1**, **2-4**, **2-5**, **2-6** and **2-2M**.

Data	**2-1**	**2-4**	**2-5**	**2-6**	**2-2M**
CCDC number	1476260	1476259	1476261	1476262	1476258
Empirical formula	$C_{48}H_{60}B_2N_4S_2$	$C_{20}H_{28}BFN_2$	$C_{28}H_{37}BN_2$	$C_{34}H_{48}B_2N_2O_2$	$C_{72}H_{88}B_2F_{12}N_8O_{12}S_8$
Formula weight / g·mol^{-1}	778.82	326.25	412.40	538.36	1763.60
T / K	100(2)	100(2)	100(2)	100(2)	100(2)
λ / Å, radiation	0.71073 Mo-K_α	0.71073 Mo-K_α	0.71073 Mo-K_α	0.71073 Mo-K_α	0.71073 Mo-K_α
Crystal size / mm³	0.11x0.12x0.24	0.20×0.25×0.45	0.20×0.60×0.62	0.30×0.52×0.72	0.19x0.43x0.60
Crystal color, habit	yellow prism	yellow block	yellow block	yellow block	red block
μ / mm^{-1}	0.153	0.075	0.066	0.068	0.298
Crystal system	Monoclinic	Monoclinic	Orthorhombic	Monoclinic	Monoclinic
Space group	$P2_1/n$	$P2_1/n$	$Pbcn$	$P2_1/n$	$P2_1/n$
a / Å	8.0124(6)	8.161(2)	12.388(1)	12.0780(4)	18.2185(5)
b / Å	31.519(3)	9.881(4)	10.008(1)	11.2531(3)	12.8036(3)
c / Å	9.5386(9)	22.738(6)	19.158(2)	23.7904(6)	19.0145(4)
α / °	90	90	90	90	90
β / °	108.566(2)	91.052(16)	90	102.3580(10)	106.928(1)
γ / °	90	90	90	90	90
Volume / Å^3	2283.5(3)	1833.2(10)	2375.3(4)	3158.55(16)	4243.19(18)
Z	2	4	4	4	2
ρ_{calc} / g·cm^{-3}	1.133	1.182	1.153	1.132	1.380
F(000)	837	704	896	1168	1836
θ range / °	1.29 - 26.00	1.792 - 26.000	2.824 - 26.066	1.753 - 25.998	1.95-26.000
Reflections collected	30808	11700	20370	27037	32734
Unique reflections	4488	3596	2350	6199	8349
Parameters / restraints	260 / 0	225 / 0	147 / 0	375 / 0	526 / 0
GooF on F^2	1.0637	1.042	1.043	1.021	1.033
R_1 [I>2σ(I)]	0.0627	0.0412	0.0429	0.0411	0.0491
wR^2 (all data)	0.1787	0.1161	0.1111	0.1103	0.1366
Max. / min. residual electron density / e·Å^{-3}	0.537 / –0.447	0.228 / –0.191	0.316 / –0.201	0.286 / –0.259	0.664 / –0.562

Table 7-2. Single-crystal X-ray diffraction data and structure refinements of **5-1**, **5-3**, **5-4**, **5-5** and **5-6**.

Data	**5-1**	**5-3**	**5-4**	**5-5**	**5-6**
CCDC number	1892920	1892922	1892924	189295	1892926
Empirical formula	$C_{46}H_{60}B_2N_4$	$C_{54}H_{64}B_2N$	$C_{25}H_{33}BN_2S$	$C_{31}H_{44}B_2N_2O_2S$	$C_{11}H_{18}NO$, CF_3O_3S
Formula weight / g·mol^{-1}	690.60	790.71	404.40	530.36	329.33
T / K	100(2)	100(2)	100(2)	100(2)	100(2)
λ / Å, radiation	0.71073 Mo-K_α	0.71073 Mo-K_α	0.71073 Mo-K_α	0.71073 Mo-K_α	0.71073 Mo-K_α
Crystal size / mm³	0.07×0.33×0.39	0.09×0.10×0.13	0.22×0.30×0.33	0.21×0.52×0.59	0.05×0.08×0.13
Crystal color, habit	yellow plate	orange block	yellow block	yellow block	colorless needle
μ / mm^{-1}	0.065	0.068	0.159	0.134	0.270
Crystal system	Triclinic	Monoclinic	Monoclinic	Triclinic	Monoclinic
Space group	$P\ \bar{1}$	$C2/c$	$C2/c$	$P\ \bar{1}$	$P2_1/c$
a / Å	12.174(6)	22.3197(13)	13.622(7)	10.088(3)	8.601(3)
b / Å	12.532(6)	10.0803(6)	8.904(4)	12.262(3)	24.935(12)
c / Å	15.397(9)	20.8730(13)	18.617(8)	13.589(4)	6.882(4)
α / °	70.367(11)	90	90	106.623(17)	90
β / °	70.074(16)	108.878(6)	98.536(18)	97.230(19)	97.81(2)
γ / °	72.09(2)	90	90	101.603(12)	90
Volume / Å^3	2029.9(18)	4443.6(5)	2233.1(17)	1547.4(8)	1462.2(11)
Z	2	4	4	2	4
ρ_{calc} / g·cm^{-3}	1.130	1.182	1.203	1.138	1.496
F(000)	748	1704	872	572	688
θ range / °	1.768 - 26.022	1.929 - 27.103	2.212 - 27.499	1.790 - 26.022	1.633 - 27.179
Reflections collected	26777	94221	36560	35596	15558
Unique reflections	7968	4902	2571	6100	3245
Parameters / restraints	487 / 0	280 / 0	164 / 0	415 / 24	199 / 0
GooF on F^2	1.028	1.027	1.229	1.039	1.000
R_1 [I>2σ(I)]	0.0477	0.0541	0.0587	0.0375	0.0485
wR^2 (all data)	0.1280	0.1388	0.1291	0.1039	0.1044
Max. / min. residual electron density / e·Å^{-3}	0.299 / –0.224	0.249 / –0.198	0.293 / –0.236	0.320 / –0.253	0.474 / –0.438

Table 7-3. Single-crystal X-ray diffraction data and structure refinements of **5-1M** and **5-3M**.

Data	**5-1M**[a]	**5-3M**[a, b]
CCDC number	1892921	1892923
Empirical formula	$C_{50}H_{72}B_2N_4$, $4(SO_3CF_3)$, $8(C_2H_3N)$	$C_{58}H_{76}B_2N_4 \cdot 4(CF_3O_3S) \cdot 0.545(C_4H_8O) \cdot 2.455(C_2H_3N)$
Formula weight / g·mol^{-1}	1675.44	1586.00
T / K	100(2)	100(2)
λ / Å, radiation	0.71073 Mo-K_α	0.71073 Mo-K_α
Crystal size / mm³	0.24×0.40×0.68	0.28×0.48×0.52
Crystal color, habit	colorless block	yellow block
μ / mm^{-1}	0.198	0.214
Crystal system	Orthorhombic	Monoclinic
Space group	$Pca2_1$	Cc
a / Å	30.258(19)	36.98(2)
b / Å	17.864(12)	12.339(8)
c / Å	15.858(12)	16.997(10)
α / °	90	90
β / °	90	92.12(3)
γ / °	90	90
Volume / Å^3	8572(10)	7750(8)
Z	4	4
ρ_{calc} / g·cm^{-3}	1.298	1.359
F(000)	3512	3317
θ range / °	1.764 - 26.022	1.740 - 26.069
Reflections collected	54506	84916
Unique reflections	15643	12958
Parameters / restraints	1111 / 136	1329 / 391
GooF on F^2	1.058	1.036
R_1 [I>2σ(I)]	0.0752	0.0480
wR^2 (all data)	0.2112	0.1320
Max. / min. residual electron density / e·Å^{-3}	1.446 / –0.486	0.604 / –0.264

[a] Several acetonitrile solvent molecules and triflate anions of the crystal structures of **5-1M** and **5-3M** are strongly disordered. Hence, remaining residual electron density is associated with solvent molecules or anions. Crystals of **5-1M** and **5-3M** desolvate very quickly forming cracks resulting in a decrease of the crystal quality. These are the best results that have been obtained after several trials; [b] The crystal structure of **5-3M** contains two fully occupied acetonitrile molecules. The third acetonitrile molecule shares the position with a tetrahydrofuran molecule in the ratio 0.45:0.55.

7.17 DFT Calculations

Table 7-4. Lowest energy singlet electronic transitions of **2-1M** in the gas phase. H = HOMO; L = LUMO.

state	symmetry	E / eV	λ / nm	f	major (>10%) contributions
S_1	B	3.26	380	1.326	H→L (94%)
S_2	A	4.22	294	0.000	H→L+1 (54%), H–3→L (19%)
S_3	A	4.41	281	0.000	H–3→L (34%), H→L+1 (23%), H–5→L (21%)
S_4	A	4.44	279	0.018	H–6→L (37%), H–7→L+1 (18%), H–3→L (13%), H–5→L (12%)
S_5	B	4.45	279	0.155	H–7→L (44%), H–4→L (20%), H–6→L+1 (16%)
S_6	B	4.46	278	0.040	H–9→L (75%)
S_7	B	4.68	265	0.006	H–2→L (53%), H–1→L+1 (21%)
S_8	A	4.69	265	0.002	H–1→L (50%), H–2→L+1 (22%)

Table 7-5. Lowest energy singlet electronic transitions of **2-1M** in MeCN solution. H = HOMO; L = LUMO.

state	symmetry	E / eV	λ / nm	f	major (>10%) contributions
S_1	B	3.22	385	1.379	H→L (94%)
S_2	A	4.22	293	0.000	H→L+1 (57%), H–8→L (22%)
S_3	A	4.35	285	0.020	H–5→L (44%), H–3→L (23%), H–6→L+1 (19%)
S_4	B	4.36	284	0.174	H–6→L (49%), H–5→L+1 (18%), H–4→L (16%)
S_5	A	4.42	281	0.002	H–8→L (57%), H–7→L (17%)
S_6	B	4.49	276	0.078	H–10→L (78%)
S_7	B	4.59	270	0.007	H–2→L (56%), H–1→L+1 (20%)
S_8	A	4.59	270	0.002	H–1→L (60%), H–2→L+1 (20%)

Table 7-6. Lowest energy singlet electronic transitions of **2-2M** in the gas phase. H = HOMO; L = LUMO.

state	symmetry	E / eV	λ / nm	f	major (>10%) contributions
S_1	A	2.59	478	2.336	H→L (87%)
S_2	A	3.29	377	0.001	H→L+1 (78%), H–1→L (15%)
S_3	A	4.09	303	0.000	H–1→L (71%), H→L+1 (15%)
S_4	A	4.11	302	0.012	H→L+2 (57%), H–1→L+1 (18%)
S_5	A	4.38	283	0.000	H–2→L (31%), H–4→L (29%), H–3→L+1 (16%), H–5→L+1 (14%)
S_6	A	4.41	281	0.055	H–3→L (29%), H–4→L+1 (22%), H–5→L (19%), H→L+2 (13%)
S_7	A	4.52	274	0.000	H–2→L (41%), H–4→L (19%)
S_8	A	4.58	271	0.103	H–1→L+1 (31%), H–6→L (17%), H→L+2 (13%)

Table 7-7. Lowest energy singlet electronic transitions of **2-2M** in MeCN solution. H = HOMO; L = LUMO.

state	symmetry	E / eV	λ / nm	f	major (>10%) contributions
S_1	A	2.63	472	2.334	H→L (89%)
S_2	A	3.36	369	0.001	H→L+1 (70%), H–1→L (22%)
S_3	A	4.15	299	0.082	H→L+2 (48%), H–1→L+1 (24%)
S_4	A	4.15	299	0.000	H–1→L (65%), H→L+1 (21%)
S_5	A	4.43	280	0.007	H–7→L (23%), H–6→L+1 (15%), H–9→L+1 (13%), H–11→L+1 (10%)
S_6	A	4.44	279	0.143	H–7→L+1 (27%), H–6→L (27%), H–4→L (12%), H–5→L+1 (10%)
S_7	A	4.44	279	0.004	H–9→L (26%), H–11→L+1 (19%)
S_8	A	4.49	276	0.101	H–11→L (49%), H–9→L+1 (19%), H–12→L+1 (11%)

Table 7-8. Lowest energy singlet electronic transitions of **2-3M** in the gas phase. H = HOMO; L = LUMO.

state	symmetry	*E* / eV	λ / nm	*f*	major (>10%) contributions
S_1	B	2.76	449	1.891	H→L (74%)
S_2	A	3.13	396	0.001	H→L+1 (75%), H–1→L (15%)
S_3	B	3.72	333	0.291	H→L+1 (67%), H–1→L+1 (10%)
S_4	A	3.93	316	0.000	H–3→L+1 (35%), H–4→L (28%), H–2→L (22%)
S_5	B	3.93	316	0.022	H–3→L (43%), H–4→L+1 (23%), H–2→L+1 (17%)
S_6	A	4.12	301	0.000	H–1→L (46%), H→L+1 (20%), H–6→L+1 (20%)
S_7	B	4.24	292	0.107	H–1→L+1 (31%), H–6→L (24%), H→L (20%)
S_8	B	4.40	282	0.082	H–8→L (44%), H–7→L+1 (43%)

Table 7-9. Lowest energy singlet electronic transitions of **2-3M** in MeCN solution. H = HOMO; L = LUMO.

state	symmetry	*E* / eV	λ / nm	*f*	major (>10%) contributions
S_1	B	2.97	417	2.192	H→L (78%), H→L+2 (10%)
S_2	A	3.53	351	0.001	H→L+1 (60%), H–1→L (24%)
S_3	B	3.94	315	0.017	H→L+2 (50%), H–1→L+1 (24%)
S_4	A	4.14	300	0.017	H–2→L (44%), H–3→L+1 (32%)
S_5	B	4.14	300	0.007	H–3→L (44%), H–2→L+1 (31%)
S_6	A	4.27	290	0.152	H–5→L+1 (32%), H–4→L (29%)
S_7	B	4.27	290	0.142	H–4→L+1 (32%), H–5→L (28%)
S_8	A	4.40	282	0.000	H–1→L (28%), H→L+1 (24%), H–6→L+1 (12%), H–8→L+1 (10%)

Table 7-10. Lowest energy singlet electronic transitions of **2-3M** in water. H = HOMO; L = LUMO.

state	symmetry	*E* / eV	λ / nm	*f*	major (>10%) contributions
S_1	A	2.97	417	2.182	H→L (78%), H→L+2 (10%)
S_2	A	3.54	350	0.002	H→L+1 (60%), H–1→L (23%)
S_3	A	3.95	314	0.018	H→L+2 (50%), H–1→L+1 (22%)
S_4	A	4.12	301	0.014	H–2→L (43%), H–2→L+1 (25%)
S_5	A	4.15	299	0.014	H–3→L (35%), H–3→L+1 (31%)
S_6	A	4.27	290	0.123	H–6→L (11%), H–5→L (10%), H–5→L+1 (11%)
S_7	A	4.28	289	0.151	H–6→L (10%), H–6→L+1 (16%), H–5→L (11%), H–5→L+1 (12%)
S_8	A	4.39	282	0.001	H-4→L+1 (11%), H-1→L (27%), H→L+1 (24%)

Table 7-11. Lowest energy singlet electronic transitions of **3-1** in hexane solution. H = HOMO; L = LUMO.

state	symmetry	*E* / eV	λ / nm	*f*	major (>10%) contributions
S_1	B	3.50	354	0.054	H-1 → L+1 (44%), H → L (38%)
S_2	A	3.50	354	0.736	H-1 → L (38%), H → L+1 (44%),
S_3	B	3.70	335	1.496	H-4 → L (11%), H-3 → L+1 (29%), H-2 → L (37%)
S_4	A	3.77	329	0.000	H-3 → L (33%), H-2 → L+1 (42%)
S_5	B	4.19	296	0.778	H-4 → L (55%), H-3 → L+1 (15%)
S_6	A	4.37	284	0.000	H-5 → L (31%), H-4 → L+1 (42%)
S_7	A	4.59	270	0.001	H-7 → L+1 (29%), H-6 → L (25%)
S_8	B	4.59	270	0.008	H-7 → L (25%), H-6 → L+1 (29%)
S_9	B	4.62	269	0.381	H-9 → L+1 (12%), H-8 → L (14%), H-5 → L+1 (14%), H-4 → L+2 (22%)
S_{10}	A	4.62	268	0.055	H-11 → L+1 (30%), H-10 → L (39%)

Table 7-12. Lowest energy singlet electronic transitions of **3-2** in hexane solution. H = HOMO; L = LUMO.

state	symmetry	*E* / eV	λ / nm	*f*	major (>10%) contributions
S_1	A	3.50	355	0.352	H-1 → L+1 (11%), H → L+1 (29%), H → L+2 (41%)
S_2	A	3.50	355	0.427	H-1 → L+1 (25%), H-1 → L+2 (46%), H → L+1 (11%)
S_3	A	3.71	334	0.000	H-5 → L (41%), H-4 → L+1 (25%), H-4 → L+3 (20%)
S_4	A	3.72	333	1.533	H-3 → L+2 (30%), H-2 → L+1 (36%)
S_5	A	3.78	328	0.004	H-3 → L+1 (33%), H-2 → L+2 (39%)
S_6	A	3.92	317	0.345	H-4 → L (85%)
S_7	A	4.27	290	1.072	H-6 → L+2 (16%), H-5 → L+1 (51%), H-3 → L+2 (12%)
S_8	A	4.39	282	0.000	H-6 → L+1 (31%), H-5 → L+2 (41%)
S_9	A	4.55	273	0.263	H-5 → L (41%), H-4 → L+1 (39%), H-4 → L+3 (12%)
S_{10}	A	4.59	270	0.003	H-7 → L+1 (23%), H-7 → L+2 (32%)

Table 7-13. Lowest energy singlet electronic transitions of **3-3** in hexane solution. H = HOMO; L = LUMO.

state	symmetry	*E* / eV	λ / nm	*f*	major (>10%) contributions
S_1	A	3.49	354	0.384	H-1 → L (38%), H-1 → L+1 (43%), H-1 → L+2 (10%)
S_2	A	3.50	354	0.410	H → L (36%), H → L+1 (44%), H → L+2 (11%)
S_3	A	3.67	338	1.788	H-3 → L+1 (23%), H-2 → L (46%)
S_4	A	3.77	329	0.025	H-3 → L (31%), H-2 → L+1 (43%)
S_5	A	4.09	303	0.590	H-4 → L (54%), H-3 → L+1 (19%), H-2 → L+2 (13%)
S_6	A	4.34	286	0.007	H-5 → L (28%), H-4 → L+1 (45%)
S_7	A	4.54	273	0.268	H-13 → L (12%), H-5 → L+1 (26%), H-4 → L+2 (28%), H-2 → L+2 (10%)
S_8	A	4.59	270	0.008	H-7 → L (23%), H-7 → L+1 (26%)
S_9	A	4.59	270	0.004	H-6 → L (24%), H-6 → L+1 (29%)
S_{10}	A	4.61	269	0.030	H-10 → L (14%), H-10 → L+1 (10%), H-9 → L (20%). H-9 → L+1 (15%)

Table 7-14. Lowest energy singlet electronic transitions of **3-4** in hexane solution. H = HOMO; L = LUMO.

state	symmetry	*E* / eV	λ / nm	*f*	major (>10%) contributions
S_1	A	3.51	353	0.207	H-1 → L (76%)
S_2	A	3.52	352	0.581	H → L+1 (76%)
S_3	A	3.75	331	0.571	H-3 → L (34%), H-2 → L+1 (27%)
S_4	A	3.78	328	0.438	H-3 → L (35%), H-2 → L+1 (42%)
S_5	A	4.33	287	0.233	H-5 → L+1 (17%), H-4 → L (29%), H-4 →L+1 (11%)
S_6	A	4.36	284	0.157	H-5 → L (21%), H-4 →L (32%)
S_7	A	4.45	279	0.061	H-4 → L+2 (63%)
S_8	A	4.60	270	0.002	H-8 → L (55%)
S_9	A	4.60	269	0.003	H-7 → L+1 (56%)
S_{10}	A	4.64	267	0.022	H-9 → L+1 (58%)

Table 7-15. Lowest energy singlet electronic transitions of **3-5** in hexane solution. H = HOMO; L = LUMO.

state	symmetry	*E* / eV	λ / nm	*f*	major (>10%) contributions
S_1	A	2.31	537	1.739	H → L (94%)
S_2	A	3.35	370	0.294	H-2 → L (33%), H-2 → L+1 (20%), H-2 → L+2 (27%), H-2 → L+3 (10%)
S_3	A	3.35	370	0.116	H-5 → L (34%), H → L+1 (33%)
S_4	A	3.38	367	0.260	H-1 → L (28%), H-2 → L+1 (24%), H-2 → L+2 (26%), H-2 → L+3 (13%)
S_5	A	3.58	346	0.606	H-6 → L (12%), H-4 → L (28%), H-4 → L+2 (12%), H-3 → L+1 (12%)
S_6	A	3.68	337	0.012	H-3 → L (26%), H → L+1 (24%), H → L+3 (15%)
S_7	A	3.75	331	0.015	H-5 → L (43%), H → L+1 (15%)
S_8	A	3.80	326	0.122	H-1 → L (68%), H-1 → L+2 (12%), H-1→L+3 (10%)
S_9	A	3.81	325	0.161	H-2 → L (62%), H-2 → L+2 (17%), H-2 → L+3 (10%)
S_{10}	A	3.90	318	0.451	H-6 →L (41%), H-4 → L (17%)

Table 7-16. Lowest energy singlet electronic transitions of **3-1M** in water. H = HOMO; L = LUMO.[a]

state	symmetry	*E* / eV	λ / nm	*f*	major (>10%) contributions
S_1	A	3.66	338	1.709	H-1 → L+1 (28%), H → L (53%)
S_1	A_u	3.63	341	1.857	H-1 → L+1 (26%), H → L (56%)
S_2	A	3.80	326	0.000	H-1 → L (38%), H → L+1 (40%),
S_2	A_g	3.80	326	0.000	H-1 → L (37%), H → L+1 (40%)
S_3	A	4.18	296	0.013	H-3 → L+1 (31%), H-2 → L (36%)
S_3	A_g	4.18	297	0.000	H-3 → L (36%), H-2 → L+1 (31%)
S_4	A	4.18	296	0.023	H-3 → L (36%), H-2 → L+1 (31%)
S_4	A_u	4.18	297	0.036	H-3 → L+1 (31%), H-2 → L (36%)
S_5	A	4.30	288	0.001	H-6 → L (17%), H-5 → L+1 (26%), H-4 → L (13%), H-3 → L (10%), H-2 → L+1 (12%)
S_5	A_g	4.30	288	0.000	H-6 → L+1 (23%), H-5 → L (22%), H-3 → L (12%), H-2 → L+1 (10%)
S_6	A	4.30	288	0.289	H-6 → L+1 (17%), H-5 → L (26%), H-4 → L+1 (13%), H-3 → L+1 (10%), H-2 → L (12%)
S_6	A_u	4.30	288	0.292	H-6 → L (23%), H-5 → L+1 (23%), H-2 → L (12%)
S_7	A	4.47	277	0.737	H-4 → L (10%), H → L+2 (34%)
S_7	A_u	4.39	282	0.649	H-4 → L (12%), H-1 → L+1 (12%), H → L+2 (39%),
S_8	A	4.64	267	0.000	H-7 → L (28%), H-6 → L+1 (11%), H-4 → L+1 (20%)
S_8	A_g	4.64	267	0.000	H-8 → L (24%), H-4 → L+1 (24%)

[a] black: without symmetry constraints; red: in C_i symmetry.

Table 7-17. Lowest energy singlet electronic transitions of **3-2M** in water. H = HOMO; L = LUMO.[a]

state	symmetry	*E* / eV	λ / nm	*f*	major (>10%) contributions
S_1	A	3.65	339	0.004	H-1 → L+2 (29%), H → L (33%), H → L+3 (28%)
S_1	A_u	3.51	354	0.005	H-1 → L+2 (27%), H → L (39%), H → L+3 (25%)
S_2	A	3.69	335	1.733	H-2 → L+1 (30%), H-1 → L (52%)
S_2	A_u	3.58	347	1.801	H-2 → L+1 (24%), H-1 → L (61%)
S_3	A	3.81	325	0.012	H-2 → L (38%), H-1 → L+1 (39%)
S_3	A_g	3.75	330	0.000	H-2 → L (37%), H-1 → L+1 (43%)
S_4	A	3.92	316	0.562	H → L+2 (87%)
S_4	A_u	3.86	321	0.753	H → L+2 (86%)
S_5	A	4.16	298	0.021	H-3 → L (38%), H-3 → L+1 (27%)
S_5	A_g	4.13	300	0.000	H-4 → L+1 (30%), H-3 → L (38%)
S_6	A	4.18	297	0.016	H-4 → L (32%), H-4 → L+1 (32%)
S_6	A_u	4.15	299	0.034	H-4 → L (38%), H-3 → L+1 (31%)
S_7	A	4.30	288	0.119	H-7 → L (12%), H-6 → L (14%), H-6 → L+1 (14%), H-3 → L (12%)
S_7	A_g	4.28	290	0.000	H-7 → L+1 (12%), H-6 → L (25%), H-5 → L+1 (17%), H → L+1 (18%)
S_8	A	4.31	288	0.136	H-7 → L+1 (11%), H-6 → L (11%), H-5 → L+1 (10%), H-4 → L (11%), H-4 → L+1 (10%)
S_8	A_u	4.29	289	0.086	H-6 → L+1 (19%), H-5 → L (13%), H-1 → L+2 (21%), H → L (16%)

[a] black: without symmetry constraints; red: in C_i symmetry.

Table 7-18. Lowest energy singlet electronic transitions of **3-3M** in water. H = HOMO; L = LUMO.

state	symmetry	*E* / eV	λ / nm	*f*	major (>10%) contributions
S_1	A	3.53	351	1.905	H-1 → L+1 (21%), H → L (60%)
S_2	A	3.74	332	0.023	H-5 → L+1 (11%), H-1 → L (34%), H-1 → L+1 (44%)
S_3	A	4.16	298	0.018	H-2 → L (32%), H-2 → L+1 (24%)
S_4	A	4.17	297	0.017	H-3 → L (28%), H-3 → L+1 (24%)
S_5	A	4.30	289	0.459	H-5 → L (18%), H-1 → L+1 (16%), H → L+2 (40%)
S_6	A	4.30	288	0.124	H-7 → L (10%), H-6 → L (16%), H-6 → L+1 (27%)
S_7	A	4.31	288	0.179	H-7 → L (18%), H-7 → L+1 (23%), H-6 → L (10%)
S_8	A	4.62	269	0.005	H-8 → L (22%), H-5 → L+1 (22%), H → L+1 (15%)

Table 7-19. Lowest energy singlet electronic transitions of **3-4M** in water. H = HOMO; L = LUMO.

state	symmetry	*E* / eV	λ / nm	*f*	major (>10%) contributions
S_1	A	3.58	346	1.113	H-5 → L (11%), H-2 → L+1 (12%), H-1 → L+1 (16%), H → L (48%)
S_2	A	3.70	335	0.298	H-5 → L+1 (15%), H-2 → L (14%), H-1 → L (20%), H → L+1 (40%)
S_3	A	4.19	296	0.013	H-3 → L (41%), H-3 → L+1 (23%)
S_4	A	4.20	296	0.019	H-4 → L (27%), H-4 →L+1 (34%)
S_5	A	4.23	293	0.021	H → L+2 (69%)
S_6	A	4.32	287	0.109	H-6 → L (27%), H-6 → L+1 (21%)
S_7	A	4.32	287	0.178	H-7 → L (17%), H-7 → L+1 (31%)
S_8	A	4.40	282	0.030	H-5 → L (19%), H → L (21%), H → L+5 (10%)

Table 7-20. Lowest energy singlet electronic transitions of **3-5M** in water solution. H = HOMO; L = LUMO.[a]

state	symmetry	*E* / eV	λ / nm	*f*	major (>10%) contributions
S_1	A	2.28	544	1.802	H → L (93%)
S_1	A_u	2.33	532	1.596	H → L (94%)
S_2	A	3.29	376	0.138	H-1 → L (22%), H → L+1 (53%), H → L+3 (10%)
S_2	A_g	3.36	369	0.000	H-1 → L (25%), H → L+1 (45%), H → L+3 (11%)
S_3	A	3.57	347	0.777	H-2 → L (28%), H-1 → L+1 (23%), H → L+2 (34%)
S_3	A_u	3.59	345	0.917	H-2 → L (26%), H-1 → L+1 (24%), H → L+2 (32%)
S_4	A	3.72	333	0.009	H-1 → L (54%), H →L+1 (19%)
S_4	A_g	3.77	329	0.000	H-1 → L (51%), H →L+1 (20%)
S_5	A	3.92	317	0.030	H-15 → L (23%), H-13 → L (28%)
S_5	A_g	3.90	318	0.000	H-16 → L (27%), H-13 → L (29%), H → L+3 (10%)
S_6	A	3.96	313	0.243	H-2 → L (43%), H → L+2 (25%)
S_6	A_u	3.96	313	0.355	H-2 → L (53%), H → L+2 (24%)
S_7	A	4.03	308	0.001	H-1 → L+2 (14%), H → L+3 (25%)
S_7	A_g	4.00	310	0.000	H-1 → L+2 (18%), H → L+3 (33%)
S_8	A	4.05	306	0.011	H-3 → L (36%), H-3 → L+1 (35%), H-3 → L+2 (13%)
S_8	A_u	4.04	307	0.007	H-15 → L (78%)

[a] black: without symmetry constraints; red: in C_i symmetry.

Table 7-21. Lowest energy singlet electronic transitions of **4-1** in the gas phase. H = HOMO; L = LUMO.

state	symmetry	*E* / eV	λ / nm	*f*	major (>10%) contributions
S_1	A	3.56	349	0.327	H-1 → L (86%)
S_2	A	3.75	331	0.708	H-3 → L (13%), H-2 → L (41%), H → L (32%)
S_3	A	4.15	299	0.320	H-2 → L (42%), H → L (23%), H → L+1 (24%)
S_4	A	4.44	279	0.018	H → L+2 (84%)
S_5	A	4.50	276	0.138	H-3 → L (40%), H → L+1 (35%)
S_6	A	4.55	272	0.267	H → L+3 (87%)
S_7	A	4.60	270	0.004	H-4 → L (60%)
S_8	A	4.63	268	0.025	H-5 → L (70%)
S_9	A	4.66	266	0.000	H-6 → L (51%), H-1 → L+8 (11%)
S_{10}	A	4.92	252	0.020	H → L+4 (50%), H → L+6 (14%)

Table 7-22. Lowest energy singlet electronic transitions of **4-1M** in the gas phase. H = HOMO; L = LUMO.

state	symmetry	*E* / eV	λ / nm	*f*	major (>10%) contributions
S_1	A	2.33	533	0.616	H → L (89%)
S_2	B	3.57	347	0.004	H → L+1 (94%)
S_3	A	3.60	345	0.417	H-7 → L (15%), H-3 → L (20%), H-1 → L (20%), H → L (11%), H → L+2 (14%)
S_4	A	3.69	336	0.228	H-7 → L (10%), H-3 →L (10%), H → L+2 (41%), H → L+4 (18%)
S_5	B	3.78	328	0.012	H-6 → L (89%)
S_6	B	4.02	308	0.001	H → L+3 (96%)
S_7	A	4.18	296	0.060	H → L+2 (37%), H → L+4 (54%)
S_8	B	4.26	291	0.001	H-5 → L (33%), H-2 → L (28%), H → L+11 (17%)
S_9	A	4.37	284	0.000	H-3 → L (22%), H-1 → L (65%)
S_{10}	B	4.47	277	0.012	H-2 → L (41%), H → L+7 (19%), H → L+11 (30%)

Table 7-23. Lowest energy singlet electronic transitions of **4-1M** in EtOH solution. H = HOMO; L = LUMO.

state	symmetry	*E* / eV	λ / nm	*f*	major (>10%) contributions
S_1	A	3.27	379	1.077	H-1 → L (16%), H → L (72%)
S_2	B	4.12	301	0.011	H-2 → L (82%)
S_3	A	4.20	295	0.167	H-9 → L (12%), H-1 → L (31%), H → L+1 (30%)
S_4	B	4.33	287	0.142	H-5 → L (75%)
S_5	B	4.41	281	0.053	H → L+4 (79%)
S_6	A	4.56	272	0.260	H-9 → L (14%), H → L (19%), H → L+1 (33%)
S_7	B	4.64	267	0.198	H → L+6 (81%)
S_8	A	4.70	264	0.045	H-9 → L (10%), H-6 → L (66%)
S_9	B	4.76	261	0.036	H-8 → L (61%)
S_{10}	A	4.89	253	0.020	H-11 → L (28%), H-9 → L (37%), H-1 → L (18%)

Table 7-24. Lowest energy singlet electronic transitions of **4-2** in the gas phase with C_3 symmetry. H = HOMO; L = LUMO.

state	symmetry	*E* / eV	λ / nm	*f*	major (>10%) contributions
S_1	E	3.56	348	0.161	H-3 → L (27%), H-2 → L+1 (13%), H-2 → L+2 (25%), H-1 → L (13%)
S_2	E	3.56	348	0.161	H-3 → L+1 (27%), H-2 → L (13%), H-1 → L+1 (13%), H-1 → L+2 (25%)
S_3	A	3.56	348	0.611	H-3 → L+2 (29%), H-2 → L (28%), H-1 → L+1 (28%)
S_4	E	3.67	338	1.351	H-4 → L+2 (12%), H → L (30%)
S_5	E	3.67	338	1.351	H-5 → L+2 (12%), H → L+1 (30%)
S_6	A	3.82	325	0.000	H-6 → L+2 (18%), H-5 → L+1 (22%), H-4 → L (22%), H → L+2 (12%)
S_7	E	4.04	307	0.158	H-6 → L+1 (18%), H-5 → L+2 (13%), H → L+1 (16%), H → L+4 (17%)
S_8	E	4.04	307	0.158	H-6 → L (18%), H-4 → L+2 (13%), H → L (16%), H → L+3 (17%)
S_9	A	4.29	289	0.000	H-8 → L (15%), H-7 → L+1 (15%), H-6 → L+2 (12%), H → L+2 (31%),
S_{10}	A	4.35	285	0.013	H → L+5 (84%)

Table 7-25. Lowest energy singlet electronic transitions of **4-2** in the gas phase with C_1 symmetry. H = HOMO; L = LUMO.

state	symmetry	*E* / eV	λ / nm	*f*	major (>10%) contributions
S_1	A	3.56	348	0.161	H-3 → L (12%), H-2 → L (11%), H-1 → L+1 (19%), H-1 → L+2 (26%)
S_2	A	3.56	348	0.161	H-3 → L (21%), H-3 → L+1 (15%), H-2 → L+1 (14%), H-2 → L+2 (28%)
S_3	A	3.56	348	0.611	H-3 → L+2 (27%), H-2 → L (20%), H-1 → L+1 (19%)
S_4	A	3.67	338	1.351	H → L (34%)
S_5	A	3.67	338	1.351	H → L+1 (34%)
S_6	A	3.82	325	0.000	H-6 → L+2 (18%), H-5 → L (12%), H-5 → L+1 (10%), H-4 → L (10%), H-4 → L+1 (12%), H → L+2 (12%)
S_7	A	4.04	307	0.158	H-6 → L (18%), H-4 → L+2 (10%), H → L (17%), H → L+3 (16%)
S_8	A	4.04	307	0.158	H-6 → L+1 (18%), H-5 → L+2 (10%), H → L+1 (17%), H → L+4 (16%)
S_9	A	4.29	289	0.000	H-8 → L+1 (14%), H-7 → L (14%), H-6 → L+2 (12%), H → L+2 (31%),
S_{10}	A	4.35	285	0.013	H → L+5 (84%)

Table 7-26. Lowest energy singlet electronic transitions of **4-2M** in the gas phase with C_3 symmetry. H = HOMO; L = LUMO.

state	symmetry	*E* / eV	λ / nm	*f*	major (>10%) contributions
S_1	E	3.11	398	1.054	H → L (66%)
S_2	E	3.11	398	1.054	H → L+1 (66%)
S_3	A	3.32	373	0.000	H → L+2 (70%)
S_4	E	3.96	313	0.007	H-8 → L (11%), H-5 → L (10%), H-1 → L+2 (11%)
S_5	E	3.96	313	0.007	H-8 → L+1 (11%), H-5 → L+1 (10%), H-2 → L+2 (11%)
S_6	A	3.96	313	0.028	H-5 → L+2 (28%), H-4 → L+1 (22%), H-3 → L (22%)
S_7	E	3.96	313	0.002	H-5 → L (12%), H-4 → L+2 (12%)
S_8	E	3.96	313	0.002	H-5 → L+1 (12%), H-3 → L+2 (12%)
S_9	A	3.99	311	0.000	H-8 → L+2 (16%), H-2 → L+1 (18%), H-1 → L (18%), H → L+2 (27%)
S_{10}	E	4.21	294	0.622	H → L+1 (14%), H → L+6 (36%), H → L+7 (14%)

Table 7-27. Lowest energy singlet electronic transitions of **4-2M** in EtOH solution with C_3 symmetry. H = HOMO; L = LUMO.

state	symmetry	E / eV	λ / nm	f	major (>10%) contributions
S_1	E	3.40	365	1.407	H → L (54%), H → L+3 (11%)
S_2	E	3.40	365	1.408	H → L+1 (54%), H → L+4 (11%)
S_3	A	3.66	339	0.000	H-2 → L (13%), H-1 → L+1 (13%), H → L+2 (48%),
S_4	E	4.12	301	0.014	H-6 → L (14%), H-1 → L+2 (10%), H → L+3 (17%)
S_5	E	4.12	301	0.013	H-6 → L+1 (14%), H-2 → L+2 (10%), H → L+4 (17%)
S_6	E	4.15	298	0.006	H-5 → L+2 (10%), H-4 → L (26%), H-4 → L+2 (13%), H-3 → L (12%), H-3 → L+1 (12%)
S_7	E	4.15	298	0.017	H-4 → L+1 (14%), H-3 → L+1 (26%), H-3 → L+2 (22%)
S_8	E	4.15	298	0.017	H-5 → L (23%), H-5 → L+1 (18%), H-5 → L+2 (12%), H-4 → L+2 (11%)
S_9	E	4.30	288	0.012	H-10 → L+2 (12%), H-9 → L+1 (23%)
S_{10}	E	4.30	288	0.018	H-11 → L+1 (9%)

Table 7-28. Lowest energy singlet electronic transitions of **4-2M** in EtOH solution with C_1 symmetry. H = HOMO; L = LUMO.

state	symmetry	E / eV	λ / nm	f	major (>10%) contributions
S_1	A	3.40	365	1.407	H → L (56%), H → L+3 (11%)
S_2	A	3.40	365	1.408	H → L+1 (56%), H → L+4 (11%)
S_3	A	3.66	339	0.000	H-2 → L (16%), H-1 → L+1 (16%), H → L+2 (48%),
S_4	A	4.12	301	0.014	H-6 → L (18%), H-2 → L+2 (14%), H → L+3 (23%)
S_5	A	4.12	301	0.014	H-6 → L+1 (18%), H-1 → L+2 (14%), H → L+4 (23%)
S_6	A	4.15	299	0.003	H-5 → L+2 (15%), H-4 → L (11%), H-3 → L+1 (37%)
S_7	A	4.15	299	0.017	H-5 → L (10%), H-5 → L+1 (11%), H-4 → L (22%), H-3 → L+2 (14%)
S_8	A	4.15	299	0.020	H-5 → L (26%), H-4 → L+1 (17%), H-4 → L+2 (23%)
S_9	A	4.30	288	0.013	H-10 → L+2 (10%), H-9 → L+1 (12%)
S_{10}	A	4.30	288	0.012	H-9 → L+1 (10%)

Table 7-29. Lowest energy singlet electronic transitions of **5-1M** in water. H = HOMO; L = LUMO.

state	symmetry	E / eV	λ / nm	f	major (>10%) contributions
S_1	AU	4.15	299	0.716	H-2 → L (84%)
S_2	BU	4.17	298	0.016	H-7 → L (29%), H-6 → L (42%), H-3 → L (21%)
S_3	BU	4.22	294	0.177	H-6 → L (33%), H-4 → L+1 (15%), H-3 → L (33%)
S_4	BG	4.22	294	0.000	H-6 → L-1 (11%), H-5 → L (14%), H-4 → L (61%)
S_5	AG	4.54	273	0.000	H-8 → L (32%), H-2 → L+1 (10%), H-1 → L (40%)
S_6	AU	4.56	272	0.047	H-1 → L+1 (18%), H → L (69%)
S_7	AG	4.59	270	0.000	H-8 → L (41%), H-1 → L (30%), H → L+1 (11%)
S_8	BG	4.68	265	0.000	H-5 → L (54%), H-4 → L (12%)

Table 7-30. Lowest energy singlet electronic transitions of **5-2M** in water. H = HOMO; L = LUMO.

state	symmetry	E / eV	λ / nm	f	major (>10%) contributions
S_1	A	2.68	463	2.212	H → L (88%)
S_2	A	3.42	362	0.000	H-1 → L (25%), H → L+1 (66%)
S_3	A	4.16	298	0.040	H-1 → L (45%), H → L+1 (17%), H → L+2 (10%)
S_4	A	4.17	297	0.147	H-1 → L (11%), H-1 → L+1 (19%), H → L+2 (40%)
S_5	A	4.32	287	0.132	H-5 → L+1 (18%), H-4 → L (35%)
S_6	A	4.35	285	0.002	H-5 → L (37%), H-4 → L+1 (10%)
S_7	A	4.44	279	0.088	H-9 → L (15%), H-9 →L+1 (13%), H-7 → L (16%), H-7 → L+1 (14%)
S_8	A	4.48	277	0.087	H-8 → L (26%), H-8 → L+1 (21%)

Table 7-31. Lowest energy singlet electronic transitions of **5-3M** in water. H = HOMO; L = LUMO.

state	symmetry	E / eV	λ / nm	f	major (>10%) contributions
S_1	A	2.72	455	0.333	H → L (97%)
S_2	A	3.37	368	0.000	H → L+1 (93%)
S_3	A	3.73	332	0.057	H → L+2 (94%)
S_4	A	3.76	329	0.046	H-1 → L (68%), H → L+5 (15%)
S_5	A	4.09	303	0.180	H-3 → L+1 (12%), H-2 → L (60%)
S_6	A	4.16	298	0.000	H-7 → L (14%), H-3 → L (40%), H-2 → L+1 (29%)
S_7	A	4.50	276	0.000	H-10 → L (58%), H-3 → L (25%)
S_8	A	4.54	273	0.016	H-5 → L+1 (28%), H-4 → L (49%)

8 REFERENCES

[1] a) A. D. Buckingham, *Q. Rev. Chem. Sci.* **1959**, *13*, 183-214; b) D. J. Griffiths, in *Introduction to Electrodynamics*, 3rd ed., Prentice Hall, Inc., Upper Saddle River, **1999**, pp. 146-159.

[2] a) G. M. Cooper, R. E. Hausman, *The cell*, 7th ed., Oxford University Press, New York, **2018**; b) H. Plattner, J. Hentschel, *Zellbiologie*, 3rd ed., Thieme, Stuttgart, **2006**.

[3] J. Walker-Daniels, O. Faklaris, *Materials and Methods* **2012**, *2*, 124.

[4] M. Fernández-Suárez, A. Y. Ting, *Nat. Rev. Mol. Cell Biol.* **2008**, *9*, 929.

[5] Z. Yang, A. Sharma, J. Qi, X. Peng, D. Y. Lee, R. Hu, D. Lin, J. Qu, J. S. Kim, *Chem. Soc. Rev.* **2016**, *45*, 4651-4667.

[6] R. Cole, *Cell Adh. Migr.* **2014**, *8*, 452-459.

[7] M. M. Frigault, J. Lacoste, J. L. Swift, C. M. Brown, *J. Cell Sci.* **2009**, *122*, 753-767.

[8] T. Terai, T. Nagano, *Curr. Opin. Chem. Biol.* **2008**, *12*, 515-521.

[9] L. Ji, S. Griesbeck, T. B. Marder, *Chem. Sci.* **2017**, *8*, 846-863.

[10] a) G. C. Welch, R. R. S. Juan, J. D. Masuda, D. W. Stephan, *Science* **2006**, *314*, 1124-1126; b) D. W. Stephan, *J. Am. Chem. Soc.* **2015**, *137*, 10018-10032; c) G. C. Welch, D. W. Stephan, *J. Am. Chem. Soc.* **2007**, *129*, 1880-1881; d) D. W. Stephan, G. Erker, *Chem. Sci.* **2014**, *5*, 2625-2641; e) D. W. Stephan, G. Erker, *Angew. Chem. Int. Ed.* **2015**, *54*, 6400-6441; f) D. W. Stephan, G. Erker, *Angew. Chem. Int. Ed.* **2010**, *49*, 46-76; g) D. W. Stephan, *Acc. Chem. Res.* **2015**, *48*, 306-316; h) G. Erker, D. W. Stephan, *Frustrated Lewis Pairs I: Uncovering and Understanding, Vol. 332*, Springer-Verlag, Berlin, **2013**; i) D. W. Stephan, G. Erker, *Frustrated Lewis Pairs II: Expanding the Scope Preface, Vol. 334*, Springer-Verlag, Berlin, **2013**; j) S. Mukherjee, P. Thilagar, *J. Chem. Sci.* **2015**, *127*, 241-255; k) S. Mukherjee, P. Thilagar, *Resonance* **2014**, *19*, 1017-1027.

[11] P. J. Grisdale, J. L. Williams, M. Glogowski, B. Babb, *J. Org. Chem.* **1971**, *36*, 544-549.

[12] J. C. Doty, B. Babb, P. J. Grisdale, M. Glogowski, J. L. R. Williams, *J. Organomet. Chem.* **1972**, *38*, 229-236.

[13] a) T. W. Hudnall, C.-W. Chiu, F. P. Gabbaï, *Acc. Chem. Res.* **2009**, *42*, 388-397; b) Z. M. Hudson, S. Wang, *Acc. Chem. Res.* **2009**, *42*, 1584-1596; c) C. R. Wade, A. E. J. Broomsgrove, S. Aldridge, F. P. Gabbaï, *Chem. Rev.* **2010**, *110*, 3958-3984; d) F. Jäkle, *Chem. Rev.* **2010**, *110*, 3985-4022.

[14] a) Z. Yuan, N. J. Taylor, T. B. Marder, I. D. Williams, S. K. Kurtz, L.-T. Cheng, *J. Chem. Soc., Chem. Commun.* **1990**, 1489-1492; b) M. Lequan, R. M. Lequan, K. C. Ching, *J. Mater. Chem.* **1991**, *1*, 997-999; c) M. Lequan, R. M. Lequan, K. C. Ching, M. Barzoukas, A. Fort, H. Lahoucine, G. Bravic, D. Chasseau, J. Gaultier, *J. Mater. Chem.* **1992**, *2*, 719-725; d) M. Lequan, R. M. Lequan, K. Chane-Ching, A.-C. Callier, M. Barzoukas, A. Fort, *Adv. Mater. Opt. Electron.* **1992**, *1*, 243-247; e) C. Branger, M. Lequan, R. M. Lequan, M. Barzoukas, A. Fort, *J. Mater. Chem.* **1996**, *6*, 555-558; f) Z. Yuan, N. J. Taylor, Y. Sun, T. B. Marder, I. D. Williams, L.-T. Cheng, *J. Organomet. Chem.* **1993**, *449*, 27-37.

[15] Z. Yuan, C. D. Entwistle, J. C. Collings, D. Albesa-Jové, A. S. Batsanov, J. A. K. Howard, N. J. Taylor, H. M. Kaiser, D. E. Kaufmann, S.-Y. Poon, W.-Y. Wong, C. Jardin, S. Fathallah, A. Boucekkine, J.-F. Halet, T. B. Marder, *Chem. Eur. J.* **2006**, *12*, 2758-2771.

[16] Z. Yuan, N. J. Taylor, R. Ramachandran, T. B. Marder, *Appl. Organomet. Chem.* **1996**, *10*, 305-316.

[17] a) C. D. Entwistle, T. B. Marder, *Angew. Chem. Int. Ed.* **2002**, *41*, 2927-2931; b) C. D. Entwistle, T. B. Marder, *Chem. Mater.* **2004**, *16*, 4574-4585.

[18] a) S. Yamaguchi, A. Wakamiya, *Pure Appl. Chem.* **2006**, *78*, 1413-1424; b) F. Jäkle, *Coord. Chem. Rev.* **2006**, *250*, 1107-1121; c) M. Elbing, G. C. Bazan, *Angew. Chem. Int. Ed.* **2008**, *47*, 834-838; d) F. Jäkle, *Boron: Organoboranes*, 2nd ed., John Wiley & Sons, Ltd, Chichester, **2011**; e) Y. Ren, F. Jäkle, *Dalton Trans.* **2016**, *45*, 13996-14007.

[19] R. Stahl, C. Lambert, C. Kaiser, R. Wortmann, R. Jakober, *Chem. Eur. J.* **2006**, *12*, 2358-2370.
[20] U. Megerle, F. Selmaier, C. Lambert, E. Riedle, S. Lochbrunner, *Phys. Chem. Chem. Phys.* **2008**, *10*, 6245-6251.
[21] a) X. Y. Liu, D. R. Bai, S. Wang, *Angew. Chem. Int. Ed.* **2006**, *45*, 5475-5478; b) D. R. Bai, X. Y. Liu, S. Wang, *Chem. Eur. J.* **2007**, *13*, 5713-5723.
[22] H. Pan, G. L. Fu, Y. H. Zhao, C. H. Zhao, *Org. Lett.* **2011**, *13*, 4830-4833.
[23] M. Steeger, C. Lambert, *Chem. Eur. J.* **2012**, *18*, 11937-11948.
[24] T. Taniguchi, J. Wang, S. Irle, S. Yamaguchi, *Dalton Trans.* **2013**, *42*, 620-624.
[25] A. Proń, M. Baumgarten, K. Müllen, *Org. Lett.* **2010**, *12*, 4236-4239.
[26] S. M. Cornet, K. B. Dillon, C. D. Entwistle, M. A. Fox, A. E. Goeta, H. P. Goodwin, T. B. Marder, A. L. Thompson, *Dalton Trans.* **2003**, *32*, 4395-4405.
[27] L. Weber, V. Werner, M. A. Fox, T. B. Marder, S. Schwedler, A. Brockhinke, H.-G. Stammler, B. Neumann, *Dalton Trans.* **2009**, *38*, 1339-1351.
[28] a) Y. Qin, G. Cheng, A. Sundararaman, F. Jäkle, *J. Am. Chem. Soc.* **2002**, *124*, 12672-12673; b) A. Sundararaman, K. Venkatasubbaiah, M. Victor, L. N. Zakharov, A. L. Rheingold, F. Jäkle, *J. Am. Chem. Soc.* **2006**, *128*, 16554-16565.
[29] J. Wang, Y. Wang, T. Taniguchi, S. Yamaguchi, S. Irle, *J. Phys. Chem. A* **2012**, *116*, 1151-1158.
[30] P. Sudhakar, S. Mukherjee, P. Thilagar, *Organometallics* **2013**, *32*, 3129-3133.
[31] Z. Zhang, R. M. Edkins, J. Nitsch, K. Fucke, A. Steffen, L. E. Longobardi, D. W. Stephan, C. Lambert, T. B. Marder, *Chem. Sci.* **2015**, *6*, 308-321.
[32] Z. Lu, Z. Cheng, Z. Chen, L. Weng, Z. H. Li, H. Wang, *Angew. Chem. Int. Ed.* **2011**, *50*, 12227-12231.
[33] Z. Zhang, R. M. Edkins, J. Nitsch, K. Fucke, A. Eichhorn, A. Steffen, Y. Wang, T. B. Marder, *Chem. Eur. J.* **2015**, *21*, 177-190.
[34] I. A. I. Mkhalid, J. H. Barnard, T. B. Marder, J. M. Murphy, J. F. Hartwig, *Chem. Rev.* **2010**, *110*, 890-931.
[35] A. Wakamiya, S. Yamaguchi, *Bull. Chem. Soc. Jpn.* **2015**, *88*, 1357-1377.
[36] X. Yin, J. Chen, R. A. Lalancette, T. B. Marder, F. Jäkle, *Angew. Chem. Int. Ed.* **2014**, *53*, 9761-9765.
[37] a) A. Steffen, R. M. Ward, W. D. Jones, T. B. Marder, *Coord. Chem. Rev.* **2010**, *254*, 1950-1976; b) H. Braunschweig, I. Krummenacher, in *Organic Redox Systems: Syntheis, Properties, and Applications* (Ed.: T. Nishinaga), John Wiley & Sons, Inc., Hoboken, **2016**, pp. 503-522; c) H. Braunschweig, I. Krummenacher, J. Wahler, *Adv. Organomet. Chem.* **2013**, *61*, 1-53; d) H. Braunschweig, T. Kupfer, *Chem. Commun.* **2011**, *47*, 10903-10914.
[38] Z. Zhang, Z. Wang, M. Haehnel, A. Eichhorn, R. M. Edkins, A. Steffen, A. Krueger, Z. Lin, T. B. Marder, *Chem. Commun.* **2016**, *52*, 9707-9710.
[39] Z. Zhang, R. M. Edkins, M. Haehnel, M. Wehner, A. Eichhorn, L. Mailänder, M. Meier, J. Brand, F. Brede, K. Müller-Buschbaum, H. Braunschweig, T. B. Marder, *Chem. Sci.* **2015**, *6*, 5922-5927.
[40] Z. Xi, *Acc. Chem. Res.* **2010**, *43*, 1342-1351.
[41] H. Braunschweig, V. Dyakonov, J. O. C. Jimenez-Halla, K. Kraft, I. Krummenacher, K. Radacki, A. Sperlich, J. Wahler, *Angew. Chem. Int. Ed.* **2012**, *51*, 2977-2980.
[42] K. Schickedanz, T. Trageser, M. Bolte, H. W. Lerner, M. Wagner, *Chem. Commun.* **2015**, *51*, 15808-15810.
[43] a) L. Weber, V. Werner, M. A. Fox, T. B. Marder, S. Schwedler, A. Brockhinke, H. G. Stammler, B. Neumann, *Dalton Trans.* **2009**, *38*, 2823-2831; b) L. Weber, J. Halama, L. Böhling, A. Chrostowska, A. Dargelos, H.-G. Stammler, B. Neumann, *Eur. J. Inorg. Chem.* **2011**, *2011*, 3091-3101; c) L. Weber, D. Eickhoff, J. Kahlert, L. Böhling, A. Brockhinke, H.-G. Stammler, B. Neumann, M. A. Fox, *Dalton Trans.* **2012**, *41*, 10328-10346; d) L. Weber, D. Eickhoff, T. B. Marder, M. A. Fox, P. J. Low, A. D. Dwyer, D. J. Tozer, S. Schwedler, A. Brockhinke, H.-G. Stammler, B. Neumann, *Chem. Eur. J.* **2012**, *18*, 1369-1382.

[44] a) P. Bissinger, H. Braunschweig, A. Damme, T. Kupfer, A. Vargas, *Angew. Chem. Int. Ed.* **2012**, *51*, 9931-9934; b) H. Braunschweig, A. Damme, R. D. Dewhurst, A. Vargas, *Nature Chem.* **2013**, *5*, 115-121.

[45] J. E. Leffler, G. B. Watts, T. Tanigaki, E. Dolan, D. S. Miller, *J. Am. Chem. Soc.* **1970**, *92*, 6825-6830.

[46] a) H. C. Brown, V. H. Dodson, *J. Am. Chem. Soc.* **1957**, *79*, 2302-2306; b) S. I. Weissman, H. v. Willigen, *J. Am. Chem. Soc.* **1965**, *87*, 2285-2286; c) T. J. DuPont, J. L. Mills, *J. Am. Chem. Soc.* **1975**, *97*, 6375-6382.

[47] M. M. Olmstead, P. P. Power, *J. Am. Chem. Soc.* **1986**, *108*, 4235-4236.

[48] a) P. Y. Feng, Y. H. Liu, T. S. Lin, S. M. Peng, C. W. Chiu, *Angew. Chem. Int. Ed.* **2014**, *53*, 6237-6240; b) Y. Zheng, J. Xiong, Y. Sun, X. Pan, J. Wu, *Angew. Chem. Int. Ed.* **2015**, *54*, 12933-12936; c) L. E. Longobardi, L. Liu, S. Grimme, D. W. Stephan, *J. Am. Chem. Soc.* **2016**, *138*, 2500-2503; d) C. W. Chiu, F. P. Gabbaï, *Angew. Chem. Int. Ed.* **2007**, *46*, 1723-1725; e) D. Scheschkewitz, H. Amii, H. Gornitzka, W. W. Schoeller, D. Bourissou, G. Bertrand, *Science* **2002**, *295*, 1880-1881.

[49] a) W. Kaim, A. Schulz, *Angew. Chem. Int. Ed.* **1984**, *23*, 615-616; b) A. Schulz, W. Kaim, *Chem. Ber.* **1989**, *122*, 1863-1868; c) A. Lichtblau, W. Kaim, A. Schulz, T. Stahl, *J. Chem. Soc., Perkin Trans. 2* **1992**, 1497-1501; d) J. Fiedler, S. Záliš, A. Klein, F. M. Hornung, W. Kaim, *Inorg. Chem.* **1996**, *35*, 3039-3043; e) S. Záliš, W. Kaim, *Main Group Chem.* **2007**, *5*, 267-276; f) W. Kaim, N. S. Hosmane, S. Záliš, J. A. Maguire, W. N. Lipscomb, *Angew. Chem. Int. Ed.* **2009**, *48*, 5082-5091.

[50] a) A. P. Kulkarni, C. J. Tonzola, A. Babel, S. A. Jenekhe, *Chem. Mater.* **2004**, *16*, 4556-4573; b) P. J. Low, M. A. J. Paterson, H. Puschmann, A. E. Goeta, J. A. K. Howard, C. Lambert, J. C. Cherryman, D. R. Tackley, S. Leeming, B. Brown, *Chem. Eur. J.* **2004**, *10*, 83-91.

[51] a) T. Noda, Y. Shirota, *J. Am. Chem. Soc.* **1998**, *120*, 9714-9715; b) M. Kinoshita, Y. Shirota, *Chem. Lett.* **2001**, 614-615.

[52] L. Ji, R. M. Edkins, A. Lorbach, I. Krummenacher, C. Brückner, A. Eichhorn, H. Braunschweig, B. Engels, P. J. Low, T. B. Marder, *J. Am. Chem. Soc.* **2015**, *137*, 6750-6753.

[53] a) T. M. Figueira-Duarte, K. Müllen, *Chem. Rev.* **2011**, *111*, 7260-7314; b) J. M. Casas-Solvas, J. D. Howgego, A. P. Davis, *Org. Biomol. Chem.* **2014**, *12*, 212-232.

[54] a) D. N. Coventry, A. S. Batsanov, A. E. Goeta, J. A. K. Howard, T. B. Marder, R. N. Perutz, *Chem. Commun.* **2005**, *41*, 2172-2174; b) A. S. Batsanov, J. A. K. Howard, D. Albesa-Jové, J. C. Collings, Z. Liu, I. A. I. Mkhalid, M.-H. Thibault, T. B. Marder, *Cryst. Growth Des.* **2012**, *12*, 2794-2802; c) Z. Liu, Y. Wang, Y. Chen, J. Liu, Q. Fang, C. Kleeberg, T. B. Marder, *J. Org. Chem.* **2012**, *77*, 7124-7128.

[55] A. G. Crawford, Z. Liu, I. A. I. Mkhalid, M.-H. Thibault, N. Schwarz, G. Alcaraz, A. Steffen, J. C. Collings, A. S. Batsanov, J. A. K. Howard, T. B. Marder, *Chem. Eur. J.* **2012**, *18*, 5022-5035.

[56] M. Kreyenschmidt, M. Baumgarten, N. Tyutyulkov, K. Müllen, *Angew. Chem. Int. Ed.* **1994**, *33*, 1957-1959.

[57] A. G. Crawford, A. D. Dwyer, Z. Liu, A. Steffen, A. Beeby, L.-O. Pålsson, D. J. Tozer, T. B. Marder, *J. Am. Chem. Soc.* **2011**, *133*, 13349-13362.

[58] a) L. Ji, A. Lorbach, R. M. Edkins, T. B. Marder, *J. Org. Chem.* **2015**, *80*, 5658-5665; b) R. Kurata, K. Tanaka, A. Ito, *J. Org. Chem.* **2016**, *81*, 137-145; c) B. R. Kaafarani, C. Risko, T. H. El-Assaad, A. O. El-Ballouli, S. R. Marder, S. Barlow, *J. Phys. Chem. C* **2016**, *120*, 3156-3166; d) B. R. Kaafarani, A. O. El-Ballouli, R. Trattnig, A. Fonari, S. Sax, B. Wex, C. Risko, R. S. Khnayzer, S. Barlow, D. Patra, T. V. Timofeeva, E. J. W. List, J.-L. Brédas, S. R. Marder, *J. Mater. Chem. C* **2013**, *1*, 1638.

[59] J. Merz, J. Fink, A. Friedrich, I. Krummenacher, H. H. Al Mamari, S. Lorenzen, M. Haehnel, A. Eichhorn, M. Moos, M. Holzapfel, H. Braunschweig, C. Lambert, A. Steffen, L. Ji, T. B. Marder, *Chem. Eur. J.* **2017**, *23*, 13164-13180.

[60] E. C. Neeve, S. J. Geier, I. A. I. Mkhalid, S. A. Westcott, T. B. Marder, *Chem. Rev.* **2016**, *116*, 9091-9161.

[61] a) W. J. Grigsby, P. P. Power, *Chem. Commun.* **1996**, *32*, 2235-2236; b) W. J. Grigsby, P. Power, *Chem. Eur. J.* **1997**, *3*, 368-375; c) H. Asakawa, K.-H. Lee, K. Furukawa, Z. Lin, M. Yamashita, *Chem. Eur. J.* **2015**, *21*, 4267-4271; d) A. Moezzi, M. M. Olmstead, P. P. Power, *J. Am. Chem. Soc.* **1992**, *114*, 2715-2717; e) T. Kaese, A. Hübner, M. Bolte, H.-W. Lerner, M. Wagner, *J. Am. Chem. Soc.* **2016**, *138*, 6224-6233.

[62] J. D. Hoefelmeyer, F. P. Gabbaï, *J. Am. Chem. Soc.* **2000**, *122*, 9054-9055.

[63] a) A. Hübner, A. M. Diehl, M. Diefenbach, B. Endeward, M. Bolte, H. W. Lerner, M. C. Holthausen, M. Wagner, *Angew. Chem. Int. Ed.* **2014**, *53*, 4832-4835; b) A. Hübner, T. Kaese, M. Diefenbach, B. Endeward, M. Bolte, H. W. Lerner, M. C. Holthausen, M. Wagner, *J. Am. Chem. Soc.* **2015**, *137*, 3705-3714.

[64] R. Bertermann, H. Braunschweig, R. D. Dewhurst, C. Hörl, T. Kramer, I. Krummenacher, *Angew. Chem. Int. Ed.* **2014**, *53*, 5453-5457.

[65] P. Bissinger, H. Braunschweig, A. Damme, I. Krummenacher, A. K. Phukan, K. Radacki, S. Sugawara, *Angew. Chem. Int. Ed.* **2014**, *53*, 7360-7363.

[66] H. Braunschweig, V. Dyakonov, B. Engels, Z. Falk, C. Hörl, J. H. Klein, T. Kramer, H. Kraus, I. Krummenacher, C. Lambert, C. Walter, *Angew. Chem. Int. Ed.* **2013**, *52*, 12852-12855.

[67] A. Escande, M. J. Ingleson, *Chem. Commun.* **2015**, *51*, 6257-6274.

[68] a) M. J. Bosdet, W. E. Piers, *Can. J. Chem.* **2009**, *87*, 8-29; b) Z. Liu, T. B. Marder, *Angew. Chem. Int. Ed.* **2008**, *47*, 242-244.

[69] a) A. Hübner, M. Diefenbach, M. Bolte, H. W. Lerner, M. C. Holthausen, M. Wagner, *Angew. Chem. Int. Ed.* **2012**, *51*, 12514-12518; b) A. Hübner, Z. W. Qu, U. Englert, M. Bolte, H. W. Lerner, M. C. Holthausen, M. Wagner, *J. Am. Chem. Soc.* **2011**, *133*, 4596-4609; c) S. Yamaguchi, T. Shirasaka, S. Akiyama, K. Tamao, *J. Am. Chem. Soc.* **2002**, *124*, 8816-8817; d) A. Wakamiya, K. Mishima, K. Ekawa, S. Yamaguchi, *Chem. Commun.* **2008**, *44*, 579-581; e) A. Iida, S. Yamaguchi, *J. Am. Chem. Soc.* **2011**, *133*, 6952-6955; f) A. Iida, A. Sekioka, S. Yamaguchi, *Chem. Sci.* **2012**, *3*, 1461-1466; g) D. M. Chen, Q. Qin, Z. B. Sun, Q. Peng, C. H. Zhao, *Chem. Commun.* **2014**, *50*, 782-784; h) M. F. Smith, S. J. Cassidy, I. A. Adams, M. Vasiliu, D. L. Gerlach, D. A. Dixon, P. A. Rupar, *Organometallics* **2016**, *35*, 3182-3191.

[70] a) A. Caruso Jr., M. A. Siegler, J. D. Tovar, *Angew. Chem. Int. Ed.* **2010**, *49*, 4213-4217; b) A. Caruso Jr., J. D. Tovar, *J. Org. Chem.* **2011**, *76*, 2227-2239; c) A. Caruso Jr., J. D. Tovar, *Org. Lett.* **2011**, *13*, 3106-3109; d) D. R. Levine, A. Caruso Jr., M. A. Siegler, J. D. Tovar, *Chem. Commun.* **2012**, *48*, 6256-6258; e) D. R. Levine, M. A. Siegler, J. D. Tovar, *J. Am. Chem. Soc.* **2014**, *136*, 7132-7139.

[71] R. E. Messersmith, J. D. Tovar, *J. Phys. Org. Chem.* **2015**, *28*, 378-387.

[72] a) S. Saito, K. Matsuo, S. Yamaguchi, *J. Am. Chem. Soc.* **2012**, *134*, 9130-9133; b) Z. Zhou, A. Wakamiya, T. Kushida, S. Yamaguchi, *J. Am. Chem. Soc.* **2012**, *134*, 4529-4532.

[73] T. Kushida, S. Yamaguchi, *Organometallics* **2013**, *32*, 6654-6657.

[74] T. Kushida, C. Camacho, A. Shuto, S. Irle, M. Muramatsu, T. Katayama, S. Ito, Y. Nagasawa, H. Miyasaka, E. Sakuda, N. Kitamura, Z. Zhou, A. Wakamiya, S. Yamaguchi, *Chem. Sci.* **2014**, *5*, 1296-1304.

[75] a) J. F. Araneda, B. Neue, W. E. Piers, *Angew. Chem. Int. Ed.* **2012**, *51*, 9977-9979; b) C. Dou, S. Saito, K. Matsuo, I. Hisaki, S. Yamaguchi, *Angew. Chem. Int. Ed.* **2012**, *51*, 12206-12210; c) T. Kushida, Z. Zhou, A. Wakamiya, S. Yamaguchi, *Chem. Commun.* **2012**, *48*, 10715-10717; d) T. Kushida, S. Yamaguchi, *Angew. Chem. Int. Ed.* **2013**, *52*, 8054-8058; e) A. Shuto, T. Kushida, T. Fukushima, H. Kaji, S. Yamaguchi, *Org. Lett.* **2013**, *15*, 6234-6237; f) T. Kushida, A. Shuto, M. Yoshio, T. Kato, S. Yamaguchi, *Angew. Chem. Int. Ed.* **2015**, *54*, 6922-6925; g) S. Osumi, S. Saito, C. Dou, K. Matsuo, K. Kume, H. Yoshikawa, K. Awaga, S. Yamaguchi, *Chem. Sci.* **2016**, *7*, 219-227.

[76] a) U. H. F. Bunz, *Acc. Chem. Res.* **2015**, *48*, 1676-1686; b) U. H. F. Bunz, J. U. Engelhart, B. D. Lindner, M. Schaffroth, *Angew. Chem. Int. Ed.* **2013**, *52*, 3810-3821; c) U. H. F. Bunz,

Chem. Eur. J. **2009**, *15*, 6780-6789; d) L. Ji, M. Haehnel, I. Krummenacher, P. Biegger, F. L. Geyer, O. Tverskoy, M. Schaffroth, J. Han, A. Dreuw, T. B. Marder, U. H. F. Bunz, *Angew. Chem. Int. Ed.* **2016**, *55*, 10498-10501.

[77] A. H. Endres, M. Schaffroth, F. Paulus, H. Reiss, H. Wadepohl, F. Rominger, R. Krämer, U. H. F. Bunz, *J. Am. Chem. Soc.* **2016**, *138*, 1792-1795.

[78] a) A. Lorbach, M. Bolte, H. Li, H. W. Lerner, M. C. Holthausen, F. Jäkle, M. Wagner, *Angew. Chem. Int. Ed.* **2009**, *48*, 4584-4588; b) E. Januszewski, A. Lorbach, R. Grewal, M. Bolte, J. W. Bats, H. W. Lerner, M. Wagner, *Chem. Eur. J.* **2011**, *17*, 12696-12705; c) C. Hoffend, F. Schodel, M. Bolte, H. W. Lerner, M. Wagner, *Chem. Eur. J.* **2012**, *18*, 15394-15405; d) E. Januszewski, M. Bolte, H.-W. Lerner, M. Wagner, *Organometallics* **2012**, *31*, 8420-8425; e) C. Hoffend, M. Diefenbach, E. Januszewski, M. Bolte, H. W. Lerner, M. C. Holthausen, M. Wagner, *Dalton Trans.* **2013**, *42*, 13826-13837; f) C. Hoffend, K. Schickedanz, M. Bolte, H.-W. Lerner, M. Wagner, *Tetrahedron* **2013**, *69*, 7073-7081; g) C. Reus, S. Weidlich, M. Bolte, H. W. Lerner, M. Wagner, *J. Am. Chem. Soc.* **2013**, *135*, 12892-12907; h) C. Reus, F. Guo, A. John, M. Winhold, H.-W. Lerner, F. Jäkle, M. Wagner, *Macromolecules* **2014**, *47*, 3727-3735; i) V. M. Hertz, M. Bolte, H.-W. Lerner, M. Wagner, *Angew. Chem. Int. Ed.* **2015**, *54*, 8800-8804; j) V. M. Hertz, H. W. Lerner, M. Wagner, *Org. Lett.* **2015**, *17*, 5240-5243; k) V. M. Hertz, J. G. Massoth, M. Bolte, H. W. Lerner, M. Wagner, *Chem. Eur. J.* **2016**, *22*, 13181-13188.

[79] E. von Grotthuss, M. Diefenbach, M. Bolte, H. W. Lerner, M. C. Holthausen, M. Wagner, *Angew. Chem. Int. Ed.* **2016**, *55*, 14067-14071.

[80] a) S. N. Kessler, M. Neuburger, H. A. Wegner, *Eur. J. Org. Chem.* **2011**, *2011*, 3238-3245; b) S. N. Kessler, M. Neuburger, H. A. Wegner, *J. Am. Chem. Soc.* **2012**, *134*, 17885-17888.

[81] C. Dou, S. Saito, S. Yamaguchi, *J. Am. Chem. Soc.* **2013**, *135*, 9346-9349.

[82] T. Agou, J. Kobayashi, T. Kawashima, *Inorg. Chem.* **2006**, *45*, 9137-9144.

[83] S. Yamaguchi, S. Akiyama, K. Tamao, *J. Am. Chem. Soc.* **2001**, *123*, 11372-11375.

[84] S. K. Sarkar, S. Mukherjee, P. Thilagar, *Inorg. Chem.* **2014**, *53*, 2343-2345.

[85] a) Y. Sun, N. Ross, S.-B. Zhao, K. Huszarik, W.-L. Jia, R.-Y. Wang, D. Macartney, S. Wang, *J. Am. Chem. Soc.* **2007**, *129*, 7510-7511; b) Y. Sun, S. Wang, *Inorg. Chem.* **2009**, *48*, 3755-3767; c) Y. Li, Y. Kang, J.-S. Lu, I. Wyman, S.-B. Ko, S. Wang, *Organometallics* **2014**, *33*, 964-973.

[86] M. Varlan, B. A. Blight, S. Wang, *Chem. Commun.* **2012**, *48*, 12059-12061.

[87] a) G. R. Kumar, S. K. Sarkar, P. Thilagar, *Phys. Chem. Chem. Phys.* **2015**, *17*, 30424-30432; b) C. Wang, J. Jia, W. N. Zhang, H. Y. Zhang, C. H. Zhao, *Chem. Eur. J.* **2014**, *20*, 16590-16601; c) G. R. Kumar, S. K. Sarkar, P. Thilagar, *Chem. Eur. J.* **2016**, *22*, 17215-17225.

[88] T. W. Hudnall, M. Melaïmi, F. P. Gabbaï, *Org. Lett.* **2006**, *8*, 2747-27499.

[89] W. E. Piers, G. J. Irvine, V. C. Williams, *Eur. J. Inorg. Chem.* **2000**, *2000*, 2131-2142.

[90] a) S. Solé, F. P. Gabbaï, *Chem. Commun.* **2004**, *40*, 1284-1285; b) M. Melaïmi, S. Solé, C.-W. Chiu, H. Wang, F. P. Gabbaï, *Inorg. Chem.* **2006**, *45*, 8136-8143; c) M. Melaïmi, F. P. Gabbaï, *J. Am. Chem. Soc.* **2005**, *127*, 9680-9681.

[91] a) M. H. Lee, F. P. Gabbaï, *Inorg. Chem.* **2007**, *46*, 8132-8138; b) T. W. Hudnall, Y. M. Kim, M. W. Bebbington, D. Bourissou, F. P. Gabbaï, *J. Am. Chem. Soc.* **2008**, *130*, 10890-10891.

[92] a) M. H. Lee, T. Agou, J. Kobayashi, T. Kawashima, F. P. Gabbaï, *Chem. Commun.* **2007**, *43*, 1133-1135; b) Y. Kim, F. P. Gabbaï, *J. Am. Chem. Soc.* **2009**, *131*, 3363-3369.

[93] a) H. Li, R. A. Lalancette, F. Jäkle, *Chem. Commun.* **2011**, *47*, 9378-9380; b) F. Pammer, F. Jäkle, *Chem. Sci.* **2012**, *3*, 2598.

[94] a) C.-H. Zhao, A. Wakamiya, Y. Inukai, S. Yamaguchi, *J. Am. Chem. Soc.* **2006**, *128*, 15934-15935; b) A. Wakamiya, K. Mori, S. Yamaguchi, *Angew. Chem. Int. Ed.* **2007**, *46*, 4273-4276.

[95] F. Cheng, E. M. Bonder, F. Jäkle, *J. Am. Chem. Soc.* **2013**, *135*, 17286-17289.

[96] W. M. Wan, F. Cheng, F. Jäkle, *Angew. Chem. Int. Ed.* **2014**, *53*, 8934-8938.

[97] X. Yin, F. Guo, R. A. Lalancette, F. Jäkle, *Macromolecules* **2016**, *49*, 537-546.

[98] a) P. Chen, R. A. Lalancette, F. Jäkle, *J. Am. Chem. Soc.* **2011**, *133*, 8802-8805; b) P. Chen, F. Jäkle, *J. Am. Chem. Soc.* **2011**, *133*, 20142-20145.

[99] P. Chen, R. A. Lalancette, F. Jäkle, *Angew. Chem. Int. Ed.* **2012**, *51*, 7994-7998.

[100] P. Chen, X. Yin, N. Baser-Kirazli, F. Jäkle, *Angew. Chem. Int. Ed.* **2015**, *54*, 10768-10772.

[101] a) Y. Shirota, M. Kinoshita, T. Noda, K. Okumoto, T. Ohara, *J. Am. Chem. Soc.* **2000**, *122*, 11021-11022; b) H. Doi, M. Kinoshita, K. Okumoto, Y. Shirota, *Chem. Mater.* **2003**, *15*, 1080-1089; c) D. Mutaguchi, K. Okumoto, Y. Ohsedo, K. Moriwaki, Y. Shirota, *Org. Electron.* **2003**, *4*, 49-59.

[102] a) W.-L. Jia, D.-R. Bai, T. McCormick, Q.-D. Liu, M. Motala, R.-Y. Wang, C. Seward, Y. Tao, S. Wang, *Chem. Eur. J.* **2004**, *10*, 994-1006; b) W. L. Jia, X. D. Feng, D. R. Bai, Z. H. Lu, S. Wang, G. Vamvounis, *Chem. Mater.* **2005**, *17*, 164-170; c) W. L. Jia, M. J. Moran, Y.-Y. Yuan, Z. H. Lu, S. Wang, *J. Mater. Chem.* **2005**, *15*, 3326-3333; d) F. Li, W. Jia, S. Wang, Y. Zhao, Z.-H. Lu, *J. Appl. Phys.* **2008**, *103*, 034509; e) F. Miyamoto, S. Nakatsuka, K. Yamada, K. Nakayama, T. Hatakeyama, *Org. Lett.* **2015**, *17*, 6158-6161.

[103] G. Zhou, C.-L. Ho, W.-Y. Wong, Q. Wang, D. Ma, L. Wang, Z. Lin, T. B. Marder, A. Beeby, *Adv. Funct. Mater.* **2008**, *18*, 499-511.

[104] a) Z. M. Hudson, C. Sun, M. G. Helander, H. Amarne, Z.-H. Lu, S. Wang, *Adv. Funct. Mater.* **2010**, *20*, 3426-3439; b) Z. B. Wang, M. G. Helander, Z. M. Hudson, J. Qiu, S. Wang, Z. H. Lu, *Appl. Phys. Lett.* **2011**, *98*, 213301; c) Z. B. Wang, M. G. Helander, J. Qiu, D. P. Puzzo, M. T. Greiner, Z. M. Hudson, S. Wang, Z. W. Liu, Z. H. Lu, *Nat. Photonics* **2011**, *5*, 753-757; d) X. Wang, Y.-L. Chang, J.-S. Lu, T. Zhang, Z.-H. Lu, S. Wang, *Adv. Funct. Mater.* **2014**, *24*, 1911-1927.

[105] Z. M. Hudson, C. Sun, M. G. Helander, Y.-L. Chang, Z.-H. Lu, S. Wang, *J. Am. Chem. Soc.* **2012**, *134*, 13930-13933.

[106] H. Uoyama, K. Goushi, K. Shizu, H. Nomura, C. Adachi, *Nature* **2012**, *492*, 234-238.

[107] W.-L. Jia, D. Song, S. Wang, *J. Org. Chem.* **2003**, *68*, 701-705.

[108] a) H. Hirai, K. Nakajima, S. Nakatsuka, K. Shiren, J. Ni, S. Nomura, T. Ikuta, T. Hatakeyama, *Angew. Chem. Int. Ed.* **2015**, *54*, 13581-13585; b) M. Numata, T. Yasuda, C. Adachi, *Chem. Commun.* **2015**, *51*, 9443-9446; c) K. Suzuki, S. Kubo, K. Shizu, T. Fukushima, A. Wakamiya, Y. Murata, C. Adachi, H. Kaji, *Angew. Chem. Int. Ed.* **2015**, *54*, 15231-15235; d) T. Hatakeyama, K. Shiren, K. Nakajima, S. Nomura, S. Nakatsuka, K. Kinoshita, J. Ni, Y. Ono, T. Ikuta, *Adv. Mater.* **2016**, *28*, 2777-2781.

[109] a) B. Strehmel, V. Strehmel, *Adv. Photochem.* **2007**, *29*, 111-354; b) G. S. He, L.-S. Tan, Q. Zheng, P. N. Prasad, *Chem. Rev.* **2008**, *108*, 1245-1330; c) M. Rumi, S. Barlow, J. Wang, J. W. Perry, S. R. Marder, in *Photoresponsive Polymers I, Vol. 213* (Eds.: S. R. Marder, K.-S. Lee), Springer, Berlin, **2008**, pp. 1-95; d) F. Terenziani, C. Katan, E. Badaeva, S. Tretiak, M. Blanchard-Desce, *Adv. Mater.* **2008**, *20*, 4641-4678.

[110] a) M. Albota, D. Beljonne, J.-L. Brédas, J. E. Ehrlich, J.-Y. Fu, A. A. Heikal, S. E. Hess, T. Kogej, M. D. Levin, S. R. Marder, D. McCord-Maughon, J. W. Perry, H. Röckel, M. Rumi, G. Subramaniam, W. W. Webb, X.-L. Wu, C. Xu, *Science* **1998**, *281*, 1653-1656; b) D. Beljonne, W. Wenseleers, E. Zojer, Z. Shuai, H. Vogel, S. J. K. Pond, J. W. Perry, S. R. Marder, J. L. Brédas, *Adv. Funct. Mater.* **2002**, *12*, 631-641; c) Q. Zheng, G. S. He, P. N. Prasad, *Chem. Mater.* **2005**, *17*, 6004-6011.

[111] a) Z.-Q. Liu, Q. Fang, D. Wang, G. Xue, W.-T. Yu, Z.-S. Shao, M.-H. Jiang, *Chem. Commun.* **2002**, 2900-2901; b) Z.-Q. Liu, Q. Fang, D. Wang, D.-X. Cao, G. Xue, W.-T. Yu, H. Lei, *Chem. Eur. J.* **2003**, *9*, 5074-5084; c) Z.-Q. Liu, Q. Fang, D.-X. Cao, D. Wang, G.-B. Xu, *Org. Lett.* **2004**, *6*, 2933-2936; d) Z.-Q. Liu, M. Shi, F.-Y. Li, Q. Fang, Z.-H. Chen, T. Yi, C.-H. Huang, *Org. Lett.* **2005**, *7*, 5481-5484; e) M. Charlot, L. Porrès, C. D. Entwistle, A. Beeby, T. B. Marder, M. Blanchard-Desce, *Phys. Chem. Chem. Phys.* **2005**, *7*, 600-606; f) C. D. Entwistle, J. C. Collings, A. Steffen, L.-O. Pålsson, A. Beeby, D. Albesa-Jové, J. M. Burke, A. S. Batsanov, J. A. K. Howard, J. A. Mosely, S.-Y. Poon, W.-Y. Wong, F. Ibersiene, S. Fathallah, A. Boucekkine, J.-F. Halet, T. B. Marder, *J. Mater. Chem.* **2009**, *19*, 7532-7544; g) J. C. Collings, S.-Y. Poon, C. Le Droumaguet, M. Charlot, C. Katan, L.-O. Pålsson, A.

Beeby, J. A. Mosely, H. M. Kaiser, D. Kaufmann, W.-Y. Wong, M. Blanchard-Desce, T. B. Marder, *Chem. Eur. J.* **2009**, *15*, 198-208; h) L. Ji, Q. Fang, M.-S. Yuan, Z.-Q. Liu, Y.-X. Shen, H.-F. Chen, *Org. Lett.* **2010**, *12*, 5192-5195; i) L. Ji, R. M. Edkins, L. J. Sewell, A. Beeby, A. S. Batsanov, K. Fucke, M. Drafz, J. A. K. Howard, O. Moutounet, F. Ibersiene, A. Boucekkine, E. Furet, Z. Liu, J.-F. Halet, C. Katan, T. B. Marder, *Chem. Eur. J.* **2014**, *20*, 13618-13635.

[112] a) N. S. Makarov, S. Mukhopadhyay, K. Yesudas, J.-L. Brédas, J. W. Perry, A. Pron, M. Kivala, K. Müllen, *J. Phys. Chem A* **2012**, *116*, 3781-3793; b) P. Chen, A. S. Marshall, S. H. Chi, X. Yin, J. W. Perry, F. Jäkle, *Chem. Eur. J.* **2015**, *21*, 18237-18247.

[113] X. Li, X. Guo, L. Cao, Z. Xun, S. Wang, S. Li, Y. Li, G. Yang, *Angew. Chem. Int. Ed.* **2014**, *53*, 7809-7813.

[114] J. Liu, X. Guo, R. Hu, X. Liu, S. Wang, S. Li, Y. Li, G. Yang, *Anal. Chem.* **2016**, *88*, 1052-1057.

[115] J. Liu, S. Zhang, C. Zhang, J. Dong, C. Shen, J. Zhu, H. Xu, M. Fu, G. Yang, X. Zhang, *Chem. Commun.* **2017**, *53*, 11476-11479.

[116] J. Liu, S. Li, S. Zhang, C. Shen, J. Zhu, G. Yang, X. Zhang, *Sens. Actuator. B Chem.* **2018**, *261*, 531-536.

[117] a) J. Liu, X. Guo, R. Hu, J. Xu, S. Wang, S. Li, Y. Li, G. Yang, *Anal. Chem.* **2015**, *87*, 3694-3698; b) J. Liu, C. Zhang, J. Dong, J. Zhu, C. Shen, G. Yang, X. Zhang, *RSC Adv.* **2017**, *7*, 14511-14515; c) J. Liu, C. Zhang, J. Dong, J. Zhu, C. Shen, G. Yang, X. Zhang, *New J. Chem.* **2017**, *41*, 4733-4737; d) X. Guo, X. Zhang, S. Wang, S. Li, R. Hu, Y. Li, G. Yang, *Anal. Chim. Acta* **2015**, *869*, 81-88.

[118] S. Pagidi, N. K. Kalluvettukuzhy, P. Thilagar, *Langmuir* **2018**, *34*, 8170-8177.

[119] S. Griesbeck, Z. Zhang, M. Gutmann, T. Lühmann, R. M. Edkins, G. Clermont, A. N. Lazar, M. Haehnel, K. Edkins, A. Eichhorn, M. Blanchard-Desce, L. Meinel, T. B. Marder, *Chem. Eur. J.* **2016**, *22*, 14701-14706.

[120] a) S. Yamaguchi, A. Wakamiya, *Pure Appl. Chem.* **2006**, *78*, 1413-1424; b) Z. M. Hudson, S. Wang, *Dalton Trans.* **2011**, *40*, 7805-7816.

[121] Z. Zhou, A. Wakamiya, T. Kushida, S. Yamaguchi, *J. Am. Chem. Soc.* **2012**, *134*, 4529-4532.

[122] E. Galbraith, T. D. James, *Chem. Soc. Rev.* **2010**, *39*, 3831-3842.

[123] a) T. Noda, Y. Shirota, *J. Am. Chem. Soc.* **1998**, *120*, 9714-9715; b) Y. Shirota, H. Kageyama, *Chem. Rev.* **2007**, *107*, 953-1010; c) C. Sun, Z. M. Hudson, M. G. Helander, Z.-H. Lu, S. Wang, *Organometallics* **2011**, *30*, 5552-5555.

[124] Y. Chen, G.-Q. Liu, Y.-Y. Wang, P. Yu, Z. Liu, Q. Fang, *Synth. Met.* **2012**, *162*, 291-295.

[125] a) H. Zhao, L. A. Leamer, F. P. Gabbaï, *Dalton Trans.* **2013**, *42*, 8164-8178; b) T. W. Hudnall, F. P. Gabbaï, *J. Am. Chem. Soc.* **2007**, *129*, 11978-11986.

[126] C.-W. Chiu, Y. Kim, F. P. Gabbaï, *J. Am. Chem. Soc.* **2009**, *131*, 60-61.

[127] a) Y. Kim, F. P. Gabbaï, *J. Am. Chem. Soc.* **2009**, *131*, 3363-3369; b) T. Agou, M. Sekine, J. Kobayashi, T. Kawashima, *Chem. Eur. J.* **2009**, *15*, 5056-5062; c) K. C. Song, K. M. Lee, N. V. Nghia, W. Y. Sung, Y. Do, M. H. Lee, *Organometallics* **2013**, *32*, 817-823.

[128] X. Li, X. Guo, L. Cao, Z. Xun, S. Wang, S. Li, Y. Li, G. Yang, *Angew. Chem. Int. Ed.* **2014**, *53*, 7809-7813.

[129] J. Liu, X. Guo, R. Hu, X. Liu, S. Wang, S. Li, Y. Li, G. Yang, *Anal. Chem.* **2016**, *88*, 1052-1057.

[130] a) X. Zhao, Y. Li, D. Jin, Y. Xing, X. Yan, L. Chen, *Chem. Commun.* **2015**, *51*, 11721-11724; b) M. Grzybowski, E. Glodkowska-Mrowka, V. Hugues, W. Brutkowski, M. Blanchard-Desce, D. T. Gryko, *Chem. Eur. J.* **2015**, *21*, 9101-9110; c) N. Jiang, J. Fan, F. Xu, X. Peng, H. Mu, J. Wang, X. Xiong, *Angew. Chem. Int. Ed.* **2015**, *54*, 2510-2514; d) M. Homma, Y. Takei, A. Murata, T. Inoue, S. Takeoka, *Chem. Commun.* **2015**, *51*, 6194-6197.

[131] S. W. Perry, J. P. Norman, J. Barbieri, E. B. Brown, H. A. Gelbard, *BioTechniques* **2011**, *50*, 98-115.

[132] Y. Takihara, M. Inatani, K. Eto, T. Inoue, A. Kreymerman, S. Miyake, S. Ueno, M. Nagaya, A. Nakanishi, K. Iwao, Y. Takamura, H. Sakamoto, K. Satoh, M. Kondo, T. Sakamoto, J. L. Goldberg, J. Nabekura, H. Tanihara, *Proc. Natl. Acad. Sci.* **2015**, *112*, 10515-10520.

[133] Z.-H. Sheng, Q. Cai, *Nat. Rev. Neurosci.* **2012**, *13*, 77-93.

[134] C.-W. Chiu, F. P. Gabbaï, *Organometallics* **2008**, *27*, 1657-1659.
[135] Molecular Probes, Inc., Eugene, **2008**.
[136] a) C. Xu, W. W. Webb, *J. Opt. Soc. Am. B* **1996**, *13*, 481-491; b) M. A. Albota, C. Xu, W. W. Webb, *Appl. Opt.* **1998**, *37*, 7352-7356.
[137] M. Barzoukas, M. Blanchard-Desce, *J. Chem. Phys.* **2000**, *113*, 3951-3959.
[138] a) M. Elbing, G. C. Bazan, *Angew. Chem. Int. Ed.* **2008**, *47*, 834-838; b) E. von Grotthuss, A. John, T. Kaese, M. Wagner, *Asian J. Org. Chem.* **2018**, *7*, 37-53.
[139] X. Yin, J. Chen, R. A. Lalancette, T. B. Marder, F. Jäkle, *Angew. Chem. Int. Ed.* **2014**, *53*, 9761-9765.
[140] a) Y. Chen, D. Cao, S. Wang, C. Zhang, Z. Liu, *J. Mol. Struct.* **2010**, *969*, 182-186; b) J. Ohshita, Y. Tominaga, D. Tanaka, Y. Ooyama, T. Mizumo, N. Kobayashi, H. Higashimura, *Dalton Trans.* **2013**, *42*, 3646-3652; c) G. Turkoglu, M. E. Cinar, T. Ozturk, *Eur. J. Org. Chem.* **2017**, *2017*, 4552-4561.
[141] a) M. Numata, T. Yasuda, C. Adachi, *Chem. Commun.* **2015**, *51*, 9443-9446; b) I. S. Park, M. Numata, C. Adachi, T. Yasuda, *Bull. Chem. Soc. Jpn.* **2016**, *89*, 375-377; c) Y. Liu, G. Xie, K. Wu, Z. Luo, T. Zhou, X. Zeng, J. Yu, S. Gong, C. Yang, *J. Mater. Chem. C* **2016**, *4*, 4402-4407; d) Y. H. Lee, S. Park, J. Oh, J. W. Shin, J. Jung, S. Yoo, M. H. Lee, *ACS Appl. Mater. Interfaces* **2017**, *9*, 24035-24042.
[142] M. Kinoshita, Y. Shirota, *Chem. Lett.* **2001**, *30*, 614-615.
[143] a) W. Kaim, A. Schulz, *Angew. Chem. Int. Ed.* **1984**, *23*, 615-616; b) L. Ji, I. Krummenacher, A. Friedrich, A. Lorbach, M. Haehnel, K. Edkins, H. Braunschweig, T. B. Marder, *J. Org. Chem.* **2018**, *83*, 3599-3606.
[144] a) S.-Y. Li, Z.-B. Sun, C.-H. Zhao, *Inorg. Chem.* **2017**, *56*, 8705-8717; b) M. Ito, E. Ito, M. Hirai, S. Yamaguchi, *J. Org. Chem.* **2018**, *83*, 8449-8456; c) M. Meier, L. Ji, J. Nitsch, I. Krummenacher, A. Deißenberger, D. Auerhammer, M. Schäfer, T. B. Marder, H. Braunschweig, *Chem. Eur. J.* **2019**, *25*, DOI: 10.1002/chem.201805454.
[145] H. M. Kim, B. R. Cho, *Chem. Rev.* **2015**, *115*, 5014-5055.
[146] a) M. Rumi, S. Barlow, J. Wang, J. W. Perry, S. R. Marder, in *Photoresponsive Polymers I, Vol. 213* (Eds.: S. R. Marder, K.-S. Lee), Springer, Berlin, **2008**, pp. 1-95; b) M. Pawlicki, H. A. Collins, R. G. Denning, H. L. Anderson, *Angew. Chem. Int. Ed.* **2009**, *48*, 3244-3266; c) H. M. Kim, B. R. Cho, *Chem. Commun.* **2009**, 153-164.
[147] a) B. H. Cumpston, S. P. Ananthavel, S. Barlow, D. L. Dyer, J. E. Ehrlich, L. L. Erskine, A. A. Heikal, S. M. Kuebler, I. Y. S. Lee, D. McCord-Maughon, J. Qin, H. Röckel, M. Rumi, X.-L. Wu, S. R. Marder, J. W. Perry, *Nature* **1999**, *398*, 51-54; b) S. Kawata, H.-B. Sun, T. Tanaka, K. Takada, *Nature* **2001**, *412*, 697-698; c) W. Zhou, S. M. Kuebler, K. L. Braun, T. Yu, J. K. Cammack, C. K. Ober, J. W. Perry, S. R. Marder, *Science* **2002**, *296*, 1106-1109; d) S. Juodkazis, V. Mizeikis, H. Misawa, *J. Appl. Phys.* **2009**, *106*, 051101.
[148] a) D. A. Parthenopoulos, P. M. Rentzepis, *Science* **1989**, *245*, 843-845; b) S. Kawata, Y. Kawata, *Chem. Rev.* **2000**, *100*, 1777-1788; c) W. Dallari, M. Scotto, M. Allione, E. Samoylova, F. Pignatelli, R. Cingolani, A. Athanassiou, A. Diaspro, *Microelectron. Eng.* **2011**, *88*, 3466-3469.
[149] a) G. S. He, J. D. Bhawalkar, C. F. Zhao, P. N. Prasad, *Appl. Phys. Lett.* **1995**, *67*, 2433-2435; b) J. E. Ehrlich, X. L. Wu, I. Y. S. Lee, Z. Y. Hu, H. Röckel, S. R. Marder, J. W. Perry, *Opt. Lett.* **1997**, *22*, 1843-1845; c) C. W. Spangler, *J. Mater. Chem.* **1999**, *9*, 2013-2020.
[150] a) G. S. He, R. Signorini, P. N. Prasad, *Appl. Opt.* **1998**, *37*, 5720-5726; b) A. Abbotto, L. Beverina, R. Bozio, S. Bradamante, C. Ferrante, G. A. Pagani, R. Signorini, *Adv. Mater.* **2000**, *12*, 1963-1967.
[151] a) W. G. Fisher, W. P. Partridge, C. Dees, E. A. Wachter, *Photochem. Photobiol.* **1997**, *66*, 141-155; b) Y. Shen, A. J. Shuhendler, D. Ye, J.-J. Xu, H.-Y. Chen, *Chem. Soc. Rev.* **2016**, *45*, 6725-6741.
[152] a) W. Denk, J. Strickler, W. Webb, *Science* **1990**, *248*, 73-76; b) P. Ning, W. Wang, M. Chen, Y. Feng, X. Meng, *Chin. Chem. Lett.* **2017**, *28*, 1943-1951; c) Q. Zhang, X. Tian, H. Zhou, J. Wu, Y. Tian, *Materials* **2017**, *10*, 223.

[153] a) S. Yao, K. D. Belfield, *Eur. J. Org. Chem.* **2012**, *2012*, 3199-3217; b) D. Kim, H. G. Ryu, K. H. Ahn, *Org. Biomol. Chem.* **2014**, *12*, 4550-4566.
[154] a) J. A. Mindell, *Annu. Rev. Physiol.* **2012**, *74*, 69-86; b) C. Settembre, A. Fraldi, D. L. Medina, A. Ballabio, *Nat. Rev. Mol. Cell Biol.* **2013**, *14*, 283-296.
[155] F. M. Platt, B. Boland, A. C. van der Spoel, *J. Cell Biol.* **2012**, *199*, 723-734.
[156] a) H. M. Kim, M. J. An, J. H. Hong, B. H. Jeong, O. Kwon, J.-Y. Hyon, S.-C. Hong, K. J. Lee, B. R. Cho, *Angew. Chem. Int. Ed.* **2008**, *47*, 2231-2234; b) J. H. Han, S. K. Park, C. S. Lim, M. K. Park, H. J. Kim, H. M. Kim, B. R. Cho, *Chem. Eur. J.* **2012**, *18*, 15246-15249; c) H. J. Kim, C. H. Heo, H. M. Kim, *J. Am. Chem. Soc.* **2013**, *135*, 17969-17977; d) L. Yuan, L. Wang, B. K. Agrawalla, S.-J. Park, H. Zhu, B. Sivaraman, J. Peng, Q.-H. Xu, Y.-T. Chang, *J. Am. Chem. Soc.* **2015**, *137*, 5930-5938.
[157] a) H. Yu, Y. Xiao, L. Jin, *J. Am. Chem. Soc.* **2012**, *134*, 17486-17489; b) H.-J. Lee, C.-W. Cho, H. Seo, S. Singha, Y. W. Jun, K.-H. Lee, Y. Jung, K.-T. Kim, S. Park, S. C. Bae, K. H. Ahn, *Chem. Commun.* **2016**, *52*, 124-127; c) B. Zhu, P. Li, W. Shu, X. Wang, C. Liu, Y. Wang, Z. Wang, Y. Wang, B. Tang, *Anal. Chem.* **2016**, *88*, 12532-12538; d) J. Fan, Z. Han, Y. Kang, X. Peng, *Sci. Rep.* **2016**, *6*, 19562; e) L. Zhou, Y. Liu, S. Hu, H. Wang, H. Sun, X. Zhang, *Tetrahedron* **2016**, *72*, 4637-4642; f) H. Chen, Y. Tang, H. Shang, X. Kong, R. Guo, W. Lin, *J. Mater. Chem. B* **2017**, *5*, 2436-2444; g) W. Feng, Z. Mao, L. Liu, Z. Liu, *Talanta* **2017**, *167*, 134-142; h) W. Luo, H. Jiang, X. Tang, W. Liu, *J. Mater. Chem. B* **2017**, *5*, 4768-4773; i) J. Huang, N. Li, Q. Wang, Y. Gu, P. Wang, *Sens. Actuator. B Chem.* **2017**, *246*, 833-839.
[158] J. Jiang, X. Tian, C. Xu, S. Wang, Y. Feng, M. Chen, H. Yu, M. Zhu, X. Meng, *Chem. Commun.* **2017**, *53*, 3645-3648.
[159] J. H. Son, C. S. Lim, J. H. Han, I. A. Danish, H. M. Kim, B. R. Cho, *J. Org. Chem.* **2011**, *76*, 8113-8116.
[160] M. Tian, Y. Sun, L. Guo, R. Zhang, G. Zhang, R. Feng, X. Li, H. Zhang, L. He, X. Yu, X. He, *Sens. Actuator. B Chem.* **2017**, *243*, 955-962.
[161] X. Wang, D. M. Nguyen, C. O. Yanez, L. Rodriguez, H.-Y. Ahn, M. V. Bondar, K. D. Belfield, *J. Am. Chem. Soc.* **2010**, *132*, 12237-12239.
[162] a) S. Yao, H.-Y. Ahn, X. Wang, J. Fu, E. W. Van Stryland, D. J. Hagan, K. D. Belfield, *J. Org. Chem.* **2010**, *75*, 3965-3974; b) C. D. Andrade, C. O. Yanez, M. A. Qaddoura, X. Wang, C. L. Arnett, S. A. Coombs, J. Yu, R. Bassiouni, M. V. Bondar, K. D. Belfield, *J. Fluoresc.* **2011**, *21*, 1223-1230.
[163] C. S. Lim, S. T. Hong, S. S. Ryu, D. E. Kang, B. R. Cho, *Chem. Asian J.* **2015**, *10*, 2240-2249.
[164] A. L. Capodilupo, V. Vergaro, E. Fabiano, M. De Giorgi, F. Baldassarre, A. Cardone, A. Maggiore, V. Maiorano, D. Sanvitto, G. Gigli, G. Ciccarella, *J. Mater. Chem. B* **2015**, *3*, 3315-3323.
[165] S. Chen, M. Zhao, J. Su, Q. Zhang, X. Tian, S. Li, H. Zhou, J. Wu, Y. Tian, *Dyes Pigm.* **2017**, *136*, 807-816.
[166] C.-W. Chiu, Y. Kim, F. P. Gabbaï, *J. Am. Chem. Soc.* **2009**, *131*, 60-61.
[167] B. Chen, G. Feng, B. He, C. Goh, S. Xu, G. Ramos-Ortiz, L. Aparicio-Ixta, J. Zhou, L. Ng, Z. Zhao, B. Liu, B. Z. Tang, *Small* **2016**, *12*, 782-792.
[168] a) M. Grzybowski, D. T. Gryko, *Adv. Opt. Mater.* **2015**, *3*, 280-320; b) M. Kaur, D. H. Choi, *Chem. Soc. Rev.* **2015**, *44*, 58-77.
[169] a) A. Nowak-Król, M. Grzybowski, J. Romiszewski, M. Drobizhev, G. Wicks, M. Chotkowski, A. Rebane, E. Górecka, D. T. Gryko, *Chem. Commun.* **2013**, *49*, 8368-8370; b) J. Schmitt, V. Heitz, A. Sour, F. Bolze, H. Ftouni, J.-F. Nicoud, L. Flamigni, B. Ventura, *Angew. Chem. Int. Ed.* **2015**, *54*, 169-173.
[170] R. Englman, J. Jortner, *Mol. Phys.* **1970**, *18*, 145-164.
[171] S. J. Strickler, R. A. Berg, *J. Chem. Phys.* **1962**, *37*, 814-822.
[172] a) E. Sakuda, Y. Ando, A. Ito, N. Kitamura, *J. Phys. Chem A* **2010**, *114*, 9144-9150; b) A. Ito, K. Kawanishi, E. Sakuda, N. Kitamura, *Chem. Eur. J.* **2014**, *20*, 3940-3953.
[173] S. Amthor, C. Lambert, S. Dümmler, I. Fischer, J. Schelter, *J. Phys. Chem A* **2006**, *110*, 5204-5214.

[174] a) H.-J. Jo, C.-B. Kim, T.-Y. Ryoo, B.-K. Ahn, K.-Y. Park, *Bull. Korean Chem. Soc.* **2010**, *31*, 3749-3754; b) N. Agarwal, P. K. Nayak, F. Ali, M. P. Patankar, K. L. Narasimhan, N. Periasamy, *Synth. Met.* **2011**, *161*, 466-473; c) B. Kobin, S. Behren, B. Braun-Cula, S. Hecht, *J. Phys. Chem. A* **2016**, *120*, 5474-5480.

[175] J. Cortes, H. Heitele, J. Jortner, *J. Phys. Chem.* **1994**, *98*, 2527-2536.

[176] M. Li, J. Fan, H. Li, J. Du, S. Long, X. Peng, *Biomaterials* **2018**, *164*, 98-105.

[177] a) D. Scherer, R. Dörfler, A. Feldner, T. Vogtmann, M. Schwoerer, U. Lawrentz, W. Grahn, C. Lambert, *Chem. Phys.* **2002**, *279*, 179-207; b) B. Strehmel, S. Amthor, J. Schelter, C. Lambert, *ChemPhysChem* **2005**, *6*, 893-896.

[178] D. X. Cao, Z. Q. Liu, Q. Fang, G. B. Xu, G. Xue, G. Q. Liu, W. T. Yu, *J. Organomet. Chem.* **2004**, *689*, 2201-2206.

[179] a) C. Branger, M. Lequan, R. M. Lequan, M. Large, F. Kajzar, *Chem. Phys. Lett.* **1997**, *272*, 265-270; b) Z. Yuan, J. C. Collings, N. J. Taylor, T. B. Marder, C. Jardin, J.-F. Halet, *J. Solid State Chem.* **2000**, *154*, 5-12.

[180] S.-J. Chung, K.-S. Kim, T.-C. Lin, G. S. He, J. Swiatkiewicz, P. N. Prasad, *J. Phys. Chem. B* **1999**, *103*, 10741-10745.

[181] C. Le Droumaguet, A. Sourdon, E. Genin, O. Mongin, M. Blanchard-Desce, *Chem. Asian J.* **2013**, *8*, 2984-3001.

[182] F. Terenziani, C. Le Droumaguet, C. Katan, O. Mongin, M. Blanchard-Desce, *Chem. Phys. Chem.* **2007**, *8*, 723-734.

[183] V. Alain-Rizzo, D. Drouin-Kucma, C. Rouxel, I. Samb, J. Bell, P. Y. Toullec, V. Michelet, I. Leray, M. Blanchard-Desce, *Chem. Asian J.* **2011**, *6*, 1080-1091.

[184] B. R. Cho, K. H. Son, S. H. Lee, Y.-S. Song, Y.-K. Lee, S.-J. Jeon, J. H. Choi, H. Lee, M. Cho, *J. Am. Chem. Soc.* **2001**, *123*, 10039-10045.

[185] a) A. Abbotto, L. Beverina, R. Bozio, A. Facchetti, C. Ferrante, G. A. Pagani, D. Pedron, R. Signorini, *Chem. Commun.* **2003**, 2144-2145; b) A. Abbotto, L. Beverina, S. Bradamante, A. Facchetti, G. A. Pagani, R. Bozio, C. Ferrante, D. Pedron, R. Signorini, *Synth. Met.* **2003**, *139*, 795-797.

[186] a) H. Wang, Q. Zhang, J. Zhang, L. Li, Q. Zhang, S. Li, S. Zhang, J. Wu, Y. Tian, *Dyes Pigm.* **2014**, *102*, 263-272; b) M. Fanshun, L. Bo, Q. Shixiong, C. Kongchang, T. He, *Chem. Lett.* **2004**, *33*, 470-471; c) C. Yue-Zhi, F. Qi, X. Gang, X. Gui-Bao, Y. Lei, Y. Wen-Tao, *Chem. Lett.* **2005**, *34*, 644-645.

[187] a) M. Drobizhev, A. Karotki, Y. Dzenis, A. Rebane, Z. Suo, C. W. Spangler, *J. Phys. Chem. B* **2003**, *107*, 7540-7543; b) J. Yoo, S. K. Yang, M.-Y. Jeong, H. C. Ahn, S.-J. Jeon, B. R. Cho, *Org. Lett.* **2003**, *5*, 645-648; c) C. Katan, F. Terenziani, O. Mongin, M. H. V. Werts, L. Porrès, T. Pons, J. Mertz, S. Tretiak, M. Blanchard-Desce, *J. Phys. Chem. A* **2005**, *109*, 3024-3037; d) C. Katan, F. Terenziani, C. L. Droumaguet, O. Mongin, M. H. V. Werts, S. Tretiak, M. Blanchard-Desce, *Proc. SPIE-Int. Soc. Opt. Eng.* **2005**, *5935*; e) C. Sissa, V. Parthasarathy, D. Drouin-Kucma, M. H. V. Werts, M. Blanchard-Desce, F. Terenziani, *Phys. Chem. Chem. Phys.* **2010**, *12*, 11715-11727.

[188] a) F. Terenziani, C. Sissa, A. Painelli, *J. Phys. Chem. B* **2008**, *112*, 5079-5087; b) N. S. Makarov, S. Mukhopadhyay, K. Yesudas, J.-L. Brédas, J. W. Perry, A. Pron, M. Kivala, K. Müllen, *J. Phys. Chem. A* **2012**, *116*, 3781-3793.

[189] J. Xue, Y. Zhao, J. Wu, F. Wu, X. Fang, *New J. Chem.* **2009**, *33*, 634-640.

[190] C. Le Droumaguet, O. Mongin, M. H. V. Werts, M. Blanchard-Desce, *Chem. Commun.* **2005**, 2802-2804.

[191] C. Allain, F. Schmidt, R. Lartia, G. Bordeau, C. Fiorini-Debuisschert, F. Charra, P. Tauc, M.-P. Teulade-Fichou, *Chem. Bio. Chem.* **2007**, *8*, 424-433.

[192] B. Dumat, G. Bordeau, E. Faurel-Paul, F. Mahuteau-Betzer, N. Saettel, G. Metge, C. Fiorini-Debuisschert, F. Charra, M.-P. Teulade-Fichou, *J. Am. Chem. Soc.* **2013**, *135*, 12697-12706.

[193] V. Parthasarathy, S. Fery-Forgues, E. Campioli, G. Recher, F. Terenziani, M. Blanchard-Desce, *Small* **2011**, *7*, 3219-3229.

[194] X. Gan, Y. Wang, X. Ge, W. Li, X. Zhang, W. Zhu, H. Zhou, J. Wu, Y. Tian, *Dyes Pigm.* **2015**, *120*, 65-73.
[195] E. Sakuda, Y. Ando, A. Ito, N. Kitamura, *J. Phys. Chem. A* **2010**, *114*, 9144-9150.
[196] a) E. Krause, *Ber. Dt. Chem. Ges.* **1924**, *57*, 216-217; b) E. Krause, H. Polack, *Ber. Dt. Chem. Ges.* **1926**, *59*, 777-785.
[197] E. Krause, P. Nobbe, *Ber. Dt. Chem. Ges.* **1930**, *63*, 934-942.
[198] G. Wittig, W. Herwig, *Chem. Ber.* **1955**, *88*, 962-976.
[199] a) W.-L. Jia, D.-R. Bai, T. McCormick, Q.-D. Liu, M. Motala, R.-Y. Wang, C. Seward, Y. Tao, S. Wang, *Chem. Eur. J.* **2004**, *10*, 994-1006; b) H. Li, A. Sundararaman, K. Venkatasubbaiah, F. Jäkle, *J. Am. Chem. Soc.* **2007**, *129*, 5792-5793; c) Y. Kim, H. Zhao, F. P. Gabbaï, *Angew. Chem. Int. Ed.* **2009**, *48*, 4957-4960; d) M. Varlan, B. A. Blight, S. Wang, *Chem. Commun.* **2012**, *48*, 12059-12061.
[200] H. C. Brown, S. Sujishi, *J. Am. Chem. Soc.* **1948**, *70*, 2793-2802.
[201] a) T. J. Weismann, J. C. Schug, *J. Chem. Phys.* **1964**, *40*, 956-966; b) D. Gust, K. Mislow, *J. Am. Chem. Soc.* **1973**, *95*, 1535-1547; c) J. F. Blount, P. Finocchiaro, D. Gust, K. Mislow, *J. Am. Chem. Soc.* **1973**, *95*, 7019-7029; d) K. Mislow, *Acc. Chem. Res.* **1976**, *9*, 26-33.
[202] a) A. Sundararaman, R. Varughese, H. Li, L. N. Zakharov, A. L. Rheingold, F. Jäkle, *Organometallics* **2007**, *26*, 6126-6131; b) H. Braunschweig, A. Damme, J. O. C. Jimenez-Halla, C. Hörl, I. Krummenacher, T. Kupfer, L. Mailänder, K. Radacki, *J. Am. Chem. Soc.* **2012**, *134*, 20169-20177.
[203] B. Meng, Y. Ren, J. Liu, F. Jäkle, L. Wang, *Angew. Chem. Int. Ed.* **2018**, *57*, 2183-2187.
[204] a) M.-G. Ren, M. Mao, Q.-H. Song, *Chem. Commun.* **2012**, *48*, 2970-2972; b) M. Mao, M.-G. Ren, Q.-H. Song, *Chem. Eur. J.* **2012**, *18*, 15512-15522.
[205] F. Martinez, R. Voelkel, D. Naegele, H. Naarmann, *Mol. Cryst. Liq. Crys. Inc. Nonlinear Opt.* **1989**, *167*, 227-232.
[206] R. Uson, L. A. Oro, J. A. Cabeza, H. E. Bryndza, M. P. Stepro, in *Inorg. Synth., Vol. 32*, John Wiley & Sons, Inc., New York, **2007**, pp. 126-130.
[207] S. S. Zalesskiy, V. P. Ananikov, *Organometallics* **2012**, *31*, 2302-2309.
[208] Y. Shi, K. Hou, Y. Wang, K. Wang, H. Ren, M. Pang, F. Chen, S. Zhang, *J. Mater. Chem. A* **2016**, *4*, 5415-5422.
[209] K. Yang, T. He, X. Chen, S. Z. D. Cheng, Y. Zhu, *Macromolecules* **2014**, *47*, 8479-8486.
[210] P. Harrisson, J. Morris, T. B. Marder, P. G. Steel, *Org. Lett.* **2009**, *11*, 3586-3589.
[211] S. K. Sontag, G. R. Sheppard, N. M. Usselman, N. Marshall, J. Locklin, *Langmuir* **2011**, *27*, 12033-12041.
[212] S. Berger, S. Braun, in *200 and More NMR Experiments: A Practical Course, Vol. 1*, Wiley-VCH, Weinheim, **2004**, pp. 141-148.
[213] S.-F. Liu, Q. Wu, H. L. Schmider, H. Aziz, N.-X. Hu, Z. Popović, S. Wang, *J. Am. Chem. Soc.* **2000**, *122*, 3671-3678.
[214] G. Sheldrick, *Acta Crystallogr.* **2015**, *A71*, 3-8.
[215] G. Sheldrick, *Acta Crystallogr.* **2008**, *A64*, 112-122.
[216] C. B. Hübschle, G. M. Sheldrick, B. Dittrich, *J. Appl. Crystallogr.* **2011**, *44*, 1281-1284.
[217] DIAMOND, K. Brandenburg, Crystal Impact Gbr, Bonn, Germany, **2007**.
[218] N. S. Makarov, M. Drobizhev, A. Rebane, *Opt. Express* **2008**, *16*, 4029-4047.
[219] M. H. V. Werts, N. Nerambourg, D. Pelegry, Y. L. Grand, M. Blanchard-Desce, *Photochem. Photobiol. Sci.* **2005**, *4*, 531-538.
[220] S. de Reguardati, J. Pahapill, A. Mikhailov, Y. Stepanenko, A. Rebane, *Opt. Express* **2016**, *24*, 9053-9066.
[221] Gaussian 09, Revision D.01, M. J. Frisch, G. W. Trucks, H. B. Schlegel, G. E. Scuseria, M. A. Robb, J. R. Cheeseman, G. Scalmani, V. Barone, B. Mennucci, G. A. Petersson, H. Nakatsuji, M. Caricato, X. Li, H. P. Hratchian, A. F. Izmaylov, J. Bloino, G. Zheng, J. L. Sonnenberg, M. Hada, M. Ehara, K. Toyota, R. Fukuda, J. Hasegawa, M. Ishida, T. Nakajima, Y. Honda, O. Kitao, H. Nakai, T. Vreven, J. A. Montgomery, J. E. P. Jr., F. Ogliaro, M. Bearpark, J. J. Heyd, E. Brothers, K. N. Kudin, V. N. Staroverov, T. Keith, R. Kobayashi,

J. Normand, K. Raghavachari, A. Rendell, J. C. Burant, S. S. Iyengar, J. Tomasi, M. Cossi, N. Rega, J. M. Millam, M. Klene, J. E. Knox, J. B. Cross, V. Bakken, C. Adamo, J. Jaramillo, R. Gomperts, R. E. Stratmann, O. Yazyev, A. J. Austin, R. Cammi, C. Pomelli, J. W. Ochterski, R. L. Martin, K. Morokuma, V. G. Zakrzewski, G. A. Voth, P. Salvador, J. J. Dannenberg, S. Dapprich, A. D. Daniels, O. Farkas, J. B. Foresman, J. V. Ortiz, J. Cioslowski, D. J. Fox, Gaussian, Inc., Wallingford, CT, Gaussian, Inc., Wallingford, CT, **2009**.

[222] a) A. D. Becke, *J. Chem. Phys.* **1993**, *98*, 5648-5652; b) C. Lee, W. Yang, R. G. Parr, *Phys. Rev. B* **1988**, *37*, 785-789; c) P. J. Stephens, F. J. Devlin, C. F. Chabalowski, M. J. Frisch, *J. Phys. Chem.* **1994**, *98*, 11623-11627.

[223] a) G. A. Petersson, M. A. Al-Laham, *J. Chem. Phys.* **1991**, *94*, 6081-6090; b) G. A. Petersson, A. Bennett, T. G. Tensfeldt, M. A. Al-Laham, W. A. Shirley, J. Mantzaris, *J. Chem. Phys.* **1988**, *89*, 2193-2218.

[224] T. Yanai, D. P. Tew, N. C. Handy, *Chem. Phys. Lett.* **2004**, *393*, 51-57.

[225] a) S. Jungsuttiwong, R. Tarsang, T. Sudyoadsuk, V. Promarak, P. Khongpracha, S. Namuangruk, *Org. Electr.* **2013**, *14*, 711-722; b) J. Preat, *J. Phys. Chem. C* **2010**, *114*, 16716-16725; c) P. Wiggins, J. A. G. Williams, D. J. Tozer, *J. Chem. Phys.* **2009**, *131*, 091101; d) M. J. G. Peach, P. Benfield, T. Helgaker, D. J. Tozer, *J. Chem. Phys.* **2008**, *128*, 044118; e) M. J. G. Peach, A. J. Cohen, D. J. Tozer, *Phys. Chem. Chem. Phys.* **2006**, *8*, 4543-4549.

[226] a) T. Lu, F. Chen, *J. Comput. Chem.* **2012**, *33*, 580-592; b) R. L. Martin, *J. Chem. Phys.* **2003**, *118*, 4775-4777.

[227] N. M. O'Boyle, A. L. Tenderholt, K. M. Langner, *J. Comp. Chem.* **2008**, *29*, 839-845.

[228] J. Tomasi, B. Mennucci, R. Cammi, *Chem. Rev.* **2005**, *105*, 2999-3094.

Appendix

9 APPENDIX

NMR-SPECTRA

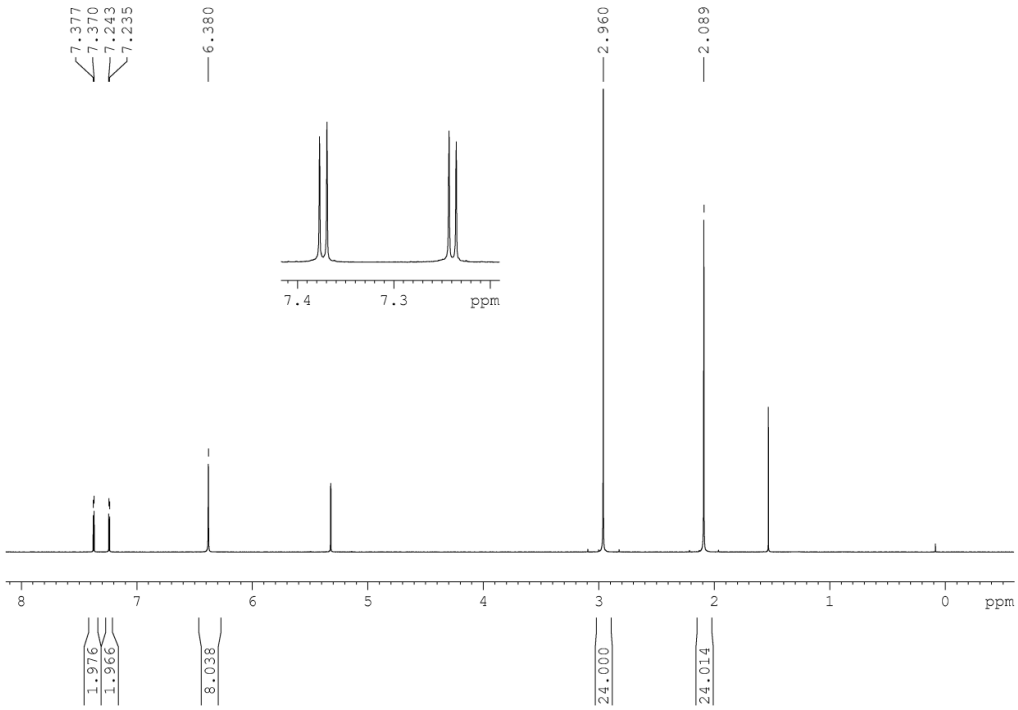

Figure A1. ^{1}H NMR spectrum of **2-1** in CD_2Cl_2 at 500 MHz.

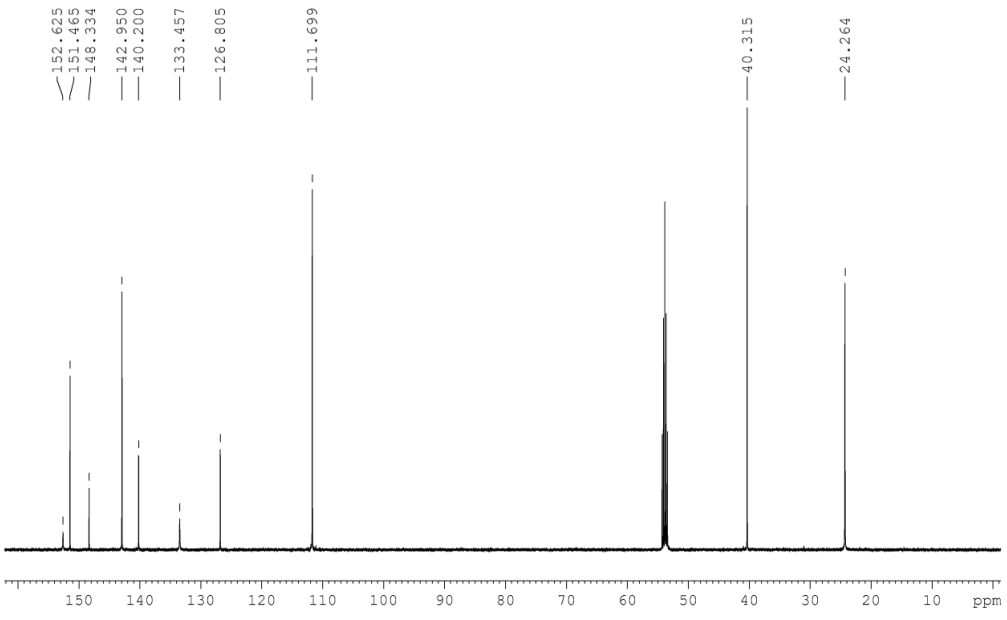

Figure A2. $^{13}C\{^{1}H\}$ NMR spectrum of **2-1** in CD_2Cl_2 at 125 MHz.

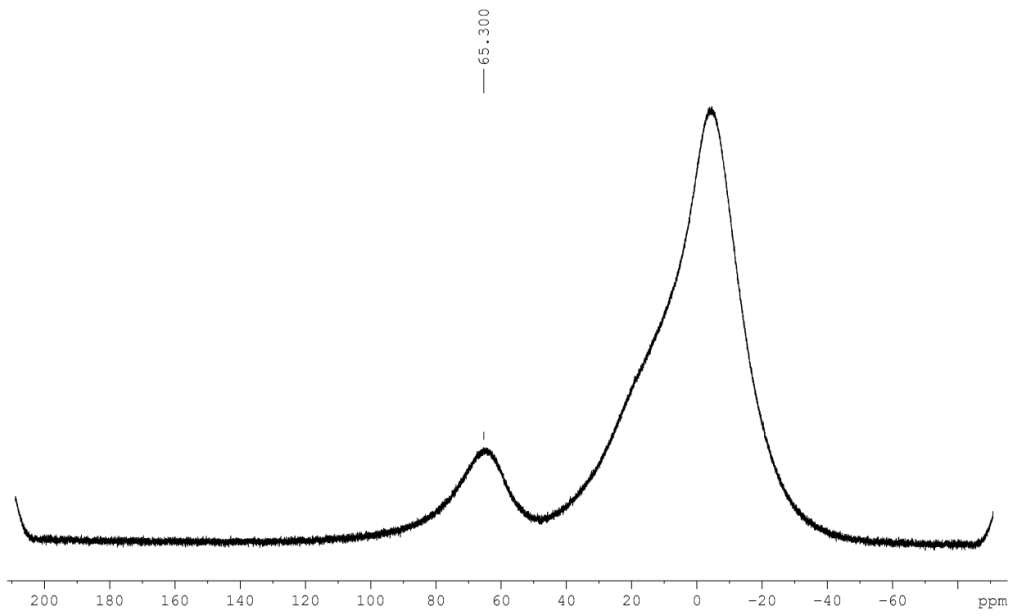

Figure A3. $^{11}B\{^{1}H\}$ NMR spectrum of **2-1** in CD_2Cl_2 at 160 MHz.

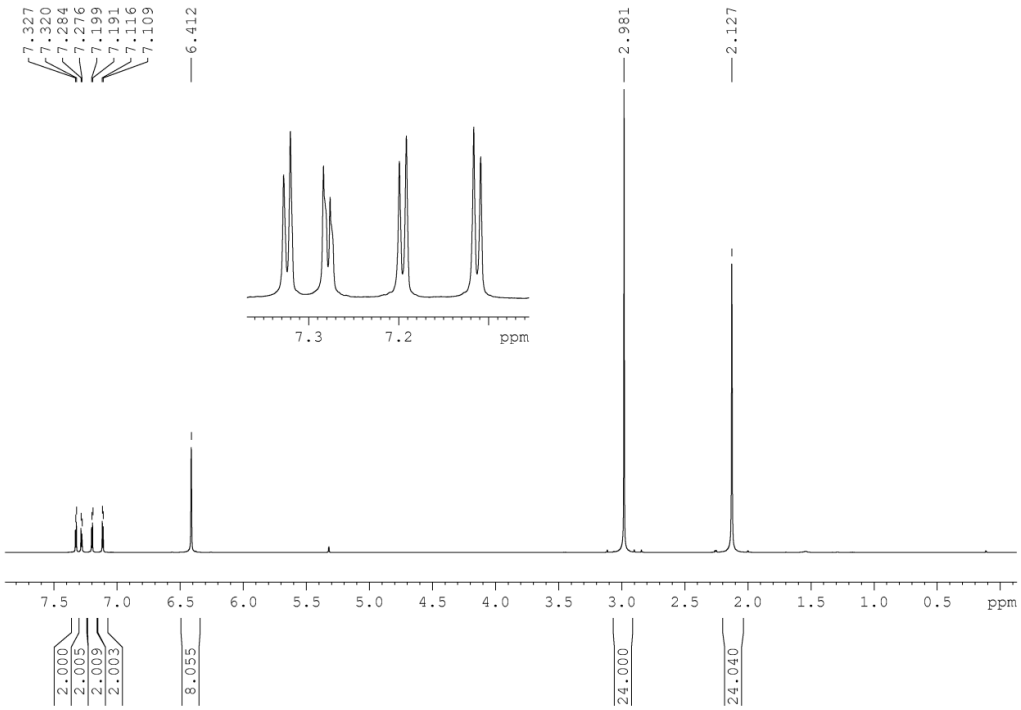

Figure A4. ^{1}H NMR spectrum of **2-2** in CD_2Cl_2 at 500 MHz.

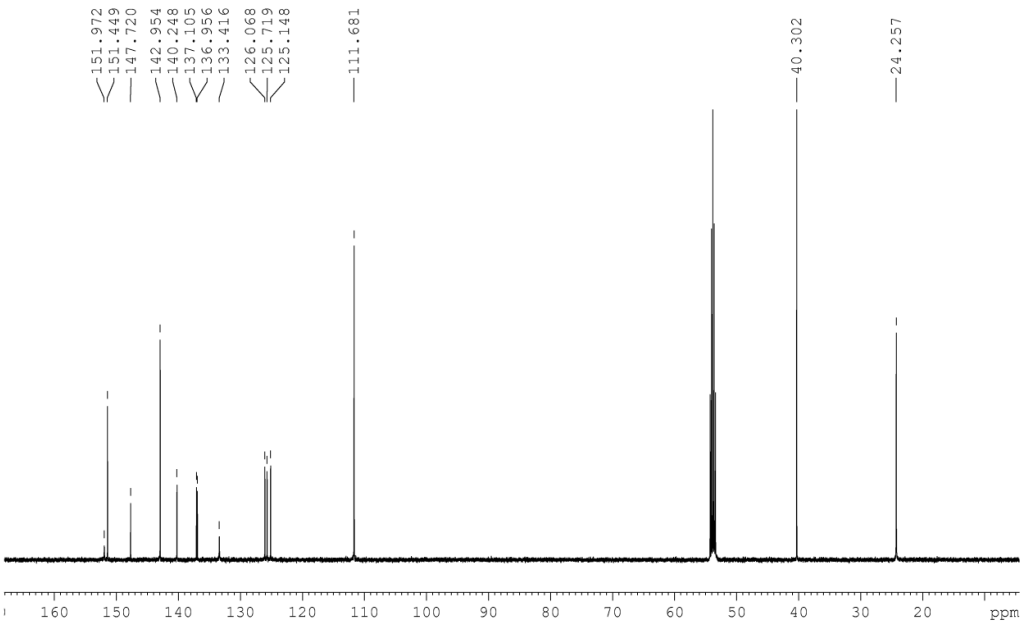

Figure A5. $^{13}C\{^{1}H\}$ NMR spectrum of **2-2** in CD_2Cl_2 at 125 MHz.

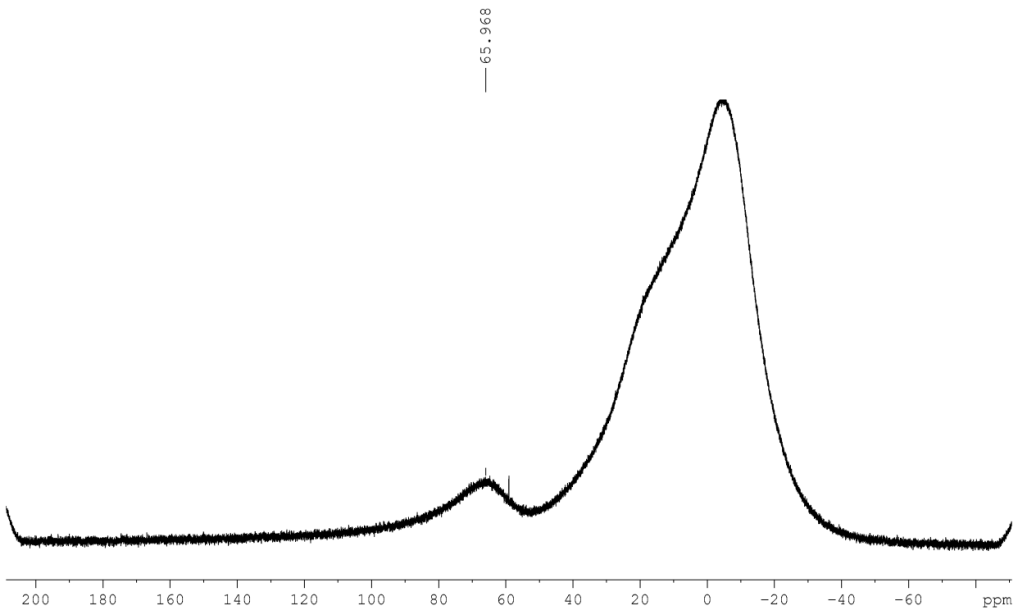

Figure A6. $^{11}B\{^{1}H\}$ NMR spectrum of **2-2** in CD_2Cl_2 at 160 MHz.

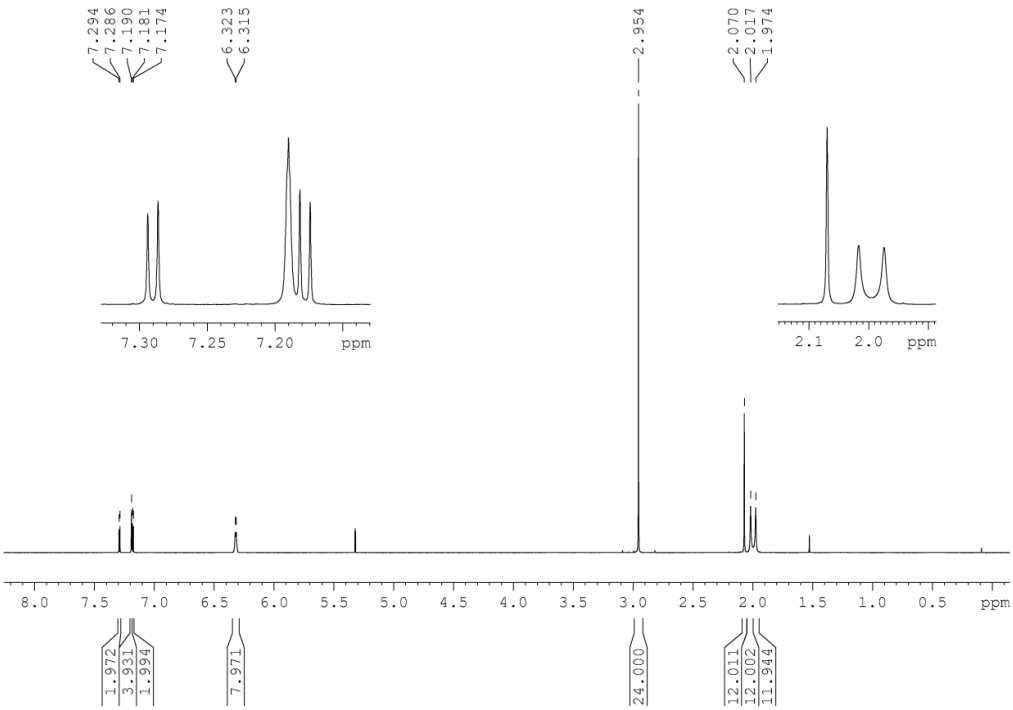

Figure A7. ^{1}H NMR spectrum of **2-3** in CD_2Cl_2 at 500 MHz.

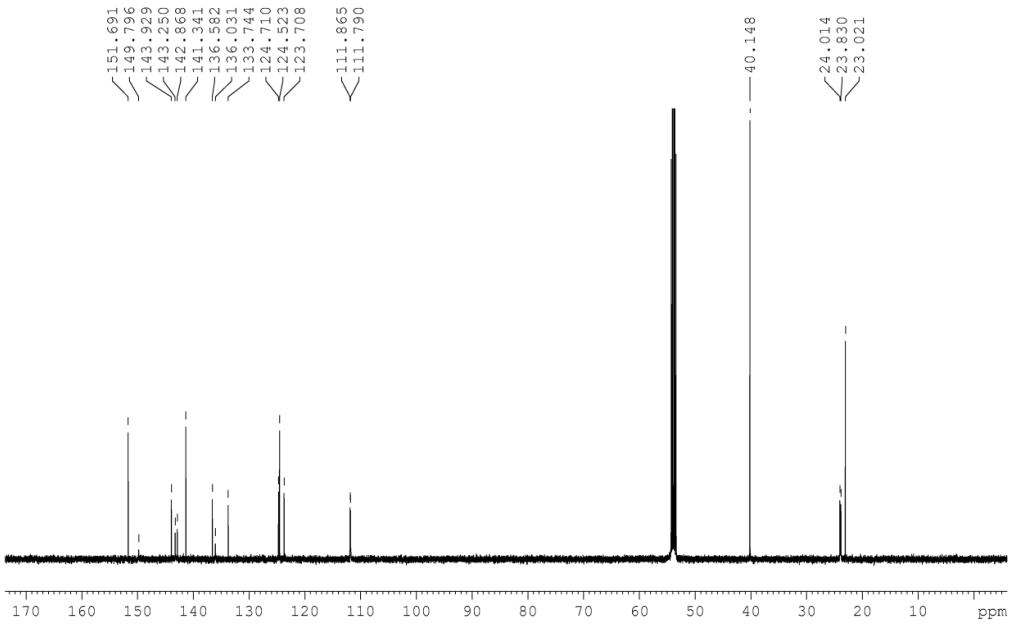

Figure A8. $^{13}C\{^{1}H\}$ NMR spectrum of **2-3** in CD_2Cl_2 at 125 MHz.

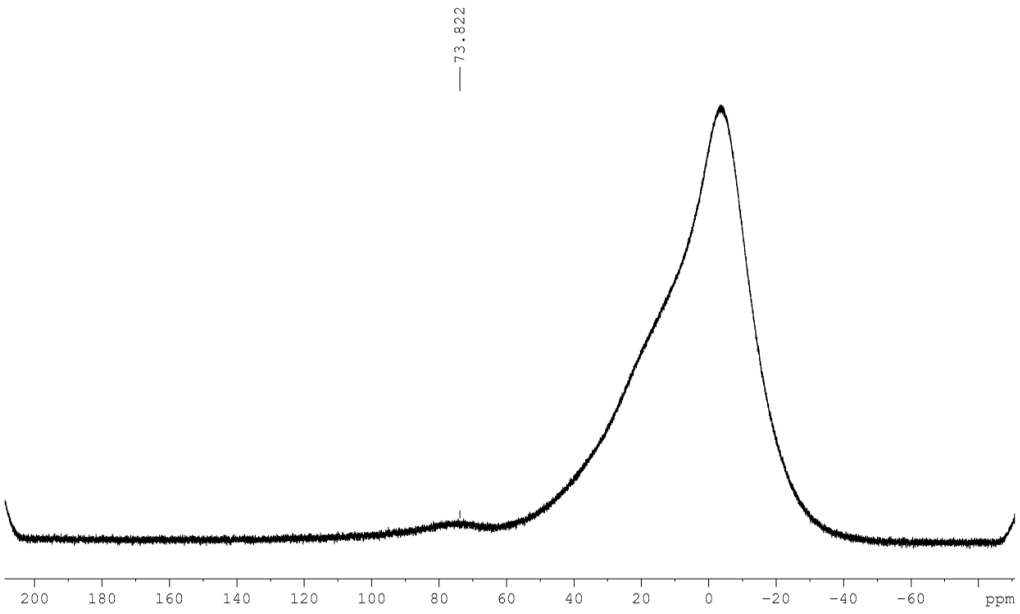

Figure A9. $^{11}B\{^{1}H\}$ NMR spectrum of **2-3** in CD_2Cl_2 at 160 MHz.

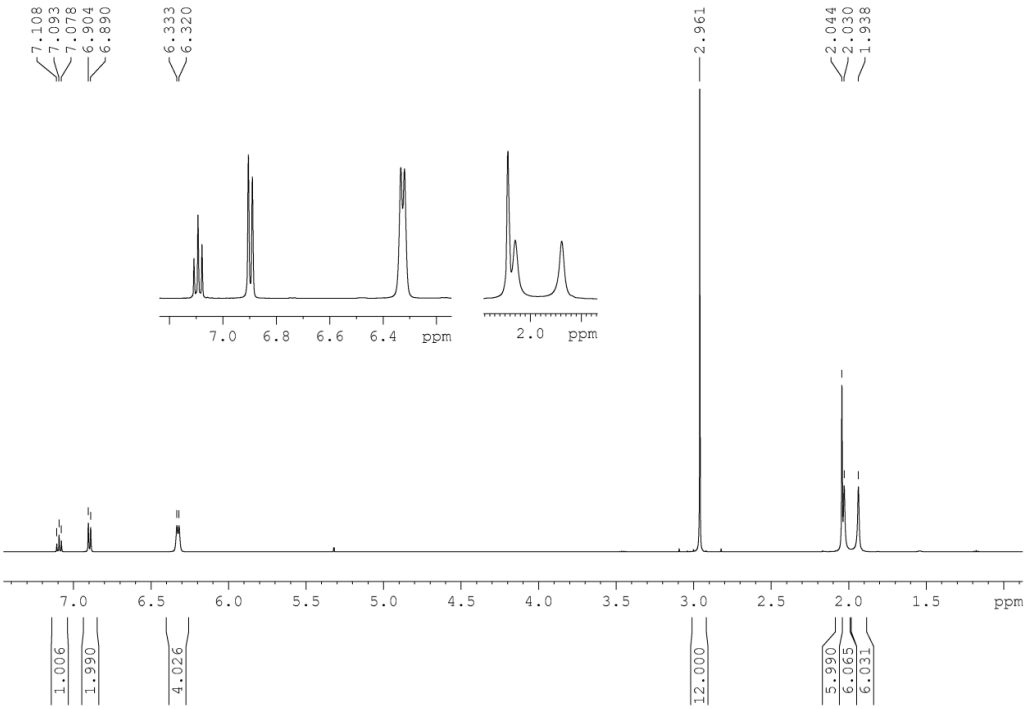

Figure A10. ^{1}H NMR spectrum of **2-5** in CD_2Cl_2 at 500 MHz.

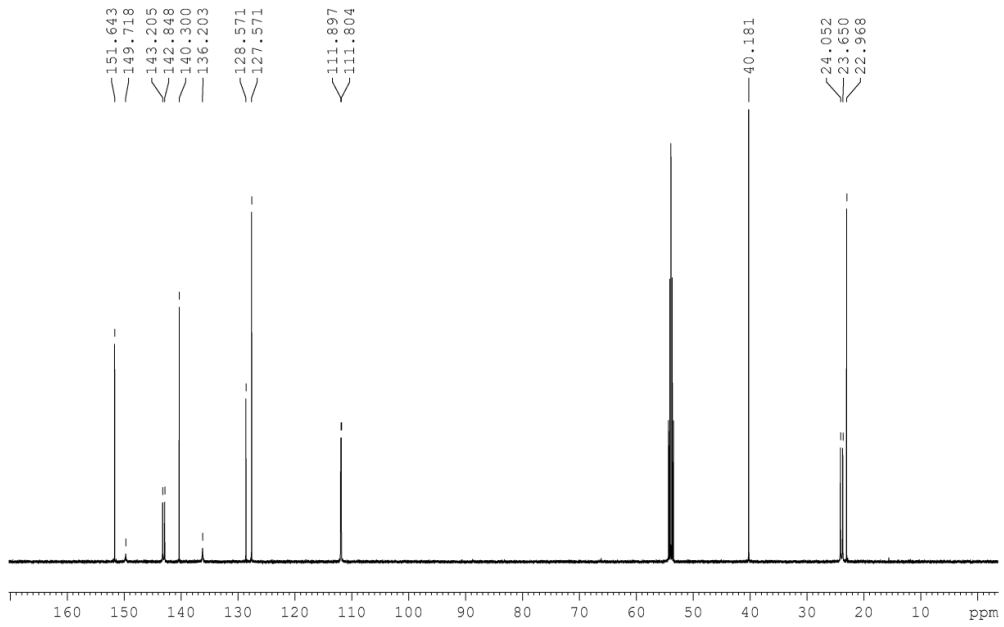

Figure A11. $^{13}C\{^{1}H\}$ NMR spectrum of **2-5** in CD_2Cl_2 at 125 MHz.

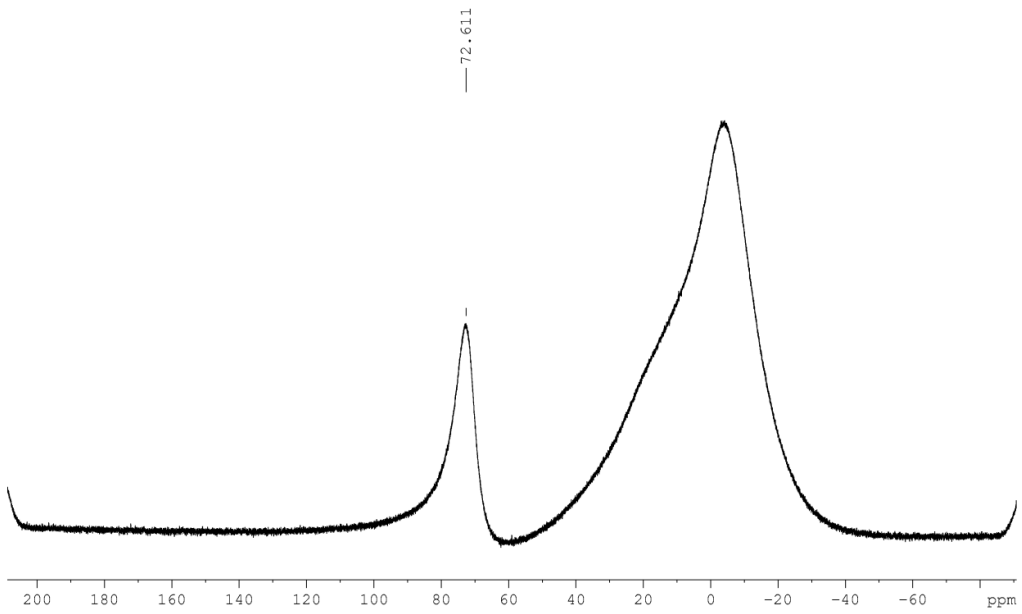

Figure A12. $^{11}B\{^{1}H\}$ NMR spectrum of **2-5** in CD_2Cl_2 at 160 MHz.

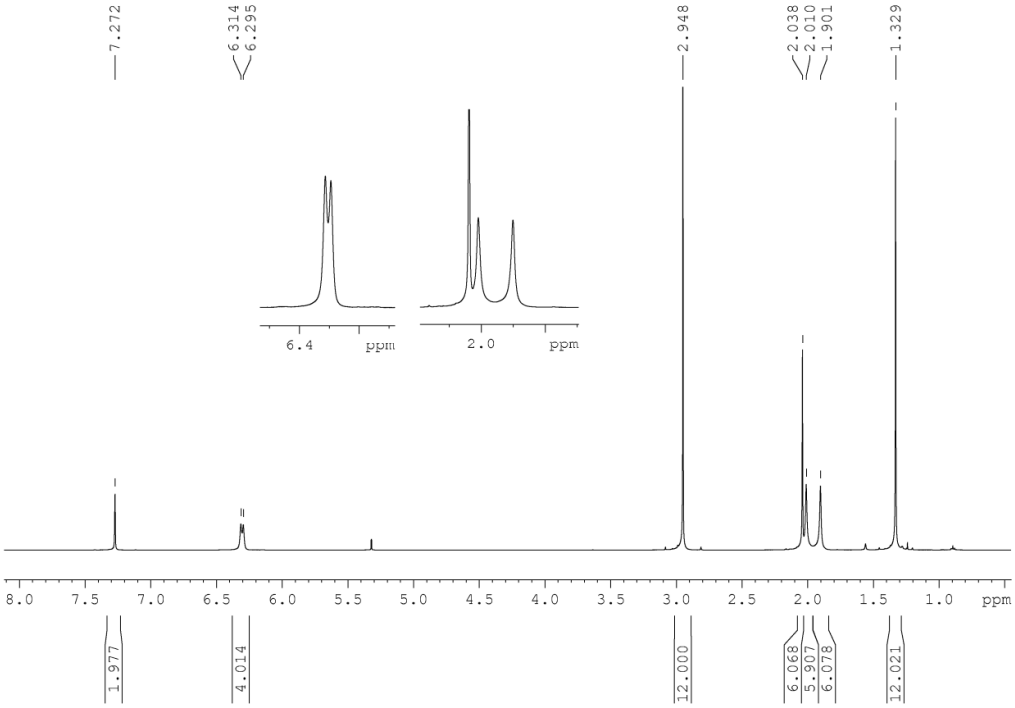

Figure A13. ^{1}H NMR spectrum of **2-6** in CD_2Cl_2 at 500 MHz.

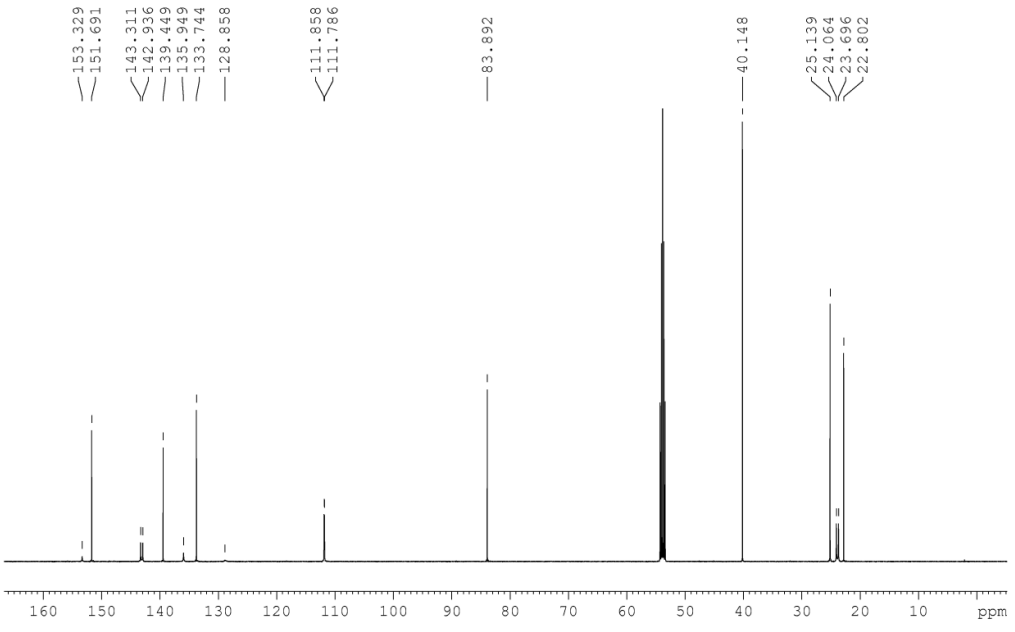

Figure A14. $^{13}C\{^{1}H\}$ NMR spectrum of **2-6** in CD_2Cl_2 at 125 MHz.

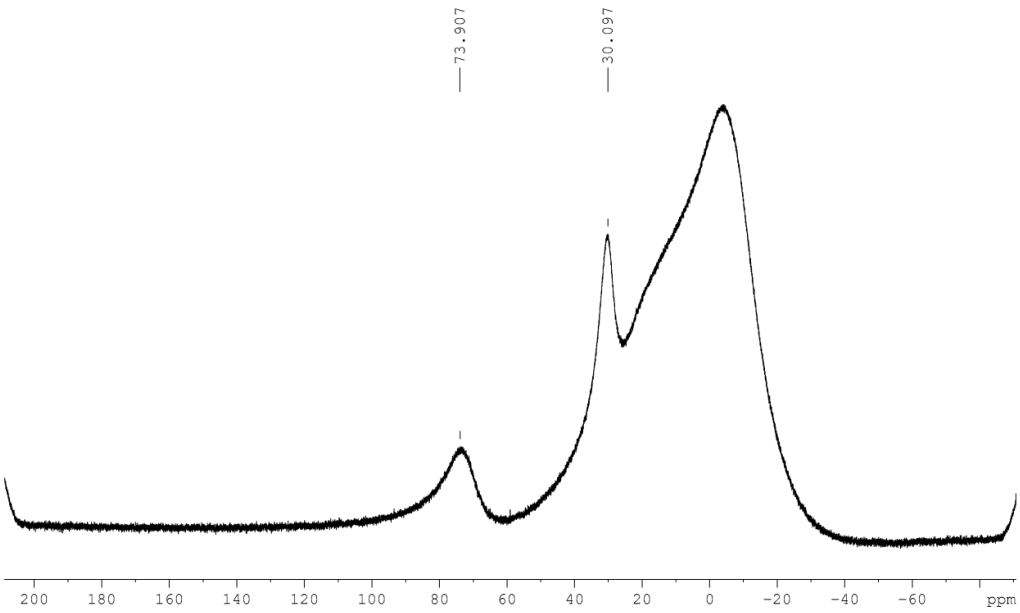

Figure A15. $^{11}B\{^{1}H\}$ NMR spectrum of **2-6** in CD_2Cl_2 at 160 MHz.

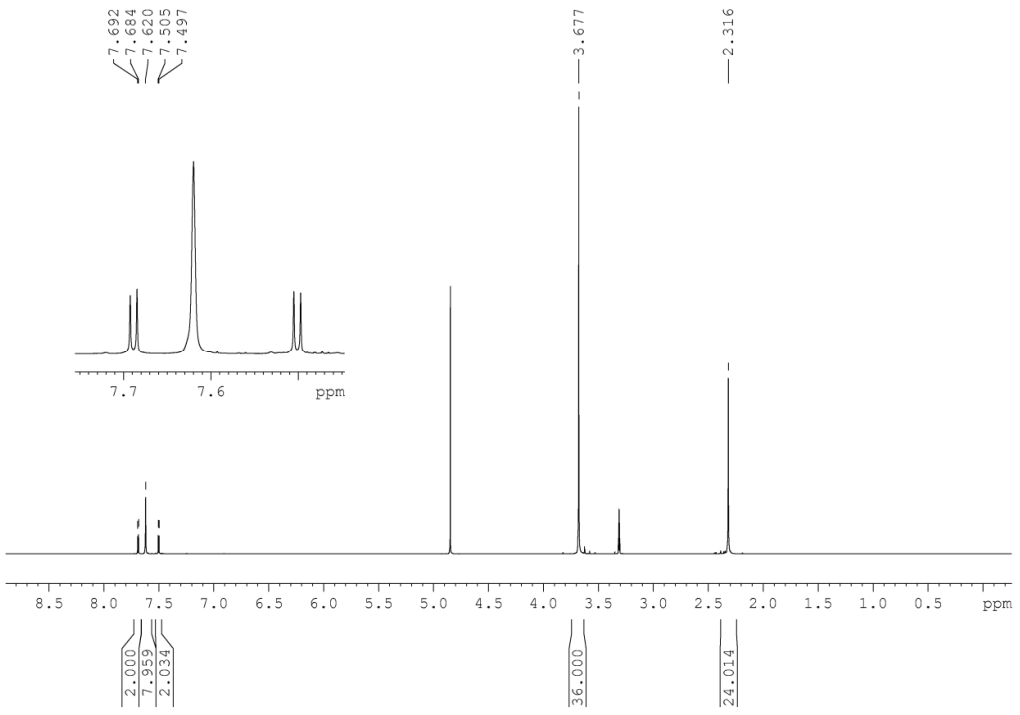

Figure A16. ^{1}H NMR spectrum of **2-1M** in CD_3OD at 500 MHz.

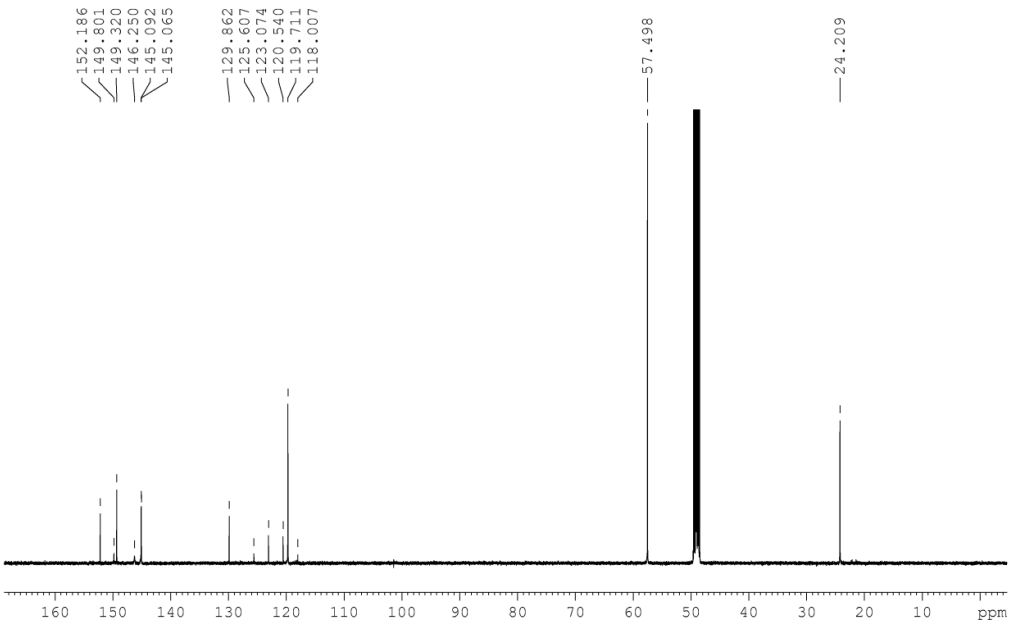

Figure A17. $^{13}C\{^{1}H\}$ NMR spectrum of **2-1M** in CD_3OD at 125 MHz.

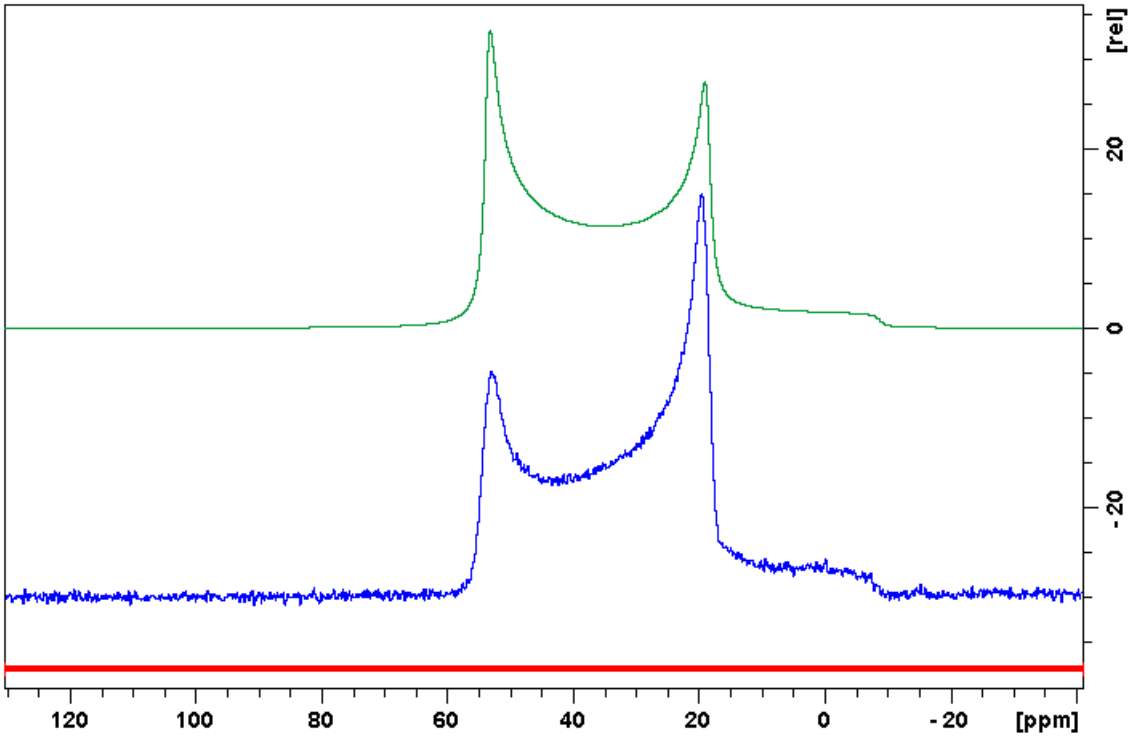

Figure A18. Solid-state $^{11}B\{^{1}H\}$ NMR spectrum of **2-1M** at 128 MHz (top: simulation). Isotropic chemical shift δ_{iso} = 64.2 ppm, quadrupolar coupling constant C_Q = 4.39 MHz, quadrupolar asymmetry parameter η_{Quad} = 0.0.

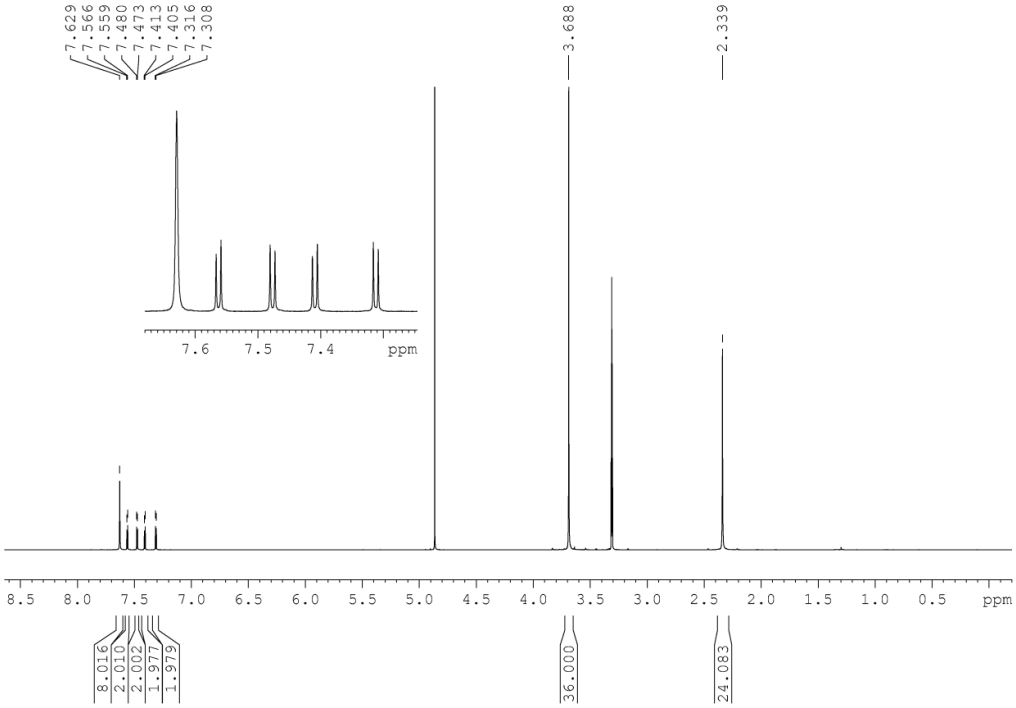

Figure A19. ^{1}H NMR spectrum of **2-2M** in CD_3OD at 500 MHz.

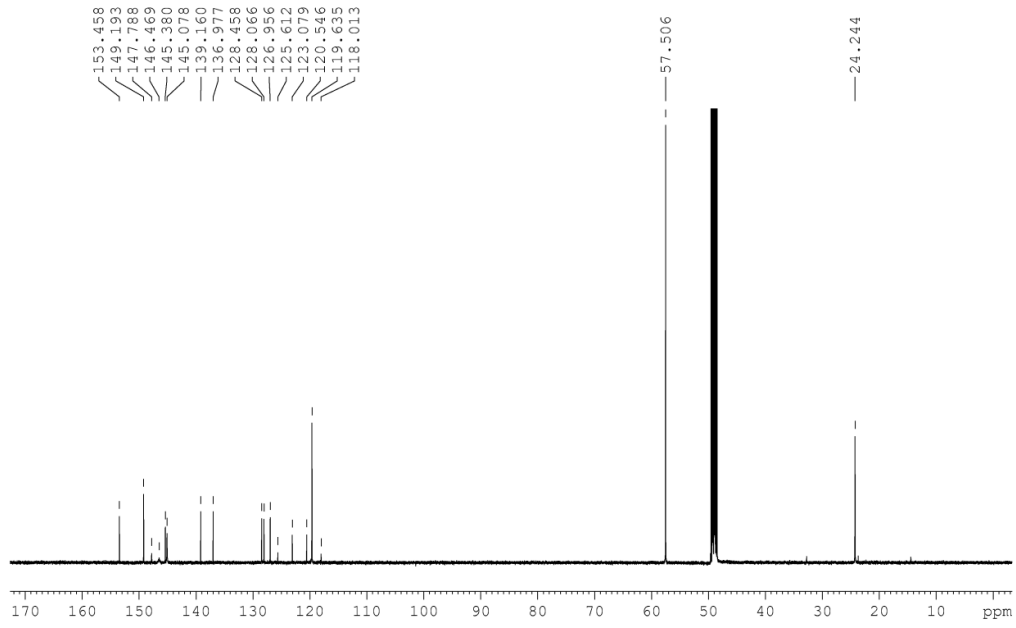

Figure A20. $^{13}C\{^{1}H\}$ NMR spectrum of **2-2M** in CD_3OD at 125 MHz.

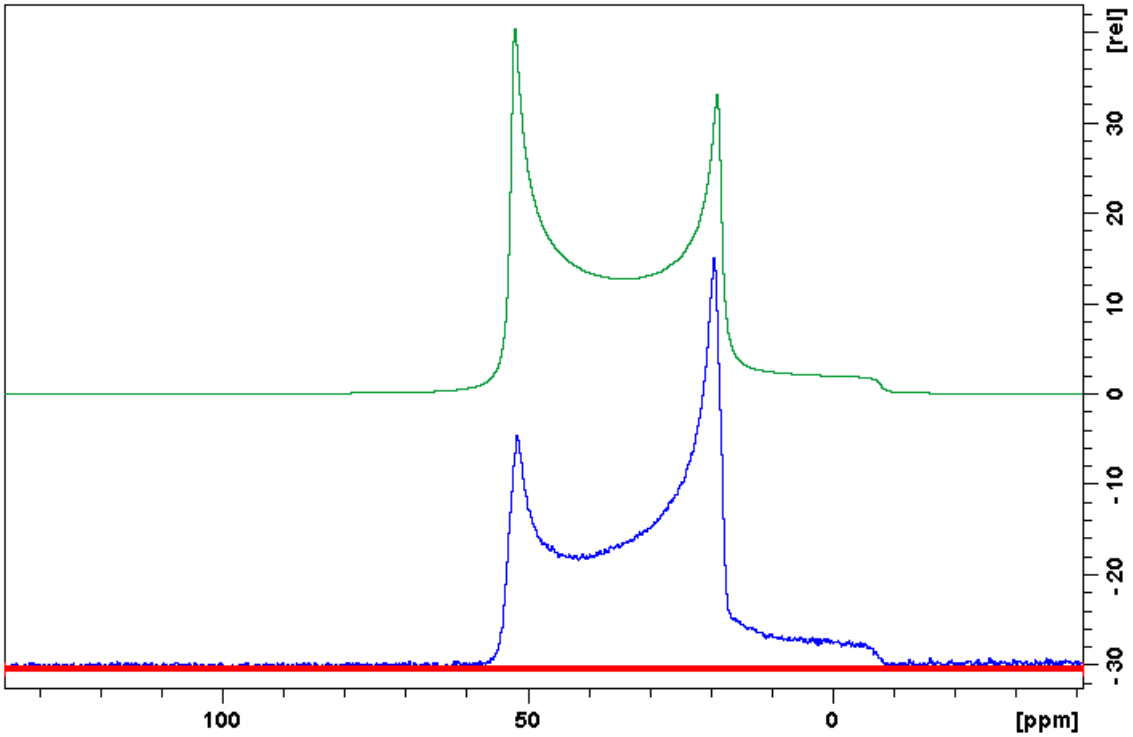

Figure A21. Solid-state $^{11}B\{^1H\}$ NMR spectrum of **2-2M** at 128 MHz (top: simulation). Isotropic chemical shift δ_{iso} = 62.6 ppm, quadrupolar coupling constant C_Q = 4.31 MHz, quadrupolar asymmetry parameter η_{Quad} = 0.0.

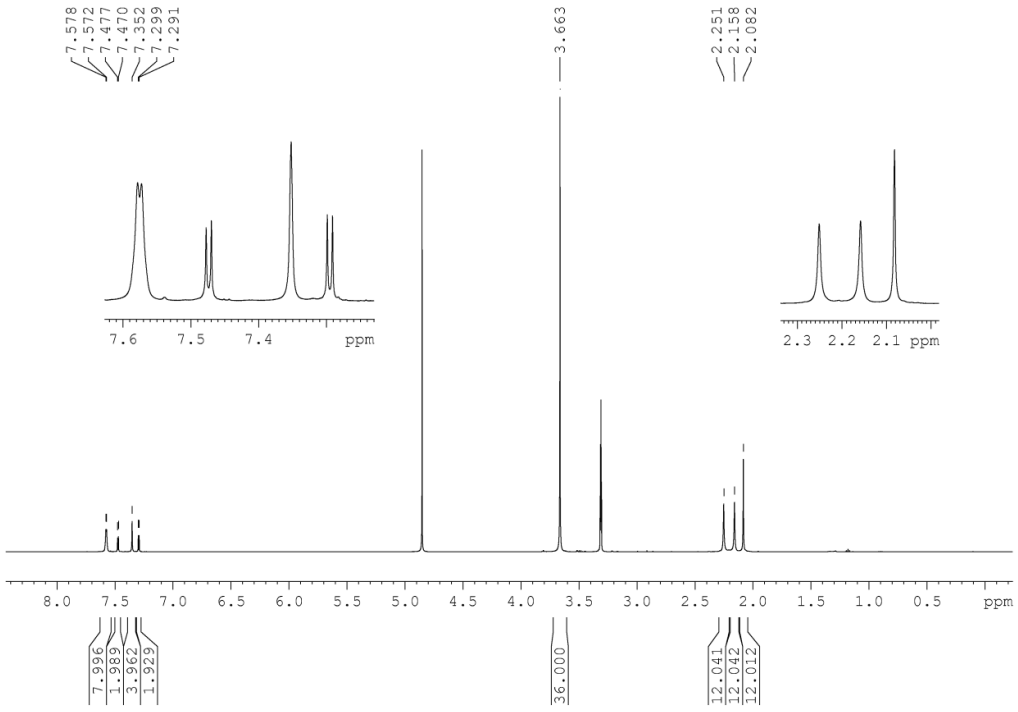

Figure A22. ^1H NMR spectrum of **2-3M** in CD_3OD at 500 MHz.

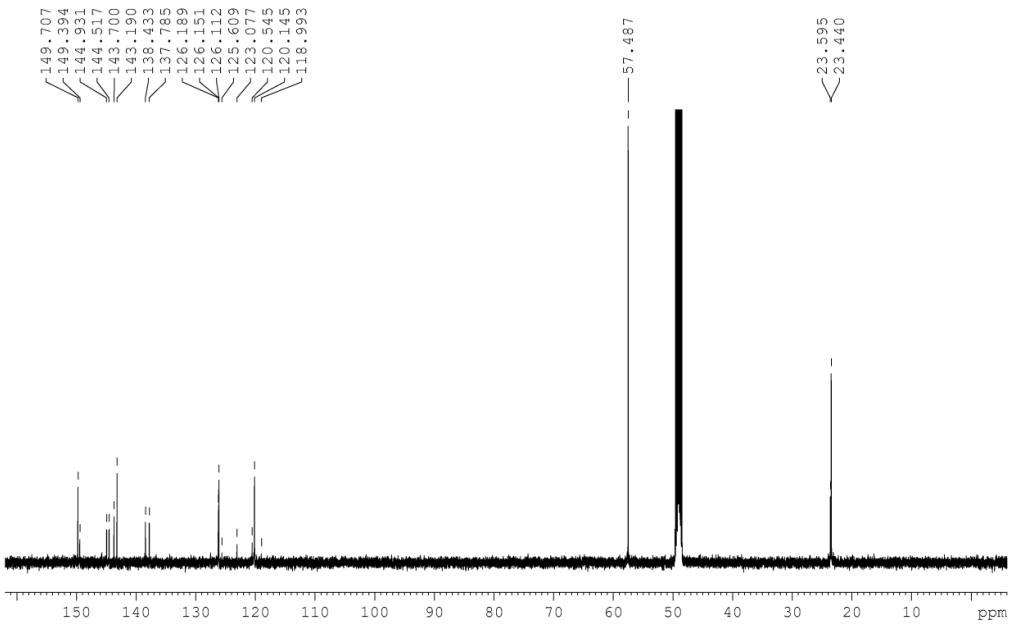

Figure A23. $^{13}C\{^{1}H\}$ NMR spectrum of **2-3M** in CD_3OD at 125 MHz.

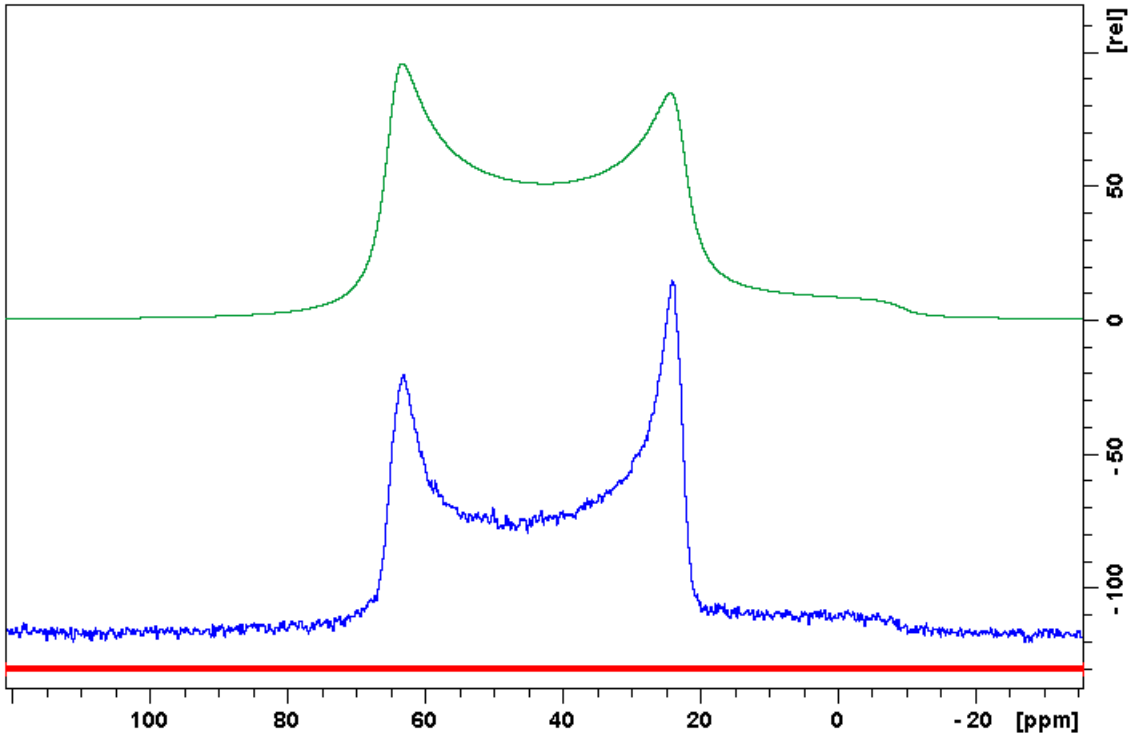

Figure A24. Solid-state $^{11}B\{^{1}H\}$ NMR spectrum of **2-3M** at 128 MHz (top: simulation). Isotropic chemical shift δ_{iso} = 77.0 ppm, quadrupolar coupling constant C_Q = 4.77 MHz, quadrupolar asymmetry parameter η_{Quad} = 0.0.

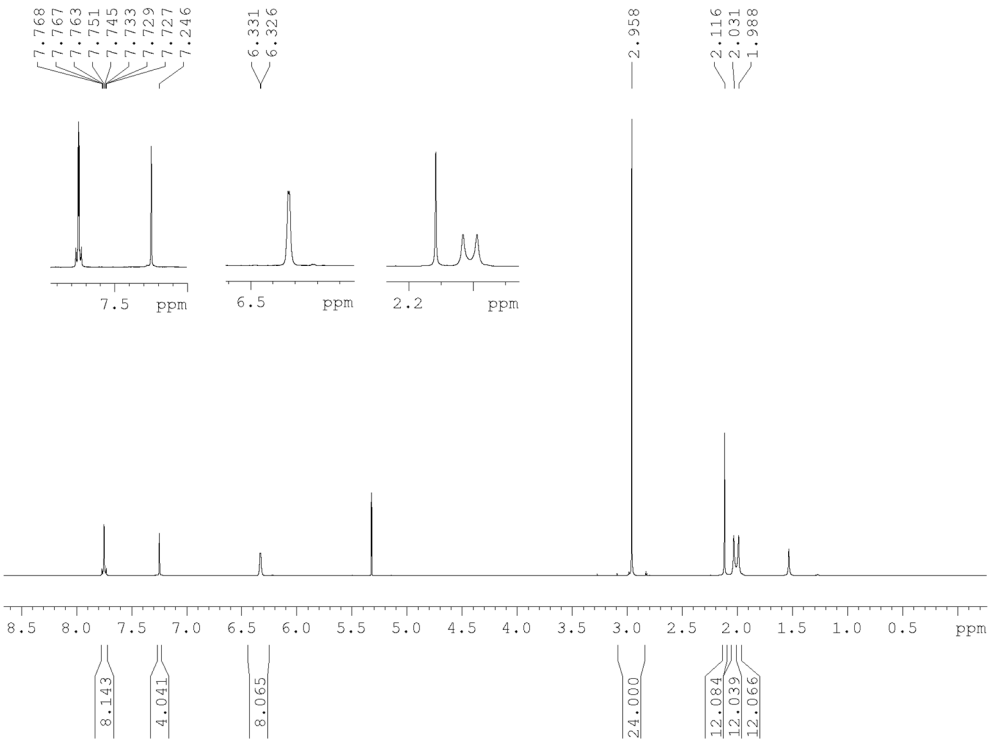

Figure A25. ^{1}H NMR spectrum of **3-1** in CD_2Cl_2 at 500 MHz.

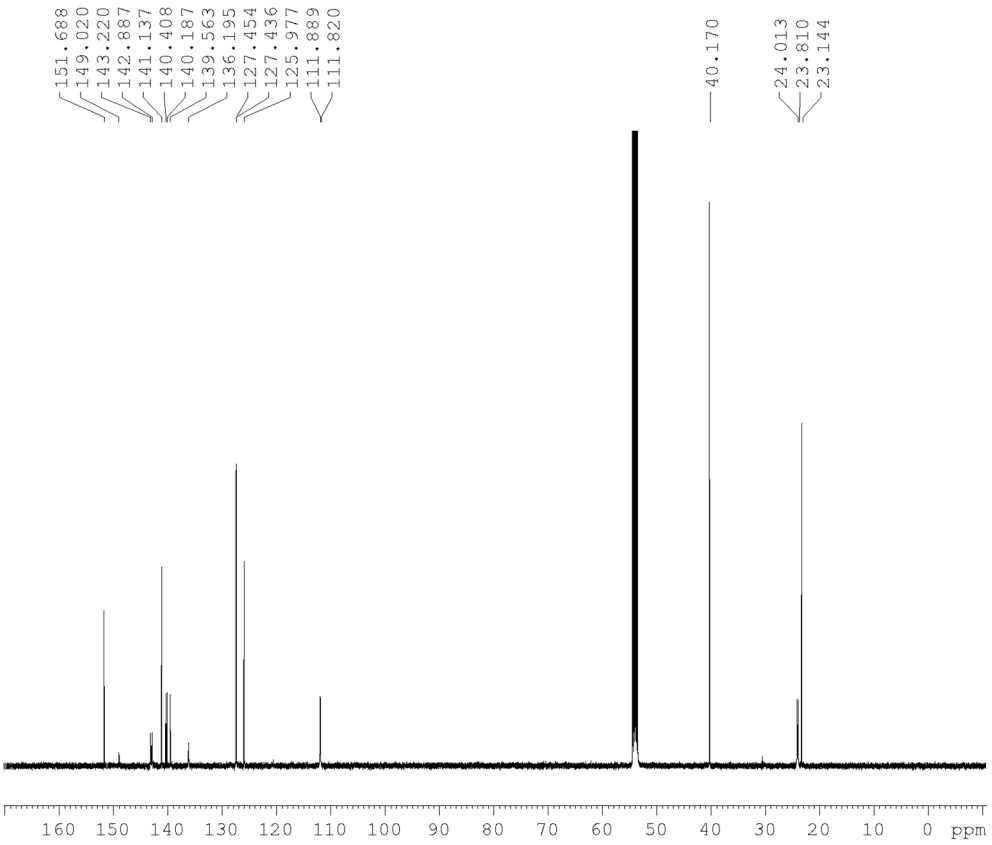

Figure A26. $^{13}C\{^{1}H\}$ NMR spectrum of **3-1** in CD_2Cl_2 at 125 MHz.

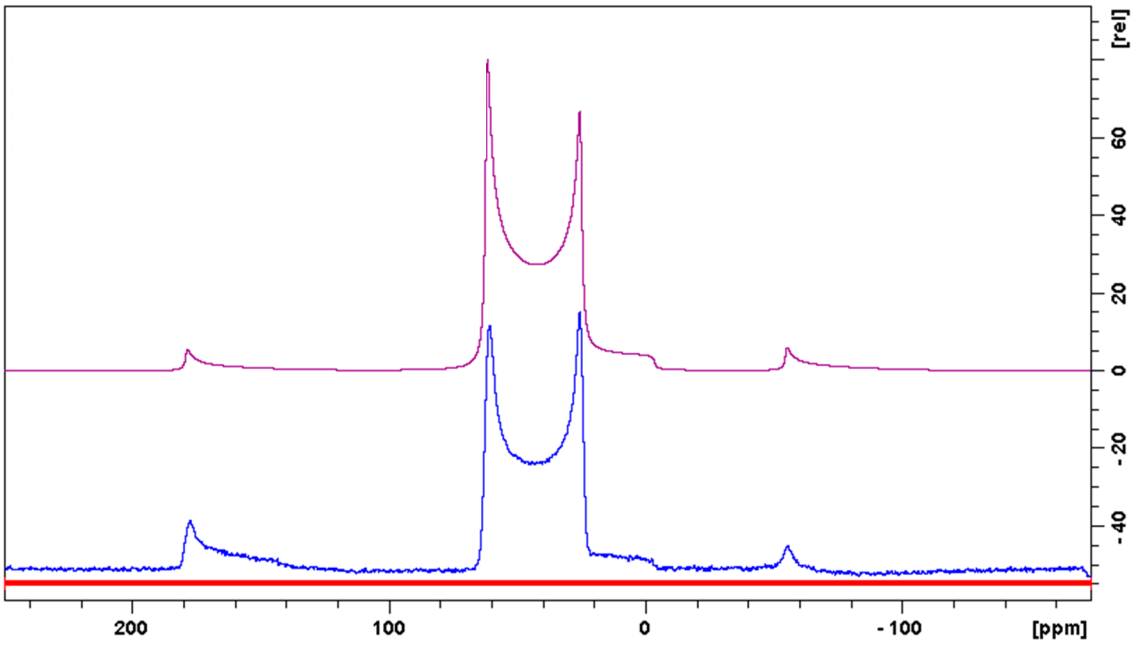

Figure A27. Solid-state $^{11}B\{^1H\}$ NMR spectrum of **3-1** at 128 MHz (top: simulation). Isotropic chemical shift δ_{iso} = 72.8 ppm, quadrupolar coupling constant C_Q = 4.49 MHz, quadrupolar asymmetry parameter η_{Quad} = 0.0.

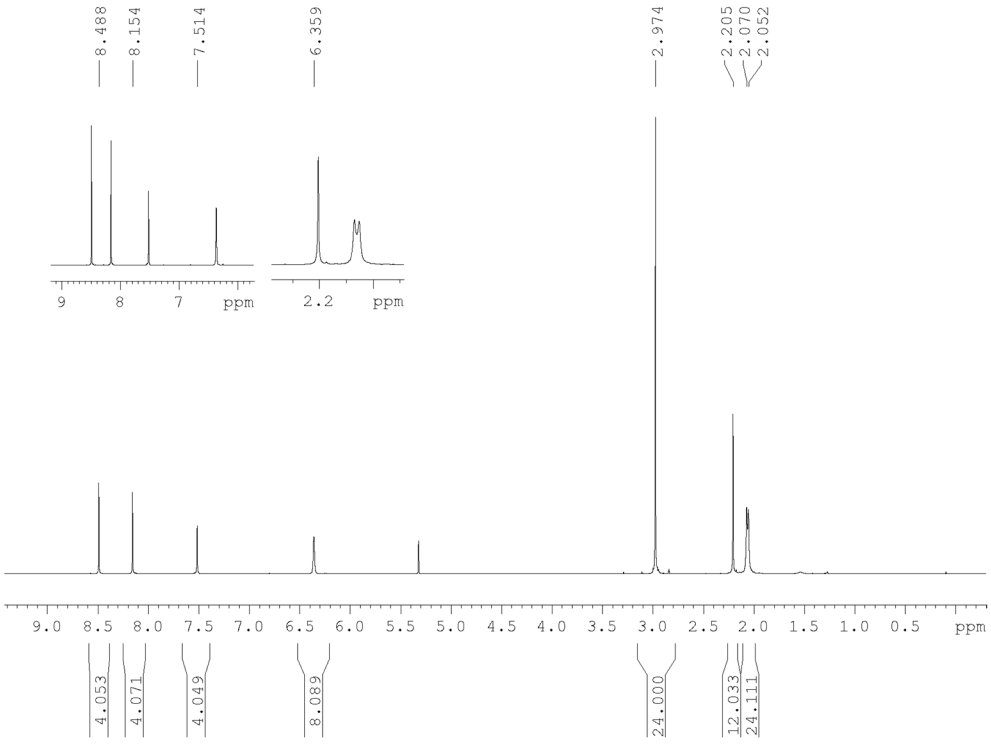

Figure A28. ^1H NMR spectrum of **3-2** in CD_2Cl_2 at 500 MHz.

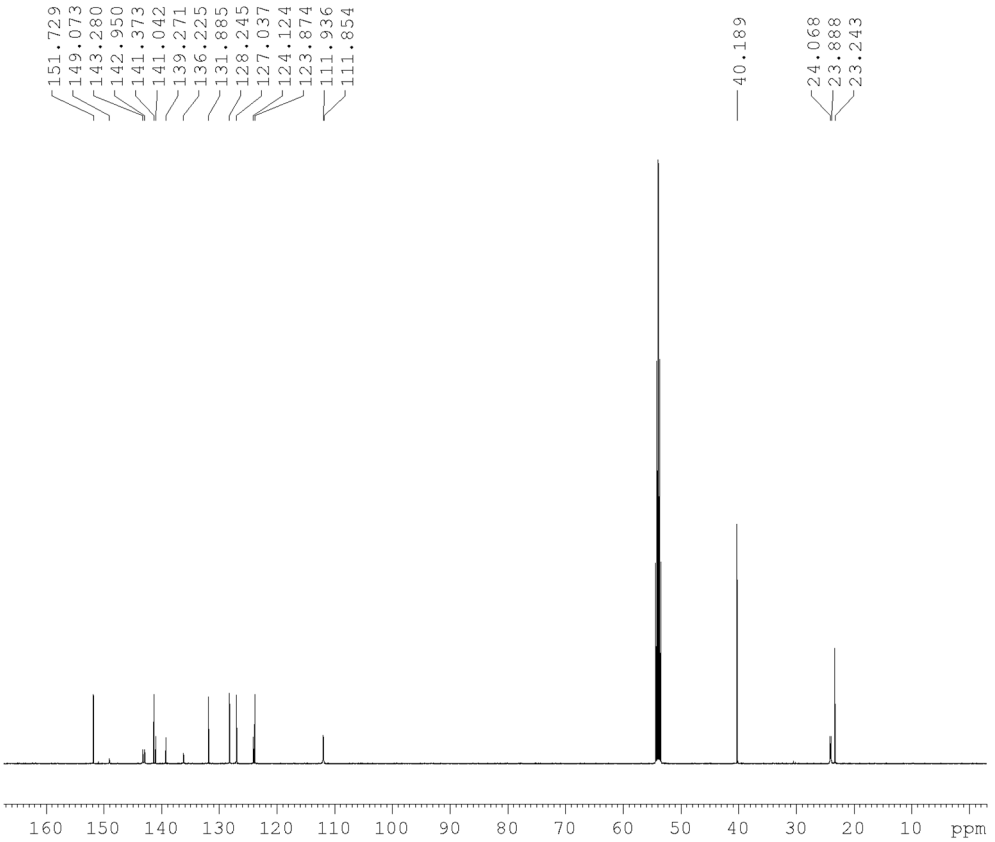

Figure A29. $^{13}C\{^{1}H\}$ NMR spectrum of **3-2** in CD_2Cl_2 at 125 MHz.

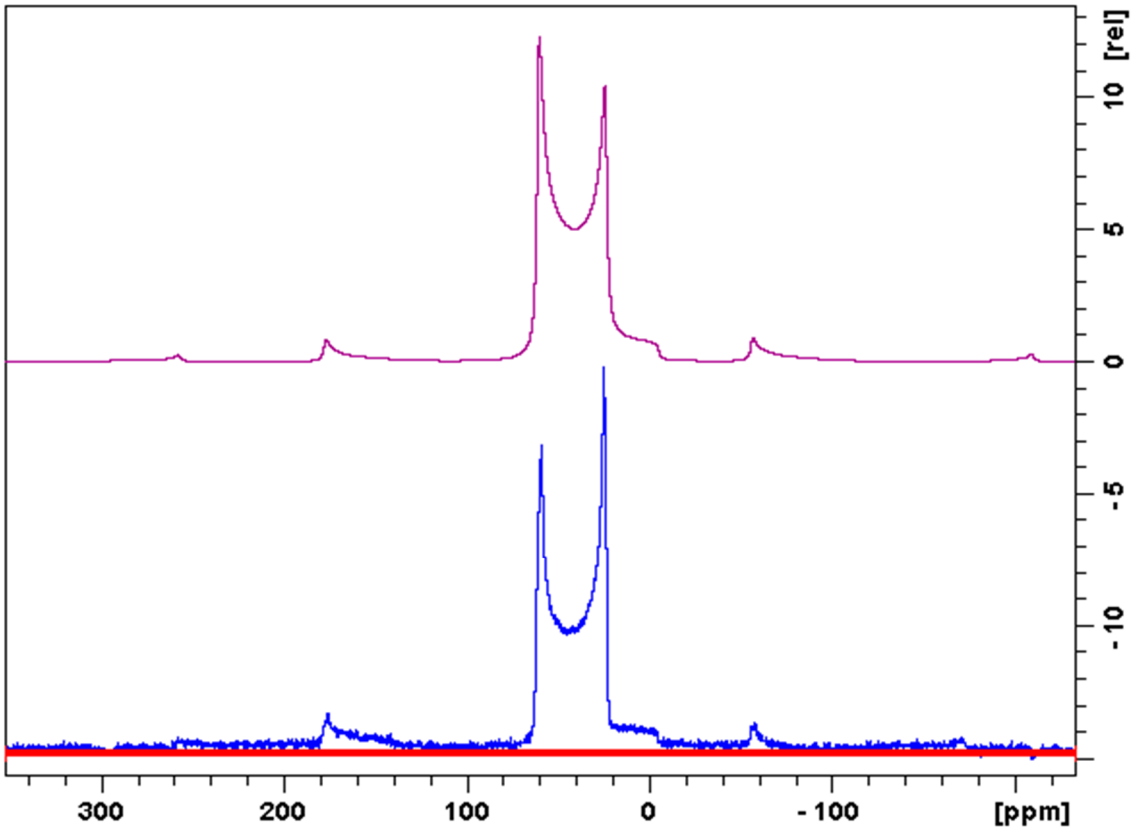

Figure A30. Solid-state $^{11}B\{^{1}H\}$ NMR spectrum of **3-2** at 128 MHz (top: simulation). Isotropic chemical shift δ_{iso} = 71.9 ppm, quadrupolar coupling constant C_Q = 4.51 MHz, quadrupolar asymmetry parameter η_{Quad} = 0.0.

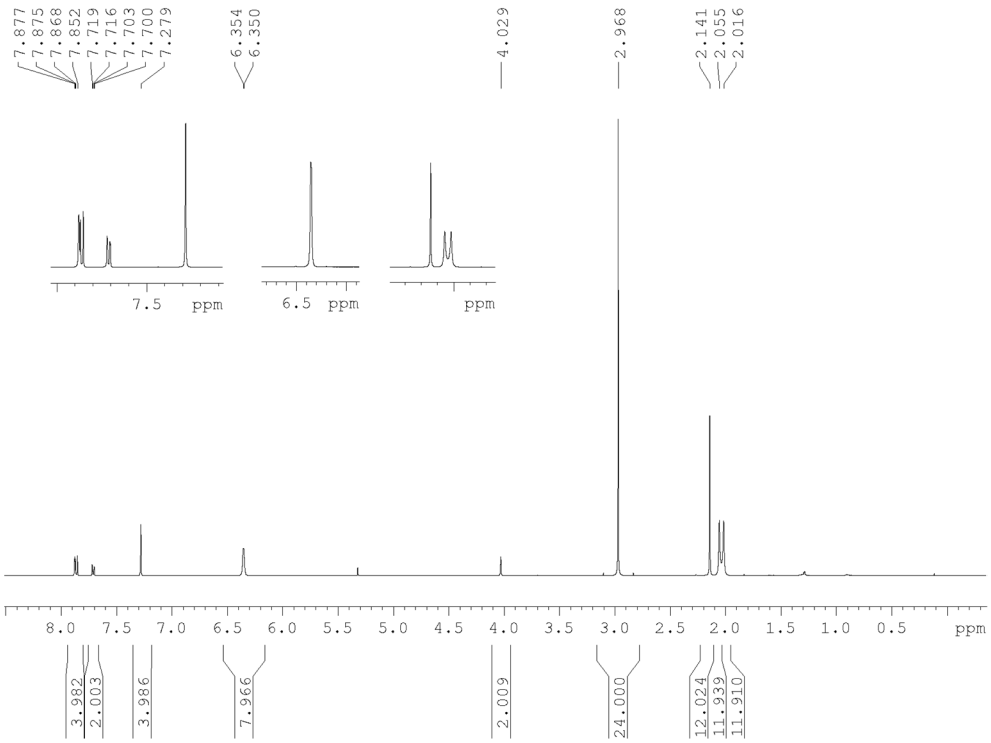

Figure A31. ^{1}H NMR spectrum of **3-3** in CD_2Cl_2 at 500 MHz.

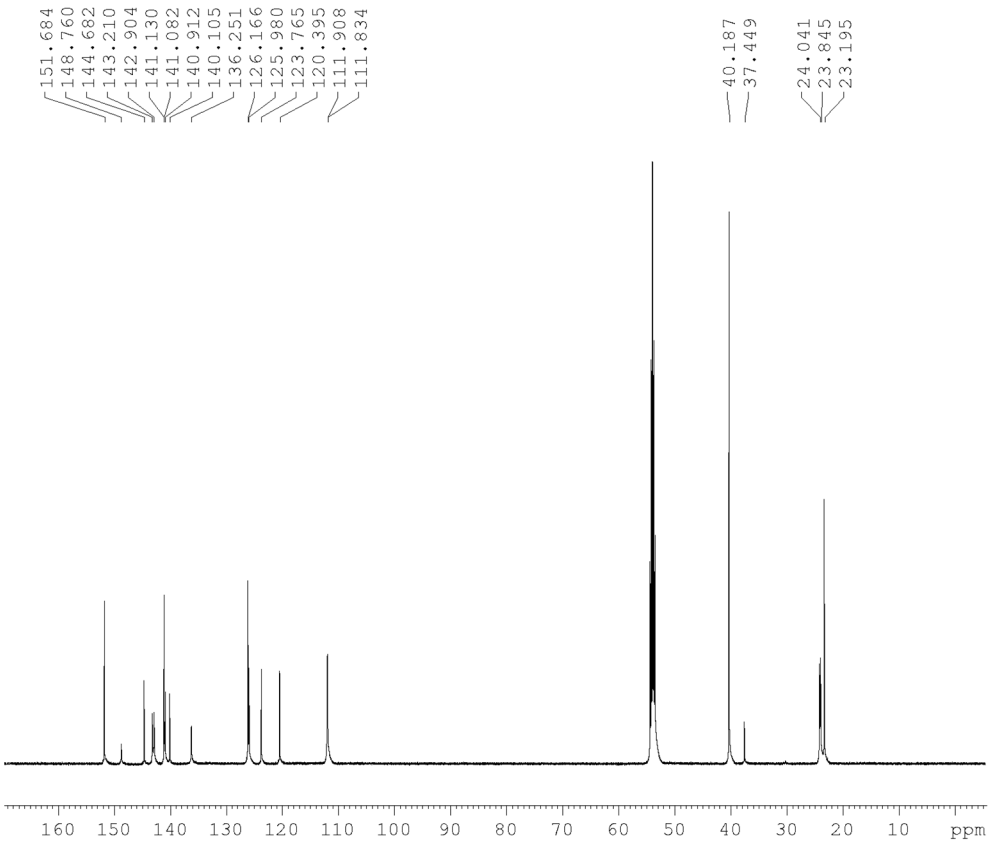

Figure A32. $^{13}C\{^{1}H\}$ NMR spectrum of **3-3** in CD_2Cl_2 at 125 MHz.

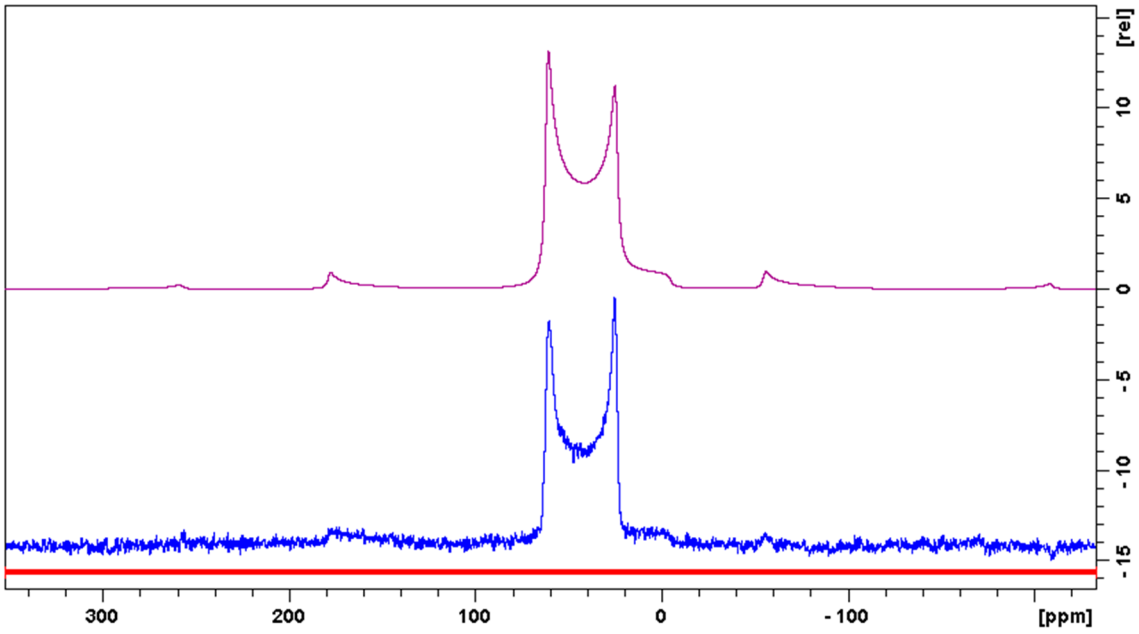

Figure A33. Solid-state $^{11}B\{^1H\}$ NMR spectrum of **3-3** at 128 MHz (top: simulation). Isotropic chemical shift δ_{iso} = 73.0 ppm, quadrupolar coupling constant C_Q = 4.53 MHz, quadrupolar asymmetry parameter η_{Quad} = 0.0.

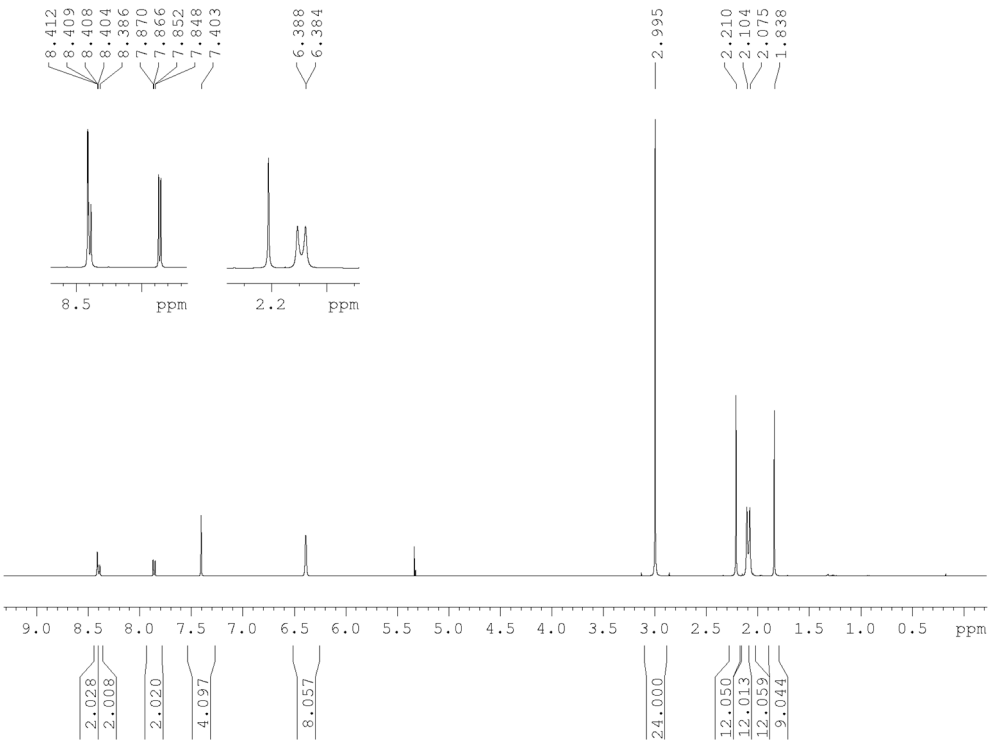

Figure A34. ^1H NMR spectrum of **3-4** in CD_2Cl_2 at 500 MHz.

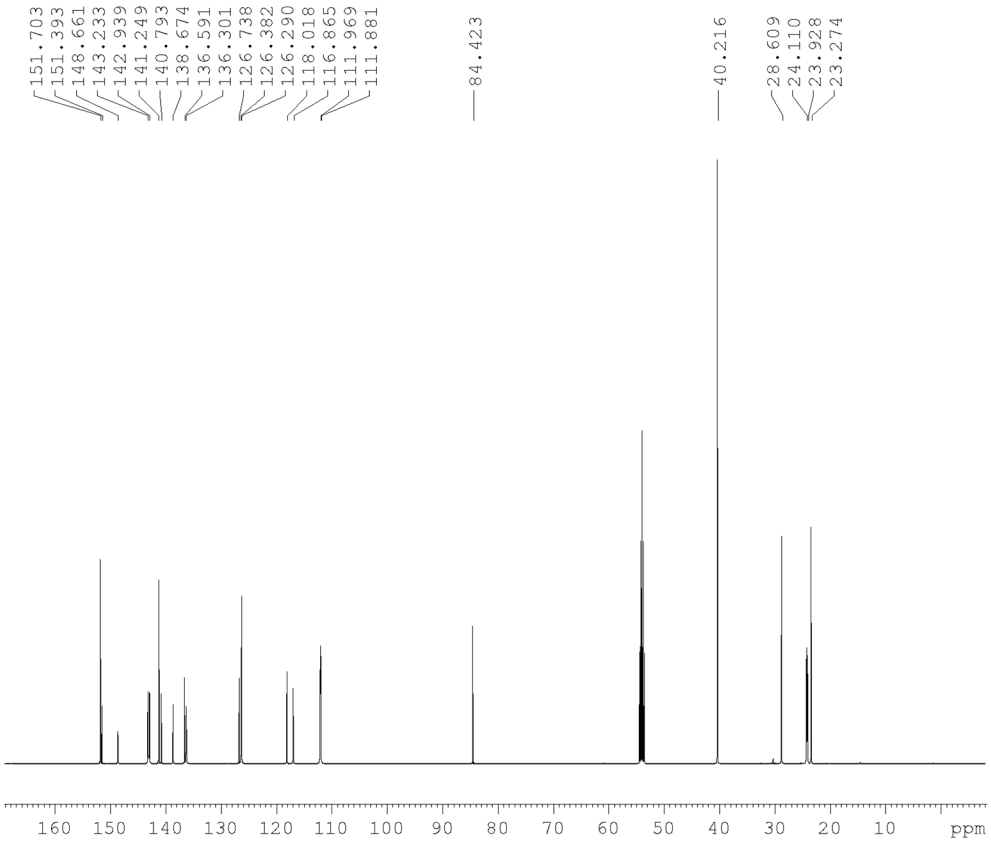

Figure A35. $^{13}C\{^{1}H\}$ NMR spectrum of **3-4** in CD_2Cl_2 at 125 MHz.

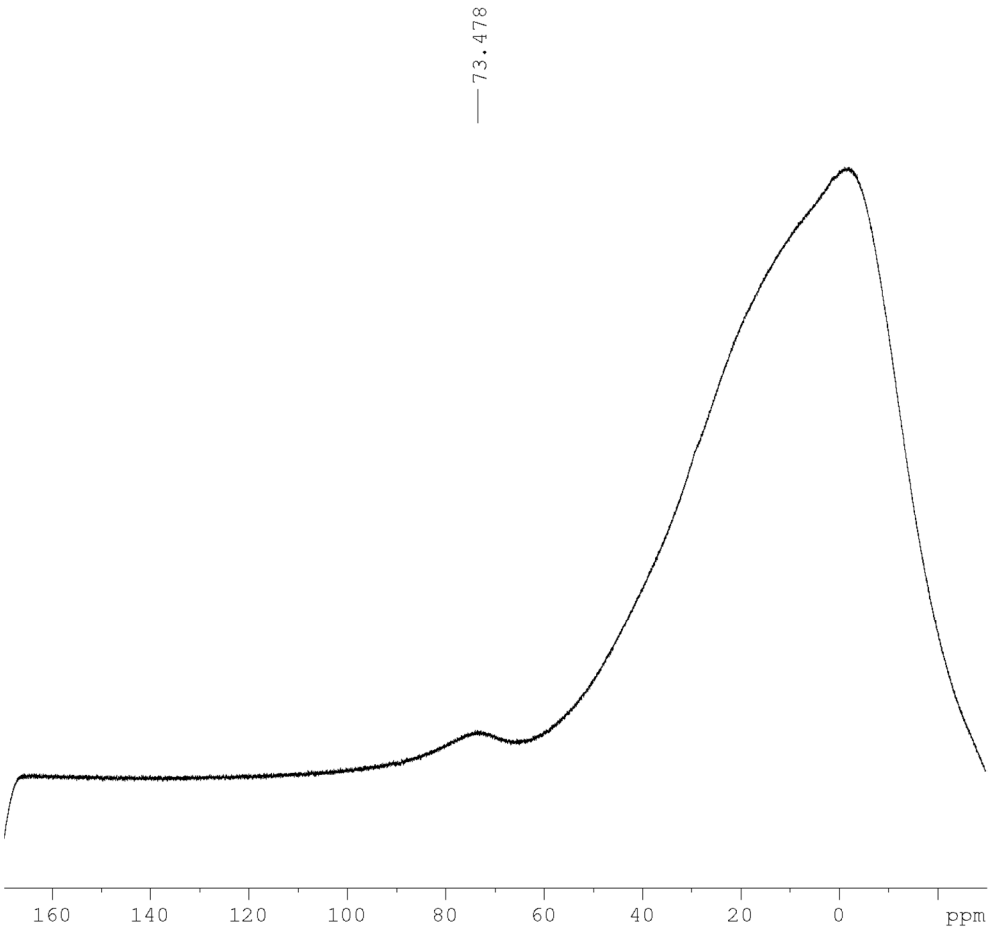

Figure A36. $^{11}B\{^{1}H\}$ NMR spectrum of **3-4** in CD_2Cl_2 at 160 MHz.

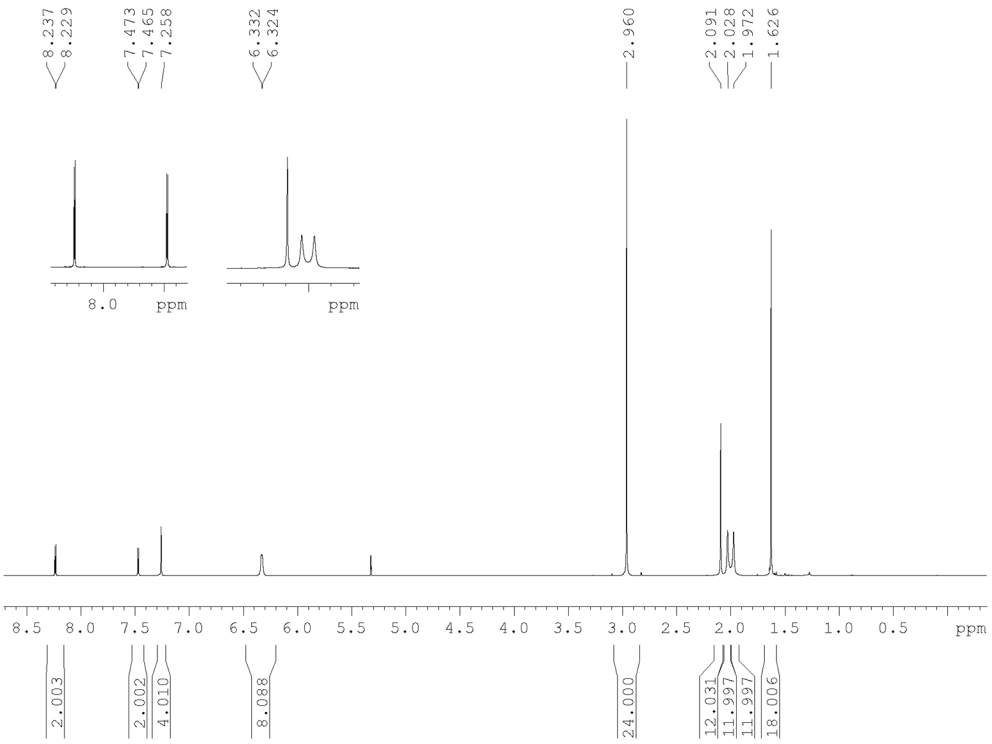

Figure A37. ^{1}H NMR spectrum of **3-5** in CD_2Cl_2 at 500 MHz.

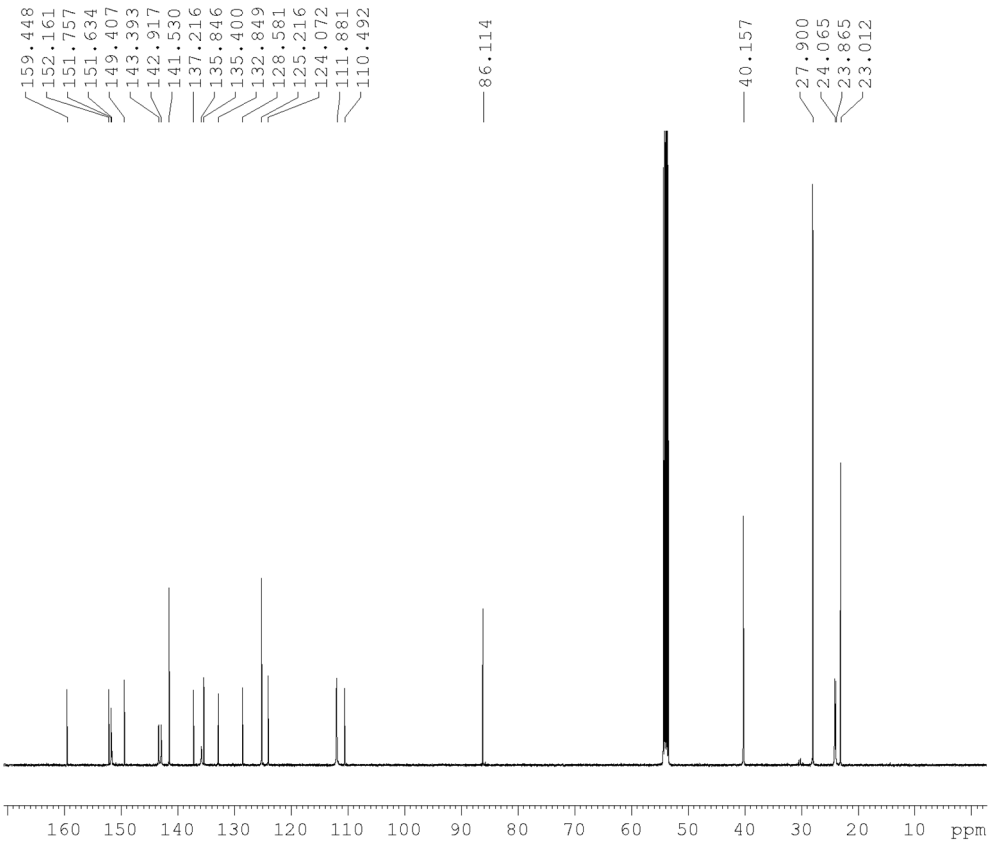

Figure A38. $^{13}C\{^{1}H\}$ NMR spectrum of **3-5** in CD_2Cl_2 at 125 MHz.

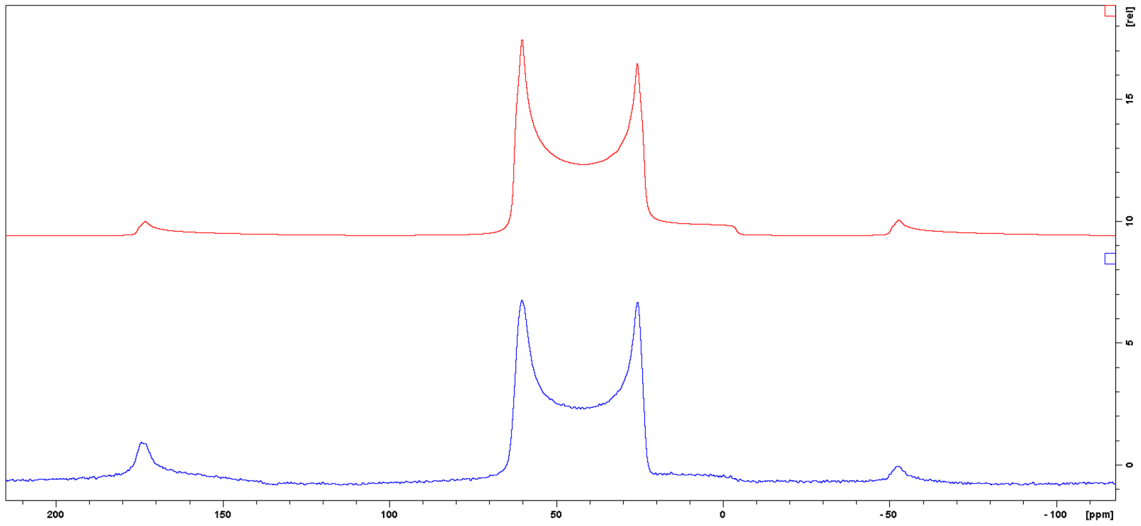

Figure A39. Solid-state $^{11}B\{^1H\}$ NMR spectrum of **3-5** at 128 MHz (top: simulation). Isotropic chemical shift δ_{iso} = 72.5 ppm, quadrupolar coupling constant C_Q = 4.49 MHz, quadrupolar asymmetry parameter η_{Quad} = 0.1.

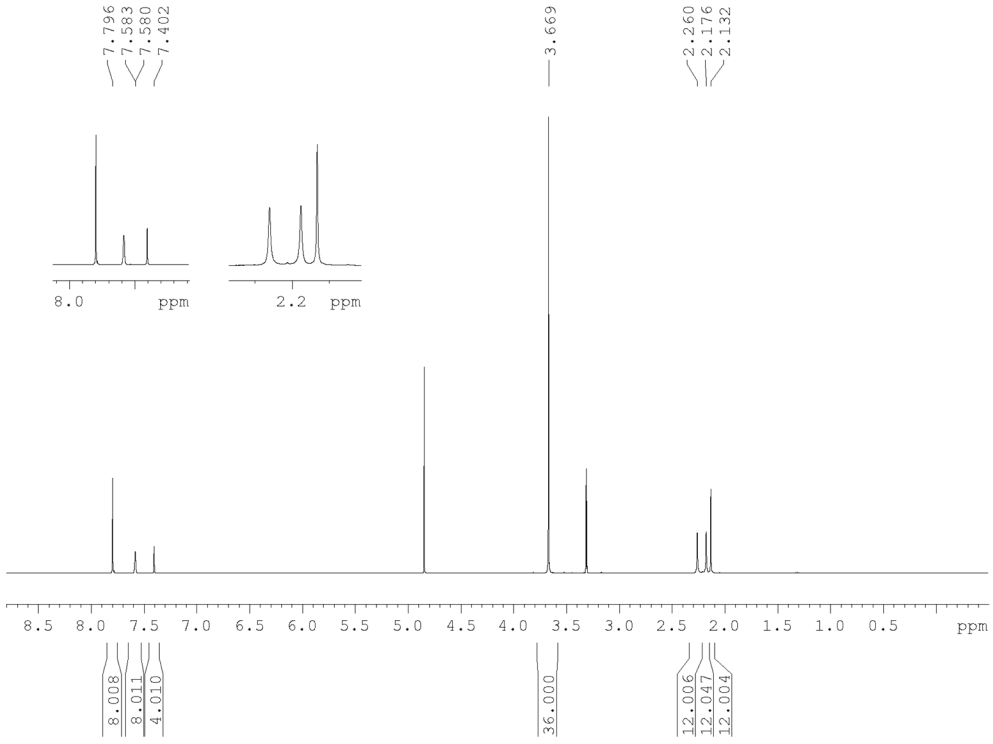

Figure A40. ^1H NMR spectrum of **3-1M** in CD_3OD at 500 MHz.

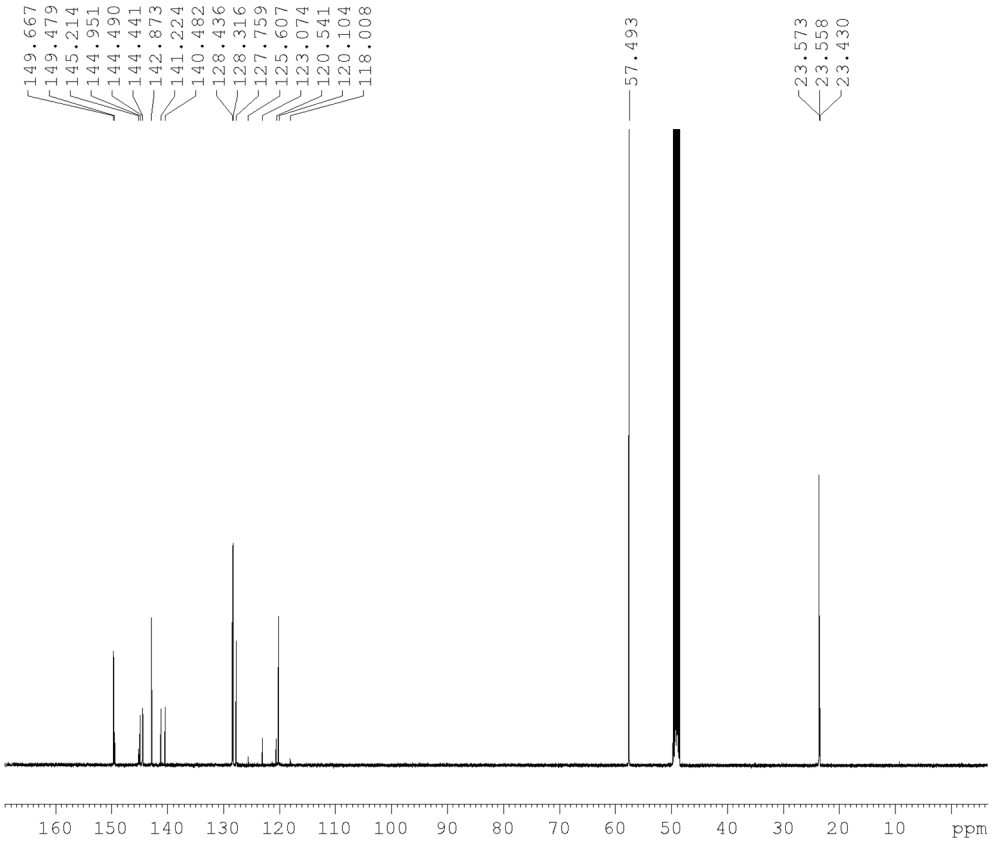

Figure A41. $^{13}C\{^{1}H\}$ NMR spectrum of **3-1M** in CD_3OD at 125 MHz.

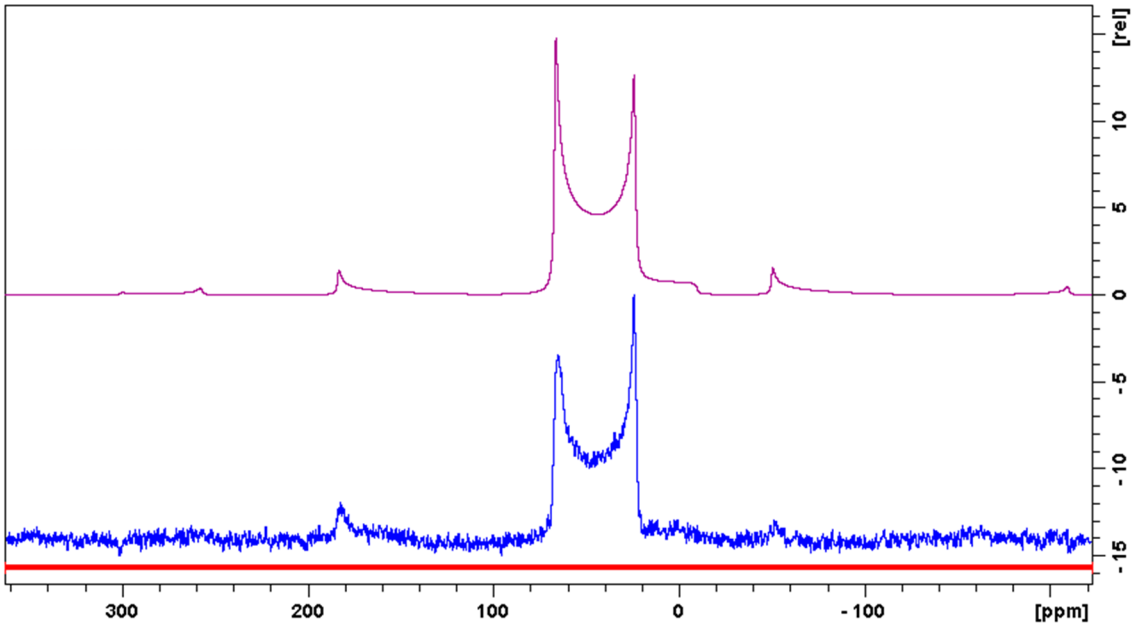

Figure A42. Solid-state $^{11}B\{^{1}H\}$ NMR spectrum of **3-1M** at 128 MHz (top: simulation). Isotropic chemical shift δ_{iso} = 79.2 ppm, quadrupolar coupling constant C_Q = 4.86 MHz, quadrupolar asymmetry parameter η_{Quad} = 0.0.

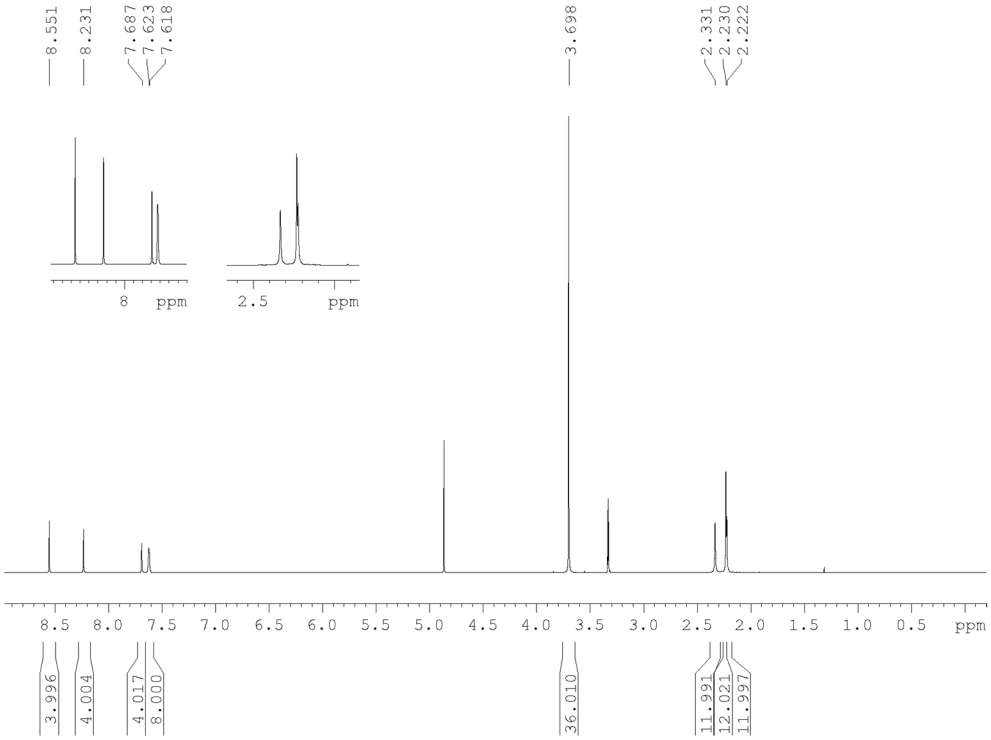

Figure A43. ^{1}H NMR spectrum of **3-2M** in CD_3OD at 500 MHz.

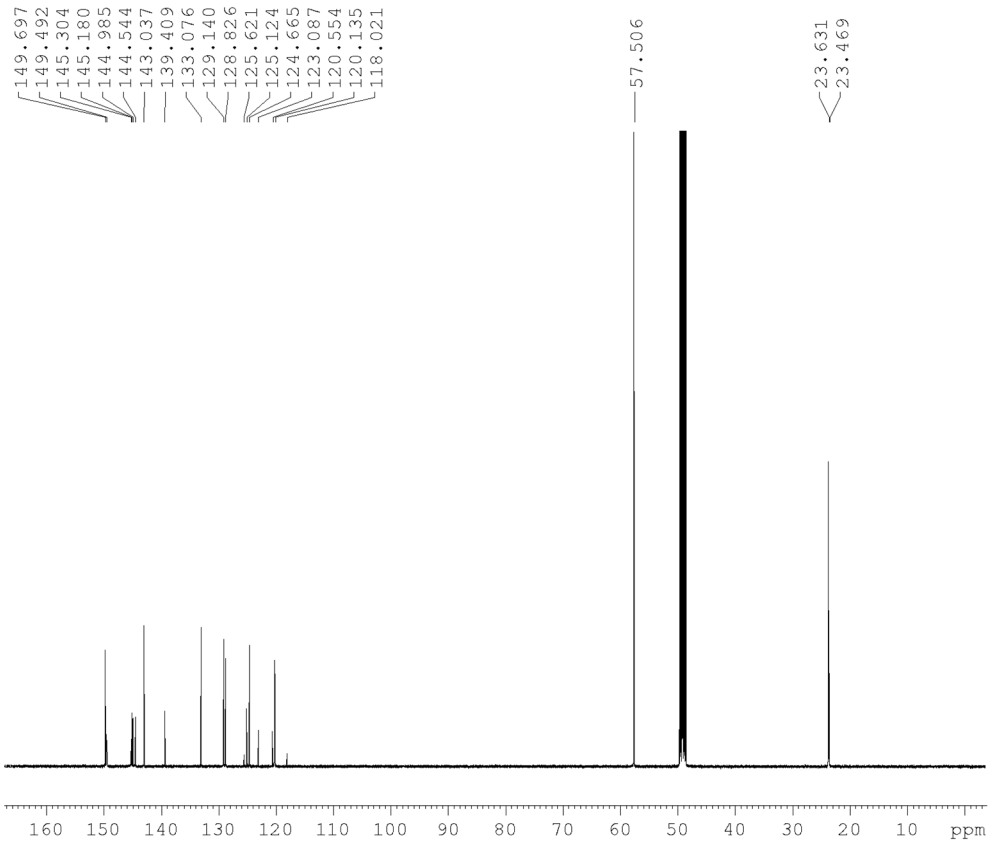

Figure A44. $^{13}C\{^{1}H\}$ NMR spectrum of **3-2M** in CD_3OD at 125 MHz.

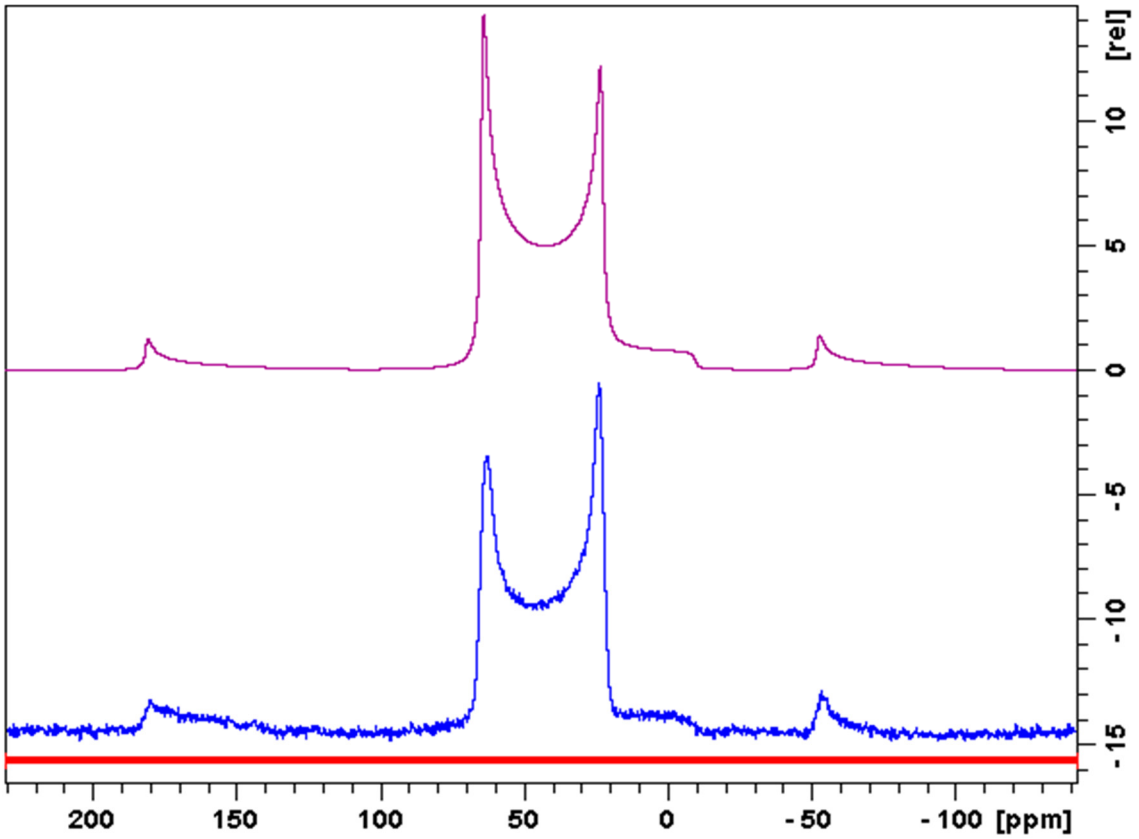

Figure A45. Solid-state $^{11}B\{^1H\}$ NMR spectrum of **3-2M** at 128 MHz (top: simulation). Isotropic chemical shift δ_{iso} = 77.2 ppm, quadrupolar coupling constant C_Q = 4.78 MHz, quadrupolar asymmetry parameter η_{Quad} = 0.0.

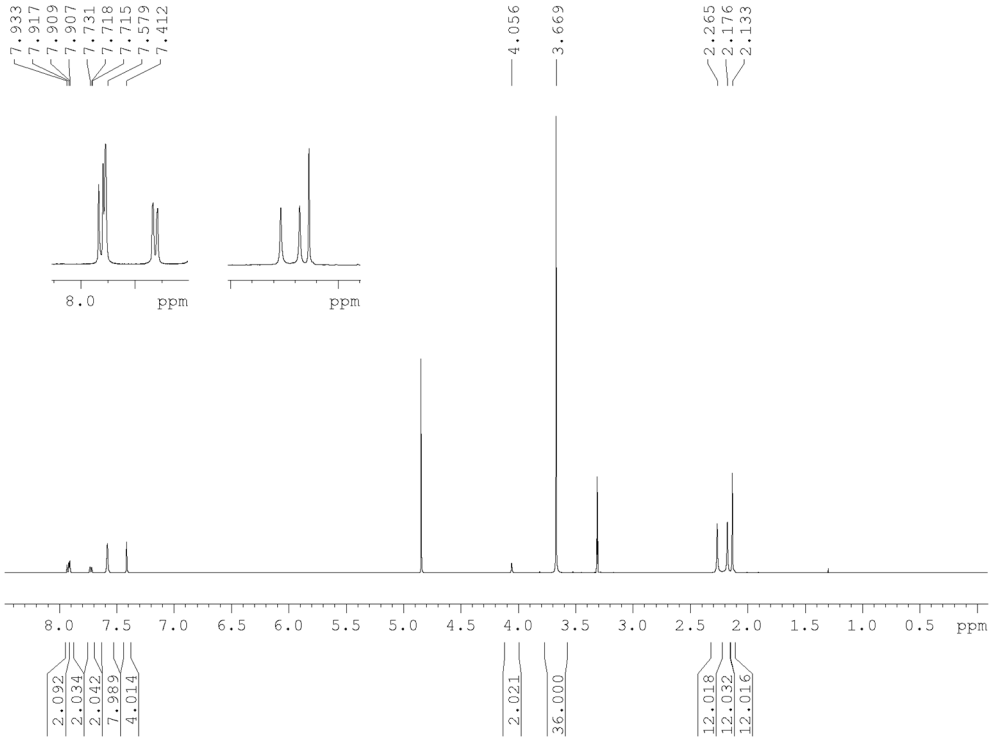

Figure A46. ^1H NMR spectrum of **3-3M** in CD_3OD at 500 MHz.

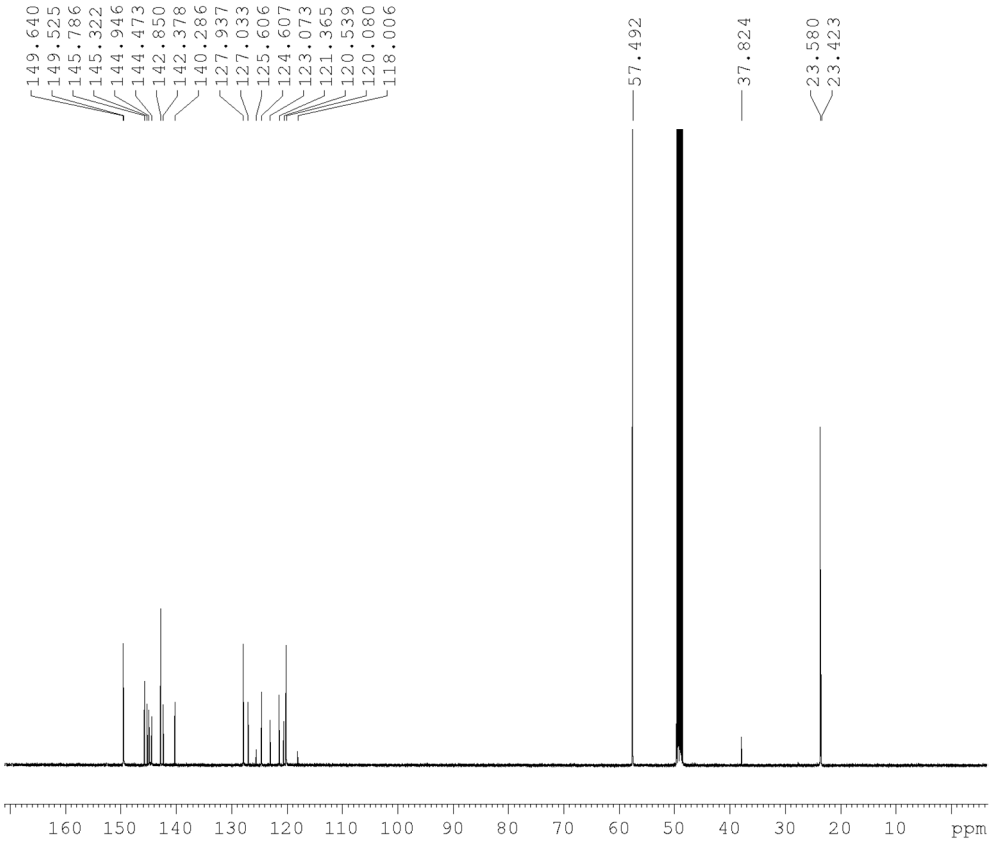

Figure A47. $^{13}C\{^{1}H\}$ NMR spectrum of **3-3M** in CD_3OD at 125 MHz.

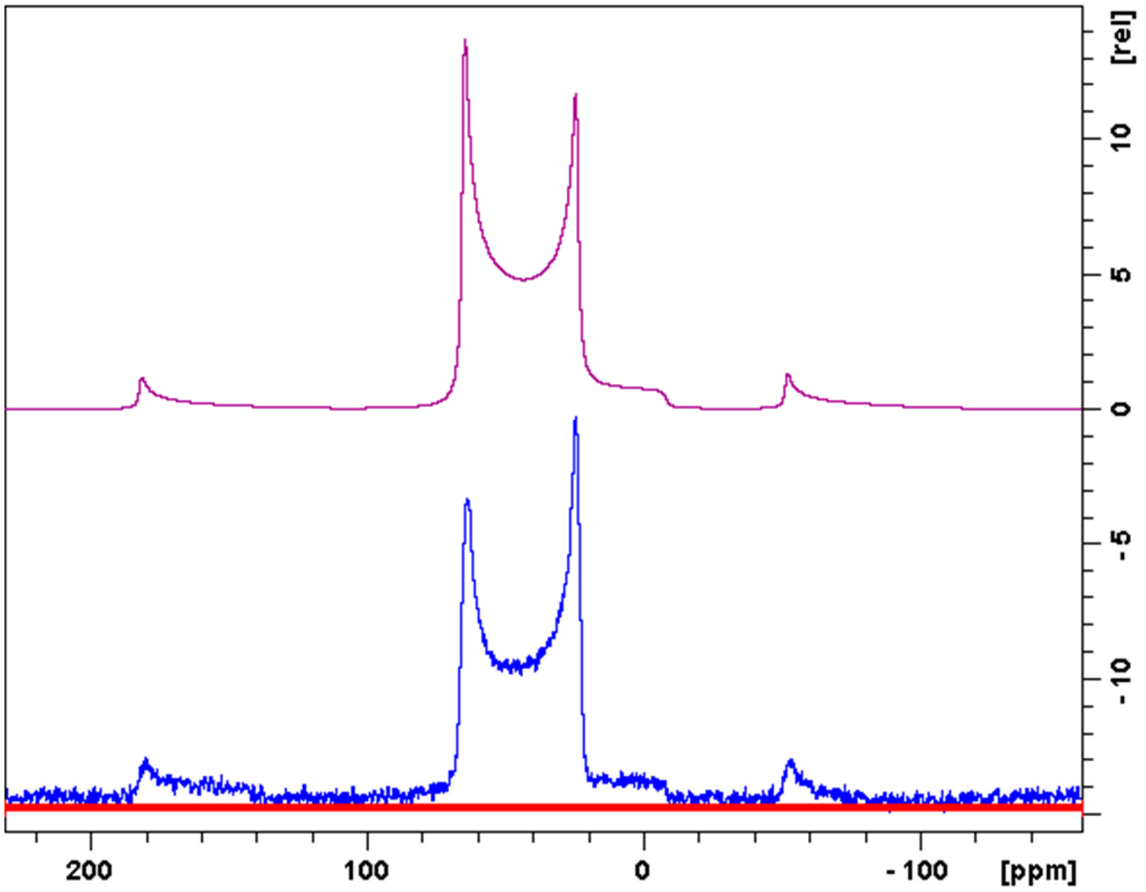

Figure A48. Solid-state $^{11}B\{^{1}H\}$ NMR spectrum of **3-3M** at 128 MHz (top: simulation). Isotropic chemical shift δ_{iso} = 77.1 ppm, quadrupolar coupling constant C_Q = 4.76 MHz, quadrupolar asymmetry parameter η_{Quad} = 0.0.

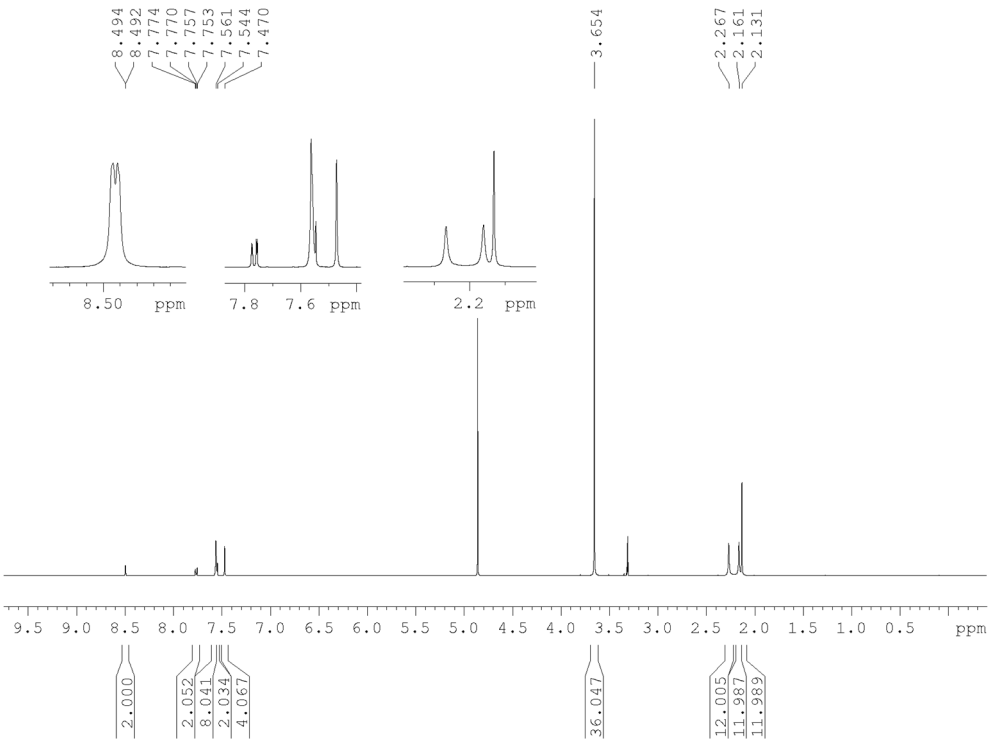

Figure A49. ^{1}H NMR spectrum of **3-4M** in CD_3OD at 500 MHz.

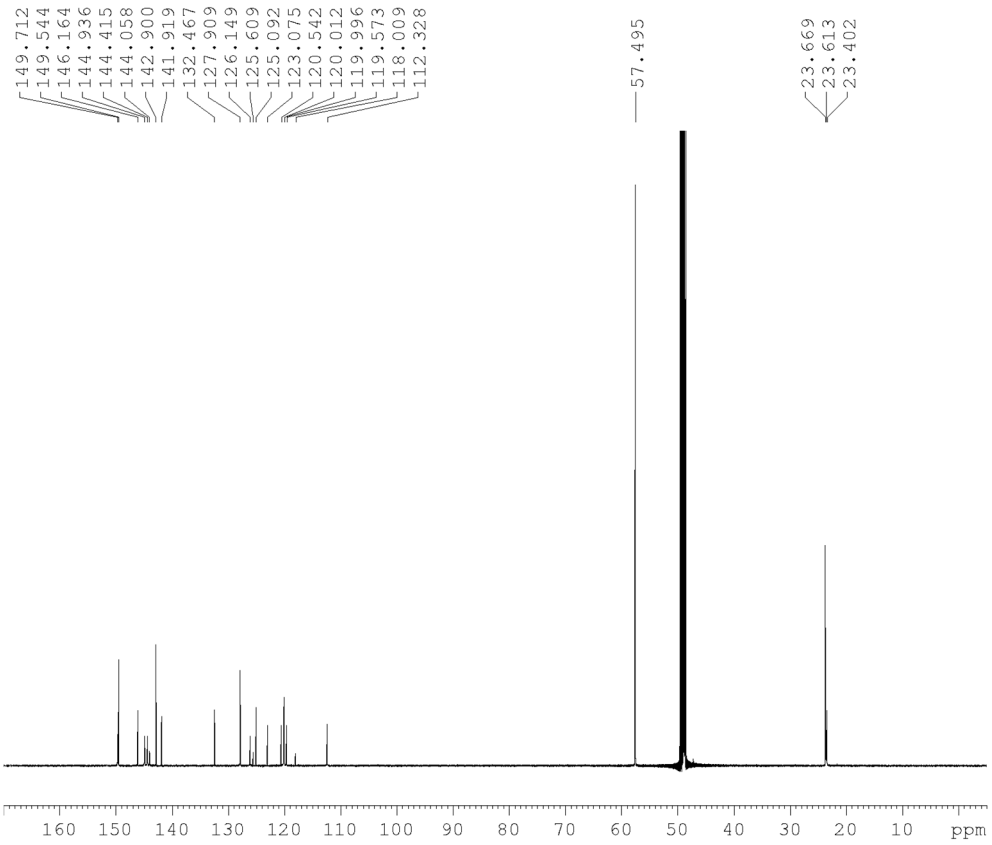

Figure A50. $^{13}C\{^{1}H\}$ NMR spectrum of **3-4M** in CD_3OD at 125 MHz.

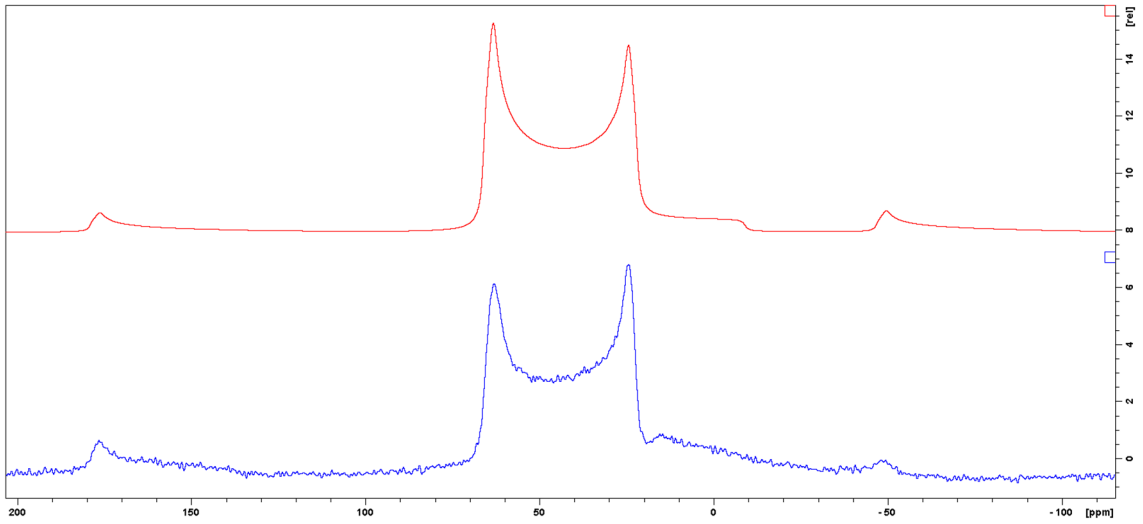

Figure A51. Solid-state $^{11}B\{^1H\}$ NMR spectrum of **3-4M** at 128 MHz (top: simulation). Isotropic chemical shift δ_{iso} = 77.0 ppm, quadrupolar coupling constant C_Q = 4.77 MHz, quadrupolar asymmetry parameter η_{Quad} = 0.1.

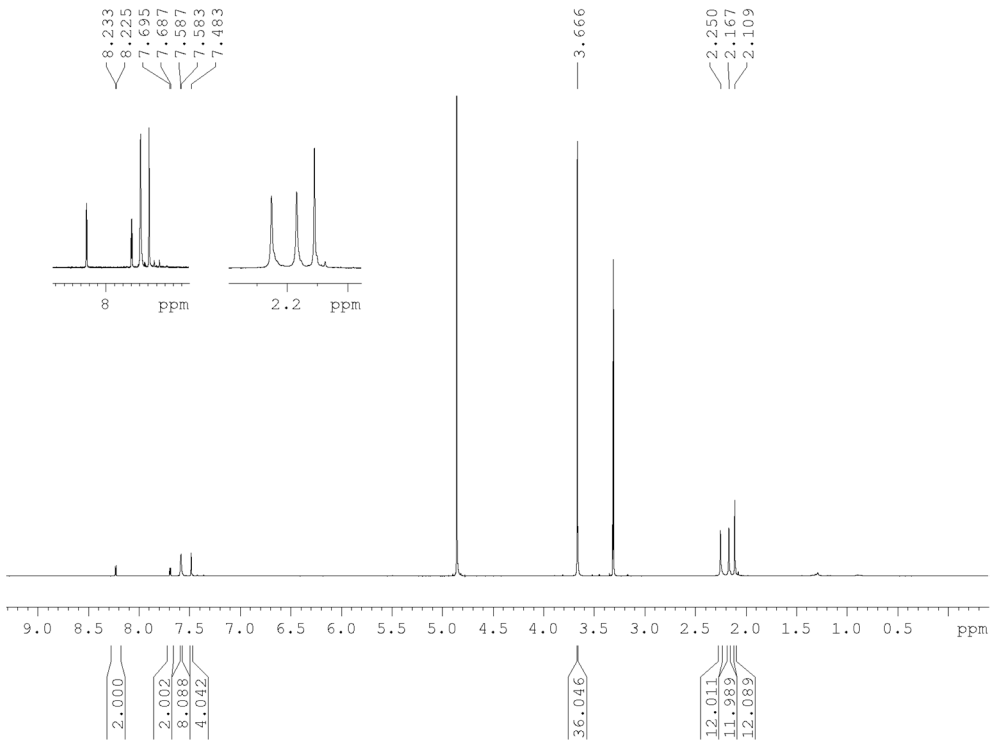

Figure A52. ^1H NMR spectrum of **3-5M** in CD_3OD at 500 MHz.

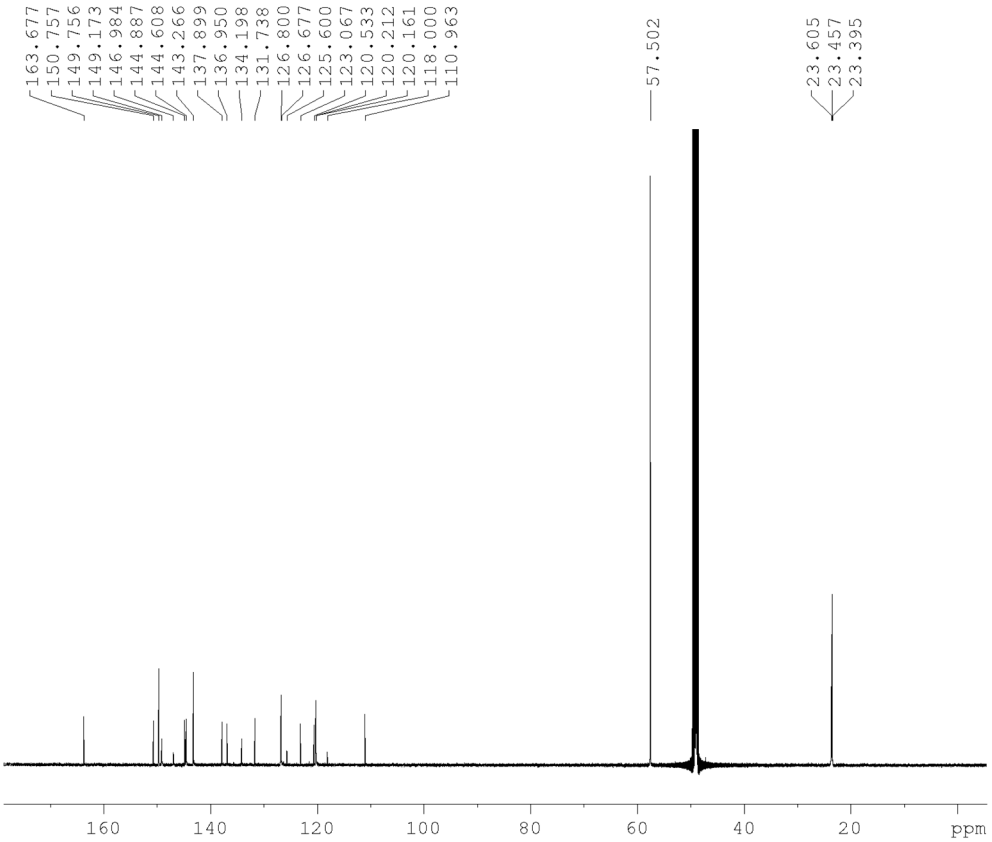

Figure A53. $^{13}C\{^{1}H\}$ NMR spectrum of **3-5M** in CD_3OD at 125 MHz.

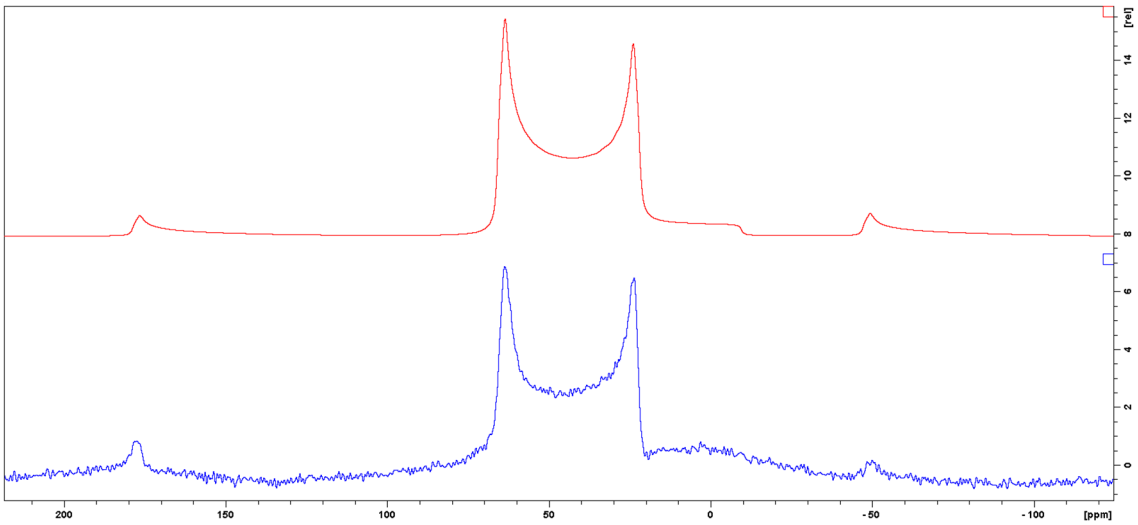

Figure A54. Solid-state $^{11}B\{^{1}H\}$ NMR spectrum of **3-5M** at 128 MHz (top: simulation). Isotropic chemical shift δ_{iso} = 77.1 ppm, quadrupolar coupling constant C_Q = 4.79 MHz, quadrupolar asymmetry parameter η_{Quad} = 0.0.

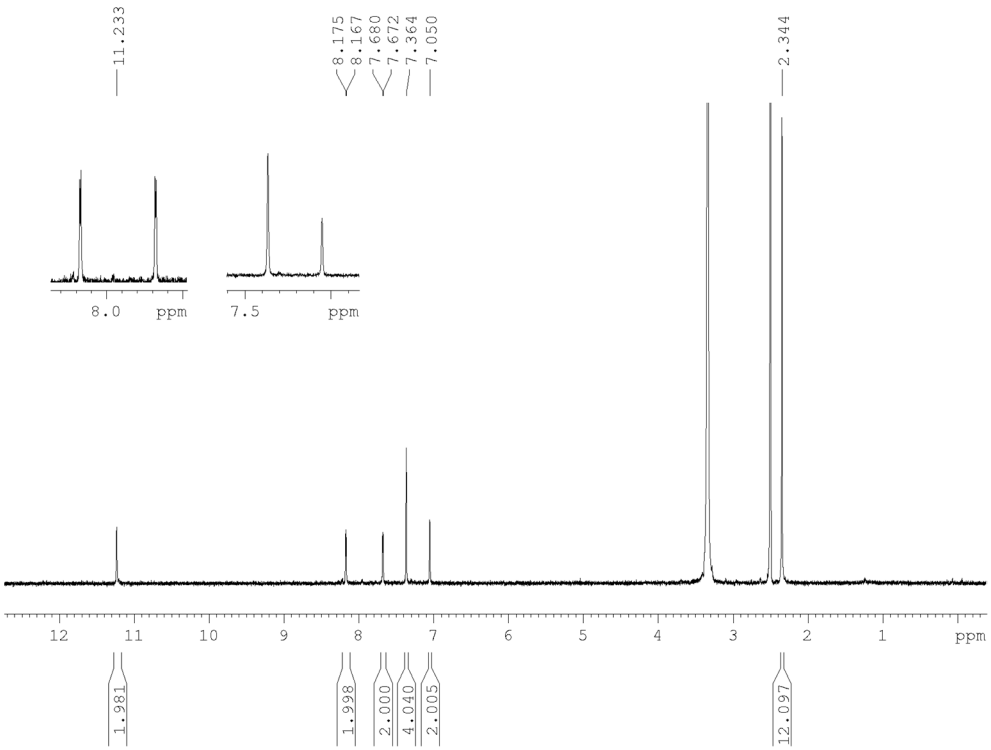

Figure A55. ^{1}H NMR spectrum of **3-5A** in d_6-DMSO at 500 MHz.

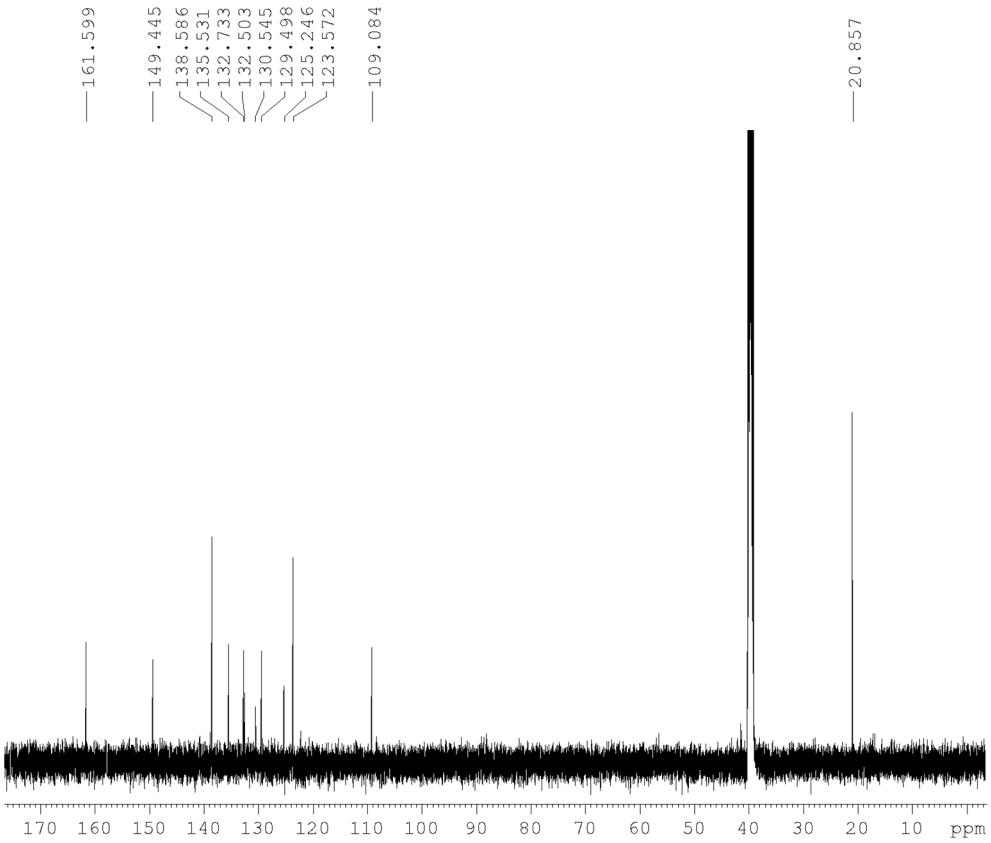

Figure A56. $^{13}C\{^{1}H\}$ NMR spectrum of **3-5A** in d_6-DMSO at 125 MHz.

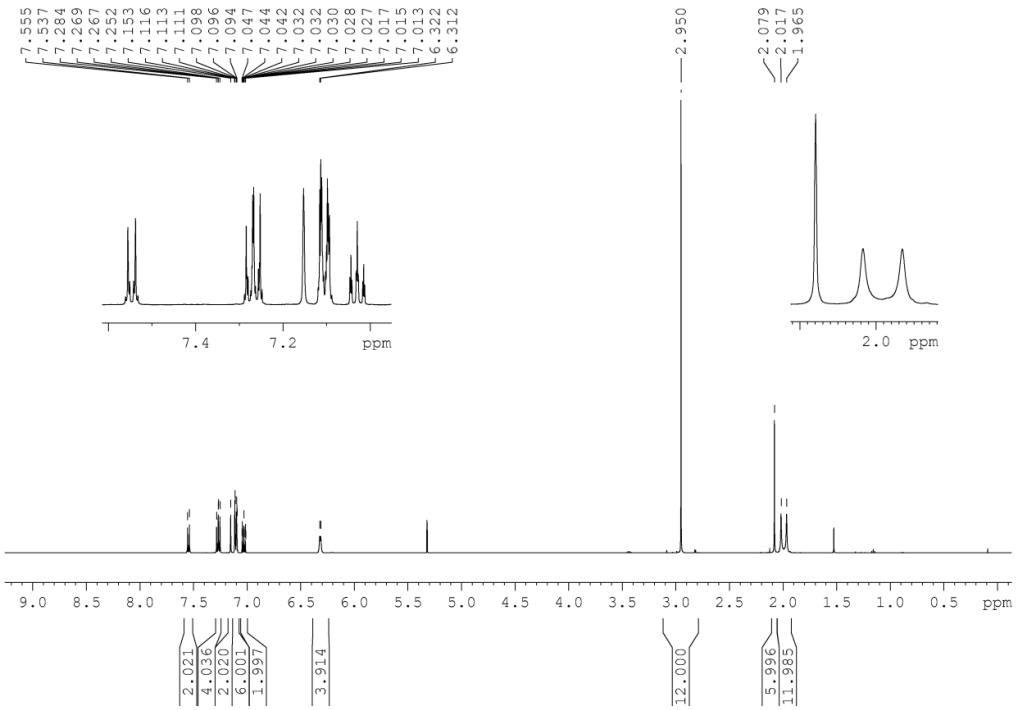

Figure A57. ^{1}H NMR spectrum of **4-1** in CD_2Cl_2 at 500 MHz.

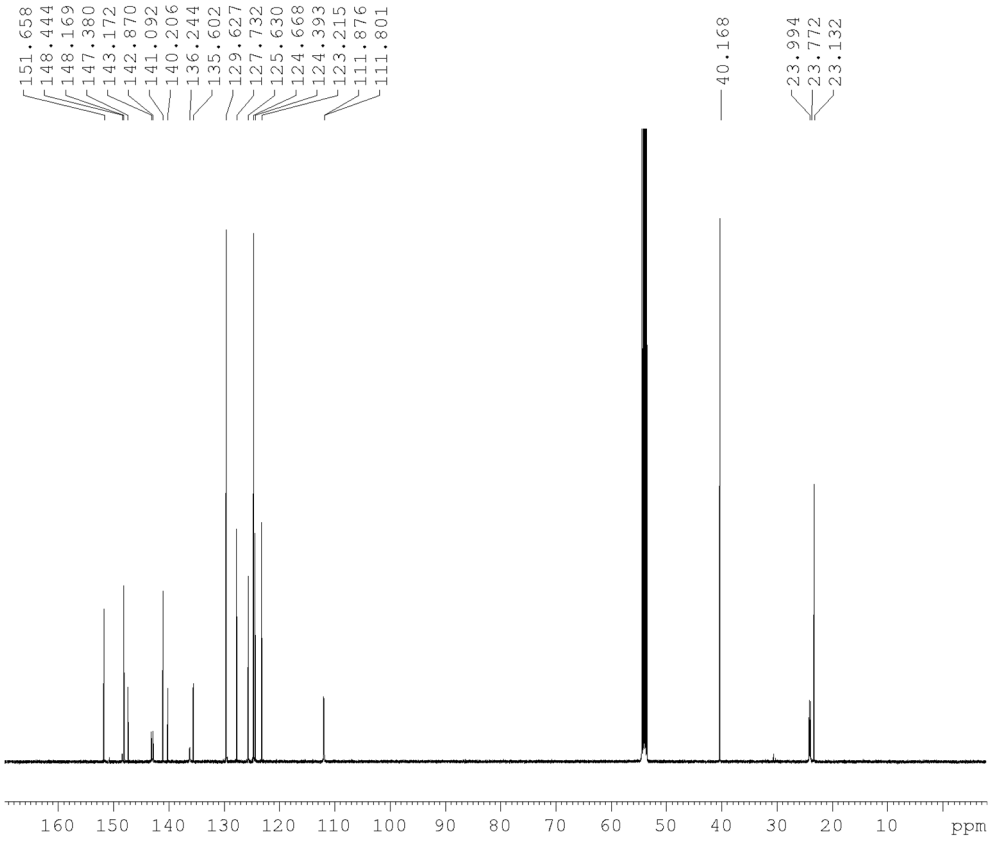

Figure A58. $^{13}C\{^{1}H\}$ NMR spectrum of **4-1** in CD_2Cl_2 at 125 MHz.

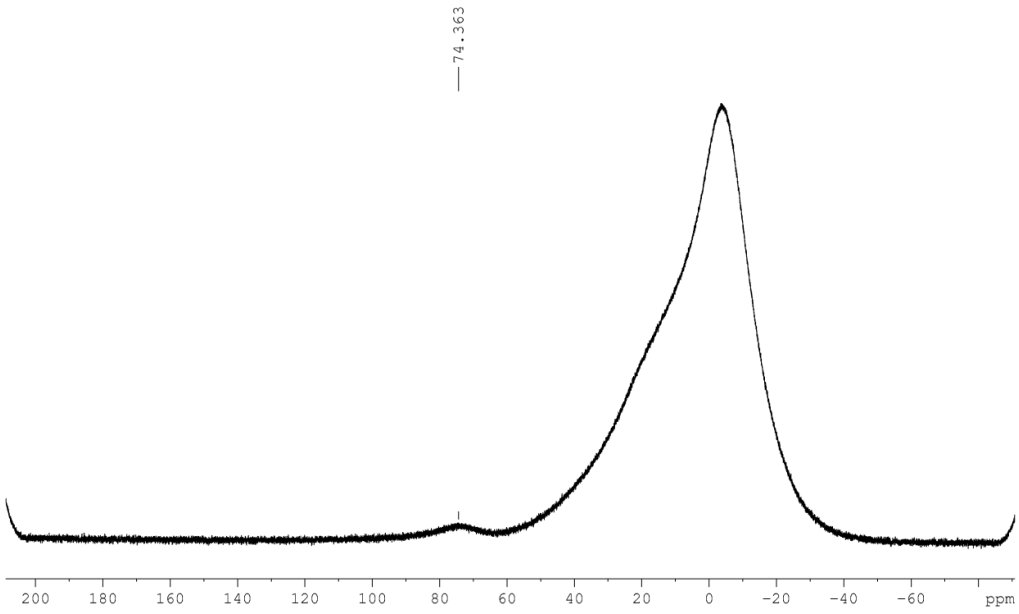

Figure A59. $^{11}B\{^{1}H\}$ NMR spectrum of **4-1** in CD_2Cl_2 at 160 MHz.

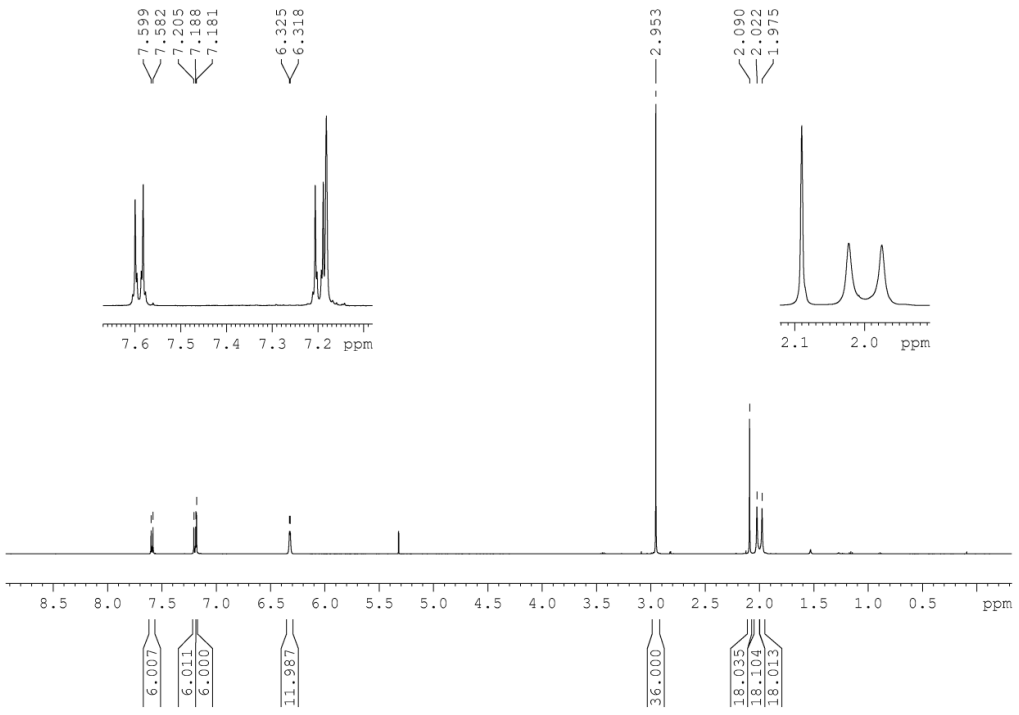

Figure A60. ^{1}H NMR spectrum of **4-2** in CD_2Cl_2 at 500 MHz.

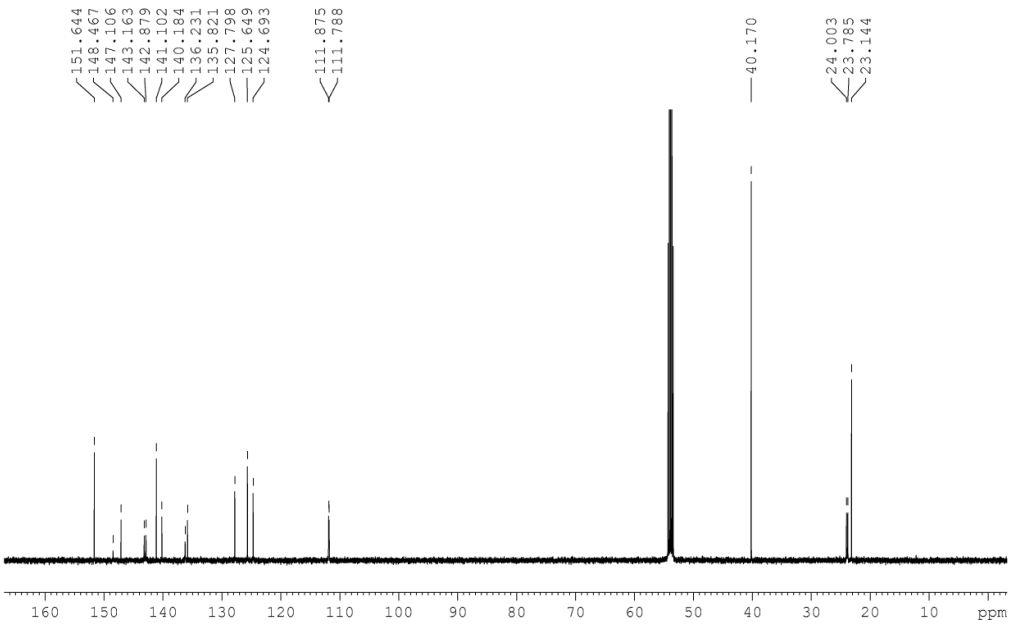

Figure A61. $^{13}C\{^{1}H\}$ NMR spectrum of **4-2** in CD_2Cl_2 at 125 MHz.

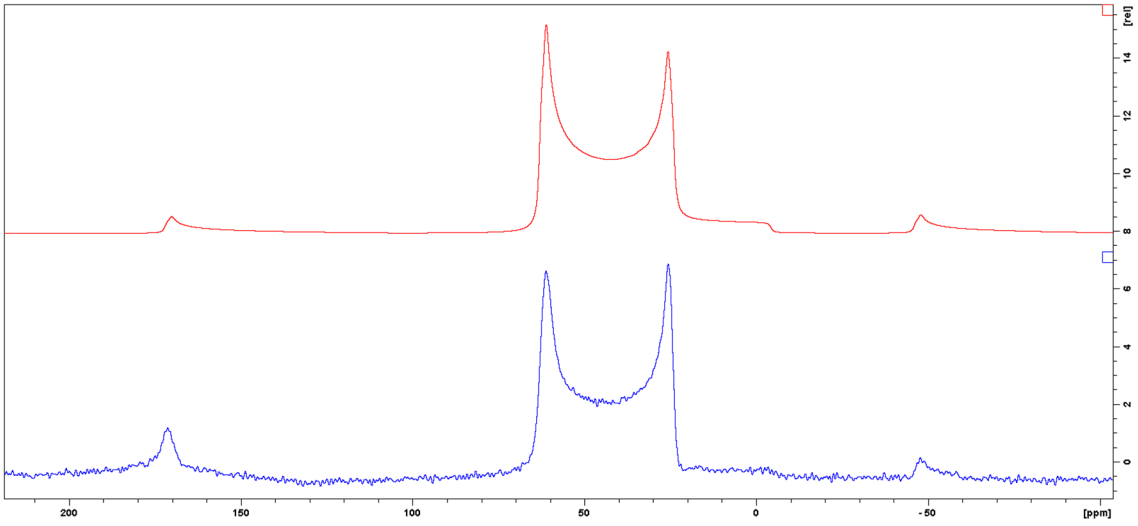

Figure A62. Solid-state $^{11}B\{^{1}H\}$ NMR spectrum of **4-2** at 128 MHz (top: simulation). Isotropic chemical shift δ_{iso} = 73.2 ppm, quadrupolar coupling constant C_Q = 4.53 MHz, quadrupolar asymmetry parameter η_{Quad} = 0.0.

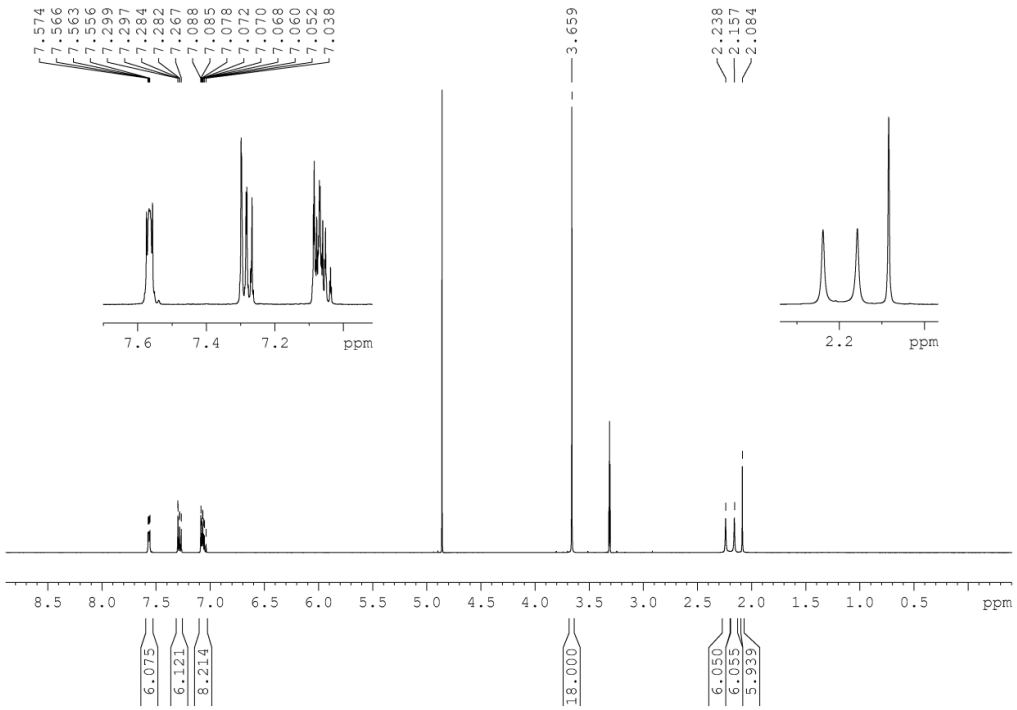

Figure A63. ^{1}H NMR spectrum of **4-1M** in CD_3OD at 500 MHz.

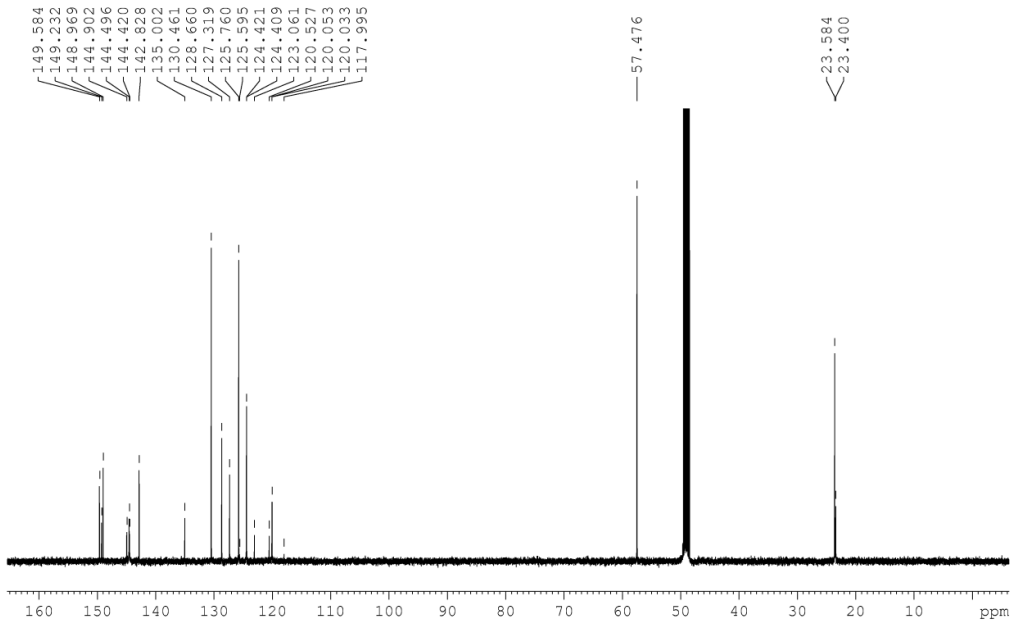

Figure A64. $^{13}C\{^{1}H\}$ NMR spectrum of **4-1M** in CD_3OD at 125 MHz.

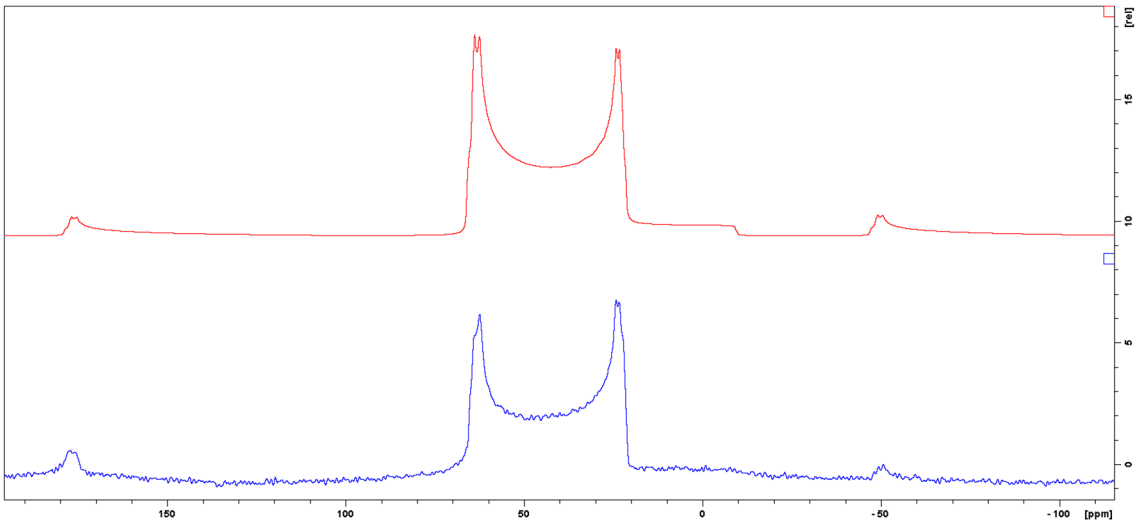

Figure A65. Solid-state $^{11}B\{^1H\}$ NMR spectrum of **4-1M** at 128 MHz (top: simulation). Isotropic chemical shift δ_{iso} = 76.0 and 77.6 ppm, quadrupolar coupling constant C_Q = 4.76 and 4.78 MHz, quadrupolar asymmetry parameter η_{Quad} = 0.0 and 0.0. Since no further side products are observable via NMR spectroscopy in solution, it can be assumed that the two signals correspond to two isomers, which exist in the solid state. An integration of the signals gives a ratio of 1:1.

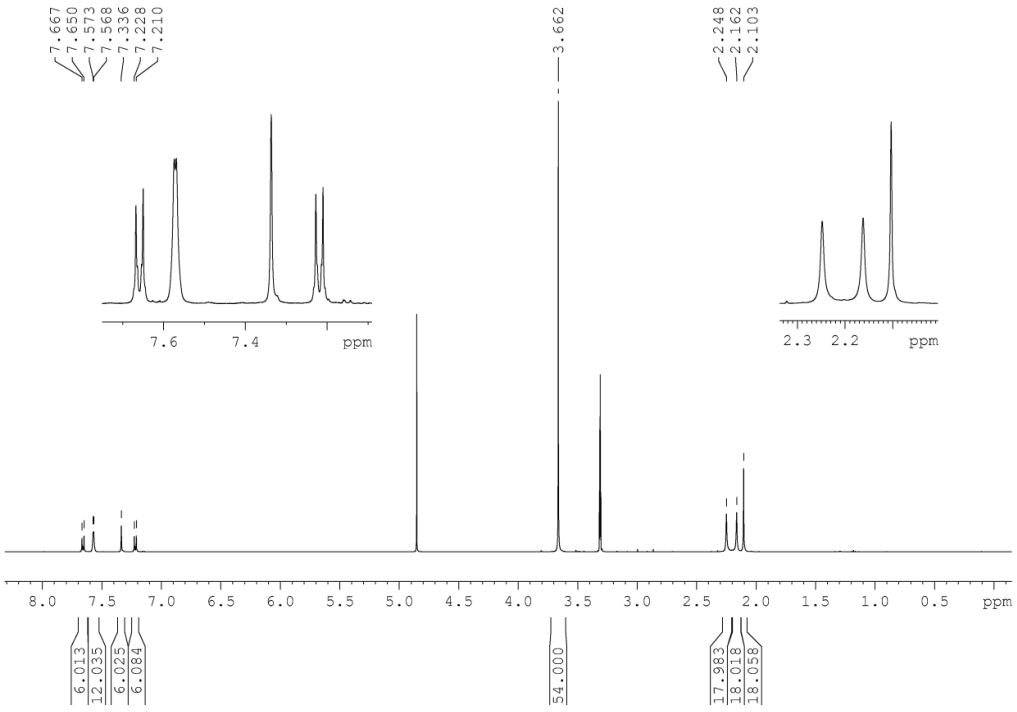

Figure A66. ^1H NMR spectrum of **4-2M** in CD_3OD at 500 MHz.

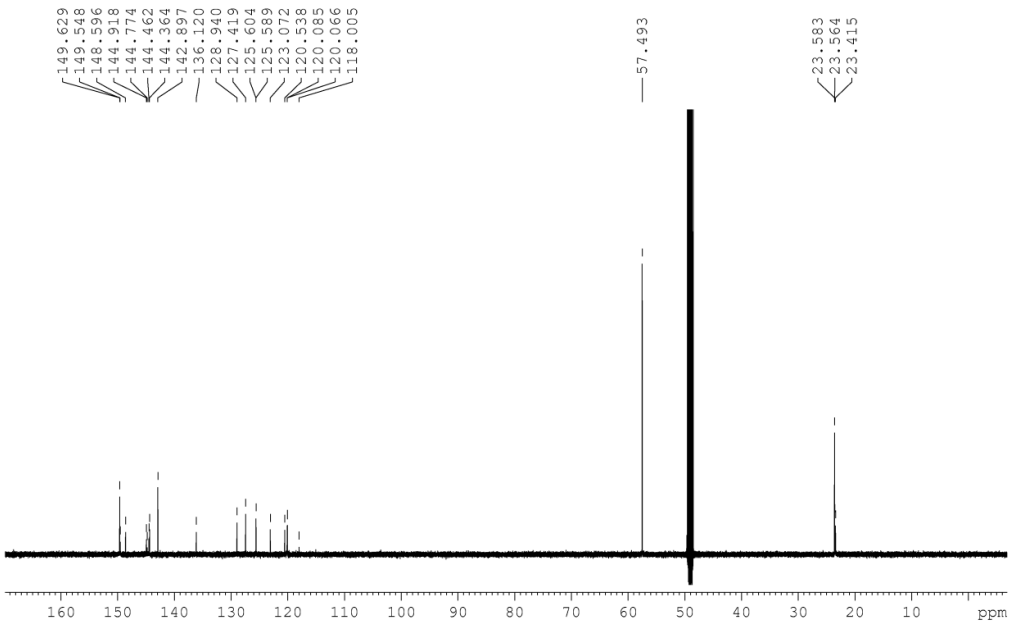

Figure A67. $^{13}C\{^{1}H\}$ NMR spectrum of **4-2M** in CD_3OD at 125 MHz.

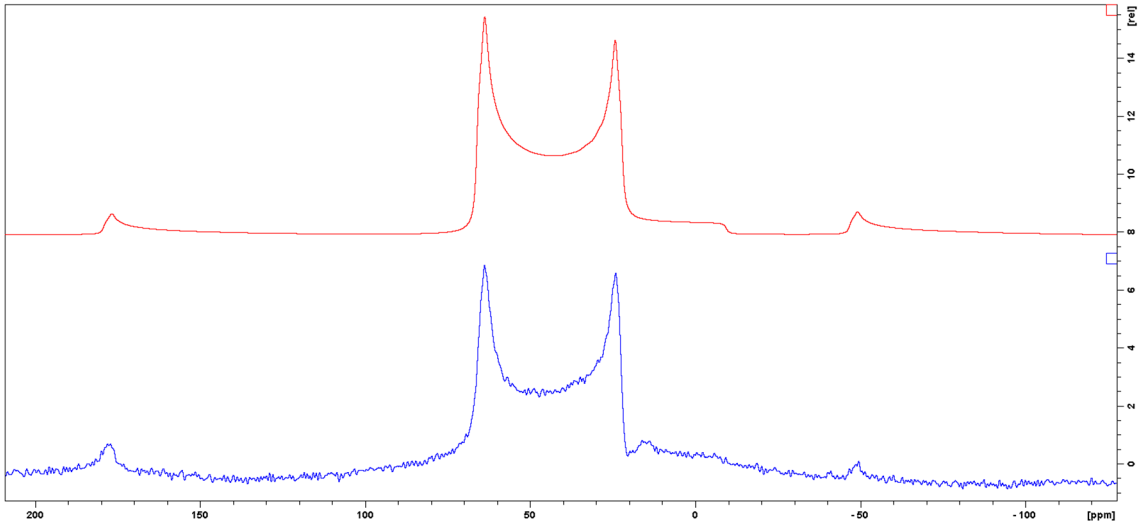

Figure A68. Solid-state $^{11}B\{^{1}H\}$ NMR spectrum of **4-2M** at 128 MHz (top: simulation). Isotropic chemical shift δ_{iso} = 77.6 ppm, quadrupolar coupling constant C_Q = 4.79 MHz, quadrupolar asymmetry parameter η_{Quad} = 0.1.

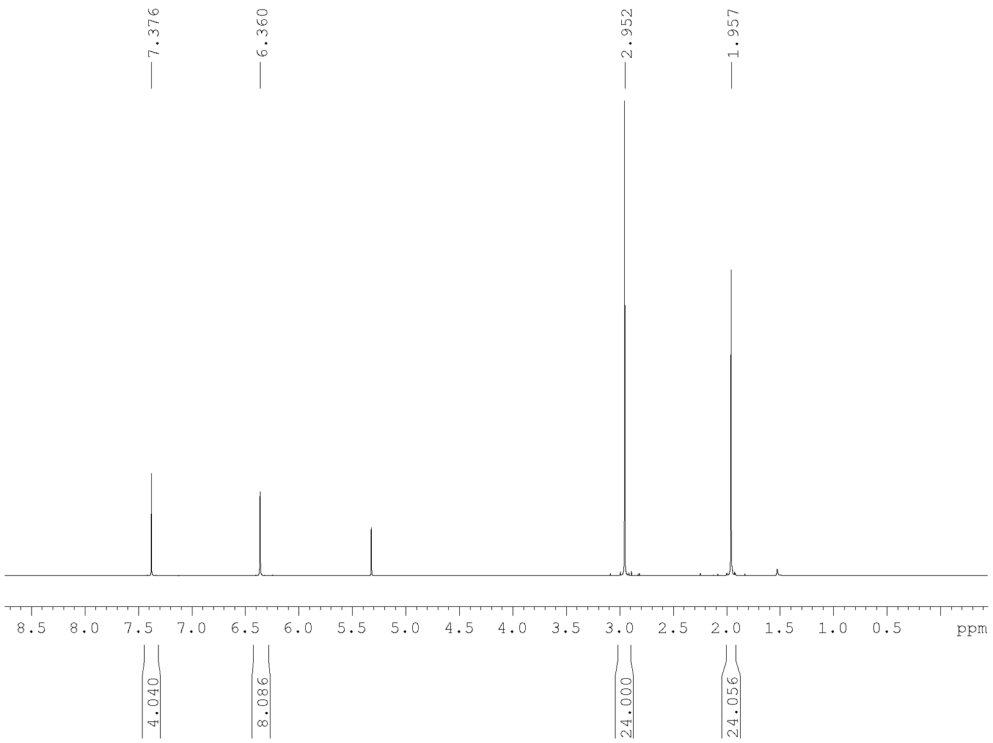

Figure A69. ^{1}H NMR spectrum of **5-1** in CD_2Cl_2 at 500 MHz.

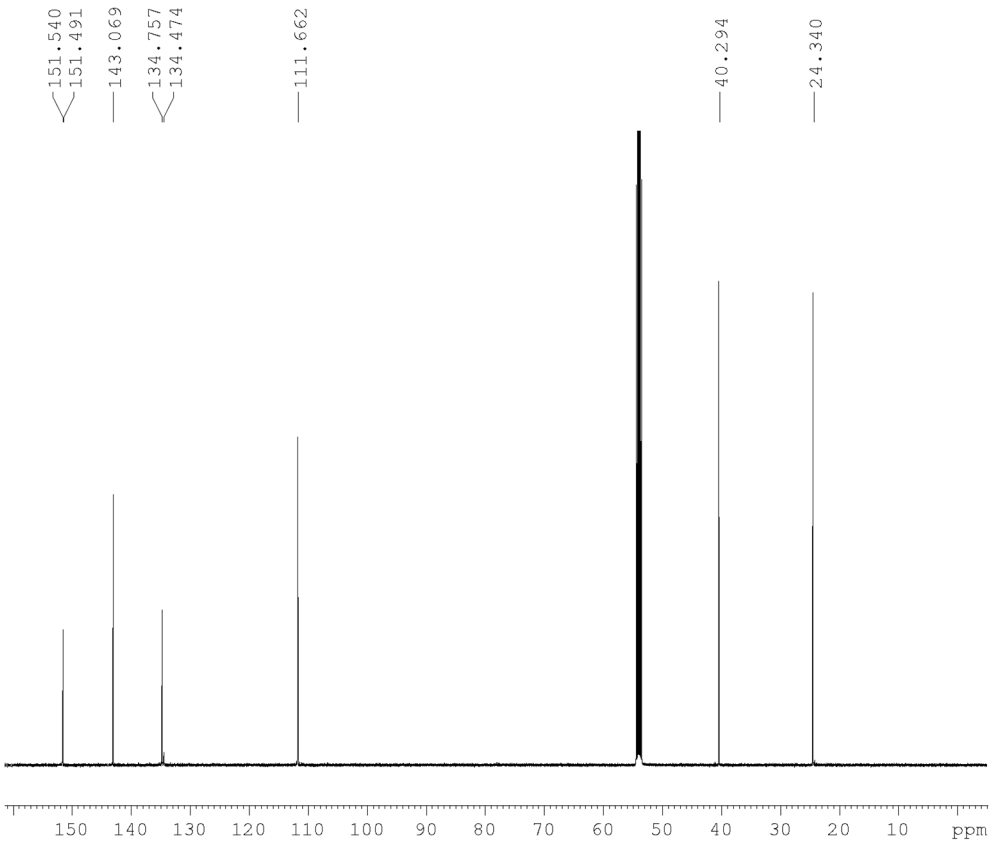

Figure A70. $^{13}C\{^{1}H\}$ NMR spectrum of **5-1** in CD_2Cl_2 at 125 MHz.

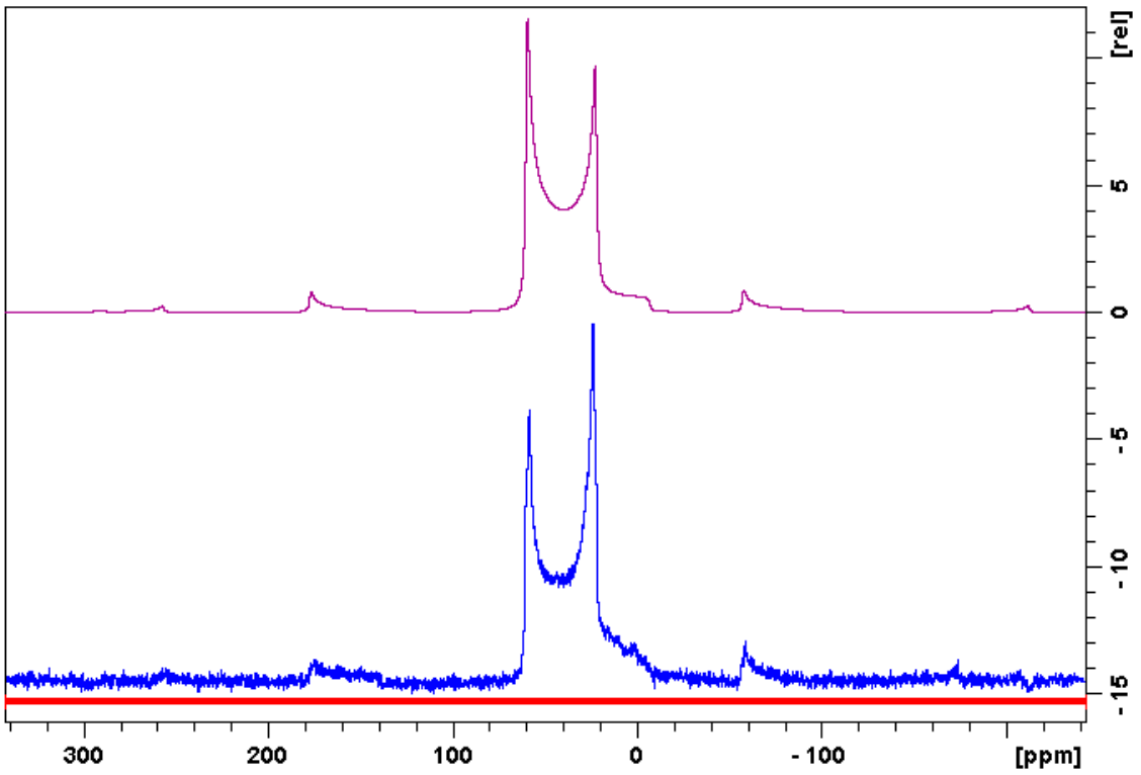

Figure A71. Solid-state $^{11}B\{^1H\}$ NMR spectrum of **5-1** at 128 MHz (top: simulation). Isotropic chemical shift δ_{iso} = 71.2 ppm, quadrupolar coupling constant C_Q = 4.54 MHz, quadrupolar asymmetry parameter η_{Quad} = 0.0.

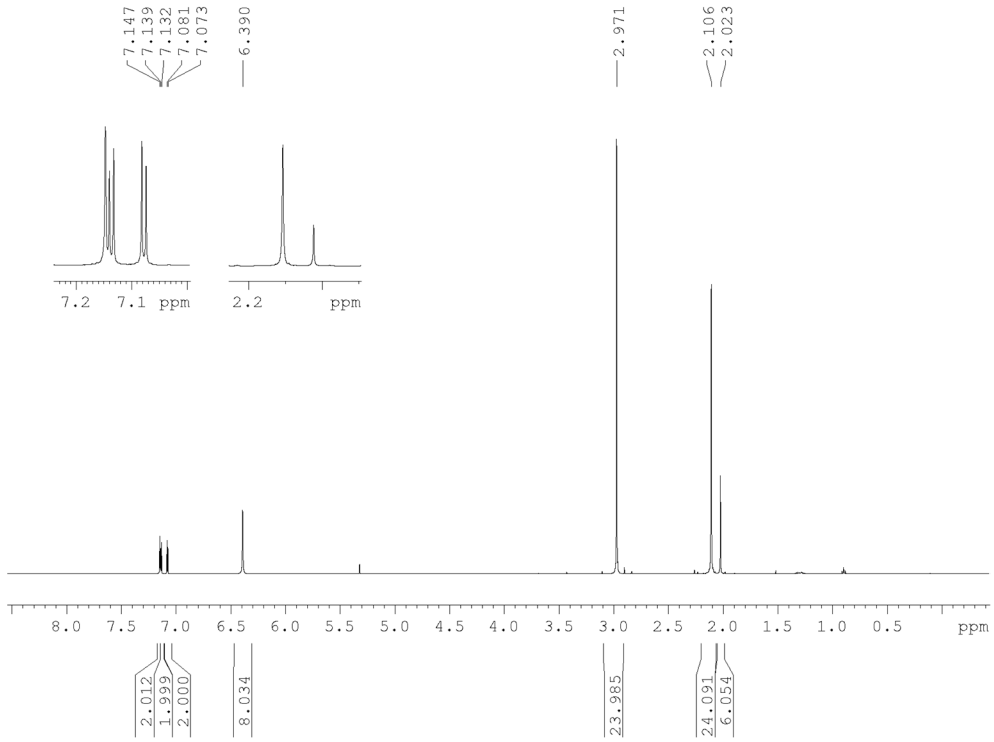

Figure A72. ^1H NMR spectrum of **5-2** in CD_2Cl_2 at 500 MHz.

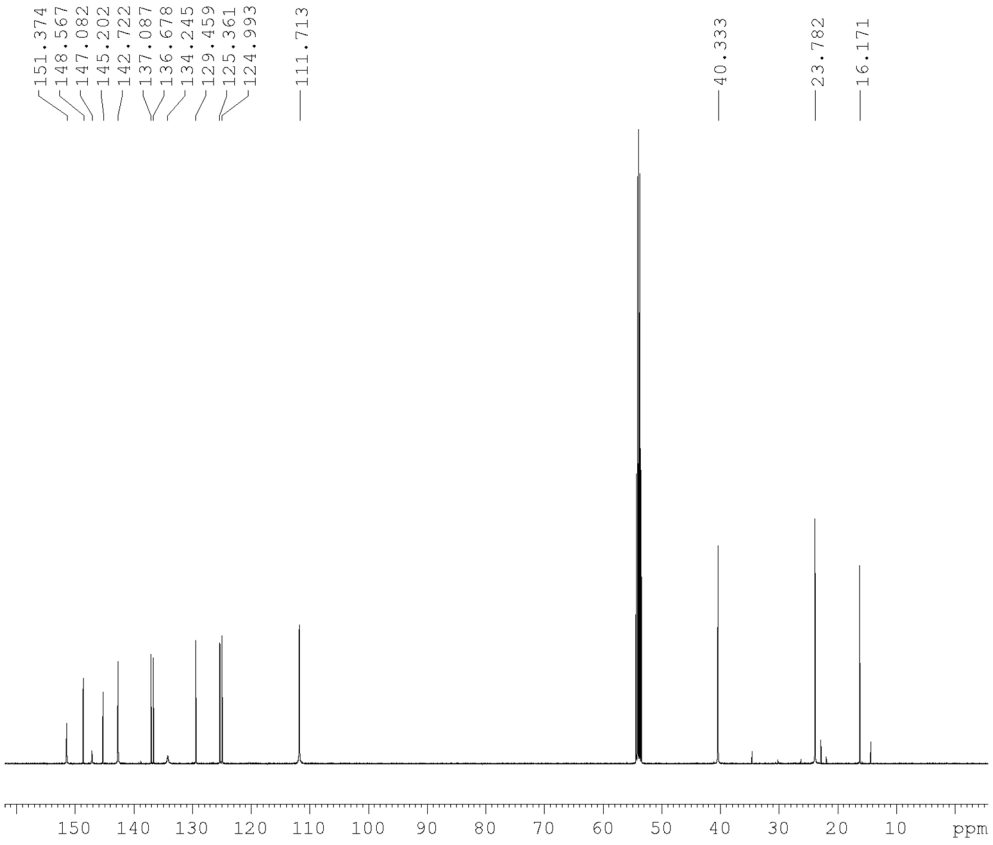

Figure A73. $^{13}C\{^{1}H\}$ NMR spectrum of **5-2** in CD_2Cl_2 at 125 MHz.

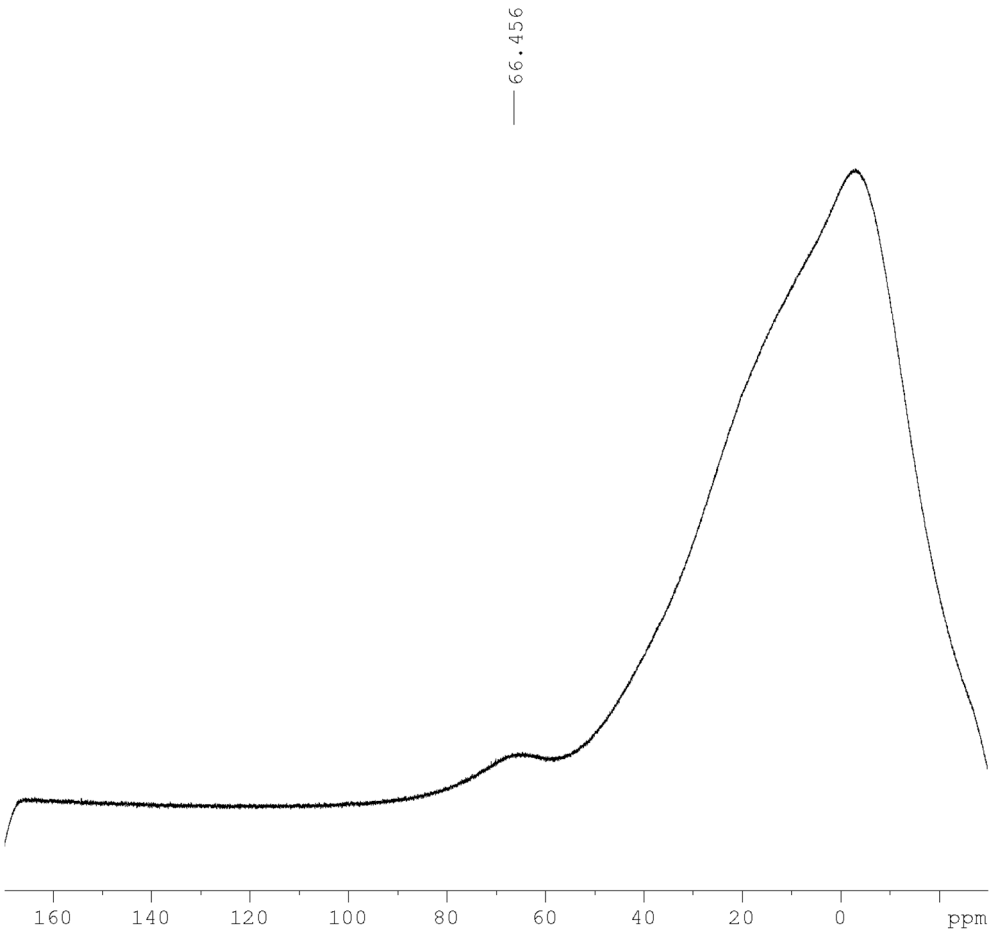

Figure A74. $^{11}B\{^{1}H\}$ NMR spectrum of **5-2** in CD_2Cl_2 at 160 MHz.

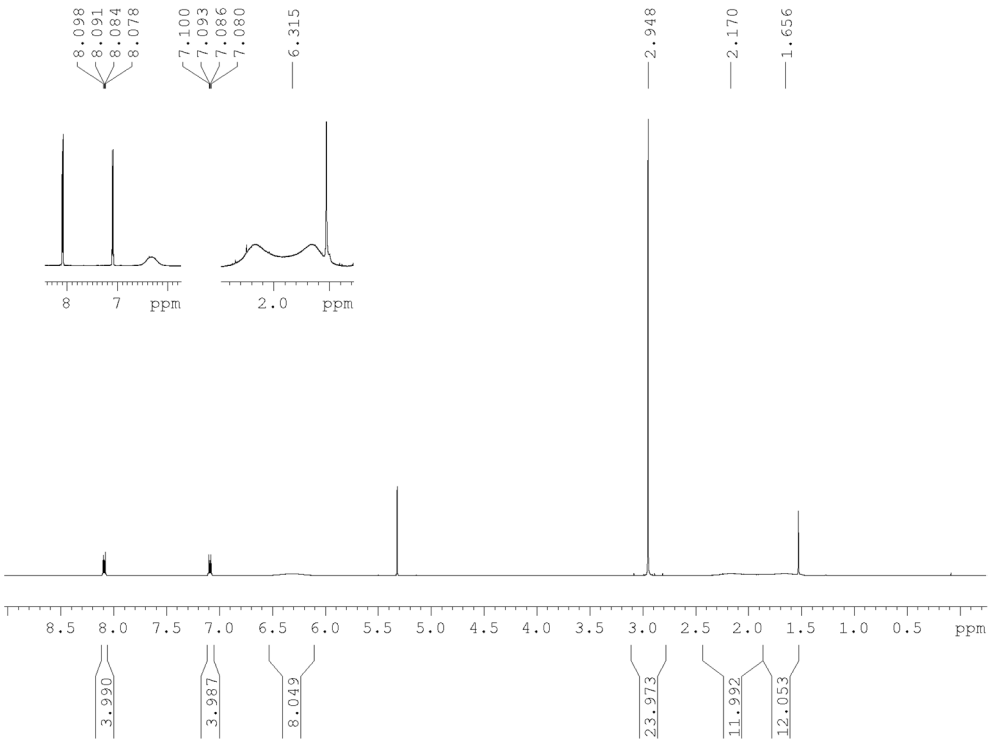

Figure A75. ^{1}H NMR spectrum of **5-3** in CD_2Cl_2 at 500 MHz.

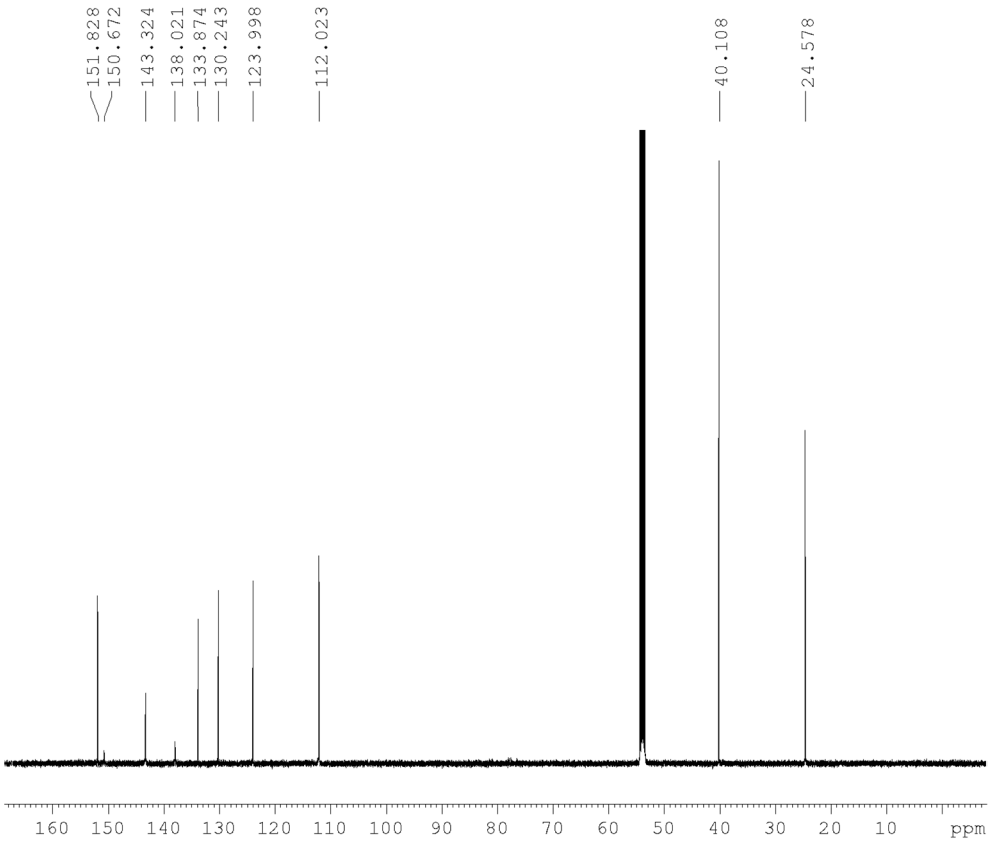

Figure A76. $^{13}C\{^{1}H\}$ NMR spectrum of **5-3** in CD_2Cl_2 at 125 MHz.

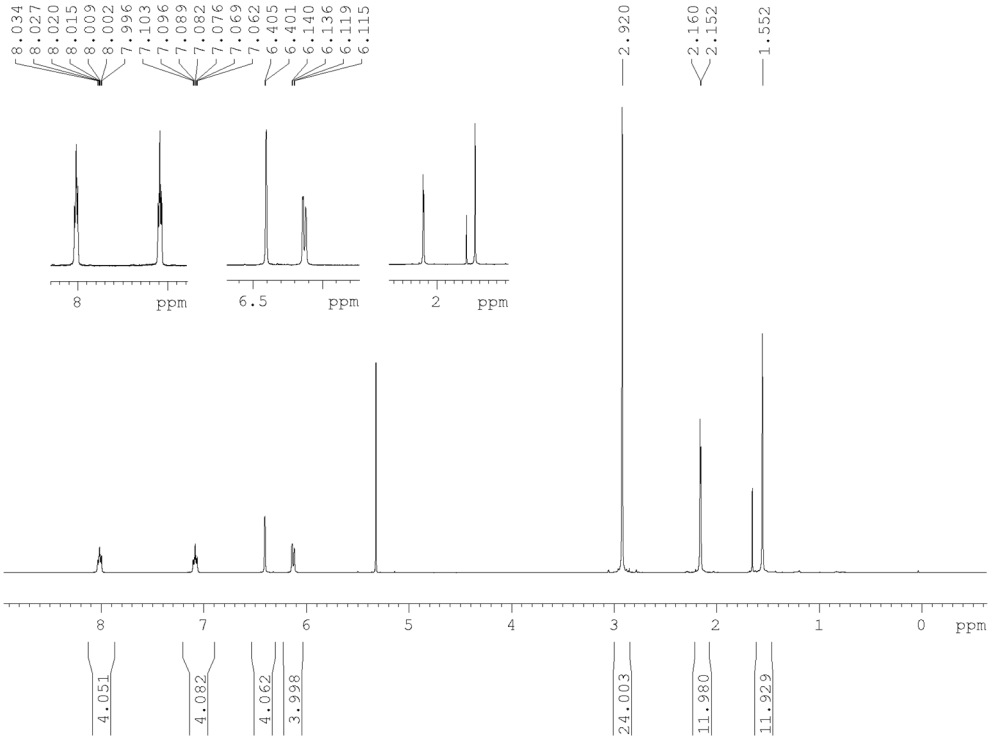

Figure A77. ^{1}H NMR spectrum of **5-3** in CD_2Cl_2 at 500 MHz at 235 K.

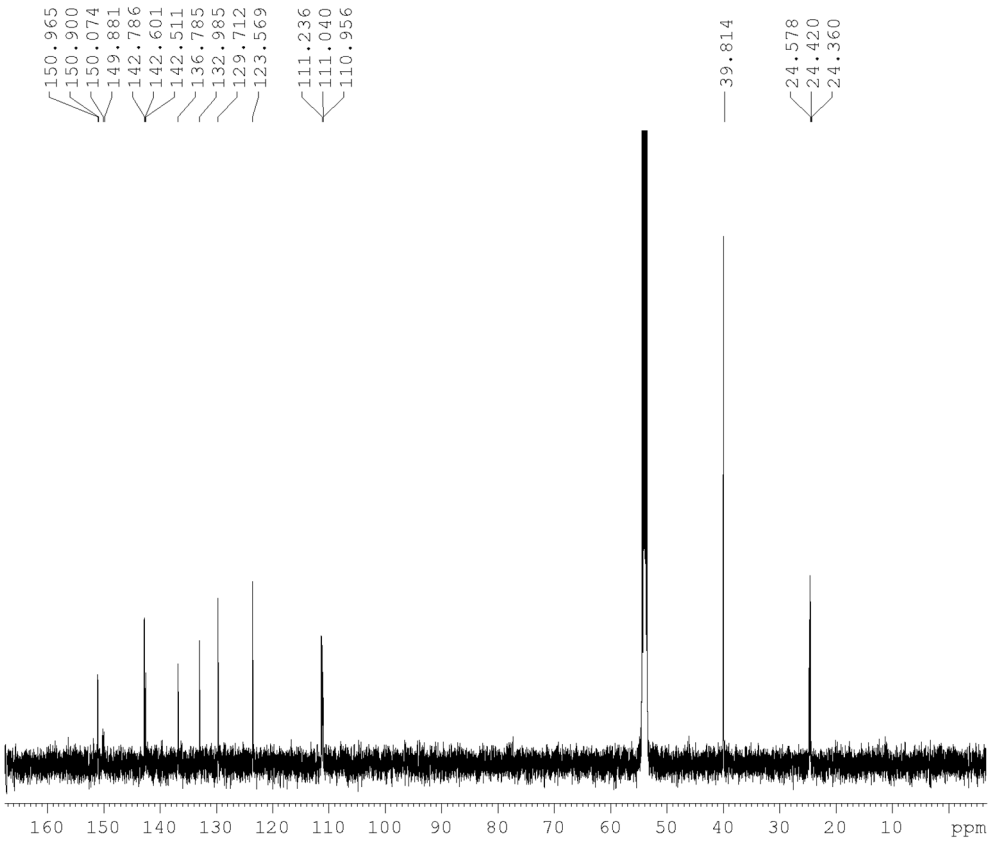

Figure A78. $^{13}C\{^{1}H\}$ NMR spectrum of **5-3** in CD_2Cl_2 at 125 MHz at 235 K.

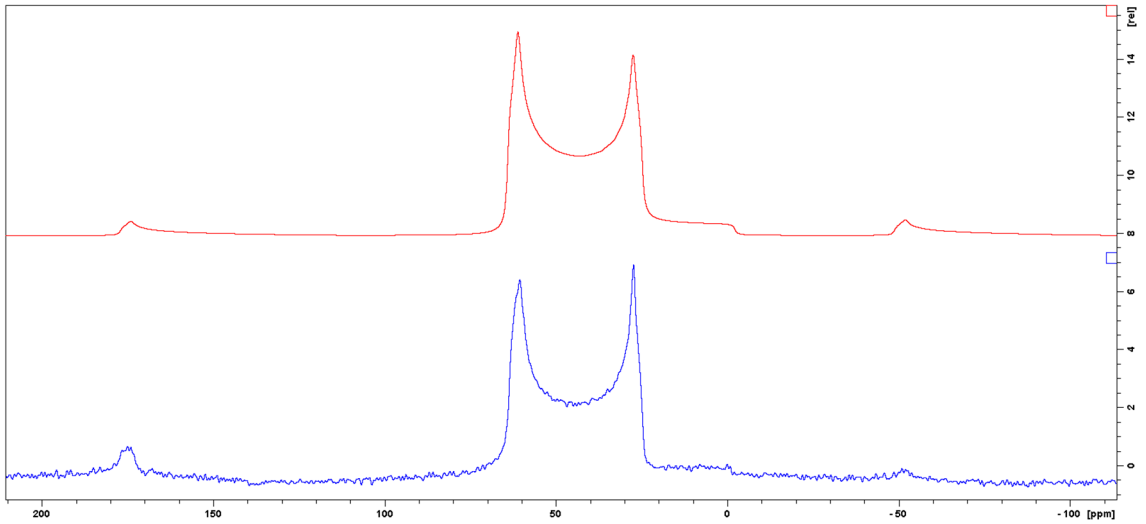

Figure A79. Solid-state $^{11}B\{^1H\}$ NMR spectrum of **5-3** at 128 MHz (top: simulation). Isotropic chemical shift δ_{iso} = 73.6 ppm, quadrupolar coupling constant C_Q = 4.47 MHz, quadrupolar asymmetry parameter η_{Quad} = 0.1.

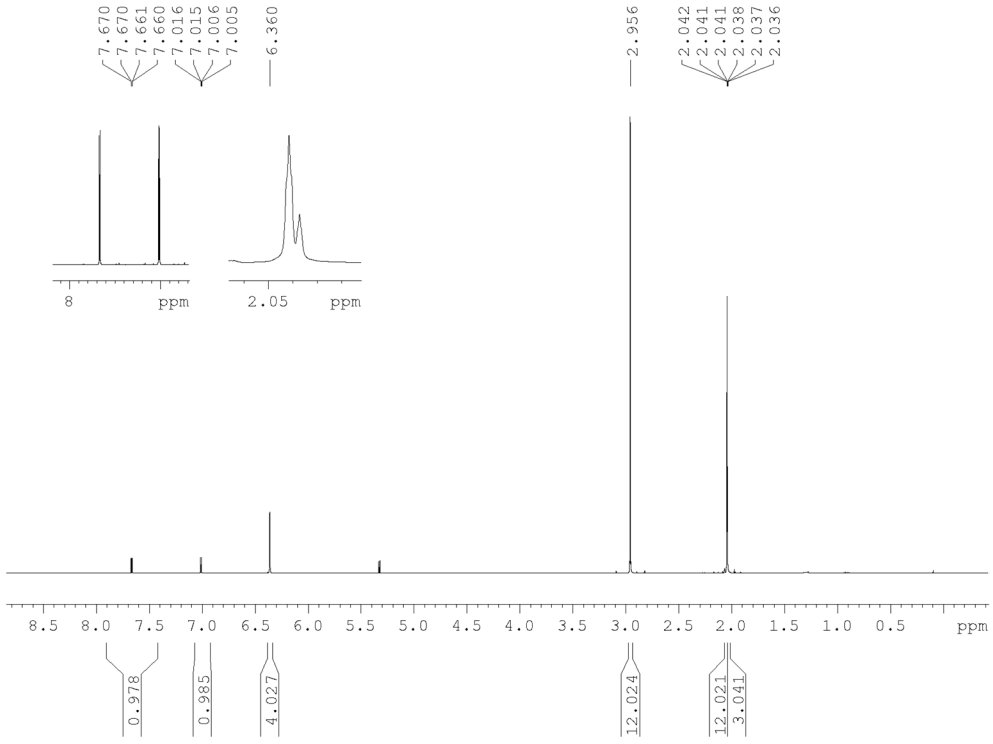

Figure A80. ^1H NMR spectrum of **5-4** in CD_2Cl_2 at 500 MHz.

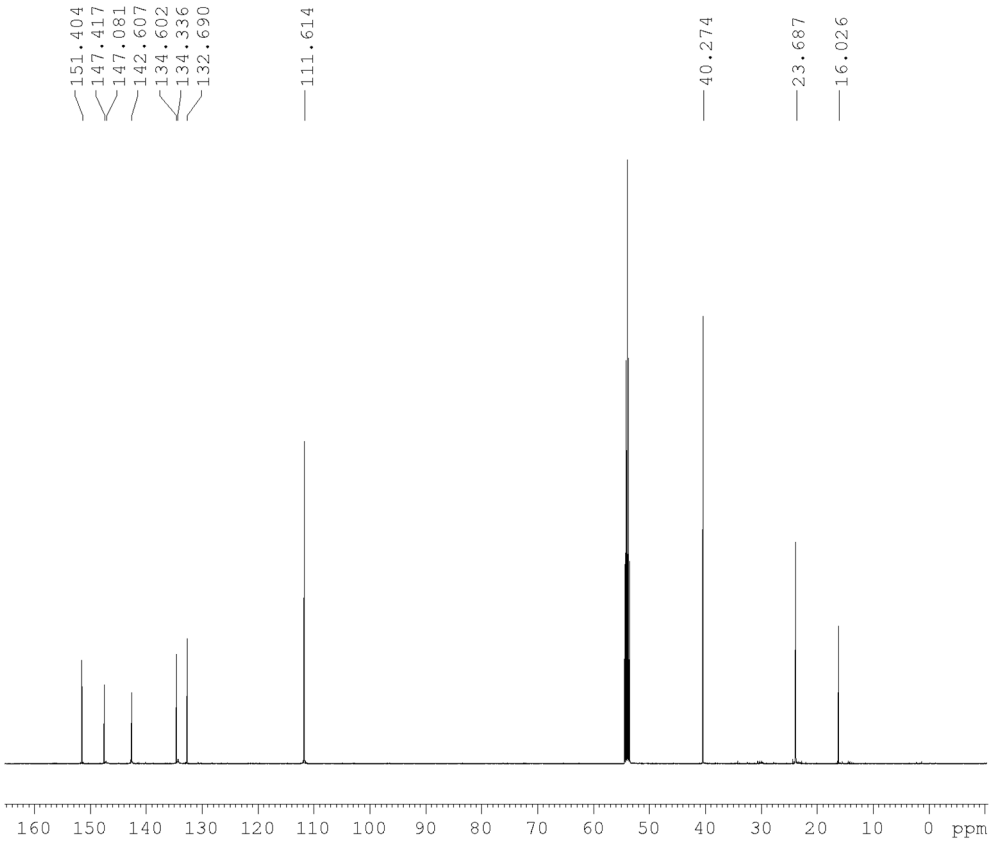

Figure A81. $^{13}C\{^{1}H\}$ NMR spectrum of **5-4** in CD_2Cl_2 at 125 MHz.

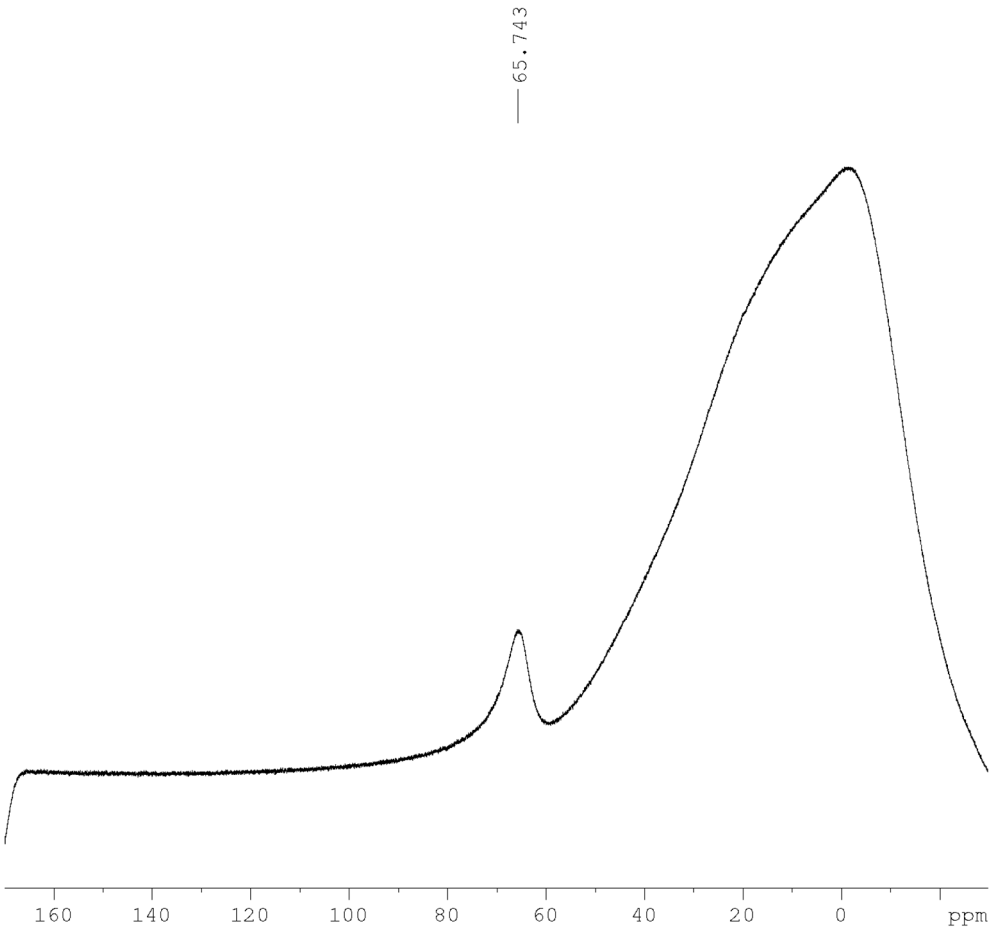

Figure A82. $^{11}B\{^{1}H\}$ NMR spectrum of **5-4** in CD_2Cl_2 at 160 MHz.

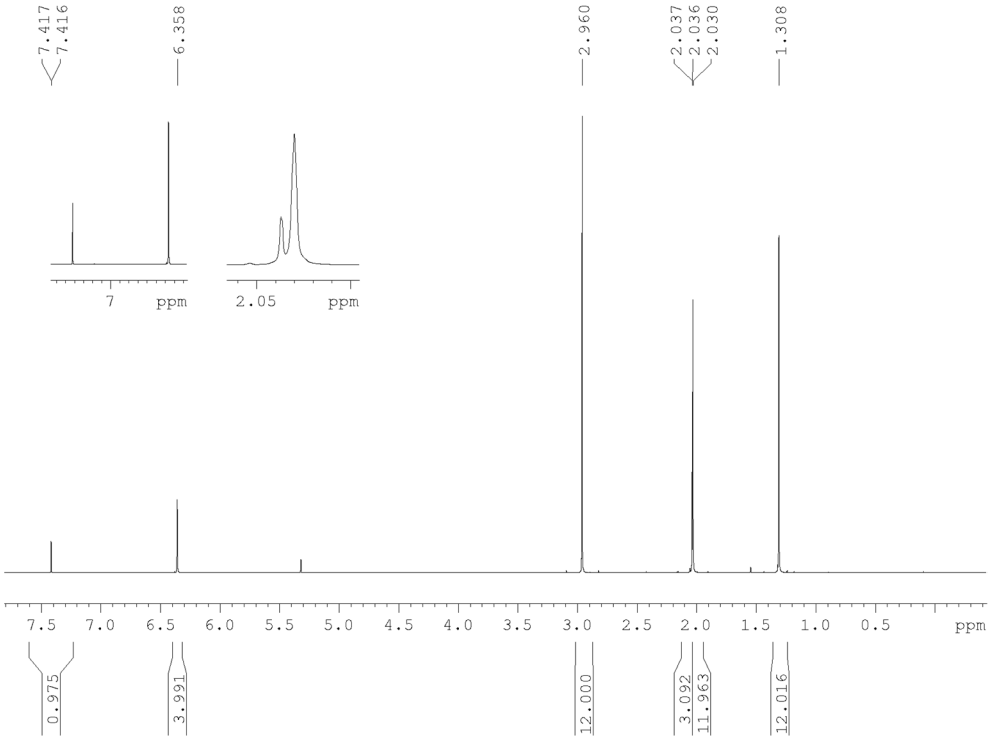

Figure A83. ^{1}H NMR spectrum of **5-5** in CD_2Cl_2 at 500 MHz.

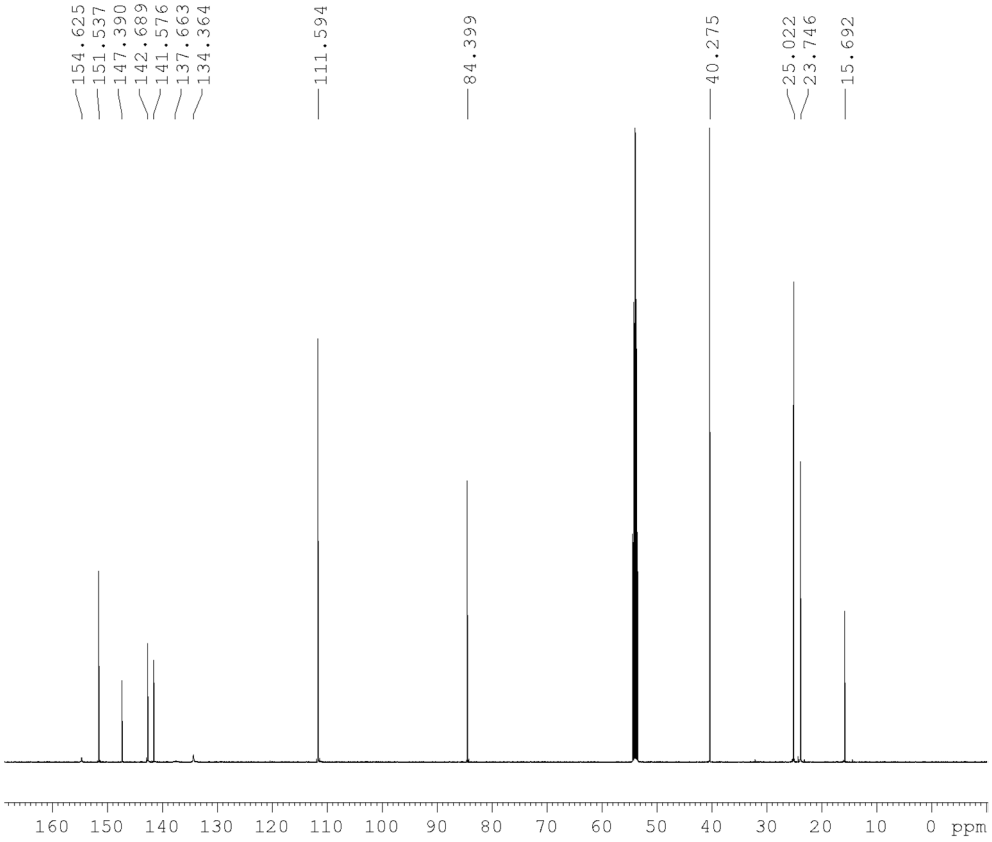

Figure A84. $^{13}C\{^{1}H\}$ NMR spectrum of **5-5** in CD_2Cl_2 at 125 MHz.

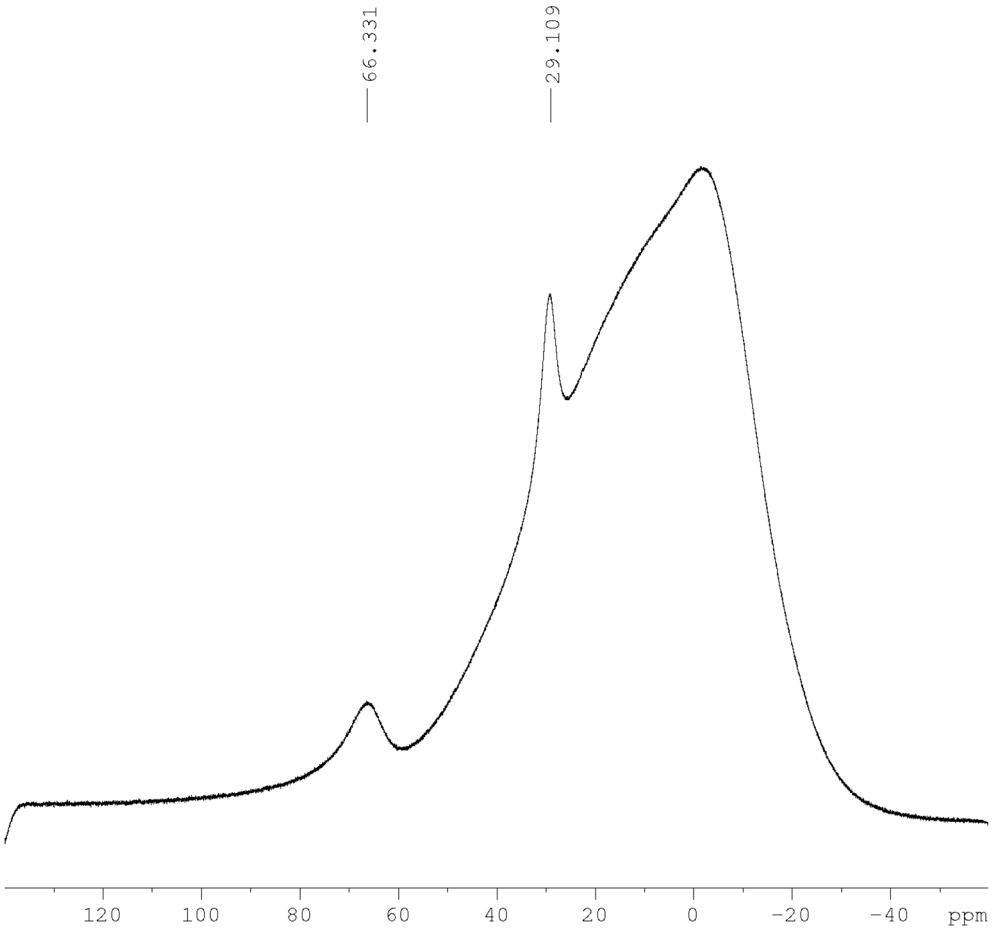

Figure A85. $^{11}B\{^{1}H\}$ NMR spectrum of **5-5** in CD_2Cl_2 at 160 MHz.

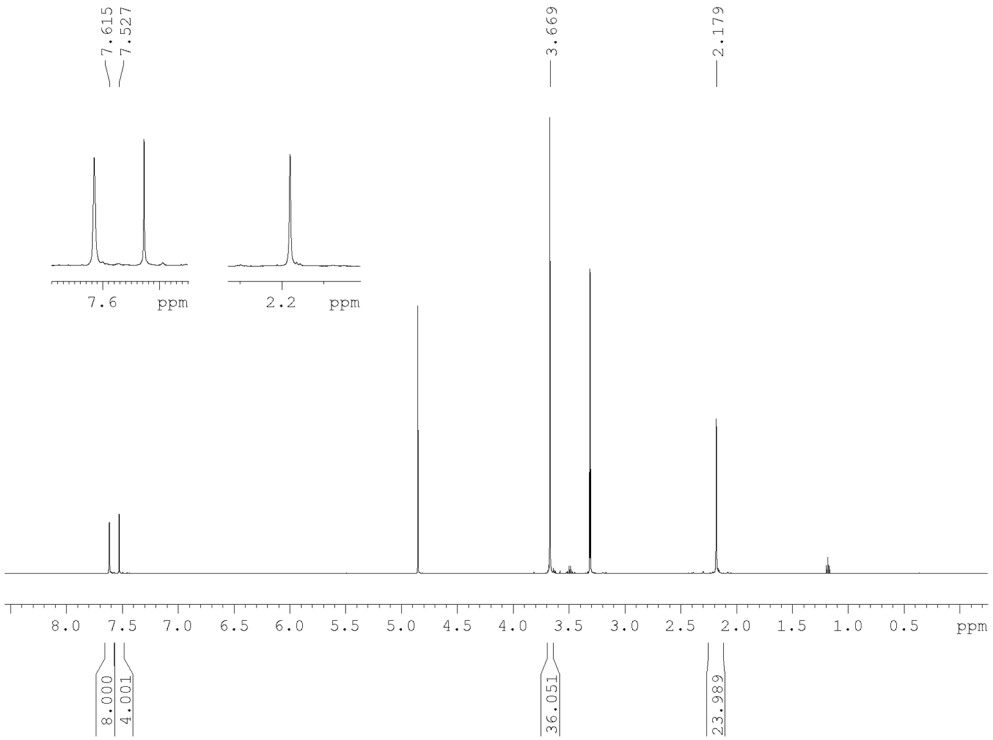

Figure A86. ^{1}H NMR spectrum of **5-1M** in CD_3OD at 500 MHz.

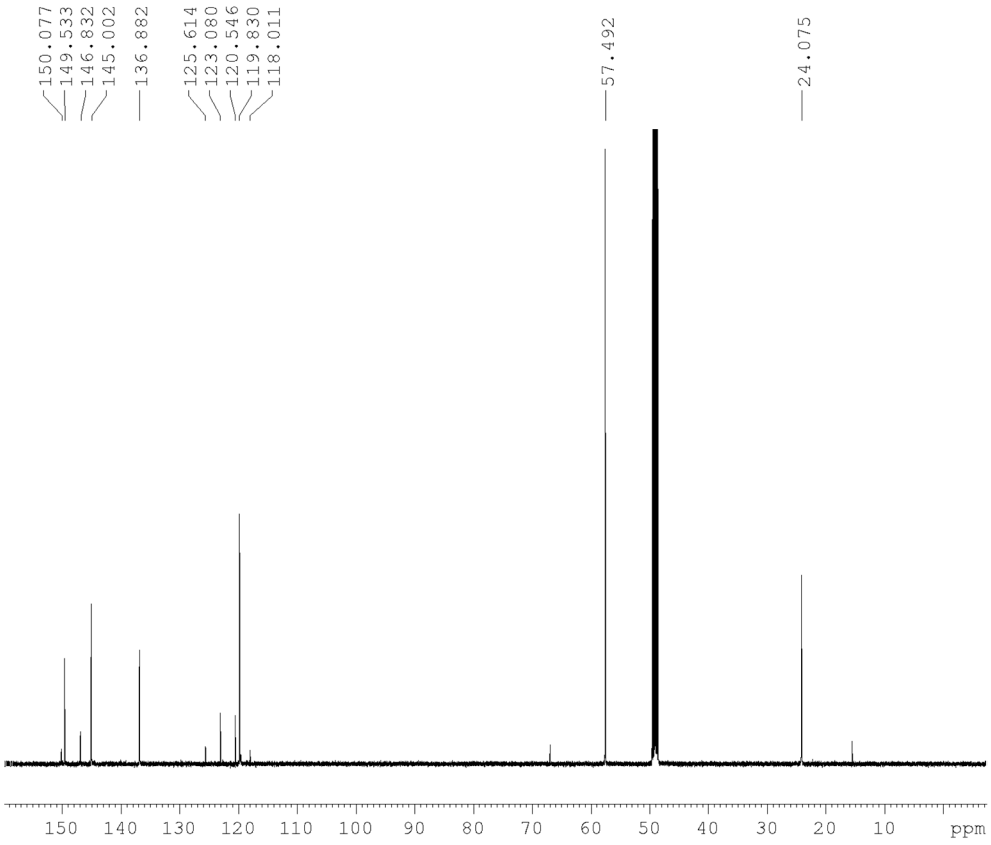

Figure A87. $^{13}C\{^{1}H\}$ NMR spectrum of **5-1M** in CD_3OD at 125 MHz.

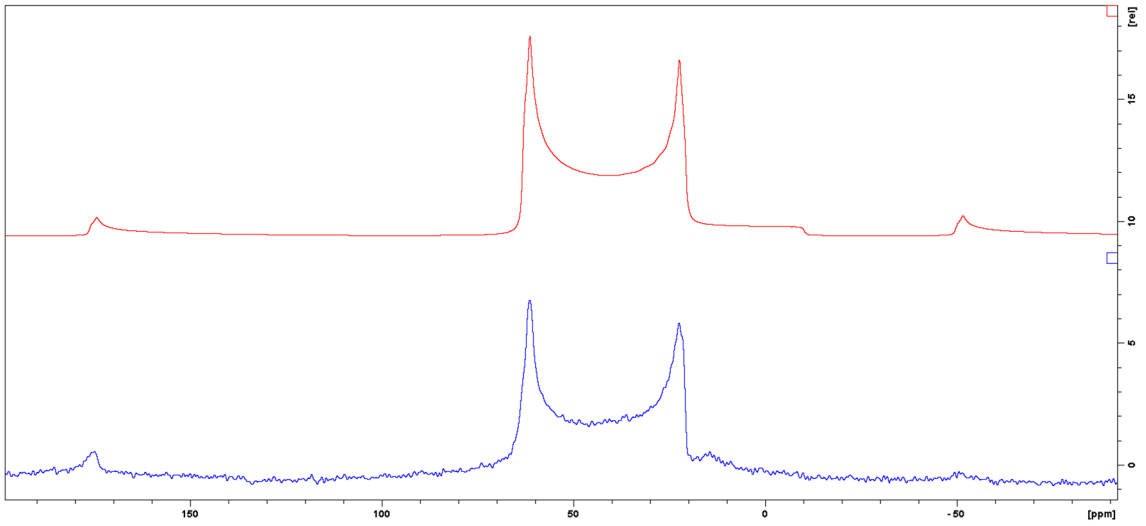

Figure A88. Solid-state $^{11}B\{^{1}H\}$ NMR spectrum of **5-1M** at 128 MHz (top: simulation). Isotropic chemical shift δ_{iso} = 74.6 ppm, quadrupolar coupling constant C_Q = 4.73 MHz, quadrupolar asymmetry parameter η_{Quad} = 0.0.

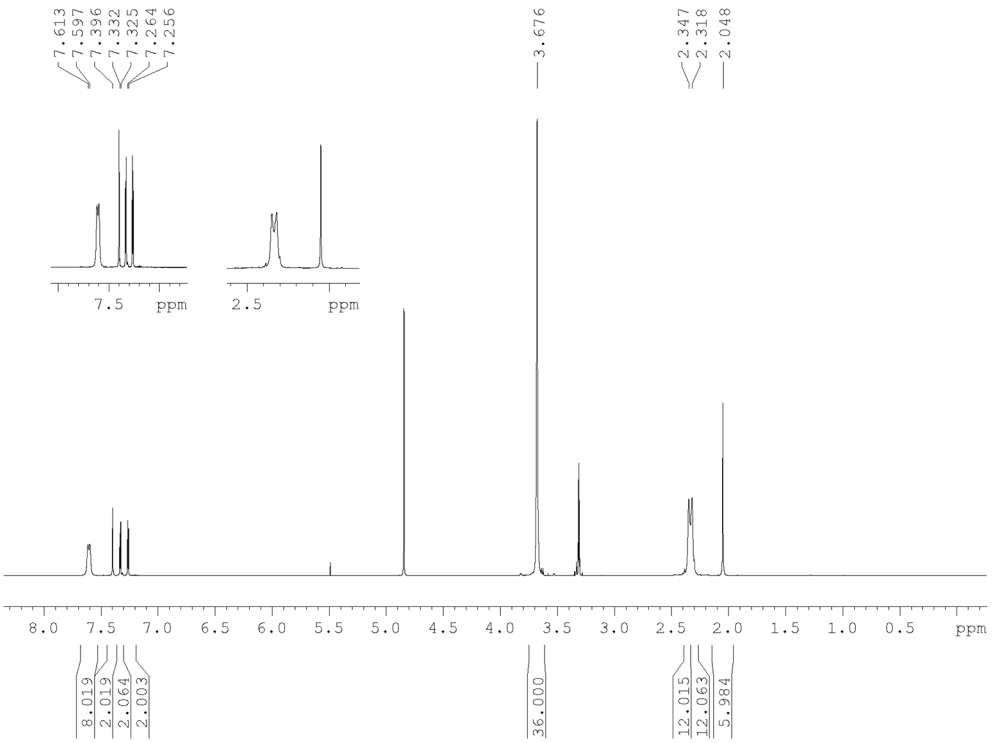

Figure A89. ^{1}H NMR spectrum of **5-2M** in CD_3OD at 500 MHz.

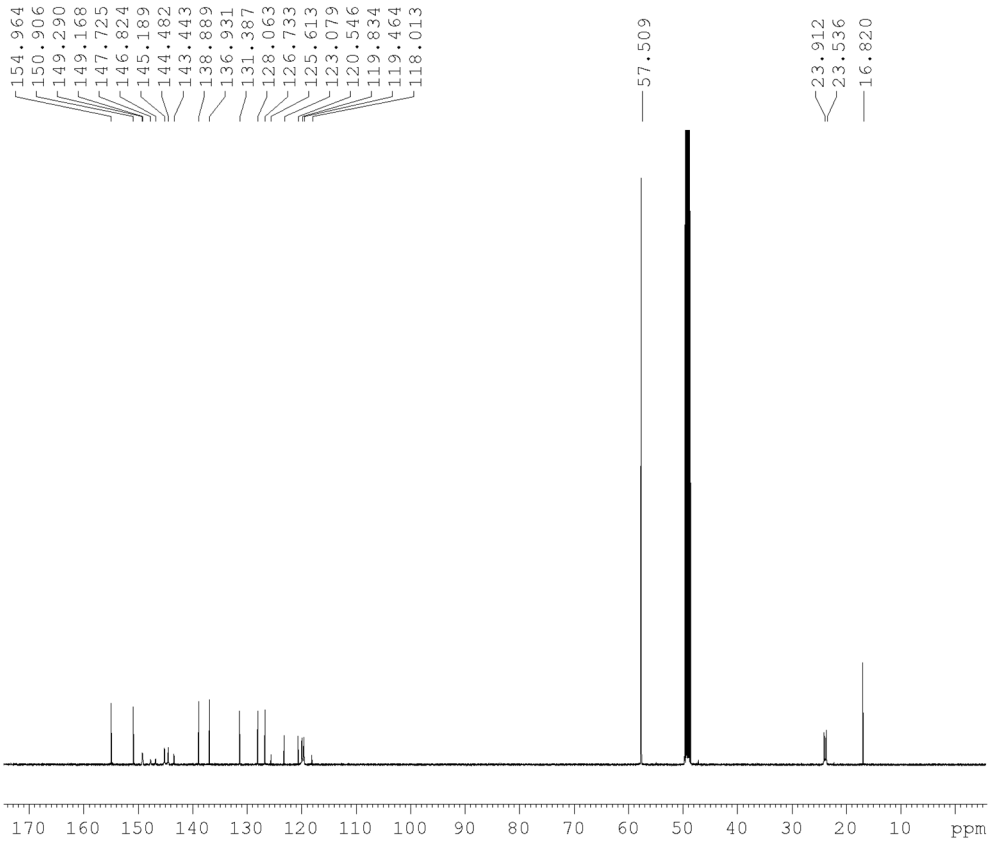

Figure A90. $^{13}C\{^{1}H\}$ NMR spectrum of **5-2M** in CD_3OD at 125 MHz.

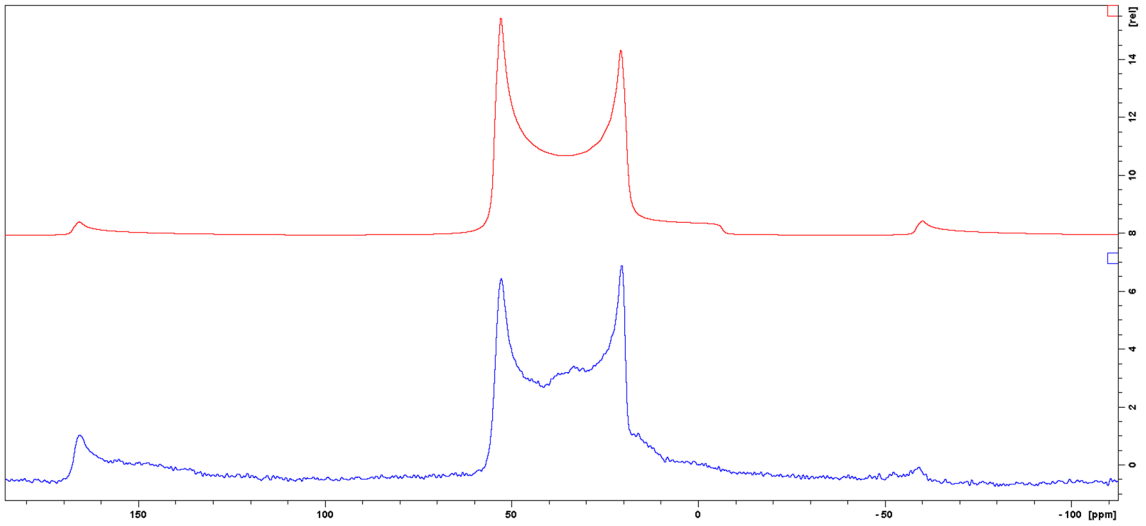

Figure A91. Solid-state $^{11}B\{^1H\}$ NMR spectrum of **5-2M** at 128 MHz (top: simulation). Isotropic chemical shift δ_{iso} = 64.0 ppm, quadrupolar coupling constant C_Q = 4.31 MHz, quadrupolar asymmetry parameter η_{Quad} = 0.0.

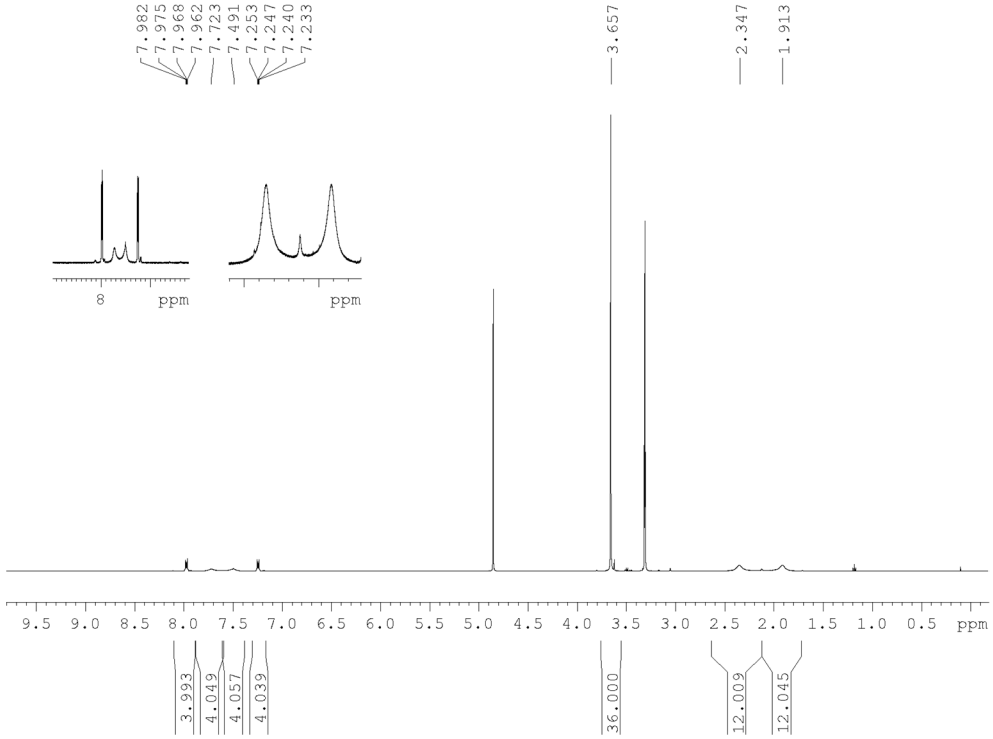

Figure A92. ^1H NMR spectrum of **5-3M** in CD_3OD at 500 MHz.

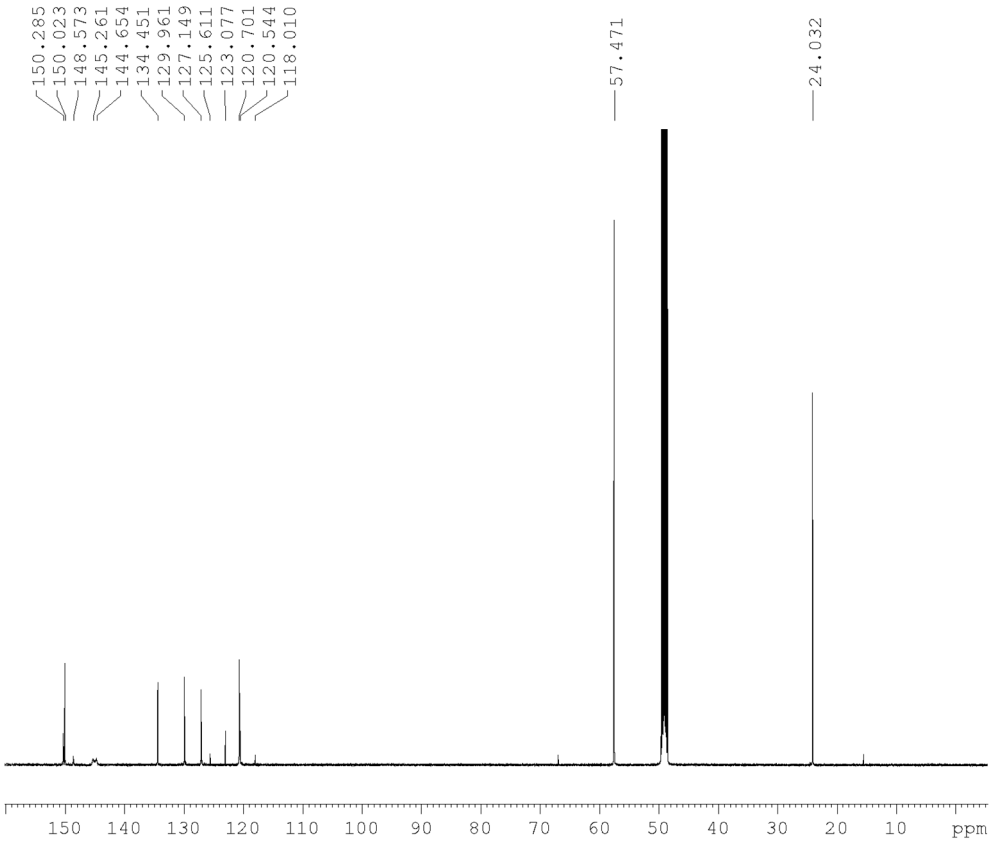

Figure A93. $^{13}C\{^{1}H\}$ NMR spectrum of **5-3M** in CD_3OD at 125 MHz.

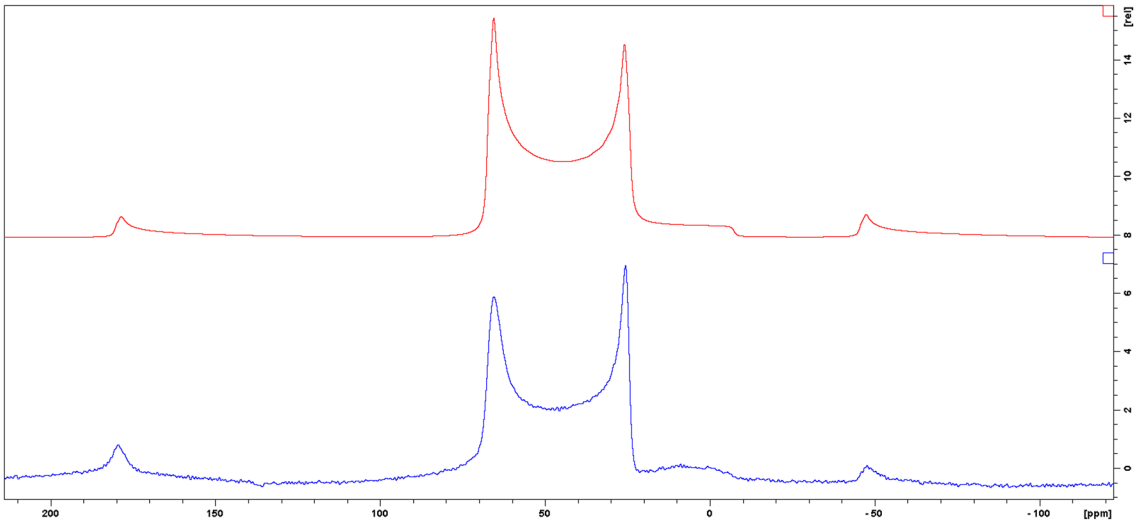

Figure A94. Solid-state $^{11}B\{^{1}H\}$ NMR spectrum of **5-3M** at 128 MHz (top: simulation). Isotropic chemical shift δ_{iso} = 79.0 ppm, quadrupolar coupling constant C_Q = 4.78 MHz, quadrupolar asymmetry parameter η_{Quad} = 0.0.

CARTESIAN COORDINATES FOR ALL DFT-OPTIMIZED STRUCTURES

Compound 2-1M

DFT B3LYP/6-31G(d), gas phase, S_0

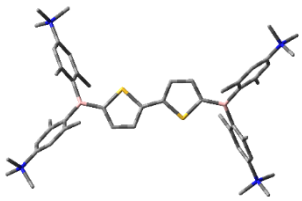

Point group: C_2
Total energy: –1 938 287.96 kcal mol^{-1}
Imaginary frequencies: 0

Symbol	X	Y	Z
C	3.084786	7.563626	-1.491846
C	-1.791898	5.062777	1.877032
C	-3.510724	6.510056	0.203880
H	-4.154514	7.056747	-0.472432
C	1.120350	5.752353	-0.556140
C	-2.301253	6.013913	-0.302444
C	1.694232	6.722993	0.304807
C	2.538401	6.619005	-2.354412
C	1.574896	5.706498	-1.901269
C	1.065504	4.705178	-2.921083
C	2.672798	7.611968	-0.165269
C	-1.409891	5.283803	0.527978
C	-3.002081	5.578886	2.364997
C	-3.852544	6.300049	1.535656
C	-0.934459	4.317187	2.881729
C	1.307967	6.831038	1.764099
C	-2.013143	6.261022	-1.767066
B	-0.010637	4.744411	-0.032502
H	2.840762	6.563208	-3.395404
H	3.081666	8.328536	0.534806
H	-3.244423	5.401880	3.408496
H	-1.475243	3.455226	3.289085
H	-0.677890	4.964912	3.728306
H	-0.004167	3.944427	2.453069
H	0.075252	4.317523	-2.679639
H	1.014959	5.155420	-3.917602
H	1.737098	3.840992	-2.989765
H	1.513891	5.900267	2.304004
H	-1.036654	6.731935	-1.912380
H	1.866539	7.625745	2.265747
H	0.242123	7.050415	1.880699
H	-2.016822	5.324317	-2.336956
H	-2.766437	6.913170	-2.217140
C	-5.992533	5.715725	2.648325
H	-5.450294	5.190190	3.432000
H	-6.915192	6.135287	3.052454
H	-6.211322	5.036950	1.823698
C	-4.816314	7.812840	3.248800
H	-4.200708	8.619128	2.849488
H	-5.752863	8.208749	3.644803
H	-4.276711	7.282892	4.031369
C	5.314289	7.758909	-2.563947
H	4.993720	7.099686	-3.368343
H	6.048019	8.473702	-2.939899
H	5.736019	7.174880	-1.745604
C	3.510724	9.352365	-3.157142
H	2.653135	9.895387	-2.759407
H	4.266224	10.048903	-3.524150
H	3.194298	8.690644	-3.961158
C	4.628365	9.495327	-0.989466
H	3.798912	10.093857	-0.614406
H	5.101161	8.937890	-0.181534
H	5.362653	10.144579	-1.466610
C	-5.967574	7.607301	1.104078
H	-5.396515	8.456134	0.729608
H	-6.244057	6.936928	0.290950
H	-6.865914	7.963794	1.608372
N	-5.138113	6.851817	2.117770
N	4.118180	8.529168	-2.034760
C	0.288980	3.235524	-0.081279
C	1.526580	2.612286	-0.235352
S	-0.950060	1.995273	0.083945
C	1.489565	1.206697	-0.220114
H	2.444674	3.179370	-0.347103
C	0.204773	0.695878	-0.074867
H	2.366527	0.579188	-0.337212
C	-0.204773	-0.695878	-0.074867
S	0.950060	-1.995273	0.083945
C	-1.489565	-1.206697	-0.220114
C	-0.288980	-3.235524	-0.081279
C	-1.526580	-2.612286	-0.235352
H	-2.366527	-0.579188	-0.337212
B	0.010637	-4.744411	-0.032502
H	-2.444674	-3.179370	-0.347103
C	-1.120350	-5.752353	-0.556140
C	1.409891	-5.283803	0.527978
C	-1.694232	-6.722993	0.304807
C	-1.574896	-5.706498	-1.901269
C	1.791898	-5.062777	1.877032
C	2.301253	-6.013913	-0.302444
C	-2.672798	-7.611968	-0.165269
C	-1.307967	-6.831038	1.764099
C	-2.538401	-6.619005	-2.354412
C	-1.065504	-4.705178	-2.921083
C	3.002081	-5.578886	2.364997
C	0.934459	-4.317187	2.881729
C	3.510724	-6.510056	0.203880
C	2.013143	-6.261022	-1.767066
C	-3.084786	-7.563626	-1.491846
H	-3.081666	-8.328536	0.534806
H	-1.513891	-5.900267	2.304004
H	-1.866539	-7.625745	2.265747
H	-0.242123	-7.050415	1.880699
H	-2.840762	-6.563208	-3.395404
H	-0.075252	-4.317523	-2.679639
H	-1.014959	-5.155420	-3.917602
H	-1.737098	-3.840992	-2.989765
C	3.852544	-6.300049	1.535656
H	3.244423	-5.401880	3.408496
H	1.475243	-3.455226	3.289085
H	0.677890	-4.964912	3.728306
H	0.004167	-3.944427	2.453069
H	4.154514	-7.056747	-0.472432
H	1.036654	-6.731935	-1.912380
H	2.016822	-5.324317	-2.336956
H	2.766437	-6.913170	-2.217140
N	-4.118180	-8.529168	-2.034760
N	5.138113	-6.851817	2.117770
C	-5.314289	-7.758909	-2.563947
C	-3.510724	-9.352365	-3.157142
C	-4.628365	-9.495327	-0.989466
C	5.992533	-5.715725	2.648325
C	4.816314	-7.812840	3.248800
C	5.967574	-7.607301	1.104078
H	-4.993720	-7.099686	-3.368343
H	-6.048019	-8.473702	-2.939899
H	-5.736019	-7.174880	-1.745604
H	-2.653135	-9.895387	-2.759407
H	-4.266224	-10.048903	-3.524150
H	-3.194298	-8.690644	-3.961158

H	-3.798912	-10.093857	-0.614406
H	-5.101161	-8.937890	-0.181534
H	-5.362653	-10.144579	-1.466610
H	5.450294	-5.190190	3.432000
H	6.915192	-6.135287	3.052454
H	6.211322	-5.036950	1.823698
H	4.200708	-8.619128	2.849488
H	5.752863	-8.208749	3.644803
H	4.276711	-7.282892	4.031369
H	5.396515	-8.456134	0.729608
H	6.244057	-6.936928	0.290950
H	6.865914	-7.963794	1.608372

Compound 2-2M

DFT B3LYP/6-31G(d), gas phase, S_0

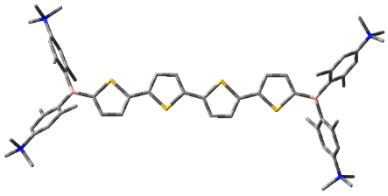

Point group: C_1
Total energy: –2 630 858.07 kcal mol^{-1}
Imaginary frequencies: 0

Symbol	X	Y	Z
C	-11.391098	-3.366988	1.228409
C	-8.998808	1.858472	-1.708103
C	-10.366936	3.435166	0.161080
H	-10.883579	4.020171	0.910585
C	-9.642616	-1.277828	0.458538
C	-9.890871	2.169668	0.531605
C	-10.621588	-1.784527	-0.434122
C	-10.443100	-2.885001	2.124191
C	-9.562543	-1.858829	1.752477
C	-8.553900	-1.429699	2.801421
C	-11.480403	-2.824511	-0.048052
C	-9.197587	1.350480	-0.397543
C	-9.491632	3.123765	-2.060673
C	-10.169985	3.904629	-1.132979
C	-8.293896	1.089972	-2.809276
C	-10.766965	-1.258221	-1.845321
C	-10.115035	1.740478	1.964868
B	-8.648252	-0.096849	0.019455
H	-10.357319	-3.288799	3.128253
H	-12.202907	-3.178244	-0.771768
H	-9.327001	3.466446	-3.077861
H	-7.417448	1.641974	-3.167556
H	-8.959381	0.947598	-3.669044
H	-7.947741	0.108881	-2.485425
H	-8.169978	-0.423387	2.634555
H	-8.996016	-1.462525	3.802642
H	-7.686718	-2.100824	2.807466
H	-9.854079	-1.421954	-2.428544
H	-10.585640	0.754775	2.021933
H	-11.583763	-1.756762	-2.374453
H	-10.972439	-0.183420	-1.852549
H	-9.168024	1.686212	2.514713
H	-10.756823	2.447688	2.497598
C	-9.523570	6.129809	-2.015950
H	-9.022720	5.656247	-2.858075
H	-9.912777	7.104797	-2.313969
H	-8.831219	6.233735	-1.180244
C	-11.663901	5.096220	-2.714959
H	-12.487306	4.468115	-2.374375
H	-12.030485	6.082337	-3.004890
H	-11.159237	4.625164	-3.556181
C	-11.495889	-5.699196	2.065866
H	-10.827171	-5.442116	2.884998
H	-12.178487	-6.491646	2.377156
H	-10.918085	-6.012774	1.196160
C	-13.126151	-4.018836	2.876912
H	-13.703559	-3.142575	2.581475
H	-13.790620	-4.829731	3.179857
H	-12.454097	-3.764141	3.694082
C	-13.288364	-4.909187	0.609037
H	-13.917786	-4.063650	0.333881
H	-12.736234	-5.277555	-0.254899
H	-13.905441	-5.708592	1.019722
C	-11.402508	6.000854	-0.462593
H	-12.263776	5.417579	-0.138817
H	-10.715467	6.167996	0.366209
H	-11.736186	6.958259	-0.863276
N	-10.684431	5.262371	-1.567972
N	-12.313810	-4.480531	1.681226
C	-7.152428	-0.389169	0.007748
C	-6.513655	-1.630400	0.080119
S	-5.915051	0.865183	-0.130303
C	-5.115005	-1.587247	0.019365
H	-7.072581	-2.557375	0.155810
C	-4.607924	-0.291600	-0.084776
H	-4.482933	-2.468139	0.049549
C	-3.226127	0.114000	-0.135969
C	-2.69722	1.389484	-0.252290
S	-1.931646	-1.070737	-0.041398
C	-1.289244	1.422475	-0.274007
H	-3.312858	2.279516	-0.326254
C	-0.701369	0.170580	-0.175884
H	-0.716787	2.338006	-0.375228
C	0.701374	-0.170514	-0.175896
C	1.289245	-1.422407	-0.274065
S	1.931657	1.070796	-0.041385
C	2.697220	-1.389421	-0.252361
H	0.716784	-2.337933	-0.375309
C	3.226133	-0.113943	-0.136002
H	3.312855	-2.279453	-0.326359
C	4.607933	0.291647	-0.084807
S	5.915045	-0.865153	-0.130339
C	5.115030	1.587285	0.019340
C	7.152437	0.389179	0.007722
C	6.513681	1.630420	0.080099
H	4.482970	2.468187	0.049521
B	8.648262	0.096845	0.019432
H	7.072619	2.557387	0.155792
C	9.642628	1.277815	0.458537
C	9.197591	-1.350481	-0.397572
C	10.621602	1.784514	-0.434120
C	9.562556	1.858812	1.752478
C	8.998829	-1.858474	-1.708134
C	9.890840	-2.169677	0.531592
C	11.480421	2.824494	-0.048048
C	10.766967	1.258209	-1.845320
C	10.443120	2.884977	2.124196
C	8.553892	1.429706	2.801412
C	9.491629	-3.123784	-2.060682
C	8.293979	-1.089961	-2.809337
C	10.366895	-3.435184	0.161085
C	10.114952	-1.740489	1.964864
C	11.391121	3.366963	1.228417
H	12.202926	3.178226	-0.771763
H	9.854038	1.421842	-2.428500
H	11.583696	1.756821	-2.374493
H	10.972547	0.183426	-1.852540
H	10.357336	3.288776	3.128258
H	8.169975	0.423389	2.634566
H	8.995986	1.462560	3.802642
H	7.686709	2.100830	2.807421
C	10.169957	-3.904653	-1.132974
H	9.327004	-3.466471	-3.077868

H	7.417802	-1.642156	-3.167973
H	8.959653	-0.947199	-3.668894
H	7.947440	-0.109041	-2.485365
H	10.883511	-4.020193	0.910606
H	10.585531	-0.754774	2.021948
H	9.167920	-1.686249	2.514677
H	10.756740	-2.447685	2.497613
N	12.313839	4.480498	1.681241
N	10.684384	-5.262408	-1.567950
C	11.495922	5.699149	2.065932
C	13.126211	4.018775	2.876895
C	13.288367	4.909185	0.609040
C	9.523509	-6.129836	-2.015914
C	11.663854	-5.096287	-2.714939
C	11.402454	-6.000885	-0.462562
H	10.827225	5.442044	2.885073
H	12.178523	6.491594	2.377227
H	10.918097	6.012747	1.196248
H	13.703615	3.142523	2.581422
H	13.790685	4.829664	3.179844
H	12.454178	3.764059	3.694075
H	13.917767	4.063650	0.333827
H	12.736215	5.277599	-0.254863
H	13.905468	5.708563	1.019740
H	9.022667	-5.656280	-2.858046
H	9.912702	-7.104836	-2.313916
H	8.831156	-6.233736	-1.180205
H	12.487268	-4.468188	-2.374367
H	12.030423	-6.082414	-3.004857
H	11.159195	-4.625237	-3.556169
H	12.263706	-5.417597	-0.138768
H	10.715401	-6.168043	0.366227
H	11.736151	-6.958284	-0.863243

Compound 2-3M

DFT B3LYP/6-31G(d), gas phase, S_0

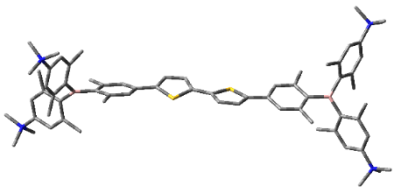

Point group: C_2
Total energy: –2 326 963.58 kcal mol^{-1}
Imaginary frequencies: 0

Symbol	X	Y	Z
C	0.263841	0.672765	0.200664
C	1.578494	1.088493	0.315912
C	1.734441	2.491353	0.282156
C	0.547261	3.186916	0.144489
S	-0.796024	2.060340	0.035390
H	2.406458	0.399850	0.445221
H	2.696575	2.978164	0.393521
C	-0.263841	-0.672765	0.200664
C	-1.578494	-1.088493	0.315912
S	0.796024	-2.060340	0.035390
C	-1.734441	-2.491353	0.282156
H	-2.406458	-0.399850	0.445221
C	-0.547261	-3.186916	0.144489
H	-2.696575	-2.978164	0.393521
C	0.347999	4.632489	0.093872
C	-0.901838	5.226627	0.335360
C	1.419696	5.494555	-0.198727
H	-1.754565	4.593254	0.565105
C	-1.087377	6.607951	0.318746
C	1.269670	6.877724	-0.257504
H	2.397029	5.070378	-0.407012
C	0.001273	7.484542	0.013583
C	-2.495013	7.100815	0.602305
C	2.519951	7.675770	-0.581688
B	-0.183351	9.038464	-0.016839
H	-2.578495	7.548849	1.598472
H	-2.834432	7.851082	-0.118825
H	-3.204528	6.269770	0.559523
H	2.489524	8.091537	-1.594586
H	2.678476	8.512606	0.106041
H	3.405178	7.036820	-0.519281
C	-1.030389	9.789714	1.120121
C	0.473920	9.925725	-1.181061
C	-2.095986	10.671011	0.810280
C	-0.706503	9.594479	2.491621
C	0.216755	9.611097	-2.544454
C	1.306077	11.038774	-0.903816
C	-2.814615	11.318311	1.828804
C	-2.536704	10.942587	-0.613740
C	-1.419696	10.269902	3.489330
C	0.399800	8.665749	2.951684
C	0.768768	10.392478	-3.566644
C	-0.644995	8.438261	-2.968330
C	1.870389	11.792999	-1.945760
C	1.656173	11.460109	0.508936
C	-2.471970	11.120112	3.159826
H	-3.629995	11.967788	1.538176
H	-2.728443	10.017069	-1.166641
H	-3.460110	11.528027	-0.636749
H	-1.775986	11.500259	-1.168973
H	-1.132628	10.102335	4.522307
H	1.323442	8.798426	2.381346
H	0.638118	8.834549	4.005885
H	0.108366	7.616611	2.838213
C	1.597803	11.470857	-3.268630
H	0.539040	10.124704	-4.592841
H	-0.126589	7.487602	-2.807227
H	-0.900153	8.504506	-4.029988
H	-1.582979	8.383671	-2.408473
H	2.513721	12.621403	-1.679320
H	0.784316	11.863385	1.033714
H	2.034969	10.623376	1.104767
H	2.430472	12.232383	0.510163
N	-3.221054	11.809281	4.282019
N	2.186978	12.266675	-4.415250
C	-3.839991	10.769567	5.197914
C	-2.265924	12.679550	5.077808
C	-4.337557	12.697701	3.785375
C	3.037169	11.358281	-5.284348
C	1.071213	12.866361	-5.250791
C	3.067443	13.403409	-3.951196
H	-3.053690	10.151206	5.626382
H	-4.383000	11.285234	5.991692
H	-4.519245	10.153939	4.607854
H	-1.831668	13.417759	4.403273
H	-2.826248	13.172712	5.873826
H	-1.481268	12.058515	5.505473
H	-3.922203	13.478378	3.149069
H	-5.061376	12.095982	3.236795
H	-4.817012	13.148115	4.654695
H	2.416746	10.561469	-5.689839
H	3.460350	11.951455	-6.096690
H	3.829958	10.936272	-4.666318
H	0.472439	13.513621	-4.609654
H	1.516766	13.441314	-6.064242
H	0.452842	12.067657	-5.655670
H	2.478162	14.094562	-3.349582
H	3.900979	13.002982	-3.375203
H	3.444565	13.915907	-4.836399
C	-0.347999	-4.632489	0.093872
C	0.901838	-5.226627	0.335360
C	-1.419696	-5.494555	-0.198727

H	1.754565	-4.593254	0.565105
C	1.087377	-6.607951	0.318746
C	-1.269670	-6.877724	-0.257504
H	-2.397029	-5.070378	-0.407012
C	-0.001273	-7.484542	0.013583
C	2.495013	-7.100815	0.602305
C	-2.519951	-7.675770	-0.581688
B	0.183351	-9.038464	-0.016839
H	2.578495	-7.548849	1.598472
H	2.834432	-7.851082	-0.118825
H	3.204528	-6.269770	0.559523
H	-2.489524	-8.091537	-1.594586
H	-2.678476	-8.512606	0.106041
H	-3.405178	-7.036820	-0.519281
C	1.030389	-9.789714	1.120121
C	-0.473920	-9.925725	-1.181061
C	2.095986	-10.671011	0.810280
C	0.706503	-9.594479	2.491621
C	-0.216755	-9.611097	-2.544454
C	-1.306077	-11.038774	-0.903816
C	2.814615	-11.318311	1.828804
C	2.536704	-10.942587	-0.613740
C	1.419696	-10.269902	3.489330
C	-0.399800	-8.665749	2.951684
C	-0.768768	-10.392478	-3.566644
C	0.644995	-8.438261	-2.968330
C	-1.870389	-11.792999	-1.945760
C	-1.656173	-11.460109	0.508936
C	2.471970	-11.120112	3.159826
H	3.629995	-11.967788	1.538176
H	2.728443	-10.017069	-1.166641
H	3.460110	-11.528027	-0.636749
H	1.775986	-11.500259	-1.168973
H	1.132628	-10.102335	4.522307
H	-1.323442	-8.798426	2.381346
H	-0.638118	-8.834549	4.005885
H	-0.108366	-7.616611	2.838213
C	-1.597803	-11.470857	-3.268630
H	-0.539040	-10.124704	-4.592841
H	0.126589	-7.487602	-2.807227
H	0.900153	-8.504506	-4.029988
H	1.582979	-8.383671	-2.408473
H	-2.513721	-12.621403	-1.679320
H	-0.784316	-11.863385	1.033714
H	-2.034969	-10.623376	1.104767
H	-2.430472	-12.232383	0.510163
N	3.221054	-11.809281	4.282019
N	-2.186978	-12.266675	-4.415250
C	3.839991	-10.769567	5.197914
C	2.265924	-12.679550	5.077808
C	4.337557	-12.697701	3.785375
C	-3.037169	-11.358281	-5.284348
C	-1.071213	-12.866361	-5.250791
C	-3.067443	-13.403409	-3.951196
H	3.053690	-10.151206	5.626382
H	4.383000	-11.285234	5.991692
H	4.519245	-10.153939	4.607854
H	1.831668	-13.417759	4.403273
H	2.826248	-13.172712	5.873826
H	1.481268	-12.058515	5.505473
H	3.922203	-13.478378	3.149069
H	5.061376	-12.095982	3.236795
H	4.817012	-13.148115	4.654695
H	-2.416746	-10.561469	-5.689839
H	-3.460350	-11.951455	-6.096690
H	-3.829958	-10.936272	-4.666318
H	-0.472439	-13.513621	-4.609654
H	-1.516766	-13.441314	-6.064242
H	-0.452842	-12.067657	-5.655670
H	-2.478162	-14.094562	-3.349582
H	-3.900979	-13.002982	-3.375203
H	-3.444565	-13.915907	-4.836399

Compound 3-1

DFT B3LYP/6-31G(d), gas phase, S_0

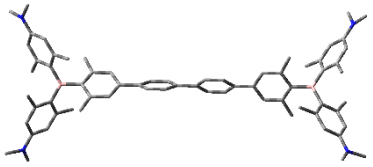

Point group: C_2
Total energy: -1823763.90 kcal mol^{-1}
Dipole moment: 0.57 D
Imaginary frequencies: 0

Symbol	X	Y	Z
C	0.000081	0.741285	-0.019291
C	0.000076	3.594646	-0.017680
C	1.144918	1.472035	0.342532
C	-1.144652	1.472447	-0.380616
C	-1.145104	2.863425	-0.377929
C	1.145355	2.863005	0.341408
H	2.043537	0.942437	0.646596
H	-2.043269	0.943193	-0.685282
H	-2.055132	3.393611	-0.644168
H	2.055393	3.392897	0.608199
C	-0.000081	-0.741285	-0.019291
C	-0.000076	-3.594646	-0.017680
C	1.144652	-1.472447	-0.380616
C	-1.144918	-1.472035	0.342532
C	-1.145355	-2.863005	0.341408
C	1.145104	-2.863425	-0.377929
H	2.043269	-0.943193	-0.685282
H	-2.043537	-0.942437	0.646596
H	-2.055393	-3.392897	0.608199
H	2.055132	-3.393611	-0.644168
C	0.000076	-5.077308	-0.016084
C	0.000577	-7.939962	-0.012238
C	0.728849	-5.807097	-0.963839
C	-0.728317	-5.804834	0.933805
C	-0.728027	-7.201991	0.959712
C	0.729159	-7.204399	-0.985947
H	1.285757	-5.272458	-1.729524
H	-1.285057	-5.268274	1.698263
C	-0.000076	5.077308	-0.016084
C	-0.000577	7.939962	-0.012238
C	0.728317	5.804834	0.933805
C	-0.728849	5.807097	-0.963839
C	-0.729159	7.204399	-0.985947
C	0.728027	7.201991	0.959712
H	1.285057	5.268274	1.698263
H	-1.285757	5.272458	-1.729524
C	-1.536761	-7.876059	2.052809
H	-0.892438	-8.339740	2.807011
H	-2.183837	-8.669865	1.664326
H	-2.177935	-7.147361	2.560120
C	1.538974	-7.881023	-2.076696
H	2.179216	-8.679706	-1.687085
H	2.186810	-7.155085	-2.579479
H	0.895387	-8.338940	-2.835091
C	-1.538974	7.881023	-2.076696
H	-0.895387	8.338940	-2.835091
H	-2.179216	8.679706	-1.687085
H	-2.186810	7.155085	-2.579479
C	1.536761	7.876059	2.052809
H	2.183837	8.669865	1.664326
H	2.177935	7.147361	2.560120
H	0.892438	8.339740	2.807011
B	0.000894	-9.533158	-0.010505

B	-0.000894	9.533158	-0.010505
C	-0.367473	-10.313887	-1.331486
C	-1.005761	-11.735162	-3.757090
C	0.427165	-11.402310	-1.793693
C	-1.495996	-9.968384	-2.128585
C	-1.809030	-10.676420	-3.288639
C	0.116846	-12.074114	-2.975868
H	-2.701998	-10.392100	-3.833574
H	0.771131	-12.879329	-3.290167
C	0.370320	-10.312661	1.311011
C	1.018832	-11.743870	3.728105
C	-0.427166	-11.396981	1.777041
C	1.498199	-9.965546	2.108482
C	1.811361	-10.673156	3.268648
C	-0.116902	-12.068215	2.959726
H	2.694944	-10.377390	3.822763
H	-0.782298	-12.859844	3.284809
C	-0.370320	10.312661	1.311011
C	-1.018832	11.743870	3.728105
C	0.427166	11.396981	1.777041
C	-1.498199	9.965546	2.108482
C	-1.811361	10.673156	3.268648
C	0.116902	12.068215	2.959726
H	-2.694944	10.377390	3.822763
H	0.782298	12.859844	3.284809
C	0.367473	10.313887	-1.331486
C	1.005761	11.735162	-3.757090
C	-0.427165	11.402310	-1.793693
C	1.495996	9.968384	-2.128585
C	1.809030	10.676420	-3.288639
C	-0.116846	12.074114	-2.975868
H	2.701998	10.392100	-3.833574
H	-0.771131	12.879329	-3.290167
C	-1.675679	-11.865386	1.049136
H	-1.430988	-12.405246	0.128617
H	-2.328259	-11.035760	0.758788
H	-2.260436	-12.537493	1.686312
C	-2.447202	-8.848514	-1.745624
H	-1.981898	-7.863958	-1.855251
H	-2.782386	-8.923999	-0.705359
H	-3.340231	-8.868560	-2.379041
C	1.667846	-11.880091	-1.058417
H	2.325676	-11.055059	-0.766830
H	2.250258	-12.557724	-1.691784
H	1.414941	-12.415963	-0.137876
C	2.443208	-8.838554	1.730986
H	3.334284	-8.854232	2.367230
H	1.971545	-7.856994	1.839984
H	2.782446	-8.910721	0.691823
C	2.447202	8.848514	-1.745624
H	3.340231	8.868560	-2.379041
H	1.981898	7.863958	-1.855251
H	2.782386	8.923999	-0.705359
C	-1.667846	11.880091	-1.058417
H	-1.414941	12.415963	-0.137876
H	-2.325676	11.055059	-0.766830
H	-2.250258	12.557724	-1.691784
C	1.675679	11.865386	1.049136
H	2.328259	11.035760	0.758788
H	2.260436	12.537493	1.686312
H	1.430988	12.405246	0.128617
C	-2.443208	8.838554	1.730986
H	-1.971545	7.856994	1.839984
H	-2.782446	8.910721	0.691823
H	-3.334284	8.854232	2.367230
N	1.345483	-12.449356	4.877800
N	-1.299280	-12.406423	-4.935631
N	-1.345483	12.449356	4.877800
N	1.299280	12.406423	-4.935631
C	0.583384	13.628529	-5.259359
H	0.940641	14.008568	-6.218606
H	0.721497	14.417322	-4.502709
H	-0.492724	13.441585	-5.358334
C	2.555655	12.144364	-5.616083
H	2.591345	12.729334	-6.537465
H	2.639030	11.086712	-5.892402
H	3.436217	12.405947	-5.007191
C	2.384204	-11.942104	5.758122
H	3.346204	-11.876353	5.235893
H	2.510857	-12.631882	6.595066
H	2.150757	-10.945098	6.164614
C	0.408455	-13.422970	5.410637
H	0.194209	-14.205020	4.672807
H	-0.550376	-12.973655	5.716196
H	0.852953	-13.906260	6.283145
C	-0.408455	13.422970	5.410637
H	-0.194209	14.205020	4.672807
H	0.550376	12.973655	5.716196
H	-0.852953	13.906260	6.283145
C	-2.384204	11.942104	5.758122
H	-3.346204	11.876353	5.235893
H	-2.510857	12.631882	6.595066
H	-2.150757	10.945098	6.164614
C	-2.555655	-12.144364	-5.616083
H	-2.591345	-12.729334	-6.537465
H	-2.639030	-11.086712	-5.892402
H	-3.436217	-12.405947	-5.007191
C	-0.583384	-13.628529	-5.259359
H	-0.940641	-14.008568	-6.218606
H	-0.721497	-14.417322	-4.502709
H	0.492724	-13.441585	-5.358334

Compound 3-2

DFT B3LYP/6-31G(d), gas phase, S_0

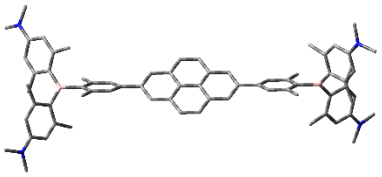

Point group: C_1
Total energy: -1919385.31 kcal mol^{-1}
Dipole moment: 0.82 D
Imaginary frequencies: 0

Symbol	X	Y	Z
C	-0.707661	0.018142	-0.029588
C	-3.546439	0.005920	-0.024199
C	-1.429136	0.911240	0.817689
C	-1.424647	-0.880777	-0.874514
C	-2.825665	-0.869664	-0.851681
C	-2.830089	0.888041	0.800191
H	-3.363528	-1.579247	-1.474821
H	-3.371698	1.592900	1.425449
C	0.715897	0.023479	-0.031466
C	3.552824	0.031500	-0.032530
C	1.432506	0.918448	0.818193
C	1.436896	-0.866644	-0.882496
C	2.837970	-0.841870	-0.866762
C	2.833705	0.901689	0.801340
H	3.381850	-1.539171	-1.498778
H	3.374101	1.601731	1.433336
C	5.037545	0.032622	-0.030714
C	7.898350	0.025093	-0.024817
C	5.766401	-0.135736	-1.214170
C	5.762432	0.200075	1.155295
C	7.159976	0.211729	1.175158
C	7.163951	-0.154347	-1.228288
H	5.230223	-0.232711	-2.155204

H	5.222959	0.299956	2.094123
C	-5.031100	-0.001043	-0.020753
C	-7.893594	-0.013993	-0.013807
C	-5.757672	0.239914	1.151885
C	-5.761126	-0.249213	-1.189671
C	-7.158583	-0.247953	-1.207431
C	-7.154898	0.225871	1.176440
H	-5.220374	0.412146	2.081302
H	-5.226884	-0.416959	-2.121664
C	7.832874	0.400429	2.522555
H	8.316213	1.379825	2.600906
H	8.610707	-0.347681	2.711233
H	7.098829	0.321719	3.331516
C	7.841646	-0.344787	-2.573054
H	8.632743	0.391620	-2.751986
H	7.113775	-0.248574	-3.385689
H	8.309099	-1.331567	-2.655472
C	-7.835671	-0.517143	-2.538950
H	-8.324234	0.378526	-2.935854
H	-8.609980	-1.289053	-2.464791
H	-7.103428	-0.857080	-3.278984
C	-7.827937	0.487945	2.511421
H	-8.603868	1.258841	2.443196
H	-7.093825	0.826160	3.250399
H	-8.313643	-0.410288	2.905969
B	9.491958	0.011878	-0.020086
B	-9.486818	-0.018928	-0.010678
C	10.260094	-1.195601	-0.684043
C	11.655941	-3.387323	-1.932352
C	11.353978	-0.979679	-1.571066
C	9.895922	-2.551227	-0.443324
C	10.591992	-3.605081	-1.034526
C	12.012921	-2.047098	-2.180756
H	10.294186	-4.616759	-0.783971
H	12.823160	-1.822163	-2.864884
C	10.279783	1.204023	0.648508
C	11.721697	3.366873	1.894290
C	11.356842	0.965721	1.549675
C	9.945253	2.566694	0.404904
C	10.658427	3.606112	1.001161
C	12.032914	2.019416	2.164624
H	10.373472	4.623919	0.760459
H	12.818436	1.777822	2.871469
C	-10.264064	-0.922784	1.023500
C	-11.690770	-2.550449	2.927604
C	-11.347031	-0.404486	1.789940
C	-9.915268	-2.283642	1.256720
C	-10.621035	-3.066745	2.169690
C	-12.016377	-1.194673	2.724220
H	-10.324935	-4.102681	2.289028
H	-12.807107	-0.735599	3.306344
C	-10.271061	0.881363	-1.042678
C	-11.702728	2.501230	-2.949492
C	-11.356538	0.359770	-1.803725
C	-9.932048	2.245136	-1.272279
C	-10.645487	3.026867	-2.180606
C	-12.033554	1.148686	-2.733374
H	-10.366668	4.069072	-2.285702
H	-12.836496	0.692100	-3.300734
C	11.810592	-0.433734	1.929518
H	12.357851	-0.919783	1.114990
H	10.972728	-1.092828	2.177900
H	12.472227	-0.397475	2.801654
C	8.767364	-2.935923	0.497091
H	7.786216	-2.700243	0.072675
H	8.827959	-2.414051	1.457961
H	8.791163	-4.010616	0.706043
C	11.851876	0.409251	-1.933914
H	11.036002	1.093735	-2.186507
H	12.522145	0.360866	-2.798798
H	12.403010	0.873531	-1.109373
C	8.825743	2.972958	-0.537145
H	8.862221	4.049181	-0.735869
H	7.839809	2.742795	-0.121101
H	8.887032	2.459716	-1.502762
C	-8.811839	2.941505	-0.520114
H	-8.851692	4.023123	-0.686514
H	-7.826286	2.590678	-0.842715
H	-8.867217	2.773920	0.560772
C	-11.823013	-1.081168	-1.682075
H	-12.353703	-1.260900	-0.741575
H	-10.991488	-1.792807	-1.711353
H	-12.501907	-1.333736	-2.503587
C	-11.812952	1.037135	1.675413
H	-10.981253	1.748637	1.703542
H	-12.488910	1.287226	2.500157
H	-12.347278	1.219485	0.737471
C	-8.786322	-2.972585	0.510798
H	-7.804828	-2.610364	0.833100
H	-8.841630	-2.810902	-0.570968
H	-8.816144	-4.053695	0.682318
N	12.432130	4.408183	2.474164
N	12.315106	-4.441210	-2.549058
N	-12.393609	-3.340889	3.826129
N	-12.380354	3.274351	-3.881649
C	-13.599395	2.762764	-4.484147
H	-13.986446	3.501023	-5.189410
H	-14.385179	2.549368	-3.742003
H	-13.406027	1.840143	-5.044695
C	-12.126144	4.703041	-3.947866
H	-12.717205	5.133895	-4.758696
H	-11.070565	4.904033	-4.165335
H	-12.386177	5.228386	-3.014693
C	11.945859	5.770454	2.338530
H	11.899945	6.069879	1.284484
H	12.637239	6.448353	2.843250
H	10.944129	5.912316	2.774551
C	13.399460	4.121637	3.519220
H	14.180419	3.443347	3.155787
H	12.943072	3.665229	4.412395
H	13.885317	5.051737	3.821337
C	-13.367135	-2.725809	4.711669
H	-14.152371	-2.218531	4.139046
H	-12.918326	-1.989388	5.397762
H	-13.846337	-3.503010	5.310690
C	-11.885119	-4.657507	4.171380
H	-11.824071	-5.301554	3.285938
H	-12.571331	-5.131733	4.876087
H	-10.885797	-4.621995	4.633747
C	12.032537	-5.803899	-2.132576
H	12.614443	-6.493637	-2.747346
H	10.972958	-6.046335	-2.276097
H	12.282358	-5.989078	-1.075423
C	13.540370	-4.185409	-3.286713
H	13.910139	-5.125053	-3.702139
H	14.333746	-3.750013	-2.658456
H	13.361391	-3.501489	-4.125250
C	-0.672640	-1.774396	-1.715269
H	-1.219882	-2.462155	-2.355745
C	0.689062	-1.766583	-1.720172
H	1.239554	-2.447960	-2.364660
C	-0.681603	1.811072	1.655800
H	-1.232289	2.494902	2.297537
C	0.680138	1.813473	1.657082
H	1.227187	2.499120	2.299982

Compound 3-3

DFT B3LYP/6-31G(d), gas phase, S_0

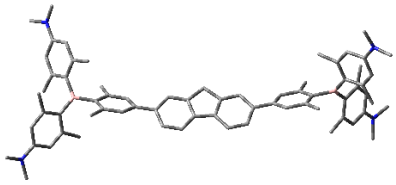

Point group: C_1
Total energy: -1847671.10 kcal mol^{-1}
Dipole moment: 1.17 D
Imaginary frequencies: 0

Symbol	X	Y	Z
C	-0.719240	-1.168415	-1.182356
C	-3.477898	-0.779274	-0.777740
C	-1.637391	-1.892335	-1.946529
C	-1.180958	-0.249979	-0.216030
C	-2.539336	-0.055864	-0.014566
C	-3.000656	-1.693010	-1.738561
H	-1.301010	-2.611050	-2.689706
H	-2.888935	0.672824	0.712407
H	-3.716295	-2.275058	-2.311981
C	0.746649	-1.159959	-1.175763
C	3.496854	-0.738821	-0.746521
C	1.679961	-1.873313	-1.931475
C	1.189003	-0.236171	-0.205499
C	2.543176	-0.026274	0.008017
C	3.038908	-1.658173	-1.711275
H	1.358613	-2.595883	-2.677562
H	2.877777	0.706174	0.738277
H	3.766378	-2.231567	-2.278521
C	4.948673	-0.525587	-0.529455
C	7.750290	-0.108426	-0.108897
C	5.465792	-0.281972	0.749474
C	5.858512	-0.557924	-1.594199
C	7.230605	-0.371142	-1.405491
C	6.827897	-0.061872	0.971466
H	4.790991	-0.287513	1.602016
H	5.484837	-0.708709	-2.604035
C	-4.933867	-0.583453	-0.573745
C	-7.744244	-0.203070	-0.178484
C	-5.832636	-0.620864	-1.647581
C	-5.466082	-0.352088	0.701149
C	-6.836310	-0.179382	0.914830
C	-7.205142	-0.422245	-1.475301
H	-5.448551	-0.775416	-2.653043
H	-4.797507	-0.339663	1.558642
C	8.114670	-0.431938	-2.637847
H	8.741495	-1.329706	-2.643288
H	8.794582	0.424269	-2.708595
H	7.504162	-0.442146	-3.547023
C	7.264845	0.193953	2.402407
H	8.114255	-0.431025	2.699378
H	6.444320	-0.016094	3.096726
H	7.574588	1.233440	2.552120
C	-7.292383	0.041794	2.345603
H	-7.839895	-0.822160	2.736125
H	-7.960247	0.904941	2.442749
H	-6.431283	0.217708	2.999071
C	-8.073125	-0.463135	-2.719852
H	-8.941639	-1.120645	-2.602120
H	-7.497424	-0.829845	-3.576309
H	-8.463625	0.527120	-2.976108
B	9.308397	0.127204	0.125114
B	-9.307519	0.008563	0.041637
C	9.791194	1.414616	0.899704
C	10.651786	3.748672	2.356625
C	10.757060	1.332559	1.944013
C	9.278875	2.711226	0.609590
C	9.718586	3.837420	1.304773
C	11.155838	2.466369	2.651653
H	9.321524	4.803214	1.014066
H	11.876755	2.340479	3.451352
C	10.347338	-0.928723	-0.418903
C	12.243637	-2.842847	-1.443873
C	11.502523	-0.523302	-1.147243
C	10.173679	-2.329878	-0.232797
C	11.104406	-3.246967	-0.719992
C	12.401941	-1.459176	-1.657961
H	10.931335	-4.299709	-0.528152
H	13.242474	-1.094698	-2.237291
C	-10.072022	1.103847	-0.798891
C	-11.473823	3.083576	-2.356734
C	-11.307401	0.812082	-1.445550
C	-9.561045	2.421796	-0.971786
C	-10.254114	3.376614	-1.715210
C	-11.966081	1.770910	-2.215216
H	-9.827484	4.370067	-1.793046
H	-12.882821	1.480666	-2.715503
C	-10.071322	-0.879452	1.099325
C	-11.441541	-2.479708	3.067128
C	-10.966108	-0.300684	2.045033
C	-9.894693	-2.290492	1.173840
C	-10.579769	-3.058825	2.114669
C	-11.613155	-1.082680	3.001653
H	-10.434559	-4.132877	2.099084
H	-12.264750	-0.584924	3.710702
C	11.808883	0.934027	-1.448247
H	12.143601	1.472251	-0.555518
H	10.937023	1.475489	-1.829244
H	12.600164	1.010725	-2.201645
C	8.263232	2.956141	-0.492382
H	7.271881	2.578288	-0.222507
H	8.540694	2.467397	-1.432192
H	8.167941	4.027936	-0.695988
C	11.386916	0.018683	2.374488
H	10.645563	-0.774508	2.514933
H	11.920310	0.143198	3.322905
H	12.102602	-0.352366	1.633818
C	8.994902	-2.908946	0.529486
H	9.155794	-3.972220	0.736216
H	8.060540	-2.815424	-0.033065
H	8.834290	-2.409169	1.490557
C	-8.991124	-3.048030	0.217042
H	-9.161342	-4.126619	0.300336
H	-7.932587	-2.860359	0.423636
H	-9.161897	-2.768791	-0.827972
C	-11.248874	1.191207	2.097207
H	-11.873774	1.517537	1.259566
H	-10.334722	1.792001	2.055480
H	-11.770991	1.448904	3.024861
C	-11.963148	-0.556552	-1.375270
H	-11.256674	-1.370185	-1.568657
H	-12.766581	-0.634105	-2.115618
H	-12.397239	-0.749342	-0.388854
C	-8.259286	2.879279	-0.337611
H	-7.388910	2.425577	-0.822346
H	-8.198910	2.618942	0.724346
H	-8.155848	3.966733	-0.414802
N	13.168600	-3.763375	-1.916487
N	11.049251	4.868304	3.073853
N	-12.160308	4.044163	-3.086339
N	-12.083589	-3.246235	4.029367
C	-13.125357	-2.645929	4.844815
H	-13.504058	-3.391820	5.546601
H	-13.972698	-2.272169	4.248074
H	-12.732386	-1.808119	5.433396
C	-12.016496	-4.695280	3.953429
H	-12.541186	-5.122692	4.810426

H	-10.977463	-5.042729	3.994903
H	-12.472050	-5.098147	3.034384
C	12.854321	-5.181212	-1.870410
H	12.692343	-5.515904	-0.838757
H	13.697766	-5.747217	-2.271103
H	11.956763	-5.439188	-2.454867
C	14.226924	-3.321866	-2.808119
H	14.846785	-2.553604	-2.331082
H	13.845197	-2.908920	-3.755905
H	14.874615	-4.169593	-3.041158
C	-13.315101	3.653692	-3.876248
H	-14.089509	3.204697	-3.243268
H	-13.067155	2.932250	-4.671625
H	-13.745598	4.542114	-4.342991
C	-11.511722	5.307472	-3.393857
H	-11.248479	5.848980	-2.477314
H	-12.202985	5.935421	-3.959676
H	-10.593031	5.182462	-3.988917
C	10.641868	6.188413	2.625107
H	11.011380	6.935456	3.330671
H	9.549172	6.273048	2.596068
H	11.027862	6.439261	1.623818
C	12.169519	4.768530	3.993515
H	12.327432	5.737895	4.470681
H	13.106408	4.472630	3.495036
H	11.965181	4.039368	4.786782
C	-0.002838	0.415091	0.469858
H	-0.006642	0.241916	1.555075
H	-0.008587	1.505267	0.330964

Compound 3-4

DFT B3LYP/6-31G(d), gas phase, S_0

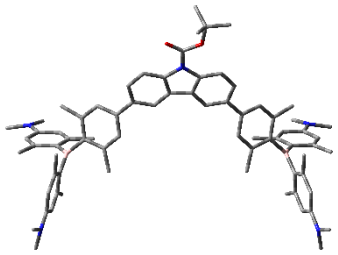

Point group: C_1
Total energy: -2075924.33 kcal mol^{-1}
Dipole moment: 4.27 D
Imaginary frequencies: 0

Symbol	X	Y	Z
C	-1.194946	5.048349	0.023218
C	-3.026125	2.908277	0.004686
C	-0.739984	3.710238	0.008320
C	-2.563475	5.325740	0.026829
C	-3.452573	4.253034	0.017367
C	-1.648711	2.652284	-0.000003
H	-2.932976	6.339946	0.027430
H	-4.517311	4.465537	-0.007134
H	-1.287254	1.628197	0.016694
C	0.710865	3.739387	0.011259
C	1.106209	5.093136	0.028301
N	-0.059822	5.906618	0.034333
C	2.457785	5.442910	0.038460
H	2.765537	6.478261	0.041821
C	3.395082	4.412081	0.032295
H	4.449144	4.672758	0.013017
C	1.667970	2.724509	0.005982
H	1.357155	1.683866	0.020336
C	3.031203	3.048097	0.016515
C	4.067302	1.985508	0.010299
C	6.062280	-0.067486	0.000946
C	3.894911	0.805781	-0.724195
C	5.255018	2.121118	0.739586
C	6.233123	1.122861	0.758705
C	4.864176	-0.200698	-0.752139
H	2.993272	0.681011	-1.319270
H	5.409135	3.016430	1.337181
C	-4.010270	1.797664	-0.003585
C	-5.903566	-0.349488	-0.014056
C	-5.208837	1.880225	0.715853
C	-3.775803	0.623525	-0.729732
C	-4.694913	-0.428973	-0.757830
C	-6.137837	0.836118	0.734058
H	-5.410374	2.770161	1.307411
H	-2.864817	0.538740	-1.317499
B	7.172317	-1.209448	-0.004882
B	-6.955068	-1.545987	-0.017430
C	7.726390	-1.748379	-1.380990
C	8.693863	-2.751520	-3.904421
C	8.118291	-0.874765	-2.434821
C	7.843800	-3.144925	-1.637033
C	8.300289	-3.619498	-2.866565
C	8.606718	-1.369712	-3.643778
H	8.347283	-4.692550	-3.013020
H	8.925324	-0.656382	-4.395152
C	7.702505	-1.785923	1.365369
C	8.691395	-2.794981	3.878132
C	9.096483	-1.945033	1.612771
C	6.823845	-2.157631	2.422342
C	7.311247	-2.666412	3.625956
C	9.564545	-2.421401	2.837250
H	6.593226	-2.967926	4.379917
H	10.636599	-2.500057	2.977303
C	-7.464118	-2.136173	1.354892
C	-8.417752	-3.167822	3.872155
C	-6.574827	-2.453330	2.420753
C	-8.850052	-2.362238	1.595592
C	-9.301695	-2.848773	2.822210
C	-7.044060	-2.973521	3.626672
H	-10.369381	-2.979354	2.956727
H	-6.316761	-3.231939	4.387705
C	-7.472299	-2.123573	-1.391948
C	-8.371772	-3.195520	-3.912291
C	-7.518778	-3.526485	-1.636002
C	-7.899683	-1.279773	-2.456256
C	-8.354803	-1.808777	-3.663712
C	-7.942753	-4.033796	-2.864055
H	-8.703236	-1.118789	-4.423597
H	-7.935428	-5.109068	-3.001197
C	4.569903	-1.422714	-1.603157
H	5.207522	-1.462504	-2.492322
H	3.527014	-1.414187	-1.937443
H	4.732763	-2.359954	-1.059496
C	7.467063	1.377979	1.605128
H	7.489810	2.418979	1.944533
H	8.396703	1.191186	1.056127
H	7.492843	0.734961	2.490916
C	5.313625	-2.064499	2.294476
H	4.967555	-1.026157	2.317536
H	4.824682	-2.597514	3.116741
H	4.946254	-2.497622	1.358254
C	10.155800	-1.581892	0.585994
H	11.148311	-1.568975	1.048951
H	9.986583	-0.595796	0.141552
H	10.181984	-2.296216	-0.243205
C	7.455103	-4.199058	-0.614303
H	8.170961	-4.248862	0.212471
H	7.413549	-5.188518	-1.082080
H	6.475319	-4.005150	-0.165921
C	8.070089	0.636749	-2.297699
H	8.612077	1.114801	-3.120500
H	8.519636	0.985748	-1.362155

H	7.042187	1.013111	-2.312100
C	-5.070272	-2.287179	2.300602
H	-4.775386	-1.233014	2.318653
H	-4.676690	-2.707925	1.369453
H	-4.560639	-2.790214	3.129146
C	-9.919561	-2.063527	0.558610
H	-10.914465	-2.095823	1.015424
H	-9.904330	-2.786964	-0.262946
H	-9.797317	-1.074919	0.104422
C	-7.085411	-4.551061	-0.601276
H	-7.802788	-4.627755	0.222102
H	-6.118737	-4.305819	-0.149562
H	-6.993316	-5.541606	-1.059378
C	-7.927285	0.233387	-2.332358
H	-8.484937	0.677016	-3.163938
H	-6.919066	0.659837	-2.341478
H	-8.401808	0.567651	-1.403742
C	-4.335217	-1.640532	-1.598542
H	-4.963620	-1.716911	-2.491864
H	-4.456412	-2.581067	-1.049790
H	-3.291561	-1.583394	-1.925478
C	-7.389159	1.036501	1.569565
H	-7.466063	2.077821	1.900078
H	-7.389571	0.400147	2.460495
H	-8.304192	0.799232	1.015611
N	9.137385	-3.235307	-5.127377
N	-8.782614	-3.711360	-5.133280
N	-8.879578	-3.642110	5.091894
N	9.169061	-3.258590	5.096037
C	10.578125	-3.583576	5.235130
H	10.768418	-3.918181	6.256967
H	10.903446	-4.378853	4.545469
H	11.205973	-2.702884	5.053697
C	8.238203	-3.797015	6.072514
H	8.787060	-4.071892	6.975659
H	7.489602	-3.047766	6.355746
H	7.703560	-4.689484	5.708929
C	-10.271512	-4.035907	5.226008
H	-10.552045	-4.853306	4.542623
H	-10.451332	-4.369520	6.250048
H	-10.941565	-3.189679	5.031892
C	-7.929431	-4.122143	6.080258
H	-7.221005	-3.333215	6.358975
H	-8.469813	-4.413578	6.983310
H	-7.348665	-4.990973	5.730504
C	-9.378141	-2.828015	-6.120673
H	-8.684928	-2.025075	-6.397809
H	-9.598528	-3.399490	-7.024697
H	-10.313595	-2.362257	-5.770712
C	-8.992709	-5.142160	-5.271880
H	-9.300598	-5.360462	-6.296489
H	-8.066757	-5.697591	-5.079796
H	-9.766658	-5.528280	-4.589447
C	9.697900	-2.314720	-6.101177
H	9.952591	-2.866019	-7.008736
H	8.969283	-1.543152	-6.376501
H	10.607135	-1.808202	-5.738885
C	9.420441	-4.652381	-5.276270
H	10.209448	-5.004804	-4.592752
H	8.522754	-5.255356	-5.093753
H	9.744063	-4.846312	-6.300959
C	-0.008764	7.300675	0.053261
O	1.035616	7.925072	0.063504
O	-1.242136	7.832696	0.058159
C	-1.433636	9.300378	0.077085
C	-2.958679	9.433063	0.076117
H	-3.240369	10.491023	0.089884
H	-3.388546	8.973898	-0.820087
H	-3.391680	8.949881	0.958065
C	-0.839282	9.888061	1.360598
H	-1.255234	9.382798	2.239056
H	0.246870	9.789524	1.376147
H	-1.097605	10.950934	1.426422
C	-0.834746	9.921563	-1.188416
H	0.251470	9.823536	-1.202700
H	-1.247490	9.439494	-2.081307
H	-1.093037	10.985768	-1.227261

Compound 3-5

DFT B3LYP/6-31G(d), gas phase, S_0

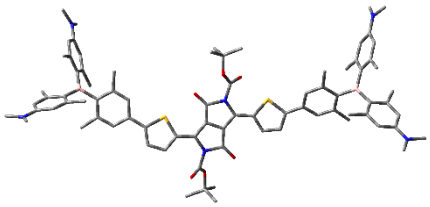

Point group: C_1
Total energy: -2968846.10 kcal mol^{-1}
Dipole moment: 3.34 D
Imaginary frequencies: 0

Symbol	X	Y	Z
C	1.374695	-1.219918	-0.622890
N	0.625081	-0.086907	-0.233258
C	-0.808036	-0.391054	-0.159122
O	-1.667888	0.442059	0.057226
C	-0.861280	-1.801159	-0.478008
C	0.456922	-2.258575	-0.766481
C	-1.768028	-2.853359	-0.517807
N	-1.008898	-3.991672	-0.881034
C	0.397932	-3.679061	-1.029279
O	1.240624	-4.526275	-1.294647
C	-3.189039	-2.839269	-0.294964
C	-4.065626	-3.879718	-0.002597
H	-3.735528	-4.897670	0.143024
C	-5.402416	-3.466435	0.143459
H	-6.205607	-4.144384	0.409553
C	-5.591767	-2.105670	-0.029413
S	-4.076908	-1.315713	-0.372021
C	2.805220	-1.306137	-0.707143
C	3.498710	-2.472677	-1.029792
H	2.987324	-3.390999	-1.296566
C	4.893428	-2.346833	-0.926372
H	5.577500	-3.165526	-1.118052
C	5.315437	-1.093504	-0.511640
S	3.947422	-0.032100	-0.296069
C	6.684350	-0.624027	-0.298170
C	9.372913	0.258878	0.111864
C	7.766192	-1.278074	-0.907998
C	6.971459	0.479647	0.518424
C	8.276658	0.934086	0.714661
C	9.084940	-0.870529	-0.703197
H	7.573644	-2.114328	-1.574332
H	6.158086	0.990241	1.028411
C	-6.842146	-1.349586	0.058018
C	-9.303115	0.094534	0.231708
C	-6.861011	0.020956	0.354578
C	-8.074905	-1.985518	-0.154105
C	-9.285509	-1.298443	-0.054962
C	-8.053418	0.743869	0.426200
H	-5.923767	0.535499	0.552572
H	-8.089216	-3.038618	-0.421813
C	8.462202	2.145737	1.609121
H	8.765375	3.027828	1.035938
H	9.232268	1.987992	2.372033
H	7.528574	2.385878	2.128430
C	10.172553	-1.661789	-1.405978

H	10.875024	-1.017632	-1.946011
H	9.734808	-2.353291	-2.133547
H	10.766813	-2.248693	-0.698207
C	-7.947756	2.223808	0.744540
H	-8.198461	2.842165	-0.123423
H	-6.929019	2.477149	1.055529
H	-8.624002	2.527180	1.551168
C	-10.555679	-2.093919	-0.293743
H	-10.318112	-3.083773	-0.697559
H	-11.229511	-1.602192	-1.003748
H	-11.124456	-2.234890	0.631035
B	10.872995	0.751939	0.339840
B	-10.676416	0.899575	0.332393
C	11.956096	-0.276631	0.844834
C	13.235850	-0.366779	0.223898
C	11.708424	-1.175174	1.921871
C	12.679114	-2.079888	2.350005
C	14.178917	-1.304269	0.643782
H	12.447813	-2.712227	3.199415
H	15.126646	-1.343942	0.119154
C	11.243384	2.257808	0.055728
C	12.010261	3.018414	0.985848
C	10.817058	2.937412	-1.121311
C	11.152085	4.271258	-1.350546
C	12.302688	4.362036	0.754279
H	10.832528	4.724628	-2.281756
H	12.868854	4.897663	1.507663
C	-10.871273	2.210010	-0.522203
C	-10.518112	2.278674	-1.900360
C	-11.395779	3.400946	0.059221
C	-11.531227	4.571133	-0.686996
C	-10.696270	3.448570	-2.637641
H	-11.912940	5.453600	-0.186415
H	-10.445490	3.430279	-3.691974
C	-11.815217	0.368803	1.285643
C	-13.165764	0.271507	0.841045
C	-11.553777	-0.056828	2.619369
C	-12.574950	-0.526659	3.444443
C	-14.165501	-0.235900	1.670428
H	-12.322942	-0.800031	4.462593
H	-15.170615	-0.308993	1.271140
C	10.015060	2.249865	-2.211966
H	9.986259	2.867638	-3.115566
H	8.981091	2.066725	-1.902223
H	10.437348	1.279295	-2.492259
C	12.526881	2.436770	2.290961
H	13.353441	1.737810	2.127287
H	11.755997	1.883754	2.837102
H	12.888299	3.234913	2.948029
C	10.401308	-1.176880	2.694534
H	9.580175	-1.595941	2.104000
H	10.092401	-0.170056	2.994497
H	10.494309	-1.775971	3.606369
C	13.644089	0.516478	-0.942998
H	14.562024	0.138226	-1.405294
H	13.828362	1.548751	-0.628441
H	12.876788	0.561623	-1.722485
C	-9.970506	1.083271	-2.659842
H	-10.556475	0.174504	-2.487050
H	-8.940065	0.854378	-2.369324
H	-9.976578	1.276916	-3.737577
C	-11.806929	3.487373	1.519357
H	-12.736606	2.943083	1.714528
H	-11.962736	4.531489	1.810863
H	-11.053130	3.066240	2.192202
C	-13.598626	0.677265	-0.557698
H	-14.612723	0.318183	-0.762908
H	-12.941737	0.271211	-1.333619
H	-13.595813	1.764453	-0.686202
C	-10.168819	0.013122	3.237931
H	-9.499264	-0.747330	2.823175
H	-10.222432	-0.145688	4.320039
H	-9.686028	0.981982	3.072777
C	-11.187511	4.632630	-2.052406
N	-11.319072	5.804313	-2.781877
C	-13.903801	-0.649542	2.991982
C	11.885260	5.028599	-0.415266
C	13.932465	-2.186708	1.714716
N	-14.904755	-1.160609	3.804584
N	14.875120	-3.120138	2.117761
N	12.175482	6.367031	-0.630643
C	16.222752	-3.058134	1.578415
H	16.730399	-2.108084	1.808701
H	16.814485	-3.872776	2.000609
H	16.218682	-3.182562	0.488662
C	14.646647	-3.897542	3.323510
H	13.720370	-4.479189	3.246487
H	15.469226	-4.603438	3.454917
H	14.580560	-3.273194	4.228949
C	11.866330	6.971932	-1.914758
H	10.794962	6.898418	-2.136098
H	12.124249	8.032389	-1.881683
H	12.417367	6.509303	-2.749200
C	13.104363	7.051281	0.252387
H	12.738415	7.053717	1.286416
H	14.107727	6.596819	0.249553
H	13.199558	8.091380	-0.065679
C	-16.290528	-1.072023	3.377274
H	-16.928133	-1.532375	4.134680
H	-16.625590	-0.033068	3.229666
H	-16.449686	-1.614204	2.437244
C	-14.628786	-1.418854	5.207260
H	-15.515772	-1.854538	5.671693
H	-13.808926	-2.138021	5.320296
H	-14.359822	-0.507756	5.765542
C	-11.104944	5.784496	-4.218523
H	-11.208822	6.798689	-4.609455
H	-10.093012	5.438445	-4.460341
H	-11.820708	5.136006	-4.748792
C	-12.018951	6.936982	-2.200672
H	-13.066020	6.706453	-1.948003
H	-11.520410	7.283797	-1.287256
H	-12.013661	7.764276	-2.913137
C	-1.450642	-5.321658	-1.170562
C	1.058697	1.267353	-0.299424
O	-2.040065	-6.023229	-0.378343
O	1.792662	1.682074	-1.171388
O	0.534659	1.943267	0.714014
O	-1.086482	-5.632537	-2.406858
C	0.516906	3.425044	0.729190
C	-0.319686	3.719525	1.975341
H	-1.312598	3.270339	1.880713
H	0.161305	3.309212	2.869114
H	-0.429580	4.801320	2.105407
C	1.944738	3.956484	0.876171
H	2.425589	3.520571	1.758582
H	2.545470	3.724243	-0.004850
H	1.916176	5.044232	1.007103
C	-0.180291	3.937952	-0.533804
H	-0.330781	5.020035	-0.451130
H	0.414381	3.739704	-1.428023
H	-1.157902	3.457837	-0.642542
C	-1.096696	-7.035843	-2.892375
C	-0.242774	-7.901741	-1.962459
H	-0.717251	-8.033843	-0.988033
H	-0.102082	-8.888940	-2.416347
H	0.738278	-7.439109	-1.817941
C	-2.541335	-7.527566	-3.006322
H	-2.551783	-8.520168	-3.470550
H	-3.013808	-7.596061	-2.024865
H	-3.128046	-6.851136	-3.637203
C	-0.443877	-6.899660	-4.268719
H	-1.026923	-6.229865	-4.908938
H	0.567421	-6.493406	-4.172713
H	-0.385836	-7.879975	-4.753146

Compound 3-1M

DFT B3LYP/6-31G(d), gas phase, S_0

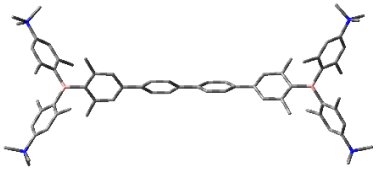

Point group: C_1
Total energy: -1923472.14 kcal mol^{-1}
Imaginary frequencies: 0

Symbol	X	Y	Z
C	7.202000	1.029646	-0.661782
C	5.806970	1.001786	-0.667812
C	5.071793	0.026002	0.020497
C	5.798649	-0.952999	0.713125
C	7.193453	-0.989458	0.711149
C	7.942237	0.016678	0.024372
H	5.272940	1.783541	-1.200498
H	5.258284	-1.730784	1.245288
C	3.589766	0.028813	0.015387
C	2.856576	-0.358803	1.150972
C	2.866716	0.418181	-1.126126
C	1.465570	-0.352988	1.146125
H	3.379524	-0.647082	2.058311
C	1.475728	0.414665	-1.133056
H	3.397747	0.705675	-2.029010
C	0.742102	0.031150	0.003379
H	0.932612	-0.671457	2.037196
H	0.950789	0.734057	-2.028550
C	-0.742221	0.031145	-0.003169
C	-1.465683	-0.353183	-1.145853
C	-1.475853	0.414860	1.133197
C	-2.856689	-0.359000	-1.150704
H	-0.932723	-0.671799	-2.036869
C	-2.866840	0.418375	1.126261
H	-0.950916	0.734410	2.028636
C	-3.589884	0.028805	-0.015187
H	-3.379631	-0.647434	-2.057997
H	-3.397875	0.706028	2.029092
C	-5.071910	0.025978	-0.020306
C	-5.807108	1.001873	0.667815
C	-5.798744	-0.953175	-0.712750
C	-7.202144	1.029714	0.661762
H	-5.273092	1.783721	1.200379
C	-7.193544	-0.989666	-0.710772
H	-5.258357	-1.731054	-1.244750
C	-7.942355	0.016609	-0.024212
B	-9.509013	0.006613	-0.018858
B	9.508900	0.006656	0.018935
C	-10.339761	1.360048	-0.245825
C	-10.094118	2.153167	-1.395948
C	-11.339120	1.799845	0.663938
C	-10.827459	3.330310	-1.623259
C	-12.039218	2.988842	0.430388
C	-11.785717	3.747665	-0.709557
H	-10.610812	3.892642	-2.522251
H	-12.781190	3.296592	1.159944
C	10.339803	1.360026	0.245773
C	10.094351	2.153203	1.395910
C	11.339152	1.799679	-0.664057
C	10.827919	3.330207	1.623186
C	12.039483	2.988553	-0.430541
C	11.786211	3.747391	0.709436
H	10.611433	3.892581	2.522190
H	12.781432	3.296197	-1.160163
C	-10.319016	-1.358499	0.215057
C	-10.045498	-2.153942	1.362446
C	-11.319706	-1.810247	-0.681407
C	-10.756107	-3.339321	1.586291
C	-12.003518	-3.014970	-0.448565
C	-11.721810	-3.771445	0.681137
H	-10.524388	-3.910979	2.479181
H	-12.746677	-3.322627	-1.172582
C	10.318831	-1.358501	-0.215053
C	10.045019	-2.154072	-1.362274
C	11.319763	-1.810150	0.681198
C	10.755590	-3.339471	-1.586186
C	12.003522	-3.014889	0.448311
C	11.721531	-3.771489	-0.681244
H	10.523630	-3.911225	-2.478950
H	12.746860	-3.322468	1.172176
C	-7.840830	-2.118639	-1.492337
H	-8.659715	-1.777153	-2.133279
H	-7.104940	-2.601795	-2.141238
H	-8.248517	-2.892185	-0.831967
C	-7.858372	2.155969	1.439683
H	-7.123466	2.655524	2.077105
H	-8.284099	2.917233	0.776636
H	-8.665727	1.808043	2.091887
C	7.840766	-2.118268	1.492926
H	7.104991	-2.601053	2.142235
H	8.248103	-2.892135	0.832713
H	8.659920	-1.776704	2.133477
C	7.858232	2.155742	-1.439921
H	7.123244	2.655456	-2.077124
H	8.284352	2.916915	-0.777026
H	8.665297	1.807609	-2.092377
C	-11.682344	-1.053380	-1.942878
H	-12.108497	-0.072027	-1.714702
H	-10.809534	-0.887682	-2.583992
H	-12.416104	-1.604795	-2.537300
C	-8.996280	-1.780908	2.390925
H	-7.985855	-1.953668	2.006614
H	-9.048362	-0.727229	2.678524
H	-9.114062	-2.375325	3.301645
C	-9.048811	1.796311	-2.434733
H	-8.038859	2.007888	-2.068299
H	-9.070483	0.737361	-2.705515
H	-9.198206	2.372351	-3.352608
C	-11.672800	1.041032	1.931611
H	-12.071746	0.046540	1.711608
H	-10.791367	0.904262	2.567983
H	-12.418365	1.575070	2.527264
C	-14.057845	4.710501	-0.973131
H	-14.367799	4.252285	-0.036090
H	-14.604554	5.641738	-1.130223
H	-14.230797	4.022460	-1.800951
C	-12.213340	5.739613	-2.196408
H	-12.423655	5.089072	-3.044613
H	-12.827041	6.638272	-2.260580
H	-11.159492	6.014668	-2.172118
C	-12.304391	5.980815	0.232020
H	-12.615459	5.519863	1.167432
H	-11.235092	6.191583	0.257884
H	-12.871075	6.897664	0.061334
C	-13.178759	-4.978689	2.286286
H	-13.894023	-4.158306	2.223813
H	-13.696010	-5.922832	2.464766
H	-12.463953	-4.789601	3.084691
C	-13.462012	-5.421940	-0.098198
H	-13.926865	-6.366905	0.183687
H	-14.218500	-4.639245	-0.143886
H	-12.960298	-5.531085	-1.059066
C	-11.440835	-6.211029	1.021644
H	-10.924479	-6.263641	0.062904
H	-10.725774	-6.021460	1.819847
H	-11.980466	-7.139220	1.216826
C	11.672648	1.040822	-1.931752
H	12.071944	0.046468	-1.711745

H	10.791076	0.903744	-2.567857
H	12.417902	1.574997	-2.527672
C	9.049034	1.796530	2.434744
H	8.039050	2.007492	2.068061
H	9.071100	0.737734	2.706124
H	9.198081	2.373124	3.352324
C	12.305116	5.980483	-0.232144
H	12.871908	6.897269	-0.061475
H	12.616071	5.519516	-1.167588
H	11.235838	6.191372	-0.257935
C	12.214258	5.739229	2.196292
H	11.160474	6.014538	2.172058
H	12.424452	5.088582	3.044444
H	12.828166	6.637746	2.260478
C	14.058506	4.709906	0.972826
H	14.605355	5.641063	1.129903
H	14.231437	4.021809	1.800602
H	14.368324	4.251695	0.035737
C	8.995508	-1.781216	-2.390521
H	7.985198	-1.954070	-2.005947
H	9.047390	-0.727555	-2.678207
H	9.113135	-2.375690	-3.301224
C	11.682805	-1.053118	1.942461
H	12.109562	-0.072089	1.713995
H	10.810099	-0.886692	2.583515
H	12.416232	-1.604792	2.537055
C	11.440444	-6.211088	-1.021463
H	10.725206	-6.021590	-1.819526
H	11.980006	-7.139314	-1.216670
H	10.924291	-6.263602	-0.062607
C	13.461895	-5.421945	0.097835
H	14.218402	-4.639258	0.143275
H	12.960403	-5.531002	1.058832
H	13.926660	-6.366946	-0.184077
C	13.178094	-4.978902	-2.286624
H	13.893436	-4.158572	-2.224364
H	13.695221	-5.923100	-2.465170
H	12.463105	-4.789803	-3.084863
N	12.443223	-5.073441	-0.962463
N	12.575357	5.024316	0.915126
N	-12.443581	-5.073360	0.962313
N	-12.574658	5.024709	-0.915294

Compound 3-1M

DFT B3LYP/6-31G(d), gas phase, S_0

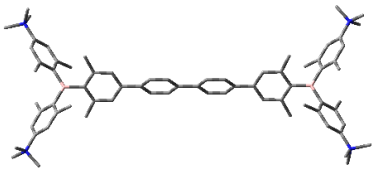

Point group: C_i

Total energy: -1923554.01 kcal mol^{-1}

Symbol	X	Y	Z
C	-0.885060	-7.227200	-0.830590
C	-0.852860	-5.832250	-0.831010
C	-0.011800	-5.099680	0.018900
C	0.827780	-5.829140	0.873010
C	0.860300	-7.224040	0.876900
C	-0.010950	-7.970140	0.023130
H	-1.527000	-5.296140	-1.492980
H	1.500960	-5.290850	1.534230
C	-0.009720	-3.617650	0.014010
C	0.173510	-2.885450	1.200470
C	-0.189750	-2.893610	-1.177970
C	0.172350	-1.494440	1.195270
H	0.295870	-3.409130	2.144200
C	-0.181360	-1.502630	-1.183570
H	-0.314930	-3.423900	-2.117630
C	-0.002320	-0.769990	0.003000
H	0.330110	-0.962300	2.128770
H	-0.336430	-0.976880	-2.121130
B	-0.004290	-9.536820	0.018870
C	-1.378660	-10.364060	0.003130
C	-2.361580	-10.116420	0.995470
C	-1.653640	-11.362270	-0.970400
C	-3.562170	-10.846800	1.011310
C	-2.866920	-12.059380	-0.950500
C	-3.814220	-11.804010	0.037900
H	-4.273690	-10.628750	1.797140
H	-3.043050	-12.800530	-1.723260
C	1.378570	-10.350440	0.028950
C	2.364710	-10.078830	-0.959870
C	1.662420	-11.352550	0.990380
C	3.569120	-10.792610	-0.971540
C	2.887520	-12.039560	0.973300
C	3.832210	-11.759670	-0.005000
H	4.289970	-10.562230	-1.749380
H	3.060650	-12.783690	1.739740
C	1.831820	-7.874360	1.845210
H	2.194490	-7.139850	2.569800
H	2.708900	-8.283810	1.331640
H	1.380470	-8.692550	2.415140
C	-1.858030	-7.880430	-1.795400
H	-2.235580	-7.144130	-2.510430
H	-2.725300	-8.304470	-1.277310
H	-1.402440	-8.688470	-2.376580
C	-0.684000	-11.697870	-2.084540
H	0.254900	-12.099830	-1.692800
H	-0.434550	-10.816700	-2.686130
H	-1.106700	-12.441710	-2.765640
C	-2.190910	-9.072020	2.081380
H	-2.331210	-8.061480	1.683670
H	-1.196630	-9.096920	2.535210
H	-2.920680	-9.219460	2.882830
C	-5.847640	-12.316930	-1.282950
H	-6.781660	-12.881240	-1.276880
H	-5.229760	-12.629170	-2.122580
H	-6.047830	-11.247090	-1.345070
C	-6.038180	-12.226610	1.150010
H	-6.302100	-11.172090	1.078050
H	-5.547870	-12.438520	2.099520
H	-6.935570	-12.838090	1.054470
C	-4.814150	-14.073680	0.126450
H	-5.759870	-14.618010	0.116620
H	-4.283280	-14.248430	1.062520
H	-4.198690	-14.384780	-0.715280
C	2.181830	-9.028370	-2.037310
H	2.286840	-8.018510	-1.627850
H	1.195280	-9.077420	-2.506320
H	2.927270	-9.147640	-2.828950
C	0.693860	-11.713490	2.098210
H	-0.232630	-12.137610	1.700140
H	0.419320	-10.840300	2.700250
H	1.130080	-12.448370	2.780460
C	6.294310	-11.485180	0.090450
H	6.250430	-10.769470	-0.728210
H	7.240980	-12.027250	0.061770
H	6.178280	-10.969120	1.043760
C	5.314770	-13.504440	1.052180
H	4.534320	-14.258830	0.958550
H	5.253980	-13.003200	2.017560
H	6.293430	-13.971760	0.941130
C	5.299930	-13.219560	-1.372920
H	4.479570	-13.932680	-1.456610
H	6.259430	-13.739240	-1.382380
H	5.256470	-12.504100	-2.191690
N	5.161420	-12.484880	-0.052530

N	-5.109510	-12.589700	0.014840
C	0.002320	0.769990	-0.003000
C	-0.172350	1.494440	-1.195270
C	0.181360	1.502630	1.183570
C	-0.173510	2.885450	-1.200470
H	-0.330110	0.962300	-2.128770
C	0.189750	2.893610	1.177970
H	0.336430	0.976880	2.121130
C	0.009720	3.617650	-0.014010
H	-0.295870	3.409130	-2.144200
H	0.314930	3.423900	2.117630
C	0.011800	5.099680	-0.018900
C	0.852860	5.832250	0.831010
C	-0.827780	5.829140	-0.873010
C	0.885060	7.227200	0.830590
H	1.527000	5.296140	1.492980
C	-0.860300	7.224040	-0.876900
H	-1.500960	5.290850	-1.534230
C	0.010950	7.970140	-0.023130
C	1.858030	7.880430	1.795400
C	-1.831820	7.874360	-1.845210
B	0.004290	9.536820	-0.018870
H	2.235580	7.144130	2.510430
H	2.725300	8.304470	1.277310
H	1.402440	8.688470	2.376580
H	-2.194490	7.139850	-2.569800
H	-2.708900	8.283810	-1.331640
H	-1.380470	8.692550	-2.415140
C	1.378660	10.364060	-0.003130
C	-1.378570	10.350440	-0.028950
C	2.361580	10.116420	-0.995470
C	1.653640	11.362270	0.970400
C	-2.364710	10.078830	0.959870
C	-1.662420	11.352550	-0.990380
C	3.562170	10.846800	-1.011310
C	2.190910	9.072020	-2.081380
C	2.866920	12.059380	0.950500
C	0.684000	11.697870	2.084540
C	-3.569120	10.792610	0.971540
C	-2.181830	9.028370	2.037310
C	-2.887520	12.039560	-0.973300
C	-0.693860	11.713490	-2.098210
C	3.814220	11.804010	-0.037900
H	4.273690	10.628750	-1.797140
H	2.331210	8.061480	-1.683670
H	1.196630	9.096920	-2.535210
H	2.920680	9.219460	-2.882830
H	3.043050	12.800530	1.723260
H	-0.254900	12.099830	1.692800
H	0.434550	10.816700	2.686130
H	1.106700	12.441710	2.765640
C	-3.832210	11.759670	0.005000
H	-4.289970	10.562230	1.749380
H	-2.286840	8.018510	1.627850
H	-1.195280	9.077420	2.506320
H	-2.927270	9.147640	2.828950
H	-3.060650	12.783690	-1.739740
H	0.232630	12.137610	-1.700140
H	-0.419320	10.840300	-2.700250
H	-1.130080	12.448370	-2.780460
N	5.109510	12.589700	-0.014840
N	-5.161420	12.484880	0.052530
C	5.847640	12.316930	1.282950
C	6.038180	12.226610	-1.150010
C	4.814150	14.073680	-0.126450
C	-6.294310	11.485180	-0.090450
C	-5.314770	13.504440	-1.052180
C	-5.299930	13.219560	1.372920
H	6.781660	12.881240	1.276880
H	5.229760	12.629170	2.122580
H	6.047830	11.247090	1.345070
H	6.302100	11.172090	-1.078050
H	5.547870	12.438520	-2.099520
H	6.935570	12.838090	-1.054470
H	5.759870	14.618010	-0.116620
H	4.283280	14.248430	-1.062520
H	4.198690	14.384780	0.715280
H	-6.250430	10.769470	0.728210
H	-7.240980	12.027250	-0.061770
H	-6.178280	10.969120	-1.043760
H	-4.534320	14.258830	-0.958550
H	-5.253980	13.003200	-2.017560
H	-6.293430	13.971760	-0.941130
H	-4.479570	13.932680	1.456610
H	-6.259430	13.739240	1.382380
H	-5.256470	12.504100	2.191690

Compound 3-2M

DFT B3LYP/6-31G(d), gas phase, S_0

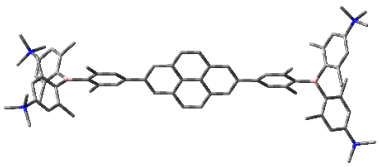

Point group: C_1
Total energy: -2019094.10 kcal mol^{-1}
Imaginary frequencies: 0

Symbol	X	Y	Z
C	0.712897	0.027240	0.071685
C	3.545794	0.024793	0.059944
C	1.429377	-1.203978	0.160054
C	1.430765	1.257366	-0.020720
C	2.832034	1.230939	-0.029167
C	2.830707	-1.179938	0.156861
H	3.370759	2.173550	-0.074053
H	3.368217	-2.123456	0.196854
C	-0.711158	0.028223	0.074262
C	-3.544068	0.029632	0.072091
C	-1.428988	-1.201933	0.165920
C	-1.427669	1.259263	-0.016285
C	-2.829003	1.234486	-0.020568
C	-2.830293	-1.175708	0.168129
H	-3.366914	2.177545	-0.066484
H	-3.369238	-2.118237	0.212778
C	-5.028577	0.028921	0.064443
C	-7.898460	0.018338	0.036469
C	-5.755122	0.932804	-0.723525
C	-5.763647	-0.876834	0.842817
C	-7.158633	-0.911654	0.830991
C	-7.150508	0.958408	-0.738329
H	-5.214599	1.620787	-1.367300
H	-5.230619	-1.559636	1.498342
C	5.029944	0.022452	0.048764
C	7.900609	0.011830	0.018178
C	5.765518	-0.883092	0.825916
C	5.755616	0.924987	-0.741180
C	7.150351	0.925140	-0.787089
C	7.161022	-0.893216	0.842511
H	5.231987	-1.584525	1.461077
H	5.213962	1.631217	-1.364013
C	-7.818377	-1.936498	1.736242
H	-8.235880	-2.775692	1.168797
H	-8.632316	-1.513925	2.334232
H	-7.087834	-2.350290	2.437059
C	-7.798260	1.985123	-1.650075
H	-8.598239	1.563316	-2.266648
H	-7.056099	2.408231	-2.332863

H	-8.231357	2.818024	-1.084740
C	7.793911	1.955883	-1.697361
H	8.225199	1.498469	-2.594432
H	8.593933	2.518526	-1.204870
H	7.049081	2.684029	-2.030284
C	7.816397	-1.925343	1.742577
H	8.596373	-2.501218	1.233533
H	7.072180	-2.641718	2.101359
H	8.277356	-1.466548	2.624099
B	-9.465222	-0.000254	0.005681
B	9.466872	-0.002371	-0.007761
C	-10.307806	1.362744	0.081664
C	-11.780965	3.771292	0.261295
C	-11.295323	1.691546	-0.879896
C	-10.079765	2.281999	1.143100
C	-10.825517	3.463770	1.226482
C	-12.014267	2.895027	-0.790242
H	-10.627772	4.132989	2.057392
H	-12.744396	3.106765	-1.560293
C	-10.265966	-1.385527	-0.110064
C	-11.662803	-3.832553	-0.368367
C	-11.295782	-1.741546	0.802379
C	-9.962694	-2.294830	-1.156160
C	-10.672015	-3.501492	-1.282539
C	-11.972311	-2.959489	0.671346
H	-10.410846	-4.155900	-2.103800
H	-12.740402	-3.199700	1.399073
C	10.314223	-0.124951	1.349287
C	11.791241	-0.298177	3.756880
C	11.307711	-1.118715	1.530382
C	10.085383	0.788852	2.415407
C	10.833316	0.699660	3.595506
C	12.027072	-1.206634	2.733609
H	10.633727	1.422617	4.379797
H	12.760232	-1.997347	2.826506
C	10.265106	0.102978	-1.395598
C	11.650421	0.240784	-3.858991
C	11.273298	1.079764	-1.615573
C	9.979876	-0.804602	-2.447660
C	10.683421	-0.735826	-3.662179
C	11.942812	1.146984	-2.842570
H	10.434948	-1.458203	-4.428926
H	12.691620	1.921414	-2.974121
C	-11.693218	-0.855657	1.965163
H	-12.155982	0.074594	1.621484
H	-10.831481	-0.580509	2.582495
H	-12.409097	-1.361097	2.619365
C	-9.042550	2.047852	2.223330
H	-8.027638	2.139338	1.824461
H	-9.118286	1.049798	2.665394
H	-9.152508	2.773499	3.034356
C	-11.613305	0.794338	-2.059150
H	-10.711537	0.494318	-2.602458
H	-12.266746	1.300912	-2.774968
H	-12.119013	-0.122624	-1.739778
C	-8.877511	-2.039870	-2.184322
H	-8.971570	-2.728484	-3.029043
H	-7.881933	-2.176425	-1.749756
H	-8.908074	-1.023225	-2.585599
C	8.915855	-1.879276	-2.341068
H	9.028347	-2.621227	-3.137050
H	7.912256	-1.449407	-2.423706
H	8.950957	-2.413097	-1.387621
C	11.653260	2.102824	-0.565367
H	12.148237	1.632670	0.290091
H	10.779029	2.637686	-0.180283
H	12.336248	2.853329	-0.973177
C	11.632008	-2.147526	0.466310
H	10.734613	-2.654041	0.097057
H	12.300644	-2.920401	0.855614
H	12.123343	-1.687951	-0.397217
C	9.040253	1.884224	2.346032
H	8.029737	1.471136	2.425977
H	9.078655	2.440793	1.405300
H	9.173278	2.604497	3.158530
N	-12.428265	-5.136598	-0.467012
N	-12.540926	5.076086	0.389474
N	12.407394	0.353265	-5.166315
N	12.553687	-0.362708	5.064188
C	-13.908882	-4.852064	-0.637631
H	-14.439078	-5.802975	-0.711569
H	-14.043294	-4.268508	-1.548645
H	-14.270791	-4.291313	0.221918
C	-12.212602	-5.952267	0.794579
H	-12.759162	-6.891924	0.698274
H	-12.580958	-5.394715	1.653524
H	-11.144286	-6.140741	0.902581
C	-11.992661	-5.987473	-1.636872
H	-12.592933	-6.897469	-1.628982
H	-10.938838	-6.240769	-1.526520
H	-12.163980	-5.442134	-2.564349
C	-11.567887	6.239790	0.339599
H	-11.033263	6.198794	-0.609633
H	-10.865108	6.159238	1.166578
H	-12.133776	7.169404	0.420270
C	-13.549601	5.280731	-0.716185
H	-14.281559	4.474260	-0.690297
H	-13.034266	5.305150	-1.675693
H	-14.046994	6.234971	-0.541651
C	-13.296016	5.104364	1.705398
H	-13.987000	4.261297	1.722451
H	-13.842082	6.046763	1.772221
H	-12.590633	5.025091	2.530208
C	13.323924	0.927997	5.272828
H	14.014473	1.054143	4.438676
H	13.871188	0.857890	6.214312
H	12.626849	1.762855	5.309058
C	11.583452	-0.564165	6.213564
H	11.038451	-1.492882	6.042973
H	10.889655	0.273309	6.252182
H	12.152922	-0.620039	7.142730
C	13.549644	-1.498151	5.108411
H	14.283149	-1.367270	4.313617
H	13.022782	-2.445128	4.996269
H	14.048258	-1.466794	6.077404
C	13.892393	0.167456	-4.917090
H	14.417302	0.244423	-5.870691
H	14.045383	-0.817754	-4.476015
H	14.243868	0.940076	-4.236041
C	11.984018	-0.682636	-6.181527
H	12.573876	-0.524675	-7.084671
H	10.925547	-0.555995	-6.406190
H	12.178426	-1.678443	-5.784770
C	12.165254	1.719292	-5.782139
H	12.711004	1.776151	-6.725274
H	12.518559	2.491001	-5.101154
H	11.094484	1.833930	-5.951989
C	0.680220	-2.429952	0.242794
H	1.227065	-3.367227	0.305160
C	-0.681139	-2.428864	0.245890
H	-1.228988	-3.365383	0.310906
C	0.682975	2.484538	-0.098273
H	1.230865	3.421129	-0.161691
C	-0.678390	2.485339	-0.096406
H	-1.225161	3.422680	-0.158487

Compound 3-2M

DFT B3LYP/6-31G(d), gas phase, S_0

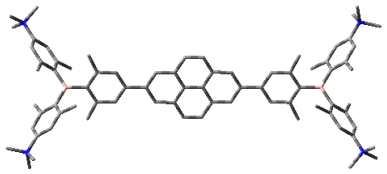

Point group: C_i
Total energy: -2019170.38 kcal mol^{-1}

Symbol	X	Y	Z
C	0.689110	0.025360	-0.025090
C	3.521930	0.009360	-0.007430
C	1.406530	-0.870400	-0.873610
C	1.406000	0.914340	0.830980
C	2.807230	0.885290	0.825720
C	2.807830	-0.857160	-0.850830
H	3.345310	1.583000	1.461660
H	3.345950	-1.561200	-1.479710
C	-0.689110	-0.025360	0.025090
C	-3.521930	-0.009360	0.007430
C	-1.406000	-0.914340	-0.830980
C	-1.406530	0.870400	0.873610
C	-2.807830	0.857160	0.850830
C	-2.807230	-0.885290	-0.825720
H	-3.345950	1.561200	1.479710
H	-3.345310	-1.583000	-1.461660
C	-5.052350	0.035500	-0.039010
C	-7.922330	0.021870	-0.026080
C	-5.783560	0.895900	0.792140
C	-5.782780	-0.828080	-0.868040
C	-7.177780	-0.864250	-0.865090
C	-7.179020	0.919910	0.801260
H	-5.246820	1.549050	1.474220
H	-5.245930	-1.474850	-1.556170
C	-7.832160	-1.839980	-1.826750
H	-8.251800	-2.708330	-1.306740
H	-8.643440	-1.386720	-2.405570
H	-7.097780	-2.215600	-2.544850
C	-7.832160	1.896450	1.762920
H	-8.634860	1.442080	2.352210
H	-7.093760	2.283140	2.470920
H	-8.263110	2.757930	1.240400
B	-9.489210	0.000810	-0.004210
C	-10.332510	1.365450	-0.012000
C	-11.806720	3.779330	-0.071000
C	-11.325090	1.642230	0.960670
C	-10.099920	2.339860	-1.022010
C	-10.846220	3.523980	-1.046330
C	-12.044560	2.848370	0.931380
H	-10.644870	4.236450	-1.839550
H	-12.778700	3.018550	1.707890
C	-10.289390	-1.389100	0.033850
C	-11.685500	-3.847150	0.154920
C	-11.314340	-1.696770	-0.901370
C	-9.990600	-2.352460	1.031740
C	-10.699560	-3.564520	1.090350
C	-11.990520	-2.920320	-0.838550
H	-10.441960	-4.261440	1.877030
H	-12.754770	-3.122000	-1.581850
C	-11.706690	-0.750650	-2.017500
H	-12.171920	0.159800	-1.627280
H	-10.842100	-0.442660	-2.615020
H	-12.418880	-1.221060	-2.701190
C	-9.057130	2.163930	-2.107910
H	-8.044300	2.234680	-1.699650
H	-9.129850	1.190700	-2.602680
H	-9.163630	2.931530	-2.879840
C	-11.648220	0.683540	2.089040
H	-10.748940	0.355610	2.620200
H	-12.305650	1.151050	2.827430
H	-12.151580	-0.215470	1.718930
C	-8.910780	-2.151820	2.077430
H	-9.008490	-2.884330	2.883940
H	-7.912930	-2.264570	1.641240
H	-8.944170	-1.157910	2.531920
N	-12.450380	-5.155010	0.180390
N	-12.567100	5.088670	-0.133590
C	-13.932060	-4.880750	0.358410
H	-14.461840	-5.834540	0.379130
H	-14.071500	-4.346430	1.298420
H	-14.290130	-4.275380	-0.471980
C	-12.227750	-5.902480	-1.121600
H	-12.774020	-6.846220	-1.078040
H	-12.592260	-5.300340	-1.951600
H	-11.158750	-6.084370	-1.234070
C	-12.019930	-6.066520	1.305630
H	-12.619410	-6.975150	1.246450
H	-10.965360	-6.313030	1.187300
H	-12.196320	-5.571260	2.259860
C	-11.595270	6.248620	-0.017150
H	-11.065360	6.157610	0.931250
H	-10.888310	6.212450	-0.843690
H	-12.161510	7.180890	-0.051230
C	-13.581450	5.233800	0.976280
H	-14.312610	4.429440	0.903950
H	-13.070940	5.207560	1.938310
H	-14.078750	6.195680	0.850120
C	-13.315630	5.186310	-1.449950
H	-14.005830	4.344960	-1.515180
H	-13.862130	6.130630	-1.469420
H	-12.606070	5.151300	-2.274240
C	0.658310	-1.762250	-1.719690
H	1.205860	-2.447270	-2.361840
C	-0.703020	-1.756250	-1.726270
H	-1.250150	-2.436440	-2.373900
C	0.703020	1.756250	1.726270
H	1.250150	2.436440	2.373900
C	-0.658310	1.762250	1.719690
H	-1.205860	2.447270	2.361840
C	5.052350	-0.035500	0.039010
C	5.783560	-0.895900	-0.792140
C	5.782780	0.828080	0.868040
C	7.179020	-0.919910	-0.801260
H	5.246820	-1.549050	-1.474220
C	7.177780	0.864250	0.865090
H	5.245930	1.474850	1.556170
C	7.922330	-0.021870	0.026080
C	7.832160	-1.896450	-1.762920
C	7.832160	1.839980	1.826750
B	9.489210	-0.000810	0.004210
H	8.634860	-1.442080	-2.352210
H	7.093760	-2.283140	-2.470920
H	8.263110	-2.757930	-1.240400
H	8.251800	2.708330	1.306740
H	8.643440	1.386720	2.405570
H	7.097780	2.215600	2.544850
C	10.332510	-1.365450	0.012000
C	10.289390	1.389100	-0.033850
C	11.325090	-1.642230	-0.960670
C	10.099920	-2.339860	1.022010
C	11.314340	1.696770	0.901370
C	9.990600	2.352460	-1.031740
C	12.044560	-2.848370	-0.931380
C	11.648220	-0.683540	-2.089040
C	10.846220	-3.523980	1.046330
C	9.057130	-2.163930	2.107910
C	11.990520	2.920320	0.838550
C	11.706690	0.750650	2.017500
C	10.699560	3.564520	-1.090350

C	8.910780	2.151820	-2.077430
C	11.806720	-3.779330	0.071000
H	12.778700	-3.018550	-1.707890
H	10.748940	-0.355610	-2.620200
H	12.305650	-1.151050	-2.827430
H	12.151580	0.215470	-1.718930
H	10.644870	-4.236450	1.839550
H	8.044300	-2.234680	1.699650
H	9.129850	-1.190700	2.602680
H	9.163630	-2.931530	2.879840
C	11.685500	3.847150	-0.154920
H	12.754770	3.122000	1.581850
H	12.171920	-0.159800	1.627280
H	10.842100	0.442660	2.615020
H	12.418880	1.221060	2.701190
H	10.441960	4.261440	-1.877030
H	9.008490	2.884330	-2.883940
H	7.912930	2.264570	-1.641240
H	8.944170	1.157910	-2.531920
N	12.567100	-5.088670	0.133590
N	12.450380	5.155010	-0.180390
C	11.595270	-6.248620	0.017150
C	13.581450	-5.233800	-0.976280
C	13.315630	-5.186310	1.449950
C	13.932060	4.880750	-0.358410
C	12.227750	5.902480	1.121600
C	12.019930	6.066520	-1.305630
H	11.065360	-6.157610	-0.931250
H	10.888310	-6.212450	0.843690
H	12.161510	-7.180890	0.051230
H	14.312610	-4.429440	-0.903950
H	13.070940	-5.207560	-1.938310
H	14.078750	-6.195680	-0.850120
H	14.005830	-4.344960	1.515180
H	13.862130	-6.130630	1.469420
H	12.606070	-5.151300	2.274240
H	14.461840	5.834540	-0.379130
H	14.071500	4.346430	-1.298420
H	14.290130	4.275380	0.471980
H	12.774020	6.846220	1.078040
H	12.592260	5.300340	1.951600
H	11.158750	6.084370	1.234070
H	12.619410	6.975150	-1.246450
H	10.965360	6.313030	-1.187300
H	12.196320	5.571260	-2.259860

Compound 3-3M

DFT B3LYP/6-31G(d), gas phase, S_0

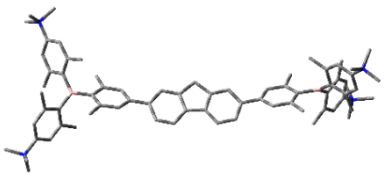

Point group: C_1
Total energy: -1947382.60 kcal mol^{-1}
Imaginary frequencies: 0

Symbol	X	Y	Z
C	-0.722957	-1.395965	-0.506400
C	-3.478062	-0.881140	-0.327342
C	-1.632553	-2.392732	-0.868008
C	-1.187115	-0.143453	-0.050765
C	-2.548027	0.113164	0.042941
C	-2.995565	-2.127301	-0.778429
H	-2.900854	1.088362	0.368570
H	-3.702625	-2.910844	-1.033028
C	0.741409	-1.382584	-0.509275
C	3.487756	-0.817872	-0.339974
C	1.667591	-2.362492	-0.874593
C	1.184666	-0.121904	-0.055414
C	2.541108	0.159222	0.033428
C	3.025744	-2.072145	-0.789702
H	2.877151	1.140280	0.359253
H	3.745847	-2.842339	-1.048487
C	4.943213	-0.547138	-0.265133
C	7.773937	-0.081449	-0.104046
C	5.496418	0.261444	0.739124
C	5.832900	-1.100428	-1.199052
C	7.211597	-0.904357	-1.128702
C	6.865991	0.517144	0.824784
H	4.841140	0.679158	1.498134
H	5.433501	-1.685009	-2.022601
C	-4.937327	-0.634548	-0.248932
C	-7.773337	-0.203778	-0.088426
C	-5.818345	-1.189981	-1.188934
C	-5.501543	0.153481	0.765239
C	-6.877538	0.358774	0.874115
C	-7.196255	-0.978426	-1.143051
H	-5.412228	-1.786359	-2.000768
H	-4.849157	0.593656	1.514379
C	8.042279	-1.560709	-2.217180
H	8.569021	-2.449565	-1.851755
H	8.795866	-0.889586	-2.641450
H	7.399809	-1.882450	-3.041738
C	7.320847	1.397519	1.974912
H	8.153114	0.963905	2.539061
H	6.501263	1.553575	2.681928
H	7.645469	2.385567	1.629999
C	-7.342633	1.225024	2.031188
H	-7.834540	0.636677	2.813458
H	-8.047427	2.003962	1.721325
H	-6.489934	1.730454	2.493204
C	-8.015669	-1.643059	-2.235139
H	-8.871130	-2.203968	-1.844338
H	-7.397453	-2.350758	-2.794371
H	-8.407961	-0.915808	-2.954318
B	9.321466	0.131439	0.009795
B	-9.322178	-0.002008	0.018015
C	9.943329	1.582676	0.292536
C	11.044205	4.152131	0.730092
C	10.850341	1.820587	1.354408
C	9.600121	2.678218	-0.547758
C	10.162480	3.941117	-0.327231
C	11.383766	3.101618	1.572203
H	9.882446	4.746459	-0.998640
H	12.059548	3.231889	2.407626
C	10.325378	-1.109661	-0.152222
C	12.061182	-3.331211	-0.402701
C	11.412128	-1.091973	-1.068162
C	10.144349	-2.273792	0.638424
C	11.020180	-3.365976	0.514687
C	12.256293	-2.201008	-1.192558
H	10.844936	-4.225940	1.147763
H	13.061259	-2.152197	-1.918487
C	-10.199823	0.341448	-1.279982
C	-11.711690	0.979288	-3.585660
C	-11.333069	-0.424776	-1.649184
C	-9.849427	1.448698	-2.101631
C	-10.613895	1.760180	-3.232371
C	-12.070490	-0.109561	-2.802378
H	-10.316212	2.617920	-3.826806
H	-12.914838	-0.739911	-3.049358
C	-10.073278	-0.149629	1.427619
C	-11.405768	-0.475316	3.902463
C	-10.933049	0.861214	1.935916
C	-9.904597	-1.327094	2.200343
C	-10.582286	-1.484015	3.421614
C	-11.577264	0.694845	3.166885

H	-10.430120	-2.406458	3.966773
H	-12.212142	1.498643	3.524893
C	11.695218	0.091340	-1.970721
H	11.971109	0.978997	-1.393809
H	10.824713	0.357813	-2.580073
H	12.515438	-0.126053	-2.660567
C	8.631592	2.549334	-1.706410
H	7.606292	2.405060	-1.352062
H	8.864421	1.696368	-2.350850
H	8.648405	3.446177	-2.332530
C	11.276879	0.731923	2.318306
H	10.421606	0.179504	2.719718
H	11.819057	1.150574	3.170891
H	11.934568	0.003067	1.833451
C	9.019219	-2.424353	1.644062
H	9.213044	-3.260303	2.322521
H	8.064584	-2.614439	1.142742
H	8.879005	-1.530071	2.256964
C	-9.001468	-2.469983	1.778789
H	-9.218175	-3.372304	2.358073
H	-7.947128	-2.218194	1.934544
H	-9.109610	-2.724552	0.721318
C	-11.175260	2.162775	1.200144
H	-11.725454	1.999206	0.268302
H	-10.237720	2.664843	0.939161
H	-11.755417	2.860262	1.810822
C	-11.796658	-1.627543	-0.852536
H	-10.980315	-2.328897	-0.653270
H	-12.572433	-2.180922	-1.389170
H	-12.211755	-1.330098	0.115842
C	-8.653749	2.335363	-1.816113
H	-7.715475	1.817269	-2.038424
H	-8.602264	2.643587	-0.767865
H	-8.687091	3.244639	-2.423411
N	13.002822	-4.505463	-0.577393
N	11.607628	5.543710	0.933982
N	-12.136466	-0.611238	5.222859
N	-12.484765	1.343709	-4.836276
C	14.427668	-4.070323	-0.290069
H	15.085264	-4.932717	-0.411061
H	14.472305	-3.697069	0.733264
H	14.714327	-3.285315	-0.986991
C	12.909865	-5.025875	-2.000050
H	13.583209	-5.878486	-2.102719
H	13.198740	-4.238082	-2.693061
H	11.879320	-5.327927	-2.187752
C	12.685954	-5.656530	0.348382
H	13.409927	-6.448382	0.155224
H	11.679887	-6.019923	0.141952
H	12.772108	-5.323334	1.382085
C	10.474851	6.520872	1.188592
H	9.934174	6.194982	2.077487
H	9.807047	6.530909	0.329417
H	10.900384	7.513925	1.342425
C	12.553181	5.628216	2.109230
H	13.395609	4.957895	1.942585
H	12.020896	5.360878	3.021329
H	12.908541	6.656542	2.178219
C	12.377621	5.972812	-0.301034
H	13.185273	5.259488	-0.466371
H	12.780212	6.972418	-0.129385
H	11.708566	5.984007	-1.159031
C	-13.038649	2.750472	-4.707518
H	-13.692551	2.783755	-3.835832
H	-13.598162	2.987515	-5.613868
H	-12.216787	3.452907	-4.584093
C	-11.566622	1.270353	-6.042642
H	-11.178627	0.254210	-6.116443
H	-10.746417	1.973928	-5.914719
H	-12.142460	1.525798	-6.933717
C	-13.651298	0.419191	-5.097172
H	-14.346059	0.468745	-4.259404
H	-13.283800	-0.597148	-5.234875
H	-14.147404	0.757262	-6.007134
C	-13.633418	-0.523662	4.991934
H	-14.140083	-0.627490	5.952813
H	-13.924181	-1.329982	4.318258
H	-13.874844	0.439747	4.547218
C	-11.861148	-1.925699	5.915292
H	-12.425789	-1.935333	6.847766
H	-10.795852	-2.005221	6.129171
H	-12.189597	-2.745900	5.277860
C	-11.704435	0.498002	6.164230
H	-12.231100	0.373835	7.111894
H	-11.952147	1.462586	5.725502
H	-10.627130	0.421287	6.312634
H	-1.291165	-3.365967	-1.209314
H	1.342594	-3.341532	-1.215312
C	-0.008715	0.759996	0.264546
H	-0.009669	1.085901	1.313694
H	-0.018343	1.674269	-0.344474

Compound 3-4M

DFT B3LYP/6-31G(d), gas phase, S_0

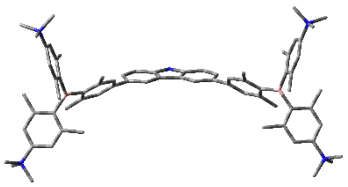

Point group: C_1
Total energy: -1957452.61 kcal mol^{-1}
Imaginary frequencies: 0

Symbol	X	Y	Z
C	-0.722957	-1.395965	-0.506400
C	-3.478062	-0.881140	-0.327342
C	-1.632553	-2.392732	-0.868008
C	-1.187115	-0.143453	-0.050765
C	-2.548027	0.113164	0.042941
C	-2.995565	-2.127301	-0.778429
H	-2.900854	1.088362	0.368570
H	-3.702625	-2.910844	-1.033028
C	0.741409	-1.382584	-0.509275
C	3.487756	-0.817872	-0.339974
C	1.667591	-2.362492	-0.874593
C	1.184666	-0.121904	-0.055414
C	2.541108	0.159222	0.033428
C	3.025744	-2.072145	-0.789702
H	2.877151	1.140280	0.359253
H	3.745847	-2.842339	-1.048487
C	4.943213	-0.547138	-0.265133
C	7.773937	-0.081449	-0.104046
C	5.496418	0.261444	0.739124
C	5.832900	-1.100428	-1.199052
C	7.211597	-0.904357	-1.128702
C	6.865991	0.517144	0.824784
H	4.841140	0.679158	1.498134
H	5.433501	-1.685009	-2.022601
C	-4.937327	-0.634548	-0.248932
C	-7.773337	-0.203778	-0.088426
C	-5.818345	-1.189981	-1.188934
C	-5.501543	0.153481	0.765239
C	-6.877538	0.358774	0.874115
C	-7.196255	-0.978426	-1.143051
H	-5.412228	-1.786359	-2.000768
H	-4.849157	0.593656	1.514379
C	8.042279	-1.560709	-2.217180
H	8.569021	-2.449565	-1.851755

H	8.795866	-0.889586	-2.641450
H	7.399809	-1.882450	-3.041738
C	7.320847	1.397519	1.974912
H	8.153114	0.963905	2.539061
H	6.501263	1.553575	2.681928
H	7.645469	2.385567	1.629999
C	-7.342633	1.225024	2.031188
H	-7.834540	0.636677	2.813458
H	-8.047427	2.003962	1.721325
H	-6.489934	1.730454	2.493204
C	-8.015669	-1.643059	-2.235139
H	-8.871130	-2.203968	-1.844338
H	-7.397453	-2.350758	-2.794371
H	-8.407961	-0.915808	-2.954318
B	9.321466	0.131439	0.009795
B	-9.322178	-0.002008	0.018015
C	9.943329	1.582676	0.292536
C	11.044205	4.152131	0.730092
C	10.850341	1.820587	1.354408
C	9.600121	2.678218	-0.547758
C	10.162480	3.941117	-0.327231
C	11.383766	3.101618	1.572203
H	9.882446	4.746459	-0.998640
H	12.059548	3.231889	2.407626
C	10.325378	-1.109661	-0.152222
C	12.061182	-3.331211	-0.402701
C	11.412128	-1.091973	-1.068162
C	10.144349	-2.273792	0.638424
C	11.020180	-3.365976	0.514687
C	12.256293	-2.201008	-1.192558
H	10.844936	-4.225940	1.147763
H	13.061259	-2.152197	-1.918487
C	-10.199823	0.341448	-1.279982
C	-11.711690	0.979288	-3.585660
C	-11.333069	-0.424776	-1.649184
C	-9.849427	1.448698	-2.101631
C	-10.613895	1.760180	-3.232371
C	-12.070490	-0.109561	-2.802378
H	-10.316212	2.617920	-3.826806
H	-12.914838	-0.739911	-3.049358
C	-10.073278	-0.149629	1.427619
C	-11.405768	-0.475316	3.902463
C	-10.933049	0.861214	1.935916
C	-9.904597	-1.327094	2.200343
C	-10.582286	-1.484015	3.421614
C	-11.577264	0.694845	3.166885
H	-10.430120	-2.406458	3.966773
H	-12.212142	1.498643	3.524893
C	11.695218	0.091340	-1.970721
H	11.971109	0.978997	-1.393809
H	10.824713	0.357813	-2.580073
H	12.515438	-0.126053	-2.660567
C	8.631592	2.549334	-1.706410
H	7.606292	2.405060	-1.352062
H	8.864421	1.696368	-2.350850
H	8.648405	3.446177	-2.332530
C	11.276879	0.731923	2.318306
H	10.421606	0.179504	2.719718
H	11.819057	1.150574	3.170891
H	11.934568	0.003067	1.833451
C	9.019219	-2.424353	1.644062
H	9.213044	-3.260303	2.322521
H	8.064584	-2.614439	1.142742
H	8.879005	-1.530071	2.256964
C	-9.001468	-2.469983	1.778789
H	-9.218175	-3.372304	2.358073
H	-7.947128	-2.218194	1.934544
H	-9.109610	-2.724552	0.721318
C	-11.175260	2.162775	1.200144
H	-11.725454	1.999206	0.268302
H	-10.237720	2.664843	0.939161
H	-11.755417	2.860262	1.810822
C	-11.796658	-1.627543	-0.852536
H	-10.980315	-2.328897	-0.653270
H	-12.572433	-2.180922	-1.389170
H	-12.211755	-1.330098	0.115842
C	-8.653749	2.335363	-1.816113
H	-7.715475	1.817269	-2.038424
H	-8.602264	2.643587	-0.767865
H	-8.687091	3.244639	-2.423411
N	13.002822	-4.505463	-0.577393
N	11.607628	5.543710	0.933982
N	-12.136466	-0.611238	5.222859
N	-12.484765	1.343709	-4.836276
C	14.427668	-4.070323	-0.290069
H	15.085264	-4.932717	-0.411061
H	14.472305	-3.697069	0.733264
H	14.714327	-3.285315	-0.986991
C	12.909865	-5.025875	-2.000050
H	13.583209	-5.878486	-2.102719
H	13.198740	-4.238082	-2.693061
H	11.879320	-5.327927	-2.187752
C	12.685954	-5.656530	0.348382
H	13.409927	-6.448382	0.155224
H	11.679887	-6.019923	0.141952
H	12.772108	-5.323334	1.382085
C	10.474851	6.520872	1.188592
H	9.934174	6.194982	2.077487
H	9.807047	6.530909	0.329417
H	10.900384	7.513925	1.342425
C	12.553181	5.628216	2.109230
H	13.395609	4.957895	1.942585
H	12.020896	5.360878	3.021329
H	12.908541	6.656542	2.178219
C	12.377621	5.972812	-0.301034
H	13.185273	5.259488	-0.466371
H	12.780212	6.972418	-0.129385
H	11.708566	5.984007	-1.159031
C	-13.038649	2.750472	-4.707518
H	-13.692551	2.783755	-3.835832
H	-13.598162	2.987515	-5.613868
H	-12.216787	3.452907	-4.584093
C	-11.566622	1.270353	-6.042642
H	-11.178627	0.254210	-6.116443
H	-10.746417	1.973928	-5.914719
H	-12.142460	1.525798	-6.933717
C	-13.651298	0.419191	-5.097172
H	-14.346059	0.468745	-4.259404
H	-13.283800	-0.597148	-5.234875
H	-14.147404	0.757262	-6.007134
C	-13.633418	-0.523662	4.991934
H	-14.140083	-0.627490	5.952813
H	-13.924181	-1.329982	4.318258
H	-13.874844	0.439747	4.547218
C	-11.861148	-1.925699	5.915292
H	-12.425789	-1.935333	6.847766
H	-10.795852	-2.005221	6.129171
H	-12.189597	-2.745900	5.277860
C	-11.704435	0.498002	6.164230
H	-12.231100	0.373835	7.111894
H	-11.952147	1.462586	5.725502
H	-10.627130	0.421287	6.312634
H	-1.291165	-3.365967	-1.209314
H	1.342594	-3.341532	-1.215312
C	-0.008715	0.759996	0.264546
H	-0.009669	1.085901	1.313694
H	-0.018343	1.674269	-0.344474

Compound 3-5M

DFT B3LYP/6-31G(d), gas phase, S_0

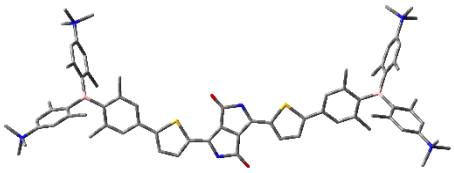

Point group: C_1
Total energy: - 2633343.06 kcal mol^{-1}
Imaginary frequencies: 0

Symbol	X	Y	Z
C	-0.722957	-1.395965	-0.506400
C	-3.478062	-0.881140	-0.327342
C	-1.632553	-2.392732	-0.868008
C	-1.187115	-0.143453	-0.050765
C	-2.548027	0.113164	0.042941
C	-2.995565	-2.127301	-0.778429
H	-2.900854	1.088362	0.368570
H	-3.702625	-2.910844	-1.033028
C	0.741409	-1.382584	-0.509275
C	3.487756	-0.817872	-0.339974
C	1.667591	-2.362492	-0.874593
C	1.184666	-0.121904	-0.055414
C	2.541108	0.159222	0.033428
C	3.025744	-2.072145	-0.789702
H	2.877151	1.140280	0.359253
H	3.745847	-2.842339	-1.048487
C	4.943213	-0.547138	-0.265133
C	7.773937	-0.081449	-0.104046
C	5.496418	0.261444	0.739124
C	5.832900	-1.100428	-1.199052
C	7.211597	-0.904357	-1.128702
C	6.865991	0.517144	0.824784
H	4.841140	0.679158	1.498134
H	5.433501	-1.685009	-2.022601
C	-4.937327	-0.634548	-0.248932
C	-7.773337	-0.203778	-0.088426
C	-5.818345	-1.189981	-1.188934
C	-5.501543	0.153481	0.765239
C	-6.877538	0.358774	0.874115
C	-7.196255	-0.978426	-1.143051
H	-5.412228	-1.786359	-2.000768
H	-4.849157	0.593656	1.514379
C	8.042279	-1.560709	-2.217180
H	8.569021	-2.449565	-1.851755
H	8.795866	-0.889586	-2.641450
H	7.399809	-1.882450	-3.041738
C	7.320847	1.397519	1.974912
H	8.153114	0.963905	2.539061
H	6.501263	1.553575	2.681928
H	7.645469	2.385567	1.629999
C	-7.342633	1.225024	2.031188
H	-7.834540	0.636677	2.813458
H	-8.047427	2.003962	1.721325
H	-6.489934	1.730454	2.493204
C	-8.015669	-1.643059	-2.235139
H	-8.871130	-2.203968	-1.844338
H	-7.397453	-2.350758	-2.794371
H	-8.407961	-0.915808	-2.954318
B	9.321466	0.131439	0.009795
B	-9.322178	-0.002008	0.018015
C	9.943329	1.582676	0.292536
C	11.044205	4.152131	0.730092
C	10.850341	1.820587	1.354408
C	9.600121	2.678218	-0.547758
C	10.162480	3.941117	-0.327231
C	11.383766	3.101618	1.572203
H	9.882446	4.746459	-0.998640
H	12.059548	3.231889	2.407626
C	10.325378	-1.109661	-0.152222
C	12.061182	-3.331211	-0.402701
C	11.412128	-1.091973	-1.068162
C	10.144349	-2.273792	0.638424
C	11.020180	-3.365976	0.514687
C	12.256293	-2.201008	-1.192558
H	10.844936	-4.225940	1.147763
H	13.061259	-2.152197	-1.918487
C	-10.199823	0.341448	-1.279982
C	-11.711690	0.979288	-3.585660
C	-11.333069	-0.424776	-1.649184
C	-9.849427	1.448698	-2.101631
C	-10.613895	1.760180	-3.232371
C	-12.070490	-0.109561	-2.802378
H	-10.316212	2.617920	-3.826806
H	-12.914838	-0.739911	-3.049358
C	-10.073278	-0.149629	1.427619
C	-11.405768	-0.475316	3.902463
C	-10.933049	0.861214	1.935916
C	-9.904597	-1.327094	2.200343
C	-10.582286	-1.484015	3.421614
C	-11.577264	0.694845	3.166885
H	-10.430120	-2.406458	3.966773
H	-12.212142	1.498643	3.524893
C	11.695218	0.091340	-1.970721
H	11.971109	0.978997	-1.393809
H	10.824713	0.357813	-2.580073
H	12.515438	-0.126053	-2.660567
C	8.631592	2.549334	-1.706410
H	7.606292	2.405060	-1.352062
H	8.864421	1.696368	-2.350850
H	8.648405	3.446177	-2.332530
C	11.276879	0.731923	2.318306
H	10.421606	0.179504	2.719718
H	11.819057	1.150574	3.170891
H	11.934568	0.003067	1.833451
C	9.019219	-2.424353	1.644062
H	9.213044	-3.260303	2.322521
H	8.064584	-2.614439	1.142742
H	8.879005	-1.530071	2.256964
C	-9.001468	-2.469983	1.778789
H	-9.218175	-3.372304	2.358073
H	-7.947128	-2.218194	1.934544
H	-9.109610	-2.724552	0.721318
C	-11.175260	2.162775	1.200144
H	-11.725454	1.999206	0.268302
H	-10.237720	2.664843	0.939161
H	-11.755417	2.860262	1.810822
C	-11.796658	-1.627543	-0.852536
H	-10.980315	-2.328897	-0.653270
H	-12.572433	-2.180922	-1.389170
H	-12.211755	-1.330098	0.115842
C	-8.653749	2.335363	-1.816113
H	-7.715475	1.817269	-2.038424
H	-8.602264	2.643587	-0.767865
H	-8.687091	3.244639	-2.423411
N	13.002822	-4.505463	-0.577393
N	11.607628	5.543710	0.933982
N	-12.136466	-0.611238	5.222859
N	-12.484765	1.343709	-4.836276
C	14.427668	-4.070323	-0.290069
H	15.085264	-4.932717	-0.411061
H	14.472305	-3.697069	0.733264
H	14.714327	-3.285315	-0.986991
C	12.909865	-5.025875	-2.000050
H	13.583209	-5.878486	-2.102719
H	13.198740	-4.238082	-2.693061
H	11.879320	-5.327927	-2.187752
C	12.685954	-5.656530	0.348382

H	13.409927	-6.448382	0.155224
H	11.679887	-6.019923	0.141952
H	12.772108	-5.323334	1.382085
C	10.474851	6.520872	1.188592
H	9.934174	6.194982	2.077487
H	9.807047	6.530909	0.329417
H	10.900384	7.513925	1.342425
C	12.553181	5.628216	2.109230
H	13.395609	4.957895	1.942585
H	12.020896	5.360878	3.021329
H	12.908541	6.656542	2.178219
C	12.377621	5.972812	-0.301034
H	13.185273	5.259488	-0.466371
H	12.780212	6.972418	-0.129385
H	11.708566	5.984007	-1.159031
C	-13.038649	2.750472	-4.707518
H	-13.692551	2.783755	-3.835832
H	-13.598162	2.987515	-5.613868
H	-12.216787	3.452907	-4.584093
C	-11.566622	1.270353	-6.042642
H	-11.178627	0.254210	-6.116443
H	-10.746417	1.973928	-5.914719
H	-12.142460	1.525798	-6.933717
C	-13.651298	0.419191	-5.097172
H	-14.346059	0.468745	-4.259404
H	-13.283800	-0.597148	-5.234875
H	-14.147404	0.757262	-6.007134
C	-13.633418	-0.523662	4.991934
H	-14.140083	-0.627490	5.952813
H	-13.924181	-1.329982	4.318258
H	-13.874844	0.439747	4.547218
C	-11.861148	-1.925699	5.915292
H	-12.425789	-1.935333	6.847766
H	-10.795852	-2.005221	6.129171
H	-12.189597	-2.745900	5.277860
C	-11.704435	0.498002	6.164230
H	-12.231100	0.373835	7.111894
H	-11.952147	1.462586	5.725502
H	-10.627130	0.421287	6.312634
H	-1.291165	-3.365967	-1.209314
H	1.342594	-3.341532	-1.215312
C	-0.008715	0.759996	0.264546
H	-0.009669	1.085901	1.313694
H	-0.018343	1.674269	-0.344474

Compound 3-5M

DFT B3LYP/6-31G(d), gas phase, S_0

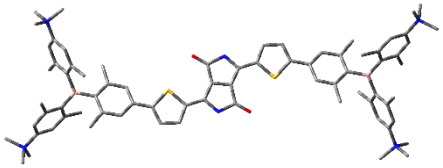

Point group: C_i

Total energy: -2633397.46 kcal mol^{-1}

Symbol	X	Y	Z
C	1.332320	0.994310	-0.567460
N	0.314620	1.831600	-1.017960
H	0.450370	2.703510	-1.510550
C	-0.980160	1.338470	-0.729070
O	-2.020840	1.916790	-1.036130
C	-0.706900	0.088170	-0.039640
C	0.706900	-0.088170	0.039640
C	-1.332320	-0.994310	0.567460
N	-0.314620	-1.831600	1.017960
H	-0.450370	-2.703510	1.510550
C	0.980160	-1.338470	0.729070
O	2.020840	-1.916790	1.036130
C	-2.714330	-1.314190	0.759080
C	-3.250230	-2.442200	1.365810
H	-2.649200	-3.247080	1.774030
C	-4.658360	-2.453550	1.388310
H	-5.235790	-3.270990	1.803720
C	-5.233700	-1.339090	0.800160
S	-3.997920	-0.246510	0.213050
C	-6.656220	-1.032850	0.643320
C	-9.442210	-0.467220	0.344540
C	-7.110530	-0.084470	-0.285180
C	-7.619130	-1.690600	1.425420
C	-8.983940	-1.443070	1.277300
C	-8.464290	0.220990	-0.430460
H	-6.394540	0.423820	-0.925600
H	-7.298680	-2.404660	2.177820
C	-8.819360	1.272510	-1.465040
H	-9.148450	2.205580	-0.996040
H	-7.948510	1.504570	-2.085040
H	-9.620540	0.950420	-2.137730
C	-9.923120	-2.228970	2.173110
H	-9.360350	-2.737840	2.961160
H	-10.669030	-1.595240	2.663160
H	-10.469900	-2.994040	1.611900
B	-10.981990	-0.162870	0.171540
C	-11.505840	1.340630	0.152590
C	-12.417060	4.012210	0.126850
C	-11.149660	2.243080	1.191500
C	-12.336470	1.818950	-0.891190
C	-12.771350	3.152810	-0.903200
C	-11.620470	3.559000	1.174430
H	-13.386880	3.478920	-1.730410
H	-11.341230	4.213480	1.992370
C	-12.026590	-1.352450	0.004250
C	-13.891830	-3.443670	-0.341570
C	-13.204480	-1.419170	0.796820
C	-11.814060	-2.368920	-0.961390
C	-12.754250	-3.395910	-1.134250
C	-14.114100	-2.466240	0.623950
H	-12.557940	-4.140630	-1.893320
H	-14.995170	-2.489420	1.255220
C	-10.270780	1.845530	2.360930
H	-10.582950	0.900830	2.816640
H	-9.227770	1.723840	2.051600
H	-10.300320	2.610650	3.141840
C	-12.787090	0.948630	-2.048000
H	-13.558000	0.237060	-1.733780
H	-13.208760	1.561160	-2.849800
H	-11.967060	0.366910	-2.479350
C	-13.533590	-0.396690	1.866110
H	-14.353470	-0.749920	2.497770
H	-12.681980	-0.191620	2.522180
H	-13.840600	0.557460	1.425780
C	-10.594990	-2.411930	-1.862660
H	-9.703430	-2.726560	-1.310270
H	-10.747370	-3.121810	-2.680640
H	-10.368000	-1.440020	-2.310390
N	-12.879660	5.448650	0.147580
N	-14.918930	-4.537190	-0.505700
C	-13.707330	5.816290	-1.060530
H	-14.600260	5.194400	-1.088460
H	-13.990250	6.863020	-0.958450
H	-13.108670	5.680650	-1.959780
C	-13.731900	5.688350	1.379090
H	-13.137940	5.498720	2.270430
H	-14.067670	6.725530	1.366970
H	-14.582950	5.009220	1.340900
C	-11.675420	6.370340	0.172380
H	-11.090100	6.176390	1.068040
H	-11.079280	6.174160	-0.718090
H	-12.032550	7.400020	0.176250

C	-14.538820	-5.546920	-1.562030
H	-13.600850	-6.024120	-1.282810
H	-15.333640	-6.290070	-1.605980
H	-14.450910	-5.045340	-2.524040
C	-16.245490	-3.925140	-0.913160
H	-16.574300	-3.231960	-0.142080
H	-16.101820	-3.400100	-1.857110
H	-16.971650	-4.729930	-1.027690
C	-15.083560	-5.286990	0.802250
H	-14.118660	-5.714320	1.073300
H	-15.421640	-4.599210	1.573680
H	-15.824220	-6.073020	0.653640
C	2.714330	1.314190	-0.759080
C	3.250230	2.442200	-1.365810
S	3.997920	0.246510	-0.213050
H	2.649200	3.247080	-1.774030
C	4.658360	2.453550	-1.388310
C	5.233700	1.339090	-0.800160
H	5.235790	3.270990	-1.803720
C	6.656220	1.032850	-0.643320
C	7.110530	0.084470	0.285180
C	7.619130	1.690600	-1.425420
C	8.464290	-0.220990	0.430460
H	6.394540	-0.423820	0.925600
C	8.983940	1.443070	-1.277300
H	7.298680	2.404660	-2.177820
C	9.442210	0.467220	-0.344540
C	8.819360	-1.272510	1.465040
C	9.923120	2.228970	-2.173110
B	10.981990	0.162870	-0.171540
H	9.148450	-2.205580	0.996040
H	7.948510	-1.504570	2.085040
H	9.620540	-0.950420	2.137730
H	9.360350	2.737840	-2.961160
H	10.669030	1.595240	-2.663160
H	10.469900	2.994040	-1.611900
C	11.505840	-1.340630	-0.152590
C	12.026590	1.352450	-0.004250
C	11.149660	-2.243080	-1.191500
C	12.336470	-1.818950	0.891190
C	13.204480	1.419170	-0.796820
C	11.814060	2.368920	0.961390
C	11.620470	-3.559000	-1.174430
C	10.270780	-1.845530	-2.360930
C	12.771350	-3.152810	0.903200
C	12.787090	-0.948630	2.048000
C	14.114100	2.466240	-0.623950
C	13.533590	0.396690	-1.866110
C	12.754250	3.395910	1.134250
C	10.594990	2.411930	1.862660
C	12.417060	-4.012210	-0.126850
H	11.341230	-4.213480	-1.992370
H	10.582950	-0.900830	-2.816640
H	9.227770	-1.723840	-2.051600
H	10.300320	-2.610650	-3.141840
H	13.386880	-3.478920	1.730410
H	13.558000	-0.237060	1.733780
H	13.208760	-1.561160	2.849800
H	11.967060	-0.366910	2.479350
C	13.891830	3.443670	0.341570
H	14.995170	2.489420	-1.255220
H	14.353470	0.749920	-2.497770
H	12.681980	0.191620	-2.522180
H	13.840600	-0.557460	-1.425780
H	12.557940	4.140630	1.893320
H	9.703430	2.726560	1.310270
H	10.747370	3.121810	2.680640
H	10.368000	1.440020	2.310390
N	12.879660	-5.448650	-0.147580
N	14.918930	4.537190	0.505700
C	13.707330	-5.816290	1.060530
C	13.731900	-5.688350	-1.379090
C	11.675420	-6.370340	-0.172380
C	14.538820	5.546920	1.562030
C	16.245490	3.925140	0.913160
C	15.083560	5.286990	-0.802250
H	14.600260	-5.194400	1.088460
H	13.990250	-6.863020	0.958450
H	13.108670	-5.680650	1.959780
H	13.137940	-5.498720	-2.270430
H	14.067670	-6.725530	-1.366970
H	14.582950	-5.009220	-1.340900
H	11.090100	-6.176390	-1.068040
H	11.079280	-6.174160	0.718090
H	12.032550	-7.400020	-0.176250
H	13.600850	6.024120	1.282810
H	15.333640	6.290070	1.605980
H	14.450910	5.045340	2.524040
H	16.574300	3.231960	0.142080
H	16.101820	3.400100	1.857110
H	16.971650	4.729930	1.027690
H	14.118660	5.714320	-1.073300
H	15.421640	4.599210	-1.573680
H	15.824220	6.073020	-0.653640

Compound 4-1

DFT B3LYP/6-31G(d), gas phase, S_0

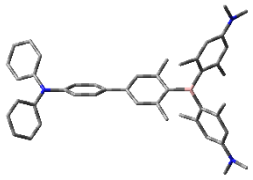

Point group: C_1
Total energy: -1237539.71 kcal mol^{-1}
Dipole moment: 2.66 D
Imaginary frequencies: 0

Symbol	X	Y	Z
N	-6.882105	0.000024	0.000068
C	-5.461794	0.000011	0.000029
C	-4.742346	0.206406	-1.188069
C	-4.742303	-0.206409	1.188099
C	-3.351855	0.213682	-1.180810
H	-5.280365	0.351133	-2.119607
C	-3.351814	-0.213713	1.180789
H	-5.280294	-0.351137	2.119654
C	-2.618801	-0.000019	-0.000025
H	-2.822651	0.347706	-2.120034
H	-2.822575	-0.347758	2.119990
C	-7.592965	-0.956888	0.774539
C	-8.733325	-0.580595	1.503115
C	-7.165948	-2.294041	0.824029
C	-9.431768	-1.524386	2.253654
H	-9.065887	0.452194	1.476245
C	-7.860625	-3.226396	1.592125
H	-6.289548	-2.594473	0.258726
C	-8.999517	-2.851213	2.308005
H	-10.311935	-1.214450	2.811167
H	-7.515213	-4.256720	1.618009
H	-9.542431	-3.582469	2.900063
C	-7.592993	0.956856	-0.774478
C	-8.733349	0.580501	-1.503016
C	-7.166002	2.294021	-0.824050
C	-9.431816	1.524237	-2.253615
H	-9.065902	-0.452289	-1.476082
C	-7.860698	3.226313	-1.592195
H	-6.289604	2.594497	-0.258765

C	-8.999591	2.851062	-2.308050
H	-10.311981	1.214242	-2.811099
H	-7.515316	4.256645	-1.618146
H	-9.542516	3.582277	-2.900149
C	-1.137192	-0.000032	-0.000050
C	-0.407879	-0.849195	0.842285
C	-0.407889	0.849127	-0.842397
H	-0.943430	-1.537721	1.491573
C	0.989345	-0.872743	0.845526
C	0.989336	0.872665	-0.845662
H	-0.943444	1.537662	-1.491671
C	1.726716	-0.000040	-0.000075
C	1.663934	-1.852220	1.788689
C	1.663915	1.852148	-1.788826
B	3.319410	-0.000014	-0.000035
H	2.144891	-2.673133	1.246932
H	2.444067	-1.378526	2.394895
H	0.931651	-2.286746	2.477459
H	2.144935	2.673025	-1.247072
H	2.443994	1.378435	-2.395089
H	0.931615	2.286723	-2.477548
C	4.099763	-1.356890	-0.201854
C	4.099669	1.356922	0.201828
C	5.184002	-1.720834	0.647516
C	3.750682	-2.289103	-1.220269
C	3.750553	2.289059	1.220293
C	5.183885	1.720950	-0.647527
C	5.853015	-2.934327	0.487849
C	5.653387	-0.843217	1.795432
C	4.456570	-3.480277	-1.385999
C	2.621062	-2.035026	-2.202742
C	4.456393	3.480259	1.386075
C	2.620970	2.034866	2.202777
C	5.852849	2.934466	-0.487805
C	5.653319	0.843377	-1.795456
C	5.526448	-3.838703	-0.542121
H	6.644997	-3.175265	1.187606
H	4.823858	-0.473476	2.406699
H	6.325274	-1.403107	2.454754
H	6.194071	0.039227	1.438248
H	4.160067	-4.140528	-2.192961
H	2.673276	-1.036208	-2.648661
H	2.653355	-2.761510	-3.021508
H	1.639845	-2.114466	-1.723940
C	5.526255	3.838770	0.542215
H	4.159852	4.140459	2.193065
H	1.639740	2.114247	1.723993
H	2.653223	2.761324	3.021566
H	2.673267	1.036037	2.648664
H	6.644826	3.175462	-1.187546
H	6.194042	-0.039050	-1.438285
H	4.823811	0.473609	-2.406734
H	6.325185	1.403308	-2.454766
N	6.228759	-5.022208	-0.721809
N	6.228567	5.022283	0.721977
C	5.720197	-6.022811	-1.644459
C	7.201295	-5.436276	0.274568
C	5.719876	6.022899	1.644551
C	7.200797	5.436571	-0.274615
H	5.660271	-5.624467	-2.664406
H	6.405652	-6.872585	-1.663146
H	4.720285	-6.392045	-1.365898
H	6.751991	-5.613731	1.265112
H	7.678400	-6.361641	-0.054849
H	7.988305	-4.682029	0.391610
H	5.659687	5.624495	2.664451
H	6.405427	6.872590	1.663457
H	4.720063	6.392262	1.365788
H	6.751217	5.614118	-1.265020
H	7.677914	6.361930	0.054803
H	7.987837	4.682406	-0.391956

Compound 4-2

DFT B3LYP/6-31G(d), gas phase, S_0

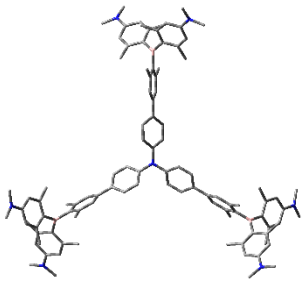

Point group: C_3
Total energy: -2771733.92 kcal mol^{-1}
Dipole moment: 0.00 D
Imaginary frequencies: 0

Symbol	X	Y	Z
C	2.603946	2.552778	0.782671
C	3.694074	2.129179	0.002286
C	3.514208	0.973509	-0.778031
C	2.308700	0.280253	-0.788704
C	1.230830	0.709341	0.002409
C	1.399849	1.857109	0.793496
N	0.000000	0.000000	0.002457
C	-1.229722	0.711260	0.002409
C	-0.001108	-1.420601	0.002409
C	-0.911644	-2.139519	-0.788704
C	-0.914021	-3.530147	-0.778031
C	-0.003114	-4.263751	0.002286
C	0.908798	-3.531472	0.782671
C	0.908379	-2.140859	0.793496
C	-2.308228	0.283750	0.793496
C	-3.512743	0.978694	0.782671
C	-3.690960	2.134573	0.002286
C	-2.600187	2.556639	-0.778031
C	-1.397056	1.859266	-0.788704
C	-0.003818	-5.746073	0.002125
C	-0.297421	-6.475265	-1.157377
C	-0.287783	-7.872468	-1.179763
C	-0.003158	-8.610169	0.001448
C	0.280406	-7.872891	1.183186
C	0.289430	-6.475675	1.161454
C	0.594632	-8.547543	2.506105
C	-0.602502	-8.546747	-2.502771
B	0.000000	-10.202587	0.000567
C	-0.860625	-10.986048	1.066722
C	0.864726	-10.979954	-1.066928
C	-0.311338	-12.069890	1.810312
C	-1.062971	-12.740669	2.775117
C	-2.409688	-12.416362	3.032756
C	-2.957214	-11.347264	2.296365
C	-2.211748	-10.639632	1.353904
C	0.319856	-12.063323	-1.814288
C	1.074646	-12.728577	-2.780486
C	2.420457	-12.398802	-3.035934
C	2.963677	-11.330242	-2.295568
C	2.214922	-10.628060	-1.351601
C	-1.113717	-12.535712	-1.641505
C	2.930670	-9.499453	-0.630551
C	1.123604	-12.537105	1.634874
C	-2.932083	-9.511005	0.637423
N	-3.163622	-13.120297	3.961676
N	3.177589	-13.097142	-3.966572
C	-4.465920	-12.612277	4.358056
C	4.478070	-12.582770	-4.360687
C	2.530038	-14.065701	-4.834075

C	-2.512447	-14.090413	4.824706
H	2.696070	3.452048	1.385028
H	4.338449	0.602520	-1.380539
H	2.199235	-0.606586	-1.404803
H	0.577624	2.206906	1.409639
H	-1.624936	-1.601300	-1.404803
H	-1.647427	-4.058468	-1.380539
H	1.641526	-4.060889	1.385028
H	1.622425	-1.603691	1.409639
H	-2.200049	-0.603216	1.409639
H	-4.337596	0.608841	1.385028
H	-2.691023	3.455947	-1.380539
H	-0.574299	2.207886	-1.404803
H	-0.507601	-5.939663	-2.080091
H	0.499252	-5.940366	2.084424
H	1.360112	-9.325235	2.407038
H	0.963387	-7.814665	3.231598
H	-0.288410	-9.031568	2.935761
H	-0.972558	-7.813843	-3.227585
H	0.280491	-9.029917	-2.933508
H	-1.367362	-9.325037	-2.403261
H	-0.580674	-13.532159	3.337175
H	-3.987992	-11.052586	2.456598
H	0.595519	-13.519998	-3.345335
H	3.993631	-11.031572	-2.453737
H	-1.829690	-11.707566	-1.633311
H	-1.396019	-13.208034	-2.458768
H	-1.253065	-13.076731	-0.699956
H	2.556960	-8.517821	-0.938854
H	2.807992	-9.555305	0.456223
H	4.004935	-9.529414	-0.840968
H	1.836788	-11.706600	1.627127
H	1.409154	-13.209906	2.450622
H	1.263510	-13.076078	0.692223
H	-2.561436	-8.529203	0.948874
H	-2.810349	-9.562481	-0.449667
H	-4.006023	-9.545393	0.848841
H	-4.412958	-11.612578	4.818050
H	-5.143958	-12.552076	3.498307
H	-4.911915	-13.298343	5.081069
H	5.155494	-12.522930	-3.500445
H	4.927026	-13.264677	-5.085812
H	4.421477	-11.581706	-4.817289
H	1.766557	-13.613729	-5.487872
H	3.284058	-14.539409	-5.466190
H	2.046655	-14.855862	-4.247623
H	-2.027100	-14.876669	4.234633
H	-1.749850	-13.638750	5.479732
H	-3.264518	-14.568967	5.455482
C	4.978154	2.869730	0.002125
C	5.756454	2.980058	-1.157377
C	5.463384	3.488491	1.161454
C	6.961649	3.687006	-1.179763
H	5.397700	2.530236	-2.080091
C	6.677920	4.179284	1.183186
H	4.894882	3.402548	2.084424
C	7.458204	4.302349	0.001448
C	7.702951	3.751592	-2.502771
C	7.105074	4.788738	2.506105
B	8.835699	5.101293	0.000567
H	7.253266	3.064661	-3.227585
H	7.679892	4.757871	-2.933508
H	8.759400	3.478349	-2.403261
H	7.395834	5.840509	2.407038
H	6.286005	4.741650	3.231598
H	7.965772	4.266014	2.935761
C	9.944509	4.747701	1.066722
C	9.076556	6.238852	-1.066928
C	10.608501	5.765319	1.810312
C	10.320066	3.404387	1.353904
C	10.287216	6.308665	-1.814288
C	8.096709	7.232209	-1.351601
C	11.565228	5.449774	2.775117
C	10.295650	7.241622	1.634874
C	11.305626	3.112610	2.296365
C	9.702813	2.216244	0.637423
C	10.485948	7.294960	-2.780486
C	11.413103	5.303348	-1.641505
C	8.330439	8.231741	-2.295568
C	6.761433	7.287761	-0.630551
C	11.957729	4.121330	3.032756
H	12.009531	6.263201	3.337175
H	9.219819	7.444005	1.627127
H	10.735537	7.825316	2.450622
H	10.692461	7.632270	0.692223
H	11.565816	2.072590	2.456598
H	8.667224	2.046332	0.948874
H	9.686526	2.347407	-0.449667
H	10.269564	1.303379	0.848841
C	9.527449	8.295579	-3.035934
H	11.410902	7.275734	-3.345335
H	11.053895	4.269225	-1.633311
H	12.136502	5.395029	-2.458768
H	11.951314	5.453179	-0.699956
H	7.556806	8.974372	-2.453737
H	6.098170	6.473303	-0.938854
H	6.871141	7.209445	0.456223
H	6.250247	8.233083	-0.840968
N	12.944321	3.820371	3.961676
N	9.753663	9.300444	-3.966572
C	13.155512	2.438539	4.358056
C	13.458879	4.869364	4.824706
C	8.657963	10.169507	-4.360687
C	10.916235	9.223927	-4.834075
H	12.263267	1.984556	4.818050
H	13.442396	1.821240	3.498307
H	13.972661	2.395329	5.081069
H	13.897123	5.682815	4.234633
H	12.686429	5.303961	5.479732
H	14.249354	4.457328	5.455482
H	8.267429	10.726253	-3.500445
H	9.024034	10.899268	-5.085812
H	7.819313	9.619965	-4.817289
H	10.906557	8.336748	-5.487872
H	10.949469	10.113782	-5.466190
H	11.842226	9.200386	-4.247623
C	-4.974336	2.876343	0.002125
C	-5.459033	3.495206	-1.157377
C	-5.752814	2.987184	1.161454
C	-6.673865	4.185461	-1.179763
H	-4.890098	3.409427	-2.080091
C	-6.958326	3.693606	1.183186
H	-5.394134	2.537818	2.084424
C	-7.455046	4.307819	0.001448
C	-7.100449	4.795155	-2.502771
C	-7.699705	3.758805	2.506105
B	-8.835699	5.101293	0.000567
H	-6.280707	4.749182	-3.227585
H	-7.960383	4.272046	-2.933508
H	-7.392038	5.846688	-2.403261
H	-8.755946	3.484725	2.407038
H	-7.249392	3.073015	3.231598
H	-7.677363	4.765554	2.935761
C	-9.083885	6.238347	1.066722
C	-9.941282	4.741102	-1.066928
C	-10.297163	6.304572	1.810312
C	-8.108318	7.235246	1.353904
C	-10.607072	5.754658	-1.814288
C	-10.311631	3.395851	-1.351601
C	-10.502257	7.290894	2.775117
C	-11.419253	5.295483	1.634874
C	-8.348412	8.234655	2.296365
C	-6.770730	7.294761	0.637423
C	-11.560595	5.433618	-2.780486
C	-10.299386	7.232363	-1.641505
C	-11.294116	3.098501	-2.295568

C	-9.692103	2.211692	-0.630551
C	-9.548041	8.295032	3.032756
H	-11.428856	7.268958	3.337175
H	-11.056607	4.262595	1.627127
H	-12.144691	5.384590	2.450622
H	-11.955970	5.443807	0.692223
H	-7.577824	8.979996	2.456598
H	-6.105788	6.482870	0.948874
H	-6.876177	7.215074	-0.449667
H	-6.263541	8.242014	0.848841
C	-11.947906	4.103224	-3.035934
H	-12.006421	6.244264	-3.345335
H	-9.224205	7.438341	-1.633311
H	-10.740483	7.813005	-2.458768
H	-10.698249	7.623552	-0.699956
H	-11.550437	2.057200	-2.453737
H	-8.655130	2.044519	-0.938854
H	-9.679132	2.345860	0.456223
H	-10.255182	1.296331	-0.840968
N	-9.780699	9.299926	3.961676
N	-12.931252	3.796698	-3.966572
C	-8.689593	10.173738	4.358056
C	-10.946433	9.221049	4.824706
C	-13.136033	2.413263	-4.360687
C	-13.446273	4.841773	-4.834075
H	-7.850309	9.628023	4.818050
H	-8.298438	10.730837	3.498307
H	-9.060746	10.903015	5.081069
H	-11.870024	9.193854	4.234633
H	-10.936579	8.334789	5.479732
H	-10.984836	10.111639	5.455482
H	-13.422923	1.796677	-3.500445
H	-13.951060	2.365409	-5.085812
H	-12.240790	1.961742	-4.817289
H	-12.673114	5.276982	-5.487872
H	-14.233527	4.425627	-5.466190
H	-13.888881	5.655476	-4.247623

Compound 4-1M

DFT B3LYP/6-31G(d), gas phase, S_0

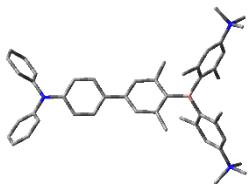

Point group: C_2
Total energy: -1287314.85 kcal mol^{-1}
Imaginary frequencies: 0

Symbol	X	Y	Z
C	2.309186	2.669883	8.380457
C	2.989741	1.995775	9.396774
C	2.681871	0.660486	9.666285
C	1.707497	-0.002687	8.921772
C	1.024189	0.674454	7.903505
C	1.323758	2.018237	7.639942
N	0.000000	0.000000	7.161104
C	0.000000	0.000000	5.769790
C	-1.024189	-0.674454	7.903505
C	-1.323758	-2.018237	7.639942
C	-2.309186	-2.669883	8.380457
C	-2.989741	-1.995775	9.396774
C	-2.681871	-0.660486	9.666285
C	-1.707497	0.002687	8.921772
C	-1.192969	-0.201384	5.036453
C	-1.183370	-0.205961	3.653245
C	0.000000	0.000000	2.910922
C	1.183370	0.205961	3.653245
C	1.192969	0.201384	5.036453
C	0.000000	0.000000	1.446414
C	0.983333	0.681671	0.702019
C	1.016168	0.677748	-0.687153
C	0.000000	0.000000	-1.444263
C	-1.016168	-0.677748	-0.687153
C	-0.983333	-0.681671	0.702019
C	-2.129743	-1.488389	-1.327349
C	2.129743	1.488389	-1.327349
B	0.000000	0.000000	-2.993712
C	-1.373852	0.119983	-3.818787
C	1.373852	-0.119983	-3.818787
C	-1.762064	-0.822296	-4.802693
C	-2.986126	-0.697740	-5.479780
C	-3.826882	0.373148	-5.206469
C	-3.456229	1.329755	-4.265441
C	-2.250804	1.211526	-3.563730
C	1.762064	0.822296	-4.802693
C	2.986126	0.697740	-5.479780
C	3.826882	-0.373148	-5.206469
C	3.456229	-1.329755	-4.265441
C	2.250804	-1.211526	-3.563730
C	0.910689	2.027524	-5.143562
C	1.953668	-2.281387	-2.532049
C	-0.910689	-2.027524	-5.143562
C	-1.953668	2.281387	-2.532049
N	-5.161908	0.532157	-5.905961
N	5.161908	-0.532157	-5.905961
C	-5.439823	-0.571814	-6.897011
C	-6.279023	0.514770	-4.879590
C	5.439823	0.571814	-6.897011
C	6.279023	-0.514770	-4.879590
C	-5.192094	1.844673	-6.664088
C	5.192094	-1.844673	-6.664088
H	2.532288	3.712822	8.173468
H	3.749899	2.508831	9.978336
H	3.205708	0.128649	10.455350
H	1.468646	-1.041500	9.127173
H	0.778863	2.546350	6.863170
H	-0.778863	-2.546350	6.863170
H	-2.532288	-3.712822	8.173468
H	-3.749899	-2.508831	9.978336
H	-3.205708	-0.128649	10.455350
H	-1.468646	1.041500	9.127173
H	-2.129263	-0.332169	5.566369
H	-2.131195	-0.322688	3.136094
H	2.131195	0.322688	3.136094
H	2.129263	0.332169	5.566369
H	1.726916	1.267910	1.232557
H	-1.726916	-1.267910	1.232557
H	-1.773078	-2.137482	-2.133424
H	-2.604185	-2.131585	-0.580778
H	-2.914210	-0.850583	-1.750024
H	2.604185	2.131585	-0.580778
H	2.914210	0.850583	-1.750024
H	1.773078	2.137482	-2.133424
H	-3.243352	-1.458726	-6.205088
H	-4.094127	2.178950	-4.041884
H	3.243352	1.458726	-6.205088
H	4.094127	-2.178950	-4.041884
H	0.714356	2.645228	-4.260117
H	1.404102	2.666785	-5.881353
H	-0.059715	1.731288	-5.552781
H	2.096061	-1.900511	-1.515665
H	0.922527	-2.640204	-2.587441
H	2.613600	-3.144308	-2.663428
H	-0.714356	-2.645228	-4.260117
H	-1.404102	-2.666785	-5.881353
H	0.059715	-1.731288	-5.552781
H	-2.096061	1.900511	-1.515665

H	-0.922527	2.640204	-2.587441
H	-2.613600	3.144308	-2.663428
H	-6.413246	-0.378537	-7.348377
H	-4.668895	-0.567981	-7.666741
H	-5.458586	-1.528176	-6.375685
H	-7.232441	0.617853	-5.400648
H	-6.142797	1.340425	-4.184048
H	-6.235941	-0.433390	-4.343315
H	6.413246	0.378537	-7.348377
H	4.668895	0.567981	-7.666741
H	5.458586	1.528176	-6.375685
H	7.232441	-0.617853	-5.400648
H	6.142797	-1.340425	-4.184048
H	6.235941	0.433390	-4.343315
H	-4.381727	1.837474	-7.393315
H	-6.157308	1.935839	-7.165234
H	-5.056082	2.668305	-5.966118
H	4.381727	-1.837474	-7.393315
H	6.157308	-1.935839	-7.165234
H	5.056082	-2.668305	-5.966118

Compound 4-2M

DFT B3LYP/6-31G(d), gas phase, S_0

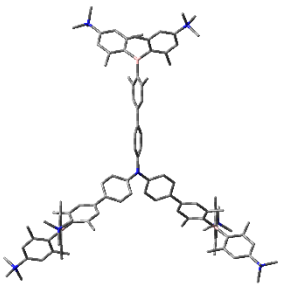

Point group: C_3
Total energy: -2920867.63 kcal mol^{-1}
Imaginary frequencies: 0

Symbol	X	Y	Z
C	-2.600782	-2.567871	0.763348
C	-3.700035	-2.136216	-0.002780
C	-3.524694	-0.968854	-0.769706
C	-2.320048	-0.273682	-0.779223
C	-1.232619	-0.711778	-0.004029
C	-1.396365	-1.872304	0.771670
N	0.000000	0.000000	-0.004513
C	1.232727	-0.711590	-0.004029
C	-0.000108	1.423368	-0.004029
C	0.923009	2.146061	-0.779223
C	0.923294	3.536901	-0.769706
C	0.000001	4.272432	-0.002780
C	-0.923451	3.536279	0.763348
C	-0.923281	2.145440	0.771670
C	2.319645	-0.273135	0.771670
C	3.524233	-0.968408	0.763348
C	3.700035	-2.136217	-0.002780
C	2.601399	-2.568047	-0.769706
C	1.397039	-1.872380	-0.779223
C	0.000157	5.755977	-0.001802
C	0.397681	6.492416	-1.128353
C	0.391444	7.888076	-1.155142
C	0.000000	8.635308	0.000284
C	-0.390604	7.886367	1.155022
C	-0.396828	6.490750	1.126031
C	-0.845998	8.535036	2.449970
C	0.847587	8.538700	-2.448848
B	-0.002884	10.204008	0.000352
C	0.535873	11.044427	1.258117
C	-0.546663	11.041099	-1.257305
C	-0.243791	12.051709	1.879398
C	0.267662	12.798858	2.953359
C	1.559806	12.575229	3.409263
C	2.346768	11.592268	2.813669
C	1.847917	10.817732	1.759144
C	0.228671	12.056579	-1.879802
C	-0.292487	12.796762	-2.947035
C	-1.587796	12.567121	-3.403690
C	-2.366995	11.581917	-2.811332
C	-1.854410	10.808612	-1.755471
C	1.646376	12.375471	-1.451509
C	-2.766132	9.732910	-1.197696
C	-1.662207	12.366787	1.448852
C	2.765354	9.749441	1.197861
H	-2.679229	-3.473971	1.356621
H	-4.349007	-0.583980	-1.362610
H	-2.220098	0.618913	-1.387977
H	-0.572948	-2.231873	1.379935
H	1.646043	1.613205	-1.387977
H	1.668762	4.058341	-1.362610
H	-1.668933	4.057266	1.356621
H	-1.646384	1.612124	1.379935
H	2.219332	0.619749	1.379935
H	4.348162	-0.583295	1.356621
H	2.680245	-3.474361	-1.362610
H	0.574055	-2.232117	-1.387977
H	0.696114	5.961523	-2.027793
H	-0.694629	5.958445	2.024831
H	-1.583078	9.328478	2.290500
H	-1.310020	7.791786	3.104396
H	-0.010609	8.978313	3.002712
H	1.321948	7.798700	-3.099574
H	0.010778	8.972913	-3.006691
H	1.576316	9.339214	-2.286897
H	-0.374755	13.546462	3.400007
H	3.358392	11.397694	3.154633
H	0.339518	13.553007	-3.400944
H	-3.376373	11.375943	-3.142940
H	2.265815	11.475511	-1.381646
H	2.132492	13.046019	-2.165665
H	1.669113	12.862362	-0.471465
H	-2.432000	8.735692	-1.502705
H	-2.797102	9.732514	-0.104495
H	-3.791506	9.865928	-1.554735
H	-2.271752	11.463525	1.346956
H	-2.161079	13.011065	2.178253
H	-1.682312	12.882979	0.483569
H	2.421365	8.747755	1.475101
H	2.816716	9.772633	0.105363
H	3.784400	9.870932	1.576443
C	-4.984900	-2.877853	-0.001802
C	-5.821437	-2.901806	-1.128353
C	-5.422740	-3.589038	1.126031
C	-7.026996	-3.605038	-1.155142
H	-5.510888	-2.377909	-2.027793
C	-6.634492	-4.281456	1.155022
H	-4.812850	-3.580789	2.024831
C	-7.478396	-4.317654	0.000284
C	-7.818524	-3.535318	-2.448848
C	-6.968559	-5.000174	2.449970
B	-8.835488	-5.104502	0.000352
H	-7.414846	-2.754509	-3.099574
H	-7.776160	-4.477122	-3.006691
H	-8.876155	-3.304477	-2.286897
H	-7.287160	-6.035224	2.290500
H	-6.092875	-5.030403	3.104396
H	-7.770142	-4.498345	3.002712
C	-9.832691	-5.058134	1.258117
C	-9.288541	-5.993974	-1.257305
C	-10.315191	-6.236984	1.879398
C	-10.292389	-3.808523	1.759144

C	-10.555639	-5.830254	-1.879802	H	11.540042	-2.763946	-3.142940
C	-8.433328	-7.010272	-1.755471	H	8.781331	-2.261673	-1.502705
C	-11.217967	-6.167627	2.953359	H	9.827155	-2.443896	-0.104495
C	-9.878848	-7.622907	1.448852	H	10.439897	-1.649424	-1.554735
C	-11.212582	-3.763774	2.813669	N	12.668081	-4.878700	-4.549361
C	-9.825941	-2.479853	1.197861	C	13.074888	-3.476615	-4.938884
C	-10.936078	-6.651682	-2.947035	C	13.930283	-5.625693	-4.157385
C	-11.540661	-4.761932	-1.451509	C	12.055037	-5.532417	-5.774703
C	-8.846737	-7.840836	-2.811332	H	12.194911	-2.922087	-5.262986
C	-7.045881	-7.261996	-1.197696	H	13.548814	-2.988206	-4.088088
C	-11.670371	-4.936783	3.409263	H	13.785711	-3.552247	-5.761975
H	-11.544203	-7.097778	3.400007	H	14.355873	-5.142464	-3.277659
H	-8.791828	-7.699157	1.346956	H	13.682938	-6.661280	-3.932401
H	-10.187373	-8.377082	2.178253	H	14.631786	-5.584184	-4.992187
H	-10.315831	-7.898414	0.483569	H	11.811957	-6.568814	-5.548704
H	-11.549888	-2.790394	3.154633	H	11.149722	-4.985331	-6.038550
H	-8.786460	-2.276914	1.475101	H	12.779242	-5.489602	-6.589842
H	-9.871706	-2.446969	0.105363	N	10.512631	-8.546796	4.553085
H	-10.440677	-1.658079	1.576443	C	11.884254	-8.229383	5.103648
C	-10.089548	-7.658632	-3.403690	C	9.521263	-8.405213	5.693283
H	-11.907007	-6.482472	-3.400944	C	10.535656	-9.988888	4.079540
H	-11.070991	-3.775503	-1.381646	H	12.627353	-8.353400	4.316691
H	-12.364430	-4.676217	-2.165665	H	11.892876	-7.209826	5.487472
H	-11.973688	-4.985687	-0.471465	H	12.087947	-8.929042	5.914472
H	-8.163669	-8.611996	-3.142940	H	9.518222	-7.364427	6.017831
H	-6.349332	-6.474020	-1.502705	H	8.529797	-8.691563	5.347865
H	-7.030053	-7.288618	-0.104495	H	9.834793	-9.058745	6.508972
H	-6.648391	-8.216504	-1.554735	H	9.543116	-10.272715	3.735122
C	4.984744	-2.878124	-0.001802	H	11.252597	-10.070392	3.262313
C	5.423756	-3.590610	-1.128353	H	10.836002	-10.623892	4.914583
C	5.819568	-2.901712	1.126031	N	-2.108963	13.410229	-4.549361
C	6.635552	-4.283039	-1.155142	C	-3.526607	13.061492	-4.938884
H	4.814774	-3.583614	-2.027793	C	-2.093148	14.876826	-4.157385
C	7.025096	-3.604911	1.155022	C	-1.236305	13.206176	-5.774703
H	5.507479	-2.377656	2.024831	H	-3.566854	12.022146	-5.262986
C	7.478396	-4.317654	0.000284	H	-4.186545	13.227720	-4.088088
C	6.970937	-5.003382	-2.448848	H	-3.816519	13.714900	-5.761975
C	7.814557	-3.534862	2.449970	H	-2.724432	15.003783	-3.277659
B	8.838372	-5.099506	0.000352	H	-1.072631	15.180412	-3.932401
H	6.092898	-5.044191	-3.099574	H	-2.479848	15.463590	-4.992187
H	7.765381	-4.495791	-3.006691	H	-0.217219	13.513862	-5.548704
H	7.299838	-6.034737	-2.286897	H	-1.257438	12.148608	-6.038550
H	8.870238	-3.293254	2.290500	H	-1.635487	13.811949	-6.589842
H	7.402895	-2.761383	3.104396	N	2.145427	13.377604	4.553085
H	7.780752	-4.479969	3.002712	C	1.184728	14.406757	5.103648
C	9.296818	-5.986293	1.258117	C	2.518497	12.448262	5.693283
C	9.835204	-5.047125	-1.257305	C	3.382803	14.118590	4.079540
C	10.558982	-5.814725	1.879398	H	0.920581	15.112309	4.316691
C	8.444472	-7.009209	1.759144	H	0.297454	13.904446	5.487472
C	10.326968	-6.226325	-1.879802	H	1.688804	14.932990	5.914472
C	10.287738	-3.798340	-1.755471	H	1.618670	11.925236	6.017831
C	10.950305	-6.631231	2.953359	H	3.262216	11.732802	5.347865
C	11.541055	-4.743880	1.448852	H	2.927707	13.046553	6.508972
C	8.865815	-7.828494	2.813669	H	4.124874	13.400939	3.735122
C	7.060587	-7.269588	1.197861	H	3.094917	14.780231	3.262313
C	11.228565	-6.145080	-2.947035	H	3.782559	14.696199	4.914583
C	9.894285	-7.613539	-1.451509	N	-10.559118	-8.531530	-4.549361
C	11.213732	-3.741081	-2.811332	C	-11.837135	-9.251132	-4.157385
C	9.812013	-2.470914	-1.197696	C	-10.818732	-7.673760	-5.774703
C	10.110565	-7.638447	3.409263	C	-9.548281	-9.584878	-4.938884
H	11.918958	-6.448684	3.400007	H	-11.631441	-9.861318	-3.277659
H	11.063580	-3.764368	1.346956	H	-12.610307	-8.519132	-3.932401
H	12.348452	-4.633983	2.178253	H	-12.151938	-9.879407	-4.992187
H	11.998143	-4.984565	0.483569	H	-11.594738	-6.945048	-5.548704
H	8.191497	-8.607299	3.154633	H	-9.892284	-7.163277	-6.038550
H	6.365096	-6.470841	1.475101	H	-11.143756	-8.322348	-6.589842
H	7.054990	-7.325664	0.105363	H	-8.628057	-9.100059	-5.262986
H	6.656278	-8.212852	1.576443	H	-9.362269	-10.239514	-4.088088
C	11.677344	-4.908489	-3.403690	H	-9.969192	-10.162653	-5.761975
H	11.567489	-7.070534	-3.400944	N	-12.658058	-4.830808	4.553085
H	8.805177	-7.700009	-1.381646	C	-13.068982	-6.177375	5.103648
H	10.231938	-8.369802	-2.165665	C	-12.039760	-4.043049	5.693283
H	10.304576	-7.876675	-0.471465	C	-13.918459	-4.129701	4.079540

H	-13.547933	-6.758908	4.316691
H	-12.190330	-6.694620	5.487472
H	-13.776750	-6.003948	5.914472
H	-11.136892	-4.560809	6.017831
H	-11.792013	-3.041239	5.347865
H	-12.762500	-3.987808	6.508972
H	-13.667990	-3.128224	3.735122
H	-14.347513	-4.709839	3.262313
H	-14.618561	-4.072307	4.914583

Compound 5-1M

DFT B3LYP/6-31G(d), gas phase, S_0

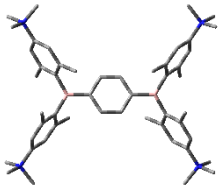

Point group: C_{2h}
Total energy: -1390126.55 kcal mol^{-1}
Imaginary frequencies: 0

Symbol	X	Y	Z
C	0.000000	0.000000	-1.439336
C	0.000000	0.000000	1.439336
C	-1.068031	-0.553810	-0.696766
C	1.068031	0.553810	-0.696766
C	1.068031	0.553810	0.696766
C	-1.068031	-0.553810	0.696766
H	-1.910558	-0.994613	-1.224015
H	1.910558	0.994613	-1.224015
H	1.910558	0.994613	1.224015
H	-1.910558	-0.994613	1.224015
B	0.000000	0.000000	-3.013128
B	0.000000	0.000000	3.013128
C	-1.384036	-0.087926	-3.812433
C	-3.783966	-0.144143	-5.315891
C	-2.372265	0.922080	-3.652380
C	-1.655712	-1.141806	-4.721682
C	-2.851654	-1.163569	-5.457951
C	-3.546739	0.891811	-4.415160
H	-3.008230	-1.991029	-6.137503
H	-4.259173	1.699842	-4.283670
C	1.384036	0.087926	-3.812433
C	3.783966	0.144143	-5.315891
C	2.372265	-0.922080	-3.652380
C	1.655712	1.141806	-4.721682
C	2.851654	1.163569	-5.457951
C	3.546739	-0.891811	-4.415160
H	3.008230	1.991029	-6.137503
H	4.259173	-1.699842	-4.283670
C	-1.384036	-0.087926	3.812433
C	-3.783966	-0.144143	5.315891
C	-1.655712	-1.141806	4.721682
C	-2.372265	0.922080	3.652380
C	-3.546739	0.891811	4.415160
C	-2.851654	-1.163569	5.457951
H	-4.259173	1.699842	4.283670
H	-3.008230	-1.991029	6.137503
C	1.384036	0.087926	3.812433
C	3.783966	0.144143	5.315891
C	1.655712	1.141806	4.721682
C	2.372265	-0.922080	3.652380
C	3.546739	-0.891811	4.415160
C	2.851654	1.163569	5.457951
H	4.259173	-1.699842	4.283670
H	3.008230	1.991029	6.137503
N	-5.061478	-0.122924	6.128670
N	5.061478	0.122924	6.128670
N	-5.061478	-0.122924	-6.128670
N	5.061478	0.122924	-6.128670
C	-6.262572	-0.146609	-5.200637
H	-6.212857	-1.053576	-4.597603
H	-7.169328	-0.141988	-5.807484
H	-6.242226	0.732593	-4.559497
C	-5.186633	-1.307547	-7.061735
H	-4.356575	-1.300969	-7.767261
H	-6.127787	-1.206675	-7.602510
H	-5.194933	-2.228460	-6.479493
C	-5.107077	1.133648	-6.981619
H	-4.242473	1.129996	-7.645681
H	-5.081053	2.010324	-6.337329
H	-6.031548	1.125162	-7.561128
C	5.186633	1.307547	-7.061735
H	4.356575	1.300969	-7.767261
H	6.127787	1.206675	-7.602510
H	5.194933	2.228460	-6.479493
C	5.107077	-1.133648	-6.981619
H	5.081053	-2.010324	-6.337329
H	6.031548	-1.125162	-7.561128
H	4.242473	-1.129996	-7.645681
C	6.262572	0.146609	-5.200637
H	6.242226	-0.732593	-4.559497
H	6.212857	1.053576	-4.597603
H	7.169328	0.141988	-5.807484
C	6.262572	0.146609	5.200637
H	6.242226	-0.732593	4.559497
H	7.169328	0.141988	5.807484
H	6.212857	1.053576	4.597603
C	5.107077	-1.133648	6.981619
H	4.242473	-1.129996	7.645681
H	6.031548	-1.125162	7.561128
H	5.081053	-2.010324	6.337329
C	5.186633	1.307547	7.061735
H	4.356575	1.300969	7.767261
H	5.194933	2.228460	6.479493
H	6.127787	1.206675	7.602510
C	-5.107077	1.133648	6.981619
H	-4.242473	1.129996	7.645681
H	-6.031548	1.125162	7.561128
H	-5.081053	2.010324	6.337329
C	-5.186633	-1.307547	7.061735
H	-5.194933	-2.228460	6.479493
H	-6.127787	-1.206675	7.602510
H	-4.356575	-1.300969	7.767261
C	-6.262572	-0.146609	5.200637
H	-6.212857	-1.053576	4.597603
H	-6.242226	0.732593	4.559497
H	-7.169328	-0.141988	5.807484
C	-2.214944	2.072324	-2.676705
H	-2.499978	1.766130	-1.663603
H	-2.851004	2.916813	-2.957404
H	-1.187944	2.441012	-2.619076
C	-0.708189	-2.305511	-4.917451
H	-1.045411	-2.963480	-5.722670
H	-0.640327	-2.919583	-4.011315
H	0.301919	-1.968555	-5.165505
C	0.708189	2.305511	-4.917451
H	-0.301919	1.968555	-5.165505
H	1.045411	2.963480	-5.722670
H	0.640327	2.919583	-4.011315
C	2.214944	-2.072324	-2.676705
H	2.851004	-2.916813	-2.957404
H	1.187944	-2.441012	-2.619076
H	2.499978	-1.766130	-1.663603
C	-2.214944	2.072324	2.676705
H	-2.499978	1.766130	1.663603
H	-1.187944	2.441012	2.619076
H	-2.851004	2.916813	2.957404

C	-0.708189	-2.305511	4.917451
H	-1.045411	-2.963480	5.722670
H	0.301919	-1.968555	5.165505
H	-0.640327	-2.919583	4.011315
C	2.214944	-2.072324	2.676705
H	2.851004	-2.916813	2.957404
H	2.499978	-1.766130	1.663603
H	1.187944	-2.441012	2.619076
C	0.708189	2.305511	4.917451
H	-0.301919	1.968555	5.165505
H	0.640327	2.919583	4.011315
H	1.045411	2.963480	5.722670

Compound 5-2M

DFT B3LYP/6-31G(d), gas phase, S_0

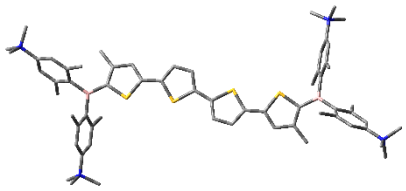

Point group: C_1
Total energy: -2679416.22 kcal mol^{-1}
Imaginary frequencies: 0

Symbol	X	Y	Z
C	-3.056379	1.079640	-0.127149
C	-2.175260	2.142351	-0.001528
H	-2.502580	3.172410	0.079153
C	-0.821630	1.756600	0.048492
H	-0.005649	2.460999	0.167693
C	-0.628572	0.387370	-0.033647
S	-2.171870	-0.434196	-0.195216
C	0.610071	-0.352461	-0.004266
C	0.798947	-1.714647	0.162510
H	-0.019952	-2.408979	0.315770
C	2.151687	-2.105245	0.149453
H	2.474977	-3.129398	0.294853
C	3.037009	-1.053715	-0.030904
S	2.156884	0.455210	-0.198579
C	4.476590	-1.143606	-0.090913
C	5.213781	-2.316442	-0.225612
H	4.748211	-3.286677	-0.359129
C	6.609268	-2.140470	-0.206749
C	7.003736	-0.792549	-0.077241
S	5.547759	0.219798	0.027438
C	-4.495891	1.159625	-0.207702
C	-5.237378	2.314477	-0.433744
H	-4.775378	3.274195	-0.638372
C	-6.633460	2.131720	-0.411844
C	-7.020498	0.796759	-0.182507
S	-5.561641	-0.198979	-0.001943
B	-8.388154	0.130218	-0.069854
B	8.376467	-0.131756	-0.006951
C	-8.516407	-1.458531	-0.279617
C	-8.801453	-4.244641	-0.697199
C	-8.195031	-2.047832	-1.531368
C	-8.966506	-2.317256	0.757478
C	-9.103029	-3.696346	0.544403
C	-8.349299	-3.428515	-1.726407
H	-9.446008	-4.303923	1.371437
H	-8.105990	-3.832087	-2.704716
C	-9.693589	0.998023	0.271633
C	-11.998848	2.515497	0.900715
C	-10.794450	1.065195	-0.618428
C	-9.781850	1.721899	1.491714
C	-10.934951	2.456945	1.796332
C	-11.930825	1.827471	-0.304149
H	-10.966745	2.982025	2.745908
H	-12.737433	1.852047	-1.025244
C	8.509147	1.451366	-0.254060
C	8.797007	4.231615	-0.702065
C	8.173838	2.028387	-1.507089
C	8.974076	2.318718	0.769003
C	9.110446	3.695055	0.542140
C	8.330393	3.406888	-1.717692
H	9.462698	4.310153	1.359673
H	8.074681	3.801941	-2.696342
C	9.689491	-0.996480	0.322614
C	12.006384	-2.528603	0.885130
C	10.741187	-1.119790	-0.628763
C	9.842837	-1.666320	1.561079
C	11.001234	-2.418806	1.833052
C	11.876162	-1.883824	-0.344515
H	11.066998	-2.904955	2.798702
H	12.643776	-1.960843	-1.107519
N	13.254195	-3.348397	1.141662
N	8.952226	5.712500	-0.986563
N	-8.958491	-5.728066	-0.966519
N	-13.215700	3.335661	1.277415
C	9.940957	5.914594	-2.119604
H	9.572483	5.416338	-3.014117
H	10.897170	5.484828	-1.820442
H	10.044840	6.985029	-2.304542
C	9.463022	6.489584	0.204114
H	8.755781	6.396020	1.027541
H	9.548147	7.535490	-0.091605
H	10.442160	6.108041	0.491256
C	7.610434	6.303004	-1.374319
H	6.913193	6.136186	-0.553015
H	7.247135	5.814181	-2.276275
H	7.740001	7.371296	-1.555839
C	7.664458	1.231651	-2.692753
H	6.681333	1.598096	-3.009678
H	7.557868	0.169933	-2.473520
H	8.339854	1.336690	-3.550244
C	9.314912	1.808671	2.151692
H	8.461707	1.296570	2.608917
H	9.600897	2.626086	2.819417
H	10.147142	1.098032	2.120732
C	10.664129	-0.468621	-1.992166
H	10.578043	0.619336	-1.910029
H	9.796053	-0.823946	-2.558239
H	11.553441	-0.687855	-2.589560
C	8.819017	-1.613331	2.678081
H	9.190020	-1.013349	3.518275
H	8.619586	-2.616627	3.071007
H	7.868775	-1.188077	2.355948
C	14.482232	-2.463872	1.034895
H	14.396353	-1.667836	1.774796
H	14.537181	-2.039638	0.034396
H	15.366666	-3.072712	1.229504
C	13.348187	-4.468928	0.122128
H	12.458824	-5.092611	0.214732
H	14.247146	-5.051977	0.328857
H	13.402306	-4.043791	-0.878256
C	13.269645	-3.980083	2.513743
H	12.418318	-4.652630	2.611590
H	13.233489	-3.198012	3.271398
H	14.197370	-4.544296	2.610927
C	7.530524	-3.326009	-0.350599
H	7.828829	-3.713498	0.631296
H	8.442565	-3.081946	-0.898286
H	7.022264	-4.138524	-0.878251
C	-7.558666	3.294438	-0.672543
H	-7.727457	3.877421	0.241913
H	-8.531900	2.979107	-1.049989
H	-7.112737	3.975038	-1.404823
C	-12.812355	4.783258	1.489236

H	-13.702866	5.357620	1.749691
H	-12.374628	5.156075	0.562989
H	-12.083978	4.841263	2.295679
C	-14.290258	3.315317	0.215222
H	-15.119733	3.928321	0.568297
H	-14.629069	2.291038	0.063564
H	-13.892407	3.731994	-0.709493
C	-13.826058	2.788616	2.554281
H	-14.705964	3.384382	2.802820
H	-13.095963	2.850215	3.358933
H	-14.105325	1.748927	2.382271
C	-8.661586	1.761405	2.512968
H	-9.053064	1.958347	3.515847
H	-7.947329	2.559713	2.280564
H	-8.091195	0.832518	2.553376
C	-10.786887	0.354545	-1.954740
H	-10.690130	-0.728446	-1.829967
H	-9.952788	0.686995	-2.582401
H	-11.708026	0.544201	-2.512680
C	-9.278918	-1.802606	2.145166
H	-8.371419	-1.446357	2.646777
H	-9.707939	-2.587021	2.774949
H	-9.989112	-0.971532	2.117875
C	-7.706499	-1.261585	-2.732778
H	-7.624811	-0.193492	-2.534843
H	-8.380061	-1.400012	-3.586855
H	-6.714884	-1.610049	-3.043992
C	-7.620757	-6.320415	-1.365476
H	-6.914143	-6.146860	-0.553639
H	-7.268392	-5.838171	-2.275281
H	-7.751573	-7.390138	-1.537369
C	-9.960790	-5.941246	-2.085663
H	-10.913603	-5.509289	-1.778898
H	-10.066105	-7.013399	-2.259386
H	-9.603493	-5.451138	-2.989179
C	-9.453749	-6.495096	0.237164
H	-8.737249	-6.392422	1.051477
H	-9.539964	-7.543900	-0.047816
H	-10.430396	-6.113088	0.532076

Compound 5-3M

DFT B3LYP/6-31G(d), gas phase, S_0

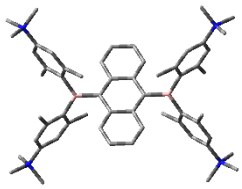

Point group: C_1
Total energy: -1582854.23 kcal mol^{-1}
Imaginary frequencies: 0

Symbol	X	Y	Z
C	0.000001	0.000020	-1.461752
C	0.000001	0.000020	1.461752
C	0.711399	0.992818	-0.726387
C	-0.711380	-0.992791	-0.726388
C	-0.711380	-0.992791	0.726388
C	0.711399	0.992818	0.726387
B	0.000005	0.000022	-3.052221
B	0.000005	0.000022	3.052221
C	1.368580	0.027496	-3.887840
C	3.722933	-0.044343	-5.463394
C	2.397163	-0.920208	-3.626236
C	1.574228	0.951474	-4.945975
C	2.750720	0.915271	-5.712830
C	3.547029	-0.955070	-4.424370
H	2.861790	1.650515	-6.499165
H	4.295853	-1.708826	-4.204663
C	-1.368572	-0.027464	-3.887841
C	-3.722951	0.044323	-5.463364
C	-2.397168	0.920226	-3.626233
C	-1.574215	-0.951443	-4.945977
C	-2.750717	-0.915266	-5.712815
C	-3.547046	0.955061	-4.424351
H	-2.861777	-1.650509	-6.499153
H	-4.295877	1.708810	-4.204644
C	1.368580	0.027496	3.887840
C	3.722933	-0.044343	5.463394
C	1.574228	0.951474	4.945975
C	2.397163	-0.920208	3.626236
C	3.547029	-0.955070	4.424370
C	2.750720	0.915271	5.712830
H	4.295853	-1.708826	4.204663
H	2.861790	1.650515	6.499165
C	-1.368572	-0.027464	3.887841
C	-3.722951	0.044323	5.463364
C	-1.574215	-0.951443	4.945977
C	-2.397168	0.920226	3.626233
C	-3.547046	0.955061	4.424351
C	-2.750717	-0.915266	5.712815
H	-4.295877	1.708810	4.204644
H	-2.861777	-1.650509	6.499153
N	4.986640	-0.127305	6.293615
N	-4.986666	0.127266	6.293576
N	4.986640	-0.127305	-6.293615
N	-4.986666	0.127266	-6.293576
C	6.199926	0.083330	-5.405526
H	6.118931	1.066141	-4.940616
H	7.096519	0.027183	-6.024870
H	6.227797	-0.691814	-4.642022
C	5.042132	0.912684	-7.390822
H	4.200539	0.770040	-8.067905
H	5.976929	0.773252	-7.933911
H	5.020860	1.908101	-6.948386
C	5.076734	-1.491558	-6.956143
H	4.198100	-1.625936	-7.587362
H	5.110032	-2.265053	-6.191212
H	5.986342	-1.524524	-7.557851
C	-5.042155	-0.912721	-7.390785
H	-4.200550	-0.770087	-8.067856
H	-5.976942	-0.773275	-7.933888
H	-5.020902	-1.908138	-6.948350
C	-5.076779	1.491519	-6.956099
H	-5.110083	2.265010	-6.191163
H	-5.986390	1.524477	-7.557803
H	-4.198148	1.625911	-7.587320
C	-6.199945	-0.083386	-5.405482
H	-6.227820	0.691752	-4.641973
H	-6.118939	-1.066200	-4.940580
H	-7.096542	-0.027242	-6.024821
C	-6.199945	-0.083386	5.405482
H	-6.227820	0.691752	4.641973
H	-7.096542	-0.027242	6.024821
H	-6.118939	-1.066200	4.940580
C	-5.076779	1.491519	6.956099
H	-4.198148	1.625911	7.587320
H	-5.986390	1.524477	7.557803
H	-5.110083	2.265010	6.191163
C	-5.042155	-0.912721	7.390785
H	-4.200550	-0.770087	8.067856
H	-5.020902	-1.908138	6.948350
H	-5.976942	-0.773275	7.933888
C	5.076734	-1.491558	6.956143
H	4.198100	-1.625936	7.587362
H	5.986342	-1.524524	7.557851
H	5.110032	-2.265053	6.191212
C	5.042132	0.912684	7.390822
H	5.020860	1.908101	6.948386

H	5.976929	0.773252	7.933911
H	4.200539	0.770040	8.067905
C	6.199926	0.083330	5.405526
H	6.118931	1.066141	4.940616
H	6.227797	-0.691814	4.642022
H	7.096519	0.027183	6.024870
C	2.309002	-1.936098	-2.505798
H	2.407701	-1.449230	-1.529914
H	3.105209	-2.681041	-2.589824
H	1.357441	-2.475791	-2.497214
C	0.572276	2.032732	-5.303885
H	1.041104	2.813418	-5.909624
H	0.149009	2.522103	-4.421832
H	-0.263892	1.626818	-5.883137
C	-0.572246	-2.032683	-5.303899
H	0.263946	-1.626743	-5.883094
H	-1.041050	-2.813343	-5.909690
H	-0.149018	-2.522094	-4.421848
C	-2.309018	1.936129	-2.505804
H	-3.105163	2.681130	-2.589910
H	-1.357418	2.475747	-2.497142
H	-2.407840	1.449283	-1.529920
C	2.309002	-1.936098	2.505798
H	2.407701	-1.449230	1.529914
H	1.357441	-2.475791	2.497214
H	3.105209	-2.681041	2.589824
C	0.572276	2.032732	5.303885
H	1.041104	2.813418	5.909624
H	-0.263892	1.626818	5.883137
H	0.149009	2.522103	4.421832
C	-2.309018	1.936129	2.505804
H	-3.105163	2.681130	2.589910
H	-2.407840	1.449283	1.529920
H	-1.357418	2.475747	2.497142
C	-0.572246	-2.032683	5.303899
H	0.263946	-1.626743	5.883094
H	-0.149018	-2.522094	4.421848
H	-1.041050	-2.813343	5.909690
C	1.397401	2.062017	1.389852
H	1.397876	2.089808	2.471982
C	1.397401	2.062017	-1.389852
H	1.397876	2.089808	-2.471982
C	2.048243	3.056397	0.708819
H	2.552378	3.851568	1.249843
C	2.048243	3.056397	-0.708819
H	2.552378	3.851568	-1.249843
C	-1.397355	-2.062009	1.389852
H	-1.397822	-2.089806	2.471982
C	-1.397355	-2.062009	-1.389852
H	-1.397822	-2.089806	-2.471982
C	-2.048177	-3.056401	-0.708820
H	-2.552292	-3.851586	-1.249841
C	-2.048177	-3.056401	0.708820
H	-2.552292	-3.851586	1.249841

PERMISSION OF ROYAL SOCIETY OF CHEMISTRY

Recent Developments in and Perspectives on Three-Coordinate Boron Materials: a Bright Future

L. Ji, S. Griesbeck and T. B. Marder, *Chem. Sci.*, 2017, **8**, 846

DOI: 10.1039/C6SC04245G

PERMISSION OF WILEY-VCH

Water-Soluble Triarylborane Chromophores for One- and Two-Photon Excited Fluorescence Imaging of Mitochondria in Cells

This Agreement between Universität Würzburg -- Stefanie Griesbeck ("You") and John Wiley and Sons ("John Wiley and Sons") consists of your license details and the terms and conditions provided by John Wiley and Sons and Copyright Clearance Center.

License Number	4526560304941
License date	Feb 12, 2019
Licensed Content Publisher	John Wiley and Sons
Licensed Content Publication	Chemistry - A European Journal
Licensed Content Title	Water-Soluble Triarylborane Chromophores for One- and Two-Photon Excited Fluorescence Imaging of Mitochondria in Cells
Licensed Content Author	Stefanie Griesbeck, Zuolun Zhang, Marcus Gutmann, et al
Licensed Content Date	Sep 15, 2016
Licensed Content Volume	22
Licensed Content Issue	41
Licensed Content Pages	6
Type of use	Dissertation/Thesis
Requestor type	Author of this Wiley article
Format	Print and electronic
Portion	Full article
Will you be translating?	No
Title of your thesis / dissertation	A Very Positive Image of Boron: Triarylborane Chromophores for Live Cell Imaging
Expected completion date	Feb 2019
Expected size (number of pages)	320
Requestor Location	Universität Würzburg Am Hubland Würzburg, 97074 Germany Attn: Universität Würzburg
Publisher Tax ID	EU826007151
Total	0.00 EUR
Terms and Conditions	

TERMS AND CONDITIONS

This copyrighted material is owned by or exclusively licensed to John Wiley & Sons, Inc. or one of its group companies (each a"Wiley Company") or handled on behalf of a society with which a Wiley Company has exclusive publishing rights in relation to a particular work (collectively "WILEY"). By clicking "accept" in connection with completing this licensing transaction, you agree that the following terms and conditions apply to this transaction (along with the billing and payment terms

and conditions established by the Copyright Clearance Center Inc., ("CCC's Billing and Payment terms and conditions"), at the time that you opened your RightsLink account (these are available at any time at http://myaccount.copyright.com).

Terms and Conditions

- The materials you have requested permission to reproduce or reuse (the "Wiley Materials") are protected by copyright.

- You are hereby granted a personal, non-exclusive, non-sub licensable (on a stand-alone basis), non-transferable, worldwide, limited license to reproduce the Wiley Materials for the purpose specified in the licensing process. This license, **and any CONTENT (PDF or image file) purchased as part of your order,** is for a one-time use only and limited to any maximum distribution number specified in the license. The first instance of republication or reuse granted by this license must be completed within two years of the date of the grant of this license (although copies prepared before the end date may be distributed thereafter). The Wiley Materials shall not be used in any other manner or for any other purpose, beyond what is granted in the license. Permission is granted subject to an appropriate acknowledgement given to the author, title of the material/book/journal and the publisher. You shall also duplicate the copyright notice that appears in the Wiley publication in your use of the Wiley Material. Permission is also granted on the understanding that nowhere in the text is a previously published source acknowledged for all or part of this Wiley Material. Any third party content is expressly excluded from this permission.

- With respect to the Wiley Materials, all rights are reserved. Except as expressly granted by the terms of the license, no part of the Wiley Materials may be copied, modified, adapted (except for minor reformatting required by the new Publication), translated, reproduced, transferred or distributed, in any form or by any means, and no derivative works may be made based on the Wiley Materials without the prior permission of the respective copyright owner.**For STM Signatory Publishers clearing permission under the terms of the STM Permissions Guidelines only, the terms of the license are extended to include subsequent editions and for editions in other languages, provided such editions are for the work as a whole in situ and does not involve the separate exploitation of the permitted figures or extracts,** You may not alter, remove or suppress in any manner any copyright, trademark or other notices displayed by the Wiley Materials. You may not license, rent, sell, loan, lease, pledge, offer as security, transfer or assign the Wiley Materials on a stand-alone basis, or any of the rights granted to you hereunder to any other person.

- The Wiley Materials and all of the intellectual property rights therein shall at all times remain the exclusive property of John Wiley & Sons Inc, the Wiley Companies, or their respective licensors, and your interest therein is only that of having possession of and the right to reproduce the Wiley Materials pursuant to Section 2 herein during the continuance of this Agreement. You agree that you own no right, title or interest in or to the Wiley Materials or any of the intellectual property rights therein. You shall have no rights hereunder other than the license as provided for above in Section 2. No right, license or interest to any trademark, trade name, service mark or other branding ("Marks") of WILEY or its licensors is granted hereunder, and you agree that you shall not assert any such right, license or interest with respect thereto

- NEITHER WILEY NOR ITS LICENSORS MAKES ANY WARRANTY OR REPRESENTATION OF ANY KIND TO YOU OR ANY THIRD PARTY, EXPRESS, IMPLIED OR STATUTORY, WITH RESPECT TO THE MATERIALS OR THE ACCURACY OF ANY INFORMATION CONTAINED IN THE MATERIALS, INCLUDING, WITHOUT LIMITATION, ANY IMPLIED WARRANTY OF MERCHANTABILITY, ACCURACY, SATISFACTORY QUALITY, FITNESS FOR A PARTICULAR PURPOSE, USABILITY, INTEGRATION OR NON-INFRINGEMENT AND ALL SUCH WARRANTIES ARE HEREBY EXCLUDED BY WILEY AND ITS LICENSORS AND WAIVED BY YOU.

- WILEY shall have the right to terminate this Agreement immediately upon breach of this Agreement by you.

- You shall indemnify, defend and hold harmless WILEY, its Licensors and their respective directors, officers, agents and employees, from and against any actual or threatened claims, demands, causes of action or proceedings arising from any breach of this Agreement by you.

- IN NO EVENT SHALL WILEY OR ITS LICENSORS BE LIABLE TO YOU OR ANY OTHER PARTY OR ANY OTHER PERSON OR ENTITY FOR ANY SPECIAL, CONSEQUENTIAL, INCIDENTAL, INDIRECT, EXEMPLARY OR PUNITIVE DAMAGES, HOWEVER CAUSED, ARISING OUT OF OR IN CONNECTION WITH THE DOWNLOADING, PROVISIONING, VIEWING OR USE OF THE MATERIALS REGARDLESS OF THE FORM OF ACTION, WHETHER FOR BREACH OF CONTRACT, BREACH OF WARRANTY, TORT, NEGLIGENCE, INFRINGEMENT OR OTHERWISE (INCLUDING, WITHOUT LIMITATION, DAMAGES BASED ON LOSS OF PROFITS, DATA, FILES, USE, BUSINESS OPPORTUNITY OR CLAIMS OF THIRD PARTIES), AND WHETHER OR NOT THE PARTY HAS BEEN ADVISED OF THE POSSIBILITY OF SUCH DAMAGES. THIS LIMITATION SHALL APPLY NOTWITHSTANDING ANY FAILURE OF ESSENTIAL PURPOSE OF ANY LIMITED REMEDY PROVIDED HEREIN.

- Should any provision of this Agreement be held by a court of competent jurisdiction to be illegal, invalid, or unenforceable, that provision shall be deemed amended to achieve as nearly as possible the same economic effect as the original provision, and the legality, validity and enforceability of the remaining provisions of this Agreement shall not be affected or impaired thereby.

- The failure of either party to enforce any term or condition of this Agreement shall not constitute a waiver of either party's right to enforce each and every term and condition of this Agreement. No breach under this agreement shall be deemed waived or excused by either party unless such waiver or consent is in writing signed by the party granting such waiver or consent. The waiver by or consent of a party to a breach of any provision of this Agreement shall not operate or be construed as a waiver of or consent to any other or subsequent breach by such other party.

- This Agreement may not be assigned (including by operation of law or otherwise) by you without WILEY's prior written consent.

- Any fee required for this permission shall be non-refundable after thirty (30) days from receipt by the CCC.

- These terms and conditions together with CCC's Billing and Payment terms and conditions (which are incorporated herein) form the entire agreement between you and WILEY concerning this licensing transaction and (in the absence of fraud) supersedes all prior agreements and representations of the parties, oral or written. This Agreement may not be amended except in writing signed by both parties. This Agreement shall be binding upon

and inure to the benefit of the parties' successors, legal representatives, and authorized assigns.

- In the event of any conflict between your obligations established by these terms and conditions and those established by CCC's Billing and Payment terms and conditions, these terms and conditions shall prevail.

- WILEY expressly reserves all rights not specifically granted in the combination of (i) the license details provided by you and accepted in the course of this licensing transaction, (ii) these terms and conditions and (iii) CCC's Billing and Payment terms and conditions.

- This Agreement will be void if the Type of Use, Format, Circulation, or Requestor Type was misrepresented during the licensing process.

- This Agreement shall be governed by and construed in accordance with the laws of the State of New York, USA, without regards to such state's conflict of law rules. Any legal action, suit or proceeding arising out of or relating to these Terms and Conditions or the breach thereof shall be instituted in a court of competent jurisdiction in New York County in the State of New York in the United States of America and each party hereby consents and submits to the personal jurisdiction of such court, waives any objection to venue in such court and consents to service of process by registered or certified mail, return receipt requested, at the last known address of such party.

WILEY OPEN ACCESS TERMS AND CONDITIONS

Wiley Publishes Open Access Articles in fully Open Access Journals and in Subscription journals offering Online Open. Although most of the fully Open Access journals publish open access articles under the terms of the Creative Commons Attribution (CC BY) License only, the subscription journals and a few of the Open Access Journals offer a choice of Creative Commons Licenses. The license type is clearly identified on the article.

The Creative Commons Attribution License

The Creative Commons Attribution License (CC-BY) allows users to copy, distribute and transmit an article, adapt the article and make commercial use of the article. The CC-BY license permits commercial and non-

Creative Commons Attribution Non-Commercial License

The Creative Commons Attribution Non-Commercial (CC-BY-NC)License permits use, distribution and reproduction in any medium, provided the original work is properly cited and is not used for commercial purposes.(see below)

Creative Commons Attribution-Non-Commercial-NoDerivs License

The Creative Commons Attribution Non-Commercial-NoDerivs License (CC-BY-NC-ND) permits use, distribution and reproduction in any medium, provided the original work is properly cited, is not used for commercial purposes and no modifications or adaptations are made. (see below)

Use by commercial "for-profit" organizations

AFFIDAVIT

I hereby confirm that my thesis entitled *"A Very Positive Image of Boron: Triarylborane Chromophores for Live Cell Imaging"* is the result of my own work. I did not receive any help or support from commercial consultants. All sources and/or materials applied are listed and specified in the thesis. Furthermore, I confirm that this thesis has not yet been submitted as part of another examination process neither in identical nor similar form.

Würzburg, 04.03.2019

Signature

EIDESSTAATLICHE ERKLÄRUNG

Hiermit erkläre ich an Eides statt, die Dissertation *"A Very Positive Image of Boron: Triarylborane Chromophores for Live Cell Imaging"* eigenständig, d.h. insbesondere selbstständig und ohne Hilfe eines kommerziellen Promotionsberaters angefertigt und keinen anderen als die von mir angegebenen Quellen und Hilfsmittel verwendet zu haben. Ich erkläre außerdem, dass die Dissertation weder in gleicher noch ähnlicher Form bereits in einem anderen Prüfungsverfahren vorgelegt hat.

Würzburg, 04.03.2019

Unterschrift